INSTITUTE OF GEOLOGY AND MINERALOGY SB RAS

V.S. SOBOLEV INSTITUTE OF GEOLOGY AND MINERALOGY
SIBERIAN BRANCH
RUSSIAN ACADEMY OF SCIENCES

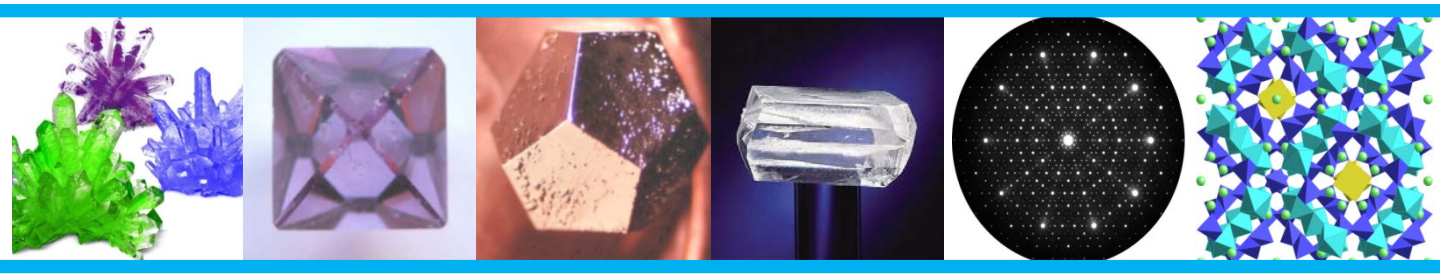

III INTERNATIONAL CONFERENCE

CRYSTALLOGENESIS AND MINERALOGY

ABSTRACT VOLUME

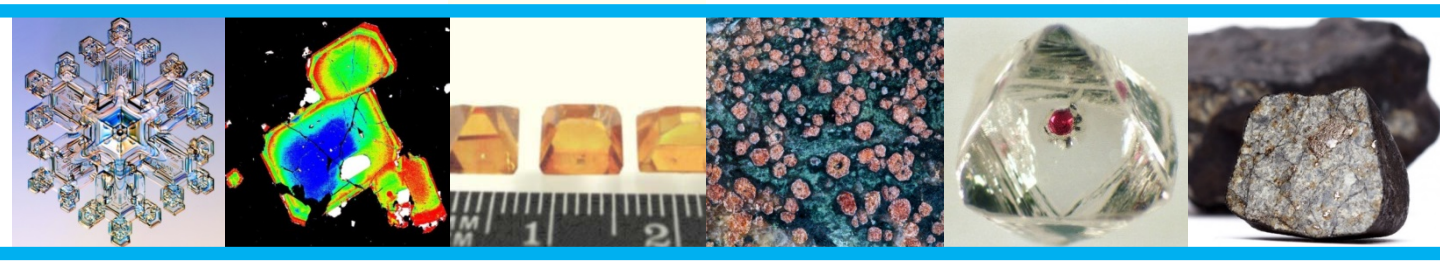

September 27 – October 1, 2013
Novosibirsk, Russia

Russian Academy of Sciences
Siberian Branch
V.S. Sobolev Institute of Geology and Mineralogy

III International Conference

CRYSTALLOGENESIS AND MINERALOGY

September 27 – October 1, 2013
Novosibirsk, Russia
http://km.igm.nsc.ru

Dedicated to the memory of
Arkady E. Glikin (1943-2012)
and to the 105th anniversary of
Vladimir S. Sobolev (1908-1982)

ABSTRACT VOLUME

Compiled and edited by
T.B. Bekker
K.D. Litasov
N.V. Sobolev

Тезисы докладов
3-ей международной конференции
«Кристаллогенезис и минералогия»

27 сентября – 1 октября 2013 г.
Новосибирск
Издательство Сибирского отделения
Российской Академии наук

УДК 548.5+549
ББК 22.37+26.303
Т29

III International Conference "Crystallogenesis and mineralogy", Abstracts Volume: Abstracts of the III International Conference "Crystallogenesis and mineralogy", Novosibirsk, 27 September – 1 October, 2013 (Ed., T.B. Bekker, K.D. Litasov, N.V. Sobolev) / Russian Academy of Sciences, Siberian Branch, V.S. Sobolev Institute of Geology and Mineralogy. - Novosibirsk: Publishing House of SB RAS, 2013. - 353 p.

Тезисы докладов 3-ей международной конференции «Кристаллогенезис и минералогия», 27 сентября – 1 октября 2013 г., Новосибирск / [под ред. Т.Б. Беккер, К.Д. Литасова, Н.В. Соболева]; Российская академия наук, Сибирское отделение, Институт геологии и минералогии им. В.С. Соболева. - Новосибирск: Из-во СО РАН, 2013. - 353 с.
ISBN 978-5-7692-1320-5

Contributors and Sponsors:

V.S. Sobolev Institute of Geology and Mineralogy SB RAS

Siberian Branch of Russian Academy of Sciences

Russian Foundation for Basic Research

Novosibirsk State University

Institute of Solid State Chemistry and Mechanochemistry SB RAS

St. Petersburg State University

Russian Mineralogical Society

International Union of Crystallography (IUCr)

International Mineralogical Association (IMA)

Ministry of Education and Science of Russian Federation

Deep Carbon Observatory

ALROSA

Almax Easy Lab

TechnoInfo

OPTEC

Huber

ISBN 978-5-7692-1320-5

ORGANIZING COMMITTEE

Chairmen:

Nikolay P. Pokhilenko (IGM SB RAS, Novosibirsk), Chair
Nikolay V. Sobolev (IGM SB RAS, Novosibirsk), Chair
Juan Manuel García-Ruiz (University of Granada), Co-chair
Elena V. Boldyreva (Novosibirsk University), Co-chair

Conference Secretary:

Tatyana B. Bekker (IGM SB RAS, Novosibirsk), *t.b.bekker@gmail.com*

Members:

Maria Bykova
Konstantin Litasov
Vasily Minkov
Yurii Palyanov
Sergey Rashchenko
Alexey Ragosin
Vadim Reutsky
Sergey Smirnov
Andrey Vishnevsky
Dmitry Zedgenizov

International Program Committee:

Askhab Askhabov (Syktyvkar)
Vladimir Balitsky (Chernogolovka)
Luca Bindi (Florence)
Andrey Bulakh (St. Petersburg)
Hanna Dabkowska (Hamilton)
Wulf Depmeier (Kiel)
Leonid Dubrovinsky (Bayreuth)
Pavel Fedorov (Moscow)
Yingwei Fei (Washington)
Karen Friese (Jülich)
Peter Gille (Munich)
Lyudmila Isaenko (Novosibirsk)
Hiroyuki Kagi (Tokyo)
Alexander Kokh (Novosibirsk)
Elena Kotelnikova (St. Petersburg)
Sergey Krivovichev (St. Petersburg)
Nicolay Leonyuk (Moscow)
Heike Lorenz (Germany)
Yury Marin (St. Petersburg)
Eiji Ohtani (Sendai)
Dmitry Pushcharovsky (Moscow)
Ramiza Rastsvetaeva (Moscow)
Dmitry Rundqvist (Moscow)
Yury Seryotkin (Novosibirsk)
Vladislav Shatsky (Irkutsk)
Steve Shirey (Washington)
Lawrence Taylor (Knoxville)
Katsuo Tsukamoto (Sendai)
Vadim Urusov (Moscow)
Alexey Voloshin (Moscow)

DEDICATION

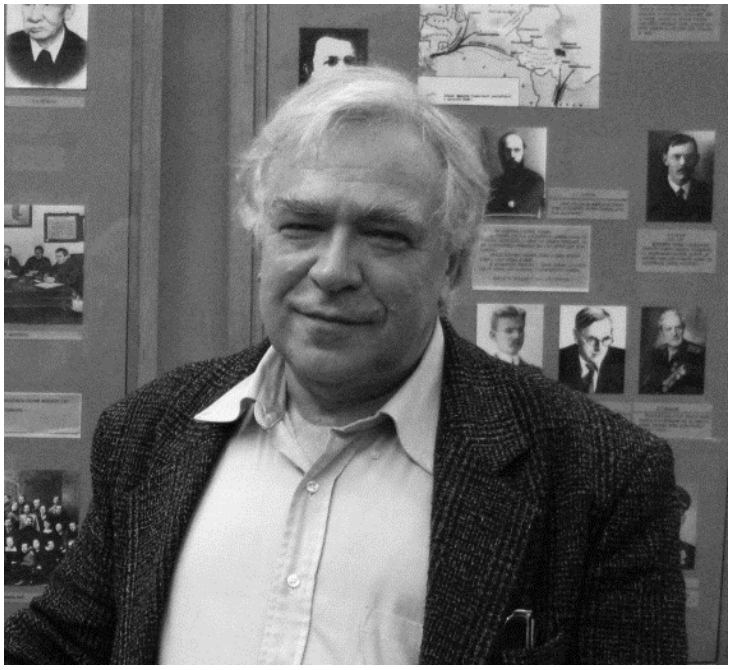

Arcady Eduardovich Glikin (1943 – 2012) was born in Kostroma, where his parents resided after the first Leningrad blockade winter of 1942-1943. During his school years, Arcady was fascinated by geology, which led him to the Club of Young Geologists of the Leningrad Palace of Pioneers. In 1960, Arcady entered the Leningrad State University (LSU) and since third year of study began to specialize in crystallography. Since 1963 and till the end of his life, i.e. for over 49 years, his scientific and teaching activities were connected with the Department of Crystallography of Faculty of Geology of the LSU. After graduation in 1965, Arcady was enrolled to Ph.D. study at the same Department, where he also worked as (successively) a technician, young, senior, leading and major scientist, being a member of the LSU Scientific Institute of the Earth Crust. In 1978, he obtained his Ph.D. degree for his dissertation 'Structural-chemical evaluation of the influence of components of crystallization media upon crystal morphology'. In 1996, he defended his Doctor of Sciences (Habilitation) dissertation 'Modeling metasomatic crystallogenesis using aqueous salt systems'. In 1999, he received a Scientific Title of Professor in 'Mineralogy and crystallography'.

A.E. Glikin created a scientific school known for its studies on fundamentals of crystallogenesis and modeling of natural mineralogenetic processes. Basic ideas and applications of his approach are described in details in his book 'Polymineral-Metasomatic Crystallogenesis' published by Springer-Verlag in 2009. His main achievements concerned with the genetic basis of isomorphism in crystals, metasomatic replacement of crystals, recrystallization of polymineral aggregates, and oriented crystal intergrowths (epitaxy and quasi-epitaxy). In addition, he worked on structural and chemical modeling of crystal morphogenesis for anomalous kinetic conditions of crystal growth.

Outstanding organizational abilities of A.E. Glikin were revealed in his active participation in and organization of numerous scientific conferences. He was a member of the Council of the Russian Mineralogical Society and Deputy Editor of its main journal, 'Proceedings of the RMS' ('Zapiski'). In 2001, under auspice of the Russian Mineralogical Society, he initiated the series of International Conferences 'Crystallogenesis and Mineralogy'. The Ist and the IInd conferences were held in St.Petersburg in 2001 and 2007, respectively. A.E. Glikin proposed and initiated the organization of present (3rd) conference in Novosibirsk, however, tragically passed away on August 26, 2012. This conference is dedicated to his bright memory.

DEDICATION

Vladimir Stepanovich Sobolev (1908-1982). Within more than 50 years of his scientific activities, beginning with graduating from Leningrad Mining Institute in 1930, Vladimir Sobolev contributed significantly to the Earth´s sciences. His critical role in the discovery of the Siberian diamond deposits received international recognition. All his scientific work was devoted to the developments in mineralogy and petrology including the application of physical and chemical methods to the analysis of the processes of mineral formation, especially, silicates. His book "Introduction to the Mineralogy of Silicates" (1949) was met with great interest not only by mineralogists, but also by chemists. He was an eminent petrologist and mineralogist and is a past President of International Mineralogical Association.

Vladimir Sobolev was the first to compare and summarize data on the formation conditions of synthetic and natural diamonds, to estimate the critical role of fluids in diamond and other crustal and mantle mineral formation. He initiated systematic study of Siberian kimberlites, their peridotite and eclogite xenoliths, diamonds and associated minerals. Fifteen years after the publication of his ideas on mineralogy, crystal chemistry and classification of silicates, Vladimir Sobolev proposed a new scheme of metamorphic facies based on the available experimental data of the most important mineral equilibria with special attention to significance of high pressure during the formation of crustal and mantle rocks.

Since Vladimir Sobolev pioneering research, the extent of scientific information available from the studies on diamonds and their inclusions, mantle xenoliths and crustal metamorphic rocks, have expanded immensely. This has arisen from the development and application of many new techniques of diffraction and spectroscopy, together with the possibilities provided by ultrahigh pressure and temperature experiments. The use of these techniques and the new types of information they provide are particularly well exemplified by the major topics of this Conference.

PLENARY LECTURES

STRUCTURAL COMPLEXITY OF MINERALS AND INORGANIC COMPOUNDS: STATISTICS AND RELATION TO CRYSTALLIZATION PROCESSES

Krivovichev S.V.

Saint-Petersburg State University (SPSU), Saint-Petersburg, Russia
s.krivovichev@spbu.ru

Evolution of matter toward states of higher complexity in the course of the evolution of the Universe is one of the most exciting and interesting topics in modern science and in modern chemistry in particular. A number of different approaches have been suggested in order to quantitatively evaluate complexity of chemical, biological, technological and even social systems. Most of these approaches are based upon the extensive use of concepts and techniques borrowed from the information theory developed in the second half of the XXth century as a theory of communication and transmission of information. Nowadays complexity theory is a well-developed field within computer science with interdisciplinary applications in many areas of theoretical and applied science. It is interesting, however, that complexity theorists have always regarded crystals as 'intuitively simple objects', in contrast to much more complex and dynamic biological systems. On the other hand, it was largely appreciated that crystal structures may possess different degrees of complexity, which has been reflected in titles of scientific papers with the use of expressions such as 'complicated structure', 'the most complex structure', 'complexity', 'complex superstructures', 'a masterpiece of structural complexity', etc. However, until recently complexity of crystal structures was destined to be 'largely a qualitative, frequently intuitive, notion', which escaped a quantitative definition.

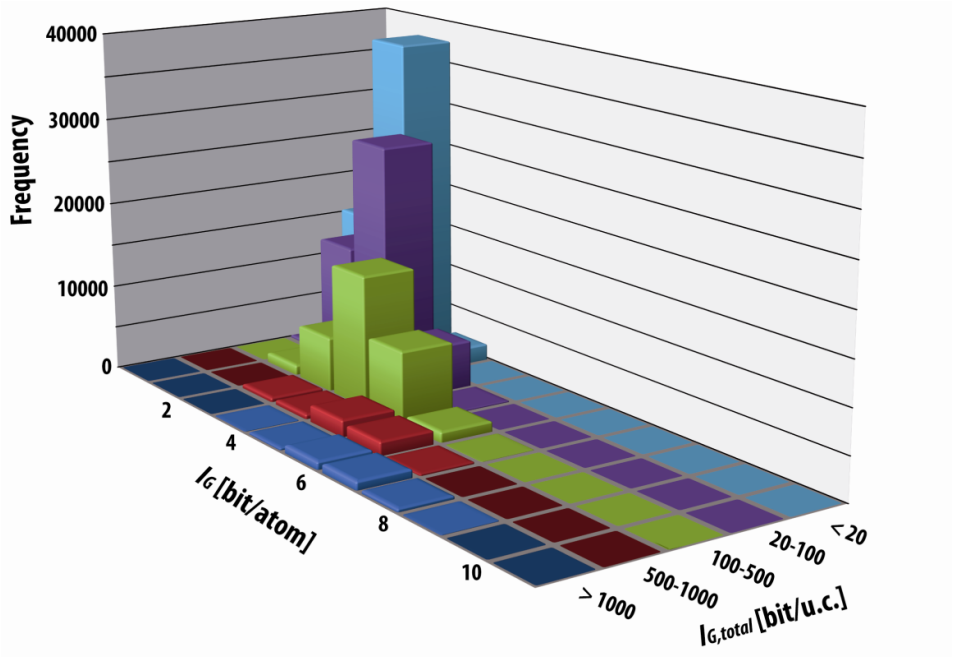

Figure 1. Histogram showing distribution of inorganic crystal-structure reports stored in the Inorganic Crystal Structure Database (ICSD) according to the values of the information-based I_G and $I_{G,total}$ parameters.

In order to analyze complexity of inorganic structures on a large-scale basis, complexity parameters have been calculated for all crystal-structure entries stored in the Inorganic Crystal Structure Database (ICSD) using the *TOPOS* program package. Figure 1 shows distribution of

the ICSD reports according to the information contents per atom (I_G) and per unit-cell ($I_{G,total}$). According to the $I_{G,total}$ values, all structures can be subdivided into very simple, simple, intermediate, complex, and very complex. It can be seen from Figure 1 that most ICSD structure reports are for very simple and simple structures that together constitute about 75% of the ICSD data. This reflects the fact that structurally and chemically simple inorganic compounds have been most studied over the last hundred years, though the general current trend is towards elucidation of structures with increasing complexity.

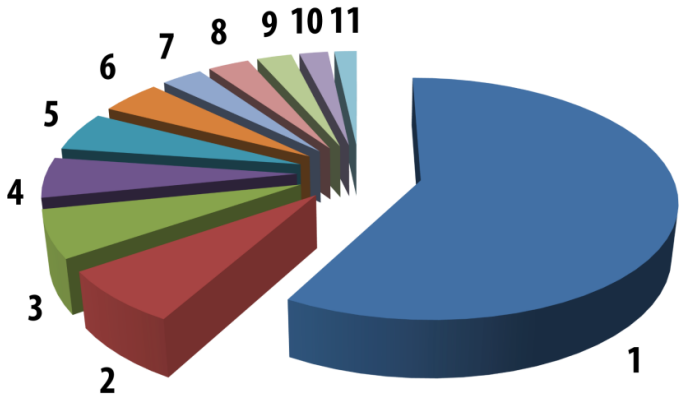

Figure 2. Classification of 1000 most complex inorganic structures: 1 – Mo-W-V-based polyoxometallates; 2 – oxides and oxysalts; 3 – structures containing (nano)clusters; 4 – zeolites and microporous framework compounds; 5 – intermetallic compounds (inc. borides and silicides); 6 – fullerene-based structures; 7 – uranyl peroxide nanospheres; 8 – superstructures of simple structure types; 9 – Nb-Ti-based polyoxometallates; 10 – sulphides and selenides; 11 – halogenides.

Analysis of 2000 most complex structures stored in the ICSD according to their belonging to specific classes of inorganic compounds is shown in Figure 2. About 90% of all these compounds are structures based upon nanoscale-sized clusters with 82% represented by Mo-, W- and V-based polyoxometallates. Among other classes are: oxides and oxysalts (e.g., silicates, sulfates, borates, etc.), zeolites and microporous framework materials, intermetallic compounds, borides and silicides, superstructures of simpler structure types, sulphides and selenides, and halogenides.

In this contribution, we shall discuss various aspects of structural complexity of minerals and inorganic solids **[1-4]**, from the reasons of complexity to the relations between complexity and the 'ease' of crystallization.

This work was supported by the Russian Federal Grant-in-Aid Program 'Cadres' (agreement 8313).

References:

[1] Krivovichev, S., Topological complexity of crystal structures: Quantitative approach. *Acta Crystallogr. A.* **2012,** *68* (3), 393-398.
[2] Krivovichev, S. V., Information-based measures of structural complexity: Application to fluorite-related structures. *Struct. Chem.* **2012,** *23* (4), 1045-1052.
[3] Krivovichev, S. V., Structural and topological complexity of zeolites: An information-theoretic analysis. *Micropor. Mesopor. Mater.* **2013,** *171*, 223-229.
[4] Krivovichev S.V., Structural complexity of minerals: information storage and processing in the mineral world. *Mineral. Mag.* **2013**, *25*, 275-326.

PATTERN FORMATION AND CHEMICAL COUPLING IN HIGHLY ALKALINE SILICA-RICH ENVIRONMENTS

García-Ruiz, J.M.

Laboratorio de Estudios Cristalográficos, Instituto Andaluz de Ciencias de la Tierra, CSIC-Universidad de Granada, Granada, Spain
juanma.garciaruiz@gmail.com

Since the pioneering book of Grigoriev **[1]**, the study of the growth of single crystals was expanded to cover also crystal aggregates with complex shapes and textures in mineral precipitation. Bizarre as it might seem, purely inorganic processes may also produce self-assembled complex crystalline materials that –like those produced by living organisms- are not controlled by crystallographic symmetry. Such a kind of crystalline materials must be -by definition- polycrystalline, because the restricted point symmetry of the single crystal has to be expanded in order to develop complexity. Complexity means in this context self-assembled shapes with either positive or negative Gaussian constant curvature. Silica biomorphs is a synthetic type of material that shares with life complexity, morphology, hierarchy and self-assembly yet they are remarkably simple in chemical terms **[2,3]**. The synthesis requires only a source of carbonate ions (e.g atmospheric CO_2), strong alkaline aqueous solutions, silica and alkaline-earth cations (Ba and Sr, Ca). Under these alkaline conditions, the precipitation of alkaline-earth carbonates (witherite, strontianite or calcite/aragonite) coupled with silica yields aggregates made of millions of nanocrystals exhibiting self-assembled complex noncrystallographic morphologies. There have been significant advances in the understanding of these fascinating and challenging structures (see reference **[2]**). A phenomenological explanation of the morphogenesis of these complex structures has been already achieved **[4]** while the chemistry triggering their formation is thought to be an autocatalytic process due to the coupling of silica and carbonate precipitation, because of their reverse solubility with respect to pH. This theory has not been ye experimentally validated because the difficulty to measure pH oscillations at the scale of a hundred of microns. Another fascinating feature, still unexplained, is the role of crystal structure in controlling the morphology of silica biomorphs. It is known that shapes with continuous curvature are only made by aragonite-type structures (aragonite, witherite, strontianite), while rombohedrical type structures (calcite) only form complex fractal shapes. I will review in this talk the latest experimental achievements towards a better understanding of silica biomorphs, namely a) high resolution pH monitoring in real time and space by fluorescence optical microscopy and b) experiments designed to relate shape with crystal structure. I will also discuss the expected scenarios for the formation of these structures in mineral environments and the plausible geochemical role that they might play, particularly during early stages of the history of the planet.

This work was supported by the Spanish Consolider-Ingenio 2010 project "Factoría de Cristalización" CSD2006-00015 and by the project CGL2010-16882 of the Ministry of Science and Innovation.

[1] D. P. Grigoriev, D.P., 1965. Ontogeny of Minerals (Israel Program for Scientific Translation, Jerusalem, Israel).
[2] M. Kellermeier, M., Cölfen, H., and García-Ruiz, J.M., 2012. European Journal of Inorganic Chemistry 5123–5144. Doi: 10.1002/ejic.20121029.
[3] García-Ruiz, J.M., Hyde, S., Carnerup, A., Christy, A., Van Kranendonk, M., Welham, N. J., 2013. Science 302: 1194-1197.
[4] García-Ruiz, J.M., Melero, E., Hyde, S., 2009 Science 323: 362-366.

BUILDING UNITS IN CRYSTALLOGENESIS

Askhabov A.M.

Institute of Geology, Komi Sci. Center, Ural Br., RAS, Syktyvkar, Russia
xmin@geo.komisc.ru

In the beginning of last century it became clear that the mechanism of crystals growth cannot be established without taking into account the sizes and the nature of building units, i.e. those structural units which joining forms the ordered (crystalline) matter from disordered environment. Within the frames of such methodical approach to the analysis of processes of crystals formation two concepts were the most distributed. The first one was formed on ideas of Kossel-Stransky-Kaishev molecular-kinetic theory of crystals growth, it assumes that crystals grow by joining of separate atoms (ions) or molecules. This concept which is often called Kossel's, is considered classical. It is namely in its frames that the majority of known theoretical models of crystals growth was developed. The second (Balarev's) concept originates from E.S.Fedorov's works and is developed most fully by D.Balarev **[3].** It asserts that growth of crystals occurs by joining of ready crystalline particles (blocks).

The concept of block or microblock growth of crystals was popular enough in the 1920-30-s. It seemed that the data on mosaic, imperfect structure of crystals also confirmed the assumption on formation of crystals from separate blocks. However in the discussion arisen the main provisions of the theory of microblock growth of crystals were subjected to serious criticism and lost popularity. In particular, theorists - physicists and chemists, unlike mineralogists and practitioners-growers completely lost interest to growth of crystals from separate crystal particles. This also occurred because the conceptual assumptions of ultra-micro-heterogeneous (colloidal-disperse) structure of real crystals had no universal corroboration.

Nevertheless, we have no grounds for complete refusal of the possibility of formation of crystals in certain conditions from separate crystal blocks. Moreover, interest to the ideas stated by E.S.Fedorov, D.Balarev, A.V.Shubnikov, N.P.Sheftal, I.Sunagava, periodically arises **[6,7]**. For example, N.P.Yushkin **[6]** considers microblock growth the only possible mechanism of growth from natural heterogeneous solutions. He asserts: " … in the nature we constantly meet perfectly faceted crystals of sparingly soluble and insoluble minerals in water, but cryslallized namely from water solutions" (P. 4). In such cases Kossel's concept of atomic growth of crystals basically cannot be used for explanation of their genesis. Hence, if crystal forming crystalline particles are formed or exist in environment, then we, obviously, cannot exclude their participation in the growth process. By the way, the same concerns growth of crystals by joining particles of another nature which existence in crystal-forming medium is also possible.

On this basis various models of crystals growth, that greatly differ both from models of atomic growth, and from microblock growth were built. Various molecular complexes, associations of molecules and other groupings of particles, which existence in crystal forming medium is practically not debated now, can be considered as building units in these models. In particular, the idea on growth of crystals from molecular complexes was stated by R.O.Grisdale in 1968 **[4]**. Finally these ideas were transformed to various variants of cluster growth of crystals or preliminary cluster self-organization in crystal-forming systems. So, in the concept of matrix assemblage of crystalline structures developed by G.D.Ilyushin **[5]**, a key building element is polyhedral cluster - precursor or super (over) precursor. Thus «simply ensemble from n atoms even if atoms have dense packing and are characterized by the minimum energy as a whole, is not the precursor of structure. For this purpose it should possess special crystallographic properties to be integrated into three-dimensional-periodic lattices» (P. 44).

In this case the new concept **[1-2]** proposed by us in which the main building units are special nanosize clusters of proto-phase or «hidden phase» named quatarons, does not have any structural and symmetrical limitations on building units. Quatarons are amorphous formations

(pre-nucleation clusters) of dynamic structure and mainly quasispherical form. The arrangement of atoms and angles between them in quatarons are not strictly fixed. On this and other reasons they represent ideal formations as building units in growth of crystals. Complementary structures necessary for problemless incorporation in crystal's lattice potentially already exist or can easily be formed in quatarons. Quatarons are the only nonequilibrium structures from all those considered in various concepts and models of building units of crystals growth which in turn also occur in nonequilibrium conditions.

Structurally stabilized and energetically minimized cluster structures formed on the basis of quatarons, for example fullerene-like or magic icosahedral clusters cannot serve as building units for crystals growth. Similar formations in the condensed state form amorphous substances, they can be considered as the structural units forming mineraloides. Only very seldom they or their aggregates form three-dimensional ordered objects of the type of fullerites or noble opals.

Thus, owing to variety in the nature and structure of building units, growth of crystals represents polyrouting process. Depending on conditions of growth these or other building units can appear the predominating ones. However it should be noted that the growth of a crystal occurring with participation of all other types of building units, can be interpreted in terms of the quataron concept. And this is the indisputable relative universality of the quataron concept of crystals and quatarons formation as basic building units at growth of crystals.

The work on non-classical mechanisms of crystallization is supported by the Program of Basic Researches of the Ural Branch, RAS (№ 12-T-5-1022) and the RFBR (Project 11-25-004320).

References:

[1] A.M. Askhabov. Processes and mechanisms of crystallogenesis. L.: Nauka, 1984. 168 p.

[2] A.M. Askhabov. The quataron concept: main ideas and some applications // Proceedings of the Komi Sci.Centre, Ural Br., RAS, 2011, No. 3. P. 70-77.

[3] D. Balarev. Stroezh na realnokrystalnite systemi. Sofia, 1964. 266 p.

[4] R.O. Grisdale. The growth of crystals from molecular complexes // Theory and practice of growing crystals, 1968, P. 176-189.

[5] G.D. Ilyushin. Modelling of processes of self-organization in crystal forming systems. Editorial URSS, 2003, 376 p.

[6] N.P. Yushkin. Theory of microblock growth of crystals in natural heterogeneous solutions. Syktyvkar, 1971, 52 p.

[7] M. Niederberger and H. Gölfen. Oriented attachment and mesocrystals: non-classical crystallization mechanisms based on nanoparticle assembly // Phys.Chem. Chem.Phys., 2006. V.8, p. 3271-3287.

PHASE RELATIONS AND PHYSICAL PROPERTIES OF IRON ALLOYS AT HIGH PRESSURE: APPROACH TO THE EARTH'S CORE

Ohtani E.

Department of Earth and Planetary Materials Science, Graduate School of Science, Tohoku University, Sendai, Japan
ohtani@m.tohoku.ac.jp

Compositional and thermal structures of the core are the key issues for better understanding the central part of the Earth. The partitioning of light elements between the inner and outer core is an important clue to determine the light element abundances in the inner and outer cores because the inner core was crystallized from the molten outer core. We have conducted in situ X-ray diffraction studies on melting and phase relations of several iron-light element binary and ternary systems such as Fe-S, Fe-Si, and Fe-S-Si systems to the core pressures based on the in situ X-ray powder diffraction using the synchrotron X-ray radiation combined with the laser heated diamond anvil cell at BL10XU, SPring-8. The recovered samples were excavated by a FIB system for textural observations with FEG-SEM and chemical analysis with EDS. Our results on melting relations in the Fe–S–Si system to 135 GPa revealed that silicon is partitioned into the solid hcp-iron alloy, whereas the coexisting metallic liquid is enriched in sulfur, i.e., D(Si)S/L> 1 and D(S)S/L< 1. If the Earth's core contains both sulfur and silicon as light elements, the core is divided by a sulfur-rich outer core and a silicon-rich inner core.

Sound velocity is the most accurate information in seismology and can provide important clues on the structure and composition of the core. In spite of its importance, the sound velocity data of the core materials at high pressure and temperature are still very limited due to technical difficulties. We measured the compressional velocity of hcp-iron and the other alloys by the inelastic X-ray scattering (IXS) method using DAC at high pressure and temperature. Inelastic X-ray scattering spectra were taken at BL35XU, Spring-8. We made the IXS measurement to 174 GPa, the highest pressure at room temperature in this method. Compressional velocity measurements at high temperature were made by using both external heating and laser heating. We developed a portable laser heating system and successfully measured the IXS spectra to temperatures up to 3000 K at 100 GPa. We also measured the compressional velocity and density of $Fe_{0.83}Ni_{0.09}Si_{0.08}$ to 151 GPa and Fe_3S to 85 GPa at room temperature. These data could provide new clues for understanding the compositional and thermal structures of the inner core.

Our IXS measurements revealed that the compressional velocity-density relation of hcp-Fe at 300 K is consistent with recent IXS results [1, 2]. We obtained following Birch's law by fitting our results and the recent hcp-Fe data-sets at 300 K [1, 2]: V_p [km/s] = 1.174($\pm$0.031)ρ [g/cm^3] – 3.591($\pm$0.326) (R^2 = 0.989). The sound velocity of hcp-Fe was measured up to 3000 K at 100 GPa by using a double sided portable laser heating system, and the results revealed that there is a temperature dependency in Birch's law which is consistent with the shock compression experiments [3] and the *ab-initio* calculations [4, 5].

The present experimental results on partitioning of Si and S between the liquid and solid iron alloys and the compressional velocity data of hcp-Fe, Fe_3S, and $Fe_{0.83}Ni_{0.09}Si_{0.08}$ revealed that the PREM outer and inner cores can be accounted for by a pair of the sulfur-enriched outer core (with 0.4–1.7 at.% Si and 9.5 at.% S) and silicon-enriched inner core (with 2.4–4.5 at.% Si and 0.3–1.3 at.% S), which are consistent with the compositions of the outer and inner cores proposed by previous studies [6, 7, 8].

This work was conducted by collaboration with T. Sakai (GRC), S. Kamada, T. Sakamaki, S. Takahashi, T. Sakairi, (Tohoku Univ), K. Mibe (ERI), Y. Shibazaki (CIW), H. Fukui (Riken, Univ Hyogo), S. Tsutsui (SPring-8), A.Q.R. Baron (Riken, SPring-8). I appreciate them for their

important contributions. This work was supported by JSPS KAKENHI Grants Nos. 18104009 and 22000002 and Ministry of Education and Science of RF (No 14.B25.31.0032).

References:

[1] Mao, Z., et al. (2012), Sound velocities of Fe and Fe-Si alloy in the Earth's core, www.pnas.org/cgi/doi/ 10.1073/pnas.1207086109.
[2] Antonangeli, D., et al. (2012), *Earth Planet. Sci. Lett.*, *331–332*, 210–214.
[3] Brown, J. M., and R. G. McQueen (1986), *J. Geophys. Res.*, *91*, 7485-7494.
[4] Ono, S., Mibe, K., 2010. Physics of the Earth and Planetary Interiors, 180: 1-6.
[5] Vočadlo, L., Dobson. D. P., and Wood, I. G. (2009), *Earth Planet. Sci. Lett., 288*, 534–538.
[6] Sha, X., R. E. Cohen (2010), *Geophys. Res. Lett.*, *37*, L10302, doi:10.1029/2009GL042224.
[7] Antonangeli, D. et al. *Earth Planet. Sci. Lett.* **295,** 292–296 (2010).
[8] Huang, H. et al. *Nature* **479,** 513–516 (2011).

CARBON AT HIGH PRESSURE: SOLUBILITY AND MELTING IN THE Fe-C SYSTEM AND DYAMOND SYNTHESIS

Fei Y.

Geophysical Geophysical Laboratory, Carnegie Institution of Washington, Washington, DC 20015, USA
fei@gl.ciw.edu

It is important to understand the behavior of the Fe-C system at high pressure because of its applications to geophysics and super-hard materials synthesis. The phase relations in the Fe-C system at ambient pressure have been well established, with a eutectic point at 1420 K and 4.3 wt% carbon. The maximum carbon solubility in fcc-Fe is about 2.14 wt% C. We have determined the effect of pressure on the eutectic temperature up to 25 GPa in the multi-anvil device. The eutectic temperature increases linearly with increasing pressure, with a measured value of 1975K at 25 GPa. By careful calibrations and measurements of carbon content in the quenched sample, we were able to establish melting and phase relations in the Fe-C system at 5, 10, 20, and 25 GPa. The solubility of carbon in metallic iron and the eutectic composition seem to slightly decrease with increasing pressure. At 5 GPa, iron carbide Fe_3C coexists with graphite whereas Fe_3C coexists with Fe_7C_3 at 10 GPa, indicating that a reaction $3Fe_7C_3 = 7Fe_3C + 2C$ occurs at a pressure between 5 and 10 GPa, consistent with previous study of the system at high pressure. We have also invested the carbon solubility in metallic iron and stability of Fe_3C in the laser-heated diamond anvil cell by in-situ synchrotron X-ray diffraction. It is clear that the solubility of carbon in iron is substantially decreased at higher pressure and Fe_3C is stable to very high pressure.

Diamond can easily form in the Fe-C system at pressures higher than 5 GPa. We have been also exploring diamond synthesis with different carbon precursors, including graphene and mesoporous carbon. We were able to synthesize transparent, mesoporous diamond monoliths from periodic mesoporous carbon CMK-8 at temperatures as low as 1600 K. We are developing new techniques to produce nanocrystalline diamonds and diamond composites. This development will lead to new applications of diamond-related materials and further development of high-pressure techniques.

THE IMPOSSIBLE FALLEN FROM THE SKY

Bindi L.

Dipartimento di Scienze della Terra, Università di Firenze, Firenze, Italy
luca.bindi@unifi.it

The regularly repeating atomic arrangement in crystals is called periodic. The hexagons in a honeycomb lattice or the square tiles in a bathroom tiling are examples of periodic tessellations. According to the laws of mathematics discovered in the 19th century, periodicity can only occur for certain rotational symmetries: one-, two-, three-, four- and six-fold symmetry are allowed; but crystals or periodic tilings with five-, seven-, eight- or higher-fold symmetry axes are strictly forbidden. About thirty years ago, however, a new kind of material that violates these rules was hypothesized **[1]** and dubbed *quasicrystals* (short for *quasiperiodic crystals*), and, independently, a synthetic example was discovered in the laboratory **[2]**. Since then, over a hundred different types have been made in the laboratory using highly controlled synthetic methods.

Quasicrystals have an atomic arrangement that is quasiperiodic, two or more types of atomic clusters each repeat at regular intervals like in a crystal; however, the ratio of intervals is irrational (not expressible as a fraction) so that the combined arrangement of atoms never exactly repeats. Because they are quasiperiodic, they can violate the mathematical theorems and have any of the rotational symmetries forbidden to crystals, including five-fold symmetry in the plane and icosahedral symmetry in three dimensions. An example is the five-fold symmetric Penrose tiling composed of two tile shapes that repeat with frequencies whose ratio is the famous irrational number known as the "golden ratio".

Are quasicrystals energetically stable and robust like crystals? Or are they metastable oddities? If some are truly stable materials, then it is conceivable that they formed under natural conditions, just like crystalline minerals. Thus, the question arises: Is it possible that quasicrystals formed through natural geologic processes long before they were discovered in the laboratory? Now the answer is known. In 2009, a new kind of mineral was discovered in a sample labeled "khatyrkite" (and catalogued as coming from the Khatyrka region of the Koryak mountains in the Chukotka autonomous okrug on the northeastern part of the Kamchatka peninsula) belonging to the collection of the Museo di Storia Naturale of the Università degli Studi di Firenze, Italy **[3]**. The mineral, the first naturally forming quasicrystal, has chemical composition $Al_{63}Cu_{24}Fe_{13}$ and has the symmetry of an icosahedron. In 2010, the new mineral was officially accepted by the Commission on New Minerals, Nomenclature and Classification of the International Mineralogical Association as the first natural quasicrystal and named *icosahedrite* for the symmetry of its atomic structure **[4]**.

A puzzling aspect for geologists was the presence of metallic aluminum in the quasicrystal grains as well as some of the other mineral phases found in the rock. Aluminum normally oxidizes unless placed in a highly reducing environment, as is done in the laboratory or in industry. Hence, serious consideration had to be given to the possibility that the sample was slag or an accidental byproduct of some anthropogenic process. Over the next two years, more data was collected that provided overwhelming evidence that the rock was formed by some natural process. Among the data was the discovery of a grain of icosahedrite trapped within stishovite, which indicated that the quasicrystal had to have formed at pressures that only occur under exotic conditions, either very deep under the surface of the Earth, near the boundary between core and mantle, or in space, through the collisions of meteors and asteroids. To distinguish the two possibilities, a series of ion probe experiments that measure the ratio of oxygen isotopes were carried out. The results were unmistakable: the oxygen isotopes matched precisely the known abundances in a form of meteorite known as carbonaceous chondrite, among the oldest meteorites to have formed in our solar system **[5]**.

Establishing that the material is indeed natural and meteoritic was based on the analyses of the sample of the Florence Museum only. The only hope for pushing the exploration further was to find new samples; but the only real chance of finding more samples with the same remarkable properties would have been to return to the place where the original samples were found: the Listvenitovyi stream in the Koryak Mountains in far eastern Russia. Despite the difficulties and the unlikely possibility of finding more samples, a geological expedition to Chukotka in far eastern Russia was undertaken in 2011 **[6,7]**. The extraordinary journey to one of the most remote places on the planet resulted in the unexpected discovery of new samples that have firmly established that the quasicrystal and the rock containing it are definitely part of a CV3 carbonaceous chondritic meteorite (officially named *Khatyrka*, after a river in Chukotka) with calcium aluminum inclusions that date back 4.5 Gya to the formation of the solar system.

What does it mean to have found the first mineral with forbidden symmetry in Nature? In geology, the discovery of a natural quasicrystal has opened a new chapter in the study of mineralogy, forever altering the conventional classification of mineral forms. In condensed matter physics, the discovery has pushed back the age of the oldest quasicrystals by orders of magnitude and has had an impact on our view of how difficult it is for quasicrystals to form. To have found a natural quasicrystal has been also a way of studying quasicrystal stability over annealing times and conditions not accessible in the laboratory and demonstrates that these materials are not inherently delicate, metastable oddities that may only be synthesized for ideal compositions and under highly controlled laboratory conditions. Identifying materials that form quasicrystals has always relied significantly on trial-and-error and serendipity, and searching through Nature has proved to be an effective complement to laboratory methods. Finally, the discovery has suggested new geologic or extra-terrestrial processes of formation. What remains is determine exactly how the collisions of asteroids produced quasicrystals and never-before-seen combinations of aluminum and copper metallic alloys. The research team will be performing a series of follow-up experiments to determine more precisely the conditions under which the novel minerals formed and the implications for the evolution of the early solar system.

References:

[1] D. Levine, P.J. Steinhardt (1984) Quasicrystals: A new class of ordered structures. *Physical Review Letters*, 53:2477-2480.

[2] D. Shechtman, I. Blech, D. Gratias, J.W. Cahn (1984) Metallic phase with long-range orientational order and no translational symmetry. *Physical Review Letters*, 53:1951-1954.

[3] L. Bindi, P.J. Steinhardt, N. Yao, P.J. Lu (2009) Natural quasicrystals. *Science*, 324:1306-1309.

[4] L. Bindi, P.J. Steinhardt, N. Yao, P.J. Lu (2011) Icosahedrite, $Al_{63}Cu_{24}Fe_{13}$, the first natural quasicrystal. *American Mineralogist*, 96:928-931.

[5] L. Bindi, J.M. Eiler, Y. Guan, L. Hollister, G.J. MacPherson, P.J. Steinhardt, N. Yao. (2012) Evidence for the extra-terrestrial origin of a natural quasicrystal. *Proc. Nat Acad. Sci. USA*, 109:1396-1401.

[6] L. Bindi, P.J. Steinhardt (2012) The discovery of the first natural quasicrystal. A new era for mineralogy? *Elements*, 8:13-14.

[7] P.J. Steinhardt, L. Bindi (2012) In search of natural quasicrystals. *Reports on Progress in Physics*, 75:092601-092611.

MORPHOTROPIC CHANGES IN CRYSTALS OF DOUBLE HALOGENIDES AND CHALCOGENIDES AS A TOOL TO CONTROL THEIR FUNCTIONAL PROPERTIES.

Isaenko L.I.

V.S. Sobolev Institute of Geology and Mineralogy of SB RAS, Novosibirsk, Russia
lisa@igm.nsc.ru

Crystals undergoing sharp structural changes when varying composition, temperature or pressure attract attention of specialists in different fields of physics and chemistry. Analysis of the composition-structure-property correlation in crystals of a morphotropic set allows one to change the structure by replacing certain atoms and producing defects in the single crystal matrix to optimize a complex of properties providing the effective application of functional materials.

From this point of view the particularly important feature is the existence of phase transition in crystals with a friable (porous?) structure (with a large number of cavities in the lattice). In the range of phase transitions the physical properties vary because the system is in the extreme conditions and it loses the stability: as a result crystal is capable to obtain a new property which can be used in a set of applications. The important task is to establish the effect of impurity and native defects on nature and temperature of phase transitions. On example of three systems: APb_2Br_5 (A=K, Rb, Cs); $BMgF_4$ (B=Ba, Sr) и CMX_2 (C=Li, Ag; M=Ga, In; X=S, Se, Te) we showed the evolution of the structure and the extension of the stability region for different phases at replacing atoms in the lattice.

Depending on the ratio between the alkali metals (x) crystals $K_xRb_{1-x}PbBr_5$ may have both monoclinic ($P2_1/c$) and tetrahedral (I4/mcm) structure. Only compounds of solid solutions with a low symmetry undergo the high-temperature ferroelastic phase transition of type II ($P2_1/c \leftrightarrow$ mmm). This is a reason why twins form and the crystal quality lowers. One should note that the level of doping by Rare elements depends strongly on lattice structure and it is particularly high in crystals of low (monoclinic) symmetry and decreases considerably in the case of tetrahedral symmetry. The partial potassium substitution for rubidium allows one to avoid the twins' formation at phase transition whereas high segregation coefficient for Rare Earth elements is saved and such crystals can be used as active media for laser systems operating in the IR region.

Similar regularities are observed for compounds of variable composition $Ba_xSr_{1-x}MgF_4$, but in our case in the whole "x" range the crystal is related to noncentrosymmetric ferroelectrics and existence of phase transition is observed an opportunity to form periodic structures. The latter give an opportunity to increase considerably the efficiency of nonlinear conversion of laser radiation frequency in the UV.

For ternary chalcogenides of the CMX_2 family where C=; M=Ga, In; X=S, Se, Te, the Ag replacing for Li produces a transition from the chalcopyrite, I 42d structure to the wurtzite, $Pna2_1$ structure (besides tellurides). In each case there are some specific features of real structure forming. The main field of their application is nonlinear conversion of coherent radiation in the mid-IR. Thus, changing composition, one can trace the regularities of structural transformations, formation conditions for phase transitions and defects, and use them to increase the nonlinear conversion efficiency (in nonlinear $BMgF_4$ and CMX_2 crystals) or to exclude them in the case of laser crystals APb_2Br_5.

CRYSTAL GROWTH OF MAGNETIC OXIDES

***Dąbkowska H.A.*[1], *Couchman M.M.P.*[2], *Fritsch K.*[2], *Ganshow S.*[3], *Gaulin B.D.*[1,2], *Luke G.M.*[1,2], *Marjerrison C.*[2], *Medina T.*[2], *Millington A.L.*[2], *Morningstar A.*[2], *Munsie T.*[2], *d'Ortensio R.*[2], *Dąbkowski A.B.*[1]**

[1] *BIMR, McMaster University, Hamilton, Ont., Canada,*
[2] *Department of Physics and Astronomy, McMaster University, Hamilton, Ont., Canada,*
[3] *IKZ Berlin Germany*
email: dabkoh@mcmaster.ca

In the last years a significant part of solid state research was devoted to magnetic materials. High quality, well characterized crystals or thin films of magnetic metals, intermetallic compounds and complex oxides are essential for understanding both known and emerging magnetic phenomena and interactions.

As obtaining single crystals of materials from each of the above groups comes with different challenges, in this presentation I would like to concentrate on the growth of crystals of complex oxides and their solid solutions for understanding geometrically frustrated magnetism (1) and high temperature superconductivity (2).

My example of (1) are cubic rare earth pyrochlores $RE_2M_2O_7$ (where RE is an rare earth element and M = Ti, Sn, V or Zr), hosting many of the unusual, magnetic, frustrated states which are in the centre of attention of solid state physics.

As the rare earth pyrochlores melt congruently at temperatures above the melting point of Pt, the Optical Floating Zone [OFZ] technique proved to be an efficient, crucible-free method for growth of relatively big single crystals. Using oxidizing or neutral growth atmosphere it was possible to crystallize $Y_2Ti_2O_7$ – diamagnet, a potential inert matrix for actinides transmutation, $Tb_2Ti_2O_7$ - a spin liquid, with thermal longitudinal spin fluctuations which break spin ice rules, $Ho_2Ti_2O_7$ and $Dy_2Ti_2O_7$ – classical, but still not well enough understood, spin ice systems, $Er_2Ti_2O_7$ and $Yb_2Ti_2O_7$ which displays unexpected, quasi-two-dimensional (2D) magnetic correlations within a cubic lattice environment at low temperatures before entering an exotic disordered ground state below T = 265 mK. Moreover, $Lu_2V_2O_7$ melts congruently only in reducing conditions and shows ferromagnetic properties.

My example of (2) are incongruently melting $Bi_2Sr_2Ca_{n-1}Cu_nO_{4+2n+x}$ (n = 1, 2, T_c = 20 and 85, respectively) and Ba or Sr doped $LaCu_2O_4$ oxides. As in the case of pyrochlores only small crystals can be obtained from high temperature solutions. By the OFZ method when applying oxygen overpressure it was possible to grow high quality crystals of 1-2 cc in volume.

To investigate even further physical, crystallographic and optical properties of these magnetics by directionally sensitive methods such as neutron scattering or muon experiments, those high quality single crystals are essential.

In this presentation the effects of growth conditions and composition on crystal properties of these oxides will be discussed. I will also make an effort to show great possibilities of OFZ in producing crystals of exotic magnetic oxides like nickelates, cobaltites, chromates, rhodates etc.

CATHODOLUMINESCENCE MICROSCOPY OF THE KOKCHETAV UHP-ROCKS: WHAT CAN WE LEARN FROM DIAMOND, CARBON-HOSTING MINERALS AND SILICATES?

Schertl, H.-P. [1], ***Neuser, R.D.*** [1], ***Sobolev, N.V.*** [2]

[1] *Ruhr-University Bochum, Institute of Geology, Mineralogy and Geophysics, Bochum, Germany*
[2] *V.S. Sobolev Institute of Geology and Mineralogy, Novosibirsk 630090, Russia*
hans-peter.schertl@rub.de

During the last 50 years cathodoluminescence (CL) microscopy has become a standard tool in geoscience. While early studies mainly focused on sedimentary rocks, within the last 2 decades this technique has also been applied to various metamorphic and magmatic rocks **[1, 2]**. In addition, CL is indispensable as a scientific tool for the identification of different zircon domains, which need to be characterized prior to ion probe dating (SHRIMP; e.g. **[3]**).

Here, we would like to show results on UHP-metamorphic rocks from the Kokchetav Massif/Kazakhstan using a "hot cathode" CL microscope. It is important to note, that the investigations presented were entirely made just using normal polished thin sections. This makes CL-microscopy an important petrological tool to contribute to other techniques like e.g. electron microprobe and oxygen isotope analysis. Particularly layered calcsilicate rocks from the Kokchetav massif offer a huge potential by applying CL-microscopy. Different carbonates show different luminescent colours (calcite - yellow, aragonite - green, Mg-calcite - orange, dolomite - red). Thus different lithologies like dolomite- and Mg-calcite-enriched layers (even if they are very thin) can instantly be distinguished. Further petrographical observations reveal dolomite exsolution patterns within Mg-bearing calcite, concentric zonations of dolomite and Mg-calcite, and rare occurrences of calcite (yellow luminescence) in talc-bearing pseudomorphs after forsterite. Diamond can be easily identified by its greenish-blue luminescence colors, even zonation of diamond easily becomes visible. Very interesting results were derived from garnet. Although the calcsilicates generally contain garnets lacking luminescence, through very careful CL-studies about 10% of these garnets were disclosed to show complex growth structures (see **[4]**; their Fig. 8). Typically, yellowish-brown luminescent garnet of an earlier generation may contain some "veining" of a second garnet generation lacking luminescence. Electron microprobe analyses reveal that the later garnet is typically lower in Ca and Mn and higher in Fe and Mg ($Gros_{52.1}And_{5.9}Py_{37.7}Alm_{3.1}Spes_{1.2}$) than the earlier one ($Gros_{58.5}And_{2.7}Py_{35.6}Alm_{1.4}Spes_{1.9}$). A recent paper on in situ ion microprobe oxygen isotope studies of these garnets **[5]** demonstrate a $\delta^{18}O$ gradient from 11.3 (rim) to 12.8‰ (core) VSMOW. The high $\delta^{18}O$ values in the luminescent portion of the zoned garnet are significantly higher than would be in equilibrium with mantle-derived magmas and indicate formation in, or exchange with, a crustal reservoir. Garnet is partly altered and forms reaction rims which mainly consist of bluish luminescent pyroxene and small spinel crystals lacking luminescence. Locally an inner rim of greenish luminescent secondary pyroxene higher in $Al^{[4]}$ is developed. Matrix clinopyroxenes locally exhibit greenish luminescent core- and bluish rim-zones. EMP-analyses demonstrate the greenish domains to be higher in iron (2.27 wt.% $FeO_{tot.}$) and potassium (0.44 wt.% K_2O) than the bluish ones (0.81 wt.% $FeO_{tot.}$ and 0.20 wt.% K_2O). When the iron content of clinopyroxene is higher than about 2.5–3 wt.% $FeO_{tot.}$, it completely lacks luminescence. Exsolution lamellae of K-feldspar (blue luminescence) within clinopyroxene (diopsidic) could immediately be recognized under the CL microscope, although being extremely fine-grained and not to distinguish from quartz under the polarizing microscope **[6]**. Recent studies on clinopyroxene (omphacite) from Weihai, Shandong Province (China) demonstrated enclosed quartz exsolution lamellae to show violet luminescence. Accessory luminescent minerals like diamond (greenish-blue), zircon (blue), apatite (green), are easily identified in thin section, even when they occur in very small abundance

In essence, CL enables color images of important but otherwise invisible growth features and internal structures of minerals, like small-scale growth zoning, inhomogeneities, exsolution lamellae, dissolution and deformational effects etc. being easily achieved within seconds. It is easy to identify e.g. interstitial phases and different annealed crack systems of rock matrices; in addition the technique helps to gain valuable insights into the understanding of mineral reactions. Since several REE activators like Dy^{3+}, Sm^{3+}, Eu^{3+} produce sharp peaks whose wavelength is not dependent on the respective mineral investigated, it is possible, using a spectrometer unit, to qualitatively analyse the element content. The present results demonstrate the advantages of using a "hot cathode" CL microscope - the conclusions drawn above open new avenues for petrological applications. Thus, we propose that the CL-technique should be used more intensively for routine investigations of thin sections as a pathfinder prior to further studies using different other techniques like electron microprobe, ion microprobe, Raman spectroscopy etc..

References:

[1] Schertl, H.-P., Neuser, R.D., Sobolev, N.V., Shatsky, V.S. (2004): UHP-metamorphic rocks from Dora Maira/Western Alps and Kokchetav/Kazakhstan: New insights using cathodoluminescence petrography. European Journal of Mineralogy, 16:49-57.

[2] Götze, J., Schertl, H.-P., Neuser, R.D., Kempe, U., Hanchar, J. (2013): Cathodoluminescence (OM–CL) imaging as a powerful tool to reveal internal textures of minerals. Mineralogy and Petrology 107:373–392.

[3] Gebauer, D., Schertl, H.-P., Brix, M., Schreyer, W. (1997): 35 Ma old ultrahigh-pressure metamorphism and evidence for very rapid exhumation in the Dora Maira Massif, Western Alps. Lithos 41:5-24.

[4] Schertl, H.-P., Sobolev, N.V. (2013): The Kokchetav Massif, Kazakhstan: "Type locality" of diamond-bearing UHP-metamorphic rocks. Journal of Asian Earth Sciences 63:5-38.

[5] Sobolev, N.V., Schertl, H.-P., Valley, J.R., Page, Z., Kita, N.T., Spicuzza, M.J., Neuser, R.D., Logvinova, A.M. (2011): Oxygen isotope variations of garnets and clinopyroxenes in a layered diamondiferous calcsilicate rock from Kokchetav Massif, Kazakhstan: a window into the geochemical nature of deeply subducted UHPM rocks. Contributions to Mineralogy & Petrology 162:1079–1092.

[6] Schertl, H.-P., O´Brien, P. (2013): Continental crust at mantle depths: key minerals and microstructures. Elements 9, Number 4.

WHERE DO DIAMONDS GROW? A CRYSTALLOGRAPHIC APPROACH

Angel R.J. [1], ***Milani S.*** [1], ***Nimis P.*** [1], ***Bruno M.*** [2], ***Harris J.W.*** [3], ***Nestola F.*** [1]

[1] *Dipartimento di Geoscienze, Università di Padova, Italy*
[2] *Dipartimento di Scienze della Terra, Università di Torino, Italy*
[3] *School of Geographical and Earth Sciences, University of Glasgow, UK*
rossjohn.angel@unipd.it.

The inclusions in diamonds are the only direct samples we have of the Earth's interior below the crust, apart from the diamonds themselves. Many of these inclusions are single crystals, or clusters of a few single crystals. We have adapted the methods of high-pressure single-crystal diffraction to characterizing these diamonds and their inclusions *in-situ,* in order to place constraints on the growth conditions and source regions of the diamonds themselves.

The orientations of both inclusion crystals and diamonds can be determined by single-crystal diffraction of both the diamond and inclusion. Appropriate manipulation of the orientation matrices allows the orientation of the inclusion crystals relative to their diamond host crystal to be determined unambiguously. For example, we have studied 21 diamonds, all from the same kimberlite source (Udachnaya, Yakutia), containing a total of 51 olivine inclusions with diamond-imposed morphology. Each diamond contained up to nine individual olivines. On a statistical basis, no preferential orientation could be found between olivines and the diamond host. In particular, only 3 olivines show an orientation comparable to that found by Mitchell and Giardini **[1]**, i.e. (101)oli // (101)dia *and* (010)oli // (111)dia, which is believed to be the most favourable in the case of epitaxy. Based on our data, such a special orientation does not appear to be "typical" of olivines included in diamonds.

Measurement of the stress state of single crystal inclusions *in-situ* within the diamond, in combination with knowledge of the elasticity of the inclusion, allows the conditions of entrapment of the inclusion to be constrained. The average stress state of the inclusion is determined by precisely measuring the unit-cell parameters of the inclusion crystal by single-crystal diffraction, and combining these with the known compressibility of the mineral previously determined on other crystals of the same composition by diamond-anvil cell experiments. In the case of mineral inclusions that exhibit solid solution, such as olivine and spinels, the composition of the inclusion can be determined by collecting diffraction intensity data from the inclusion crystal and performing a structure refinement **[2]**. When combined with knowledge of the thermoelastic equations of state of both the inclusion and the diamond, the current stress state of the inclusion defines a line (isomeke) in *P-T* space that represents possible conditions of entrapment of the inclusion by the diamond. Such a series of measurements on one olivine in the Udachnaya suite showed that it had a composition Fo92.7, is currently under homogeneous stress of 0.4 GPa, and appears to have been entrapped at conditions close to the graphite-diamond equilibrium phase boundary.

This work was supported by ERC starting grant 307322 to Fabrizio Nestola.

References:

[1] Mitchell and Giardini (1953) American Mineralogist 38, 136–138.
[2] Nestola et all. (2011) Earth and Planetary Science Letters 305, 249–255

A MEMORY OF PROFESSOR ARKADY GLIKIN ON THE DISCUSSION OF REPLACEMENT OF MINERALS

Tsukamoto K.

Graduate School of Science, Tohoku University, Sendai, Japan/
Graduate School of Engineering, Osaka University
ktsuka@m.tohoku.ac.jp

I remember the days when we met each other in Saint-Petersburg and then in Sendai. We had a common interest on the replacement of minerals and wanted to understand the mechanism based on crystal growth mechanism.

The most exciting idea of replacement of minerals was independently developed by Arkady Glikin in Russia and Andrew Putnis in Germany. Among others Arkady did a pioneering work for the visualization of a coupled dissolution and precipitation mechanism, which is one of the most updated ideas of mineral replacement. He started, for the study, to use atomic force microscope (AFM) to visualize the process and found many interesting phenomena, which have not been recognized. The use of AFM was the most exciting idea in those days for the geological and mineralogical processes.

I want to introduce how the idea to use AFM by Arkady encouraged scientists in many countries to study elemental process of mineral replacement, leading to a new concept of mineral replacement. I also want to stress the importance of international collaboration for the progress of sciences, along which Arkady had been walking.

CHELYABINSK METEORITE: RECENT EVENTS SIMILAR TO TUNGUSKA EVENT

Taylor L.*[1], Liu Y.[2], Day J.M.D.[3], Patchen A.[1], Taylor D.[1], Pokhilenko L.N.[4], Pokhilenko N.P.[4], Podgornykh N.M.[4]

[1] *Earth & Planetary Sci., Univ. of Tenn., Knoxville, TN, USA*
[2] *Dept. of Geological & Planetary Sci., California Inst. of Technology, Pasadena, CA USA*
[3] *Scripps Oceanographic Institute, University of California, La Jolla, CA USA*
[4] *Sobolev Inst. of Geol. & Mineralogy, Novosibirsk, Russia*
lataylor@utk.edu

Introduction: The explosion of the large asteroidal fireball over the Ural Region of Russia on February 15, 2013, brought back the numerous stories and experiences from the Tusguska event in 1908. Of smaller size, this explosion over Chelyabinsk still yielded a shock wave that damaged buildings, injured more than a 1500 person, mainly from flying glass, and disintegrated the initial mass of this of this 18-20 meter bolide (~10,000 tonnes) into a shower of small meteorites, down to dust sizes, over a large region of 1000s of km^2. The initial velocity of the meteoroid of ~18.6 km/sec, some 50 X the speed of sound, in the upper-most portions of the atmosphere at the time of the explosion, caused the air burst ~23 km above the Earth [1-2]. The kinetic energy from the explosion and shock waves of this Near-Earth Asteroid (NEA) have been estimated at ~440 kilo-tonnes (~1.8 PJ) of TNT, 20–30 times more than was released from the atomic bomb detonated at Hiroshima [1-2]. Although huge, this explosion is estimated to be only 1/50th that of the Tunguska event. The 6-m diameter hole in the ice of Lake Chebarkul was reportedly made by a large fragment, but only a ~60 cm fragment (~300 kg). Because almost all the fragments of this meteorite have black fusion crusts, they were easy to spot in the snow and literally 1000s of pieces have been found, of which we have three.

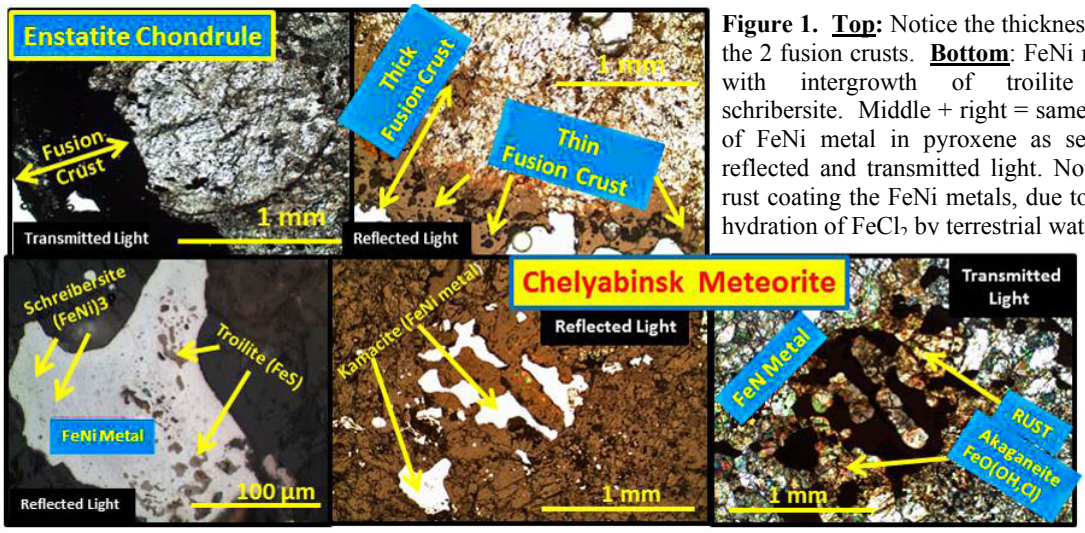

Figure 1. Top: Notice the thicknesses of the 2 fusion crusts. **Bottom**: FeNi metal, with intergrowth of troilite and schribersite. Middle + right = same view of FeNi metal in pyroxene as seen in reflected and transmitted light. Note the rust coating the FeNi metals, due to oxy-hydration of FeCl$_2$ by terrestrial water.

Petrographic description: The Chelyabinsk bolide was a fragmental stony meteoroid that shattered and produced a huge meteorite shower with its air burst [3-10]. This meteorite is a LL-5 chondrite, which consists of a breccia of light-colored chondrule-bearing clasts of various types (see Figures1-2) cross-cut by shock-produced dark impact-melt veins and some melt pockets; however, we have not defined any high-pressure phases to date. These melt veins predate the recent events and are from an older collisional event, perhaps at 4.35-3.9 Ga, as suggested for other LL chondrites. The fusion crusts on almost all stones recovered are of two types and thicknesses – Figure 1 – again representing two related melting events, perhaps one before and

one after a fragmentation at high velocity. The numbers and variety of the chondrules are displayed in Figures 1 - 2 and are of several textures and mineralogy.

Silicate minerals are remarkably homogenous [6] with compositions of: Fo $_{71.0\ \pm0.4}$ for olivine, En $_{74.7\ \pm0.3}$ Wo $_{1.4\ \pm0.2}$ for orthopyroxene, En $_{46.4\ \pm0.5}$ Wo $_{45.1\ \pm0.9}$ for diopside. The matrix plagioclase compositions are largely albitic (Ab $_{83\ \pm4}$ Or $_{6\ \pm3}$), but K-rich compositions are also observed (Ab $_{34\text{-}42}$ Or $_{56\text{-}47}$). Accessory minerals include ilmenite, chromite, chlor-apatite, merrillite, troilite, FeNi metals - kamacite, 4-5.6 wt% Ni, 1.7-2.5 wt% Co; taenite 30-54 wt% Ni, 0.4-0.6 wt% Co, within the compositional range for equilibrated LL chondrites. Taenite grains often contain native Cu, troilite, schreibersite, cohenite, and lawrencite ($FeCl_2$), which quickly oxyhydrates to rust consisting of akaganéite [FeO(OHCl)], from terrestrial water vapor [6].

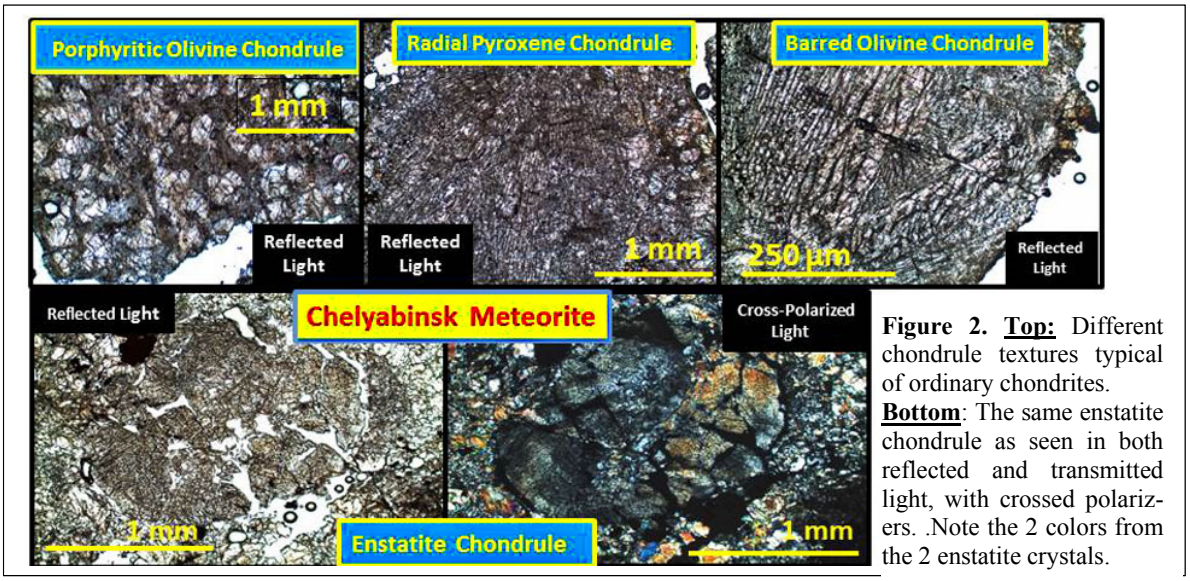

Figure 2. **Top:** Different chondrule textures typical of ordinary chondrites. **Bottom**: The same enstatite chondrule as seen in both reflected and transmitted light, with crossed polarizers. .Note the 2 colors from the 2 enstatite crystals.

Conclusion: The greatest importance of the Chelyabinsk is in the recorded demonstration of the extreme explosion/air burst that the initial meteoroid created. In many respects, this "Baby Tunguska" demonstrated to the world the dynamics that a large fragmental bolide has upon entering the atmosphere at such high velocities. Yes, the meteorite science is fine for this typical LL5 ordinary chondrite, but the dynamics of its entry gave witness to the type of explosion that caused the Tunguska devastation in 1908 – and emphasizes the importance of the mapping of the routes in space of all NEAs of any size. How this small asteroid slipped through the astronomer's observations is of serious concern to mankind the world over.

References:

[1] http://neo.jpl.nasa.gov/news/fireball_130301.html. [2] Zuluaga, J.I and Ferrin I. (2013), Astrophys. (http://arxiv. org/abs/1302.5377). [3] Galimov E. M., et al. 2013. Science (submitted). [4] Ivanova, M.A., et al., 2013, 76th Annual Mtg. Meteor. Society, Abstract #5366. [5] Jones, R.H., et al. 2013, 76th Annual Mtg. Meteor. Society, Abstract #5119. [6] Liu, Y., Taylor, L.A., et al, 2013, 76th Annual Mtg. Meteor. Society, Abstract #5103. [7] Kohout, T., et al., 3013, 76th Annual Mtg. Meteor. Society, Abstract #5273. [8] Kring, D.A., et al., 2013, 76th Annual Mtg. Meteor. Society, Abstract #5224. [9] Provinec, P.P., et al., 2013, 76th Annual Mtg. Meteor. Society, Abstract #5196. [10] Righter, K. et al., 2013, #5235.

COMPLEX ZONING OF OLIVINE MACROCRYSTS FROM UDACHNAYA ULTRAFRESH KIMBERLITE: LINK TO KIMBERLITE FORMATION AND EVOLUTION

Sobolev N.V. [1], ***Sobolev A.V.*** [2], ***Tomilenko A.A.*** [1], . ***Kovyazin S.V.*** [1], ***Batanova V.G.*** [2], ***Kuzmin D.V.*** [1]

[1] *V.S. Sobolev Institute of Geology and Mineralogy, SB RAS, Russia*
[2] *Vernadsky Institute of Geochemistry and Analytical Chemistry, RAS, Moscow, Russia*
sobolev@igm.nsc.ru

The mineral olivine, one of the main constituent of the Earth´s mantle, is also dominant mineral of kimberlites, their peridotite xenoliths and diamond inclusions. The range in forsterite (Fo) contents of olivines associated with kimberlites is 85 – 95 [**4, 7**]. The origin and growth history of olivines occurring in kimberlites is complicated and requires further concentrated and systematic study. Indeed mantle olivines continue to grow even during the formation and evolution of kimberlites as they ascend from depths up to the Earth surface.

Olivine is completely altered in overhelming majority of kimberlites compared to its fresh appearance in diamonds and many peridotite xenoliths. However, as an exception, olivine is absolutely fresh in a huge block from Udachnaya-East kimberlite in Yakutia (Russia) demonstrating complete lack of serpentine presence in thin sections even in smallest grains which are embedded in chloride-carbonate matrix. [**3**]. Two main olivine populations are clearly distinguished in any kimberlites worldwide: rounded or anhedral olivine-I macrocrysts and euhedral olivine-II phenocrysts [**1-2, 4-5**]. In contrast to previous studies [**4**], we found that unzoned phenocrysts crystallized in groundmass prior to kimberlite emplacement, represent only very limited portion (less than 5%) of all olivine population, which approaches to 60 vol. % [**4**]. Fresh olivine macrocrysts from Udachnaya kimberlite include homogeneous, resorbed, irregularly shaped cores, mostly Ti-bearing (100-450 ppm TiO_2) and rims of different width, which sometimes include several zones (up to seven). Some zones, up to three, which separate cores from the rims, are very thin, about 5 μm each and even less. The innovative method for the EPMA study of trace elements in olivine with Jeol 8200 published recently [6] using the high sample current and high counting time, was considerably developed and concentrations of Ni, Mn, Co, Ca, Al, Ti, P and Zn are measured with Jeol 8230 with an external precision down to 10 ppm (2 standard errors) and detection limit down to 2 ppm. In addition high resolution compositional maps of olivine zoning for all mentioned elements are produced.

We report here the results of integrated approach to carefully selected olivine grains with normal and reverse zoning after examination of many hundreds olivines from the most fresh samples of Udachnaya kimberlite. These results include BSE images, EPMA analyses and X-ray element maps of three olivine grains with complex zoning and wide variations of “core” and “rim” ratios which led to finding the fine-scale compositional heterogeneities in terms of Ca, Cr, Ti, Mn, Ni, Co. Along with narrow range in Fo (89-91) in rim zones, variations in some trace elements in direction from outer rim towards the core are very wide (in ppm) for NiO (1300-3200), MnO (2350-1100), TiO_2 (550-300), Cr_2O_3 (100-500), CaO (900-150). An example of olivine complex zoning showing positive correlation of Fo and NiO contents and significant difference in TiO_2 contents in the core and rim parts, is presented in Fig.1.

We conclude, that the whole range in Fo and trace element contents for the rim part zones of three carefully selected olivine II samples covers major variations typical of all previously studied olivine II grains from Udachnaya kimberlite [**4**]. In addition, detection of Na, Cl and P indicated their relation to micro- and submicrometer sized carbonate and halide melt inclusions in the outermost parts of grains. Complex composition of some outer zones within the rim parts of the studied grains indicates rapid change of growth and resorption conditions.

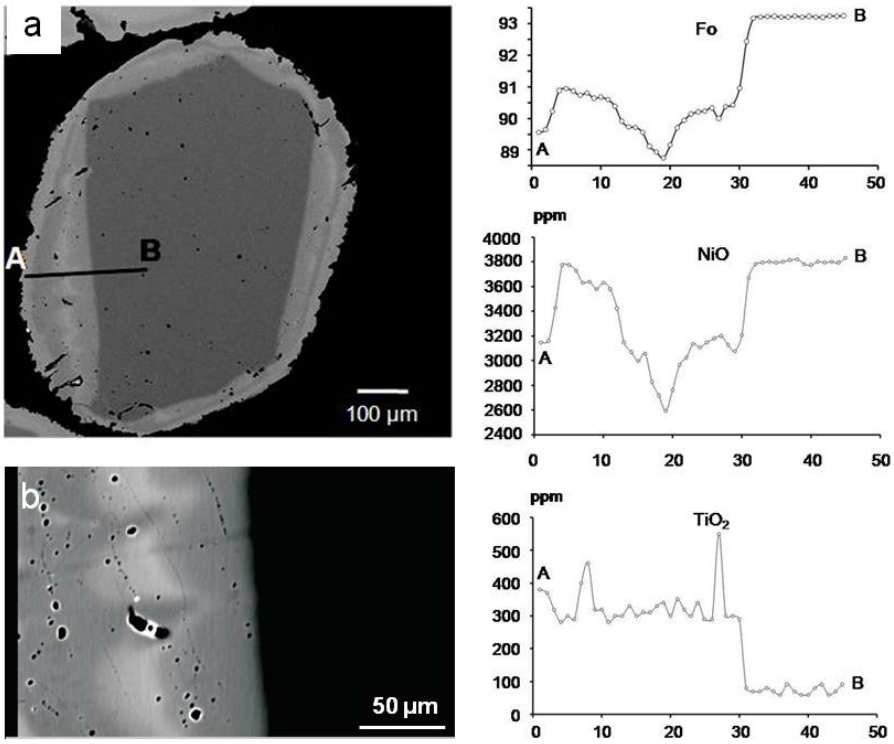

Figure 1. BSE image (a), its detail (b) and profiles of Fo, NiO and TiO_2 concentrations vs number of analyses of one of the studied olivine macrocryst with complex zoning from Udachnaya ultrafresh kimberlite. Note complex composition of some outer zones within rim part, which indicates rapid change of growth and resorption conditions.

References:

[1] Arndt N.T. et al. (2010), Journ. Petrol., 51:573-602.
[2] Brett, R.C. et al., (2009), Lithos, 112S:201-212.
[3] Kamenetsky, M.B. et al., (2004), Geology, 32: 845-848.
[4] Kamenetsky, V.S. et al., (2008), Journ. Petrol., 49: 823-839.
[5] Sobolev, A.V. et al., (1989), GSA Spec. Publ. N14, Proc. Fourth Intern. Kimb. Conf. 1: 220-240.
[6] Sobolev A.V. et al., (2007) Science,316:412-417.
[7] Sobolev, N.V. et al., (2009), Lithos, 112S; 701-713.

Special Lecture

GIANT CRYSTALS OF NAICA: THE SCIENCE BEHIND THE BEAUTY

García-Ruiz, J.M.

Laboratorio de Estudios Cristalográficos, Instituto Andaluz de Ciencias de la Tierra, CSIC-Universidad de Granada, Granada, Spain
juanma.garciaruiz@gmail.com

The Cave of Giant Crystals in the Naica mine (Mexico) is one of the most amazing displays of mineral beauty ever created by Nature (Figure 1). In addition to the colossal crystals, which in some cases exceed eleven meters in length and one meter in thickness, the scenery developed by the crystalline beams of moonlight luster going through the darkness of the cave, from the floor to the ceiling, is a unique example of harmony based on crystal symmetry. But at the same time, deciphering the mechanism of formation of these crystals is a fascinating challenge as mineralogical processes taking place close to equilibrium, or with very slow kinetics, are difficult to quantify precisely.

I will discuss in this lecture the scientific basis for the formation of this remarkable phenomenon of mineralization. The study is supported by data obtained with a number of techniques including fluid inclusions analysis, confocal differential interference contrast microscopy, atomic force microscopy, stable isotopic analysis, fluid inclusions, etc., as well as experimental and theoretical nucleation and crystal growth studies of calcium sulfate. The genesis of the Giant Gypsum Crystals in the Cave of Crystals in Naic mines requires a) a coupled set of dissolution/precipitation reactions providing a large enoug amount of material to crystallize, b) the right context for an steady, close to equlibrium nucleation giving rise to the right number of crystals a c) crystal growth mechanisms compatible with the development of elongated crystals (beams) with a particular growth morphology that makes these crystals unique.We propose that these giant crystals are the result of a self-feeding mechanism based on a solution mediated anhydrite-gypsum phase transition occurring in a slow and smooth cooling scenario. Therefore they must be the result of an extremely slow crystallization process close to equilibrium, which has been studied by confocal differential interference contrast microscopy. The talk will be illustrated by microvideos from the movie “The Mistery of the giant crystals” (Figure 2)

This work was supported by the Spanish Consolider-Ingenio 2010 project “Factoría de Cristalización” CSD2006-00015 and by the project CGL2010-16882 of the Ministry of Science and Innovation.

References:

[1] García-Ruiz, J.; Villasuso, R.; Ayora, C.; Canals, A.; Otálora, F., 2007. Geology, 35, 327–330.

[2] García-Ruiz, J.; Villasuso, R.; Ayora, C.; Canals, A.; Otálora, F., 2008. Mcgraw-Hill Yearbook of Science &Technology. New York, 154-156.

[3] Van Driessche, A.E.S., García-Ruiz, J.M., Tsukamoto, K., Patiño, L.D., Satoh, H., 2011. PNAS. 108, 15721-15726

[4] Yves Krüger, Y., García-Ruiz, J.M., Canals, A., Martí, D., Frenz M., van Driessche, A., 2013. Geology, 41 (2013) 119-122.

Figure 1. Large beams of gypsum in the Cave of Giant Crystals of Naica.

Figure 2. The poster of "The Mistery of the giant crystals".

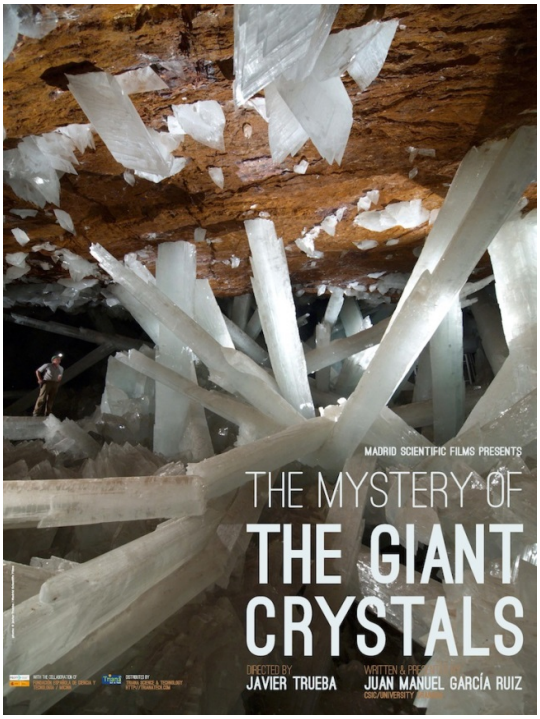

SESSION 1

Formation of the ideal and real structure of crystals; aperiodic structures

INVESTIGATION OF NANO-DOMAIN STATE OF STRONGLY OXYGEN-DEFICIENT PEROVSKITE-LIKE OXIDES: MONTE CARLO STRUCTURE SIMULATION AND DEBYE CALCULATION OF XRD PATTERNS

Ancharova U.V. [1], ***Cherepanova S.V.*** [2], ***Lyakhov N.Z.*** [1]

[1] *Institute of Solid State Chemistry and Mechanochemistry SB RAS, Novosibirsk, Russia*
[2] *Boreskov Institute of catalysis SB RAS, Novosibirsk, Russia*
ancharova@gmail.com

Strongly non-stoichiometric oxygen-deficient perovskite-like oxides $ABO_{3-\delta}$ can not be considered in the approximation of the model of point defects, as the vacancy concentration reaches such values that vacancies begin to interact with each other **[1]**. In this case, the system tends to form a heterogeneous state, consisting of domains with local ordering of vacancies **[2]**.

Indeed HRTEM studies of many nonstoichiometric perovskite-like compounds $ABO_{3-\delta}$ with stoichiometry close to vacancy-ordered brownmillerite structure $ABO_{2.5}$ show **[3-8]** that the crystals are composed of domains with brownmillerite structure of dimensions ~10nm perpendicularly oriented relative to each other. In this case X-ray diffraction patterns have some peculiarities. Despite the low local symmetry within each domain on the powder X-Ray diffraction patterns along with the strong peaks corresponding to high-symmetric cubic perovskite structure the additional weak broadened peaks are also observed. With that computer modeling of such micro-domain structures and their deceptively simple diffraction patterns have not been done until now.

The same features are observed on the XRD patterns for modified strontium ferrites with compositions $Sr(Fe_{0.95}Mo_{0.05})O_{2.5+x}$, $Sr(Co_{0.8}Fe_{0.2})O_{2.5+x}$, $Sr(Co_{0.75}Nb_{0.05}Fe_{0.2})O_{2.5+x}$, $Sr(Co_{0.7}Nb_{0.1}Fe_{0.2})O_{2.5+x}$, $(Sr_{0.7}La_{0.3})(Co_{0.5}Al_{0.3}Fe_{0.2})O_{2.5+x}$, ($x$<0.2). It is clear that traditional Rietveld analysis is not suitable in the case of microdomain structure because it developed for the perfect crystals and can not fit simultaneously widths of relatively narrow main peaks and broadened superstructural ones. So it was decided to build the nano-domain structure by Monte Carlo technique and then calculate the intensity diffracted on the generated particles by the Debye formula. This approach makes it possible to consider materials that have any structure and condition of 3D periodicity is not obligatory.

Formation of the domain structure is energetically favorable process since mutual orientation of domains minimizes the total energy of deformation fields in the crystal. At the same time the domain partition leads to the increase of the domain-wall energy. The balance of this counteracting factors defines the system state in which long range order parameter is characterized by the equilibrium value of the average domain size, which can be estimated from the HRTEM data as ~10nm **[3-8]**. The domain formation leads to the stress relaxation because deformations in various domains compensate each other, while the released energy is sufficient for the domain wall formation. Superstoichiometric oxygen x is localized at the domain walls and prevents further growth of domains **[6]**.

As a result of above mentioned simulations it was shown that the experimental diffraction patterns correspond to the microdomain structure, where in the matrix of the cubic perovskite structure the nano-domains with orthorhombic brownmillerite structure are distributed in a certain way. A systematic analysis of the impacts of different types of disorder in strongly nonstoichiometric oxides on the diffraction patterns was made.

This work was carried out with the involvement of equipment belonging to the shared research center "SSTRC" and supported by the Ministry of Education and Science of the Russian Federation.

References:

[1] Гусев А.И., Нестехиометрия, беспорядок, ближний и дальний порядок в твердом теле - Москва: Физматлит, 2007.
[2] Anderson J.S. Problems of Nonstoichiometry / Ed. Rabenau A. Amsterdam: North-Holland, 1970. - P.11.
[3] Lindberg F. et. al. // J. Solid State Chemistry. - 2004. - 177. - P.1592.
[4] Doorn R. H. E. et. al. // Solid State Ionics. - 2000. - 128. - P.65.
[5] Liu Y. et al. // J. Solid State Chemistry. - 2003. - 170. - P.247.
[6] Nakayama N. et al. // J. Solid State Chemistry. - 1987. - 71. - P.403.
[7] Alario-Franco M.A. et al. // Materials Res. Bull. - 1982. - 17. - P.733.
[8] D'Hondt H. et al. // J. of Solid State Chemistry. - 2009. - 182. - P.356.

ON THE CRYSTAL STRUCTURE OF 'BETA-LOMONOSOVITE'

***Avdontseva M.S.*,[1] *Zolotarev A.A. Jr.*,[1] *Krivovichev S.V.*,[1] *Pekov I.V.*[2]**

[1] *Saint-Petersburg State University, St.Petersburg, Russia*
[2] *Moscow State University, Moscow, Russia*
ritta89@rambler.ru

'Beta-lomonosovite', $Na_4Ti_4Si_4O_{18}{\cdot}Na_3[PO_3(OH)PO_2(OH)_2]$, is a titanosilicate from the murmanite-lomonosovite family, which is currently discredited as a mineral species [1]. The purpose of this work is to study the crystal structure of 'beta-lomonosovite' in order to establish its possible identity as a separate mineral species. The sample of the mineral originated from the Apatite Circus mineral deposit, Khibiny Massif.

The crystal structure of mineral was studied by single crystal X-ray diffraction analysis by means of the Bruker Smart Apex II diffractometer equipped with the CCD area detector. Beta-lomonosovite is triclinic, *P*-1, a = 5.327(2), b = 14.161(4), c = 14.495(4) Å, α = 102.94(2), β = 96.32(2), γ = 90.28(3)°, V = 1058.8(5) Å^3. The structure consists of chains of PO_4 tetrahedra and TiO_6 octahedra running parallel to the c axis. The $P1O_4$ tetrahedron occupies a position analogous to that in lomonosovite and the $P2O_4$ is turned towards the opposite side [2].

In agreement with previous reports [3], structure refinement indicated that there are several under-occupied Na sites, which is most probably related to the protonation of some of the PO_4 tetrahedra. Analysis of tetrahedra distortion indicated that each of the two PO_4 tetrahedra has two potential O sites available for protonation. Ordering of the under-occupied Na sites and distortions of the PO_4 tetrahedra result in doubling of the unit cell compared to that in lomonosovite.

In conclusion, our studies confirmed previous results and allowed to obtain precise structural information that can be used to investigate status of 'beta-lomonosovite' either as a new mineral species or a variety of lomonosovite.

We thank Russian foundation for basic research for financial support through the grant № 12-05-31190 and SPbSU X-Ray Diffraction Resource Centre for instrumental support.

References:

[1] Pekov I.V. Lovozero Massif: History, Pegmatites, Minerals. Moscow, OP, 2000. - 480 pp.

[2] Ferraris G. Heterophyllosilicates, a potential source of nanolayers for material science // Minerals as Advanced Materials I. (Ed. By S.V. Krivovichev). Springer – Verlag, Berlin. 2008. P. 157 – 163.

[3] Rastsvetaeva R.K., Sirota M.I., Belov N.V. Crystal structure of betalomonosovite. Kristallografia.1975. 20.2. P. 259 - 264 (in Russ.).

INVESTIGATION OF DEFECT STRUCTURE OF TRANSPARENT MEDIA BY DYNAMIC HOLOGRAPHY METHOD

Bogodaev N.V., Ivleva L.I., Lykov P.A.

Prokhorov General Physics Institute, Russian Academy of Sciences, Moscow, Russia
ivleva@ran.gpi.ru

Optical quality of active media is the important factor to define the efficiency of applications of the materials in optics, optoelectronics and quantum electronics devices. Investigations of optical homogeneities of the materials during different stages of their production allows to define influence of technological regimes on defect structure of the medium and to optimize the processes of crystal growth, creation of laser glasses and formation of optically perfect transparent ceramics. To control optical quality of visible diapason transparent media the interference methods, polarization–optical technique and holographic interferometer method can be used. It should be noted the images obtained by interferometer techniques must be treated using special program to define microstructure of defects.

A dynamic holography method bases on image recording in regime of two-wave mixing of laser radiation in reversible photosensitive medium **[1, 2]**. The technique suggested by us allows to realize the regime of two-exposure interferometry, image recording in amplification regime and to obtain contrast images of phase defects **[3]**. It is a high speed non-destructive method for testing the optical quality of materials which allows to obtain a magnified image of the object under study in sizes of from 1 to 40 mm and to determine the presence of optical inhomogeneities of $\Delta n \sim 10^{-5}$ /cm. The method can be used for studies of optically dense and photosensitive materials.

In our scheme recording was performed by the second harmonic radiation of the Nd:YAG laser (TEM_{oo} mode) with diode pumping ($\lambda = 532$nm, $\Delta\lambda \sim 0.1$nm). Photorefractive barium–strontium niobate crystal SBN:61, doped with Ce (0.07 at.%) or Co (0.03 at.%), was used as a recording medium. A 1mm thick layer of this solid solution made it possible to magnify an image by a factor of 20–30. The gain coefficients were found to be 35 cm^{-1} for SBN:Ce and 27 cm^{-1} for SBN:Co. The sample was placed in a wide homogeneous (object) neodymium laser beam. The hologram was recorded in the SBN crystal as a result of the interference of the signal and pump beams. Holograms were recorded and read simultaneously, i.e. in real time (dynamic holography). The magnified sample image was projected on a screen and recorded with a digital camera to be processed on a personal computer.

The optimization of temporal and spectral parameters of the output radiation of solid state diode pumped laser was carried out for correction of laser radiation and increasing of efficiency of optical image recording. In the recording experiments the optical delay between writing beams was chosen so that defect free area exhibit minimal amplification. In this case any phase distortions provide additional phase changes for the interacting beams, resulting in additional energy exchange and amplification of the phase distorted area images. This selective amplification leads to increasing of the image contrast of defect regions, easily reveals the areas with different phase distortions and proceeds more detailed investigations of defect structure of transparent material.

The experimental images of multicomponent oxide crystals such as lithium niobate, strontium barium niobate, strontium molibdate, barium tungstate and complex transparent fluoride ceramic will be shown. The results of comparison of this technique with other ones are given in figure for strontium molibdate crystal. The technique allows not only to study the nature of microdefects in different media but it is a quick non-destructive method to identify the regions of high optical quality in bulk transparent materials which are available for preparing of optical elements.

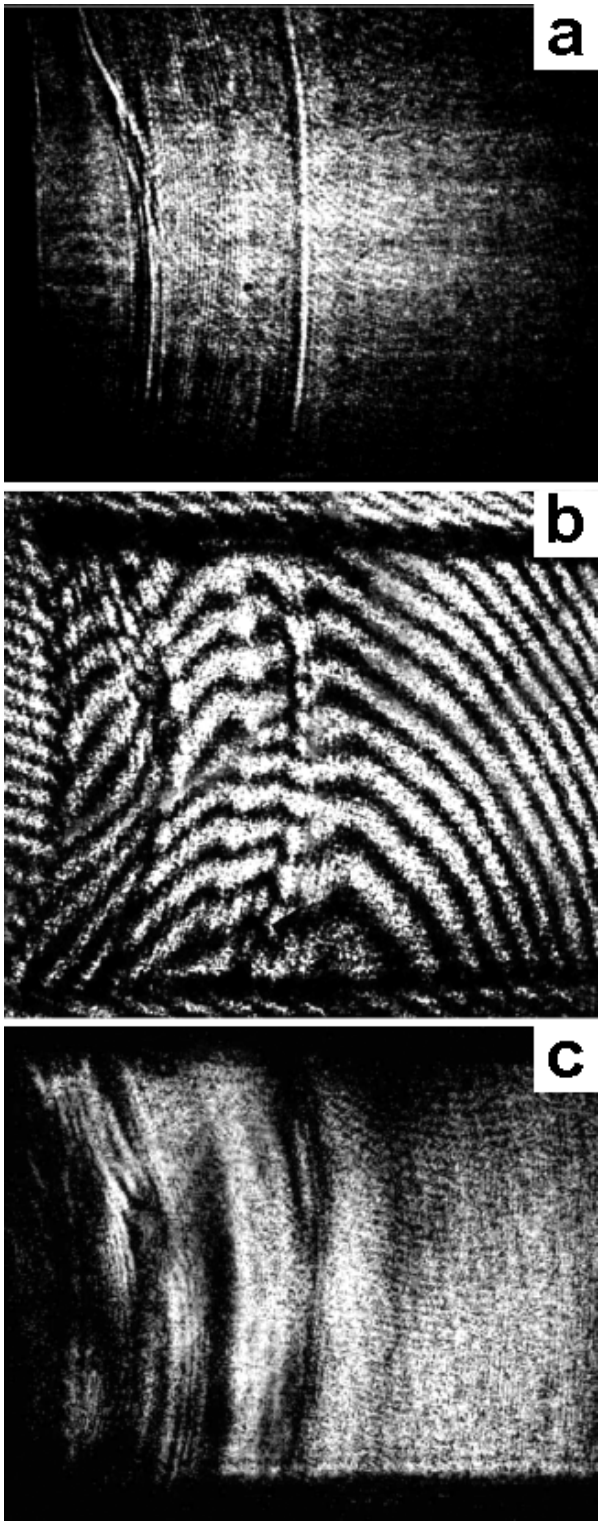

Images of crystal element obtained by
a) dynamic holographic method;
b) interference method;
c) polarization–optical technique.

References:
[1] V.L.Vinnitskii, N.V.Kukhtarev, S.G.Odulov, M.S.Soskin "Uspehi fizicheskih nauk", 1979, v.129, n.1, p.113-137, in Russian
[2] C. West "Holographic interferometry", Moscow, MIR, 1982, p.504, in Russian
[3] N.V. Bogodaev, L.I. Ivleva, P.A. Lykov, V.V. Osiko, A A. Gordeev "Crystallography Reports", 2010, v.55, n.6, pp.1000–1005.

STRUCTURAL ANALYSIS OF APERIODIC CRYSTALS

Bolotina N.B.

Shubnikov Institute of Crystallography RAS, Moscow, Russia
bolotina@ns.crys.ras.ru

The name 'crystals' is usually assigned to the solids with 3D periodicity of their atomic structure. Combining a translational symmetry of a 3D crystal lattice and a pointed symmetry of corresponding unit cell, one can derive 230 crystallographic space groups, which form a theoretical base of the structure analysis. An experimental approach to the single-crystal structure analysis is based on properties of the reciprocal crystal lattice. Using X-ray diffraction techniques one can observe sharp peaks ('reflections') at points of a reciprocal lattice and a weak background between them. All the reflections have integer coordinates (h, k, l) in the reciprocal basis, which are known as Miller's indexes. There are, however, some solids, which diffraction patterns contain additional peaks (so-called 'satellites') with non-integer coordinates ($h + \alpha$, $k + \beta$, $l + \gamma$). Moreover, it is hard sometimes to choose easy rational α-, β-, γ-values.

After discussions, most crystallographers agreed that such solids had to be considered as crystals as well, and International Union of Crystallography (IUCr) proposed a new definition. According to that, a material is a crystal if it has 'essentially' a sharp diffraction pattern. New crystals were called 'aperiodic' in contrast to usual 'periodic' crystals.

Aperiodic crystals form three main groups: (1) incommensurate modulated crystals; (2) incommensurate composites; (3) quasicrystals. Two first groups will be discussed here.

Atoms of usual crystals are located in the points of the crystal lattices. We must keep an idea of a basic 3D-periodic lattice to determine a modulated structure. An atom of the modulated crystal is displaced from the point **n** of the basic lattice. Its displacement is given by a modulation wave $\mathbf{A}\cos(2\pi\mathbf{q}\cdot\mathbf{n})$, which length λ is equal to $1/|\mathbf{q}|$. The modulation is incommensurate in case the wave length is incommensurate to the period of the basic lattice.

Symmetry of incommensurate modulated crystals cannot be presented in the 3D space using one of 230 groups mentioned above, since translational 3D symmetry of the crystal is broken. Because of that, the conventional structure analysis does not work. Special techniques will be considered that allow to describe a modulated crystal structure in a (3+d)D space as a fully ordered, periodic structure. Several examples of modulated crystals will be given to show possibilities of the (3+d)D structure analysis.

Similar approach is used for the crystal structure analysis of the incommensurate composites. Atoms of such a composite form two subsystems, each of them is attached to an own basic lattice, One of two incommensurate lattices can be selected as 'main'. X-ray scattering on the first atomic subsystem results in reflections located at points of the 'main' reciprocal lattice. Other atoms give the diffraction reflections, which look like 'satellites' with non-integer indexes in the reciprocal basis of the first subsystem. True satellites are also present in the diffraction pattern, since incommensurate subsystems modulate adjusting one to other. Some examples will be presented.

Special software (see: http://jana.fzu.cz/) is used for the structure analysis of modulated crystals. Its possibilities will be shortly enumerated.

A partial financial support through the grants No 13-02-00105 from Russian Fund of Basic Research and No 2883.2012.5 of Leading Scientific Schools is greatly appreciated.

CRYSTALLOGRAPHIC ANALYSIS OF SULFIDE STRUCTURES WITH HEAVY METALS

***Borisov S.V.*, Magarill S.A., Pervukhina N.V.**
Nikolaev Institute of Inorganic Chemistry SB RAS, Novosibirsk, Russia
borisov@niic.nsc.ru

A crystal in the crystallographic analysis is represented as a mutually concordant set of atomic planes. The wave-mechanical concept of the crystalline state asserts that it is these systems of parallel equidistant planes that create ordering of atomic positions providing the long-range ordering **[1].** The intensity of X-ray reflection F_{hkl}^2 characterizes the degree of ordering of atomic positions by the given system of (*hkl*) planes, i.e., the proximity degree of atoms to planes of this system. The experience of the work with structures of different types showed that various groups of atoms (only cations, for instance) are ordered by their (own) (*hkl*) planes. To the fullest extent, a structure is governed by crystallographic planes within the range $d_{hkl} \approx 2 – 4.5$ Å with the high filling density of atoms. Any three such noncoplanar planes form three-dimensional lattice of intersection points in the nearest vicinity of which, atoms ordered by these planes (pseudotranslational sublattice) are arranged. Such sublattices characterize "force skeleton", and planes forming the sublattice will be termed, correspondingly, as "skeletal".

Considerable amount of natural and synthetic sulfides are crystallized with the mirror symmetry plane perpendicular to a short translation ~ 4 Å. In the present work, structures of sulfides with "heavy" cations, contribution of which into formation of the structure and intensities of diffraction reflects is substantially greater than that of anions, will be considered. Virtually, all these structures possess planes occupied by cations within the range $d_{hkl} \approx 1.9–4.5$ Å perpendicular to the mirror symmetry planes. Such planes can be found on experimental powder diffraction patterns or by calculation of a diffraction pattern only for cations positions. Two such (*hkl*) planes, in combination with the family of mirror symmetry planes, form the sublattice of intersection points as a sublattice sites of this structure. The neighboring sites along a short translation (~ 4 Å) are separated by distances of ~ 2 Å, so that, as a rule, the sites occupied by atom is are alternated with the vacant sizes.

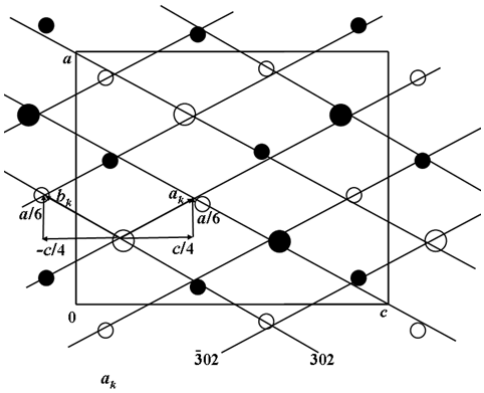

Vector expressions for parameters of cationic sublattices and their numerical values can be obtained either from geometric constructions, or by means of the program **[2].** (See Fig.1: projection of the cationic $PbBi_2S_4$ structure onto the *xz* plane. Pb is denoted as large circle, solid and open circles correspond to *y*=1/4 and *y*=3/4, respectively. The cationic sublattice is formed by intersection of (302), (-302), and (020) planes. Translations of the cationic sublattice are defined as the vector sum: $\boldsymbol{a}_k$ = 1/6$\boldsymbol{a}$ + 1/4$\boldsymbol{c}$; $\boldsymbol{b}_k$ = 1/6$\boldsymbol{a}$ – 1/4$\boldsymbol{c}$; $\boldsymbol{c}_k$ = 1/2$\boldsymbol{b}$). Thus, structures of sulfides of heavy cations investigated by the method of crystallographic analysis form the basis of the pseudohexagonal sublattice, i.e., the three-dimensional matrix ("skeleton") with half-occupancy by of cations in sites (see Table 1). The number of cells of this skeleton necessary to form the unit cell of a crystalline structure depends on the composition of a compound.

Parameters of cationic sublattices of all structures turn to be within the fairly limited ranges: $a_k, b_k \approx 3.9\text{-}4.2$ Å. $2c_k \approx 4$ Å, $\gamma_k \approx 105\text{-}128°$ The greatest deviations from average values are specific for structures with relatively small cations (Cu^{1+}, Fe^{2+}). The pseudohexagonal sublattice can be considered as a relict of the cubic cationic skeleton with the *F*-cell, in which,

among all the symmetry elements, only the system of mirror planes perpendicular to the diagonal of one of cubic cell faces is retained.

Table 1. Data on cationic sublattices of investigated compounds.

Standard characteristics of compounds (Å, °)	Skeletal planes of cationic sublattice	Sublattice parameters (Å, °) (α_k, β_k=90)	Standard characteristics of compounds (Å, °)	Skeletal planes of cationic sublattice	Sublattice parameters (Å, °) (α_k, β_k=90)
Kudriavite, (Cd,Pb)Bi_2S_4 *C*2/*m*, *a*=13.095, *b*=4.003,*c*=14.711, β=115.59, *Z*=4	$\bar{2}$02, 204, 020	a_k=-3.92 b_k=3.98 c_k=2.01 γ_k=111.92	Heyrovskyite, $Pb_6Bi_2S_9$ *Bbmm, a*=13.749, *b*=31.505, *c*= 4.1475, *Z* = 4	002, 280, $\bar{2}$80	a_k =3.96 b_k =3.96 c_k =2.07 γ_k =120.37
$Bi_3In_5S_{12}$ *C*2/*m, a*=33.13, *b*=3.873, *c*=14.413, β=91.21, *Z*=4	$\bar{8}$02, 004, 020	a_k=4.14 b_k =4.12 c_k =1.94 γ_k =118.97	Kupcikite. $(Cu,Fe)_4Bi_5S_{10}$ *C*2/*m, a* = 17.512, *b* = 3.910, *c* = 12.869 , β = 108.56, *Z* = 2	401, $\bar{2}$04, 020	a_k = 3.69 b_k = 3.19 c_k = 1.96 γ_k = 104.68
$Pb_4In_3Bi_7S_{18}$ $P2_1/m$, *a*=21.021, *b*=4.014, *c*=18.898, β=97.07, *Z*=2	$\bar{6}$01, $\bar{3}$05, 020	a_k =4.19 b_k =4.18 c_k =2.00 γ_k =123.42	Felbertalite, $Cu_2Pb_6Bi_8S_{19}$ *C*2/*m, a* = 27.64, *b* = 4.05, *c* = 20.74 , β = 131.26, *Z* = 2	$\bar{8}$03, 203, 020	a_k = 3.82 b_k = 4.25 c_k = 2.03 γ_k = 117.78
$Pb_{1.6}In_8Bi_4S_{19}$ *C*2/*m, a*=29.167, *b*=3.872, *c*=15.554, β=121.6°, *Z*=2	$\bar{8}$03, 601, 020	a_k = 4.29 b_k =4.17 c_k =1.94 γ_k =123.6	Moëloite, $Pb_6Sb_6S_{14}(S_3)$ $P2_122_1$, *a*=15.328, *b*=4.04, *c*=23.054 , *Z*=2	403, 40$\bar{3}$, 020	a_k = 4.29 b_k = 4.29 c_k = 2.02 γ_k = 126.99
$Pb_4In_2Bi_4S_{13}$ *Pbam, a*=21.344, *b*=26.494, *c*=4.002, *Z*=4	$\bar{6}$10, $\bar{4}$60, 002	a_k = 4.16 b_k =4.01 c_k =2.00 γ_k =122	$Pb_4In_9S_{17}$ *Pbam, a* = 22.761, *b*=15.201, *c*=3.858, *Z*=2	340, $\bar{3}$40, 002	a_k = 4.30 b_k = 4.30 c_k = 1.99 γ_k = 123.81
Marrucciite, $Hg_3Pb_{16}Sb_{18}S_{46}$ *C*2/*m. a* = 48.124, *b*=4.108,*c*=23.990, β=118.76, *Z* = 2	803, $\bar{6}$07, 020	a_k =4.00 b_k =3.92 c_k =2.05 γ_k =119.35	Galenobismuthite, $PbBi_2S_4$ *Pnma, a*=11.742, *b*=4.081, *c*=19.522, *Z*=2	302, $\bar{3}$02, 020	a_k = 4.12 b_k = 4.12 c_k = 2.04 γ_k = 123.35
Lillianite, $Pb_3Bi_2S_6$, *Bbmm,* a=13.540, *b*=20.637, *c*=4.1103, *Z*=4	002, 250, $\bar{2}$50	a_k =3.96 b_k =3.96 c_k =2.05 γ_k =117.26	Rouxelite, $Cu_2HgPb_{22}Sb_{28}S_{64}(O,S)_2$ *C*2/*m, a*= 43.113, *b* =4.059, c =37.874, γ=117.35°,Z = 2	10 0 2, 0 0 10, 020	a_k =4.25 b_k =4.31 c_k =2.03 γ_k =127.72

The crystallographic analysis of a wide range of sulfide structures clearly demonstrates the presence of a "skeleton", i.e., cationic matrix unified for all such structures created by ordering of atomic positions by systems of parallel planes. Certainly, this is not the only factor to define a structure, but it is most important. One more structure-forming factor is related to features of chemical bonds. As a result of this, each crystal structure is a compromise of chemical interactions and forces creating the long-range ordering, i.e., the crystalline state. Analysis of these forces is not usually available in description of structures due to which those fail in the internal unity.

This work is financially supported by the RFBR (grant 13-05-00030).

[1] Borisov, S. V., Magarill, S. A. & Pervukhina, N. V. (2011). *Crystallogr. Rep.* **56**, 935–940.
[2] Gromilov, S. A., Bykova, E. A. & Borisov, S.V. (2011). *Crystallogr. Rep.*. **56**, 947-952.

STABILIZING ROLE OF Tl^+ IN ANION PACKINGS OF SULFIDE CRYSTAL STRUCTURES

***Borisov S.V.*, Magarill S.A., Pervukhina N.V.**

Nikolaev Institute of Inorganic Chemistry SB RAS, Novosibirsk, Russia
borisov@niic.nsc.ru

In classic crystallography, the close-packed anions, as the most bulk components, were believed to be the main factor to define the crystal structure. Later on this role turned to "heavy" (massive) atoms such as the cations. Of great interest are the structures where large and relatively light anions are situated nearby large and "heavy" cations. A crystallographic analysis was performed for some sulfide structures containing the "heavy" univalent Tl^+ cation closely related to the S^{2-} anion in size (the ionic radii 1.70 and 1.84 Å, respectively).

With the supposition of the layer character of the packings of the large cations, the intensities of the reflections were calculated with regard to the contributions of S^{2-} and Tl^+ alone. The strongest of them are known to define the planes of dense atomic layers **[1]**. When intersecting the families of the planes form pseudotranslational sublatticies of the atomic positions approaching the plane intersection points. Table 1 shows conventional structure characteristics, intensities for close-packed anion thallium-containing planes, and the parameters of the anion Tl^+ subcells formed by these planes.

Table 1.

Standard characteristics from the ICSD Database	Intensity planes for S + Tl			Parameters of the anion Tl-containing subcells (Å, °)
	hkl	d_{hkl}	I_{rel}	
Tl_2S *R*3, *Z*=27, a_H=12.15 Å, c_H=18.19 Å	303 $\bar{3}$ 33 0 $\bar{3}$ 3	3.04 3.04 3.04	Σ100	a_a=3.09, α_a=81.27 b_a=3.09, β_a=81.27 c_a=3.09, γ_a=81.27
$TlTaS_3$ *Pnma*, *a*=9.228; *b*=3.503; *c*=14,209 Å, *Z*=4	$\bar{2}$ 04 204 020	2,81 2,81 1,75	90 90 100	a_a= 2,91, α_a =β_a= 90 b_a= 2,91 γ_a =104,82 c_a= 1,75
$TlIn_3S_5$ *C*2/*m*, *a*=20, 258; *b*=3.8259; *c*=12,821 Å, β=121, 39°, *Z*=4	600 $\bar{6}$ 04 020	2,88 2,86 1,91	96 84 100	a_a= 3,21 α_a =β_a= 90 b_a= 3,22 γ_a =116,66 c_a=1,91
$TlIn_5S_8$ *C*2/*m*, *a*=19,050; *b*=3.839; *c*=9,192 Å, β=102, 94°, *Z*=2	003 $\bar{6}$ 02 020	2.99 2.86 1.92	100 71 100	a_a=3,18 α_a =β_a= 90° b_a= 3,31 γ_a =115,6 c_a=1,92
$TlCr_2V_3S_8$ *C*2/*m*, *a*=17,643; *b*=3.371; *c*=8,546 Å, β=104,4°, *Z*=2	003 $\bar{6}$ 02 020	2.76 2.68 1.69	100 100 100	a_a=2,95 α_a =β_a= 90° b_a= 3,03 γ_a =114,46 c_a= 1,87

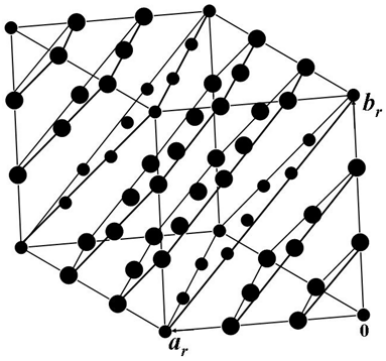

In the Tl_2S structure, all atoms occupy the nodes of the primitive rhombohedral subcell (approximating to the cube) so that the double Tl layers alternate with the S layers along the $c_н$-axis (Fig. 1).

Fig. 1. Structure of Tl_2S in rhombohedral axes (a_r=b_r=c_r=9.27 Å, α_r= β_r=γ_r=81.9°, $\boldsymbol{c_H}$=$\boldsymbol{a_r}$+$\boldsymbol{b_r}$+$\boldsymbol{c_r}$),
Tl - the large circles.

Typical of the remaining structures are pseudohexagonal subcells, having the close geometric parameters, with half-filled nodes (Fig. 2).

Thus, the large and heavy Tl^+ cation when entering into the anion sublattice stabilizes its regularity and recognizes its decisive function in the organization of the structures **[2, 3]**.

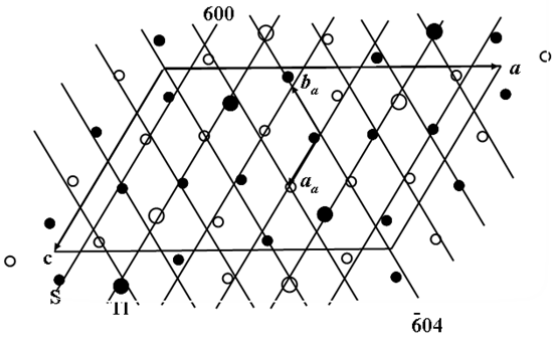

Fig. 2. Structure of $TlIn_3S_5$. Projection of anionic and Tl positions onto the *xz* plane (open and closed circles have the *y*=0 and *y*=1/2 respectively, Tl circles is large). The traces of (600) and ($\bar{6}$ 04) cristallographic planes oriented perpendicularity to the projection plane.

This work is financially supported by the RFBR (*grant 13-05-00030*).

References:

[1] Borisov, S. V., Magarill, S. A. & Pervukhina, N. V. (2011) *Cristallografiya,* (2011), **56**, 1001–1006.

[2] Borisov, S. V., Magarill, S. A. & Pervukhina, N. V. (2013) *J. Struct. Chem.* (in press).

[3] Borisov, S. V., Magarill, S. A. & Pervukhina, N. V. (2013) *J. Struct. Chem.* (in press).

CRYSTAL CHEMISTRY OF SOME NATURAL PHOSPHATES AND SULFATES CONTAINING MIXED ANIONIC RADICALS

***Chernyatieva A.P.*[1], *Yakovenchuk V.N.*[2], *Britvin S.N.*[1,2], *Murashko M.N.*[3], *Pekov I.V.*[4], *Krivovichev S.V.*[1,2]**

[1]*Crystallography Department, St. Petersburg State University, Faculty of Geology, St. Petersburg, Russia*
[2]*Nanomaterials Research Centre, Kola Science Centre, RAS, Apatity, Russia*
[3]*"Systematic Mineralogy" St. Petersburg, Russia*
[4]*Mineralogy Department, Faculty of Geology, Moscow State University and Institute of Geochemistry and Analytical Chemistry RAS, Moscow, Russia*
nastya250@yandex.ru

Sulfates and phosphates consisting of mixed anionic radicals (or heteropolyhedral units) constitute a large group of mineral species. In this contribution, we will summarize our recent results on some novel or poorly studied minerals, whose structures are based upon octahedral-tetrahedral structural units.

During investigations of secondary pegmatite phosphates from Hagendorf (Germany), we have located a new whiteite-jahnsite-group mineral that was named *whiteite-(CaMnMn)* [**1**]. The X-ray diffraction data were collected using Bruker Smart APEX II diffractometer. *Whiteite*-(CaMnMn), $CaMnMn_2Al_2[PO_4]_4(OH)_2(H_2O)_8$, is a new hydrous phosphate of Ca, Mn and Al, closely related to jahnsite-(CaMnMn) and other minerals of the whiteite group. Its structure is formed by alternating anionic layers $[M1_2M3_2(PO_4)_4(OH)]^{3-}$ composed from MO_6 octahedra and PO_4 tetrahedra, and linked together thorugh M(2) cations and water molecules [**1**].

The crystal structure of *bonshtedtite*, $Na_3Fe(PO_4)(CO_3)$, is similar to that of the other minerals of the bradleyite group. It is based upon the $[Fe(PO_4)(CO_3)]^{3-}$ layers oriented parallel to (001). The layers are formed by corner linkage of PO_4 tetrahedra and $FeO_4(CO_3)$ groups consisting of FeO_6 octahedra sharing edges with CO_3 triangles [**2**]. Topology of octa-tetrahedral layer in bonshtedtite is similar to that observed in the autunite-group minerals, but differs from the latter in terms of local topological properties.

Refinement of the crystal structure of *girvasite* at 100 K allowed to determine positions of H atoms and to reveal the hydrogen bonding scheme. The refinement confirmed that the proper chemical formula of the mineral should be written as $NaCa_2Mg_3(PO_4)_4(CO_3)(H_2O)_6$, in contrast to the formula $NaCa_2Mg_3(PO_4)_2[PO_2(OH)_2](CO_3)(OH)_2(H_2O)_4$ proposed in the original works [**3,4**].

The crystal structure of *cattiite*, $Mg_3(PO_4)_2(H_2O)_{22}$ [5] contains two symmetrically independent Mg sites, tetrahedrally coordinated by water molecules to form octahedral complexes $[Mg(H_2O)_6]^{2+}$. From 22 H_2O molecules present in the structure, four are not bonded to the Mg^{2+} cations and are located in between the $[Mg(H_2O)_6]^{2+}$ complexes [**6**]. The structure consists of layers of the two types. The **A** layer contains $[Mg1(H_2O)_6]^{2+}$ groups and the H_2O13 molecules. The **B** layer contains $[Mg2(H_2O)_6]^{2+}$ groups, $(PO_4)^{3-}$ tetrahedra and the H_2O6 molecules. The layers alternate according to the ...**ABB'ABB'A**... or [**ABB'**] sequence, where **B'** is a layer symmetrically equivalent to **B**. Natural cattiite is an analogue of synthetic $Mg_3(PO_4)_2(H_2O)_{22}$-1*A*2. The difference between the $Mg_3(PO_4)_2(H_2O)_{22}$ polytypes (cattiite and $Mg_3(PO_4)_2(H_2O)_{22}$-1*A*1) is in mutual relationships of the octahedra located in the adjacent layers.

The crystal structure of *vendidaite*, $Al_2(SO_4)(OH)_3Cl(H_2O)_6$, contains one symmetrically independent Al site octahedrally coordinated by three OH groups and three H_2O molecules. Two adjacent $[Al(OH)_3(H_2O)_3]$ octahedra share the $O_h1\cdots O_h1$ edge to form a $[Al_2(OH)_4(H_2O)_6]$ dimer with the O_h1-Al-O_h1 bond angle equal to 76.96(6)°, i.e. considerably shorter than the ideal angle of 90°. The dimers are further linked by sharing the O_h4 atoms to form $[Al_2(OH)_3(H_2O)_6]^{3+}$ chains running parallel to the *a* axis. The crystal structure contains $(SO_4)^{2-}$ groups and Cl^- anions

held in the structure by hydrogen bonds only. Together with the $[Al_2(OH)_3(H_2O)_6]^{3+}$ chains, Cl^- anions and $(SO_4)^{2-}$ groups form pseudo-layers parallel to (010).

Steklite, $KAl(SO_4)_2$, was first described as a technogenic phase in products of burning coal dumps (Chelyabinsk region, Russia). Steklite of natural origin was found in sublimates of the Yadovitaya (Poisonous) fumarole of the Second scoria cone of the Northern Breakthrough of the Great Tolbachik Fissure Eruption, Kamchatka, Russia [**7**]. In the structure of steklite, SO_4 tetrahedral anions share corners with distorted AlO_6 trigonal prisms to form $^2_\infty[(Al,Fe)(SO_4)_2]^-$ layers parallel to (001), with K^+ cations located in the interlayer space.

This work was supported by the Russian Federal Grant-in-Aid Program 'Cadres' (agreement no. 8313)..

References:

[1] Yakovenchuk V.N., Keck E., Krivovichev S. V., Pakhomovsky Y. A., Selivanova E. A., Mikhailova J. A., Chernyatieva A. P., Ivanyuk G. Yu. (2012) Whiteite-(CaMnMn), $CaMnMn_2Al_2[PO_4]_4(OH)_2 \cdot 8H_2O$, a new mineral from the Hagendorf-Süd granitic pegmatite, Germany. Mineralogical Magazine, 76, 2761-2771.

[2] Krivovichev S.V., Chernyatieva A.P., Britvin S.N., Yakovenchuk V.N., Krivovichev V.G. (2013) Refinement of the crystal structure of bonshtedtite, $Na_3Fe(PO_4)(CO_3)$. Proc. Russ. Mineral. Soc., in press.

[3] Britvin, S.N., Pakhomovsky, Ya.A., Bogdanova, A.N., Sokolova, E.V. (1990) Girvasite, a new carbonate phosphate of sodium, calcium and magnesium. Mineral. Zh. 12(3), 79-83 (in Russian).

[4] Sokolova E.V., Yegorov-Tismenko Y.K. (1990) Crystal structure of girvasite. Doklady Acad. Nauk SSSR, 311, 1372–1376 (in Russian).

[5] Britvin, S.N., Ferraris, G., Ivaldi, G., Bogdanova, A.N., Pakhomovsky, Ya.A., Chukanov,N.V., (2000) Cattiite, $Mg_3(PO_4)_2(22H_2O)$, a new mineral from Zhelezny Mine (Kovdor, Kola Peninsula, Russia). Neues Jahrbuch fur Mineralogie-Monatsherte, 160-168

[6].Chernyatieva A.P., Krivovichev S.V., Britvin S.N. (2013) Crystal structure of cattiite, $Mg_3(PO_4)_2(H_2O)_{22}$. Proc. Russ. Mineral. Soc., in press.

[7] Murashko M.N., Pekov I.V., KrivovichevS.V., Chernyatieva A.P., Yapaskurt V.O., Zadov A.E., Zelensky M.E. (2012) Steklite, $KAl(SO_4)_2$: the find at Tolbachik volcano (Kamchatka, Russia), validation as a mineral species and crystal structure. Proc. Russ. Mineral. Soc. 141(4), 36-44.

MINERALS IN SUPERSPACE

Friese K.

Jülich Center for Neutron Science, Research Centre Jülich, Jülich, Germany
k.friese@fz-juelich.de

Aperiodic structures are not periodic in three dimensions. However, the peridodicity can be regained by adding one or more additional dimensions to the *3*-dimensional space and, this way, one can recover the periodicity in a higher *3+d* -dimensional superspace **[1,2]**. The description in superspace has been used successfully for the determination of aperiodic structures since its development in the 1970s and the implantation into structure refinement programmes in the subsequent years.

Aperiodic structures are frequently observed in mineral systems. Their existence is generally restricted to certain pressure/temperature conditions or depends on the chemical composition. Thus minerals of the same group may show modulations if they are from one type location, while they have regular structures if they are from a different location, where the formation conditions were different.

The list of minerals exhibiting aperiodic structures is long and comprises framework alumosilicates (e.g. plagioclase, nepheline, sodalites), silica polymorphs (e.g. quartz, tridymite), layered alumosilicates (e.g. melilites, antigorite, fresnoite), iron oxides and sulfides (pyrrothite, wüstite), calaverite, sulfosalts (cannizzarite, cylindrite, franckeite), elements (e.g. sulphur under high pressure) or the quasicrystalline mineral icosahedrite **[3]**.

There are several underlying reasons for the formation of aperiodic structures in minerals. They arise from, for instance, vacancy ordering, clustering of ions with different sizes and charges, rigid unit modes, intergrowths of domains with slight compositional variations, or internal misfits of different building units.

In this presentation an overview over aperiodic mineral structures will be given and selected examples (e.g. nepheline **[4]**) will be discussed in detail to illustrate the complexity of these structures.

References:

[1] P. M. de Wolff, *Acta Crystallogr*. 1974, ***A30***,777-785.
[2] P. M. de Wolff, T. Janssen, A. Janner, *Acta Crystallogr*.1981, ***A37***,625-636.
[3] L. Bindi, P. J. Steinhardt,N. Yao, P. J. Lu, *Am. Miner*. 2011, ***96***, 928-931.
[4] K. Friese, A. Grzechnik, V. Petricek, A. Schönleber, S. van Smaalen, W. Morgenroth, *Acta Crystallogr*. 2011, ***B67***, 18-29.

STUDIES OF THE STRUCTURE AND PROPERTIES OF SYNTHETIC LAYERD Li-SILICATES

Palchik N.A., Grigoreva T.N., Moroz T.N., Solotchin P.A.

V.S. Sobolev Institute of Geology and Mineralogy SB RAS, Novosibirsk, Russia
nadezhda@igm.nsc.ru

Crystallochemical features of lithium micas and their properties attract the attention of a scientific community over a half of the century. But it is not clear what changes occur in these structures and how the properties of the compounds vary when monovalent lithium enters a crystal cell. Bujdak at al. **[1]** showed that even partial lithium implantation into positions of cations in the interlayer space and octahedra of smectites produces changes in negatively-charged ground layer. As a consequence, there is the tendency for mineral to possess, for example, hydrophobic properties and the sorption mechanism of alkylammonium cations in the interlayer is displayed. On sintering of fluorophlogopite, which is indispensable material in many areas of application, an effort has been made to introduce lithium into the interlayer space instead of potassium, as well as to substitute partly octahedral magnesium by lithium to produce trioctahedral mica with the formula $Li(Mg_2Li)[Si_4O_{10}]F_2$. Bobr-Sergeev **[2]** has revealed that during the crystallization of Li-fluorophlogopite, immiscible phases of various composition occurred repeatedly **[2]**. Several samples of layered lithium silicates synthesized by the researcher **[2]** differed noticeably from each other in their X-ray diffraction and IR spectroscopic data and these exhibited unusual properties. Samples obtained were represented macroscopically as powder-like substance with crystals (less than 1mm in size) in the form of translucent flakes. The samples readily adsorbed air moisture and swelled in water into jelly-like substance such as colloidal solution. After drying, the samples reverted to their original crystalline state with variable amount of water molecules in the interlayer space. The region of stretch vibrations of OH-groups in the IR spectrum of the synthesized sample shown in Fig. 1 (insertion) corresponds to the spectrum of adsorbed H_2O. According to the X-ray diffraction analysis, the original material had an obviously layered structure with the d_{001}= 12.3A and all orders of 00l up to d_{00l0} (Fig.2, curve 1). The value of the d_{060} 1.514A reflection and that of the parameter b = 9.08A were valid for the extreme terms of representatives of dioctahedral smectite **[3,4]**. There was essential decrease in the intensity of the d_{001}=12.3A peak after impregnation with ethylene glycol and two additional peaks occurred: the intense peak with d = 16.8A and another weak one with d =14.7A (Fig.2, curve 2). Some 001 reflections in the XRD pattern may be related to the presence of three layered phases in the sample. After wetting of original material with water,

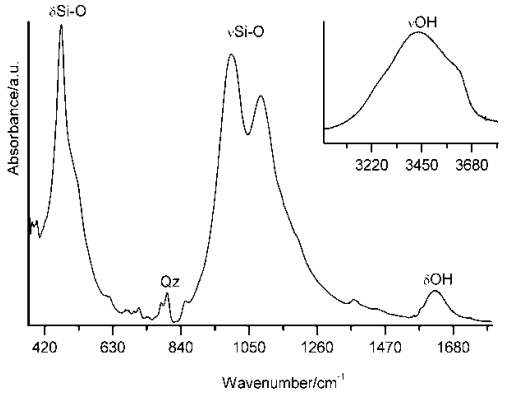

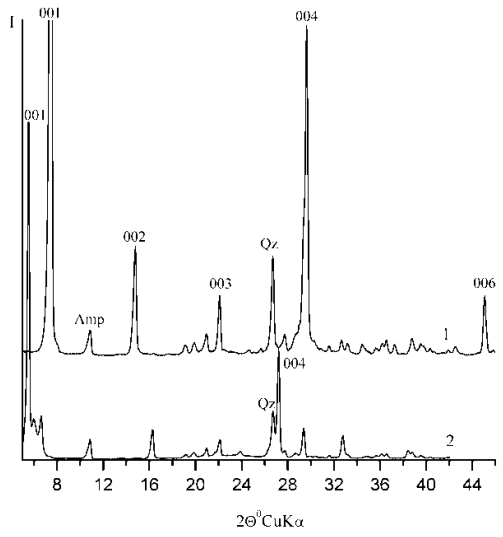

intensities of all peaks decreased abruptly and the phase with the d_{001}=18.7A and very weak 00l orders became apparent. After heating the sample at 550^0C for one hour, the band 001 shifted towards high angles and two peaks with d=12,28A and d=9.68A appeared. According to the data obtained, it can be inferred that two or three layered silicates with different characteristic properties are present in the sample. One of these silicates has a mobile structure similar to that of smectite minerals, another one is stable (d = 12.3A), and the third silicate seems to be a mixed-layer compound of the first two minerals (d = 14.7A after impregnation with ethylene glycol). The DTA curve for this mineral shows two distinct endothermic peaks at 140^0C and 200^0C due to the maximum loss of adsorbed water from the interlayer space, whereas DTA curves of naturally occurring smectites exhibit only single endothermic peaks at 140^0C **[5]**. According to the thermogravimetric data, the loss of adsorbed water is about 2.0 %. Besides, there is one more endothermic peak at 380^0C on the DTA curve related to the subsequent loss of water molecules. Thus, the thermal analysis substantiates the presence of two mobile structures in the investigated sample. One of these phases is similar to smectite and another appears to be mixed-layer compound, whereas the third phase is stable. The structures of these compounds differ in positions and the content of lithium, which can be just as in the interlayer space, so in octahedral and tetrahedral positions. The content of water molecules may be different in these compounds as well.

The work is carried out at support of the Russian Fund of Fundamental Research, the project № 13-05-00074.

References:

[1]. J.Bujdak, H.Slosiarikova. L. Novakova, B.Cicel. Fixation of lithium cations in montmorillonite. Chem. Papers. 1991. V. 45. No 4, 499-507.

[2]. A.A. Bobr-Sergeev. Some problems of synthesis of fluorophlogopite and isomorphism in its structure. Unpublished PhD thesis, 1967, 16 p (in Russian).

[3]. Alberto Viani, Alessandro F. Gualtieri, Gilberto Artioli. American Mineralogist. 2002. V. 87, 966-975.

[4]. N.A. Palchik, T.N. Grigoreva, T.N. Moroz. The composition, structure and properties of high-iron nontronites of various genesis. Kristallografiya. 2013. V. 58, No 2, 275-300 (in Russian).

[5]. V.I. Ivanova V.I., B.K. Kasatov, T.N. Krasavina, E.L. Rosinova 1974. Thermal analysis of minerals and rocks. Moscow, Nedra, 168 p (in Russian).

CRYSTAL CHEMISTRY OF LOW SYMMETRY VESUVIANITE FROM THE KHARMANKULSKIY MINES (SOUTH URALS, RUSSIA)

Panikorovskiy T.L., Zolotarev A.A. Jr., Krivovichev S.V., Antonov A.A.

Saint-Petersburg State University (SPSU), Saint-Petersburg, Russia
rotor_vlg@list.ru, aazolotarev@gmail.com

Vesuvianite is a complex mineral with a range of crystal chemical phenomena arising due to so-called 'rod polytypism' **[1-3]**. In the structures of 'high' vesuvianites (space group *P*4*/nnc*), rods are disordered, whereas in the structures of 'low' vesuvianites (space groups *P*4*/n* and *P*4*nc*), there is an ordered arrangement of rods. In this contribution, we report on the structure, composition and IR spectra of 'low' vesuvianite from the Kharmankulskiy mine. The sample was taken from collections of Mineralogical Museum of St. Petersburg State University.

The crystal of vesuvianite selected for data collection was studied using a Bruker SMART APEX X-ray diffractometer (MoKα X-radiation) equipped with a CCD type area detector. The unit-cell parameters were refined using least-squares techniques. The SHELXL program package was used for all structural calculations **[4]**. The chemical composition was studied by the wave-length dispersion spectrometry using a Cameca MS-46 electron microprobe. Infrared spectrum of vesuvianite was collected using Bruker Vertex 70 IR spectrometer at room temperature.

The unit-cell parameters are as following: a = 15.621(1), b = 11.877(1) Å, V = 2898.6(3) Å^3. Crystal chemical formula can be written as $Ca_{18.84}Mg_{2.75}Fe_{1.83}Al_{8.52}Si_{17.32}(O_{67.17}(OH)_9)$. The structure of examined sample was refined in the *P*4/*nnc*, *P*4/*n* и *P*4*nc* space groups with the R-indices equal to 0.093, 0.012 and 0.034, respectively. However, the *P*4/*nnc* and *P*4/*n* models corresponded to a high number of systematic absence violations, whereas the number of violations for the *P*4*nc* was essentially smaller. It is noteworthy that the *P*4*nc* space group is quite rare for 'low' vesuvianites **[3,5,6]**.

Interpretation of the IR spectrum obtained was done on the basis of methodology developed by Kurazhkovskaya et al. **[7]**. In the IR spectrum, two absorption bands at 438 and 476 cm^{-1} belong to the ν_2 symmetric deformation vibrations of the Si-O bonds. The bands at 563, 607 and 632 cm^{-1} correspond to the ν_4 asymmetric deformation vibrations of the same bonds. The bands 800, 881, 918, 964 and 1016 cm^{-1} may be attributed to asymmetric stretching vibrations of the Si-O and Si-O-Si bonds. The bands in the range 1610-3637 cm^{-1} correspond to regions of the hydroxyl vibrations. In terms of the group-theoretic analysis for the space group *P*4*nc* lowering of the symmetry of the tetrahedron to *C*2 results in the appearance of three bands in the 620-570 cm^{-1} region **[7]**. Therefore, IR data correspond to the 'low' vesuvianite, which is in good agreement with the results of structure refinement.

According to **[8]**, formation of contact metasomatic rocks at the Polyakovskiy and Kharmankulskiy mines happened at the temperatures near 300 °C in the course of hydrothermal alteration of primary rocks. This is in accordance with our results that vesuvianite belongs to the 'low-symmetry' arrangement.

This work was supported by the Russian Federal Grant-in-Aid Program 'Cadres' (agreement no. 8313).

References:

[1] L.A. Groat, F.C. Hawthorne, T.S. Ercit The role of fluorine vesuvianite: a crystal-structure study // Can. Mineral. 1992. Vol. 30. P. 1065-1075.
[2] F.M. Allen and C.W. Burnham. A comprehensive structure-model for vesuvianite: symmetry variations and crystal growth // Can. Mineral. 1992. Vol. 30. P. 1-18.
[3] T. Armbruster and E.Gnos. *P*4/*n* and *P*4*nc* long-range ordering in low-temperature vesuvianites // Amer. Mineral. 2000. Vol. 85. P. 563–569.
[4] Sheldrick G.M. SHELXL-97, Program for the refinement of crystal structures. Universität

Göttingen, Germany, 1997.
[5] T. Armbruster, E. Gnos. Rod polytypism in vesuvianite: crystal structure of a low-temperature *P*4*nc* vesuvianite with pronounced octahedral cation ordering // Schweiz. Mineral. Petrogr. Mitt. 2000. Bd. 80. S. 109-116.
[6] M.Ohkawa, A. Yoshiasa, S. Takeno. Structural investigation of high- and low-symmetry vesuvianite // Mineral J. 1994. Vol. 17. P. 1–20.
[7] V.S., Kurazhkovskaya, E.Ya Borovikova, G.I. Dorokhova, O.V. Kononov, S.Yu. Stefanovich. IR spectra of high-symmetric and low symmetric vesuvianites // Proc. RMS. No. 1, 2003, P. 109–121.
[8] S.V. Krivovichev, A.A. Zolotarev, Jr., T.L Panikorovsky, A.A. Antonov, V.G. Krivovichev. Crystal chemistry of low-symmetry vesuvianite from Monetnaya Dacha (Middle Ural, Russia) // Vestnik SPbSU, Ser. 7, Vol. 2013, P. 1–13.

CRYSTALLOGRAPHIC ANALYSIS OF STRUCTURAL PECULIARITIES IN OXYGEN-RICH $YBaCo_4O_{7+x}$ (x = 1.4) SINGLE CRYSTALS

***Podberezskaya N.V.*, Komarov V.Yu., Kameneva M.Yu., Smolentsev A.I., Kozeeva L.P., Lavrov A.N.**

Nikolaev Institute of Inorganic Chemistry, SB RAS, Novosibirsk, Russia
podberez@niic.nsc.ru

The X-ray diffraction was used to study in detail the reciprocal lattices of two $YBaCo_4O_{7+x}$ single crystals with high oxygen content ($x \approx 1.4$). Based on the data obtained we performed a lattice reconstruction that clarified the crystallographic peculiarities of the oxygen-rich phase. The crystal structure of $YBaCo_4O_{7+x}$ has been found to evolve with oxygen intercalation in a crystallographically regular way, inheriting the axes orientation from the parent (x = 0) phase. Both crystals studied exhibited virtually the same unit-cell parameters: a_o = 10.9233(4) and 10.9239(5) Å, b_o = 31.843(1) and 31.842(2) Å, c_o = 10.0959(4) and 10.0960(5) Å, V = 3511.7 and 3511.8 Å^3, d_{calc} = 5.428 and 5.579 for Z = 4, compositions $Y_5Ba_5Co_{20}O_{35}$ and $Y_5Ba_5Co_{20}O_{40}$ ($Pca2_1$), which are related to the unit-cell parameters of the parent hexagonal crystals [a_h = 6.3058(4) Å, c_h = 10.2442(7) Å, ($P6_3mc$)] as $a_o \approx \sqrt{3}a_h$, $b_o \approx 5b_h$, $c_o \approx c_h$. Most prominent structural changes take place in the basal plane where domains of the orthorhombic phase emerge following the rules of pseudo-hexagonal non-merohedral twinning. We have revealed a new type of superstructural oxygen ordering in $YBaCo_4O_{7+x}$ [$b_r \approx 5(a,b)_h$], and have demonstrated the absence of disorder in the layer stacking along the c axis.

The behavior of $R BaCo_4O_{7+x}$ upon variation of the oxygen content is rather complicated. Structural and thermogravimetric investigations of ceramic $YBaCo_4O_{7+x}$ samples have shown that changes of their oxygen content occur through a first-order phase transition [**1**] between two phases - a parent hexagonal phase with low oxygen concentration and an oxygen-rich one; the transition is accompanied with a significant rearrangement of the crystal structure [**1**, **2**]. Thus far several structural models were suggested to describe the lattice of the oxygen-rich phase [**2** - **5**]. According to the neutron scattering data and the high-resolution synchrotron X-ray scattering [**2**], the crystal structure of $YBaCo_4O_{7+x}$ enriched with oxygen up to $x \approx 1.1$ is orthorhombic ($Pbc2_1$, a_r = 12.790, b_r = 10.845, c_r = 10.149 Å) with the unit-cell parameters being related to those of the parent hexagonal lattice through the matrix 200/210/001. The authors of Ref. [**2**] have drawn a conclusion that, upon oxygen intercalation a half of the cobalt ions in the triangular-lattice layers acquire an octahedral oxygen coordination. This results in the formation of alternating zigzag chains of the emerged cobalt-oxygen octahedra and original tetrahedra running along the b_r axis. At the same time, zigzag chains of cobalt-oxygen octahedra are formed also along the c axis owing to the octahedra that appear in the kagome-lattice layers. An electron-diffraction study of a ceramic sample with similar oxygen content ($x \approx 1$) indicated that different grains of ceramic could possess different crystal structures with the symmetry being or being not reduced from the parent hexagonal one [**3**]. Structural modulations with different periodicities $q_A = (1/3)g_{210}$, $q_B = (1/6)g_{210}$, and $q_C=(1/10)g_{210}$ were observed, which was attributed by the authors to some dispersion in the oxygen composition from one ceramic grain to another. The smallest Niggly unit cell was determined for the oxygen-enriched samples as a=10.90(4), c=10.02(6) Å for the hexagonal structure and a = 18.90(4), b = 10.90(5) and c = 10.05(0) Å for the orthorhombic one [**4**], which corresponded to the $\sqrt{3}\times\sqrt{3}\times1$ and $3\times\sqrt{3}\times1$ supercells of the parent hexagonal lattice. By now the crystal structure of fully oxygenated (x = 1.5) $YBaCo_4O_{7+x}$ has not been determined experimentally. However, a computer simulation of the crystal structure (~ 11600 atoms) [**5**] has shown that the Co^{3+} ions in $YBaCo_4O_{8.5}$ should predominantly possess a pyramidal oxygen coordination. A small fraction of Co^{3+} ions with octahedral coordination together with remaining tetrahedrally coordinated cobalt ions are predicted to be distributed randomly over the lattice with the octahedra being located mostly in

the kagome layers. In general, the oxygen sublattice in $YBaCo_4O_{8.5}$ is expected to be highly disordered, while the heavy ions retain the long-range order.

Our investigations of $YBaCo_4O_{7+x}$ single crystals with $x \approx 1.4$ have revealed a superstructure that was not observed previously [**2** - **5**]. To prove the existence of a superstructure with the 5-fold increase in the unit-cell size along one of the axes ($b_r \approx 5b_h$) we have carried out a detailed experimental investigation of the reciprocal lattice and performed its further reconstruction, employing standard techniques developed for studying single crystals (see figure).

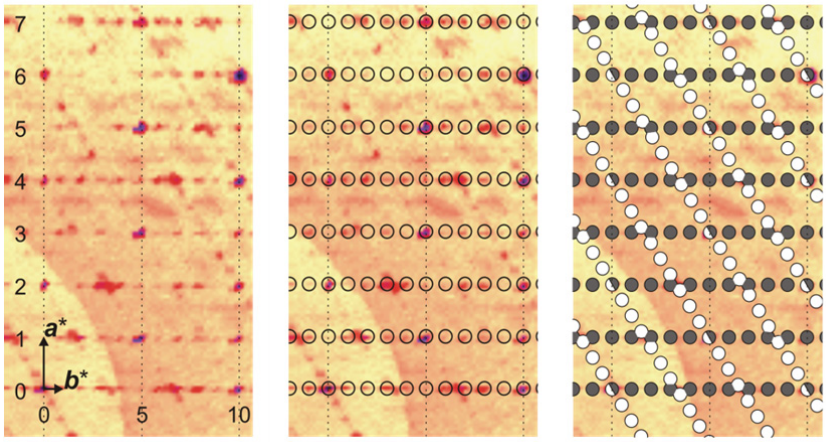

a b c

Reconstruction of the reciprocal lattice for one fragment of the hk4 plane performed for the **1** single crystal: (a) distribution of the diffraction intensities; the Miller indices are indicated for the dominant crystal twin domain; (b) positions of the Bragg peaks for the dominant twin domain shown by the open circles; (c) superposition of the Bragg peaks for the dominant (black circles) and minor (white circles) twin domains.

The obtained results demonstrate that the cation sublattices are only weakly distorted with increasing oxygen content in $YBaCo_4O_{7+x}$ [**6**, **7**] (the structure was analyzed within the $Pca2_1$ type). The distortions of the crystal lattice are predominantly restricted to the {00l} layers and manifest themselves as the formation of superstructures, while the stacking of the "hexagonal" and "kagome" layers is kept unaffected.

References:

[**1**] A.V. Alekseev, M.Yu. Kameneva, L.P. Kozeeva, A.N. Lavrov, N.V. Podberezskaya // *Bulletin of the Russian Academy of Sciences, Physics, 2013, V.77, No.2, 151;*L.P. Kozeeva, M.Yu. Kameneva, A.N. Lavrov and N.V. Podberezskaya // *Inoranic Materials, 2013,V.49, No6, P. 626*

[**2**] Chmaissem O., Zheng H., Hug A. et al. // *J. Solid State. Chem. 2008. V. 181. P. 664*

[**3**] Y. Jia, H. Jiang, M. Valkeapää, H. Yamauchi, M. Karppinen, E. I. Kauppinen // *J. Am. Chem. Soc. 2009,* ***131****, 4880*

[**4**] Y. Jia, H. Jiang, M. Valkeapää, R.Da, H. Yamauchi, M. Karppinen, E. I. Kauppinen *Sol. St. Ionics 2011,* ***204-205,*** *7*

[**5**] J. C. Waerenborgh, E. V. Tsipis, L. C. J. Pereira, M. Avdeev, E. N. Naumovich, V. V. Kharton // *Dalton Trans., 2012, 41, 667*

[**6**] Н. В. Подберезская, А. И. Смоленцев, Л. П. Козеева, М. Ю. Каменева, А. Н. Лавров // *Кристаллография, 2013, том 58, № 4, с. 598–602*

[**7**] N.V. Podberezskaya, L.P. Kozeeva, M..Yu. Kameneva, et al // *Crystallogr. Rep., 2011, V.56, No 3, P. 425.*

GENESIS AND CONFORMATION OF POLAR TWIN STRUCTURES IN CZOCHRALSKI GROWN α-SrB_4O_7 CRYSTALS

***Radionov N.V.*, Zaitsev A.I., Cherepakhin A.V., Zamkov A.V.**

L.V.Kirensky Institute of Physics SB RAS, Krasnoyarsk, Russia
az@iph.krasn.ru

Recently a number of papers emerged which report fabrication of regular twinned structures in nonferroelectric crystals such as quartz **[1]** and $Li_2B_4O_7$ **[2]**. These structures were utilized for SHG in deep UV region under QPM conditions. Orthorhombic α-SrB_4O_7, featuring favorable physical properties (fundamental absorption edge close to 120 nm, high damage threshold and chemical stability as well as sufficiently high nonlinearity **[3, 4, 5]**) and intrinsic growth twin structure **[6]** was shown to be a promising QPM SHG host **[7, 8]**.

Twin structures in SBO crystals were observed by preparing polished cross-sections and visualizing twinned areas via etching in nitric acid solution. Space group $Pmn2_1$ is used to define plane and direction indices.

The crystals under investigation have been grown from the seeds oriented in [100] direction. Twin structure appeared on the one and the same side of crystals towards direction of polar axis [001]. In addition to "plain" twins described in **[8]**, another distinctive twin structures were observed. These new "microtwins" were seen to develop exceptionally in the growth pyramids (101) on the forementioned side of crystal and appear as uneven, wavelike sheets parallel to the plane (010). The observations of several crystals show that their average extensions along the axes [100] and [001] are up to 20 μm and 200 μm correspondingly, while their extension along the axis [010] is quite uniform and comprises about 1 μm.

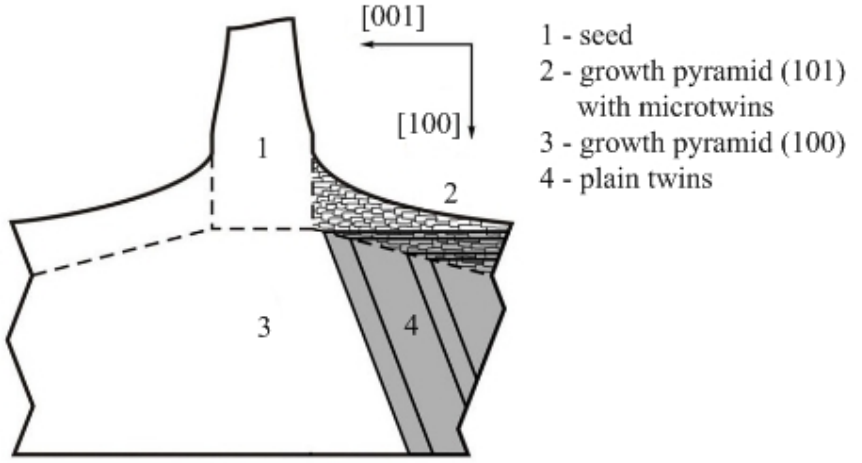

Fig. 1. Arrangement of polar twin structures in a typical α-SrB_4O_7 crystal. View direction is [010].

It was established that these microtwins can occasionally propagate in growth pyramid (100). Once they do their subsequent conformation becomes entirely different. From its propagation point these twins expand into the growth pyramids (100) and (101) along the axes [101] and [100] respectively, forming a plain twin with constant extension along the axis [010] (see Fig. 1). Such multiple plain twins compose a laminated structure with twin boundaries parallel to the plane (010). As opposed to the original microtwins, diverse plain twins vary in thickness (extension along the axis [010]) from sub-micron values to several hundreds of microns. Thickness of each individual twin, however, remains constant through several millimeters along axes [100] and [001]. This dimensional stability is favorable for organizing QPM conditions for NLO doubling of high aperture beams.

This study is supported by PSB RAS Project 2.5.2, by Grant of the President of the Russian Federation for the support of leading scientific schools SS-4828.2012.2.

References:

[1] S. Kurimura, M. Harada, K. Muramatsu, M. Ueda, M. Adachi, T. Yamada, and T. Ueno. Quartz revisits nonlinear optics: twinned crystal for quasi-phase matching // Optical Materials Express. – 2011. - V. 1, No. 7. – pp. 1367-1375.

[2] Kensaku Maeda, Satoshi Uda, Kozo Fujiwara, Jun Nozawa, Haruhiko Koizumi, Shun-ichi Sato, Yuichi Kozawa, and Takahiro Nakamura. Fabrication of quasi-phase-matching structure during paraelectric borate crystal growth // Applied Physics Express – 2013. - No.6. - pp. 015501-1 - 015501-3.

[3] Oseledchik Yu.S., Prosvirnin A.L., Pisarevskiy A.I., et al. New nonlinear optic crystals: strontium and lead tetraborates // Optical Materials. – 1995. – V. 4. – pp. 669-674.

[4] Petrov V., Noack F., Shen D., Pan F., Shen G., Wang X., Komatsu R., Alex V.. Application of the nonlinear crystal SrB4O7 for ultrafast diagnostics converting to wavelengths as short as 125 nm // Optical Letters. – 2003. –V. 29, No. 4. – pp. 373-375

[5] Zaitsev A.I., Aleksandrovskii A.S., Zamkov A.V., Sysoev A.M.. Nonlinear optical, piezoelectric, and acoustic properties of SrB4O7 // Inorganic Materials. – 2006. – V. 42, No. 12. – pp. 1360-1362

[6] Zaitsev A.I., Aleksandrovsky A.S., Vasiliev A.D., Zamkov A.V. Domain structure in strontium tetraborate single crystal // Journal of Crystal Growth. – 2008. – V. 310 – №1. – pp. 1-4.

[7] Aleksandrovsky A.S., Vyunishev A.M, Zaitsev A.I., and Slabko V. V. Random quasi-phase-matched conversion of broadband radiation in a nonlinear photonic crystal // Phys. Rev. A – 2010. – V. 82. – p. 055806.

[8] Aleksandrovsky A.S., Vyunishev A.M., Zaitsev A.I. Applications of random nonlinear photonic crystals based on strontium tetraborate // Crystals. – 2012. - V.2., No.4. – pp.1393 - 1409.

CRYSTAL CHEMISTRY OF SILICATES WITH LAYERED *HOH* MODULES

R.K. Rastsvetaeva, Aksenov S.M.
Shubnikov Institute of Crystallography RAS, Moscow, Russia
rast@ns.crys.ras.ru

A large group of minerals is formed by three-layer modules (*HOH* modules) which belong to the most stable structural fragments under natural conditions. These minerals named heterophyllosilicates are characterized by a large chemical and structural variety with the preservation of the unified basis: threelayer blocks composed of the central *O* (octahedral) layer of edge sharing *M* octahedra and two *H* (hetero) nets of Si tetrahedra and *D* octahedra (half-octahedra or fivevertex polyhedra). The minerals of these families differ in chemical composition, symmetry, and unit cell parameters, as well as in the topological features associated with the type of condensation of the three-layer blocks **[1]**.

The *D*:Si ratio in heterophyllosilicates is variable and has the follow values: 1:2, 1:4, 1:6 and 1:8 (fig. 1).

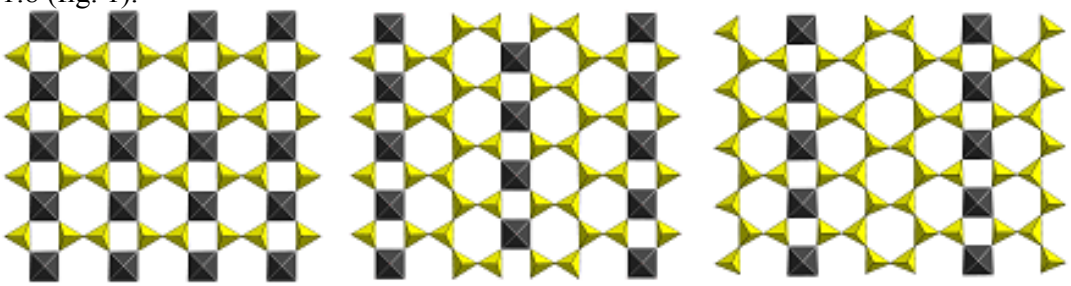

(a) (b) (c)

Fig. 1. Topology of *H* nets with different *D*:Si ratio: 1:2 (a), 1:4(b), 1:6(c).

The most minerals (40 representatives) named by N.V. Belov titanosilicate micas have ***D*:Si = 1:2** with the constant values of two lattice parameters : *a*~5.4 Å and *b*~7.1 Å. The *O* and *H* layers are connected through vertices of the polyhedra entering their composition. The *O* layer most often contains Fe, Mn, Na and Mg cations and sometimes Ti atoms. *HOH* modules are characterized by the presence of *D* cation in *H* nets in octahedra (minerals of the bafertisite group with $[DOSi_2O_7]$-radical) or half-octahedra (minerals of the lamprophyllite group with $[DSi_2O_7]$-radical). In very rare cases (bykovaite $BaNa[(Na,Ti)_4][(Ti,Nb)_2(OH,O)_3Si_4O_{14}](OH,F)_2\cdot 3H_2O$ and nechelyustovite $(Ba,Na)_2[(Na,Ti,Mn)_4][(Ti,Nb)_2(OH)_3Si_4O_{14}](OH,O,F)_2\cdot 3H_2O$), both variant of coordination are implemented in the same module.

H nets most often contain *D*=Ti in the octahedral coordination. Titanium atoms in *H* nets are partially replaced with Nb in bornemanite, perraultite, jinshajiangite, bykovaite, and nechelyustovite. Complete isomorphic substitution is observed in vuonnemite $Na_8[(Na,Ti)_4][Nb_2Si_4O_{14}]O_2(O,OH,F)_2(PO_4)_2$ and epistolite $(Na,\square)_2[(Na,Ti)_4][Nb_2(O,H_2O)_2Si_4O_{14}]O_2(OH,F)_2\cdot 2H_2O$. Another substitution ($D$=$Fe^{3+}$) was found in ericssonite $Ba_2[Mn_4][Fe_2Si_4O_{14}]O_2(OH)_2$ and ferroericssonite $Ba_2[Fe_4][Fe_2Si_4O_{14}]O_2(OH)_2$.

HOH modules are differing in the mutual position of *H* nets with respect to the *O* layer. In most minerals (bafertisite, surkhobite, schullerite, etc.), *H* nets are shifted with respect to each other along the [010] direction, whereas in other minerals (lamprophyllite, nabalamprophyllite, barytolamprophyllite, vuonnemite, etc.) they are fixed exactly opposite each other. In addition, neighboring modules can be mutually arranged in two different ways. When the *H* nets of neighboring modules face each other, there are prerequisites for their aggregation through *D* octahedra with the formation of pseudolayered (heteroframework) structures.

The rosenbuschite group contains ten minerals based on *HOH* packets combined by edge-sharing *D* polyhedra (most often Zr octahedra) to form framework structures with reduced interlayer gap occupied by Na, Ca or *REE* elements.

Generally, each structure is characterized by a module of one type. Transformations of layered silicates under natural conditions form hybrid structures, which contain simultaneously isolated and linked *HOH* modules. Modules of two types are present in the bornemanite, bykovaite, camaraite and nechelyustovite structures. Bornemanite $BaNa_3[(Na,Ti,Mn)_4][(Ti,Nb)_2O_2Si_4O_{14}](F,OH)_2(PO_4)$ is the only example of a structure with two modules isolated and linked by edges of *D* polyhedra. In the camaraite crystal structure $KNa(Fe^{2+}_5Fe^{3+}_4Mn_7)Nb_4(Si_2O_7)_2O_6(Si_8O_{22})_2O_6(OH)_{10}(H_2O)_3$ bafertisite and surkhobite parts are alternated and all channels are occupied by Ba and one of them occupied by Na. Recently discovered kazanskyite $Ba\square TiNbNa_3Ti(Si_2O_7)_2O_2(OH)_2(H_2O)_4$ contains nechelyestovite-like *HOH* modules and differs by amount of these modules in the structure.

Heterophyllosilicates are layered minerals and not considered mesoporous materials, because they do not contain channels of cavities and their intermodule space extends in two directions and is filled with large cations Ba, Sr and K and water molecules. Intermodule composition can be represented by both single large cations and complex aggregates: Na_3PO_4 and $BaSO_4$ groups in lomonosovite $Na_8[(Na,Ti)_4][Ti_2Si_4O_{14}]O_2(O,OH)_2(PO_4)_2$ and in innelite $(Ba,K)_2Ba_2[(Na,Ca,Ti)_4][Ti_2Si_4O_{14}]O_4(SO_4)_2$ respectively.

If three-layer packets in heterophyllosilicates are linked through shared vertices of *D* octahedra (or their edges), the interpacket space is divided into channels and the minerals become an intermediate between true layered titanosilicates and framework mesoporous titanosilicates. In the jinshajiangite group (surkhobite, perraultite) Ca, Na, Ba and K are distributed in different channels.

The minerals of the astrophyllite group have ***D*:Si = 1:4**. These minerals are triclinic and monoclinic heterophyllosilicates with the unit cell parameters *a*~5.4, *b*~11.9, and *c*~11.7 Å. Their modules contain *D* cations, which can be in two coordinations: DO_6 and DO_5 (magnesioastrophyllite $K_2Na[Na(Fe,Mn)_4Mg_2][Ti_2Si_8O_{24}]O_2(OH)_4$). In the first case *HOH* blocks can aggregate by sharing *X* vertex of *D* octahedra (astrophyllite $K_2Na[(Fe^{2+},Mn)_7][Ti_2FSi_8O_{24}]O_2(OH)_4$, tarbagataite $KCa(Fe^{2+},Mn)_7Ti_2(Si_4O_{12})_2O_2(OH)_5$). The structure with unshared vertices has svanbergite $Ca(Fe^{3+})Ti_2(Si_4O_{12})_2O_2(OH)_5(H_2O)_4$.

Nafertisite $(Na,K)_4(Fe^{2+},Fe^{3+})_{10}[Ti_2O_3Si_{12}O_{34}](O,OH)_6$ as well as caryochroite $(Na,Sr)_3[(Fe^{3+},Mg)_{10}][Ti_2Si_{12}O_{37}](H_2O,O,OH)_{17}$ with **Ti:Si=1:6** has modules which aggregate by sharing the vertices of Ti octahedra into a framework. Their channels are extended along the *b* axis but contracted along the *c* axis.

Obviously hypothetical mineral with ***D*:Si > 1:6** will have the most layered character, which is similar to mica with *TOT* modules. Formally, structure of the veblenite $KNa(Fe^{2+}_5Fe^{3+}_4Mn_7)Nb_4(Si_2O_7)_2(Si_8O_{22})_2O_6(OH)_{10}(H_2O)_3$ is characterized by average ***D*:Si = 1:5**, but it contains alternated fragments with ***D*:Si = 1:2** and ***D*:Si = 1:8** (fig. 2).

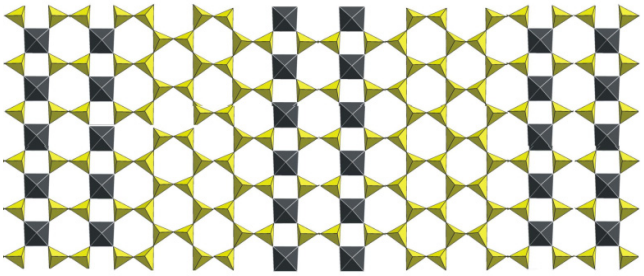

Fig. 2. Heterosilicate radical in the crystal structure of veblenite.

Thus, based on new data about chemical composition and crystal structures the features of natural layered silicates with triple layer *HOH* modules were considered. Modular approach allows not only to describe structural related minerals but simulate new structures with useful properties especially ion-exchange ones.

[1] *Rastsvetaeva R.K., Aksenov S.M.* // Crystallography Reports. 2011. V. 56. № 6. P. 910–934.

STRUCTURE ORDER - DISORDER IN THE POTASSIUM CALCIUM SILICATES: CHAROITE AND DENISOVITE

Rozhdestvenskaya I. [1], ***Mugnaioli E.***[2], ***Czank M.*** [3], ***Depmeier W.*** [3], ***Kolb U.***[2], ***Merlino S.***[4]

[1] *Saint Petersburg State University, Saint Petersburg, Russia*
[2] *Johannes Gutenberg-University, Mainz, Germany*
[3] *Christian-Albrechts-University, Kiel, Germany*
[4] *Dipartimento di Scienze della Terra, University of Pisa, Italy*
ivrozhdestvenska@mail.ru

Polytypism is a relatively common phenomenon in silicate minerals **[1]**. In chain silicates the polytypism is mostly connected with stacking faults or shifts of crystal structure blocks. The best known examples are polytypism in the *dreier* chain silicate wollastonite, $CaSiO_3$ **[2, 3]** and in calcium silicate hydrates (CSH: xonotlite, foshagite, tobermorite *etc*. **[1]**). In all structures the 'octahedral' bands and tetrahedral silicate chains run along the *z* axis. The lattice parameter $c \approx$ 7.3 Å spans two 'octahedra' edges and one repeat period of the tetrahedral silicate chains, respectively. Thus, the metrical relationships between 'octahedral' fragments and tetrahedral silicate chains permit the tetrahedral chain to be connected to the 'octahedral' fragment in two distinct positions, shifted by ≈ 3.65 Å along the chain axis *z*. The means of forming of ordering and disordering polytypes of charoite and denisovite will be briefly review.

From [010] SAED patterns on various single fibres of charoite, a rare mineral from the Murun massif in Yakutia, Russia, it was found that charoite can form four different polytypes **[4]**. Two polytypes have monoclinic symmetry. Both polytypes of charoite were studied using high-resolution transmission electron microscopy, precession electron diffraction, the newly developed technique of automated electron diffraction tomography **[5]** and the structures were determined from electron diffraction intensities *ab-initio* by direct methods. In overall form the crystal chemical formulae of charoite maybe presented as $(K,Sr,Ba,Mn)_{15\text{-}16}(Ca,Na)_{32}[(Si_{70}(O,OH)_{180})](OH,F)_{4.0}\cdot nH_2O$. Unit cell parameters of charoite-90: a = 31.96(6), b = 19.64(4), c = 7.09(1) Å, β = 90.0(1)°, V = 4450 Å^3 and of charoite-96: a = 32.11(6), b = 19.77(4), c = 7.23(1) Å, β = 95.85(9)°, V = 4566 Å^3, space group $P2_1/m$ **[4, 6]**. In a general way the structures of charoite polytypes can be visualized as being composed of three different dreier silicate chains: a dreier double chain, $[Si_6O_{17}]^{10-}$, a tubular loop-branched dreier triple chain, $[Si_{12}O_{30}]^{12-}$ and a tubular hybrid dreier quadruple chain, $[Si_{17}O_{43}]^{18-}$. The chains are bonded by their apical oxygens to edge-sharing Ca and Na-octahedral bands of various widths. All chains and octahedral bands run parallel the *z* axis. The cations K^+, Ba^{2+}, Sr^{2+}, Mn^{2+} and H_2O molecules are located inside the silicate chains. The silicate chains lie on the mirror plane and alternate along the *x* axis. Horizontal Si_2O_7 groups of each chain connect the separate bands of Ca-octahedra in such a way that apical oxygens of neighbouring Si_2O_7 groups are joined to different apices of vertical edges of octahedra and, therefore, the Si_2O_7 groups of adjacent chains are shifted relative to each other by ≈ ½ *c* and the mutual position of the three chains are fixed. It can be said approximately that the three different silicon chains form a module which can be shifted only as a rigid block.

The comparision of the unit cell parameters of charoite-90 and charoite-96 shows that they differ mainly by angle β. In the structure of charoite-96 polytype angle β is determined by the shift on *c*/2 of the rigid block along the octahedral bands in the neighbouring unit cell. The shift takes place between a hybrid dreier quadruple chain, $[Si_{17}O_{43}]^{18-}$, and a double dreier chain, $[Si_6O_{17}]^{10-}$ of nearby cell (Fig. 1).

The periodic repetition of shifts of adjacent modules results in an ordered polytype charoite-96. A sequence of shifts of adjacent modules on +½ *c* and -½ *c* results in an ordered charoite-2a polytype with twice parameter *a*. The stacking disorder in the structure is connected

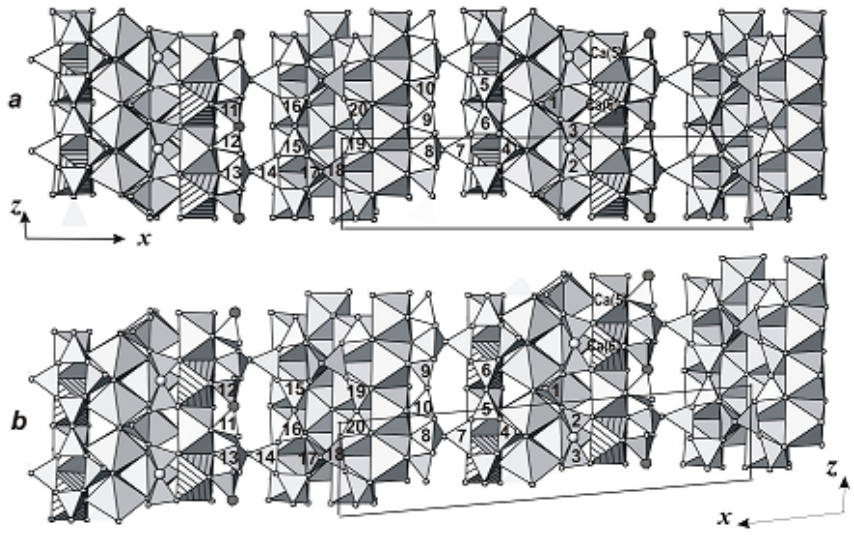

Figure 1. Cut of the structures of charoite-90 (*a*) and *(b)* charoite-96 polytypes in [010] projection ($0.32 < y < -0.25$). Note that in comparison to charoite-90, in charoite-96 the chains on both side of the octahedral column (Ca(5)-Ca(6)) are shifted by $z = ½$ with respect to each other.

with nonperiodic shifts of subsequent modules.

Charoite polytypism can be explained on the basis of order-disorder theory as a sequence of layers with parameters *b, c, a*/2 connected by a screw axis $2_{1/2}$ or $2_{-1/2}$ parallel to *c*, namely screw axes comprising a 180° rotation plus a shift of +¼ or -¼ along *c*, respectively. When the screw axes with the same translational component are constantly applied, charoite-96 polytype is formed. When the screw axes $2_{1/2}$ or $2_{-1/2}$ regularly alternate, charoite-90 polytype is formed. More complicate charoite polytypes can easily be predicted as more complicate stacking sequences along *a* are realized.

Denisovite is a thin needle- or fiber-like mineral, found in the Eveslogchorr and Yukspor Mountain in Khibini massive, Kola peninsula **[7]** and in Murun massive, Russia. The composition is $(Ca_{19.0}Mn_{0.5}Fe_{0.4})(K_{7.2}Na_{3.0})$ $(Si_{29.4}Al_{0.5})O_{80}(F,OH)_{20}$, Z = 2. Unit cell parameters: $a = 31.052(14)$, $b = 18.575(8)$, $c = 7.195(3)$ Å, $\beta = 94.2(1)°$, V = 4139(3) Å^3.

In [001] precession electron diffraction pattern the extinctions along the long axis *a* are present, so *h*00: $h = 2n$. It assumes that space group can be P*a*, P*2/a* or P*2/n*. The electron diffraction pattern also show strong diffuseness along *a** in *hkl*: $l = 2n + 1$ lines in all the observed crystals, i.e. strong disorder along *a*. One can suppose that the denisovite structure also consist from dreier silicate chains which are bonded by their apical oxygens to edge-sharing Ca and Na-octahedral bands and that all chains and octahedral bands run parallel the *z* axis. But the structure of denisovite is more disordered in comparison with the charoite structure.

In spite of similar unit cell of charoite and denisovite, their space groups are different and thus one can expect that the denisovite structure differ from the charoite structure.

The authors thank the RFBR for financial support (№ 12-05-01119-a)

[1] Ferraris, G., Makovicky, E., Merlino, S. (2004) Crystallography Of Modular Materials. Oxford University Press, New York. 370pp.

[2] Jefferson, D.A. and Bown, M.G. (1973) Nature Physical Science*,* 245**,** 43-44.

[3] Wenk, H.R., Muller, W.F., Liddell, N.A., Phakey, P.P. (1976) Wenk, H.R., *et al* (Eds.). Electron Microscopy in Mineralogy. Berlin, Heidelberg, New York: Springer-Verlag. 564 pp. (pp. 324-331).

[4] I. Rozhdestvenskaya, E. Mugnaioli, M. Czank, W. Depmeier, U. Kolb, A. Reinholdt and T. Weirich (2010) Mineralogical Magazine, 74, 159-177.

[5] Mugnaioli, E., Gorelik, T., and Kolb, U., (2009) Ultramicroscopy, 109, 758.

[6] I. Rozhdestvenskaya, E. Mugnaioli, M. Czank,W. Depmeier and U. Kolb, S. Merlino, (2011) Mineralogical Magazin, 75, 2833–2846.

[7] Yu.P. Menshikov. (1984) ZVMO, 113, 718-723.

BLOCK STRUCTURE AND LOCALIZATION OF DEFORMATION AND STRAIN IN THE CRYSTALS

Semukhin B.S.*, *Ploskov N.A.

Institute of Strength Physics and Materials Science SB RAS, Tomsk, Russia
bss@ispms.tsc.ru

Any real crystals' structure can be described as a superposition of strictly-ordered quantized volumes. These volumes are measured by several nanometers or dozens of nanometers and are divided by the inter-space of non-strictly ordered atoms.

In such a case, the plastic deformation of poly- and nano-crystals can be understood as a process of self-ordering of polycentric micropolyhedrons.

In this work, we conducted an analysis of block structure for flat samples of polycrystalline aluminum with the grain size of ~ 40 microns. The samples were shaped as a dumb bell with a working part measured as 50×10×2 mm. The uniaxial strain with a permanent speed of $6{,}67 \cdot 10^{-5}$ c^{-1} was applied to the samples. The deformation fields were recorded by the double-exposure speckle photography simultaneously with the sample straining during 17 minutes up to the moment of Taylor parabolic stages [1-4]. If given for Al: $\sigma=\sigma_{02}+\Theta\varepsilon^n$

$$\Theta=(\sigma-\sigma_{02})/\varepsilon^n$$
$$\Theta=\Delta\sigma/\Delta\varepsilon$$
$$\Delta\sigma=((\sigma-\sigma_{02})/\varepsilon^n)\,\Delta\varepsilon$$
$$n=0.5$$
$$\sigma_{Al}=52.4$$
$$\sigma_{02\,Al}=23$$
$$\Delta\varepsilon=0.002$$

Then, the distribution is Exx and $\Delta\sigma$ for the deformation of 0.069 on the parabolic stage. The study demonstrates that the macro-deformation localization can be described by a permanent dissipative structure represented by the stationary equidistantly localized centers of deformation. The characteristics of macro-deformation are different for the areas of sample with various extend of localized macro-deformation. The distribution of localized strains correlates with the localization of plastic macro-deformation which is recorded by the method of double-exposure speckle photography Figure 1.

The levels of localized strains in between the centers of localized macro-deformation are consistent with the strain for each given stage of material loading curve. However, inside the centers of localized macro-deformation, the levels of strain are doubled when compare to the strain of given loading stage.

References:

[1] V.I. Danilov, L.B. Zuev, V.V. Gorbatenko, K.V. Gonchikov, K.P. Pavlichev. Factory laboratory, **72**, № 12; 40 (2006).

[2] L.B. Zuev, V.I. Danilov, B.S. Semukhin. The space-time ordering during the plastic deformation of solid bodies, Successes of metal physics, 2002, volume 3, # 3 pp. 237-304.

[3] L.B. Zuev, V.I. Danilov, S.A. Barranikova. Physics of macro-localization of plastic deformation, Novosibirsk, Science, 2008

[4] B.S. Semukhin, N.A. Ploskov, V.I. Danilov. Metal physics. Newest technology, 2012, volume 34, 10, pp. 1411-1419

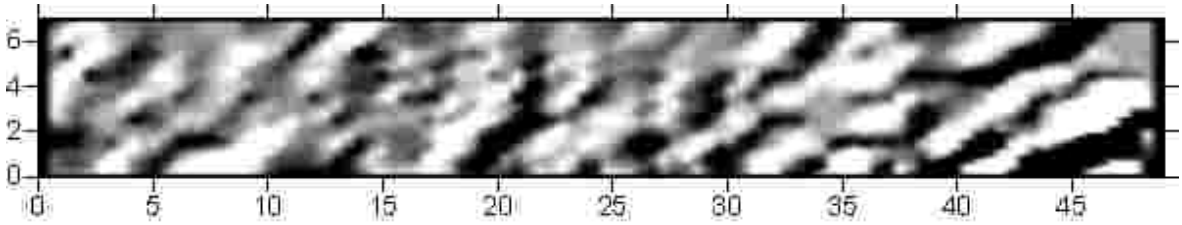

Exx

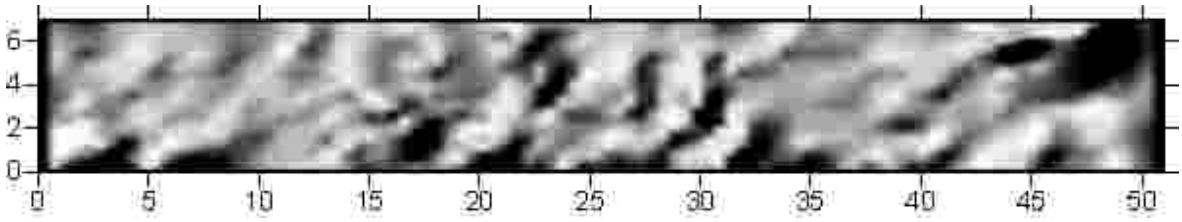

Δσ

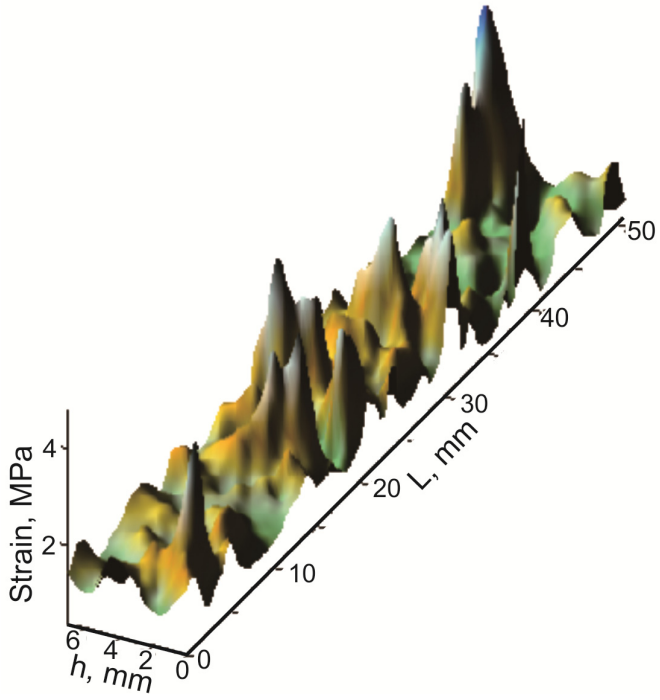

Figure 1. Strain localization during the deformation of Al at 0.002

OPTICAL PROPERTIES OF YB^{3+} ,TB^{3+} AND ND^{3+} CODOPED BAB_2O_4 , $BA_2NA_3[B_3O_6]_2F$ AND BAB_4O_7 CRYSTALS

Solntsev V.P., Davydov A.V., Yelisseyev A.P., Bekker T.B., Kokh A.E.

V.S. Sobolev Institute of Geology and Mineralogy SB RAS Novosibirsk, Russia
solntsev@igm.nsc.ru

The optical absorption and luminescence spectra of α- and β-BaB_2O_4 crystals activated by Tb^{3+}+ Yb^{3+} were studied in detail.

In BBO crystals doped with Yb^{3+} ion the dominating features are absorption bands in the 860 to 1000 nm spectral range which are associated with $^2F_{7/2} \rightarrow {}^2F_{5/2}$ in the Yb^{3+} ion **[1, 2]**. In Fig. 1 one can see six bands at 904, 920, 936, 942, 957 and 968 nm for α-BBO crystals and three bands at 901, 958 and 964 nm for β-BBO.

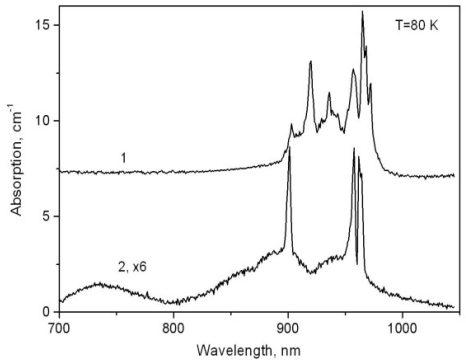

Figure 1. Fragment of absorption spectra of α- (1) and β- BBO (2), doped with Yb and Tb. T=80 K. Spectrum (1) is shifted upwards for clarity.

The emission of BBO crystals codoped with Tb and Yb has a greenish tint and a set of narrow lines associated with Tb^{3+} luminescence is observed in the 400 to 700 nm range (Fig.2). The main group near 550 nm is due to $^5D_4 \rightarrow {}^7F_5$ transitions whereas weaker groups at 500, 590 and 630 nm correspond to $^5D_4 \rightarrow {}^7F_6$, $^7F_4$, $^7F_3$ transitions, respectively (Fig.2).

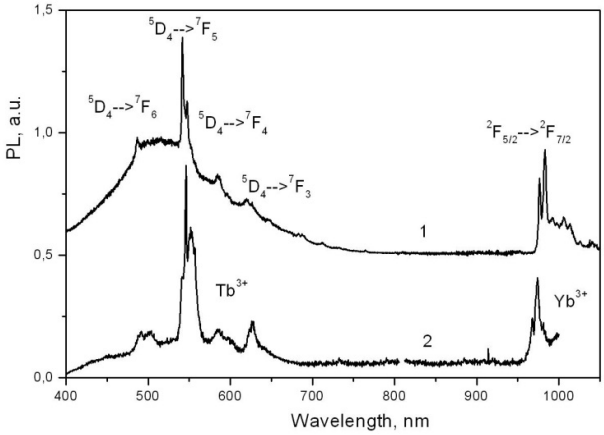

Figure 2. PL spectra at 365 nm excitation for crystals α- (1) and β- BBO (2), doped with Yb and Tb. T= 80 K. Fine structure is associated with Re^{3+}. Spectral resolution is 1.5 nm. Spectrum (1) is shifted upwards for clarity.

Analysis of these spectra showed that the replacement of Ba^{2+} position by $Yb^{3+}(Tb^{3+})$ ions in the lattice of BaB_2O_4 leads to a decrease in the symmetry of oxygen surrounding of $Yb^{3+}(Tb^{3+})$ ions.

By the present time we have preliminarily studied the optical absorption and luminescence spectra of $Ba_2Na_3[B_3O_6]_2F$ crystals activated by Nd^{3+}ions as well as the spectra of α-BaB_4O_7 crystals activated by Tb^{3+} + Eu^{3+} ions.

The preliminary analysis of recently obtained Raman light scattering spectra in Re^{3+} - activated and nonactivated BaB_2O_4 and BaB_4O_7 crystals showed that this material is transparent in the terahertz frequency range (100 GHz – 100 THz). One more important fact is that β-BBO demonstrates birefringence in the range of 0.1 - 1.5 THz (~ 3.3 – 50 cm^{-1}).

The work was supported by Grant no. 12-03-31785(mol_a) from the Russian Foundation for Basic Research.

References:

[1] F. Carrillo Romo, C. Goutaudier, Y. Guyot, M. Th. Cohen-Adad, G. Boulon, K. Lebbou, A. Yoshikawa, T. Fukuda, Optical Materials 16 (2001) 199–206.

[2] I. Nicoara, M. Stef, A. Pruna, J. Cryst. Growth 310 (2008) 1470–1475.

CRYSTAL CHEMISTRY AND ION-EXCHANGE PROPERTIES OF NATURAL TITANOSILICATES: ZORITE, IVANYUKITE AND LINTISITE AND THEIR SYNTHETIC ANALOGUES

Spiridonova D.V. [1,3], ***Krivovichev S.V.*** [1,3], ***Britvin S.N.*** [1,3], ***Yakovenchuk V.N.*** [2,3]

[1] *Saint-Petersburg State University, St.Petersburg, Russia*
[2] *Geological Institute, Kola Science Center, RAS, Apatity, Russia*
[3] *Nanomaterials Research Center, Kola Science Center, RAS, Apatity, Russia*
spiridonovadarya@mail.ru

Crystal chemistry development of zorite **[1]**, ivanyukite **[2]**, lintisite **[3]** mineral groups and their synthetic analogues ETS-4 **[4]**, GTS-1 **[5]**, AM-4 **[6]**, respectively, and investigation of new natural materials and synthesis of microporous compounds with hetero-framework structures, which possess ion-exchange, adsorptive and catalytic properties, which can contribute to their application development in ion-exchange, membrane, separating and other technologies in different industrial areas, are very important. Due to the possibility of general application of these minerals finding optimal synthesis conditions, investigation of these materials properties and their structural characteristics are quite perspective.

In this work, we report on Tl-, Cs-, Ag-, Rb-exchanged forms of zorite and their structural characteristics and provide their comparison to the previous results **[7,8]**. The exchange experiments have been done in basic, neutral and acidic solutions, since our previous results have indicated influence of pH upon cation exchange processes in zorite. It has been found that the ion-exchange capacity of zorite is higher in neutral and basic solutions compared to the acidic solutions. The most likely explanation of this observation is the reactions of protonation/deprotonation of the titanosilicate framework.

Influence of pH upon cation exchange processes in ivanyukite-Na-*T* has not been investigated.

Crystal structures of Tl-, Cs-, Ag-, Rb-exchanged zorite obtained in neutral and basic medium and Rb-, Sr-exchanged ivanyukite-Na-*T* have been investigated by single crystal X-ray diffraction. Structures of Tl-, Cs-, Ag-, Rb-zorite and Rb-, Sr-ivanyukite-Na-*T* were solved by the SHELX97 program.

According to analysis of Tl-, Cs-, Ag-, Rb-exchanged zorite crystal structures locations of the extra-framework cation sites can be divided into three groups denoted as *A*I, *A*II, *A*III. The *A*I position is located between two chains of white vertices and corresponds to the Ca1 and Na2 sites in chivruaiite and zorite, respectively. The *A*II site is in the centre of a hexagonal ring in the framework and corresponds to the Ca2 and Na1 sites in chivruaiite and zorite, respectively. The *A*III site is located in the center of large framework channel. This site is occupied by water molecules in zorite, whereas, for chivruaiite, its partial occupation by K^+ cations has been suggested. As a rule, ion exchange results in a high degree of disorder of extra-framework cations forming groups of sites around the *A*I, *A*II, *A*III positions.

Crystal structure of ivanyukite is based upon 3-dimensional framework of the pharmacosiderite type with the system of channels defined by 8-membered rings (8-MRs) with the crystallographic free diameter of 3.5 Å. The channels are occupied by Na^+, K^+ cations as well as by H_2O molecules. Asymmetric position of K^+ cation within 8-MRs is responsible for rhombohedral distortion of cubanite-like titanosilicate clusters and, as a result for the rhombohedral symmetry of the whole framework. Cation leaching of ivanyukite-Na-*T* results in disappearance of the rhombohedral distortion and relaxation of the ideal cubic symmetry. As a consequence, all exchanged forms of ivanyukite possess cubic space group P-43m. Statistical investigation of geometric parameters of pharmacosiderite type titanosilicates demonstrated that symmetry changes are associated with interactions of extra-framework cations with O atom of $[Ti_4(O,OH)_4]$ clusters of titanosilicate framework.

Within recent years, much attention has been devoted to synthesis and research of new materials, which show high thermal and radioactive stability and also ion-exchange properties. One of such materials is titanosilicate AM-4, which is the synthetic analogue of mineral lintisite. In this research AM-4 has been used to obtain new layered titanosilicate $Ti_2(OH)_2[Si_4O_{10}(OH)_2](H_2O)_2$. Decationization of AM-4 has been carried out by holding the sample in 0.5 M HCl during 3 hours. The crystal structure of new compound has been investigated by Rietveld method. In basis of this structure there are titanosilicate layers, which consist of octahedra TiO_6 and tetrahedra SiO_4. As a result of sample holding in hydrochloric acid total removal of sodium had been observed, which caused layers displacement approximately per 4.5 Å. In this structure layers are joined just by hydrogenous bonds. New layered titanosilicate can be used for getting new intercalated materials with fixed properties.

This work was supported by the Russian Federal Programme 'Scientific and Education Cadres of Innovative Russia' (state contract no. 02.740.11.0326) and President of Russian Federation grant for young doctors of sciences (to SVK, grant no. MD 407.2009.5). We thank Russian foundation for basic research for financial support through the grant № 12-05-31190 and SPbSU X-Ray Diffraction Resource Centre for instrumental support.

References:

[1] Mer'kov A.N., Bussen I.V., Goiko E.A., Kul'chitskaya E.A., Men'shikov Yu. P., Nedorezova A.P. Raite and zorite – new minerals from the Lovozero Tundra // ZVMO. 1973. Vol. 102. №. 1. P. 54–62 (in Russ.).

[2] Yakovenchuk V.N., Nikolaev A.P., Selivanova E.A., Pakhomovsky Ya.A., Korchak J.A., Spiridonova D.V., Zalkind O.A., Krivovichev S.V. Ivanyukite-Na-*T*, ivanyukite-Na-*C*, ivanyukite-K, and ivanyukite-Cu: new microporous titanosilicates from the Khibiny massif (Kola Peninsula, Russia) and crystal structure of ivanyukite-Na-*T* // Amer. Miner. 2009. Vol. 94. P. 1450–1458.

[3] Merlino S., Pasero M., Khomyakov A.P. The crystal structure of lintisite, $Na_3LiTi[Si_2O_6]_2O_2{\cdot}2H_2O$, a new titanosilicate from Lovozero (USSR) // Z. Kristallogr. 1990. Vol. 193. P. 137–148.

[4] Nair S., Jeong H.-K., Chandrasekaran A., Braunbarth C., Tsapatis M. and Kuznicki S.M. Synthesis and structure determination of ETS-4 single crystals // Chem. Mater. 2001. Vol. 13. P. 4247–4254.

[5] Behrens, E.A., Clearfield, A. Titanium silicates, $M_3HTi_4O_4(SiO_4)_3{\cdot}4H_2O$ ($M = Na^+, K^+$), with three-dimensional tunnel structures for the selective removal of strontium and cesium from wastewater solutions. Micropor. Mater. 1997. Vol. 11. P. 65–75.

[6] Dadachov M.S., Rocha J., Ferreira A., Lin Z., Anderson M.W. *Ab initio* structure determination of layered sodium titanium silicate containing edge-sharing titanate chains (AM-4) $Na_3(Na,H)Ti_2O_2[Si_2O_6]{\cdot}2.2H_2O$. Chem. Commun. 1997. P. 2371–2372.

[7] Zubkova, N.V., Pushcharovsky, D.Yu., Giester, G., Pekov, I.V., Turchkova, A.G., Chukanov, N.V. and Tillmanns, E. Crystal structures of K- and Cs-exchanged forms of zorite // Crystallogr. Rep. 2005. Vol. 50. P. 367–373.

[8] Zubkova, N.V., Pushcharovsky, D.Yu., Giester, G., Pekov, I.V., Turchkova, A.G., Tillmanns, E., and Chukanov, N.V. Crystal structure of Pb-exchanged form of zorite // Crystallogr. Rep. 2006. Vol. 51. P. 379–382.

PURE ^{208}Pb ISOTOPE IN MONAZITE: CRYSTAL CHEMICAL AND PRACTICAL ASPECTS

Valter A.A. [1], ***Podberezskaya N.V.*** [2], ***Ponevchinsky V.V.*** [1], ***Pisansky A.I.*** [1]

[1]*Institute of Applied Physics of National Academy of Science of Ukraine, Sumy-Kiev, Ukraine*
[2]*Nikolaev Institute of Inorganic Chemistry, SB RAS, Novosibirsk, Russia*
avalter@iop.kiev.ua

The accumulation of radiogenic isotopes resulting as the decay of long-life nuclides in favorable mineral matrices, apparently, is the only natural process resulting to concentration of some rare isotopes in heavily enriched, pure (> 90%) and even very pure (>>99.9%) states. The possible cases of such enrichment were developed [1].

The accumulation of the pure isotope requires the existence of the host mineral during a long geological time as a spatially closed system containing parent radioactive isotope. Degree of safety of radiogenic isotope and its purity are defined, in particular, by the crystal chemical factors [2, 3].

The formation by the decay chain of pure ^{208}Pb from ^{232}Th in ancient thorium monazites which have near zero uranium content is one of the practically important cases of natural isotope enrichment, because pure ^{208}Pb is a promising material for the nuclear power [4].

In this study we analyzed the peculiarities of cerium atoms inner surrounding by the oxygen atoms in the monazite ($CePO_4$). Ce atoms in monazite are able to be substitute by Th ones without a change of mineral structure [5]. We also analyzed the surrounding of Pb atoms by oxygen ones in the structure of $Pb_3(PO_4)_2$ for understanding the mechanism of adaptation ^{208}Pb atoms to the monazite structure.

We compared the cation-oxygen polyhedrons in the structures of monazite (a) and lead phosphate (b) were obtained by the data [6, 7] (see - figure, table- interatomic distances are given in Å).

a – nine-vertices polyhedron close to the pentagonal dipyramid with substitution of vertices which do not lie on the plane of pentagon by the pair of oxygen atoms. Coordination number of Ce (Th) atom is 7+2.

b-1 – ten-vertices polyhedron – tetragonal antiprism with two centered side faces. Atoms of bases are 2, 5, 7, 10 and 3, 4, 6, 9. The centering atoms are 1, 8. Coordination number of Pb atoms is 4+4+2.

b-2 – eight-vertices polyhedron which is the nearest to pentagonal dipyramid with Pb atom out of pentagon place. One of the O-vertices out of pentagon plane is divided in two. Coordinational number of Pb is 5+3.

Comparison of structure of obtained polyhedrons leads to the conclusion that they have obvious similarities: they can be derived from pentagonal dipyramid and polyhedron (**a**) topologically closer to polyhedron **b-1** than to polyhedron **b-2**.

This is, in our view, the main reason for the stability of radiogenic lead in monazite structure and is the causes of a high accuracy and efficiency of elemental (chemical) dating on this mineral.

The near zero uranium concentration in original monazite leads to formation of new type of monoisotope raw material.

.

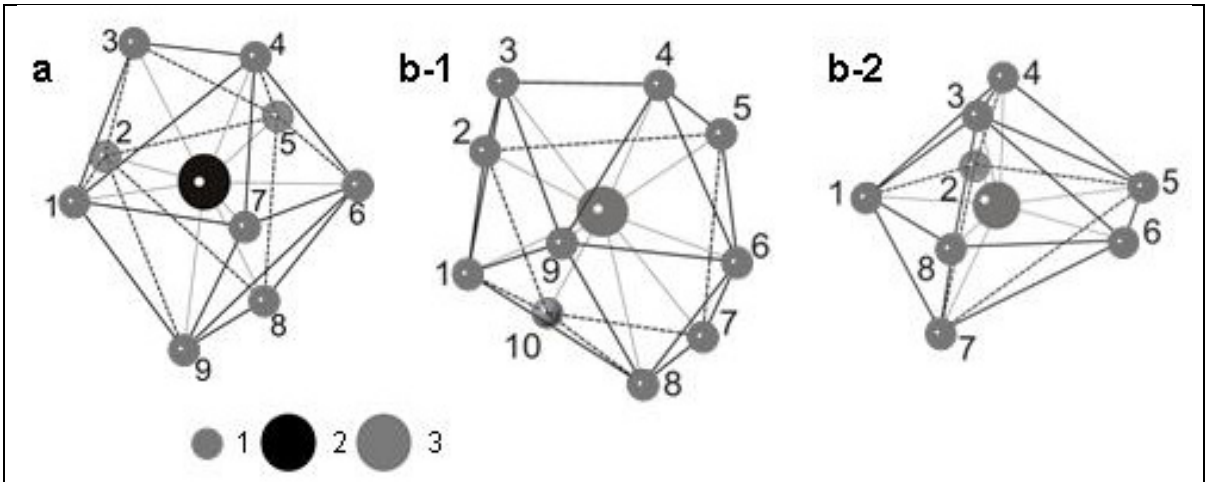

Cation-oxigen polyhedrons in the monazite ($CePO_4$) (**a**) and lead phosphate $Pb_3(PO_4)_2$ (**b**), where **b-1** and **b-2** are the polyhedrons in the two nonequivalent positions
1- Oxygen atoms (numbers – see table).2- Cerium atom, 3-Lead atoms.

Ce		Pb_1		Pb_2	
$Ce-O_1$	2.460	Pb_1-O_1	2.555	Pb_2-O_1	2.365
$Ce-O_2$	2.644	Pb_1-O_2	2.586	Pb_2-O_2	2.908
$Ce-O_3$	2.526	Pb_1-O_3	3.105	Pb_2-O_3	2.479
$Ce-O_4$	2.585	Pb_1-O_4	2.584	Pb_2-O_4	2.412
$Ce-O_5$	2.573	Pb_1-O_5	2.586	Pb_2-O_5	2.794
$Ce-O_6$	2.481	Pb_1-O_6	2.555	Pb_2-O_6	2.959
$Ce-O_7$	2.455	Pb_1-O_7	3.105	Pb_2-O_7	3.067
$Ce-O_8$	2.528	Pb_1-O_8	3.027	Pb_2-O_8	2.906
$Ce-O_9$	2.776	Pb_1-O_9	2.584		
		Pb_1-O_{10}	3.027		

References:

[1] Valter A.A., Storizhko V.E., Dikiy N.P., Dovbnya A.N. et al // Problems of atomic science and technology. (PAST)- 2005.- №6(45). – P.142-146.

[2] Valter A.A., Pisansky A.I., Podberezskaja N.V. //Reports of the National Academy of Sci of Ukraine.-2007. N 12. –P.107-110.

[3] Andreev A.V., Valter A.A., Dikiy N.P., et al. // PAST, 2011. N3 (55). –P. 54-59.

[4] Khorasanov G.L., Blokhin A.I. and Valter A.A. // Nuclear Reactors
. Amir Mesquita – editor. – InTech, 2012. –P.57-71.

[5] Votyakov S.L., Shchapova Yu.V., Khiller V.V. et al. Monazite spectroscopy and physics: the usage state and prospects for Urals geochronology problems //Lithospere.-2012.N 4, p. 158–172.

[6]. Yunxiang Ni, John M. Hughes, Anthony N. Mariano, Crystal chemistry of the monazite and xenotime structures// American Mineralogist, Volume 80, pages 21-26, 1995

[7] Angel R. J., Bismayer U. and Marshall W.G. Local and long-range order in ferroelastic lead phosphate at high pressure// Acta Crystallographica Section B Structural Science, Acta Cryst. (2004). B60, 1-9.

THE CRYSTAL STRUCTURE OF MIMETITE-2*M*, A NEW POLYMORPH OF MIMETITE FROM XIANGHUALING TIN-POLYMETALLIC OREFIELD, HUNAN PROVINCE, P.R. CHINA

***Yang Z.*[1], *Ding K.*[1], *de Fourestier J.*[2], *Li H.*[1]**

[1]*Institute of Geology and Geophysics, Chinese Academy of Sciences, Beijing, China*
[2]*Mineralogical research and consulting, Gatineau, Quebec, Canada*
yangzhm@mail.iggcas.ac.cn

Mimetite-*H* and mimetite-*M* are the polymorphs of lead arsenate with ideal formula $Pb_5(AsO_4)_3Cl$, and belong to the apatite group **[1]**. The crystal structure of mimetite-*H* was refined in the space group $P6_3/m$ with a =10.211, c = 7.4185 Å. While, mimetite-*M* crystallizes in the space group $P112_1/b$, with a =10.189(3), b = 20.372(8), c = 7.456 (1) Å, γ =119.88(3)° **[2]**.

Mimetite-2*M*, ideally $Pb_5(AsO_4)_3Cl$, is a new polymorph of mimetite in the apatite group occurring as a skarn mineral in the Xianghualing Sn-polymetallic ore field, Linwu County, Hunan Province, P.R. China. The associated minerals include fluorite, calcite, cassiterite, pyrite, sphalerite, pyrrhotite, galena, spinel, zinnwaldite and phlogopite. Mimetite-2*M* is pale yellow and forms pseudo-hexagonal columnar crystals of about 1 mm to 5 mm in size. The empirical formula is $Pb_{5.04}As_{2.97}O_{11.95}Cl_{1.05}$.

The super-structure reflections of mimetite were observed and require doubling of the *a*-axes of mimetite-*H*. The crystal structure was refined in space group $P2_1$; with a = 20.422(4), b = 7.4379(15), c = 20.435(4) Å, β = 119.95(3)°, V = 2689.5(9) Å^3, Z = 8, R1 = 0.067, wR2 = 0.180, from 17895 independent reflections.

The crystal structure of mimetite-2*M* is topologically equivalent to mimetite-*H* or mimetite-*M*, having essentially an apatite structure. The superstructure of mimetite-2*M* can be compared with mimetite-*M*. Mimetite-2*M* has AsO_4 tetrahedra linked with two types of Pb polyhedra: $Pb(1)O_9$ and $Pb(2)O_6Cl_2$. The average bond lengths for As–O, Pb(1)–O, Pb(2)–O and Pb(2)–Cl in mimetite-2*M* are respectively similar to those in mimetite-*H* and mimetite-*M*. However, the variation ranges of bond lengths increase from mimetite-*H* and mimetite-*M* to mimetite-2*M*.

The largest differences in positions of analogous atoms between the hexagonal phase mimetite-*H* and monoclinic mimetite-2*M* occur in the positions relative to the O(3) and Cl atoms in the hexagonal phase. The actual positions of the atoms $O(3)_1$ to $O(3)_{24}$ and Cl in mimetite-2*M* results in the reduction of symmetry to monoclinic with both doubled *a*-axes of the hexagonal phase.

The project was supported by the National Natural Science Foundation of China (No. 40872044 and No. 41272063).

References:

[1] PASERO, M., KAMPF, A.R., FERRARIS, C., PEKOV, I.V., RAKOVAN, J. & WHITE, T.J. (2010): Nomenclature of the apatite supergroup minerals. – Eur. J. Mineral. **22**: 163-179.

[2] DAI, Y., HUGHES, J.M. & MOORE, P.B. (1991): The crystal structures mimetite and clinomimetite, $Pb_5(AsO_4)_3Cl$. – Can. Mineral. **29**: 369-376.

PARAGENETIC SEQUENCE OF QUINTINITE, $[Mg_4Al_2(OH)_{12}][(CO_3)(H_2O)_3]$, FROM THE KOVDOR MASSIF (KOLA PENINSULA, RUSSIA): AN X-RAY SINGLE-CRYSTAL DIFFRACTION STUDY

Zhitova E.S. [1], ***Krivovichev S.V.***[1,2], ***Zolotarev A.A.*** [1], ***Yakovenchuk V.N.*** [2], ***Ivanuc*k ***G.Yu.*** [2]

[1] *St. Petersburg State University, St. Petersburg, Russia*
[2] *Nanomaterials Research Centre, Kola Science Centre, RAS, Apatity, Russia*
zhitova_es@mail.ru

The Kovdor massif of ultrabasic, alkaline rocks and carbonatites is a central-type, multiphase igneous intrusion **[1]**. This massif has a rich variety of mineral species. Many of mineral findings are of a good quality, what make them appropriate for X-ray single-crystal diffraction study. One of the most interesting examples of minerals of this kind is quintinite, $[Mg_4Al_2(OH)_{12}][(CO_3)(H_2O)_3]$, which was found in four different polytypic modifications (-2*H*-3*c* (6*R*), 1*M*, 2*H*-1*c*, 2*H*) within the Kovdor massif **[2]**,**[3]**,**[4]**. The sample of quintinite studied in this work comes from hydrothermal vein in carbonantites of the Kovdor alkaline massif, Kola peninsula, Russia.

In one of the studied samples, labeled «Q6» three different species of quintinite crystals growing consistently on each other were observed. These three generations of quintinite (denoted in the order of appearance as Q6-1, Q6-2 and Q6-3) differ in colour and crystal (Fig. 1).

Fig. 1. Three different generations of quintinite Q6.

Crystals of three generations of quintinite have been studied using single-crystal X-ray diffraction. Crystals of Q6-1 are hexagonal, space group $P6_3/mcm$, a = 3.046(5), c = 15.121(5) Å (R_1 = 0.0436). The sample can be described as Mg,Al-disordered quintinite-2*H* and is similar to the sample studied in **[4]**. The structure of quintinite Q6-2 was solved in the space group $P\text{-}3c1$, a = 5.272(1), c = 15.113(3) Å (R_1 = 0.060). The structure is characterized by the Mg,Al-ordering

and can be characterized as Mg,Al-ordered quintinite-2*H*-1*c* **[5]**. Crystal structure of quintinite Q6-3 was solved in the monoclinic space group *C*2/*m*, *a* = 5.286(5), *c* = 7.767(5) Å (R_1 = 0.057) and is identical to the structure reported by Krivovichev et al. **[3]**; it can be described as quintinite-1*M*.

The observed sequence of phases (from disordered high-temperature 2*H* polymorph through ordered 2*H* to the low-temperature ordered 1*M* polytype) is in agreement with the general trend of formation of low-entropy ordered phases with the decreasing temperature.

This work was supported by the Russian Federal Grant-in-Aid Program «Cadres» (agreement no. 8313).

References:

[1] Ivanyuk G. Yu. and Yakovenchuk V N. Minerals of the Kovdor Massif // RAS Kola Science Center Publishing, Apatity, Russia. 1997

[2] Krivovichev S.V., Yakovenchuk V.N., Zhitova E.S., Zolotarev A.A., Pakhomovsky Ya.A., Ivanyuk G.Yu.. Crystal chemistry of natural layered double hydroxides. 1. Quintinite-2*H*-3*c* from Kovdor alkaline massif, Kola peninsula, Russia // Mineralogical Magazine. 2010. Vol. 74(5). P. 821-832

[3] Krivovichev S.V., Yakovenchuk V.N., Zhitova E.S., Zolotarev A.A., Pakhomovsky Ya.A., Ivanyuk G.Yu. Crystal chemistry of natural layered double hydroxides. 2. Quintinite-1*M*: first evidence of monoclinic polytype in M^{2+}-M^{3+} layered double hydroxides // Mineralogical Magazine. 2010. Vol. 74(5). P. 833-840.

[4] Zhitova E.S., Yakovenchuk V.N., Krivovichev S.V., Zolotarev A.A., Pakhomovsky Ya.A., Ivanyuk G.Yu. Crystal chemistry of natural layered double hydroxides. 3. The crystal structure of Mg,Al-disordered quintinite-2*H* // Mineralogical Magazine. 2010. Vol. 74(5). P. 841-848

[5] Arakcheeva, A.V., Pushcharovskii, D.Yu., Atencio, D. and Lubman, G.U. Crystal structure and comparative crystal chemistry of $Al_2Mg_4(OH)_{12}(CO_3)\cdot 3H_2O$, a new mineral from the hydrotalcite-manasseite group // Crystallography Reports. 1996. Vol. 41. P. 972-981.

SESSION 2

Methods of crystal growth, synthesis of crystalline materials and experimental mineralogy

NEW FLUORIDE ORTOBORATES WITH COMPLEX ANIONIC ISOMORPHISM

Bekker T.B. [1], ***Rashchenko S.V.*** [1], ***Bakakin V.V.*** [1], ***Seryotkin Yu.V.*** [1], ***Fedorov P.P.*** [2]

[1] *V.S. Sobolev Institute of Geology and Mineralogy SB RAS, Novosibirsk, Russia*
[2] *General Physics Institute, RAS, Moscow, Russia*
t.b.bekker@gmail.com

Inorganic borates are quite famous for their nonlinear optical properties and transparency in the UV range of the electromagnetic spectrum. Fluoride borates stand out amongst other borates, as they possess much broader areas of transparency with the cut-off edges shifted further in the aforementioned UV range [1]. In the last few decades, a number of fluoride borates crystals, e. g. $KBe_2BO_3F_2$ (KBBF), $BaAlBO_3F_2$ (BABF), $BaMBO_3F$, M = Ca, Zn, Ma, possessing nonlinear optical properties have been discovered.

Recently we described two non-centrosymmetric solid-solution series $Ba_{4-x}Sr_{3+x}(BO_3)_{4-y}F_{2+3y}$ ($P6_3mc$) and $Ba_7(BO_3)_{4-y}F_{2+3y}$ ($P6_3$) [2, 3] that clearly exhibit the $(BO_3)^{3-} \leftrightarrow 3F^-$ anionic isomorphism (the former exhibits cationic $Ba^{2+} \leftrightarrow Sr^{2+}$ isomorphism, as well). Regarding $Ba_7(BO_3)_{4-y}F_{2+3y}$ and similar $Ba_{4-x}Sr_{3+x}(BO_3)_{4-y}F_{2+3y}$ structures, it is worth noting that the most convenient and best fitting depiction of them is via the model that is made up of a cation sublattice with anion-filled cavities with three types of anions in the structure: (1) isolated $(BO_3)^{3-}$ triangles, (2) isolated fluorine anions and (3) tetrahedral $[X_4]^{4-}$ anionic groups. The latter fragments are the distinguishing features in $Ba_{4-x}Sr_{3+x}(BO_3)_{4-y}F_{2+3y}$ and $Ba_7(BO_3)_{4-y}F_{2+3y}$ lattices: $[X_4]^{4-}$groups are located in the large eleven-vertex cavities of the cationic sublattice (Fig. 1a). $[X_4]^{4-}$ groups include either 4 fluoride ions each or the combination of one triangular $(BO_3)^{3-}$ and one fluoride (F^-) anions. It is these $[F_4]^{4-}$/$[(BO_3)F]^{4-}$ groups that are responsible for $(BO_3)^{3-} \leftrightarrow 3F^-$ isomorphic substitution and $[F_4]^{4-}$ group formation. Partially substituted $Ba_{4-x}Sr_{3+x}(BO_3)_{4-y}F_{2+3y}$ and $Ba_7(BO_3)_{4-y}F_{2+3y}$ solid-solutions with $0<y<1$ contain both $[(BO_3)F]^{4-}$ and $[F_4]^{4-}$ groups.

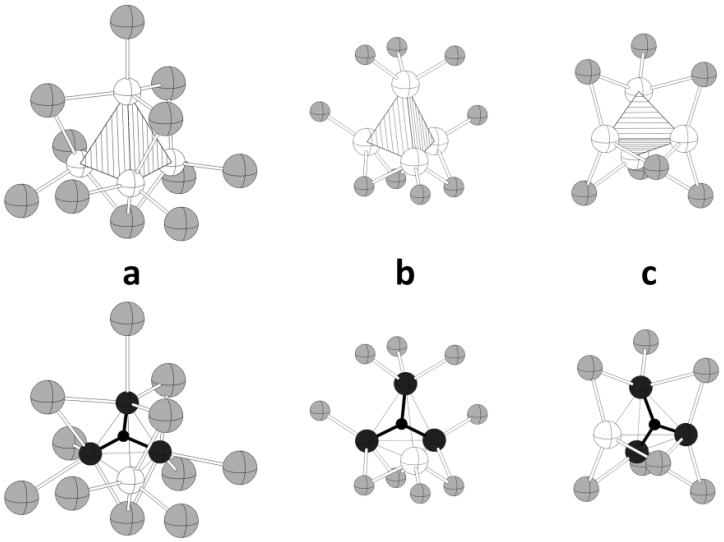

Figure 1. $[BO_3F]^{4-} \leftrightarrow [4F]^{4-}$ isomorphic substitution in $[X_4]^{4-}$ tetrahedra in fluoride borates. The top row contains a depiction of $[4F]^{4-}$ type of $[X_4]^{4-}$ groups, whereas $[BO_3F]^{4-}$ tetrahedra are given in the bottom row. White spheres represent F^- ions; $(BO_3)^{3-}$ anions are given in black, Ba^{2+} , Mg^{2+} and Eu^{3+} cations are shown in grey. Vertical couples correspond to the fragments of crystalline lattices of $Ba_7(BO_3)_{4-y}F_{2+3y}$ solid solution (a), α-$Mg_2(BO_3)_{1+y}F_{1-3y}$ solid solution (b), and $Eu_3(BO_3)_{2-y}F_{3+3y}$ (c).

The discovery of such unusual mechanism of $(BO_3)^{3-} \leftrightarrow 3F^-$ isomorphism in tetrahedral $[X_4]^{4-}$ anionic groups prompted us to look at the other phases with formally similar $(BO_3)^{3-} \leftrightarrow 3F^-$ substitutions in order to elucidate structural mechanisms. The only other previously documented examples of $(BO_3)^{3-} \leftrightarrow 3F^-$ isomorphism are α-$Mg_2(BO_3)_{1+y}F_{1-3y}$ and $Eu_3(BO_3)_{2-y}F_{3+3y}$ [5,6].

It has been found that all presently known fluoride borates that exhibit isomorphism with formal $(BO_3)^{3-} \leftrightarrow 3F^-$ stoichiometry have one similar feature of their crystalline structures, namely, the presence of tetrahedral $[(BO_3)F]^{4-}$ anionic groups, which can substitute $[F_4]^{4-}$ tetrahedra. It would seem that $[(BO_3)F]^{4-} \leftrightarrow [F_4]^{4-}$ isomorphism is the only plausible mechanism of $(BO_3)^{3-} \leftrightarrow 3F^-$ replacement of $(BO_3)^{3-}$ anions by fluoride anions (F^-). This explains why $(BO_3)^{3-} \leftrightarrow 3F^-$ substitution is unknown for pure orthoborates and can be observed only in fluoride borates. Our suggestion leads to the forecast of possible $[(BO_3)F]^{4-} \leftrightarrow [F_4]^{4-}$ isomorphism in phases containing $[(BO_3)F]$ groups in their crystalline lattices. Another important conclusion from the above observations includes the crystallographic similarities of $[(BO_3)F]^{4-}$, $[F_4]^{4-}$ and $[SiO_4]^{4-}$ four-charged tetrahedral anions that determine the existence of silicate analogs of fluoride borates as well as $[(BO_3)F]^{4-} \leftrightarrow [F_4]^{4-} \leftrightarrow [SiO_4]^{4-}$ isomorphism (e.g., Pertsevite-(F) mineral).

This work was supported by the Russian Foundation for Basic Research (grant No. 13-03-12158).

References:

[1] Wu, B. C.; Tang, D. I.; Ye, N.; Chen C. T. *Opt. Mater*. **1996**, *5*, 105-109.

[2] Rashchenko S.V., Bekker T.B., Bakakin V.V., Seryotkin Yu.V., Shevchenko V.S., Kokh A.E., Stonoga S.Yu. *Crystal Growth and Design*. **2012**, 12 (*6*), 2955-2960.

[3] Bekker T.B., Rashchenko S.V., Bakakin V.V., Seryotkin Yu.V., Fedorov P.P., Kokh A.E., Stonoga S.Yu. *CrystEngComm*. **2012**, 14, 6910-6915.

[4] Brovkin, A.A. & Nikishova, L.V. *Sov. Phys. Crystallogr.* **20**, 452–455 (1975).

[5] Antic-Fidancev, E., Corbel, G., Mercier, N., Leblane, M. *J. Solid State Chem.* **153**, 270–274 (2000).

FLUX GROWTH AND MAGNETISM OF HETEROVALENT Co-Mn LUDWIGITES

Bezmaternykh L.N., Kolesnikova E.M., Sofronova S.N., Eremin E.V.

L.V. Kirensky Institute of Physics SB RAS, Krasnoyarsk, Russia
ekoles@iph.krasn.ru

Nowadays the studies of the magnetic properties of quasi-low-dimensional structures with partially cationic disordering are actual. Based on this, there is a great interest to oxyborates of transition metals, where, at least one of them, is presented as heterovalent cation.

To synthesize a single crystals $Mn^{2+}_{2-z}Co^{2+}_{z}Mn^{3+}_{1-y}Co^{3+}_{y}BO_5$, having ludwigite structure, and to estimate their magnetic behavior depending on composition, to continue of **[1, 2]**, we studied flux crystal growth of Co–Mn oxyborates of following ratios of starting components:

$$(100-n)\%\ масс.\left(Bi_2Mo_3O_{12}+1.62\ B_2O_3+0.7\ Na_2O\right)+$$
$$+\ n\ \%\ масс.\left(\frac{(3-p)}{2}\ Mn_2O_3+\frac{p}{2}\ Co_2O_3+0.5B_2O_3\right)$$

The specificity of this approach, primarily, is using of Mn_2O_3 and Co_2O_3 in a combination with sodium carbonate in the preparation of solutions.

Fluxes, with masses 50-80 g, were prepared by the consistent melting of mixtures (in platinum tube, with volume 100 cm^3, at T=1100°C) of $Bi_2Mo_3O_{12}$ and B_2O_3, Mn_2O_3 and Co_2O_3,the latter Na_2CO_3 was added parts.

Concentration n was chosen, depending on p ($0\le p\le 3$), so, that the saturation temperature of flux was $920°C \le T_{sat}(n) \le 960°C$.

Temperature sequences of crystallizing phases have been studied in prepared fluxes. It was established, that at p=0 high-temperature crystallizing phase, in a quite wide temperature range (more, than 40°C), was mono cobalt ludwigite $Co^{2+}_2Co^{3+}BO_5$, at p=3 – mono manganese warvickite $Mn^{2+}Mn^{3+}BO_4$. Changing of high-temperature phase was observed only at about p=2.7.

Single crystals of these phases with different compositions were grown at spontaneous generation. After 3-hour homogenization at T=1100°C, the temperature in the furnace was quickly decreased down to (T_{sat}-10)°C, and further, slowly, was decreased with cooling rates about 2-4°C/day. Three days later, the tube was extracted from furnace, flux was poured. Grown single crystals (like stick, length less, than 10 mm, cross-sectional area less, than 0.5 mm^2) were separated by 20% solution acid etching.

Temperature-field dependencies of magnetization were measured for synthesized ludwigite crystals $Mn^{2+}_{2-z}Co^{2+}_{z}Mn^{3+}_{1-y}Co^{3+}_{y}BO_5$ with heterovalent Co and Mn. Temperature dependencies of magnetization, for the samples with p_1=1.5, p_2=2, p_3=2.25, shown at Figs.1,3. These dependencies were obtained at cooling in field (FC, H⊥c) and without field (ZFC).

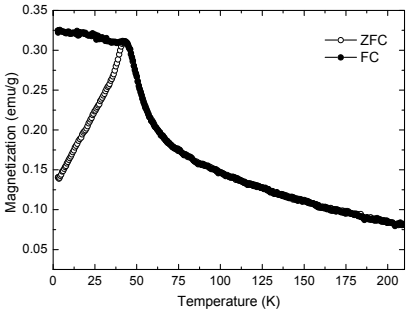

Fig.1 Temperature dependencies of magnetization of $Mn_{1.5}Co_{1.5}BO_5$, obtained at zero field cooled and at field cooled. H=1kOe

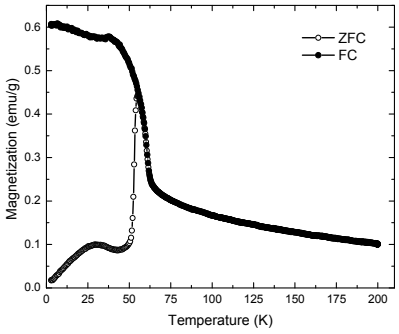

Fig.2 Temperature dependencies of magnetization of Mn_2CoBO_5, obtained at zero field cooled and at field cooled. H=1kOe

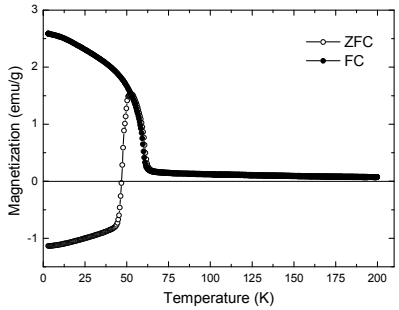

Fig.3 Temperature dependencies of magnetization of $Mn_{2.25}Co_{0.75}BO_5$, obtained at zero field cooled and at field cooled. H=1kOe

Based on these results, a general idea of the dependence of the magnetic behavior of Co-Mn heterovalent ludwigites on the relative content of manganese discusses.

The subsystem of spin glass begin to form at quite small concentration of heterovalent manganese cations in $Co_2^{2+}Co^{3+}BO_5$ (antiferromagnetic ordering at T_N=42 K). The contribution of this subsystem increases with the manganese concentration and becomes predominant. One can see the clear transition from paramagnetic phase to spin-glass state from Fig.1. The long-range antiferromagnetic order restores at high manganese concentration, at these conditions, the Neel temperature little bit increases in comparison with $Co_2^{2+}Co^{3+}BO_5$ (Fig.2). The transition to diamagnetic-like state is observed at close to the limit for ludwigite phase manganese concentration (Fig.3). This phenomena could be connected with appearance of two competing subsystems, characterized by the canted antiferromagnetism **[3]**.

The study was supported by The Ministry of education and science of Russian Federation, project no. 8365; by Russian Foundation for Basic Research (project no.13-02-98027)

References:

[1] Knyazev Yu.V., Ivanova N.B., Kazak N.V., Platunov M.S., Bezmaternikh L.N., Velikanov D.A., Vasiliev A.D., Ovchinnikov S.G., Yurkin G.Yu. Crystal structure and magnetic properties of Mn substituted ludwigite $Co_3O_2BO_3$ // Journal of Magnetism and Magnetic Materials. – 2012. – V. 324. – P. 923-927.

[2] Ivanova N.B., Kazak N.V., Knyazev Yu.V., Velikanov D.A., Bezmaternykh L.N., Ovchinnikov S.G., Vasiliev A.D., Platunov M.S., Bartolomé J., Patrin G.S. Crystal structure and magnetic anisotropy of ludwigite $Co_2FeO_2BO_3$ // Journal of Experimental and Theoretical Physics. – 2011. – V. 113, Is.6. – P. 1015-1024.

[3] Kageyama H., Khomskii D. I., Levitin R. Z., Vasil'ev A. N. Weak ferrimagnetism, compensation point, and magnetization reversal in $Ni(HCOO)_2 \cdot 2H_2O$ // Phys. Rev. B. – 2003. – V. 67. – P. 224422.

COMPARISON OF KINETIC ANOMALIES FOR SUBSTANCES WITH FIXED AND UNFIXED CHEMICAL COMPOSITIONS

Bocharov S.

St.Petersburg State University, Crystallography Dept., St.Petersburg, Russia
bocharovsergei@mail.ru

Analysis of mineral genesis based on investigation of crystal morphology, impurities composition and distribution, inclusions in bulk of crystals are performed in assumption of structureless crystallization medium. Meanwhile, crystallization kinetic, which defines mentioned crystal features, is very sensitive to changes in crystallization environment properties including changes of medium structure. For example, changes in growth rate of $Na_5P_3O_{10}$•$6H_2O$ crystals are linked to clusters of different polymorphic modifications of salt in solution **[1]**. Structure of water, which is supposed to have temperature transitions **[2]**, should have influence on structure of solution also and it should be expected that solution structure will have similar temperature transitions. Appearance of extremes on kinetic growth curves ("kinetic anomalies", fig. 1) is linked to such temperature transitions **[3-5]**. Kinetic anomalies were found in 1967 by V.V. Sipyagin and A.A. Chernov **[6]** at detailed measurements of growth rate of water-soluble salts. Now kinetic anomalies are known for dozens of water-soluble salts as well as for copper and mercury electrocrystallization cases. However relations between extremes and bulk properties of solution were established for KCl only **[4]**, kinetic anomalies of which are strongly differ from anomalies of other matters. So, mechanism of kinetic anomalies formation is unclear. Solving of this problem is limited by deficiency of data for solution structure behavior with temperature as well as kinetic data for different systems and anomalies behavior with condition changes. From this point of view it is interesting to compare kinetic anomalies for substances with fixed chemical composition and substances with varying chemical composition (mixed crystals) as well as kinetic anomalies changes in chain of intermediate solution compositions between pure members. These data can give us information about anomalies nature as well as possibility to grow mixed crystals with precision control of chemical composition distribution.

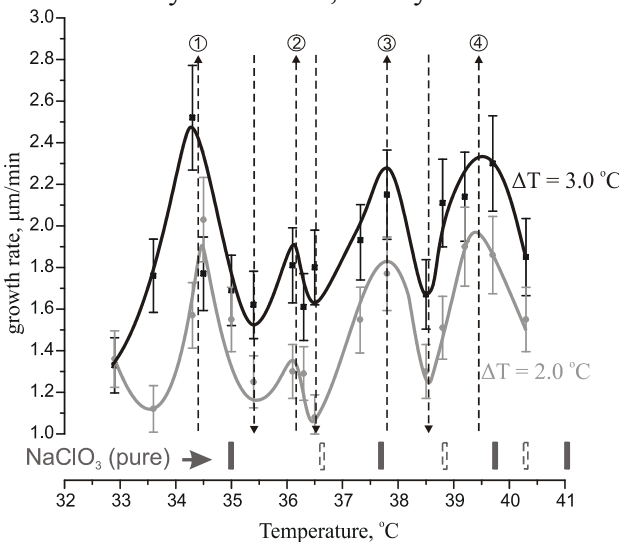

Figure 1. Kinetic anomalies of (100) face of $Na(Cl,Br)O_3$ at different supercoolings.

We investigated kinetic anomalies of mixed crystals growth for $NaClO_3$-$NaBrO_3$ system by traditional microcrystallization method and for Cu-Hg system by modified electrocrystallization

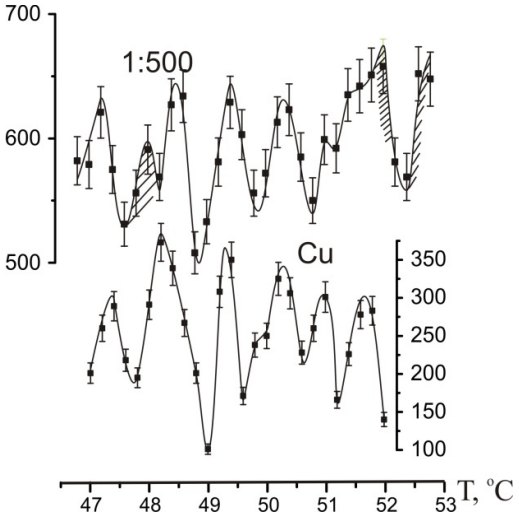

Figure 2. Kinetic anomalies of copper and Cu-amalgam electrocrystallization.

method **[5]**. Kinetic anomalies for $NaClO_3$-$NaBrO_3$ system were investigated in temperature range 33 – 41 ^oC and compound ratio in solution which responds to alyotropic point of system ($NaClO_3$:$NaBrO_3$ = 20:1). For Cu-Hg system kinetic anomalies were investigated in temperature range 45-53 ^oC and compound ratio in solution from 1:50 to 1:500 (Cu:Hg). Extreme compound ratios correspond to pure members deposition since difference of electrochemical potentials for Cu and Hg exists.

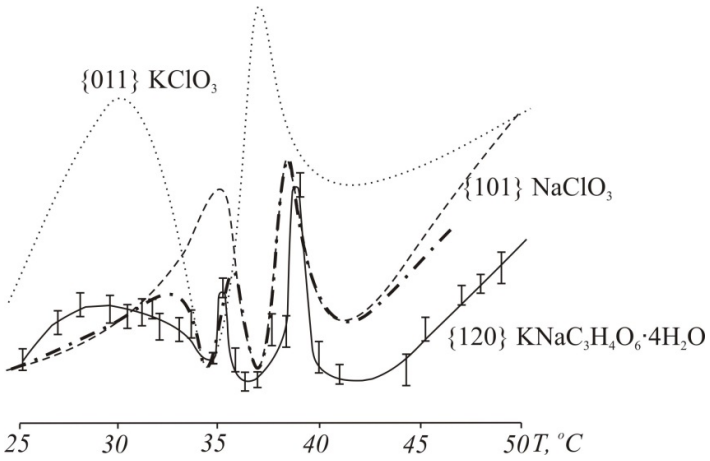

Figure 3. Kinetic anomalies of $KNaC_3H_4O_6 \cdot 4H_2O$ (solid line, data after **[7]**) as combination of kinetic curves of $KClO_3$ and $NaClO_3$ (dotted and dashed line, respectively, data after **[3]**).

Our investigations show that small deviation of solid phase chemical composition from end-members composition results in kinetic anomalies which are similar to anomalies of main phase as temperature position of peaks as well as peak intensity. For example, kinetic anomalies of $Na(Cl,Br)O_3$ (fig. 1) in the temperature range 33 – 41 ^oC are characterized by four maxima of growth rate. Three of these maxima correspond to maxima of pure sodium chlorate (fig. 1, peaks 1, 2 and 4). Kinetic anomalies of Cu-amalgams deposited from solution with compound ratio 1:500 are characterized by seven maxima in the temperature range 47 – 52 ^oC (Fig. 2). Five of them correspond to maxima of copper kinetic curve and two (Fig. 2, temperature 47.7 and 52.0 ^oC) correspond to maxima of mercury kinetic curve. So, main difference of mixed crystal kinetic anomalies is existing additional peaks which relate to kinetic anomalies of opposite end-member. Changes in compound ratio result in complication of kinetic curves. It can be described as superposition of end-member kinetic curves plotted by maximal growth rates. Thus, on one hand, kinetic anomalies of mixed crystals growth are defined by initial ratio of compounds in solution. On other hand it is defined by kinetic curves of end-members.

In contrast with kinetic anomalies of mixed crystals, kinetic anomalies of salt with fixed composition and complex cationic part ($KNaC_3H_4O_6 \bullet 4H_2O$ for example **[7]**) have kinetic curve which can be described as superposition of kinetic curves of salts with corresponding cations and plotted by minimal growth rates (fig. 3). Kinetic data which we took from different references for comparison show good agreement. So, both strong maxima of growth rate of Seignette's salt (located around 35 and 39 ^oC, fig. 3) are the same to maximums on curve plotted by minimal growth rates even by relative intensity.

The reported study was partially supported by Russian Foundation for Basic Research, research project No. 12-05-00876-a and 13-05-12053-ofi_m.

References:

[1] Troost S, J. of Crystal Growth, v.13-14, Issue C, 1972, p. 449-453
[2] Dougherty R.C., Alphonse N.K., Dillon S.R., Galligan D.K., Howard L.N., J. Phys. Chem. A, v.110, N. 24, 2006, p. 7577-7580.
[3] Sipyagin V.V., Chernov A.A., Sov. Phys. Crystallogr., v.17, 1972. p.881.
[4] Punin Yu.O., Petrov T.G., in Crystal Growth (Nauka, Moscow, 1972), v.9, p. 76 [in Russian].
[5] Bocharov S.N., Glikin A.E., Crystallography Reports, v.53, N. 1, 2008, p. 147–153.
[6] Sipyagin V.V., Sov. Phys. Crystallogr. v.12, 1967, p. 590.
[7] Kibalczyc W., Kolasinski W., Zesk. nauk. Plodz., N. 271, 1977, p. 51-62. [in Poland].

OPTICAL AND NONLINEAR OPTICAL PROPERTIES OF β-SrB_4O_7

Cherepakhin A.V.*, *Zaitsev A.I., Zamkov A.V.

L.V.Kirensky Institute of Physics SB RAS, Krasnoyarsk, Russia
a.cherepakhin@ya.ru

Borate compounds with the noncentrosymmetric crystal structure are attractive materials for nonlinear optical (NLO) applications, especially in the UV region **[1]**. Orthorhombic α-SrB_4O_7 (α-SBO) crystals have been established to possess high NLO coefficients and a very short absorption edge but they have not sufficient birefringence for the existence of the second harmonic generation (SHG) phase matching conditions. **[2, 3, 4]** Recently, strontium tetraborate crystals have been obtained with another structure modification and their structure has been established. The structure of this β-SrB_4O_7 (β-SBO) with the trigonal symmetry belongs to the noncentrosymmetric P3 space group, the unit cell parameters being: a = 17.145 (1) Å, c = 4.2527 (5) Å **[5]**.

The β-SBO single crystal has been obtained and refraction coefficients and nonlinear optical coefficients of this crystal have been measured.

β-SBO itself is a metastable crystal modification of this compound **[6]**, so β-SBO crystals cannot be obtained with a temperature higher than ~ 780°C (the stable α-SBO melting temperature is 1000°C). The single crystal β-SBO have been grown from a supercooled melt of the compositions $SrO{\cdot}2B_2O_3$ at 720°C.

The refraction indices were measured in the wavelength range between 435.8 and 1060 nm by prism method, and least square fitted to a Sellmeier equation of type

$$n^2 = A + \frac{B}{1 + C \cdot \lambda^2} + D \cdot \lambda^2 \quad (1)$$

Table 1 lists the parameters of the Sellmeier equation for the two refraction indices of β-SBO. The parameters of Sellmeier equation for the refraction indices n_e were corrected after experimental observation of phase matching type I using optical parametric oscillator Vibrant LD 355 II with 2 mm thick a-cut crystal plate of β-SBO revealed the presence of noncritical phase matching of the second type at the 0.672 μm fundamental wavelength (table 1). According to these results, β-SBO is negative one axial crystal.

Table 1. Parameters of Sellmeier equation for the refraction indices of β-SBO.

refraction indices		A	B	C	D
n_o		2.72341	0.01523	0.00772	0.01776
n_e	From 0.435 μm to 1.060 μm	2.62013	0.01396	0.00478	0.01605
	-//- + n_e (λ = 0.336 μm) = n_o (λ = 0.672 μm)	2.62188	0.01324	0.01097	0.01714

Nonlinear optical coefficients of β-SBO have been defined. The experiments have been carried out under Type I phase matching conditions using the Nd:YVO_3 with 1.085 μm and optical power 300 mW. Measurements of SHG power have been conducted using the Newport power meter (model 1918-C) with the detector 918-UV-OD3. β-BaB_2O_4 (BBO) single crystal has been used as a reference crystal. The BBO orientation was φ = 90º и θ = 20º05' and nonlinear optical coefficients was used d_{31} = 0.16 pm/V, d_{22} = -2.2 pm/V [1]. The initial orientation of the single crystal β-SBO was made with θ = 45º27'and φ = 30º. Subsequent measurements were performed with step-by-step reduction of the azimuth angle φ (the rotation step of the crystal was 7.5°, the angle θ is not changed) down to -30°. Thus, values of effective

nonlinear-optical coefficients of β-SBO crystal for each position have been defined. Using the equation

$$d_{eff} = d_{31} \cdot \sin\theta + \cos\theta \cdot (d_{11} \cdot \cos 3\varphi - d_{22} \cdot \sin 3\varphi), \quad (2)$$

nonlinear optical coefficients β-SBO have been calculated. Table 2 lists the nonlinear optical coefficients of β-SBO.

Table 2. **N**onlinear optical coefficients of β-SBO.

Coefficient	d, pm/V
d_{31}	+-0.08
d_{11}	+-0.09
d_{22}	-+1.05

This study is supported by SB RAS Project 103, by Grant of the President of the Russian Federation for the support of leading scientific schools SS-4828.2012.2 and by RFBR Grant 11-02-00596-a.

References:

[1] Chuangtian Chen, Takatomo Sasaki et al. Nonlinear Optical Borate Crystals // WILEY-VCH, 2012, 388 P.

[2] Oseledchik Yu.S., Prosvirnin A.L., Pisarevskiy A.I., et al. New nonlinear optic crystals: strontium and lead tetraborates // Optical Materials. – 1995. – Vol. 4. – pp. 669-674.

[3] Zaitsev A.I., Aleksandrovskii A.S., Zamkov A.V., Sysoev A.M. Nonlinear optical, piezoelectric, and acoustic properties of SrB_4O_7 // Inorganic Materials. – 2006. – V. 42, No. 12. – pp. 1360-1362.

[4] Petrov V., Noack F., Shen D., Pan F., Shen G., Wang X., Komatsu R., Alex V. Application of the nonlinear crystal SrB_4O_7 for ultrafast diagnostics converting to wavelengths as short as 125 nm // Optical Letters. – 2003. –V. 29, No. 4. – pp. 373-375.

[5] Vasiliev A.D., Cherepakhin A.V., Zaitsev A.I. Trigonal crystal phase of strontium tetraborate, β-SrB_4O_7 // Acta Cryst. E. – 2010. – V. 66. – pp. 48-65.

[6] Zaitsev A.I., Zamkov A.V., Koroleva N.S., Molokeev M.S., Cherepakhin A.V. Phase formation upon crystallization of $SrO \cdot 2B_2O_3$ glasses // Crystallography Reports. - 2011. - V. 56, No. 1. - pp. 44–51.

ON THE MISCIBILITY OF THE COMPOUNDS IN THE SYSTEM "CORDIERITE – BERYLLIAN INDIALITE – BERYL", ENRICHED WITH MAGNESIUM

***Demina T.V.*, Bogdanova L.A., Belozerova O. Yu., Mikhailov M.A, Mamontova S.G.**

AP Vinogradov Institute of Geochemistry, SB RAS, Irkutsk, Russia
deminat@igc.irk.ru

Five areas have been identified in the field of solid solutions of compounds with beryl (B) based on the dynamics of changes in physical properties and taking into account the "50% rule" **[1] [2-4]**: I - disordered beryllian indialite (BI) with $\Delta = 0.00$, $2V = 0°$ and well-resolved reflections; II – weakly ordered BI with $0.00 < \Delta \leq 0.14$, $0° < 2V < 20°$, and with broadened less resolved reflections of their diffraction patterns; III - ordered Be-containing cordierite (Be-Cord) with $0.14 < \Delta < 0.26$, $20° < 2V < 60°$ and diffraction patterns similar to the rhombic ordered Cord; IV - disordered Be-Cord with $\Delta = 0.00$, $2V = 0°$; III + V - where Cord and Be-Cord are jointly formed during the solid-state reaction, which suggests the miscibility gap between the last compounds.

The task of this study is to establish the relationship between the Cord and the Be-Cord in magnesium ion on the basis of material obtained by solution-melt method.

The studied phases were obtained when the temperature of the melt (Cord + $MgF_2/CaCl_2$) decreased. Moreover, BeO (1.5, 3, 6, 10, or 15%) and 2% Cr_2O_3 were added in addition to 100% of $Mg_2Al_2Si_5O_{18}$ **[5]**. The resulting material was examined using X-ray electron probe microanalysis (EPMA), X-ray diffraction (XRD) and crystal optics. When studied with RFA indialite (Ind), BI or Be-Cord diagnosed in the $2\Theta = 29\text{-}30^o$ at the appropriate mono-peak while Cord was recorded the characteristic splintered peak. The degree of deviation of the Cord orthorhombic lattice from the hexagonal symmetry (Δ) was estimated by the method of G. Afonina **[6]**. When comparing the degree of deviation of unit cell from the hexagonal symmetry Cord and solid solutions we used the half-width of the peak (B, º) at angles 2Q = 29-30º (standard - half-width of the peak of the Indus, obtained in the same s / m conditions).

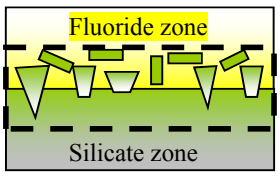

Figure 1. Productive field given as dotted line.

The segregation was observed in the solution-melt studied system (Fig. 1): sellaite (MgF_2) and hydrophilite ($CaCl_2$) are found in the upper fluoride zone, while Ind, Be-Cord, BI solid solutions, Emerald (Em) and the impurity phenacite, chrysoberyl are observed in the lower silicate zone. A productive layer, where the investigated phases formed has been revealed at the boundary of these zones. They develop as a holohedral and one-vertex individuals; the first ones are generated in the upper part of the productive layer while single-vertex originate in the silicate zone, and eventually spread into fluoride. The one-vertex individuals of the early stage are sharp-edged crystal (Fig. 2, A,V), the later have oval-base and zonal color (Fig. 2, B,G) that is associated with the change of the phase composition: colorless -Ind, pale-colored - Ind-Be-Cord (intermediate phase between the Ind and the Be-Cord) and Be-Cord, and swamp-green - BI and solid solutions. In all phases, Cr content is comparable (0.05 - 0.07 kf) and different color is associated with the form (Cr^{2+}, or

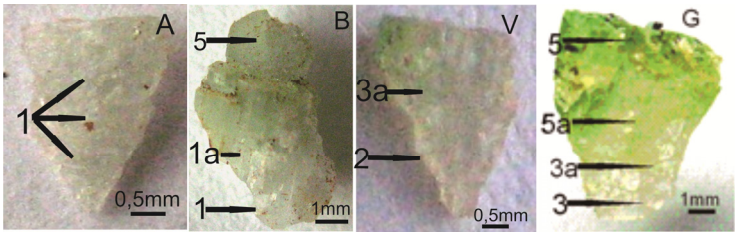

Figure 2. One-vertex individuals appearance at different stages of their nucleation in media with 1.5% (A, B) and 6% BeO (V, G): 1 – Ind/0,00, 1a – Ind/0,14, 2 – Ind-Be-Cord, 3 – Be-Cord/0,04, 3a - Be-Cord/0,09-0,18, 5 – BI/0,17-0,30 , 5a - BI/0,00

Cr^{3+}) of its occurrence **[7]**. The ratio of colorless and colored phases depends on the amount of BeO, the increase of which in the environment promotes the growth of phases with swamp-green color. Colorless indialite with Δ = 0,00 nucleated in the environments with low of BeO. The growth in the charge of BeO promotes the introduction of an isomorphic Be, which affects the structural state of the phases, as Be together with Al and Si is involved in the order-disorder processes of these compounds **[8, 9]**. The structural state of these phases responds differently to the increase of amount BeO in the environment: Ind and Ind-Be-Cord demonstrate the ordering process, as well as Be-Cord at 3% of BeO, which at 6% of BeO begins disordering; BI at 1.5-6% BeO born as ordered, but then disordering of structure starts. Crystals with 10-15% BeO nucleated as disordered. This is accompanied by the replacement of schemes of Cr introduction, and therefore the mode of its occurrence in the given phases. This process is marked by zonal change of color (Fig. 2) and the phase composition: Ind → Ind-Be-Cord → Be-Cord → BI. The reason for consistent change of phases is increasing of Mg/Be in the medium **[10]**. The character of the phase change depends on the amount of BeO in the charge. When charge was 1.5-6% BeO phases are replaced by the following scheme: Ind → Ind-Be-cord → Be-cord → Be-cord solid solution → BI When charge was 10-15% BeO: Cord → solid → BI solutions (Figure 3). Note that the Be-Cord obtained in this system is similar to Be-Cord in the granitic pegmatite **[11]**. With EPMA confirmed the picture of crystal chemical separation, identified on the basis of XRD data (Fig. 3).

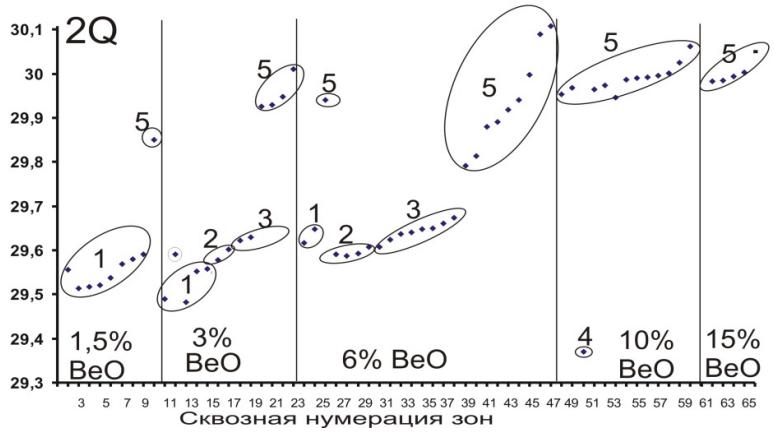

Figure 3. Areas of formation of studied phases depending on BeO content in the environments: 1 – ind, 2 – Ind –Be-cord, 3 – Be-Cord and its solid solutions, 4 –Cord, 5 –BI and its solid solutions

Conclusions. In the studied solution-melt system:

(1) it was identified four structural varieties of cordierite: Ind, Ind-Be-Cord, Be-Cord, Cord;

(2) it shown the difference in immiscibility gap of BI with Be-Cord and ordered cordierite: the gap between BI and Cord is sharper than between BI and areas enriched in Be-Cord;

(3) it was found the shift of forming regions of the studied phases depending on the increase (1.5 → 15%) BeO content in the initial compositions: cordierite varieties 2Ɵ = 29.48 → 29.69° and then sharply towards the low-angle area 29.37°, and BI with 2Ɵ = 29.85 - → 29.01° in the angles 29,99-30.06°; (4) the evolutionary scheme of phase formation reflects the changing of conditions in the formation of a particular mineral.

This work was supported by RFBR (grant № 11-05-00712).

References:

[1] EH Nickel / ZVMO. 1992. N. 4; **[2]** Demina T.V., Mikhailov, M.A / Crystallography, 98. Syktyvkar.1998;**[3]** Demina T.V. et al. / Proc. Reports. III Nat. Crystal-conf. Chernogolovka, 2003; **[4]** Pecherskaya S.P. et al. / Crystallography. 2003. V. 48. N. 3; [**5]** Demina T.V., Mikhailov, M.A. / Experiment in Mineralogy, Chernogolovka: Institute of Experimental Mineralogy RAS. 1993; **[6]** Afonina G.G., et al. / Crystal chemistry and structural properties of minerals. Leningrad. Publishing House "Nauka". 1976; **[7]** Solntsev V.P., et al. / X-ray and molecular spectroscopy of minerals. 1985. Novosibirsk. Publ. House "Nauka"; **[8]** Demina T.V. / ZVMO, no.4, 1990; **[9]** Demina T.V. / ZRMO. 2004. V. 68. Number 5; **[10]** Demina T.V., Mikhailov M.A., / Proc. Reports. II Nat. Crystal-conf. Chernogolovka, 2000b; **[11]** Yakubovich O.V.. et al.. / Crystallography. 2004. V.49. N. 6.

STUDY OF FORMATION PROCESSES OF MIXED CRYSTALS IN THE SYSTEM (Co,Ni)$K_2(SO_4)_2 \cdot 6H_2O$ BY THE EXAMPLE OF SOLID SOLUTIONS AND EPITAXIAL STRUCTURES

Grigorieva M.S., Vasilyeva N.A., Grebenev V.V., Voloshin A.E.

Shubnikov Institute of Crystallography of RAS, Moscow, Russia
labsol@crys.ras.ru

Epitaxial processes in water solutions as well as formation of solid solution crystals in multicomponent systems are of a great interest, both from point of view of mineralogy and crystallography. Initial stages of epitaxy are accompanied by simultaneous dissolution of a crystal substrate and growth of islands of the new phase that is caused by the reaction of isomorphic replacement [1-3], either by formation of a continuous-solid layer at the exchange reaction suppression. The mixed crystals can contain isomorphic components in proportion dependent on their ratio in solution which, in turn, changes during the growth because of distinction of their distribution coefficients. In this work, processes of solid solution crystals formation and a liquid-phase epitaxy are studied on the example of water-salt (Co,Ni)$K_2(SO_4)_2 \cdot 6H_2O$ system.

Isotherms of joint solubility of potassium-nickel and potassium-cobalt sulfates salts were measured at 35 и 50 ºC. Isotherms are concave that argued to solubility reduction of salts at formation of mixed structure solutions. Solubilities of individual substances differ by 2,5 times. It is revealed that at immersion of $K_2Ni(SO_4)_2 \cdot 6H_2O$ crystal (KNSH) (less soluble component) in $K_2Co(SO_4)_2 \cdot 6H_2O$ (KCSH) solution the continuous-solid layer grows on a substrate surface within several seconds. It differs from earlier studied water-salt $NiSO_4 \cdot 7H_2O/MgSO_4 \cdot 7H_2O$, $Ba(NO)_3/Pb(NO)_3$, $C_8H_5O_4K/C_8H_5O_4Rb$ systems, which reveals formation of a layer owing to islands intergrowth [1, 5-7]. Formation of a continuous-solid film blocks substrate dissolution that leads to the pure KCSH component growth. A series of bicrystalline KCSH compositions (20×30×20 mm) on KNSH substrates (10×10×10 mm) have been grown under diverse conditions (supersaturation values of mother liquor solution). The substrate surface were (001) and (110) crystal faces. The grown KCSH layers were optically transparent, without visible inclusions, block borders, cracks. Difference of lattice parameters (tab. 1), (~ 0,6 %) is rather small for the existence of a continued number of solid KCSH– KNSH solutions, but is sufficient to generate considerable misfit stresses in the epitaxial layer, leading to its possible further cracking.

Formation of a thick crystal layer without cracks in the system under study indicates the elastic stress relaxation occurs. However, development of misfit dislocations owing to intensive dislocation gliding is unlikely because of small process temperature.

Table 1. Ratio of lattice parameters of $K_2Co(SO_4)_2 \cdot 6H_2O$ and $K_2Ni(SO_4)_2 \cdot 6H_2O$ crystals [4].

	Ratio of lattice parameters:		
$K_2Co(SO_4)_2 \cdot 6H_2O$/ $K_2Ni(SO_4)_2 \cdot 6H_2O$	a_1/a_2	b_1/b_2	c_1/c_2
	1.004	1.004	1.009

Studies of defect structure of the epitaxial compositions have been conducted. At the initial stage of substrate-solution interaction the intermediate layer is formed. Its existence has been proved by energy-dispersion X-ray analysis. The layer thickness is about 4 microns, the nickel distribution is not homogeneous: its concentration decreases away from the interface. This

indicates that at the initial stage of the crystal-solution interaction the substrate actively dissolves and the supersaturated boundary solution layer forms, according to the isomorphic substitution model. Also, a large amount of defects in the interface is revealed: numerous inclusions with density of ~ $5 \cdot 10^5$ cm^{-2} and dislocation bunches inclined to a normal to the interface whose density also can be estimated at the level of 10^5-10^6 cm^{-2}. However, in pure KNSH and KCSH crystals the dislocation density is about 10^1-10^2 cm^{-2}. One can suppose that the solution inclusions reduce elastic strains on interface and, in turn, leading to formation of inclined dislocations. This assumption is in accordance with the theory of polydomain structures, which predicts that inclusions of another phase with the dissimilar from main matrix elasticity modules could relax stresses rather effectively.

The *in situ* confocal microscopy studies of crystallization of thin $K_2Co(SO_4)_2 \cdot 6H_2O$ films on $K_2Ni(SO_4)_2 \cdot 6H_2O$ substrate and $(NH_4)_2Co(SO_4)_2 \cdot 6H_2O$ films on a $(NH_4)_2Ni(SO_4)_2 \cdot 6H_2O$ substrate have been conducted for confirmation of elastic strain influence on the inclusions formation.

A growth of the mixed $K_2Ni_xCo_{(1-x)}(S0_4)_2 \cdot 6H_2O$ (KCNSH) single crystals in a wide composition range has been studied. The solid-liquid KCNSH composition dependence was measured. Basing on the studies conducted, optically clear large (15×15×20 by mm) mixed KCNSH crystals have been first grown from the solutions with a various Ni/Co content ratio varied in a wide interval. It was found that the existence of two isomorphic components in solution results in modification of the habit of mixed crystals compared to the pure ones. All the grown crystals are characterized by the well-expressed zonality and sectoriality, typical to the water-soluble crystal growth. In addition, a mosaic microinhomogeneity observed earlier by X-ray microtomography in $(Pb,Ba)(NO_3)_2$, K(Br,Cl) и $(K,Rb)HC_8H_4O_4$ single crystals [8-10] has been found in the KCNSH samples by energy-dispersion X-ray analysis. The characteristic dimension of the mosaic elements varies in the range of 70-200 microns. The mixed crystal faces demonstrate numerous signs of local development of the reaction of isomorphic replacement – the etch pits, the islands of another composition inside the pits, the pits with various edge morphology, changing a form in time. The most probable source of the mosaic microinhomogeneity is a development of the solution composition fluctuations near the growing crystal face. Possible reasons of these fluctuations are discussed.

References:

[1] Glikin A.E., Sinai M. Yu. // Zap. Vseros. mineral. o-va. 1983. № 6. P.742.
[2] Glikin A.E. // Zap. Vseros. mineral. o-va. 1995. №5. P. 125. (10)
[3] Glikin A.E. // Zap. Vseros. mineral. o-va. 1996. №5. P. 103. (11)
[4] Kirfel, A.; Klapper, H.; Schaefer, W.; Schwabenlaender, F. Zeitcschrift fuer Kristallograpfie (1998), 213, 456-460
[5] Glikin A.E., Leonteva O.A., Sinai M. Yu. // J. struct.him. 1994a. №5. P. 79-84.
[6] Glikin A.E., Leonteva O.A., Sinai M. Yu., Zorina M.L., Kirillov A.S., Tabuns E.V. //Vestnik SPSU. 1994b. Ser. 4. V. 2. №11. P.111-112.
[7] Glikin A.E., Kovalev S.I., Rudneva E.B., Kryuchkova L.Yu., Voloshin A.E. // J. Cryst. Growth. 2003. V. 255. P. 150-162.
[8] Kryuchkova L.Yu., Glikin A.E.// Fedorovskaja sessija 2010. Materials of the conference. SP.2010. P.111.
[9] Glikin A.E.// Abstracts of Proc. 17th BIWIC. International Workshop on Industrial Crystallization. Poznan. Poland. 2011. P. 233-238.
[10] Kryuchkova L.Yu., Sinai M.Yu., Glikin A.E.// Acta Crystallographica. 2011. V.67. P.469.

GROWTH AND INVERSION TWINNING OF $HoAl_{3-x}Ga_x(BO_3)_4$ SINGLE CRYSTALS

***Gudim I.A.*, Molokeev M.S., Temerov V.L.**

L.V. Kirensky Institute of Physics SB RAS, Krasnoyarsk, Russia
bezm@iph.krasn.ru

In this work we attempt to reveal dependence of structural inversion twinning [**1**] of trigonal $HoAl_{3-x}Ga_x(BO_3)_4$ single crystals on properties of small (Al^{3+}, Ga^{3+}) cation. $HoAl_{3-x}Ga_x(BO_3)_4$ ($0 \le x \le 3$) single crystals were grown from lithium molibdate and bismuth trimolibdate based fluxes [**2**]. Areas of this crystals stability were found and ratios of fluxes components were defined by direct phase probing method. Concentration (n) of crystal-forming oxides, coefficients of p, q, r and parameters of crystallization of used fluxes are given in table 1.

Table 1. Fluxes composition in a quasibinary form
(100-n)%mass.$\{Bi_2Mo_3O_{12} + pB_2O_3 + qLi_2MoO_4 + rHo_2O_3\}$+ n%mass. $HoAl_{3-x}Ga_x(BO_3)_4$.

x	n	p	q	r	T_{sat}, ^{0}C	dT_{sat}/dn, ^{0}C/mass.%	$T\Delta_{met}$, ^{0}C
0	9,8	1,5	0,4	0	975	~25	≈12
0,5	9,8	1,5	0,4	0	943	~30	
0,75	10,0	1,5	0,4	0	932	~60	
1	11,0	1,5	0,4	0	927	~80	
2,5	23	2,1	0	0,45	965	~16	
3	32	2	0	0,3	933	~3	

Crystals were grown by methods of spontaneous nucleation and group growth on seeds, Fig.1. The lattice parameters of the grown-up crystals and an inversion twinning factor (F) were measured on the monocrystal DRON autodiffractometer at the room temperature. This data are provided in table 2. The factor F is the measure of twin with the right symmetry.

Figure 1 (right) $HoAl_3(BO_3)_4$ crystal grown on seed.

Table 2. Lattice parameters and twinning factor F for $HoAl_{3-x}Ga_xFe_3(BO_3)_4$ depending on contents of gallium in flux.

x in flux	Seed			Crystal		
	a, Å	c, Å	F, %	a, Å	c, Å	F, %
0	9.290(1)	7.231(1)	0	9.287(1)	7.228(3)	0
0,5	9.316(3)	7.258(2)	≈78	9.299(2)	7.252(1)	≈12
0,75				9.307(1)	7.255(2)	≈45
1				9.315(2)	7.269(2)	≈38
2,5	9.416(2)	7.406(2)	≈44	9.413(1)	7.401(1)	≈59
3	9.445(2)	7.443(1)	100	9.448(1)	7.441(1)	100

The X-ray structural analysis confirms that these crystals have trigonal spatial group R32. Lattice parameters of a and c monotonously increase with increase in the content of the gallium. Values of these parameters depend on procedure of crystals cooling after the end of growth process too. Quickly cooled crystals have lattice parameters any more, than slowly cooled ones. Test of $HoAl_3(BO_3)_4$ sample showed, that after one hour hold at growth temperature and quickly cooled, it lattice parameters practically agrees with similar ones for seeds. It follows from table 2

that inversion twinning depends both on crystal composition and its heat treatment. There is greatest dispersion of values of twinning factor at seeds. Apparently, it is caused by their uncontrollable cooling rate. There is tendency for slowly cooled crystals to increasing part of right symmetric twins when gallium content increasing.

The study was supported by Grant of the Russian Federation president on support of sciences schools no. 4828.2012.2 and The Ministry of education and science of Russian Federation, project no. 8365

References:

[1] Bezmaternykh L.N., Gudim I.A., Zvyagina G.A., Molokeev M.S., Temerov V.L., Abstract book of Conference of CIS countries on crystal growth - 2012, Харьков, Украина, p. 122.

[2] Gudim I.A., Eremin E.V., Temerov V.L., Journal of Crystal Growth 312 (2010) 2427

QUANTITATIVE ANALYSIS OF MORPHOLOGY OF COPPER PRECIPITATE RECEIVED IN THE TEMPERATURE RANGES OF GROWTH RATE ANOMALIES

Khazikova L.A.*, *Bocharov S.N.

Saint-Petersburg State University, Saint-Petersburg, Russia
lubovkhazikova@gmail.com

Kinetic anomalies were discovered in 1967 and were found in all detailed measurements in randomly selected systems **[1]**. Anomalies represent the temperature ranges in which the growth rate undergoes sharp changes. It was subsequently shown that anomalies have a significant influence on kinetic dependent properties of crystals such as chemical composition **[2]** and morphology **[3]**. Influence of kinetic anomalies on crystals morphology was investigated only for single crystals and at quality level. Meanwhile, data for polycrystalline case are absent in literature. Obtaining these data is important for the progress in understanding the nature of the kinetic anomalies and developing methods to obtain polycrystalline samples with specified morphological characteristics.

Investigation of polycrystalline precipitate morphology in dependence on temperature was performed at copper electrocrystallization as example. The experiments were carried out in a temperature range of 46.0-51.0 ° C in solution of copper sulphate with a fixed concentration 15 g of the salt per 100 g of water. Kinetic curve for this temperature range and concentration was obtained earlier **[4]** and it reproduces kinetic curve known from the reference **[5]**.

Electrochemical copper precipitate obtained at different temperatures has been studied ex-situ by atomic force microscopy with quantitative analysis of received AFM images. Quantitative analysis consisted in statistical processing of images of the surface morphology in the NOVA program. We took the following characteristics as the main parameters that characterize morphology of the deposit: average roughness, scale height, ten point height, deviation from the mean height.

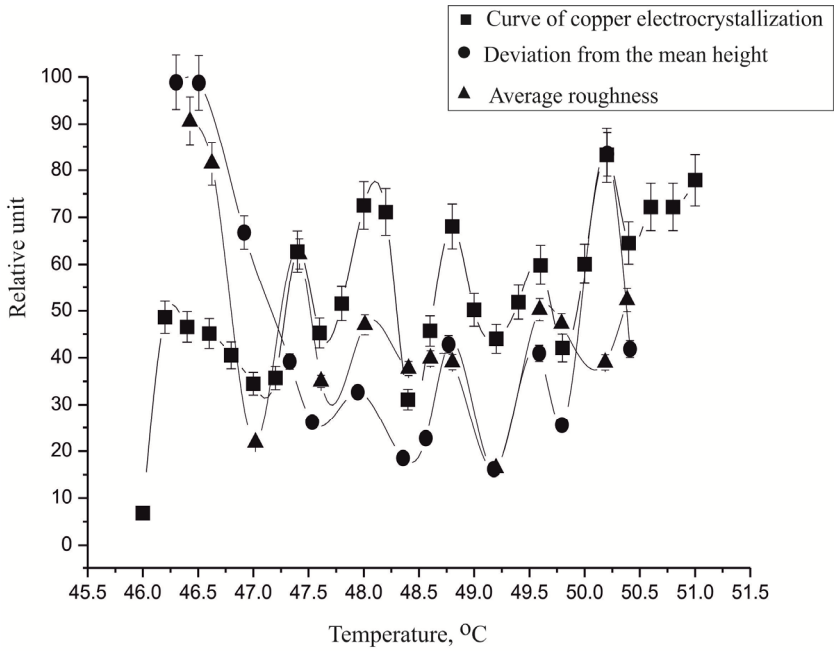

Figure 1. The dependence of the rate of electrochemical deposition of copper (squares, averaging over 14 points) and the statistical characteristics precipitate morphology (circles and triangles, averaging over 3 points) depending on the temperature.

Statistical characteristics of copper precipitate morphology in dependence on temperature vary nonmonotonically (Fig. 1). These variations have the same temperature positions but

intensities are different that what we relate to the method of curves normalization. Quantitative characteristics of copper precipitate morphology reproduce kinetic curve of copperelectrocrystallization in dependence on temperature. It confirms the data on kinetic anomalies influence on crystal morphology obtained for monocrystals case.

The data on the nonmonotonic change in the morphology of the polycrystalline deposit can serves as a theoretical basis for the creation of high-precision temperature reference points for the reconstruction of the conditions of mineralization.

This work was supported by the grant of administration of St. Petersburg for students, graduate students, young scientists, young PhD 2011(PSP №11616).

References:

[1] Chernov A.A., Sipyagin V.V., Current Topics in Materials Science, 5, p. 281 (1980).

[2] Bocharov S. N., Gille P., Glikin A. E. Kinetic anomalies of mixed crystal growth and their effects on the crystal isomorfic composition // Cryst. Res. Technol. 2009. V. 44. N. 1. P. 13-18.

[3] Glikin A.E., Bocharov S.N., Kir'yanova E.V., Sipyagin V.V., Zap. Vseross. Mineral. O–va, No. 2, p.99 (2003) [in Russian].

[4] Khazikova L. A., Bocharov S. N. // Abstracts of Young Scientists and Specialists, No 16, p. 91 (2011) [in Russian].

[5] Bocharov S.N., Glikin A.E., Crystallography Reports, Vol. 53, 1, p. 147 (2008).

THERMODYNAMIC AND CRYSTAL CHEMISTRY ASPECTS FOR IMPERFECT AND PERFECT CRYSTAL GROWTH FROM AQUEOUS SOLUTIONS

Kidyarov B.I.
A.V. Rzhanov Institute of Semiconductor Physics, SB RAS, Novosibirsk, Russia
kidyarov@isp.nsc.ru

Any elaboration of the perfect crystal growth technology from aqueous solutions is very non- trivial, and labour-consuming task, because each salt can be characterized by the some distinctive crystallisation peculiarities [1]. The search of typical peculiarities among all salts is the right way for a priory design of the perfect crystal growth technology. The perfect crystal growth from a liquid phase is possible only at high morphologically stability which predetermined by the some thermodynamic and thermo-physical criteria. For crystal growth from aqueous solutions, such thermodynamic criterion **α** is proposed by Sangwal, however one do not useful in many cases of the salt majority because there are not take into account a real salt ion activity (a_i) [2]. The more exact criterion is $\alpha = \xi\{(\Delta H_s(T, a_i)/RT_m) - \ln a_s(T)\}$, were $a_i = \gamma_i x_i$ [1].

Electrolyte systematization, and classification. According to extended Debye-Hückel electrostatic theory of solution, the electrolyte activity coefficient $\gamma_{\pm s}$ is depended on salt concentration x_i, and all salts can be divided on solubility product (SP) and thermodynamic extent of salt non-ideality (q) into four large taxons O, A, B, and C, Fig.1 [1, 3]. It is shown, that the dependence of q on SP is increasing and linear for salts, having common ion, and lines «q – SP» form a bundle with a focus which is arranged at single point ($q \geq 0$, $SP \geq 0$) [1, 3]. There are the ideal solutions according to Debye - Hückel theory near this point, strip B (line1), while other solutions have negative (O, A) or positive (C) deviation to non-ideality, Fig 1. At weak salt solubility (x_i < 1-7 mas. %), α is small and formation of perfect crystals is not possible (taxon O), or it is impeded (taxon A) owing to kinetic restrictions by salt diffusion [1]. The crystals of salts, which form ideal solutions (taxon B), can be grown more easily than salts, which having low (A), or high solubility (C). Besides, the morphologically stability of crystal growth is dependent on crystallization stability of solution, namely on maximum of possible solution supercooling ΔT_m [1]. In our works, the system studies of the nucleation kinetics in 1-1 and other 150 salts aquosystem have been early carried out by statistical method of many samples [1, 3].

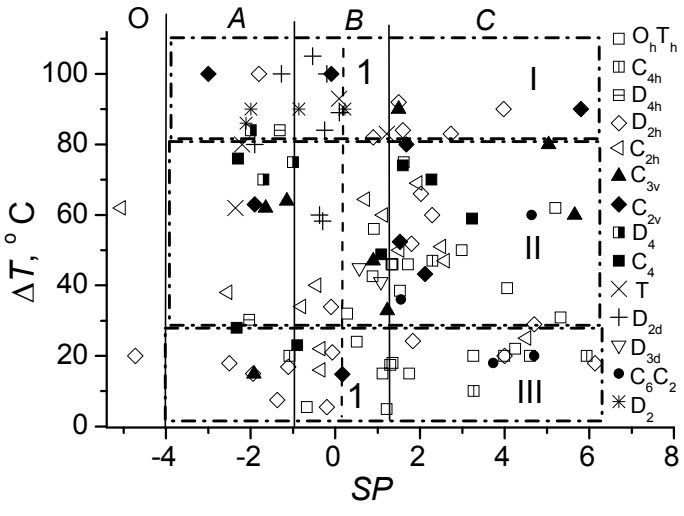

Figure 1. Indistinct set of the pair values {lg (*SP*) - ΔT_m} for crystals of 1-1, 2-1 and 1-2 electrolytes, and its taxonomy. The symbols are designated different point symmetry of crystals.

It is shown that the solution supercooling ΔT has a considerable spread and depends substantially on the upper heating temperature T^+ of the solution, the electrolyte nature, and the physical state (structure) of the solid phase [1, 3]. As an example, Fig. 2 shows the dependences of the minimum temperature T_c of the onset of crystallization on the temperature T^+ of NH_4F solutions (C_{6v}), NH_4ClO_4 (C_{2v}), crystals of which have weak acentric properties),

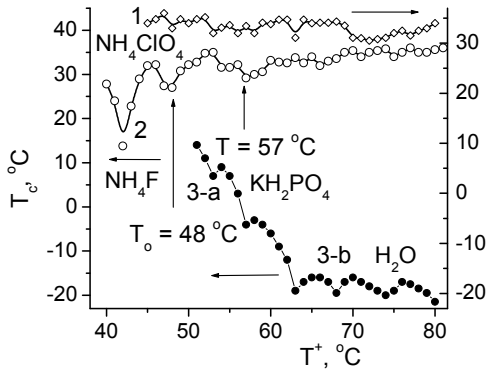

Figure 2. Dependence of the temperature T_c of the onset of crystallization on the temperature T^+ for solutions of the salts (*1*) NH_4ClO_4, (*2*) NH_4F, and (*3*) KH_2PO_4. Curves *1* –*3* correspond to the saturation temperatures of solutions T_0 = 47, 48, and 50°C (the numbers of samples is N = 12, 11, and 40), respectively.

and KH_2PO_4 (D_{2d}, crystal with moderate acentric properties). The limiting supercoolings of NH_4ClO_4 solutions ($\Delta T_m = T_o - T_c$) are minimum and depend only slightly on the temperature T^+. For the majority of electrolytes, the supercooling ΔT increases non-monotonically with an increase in the temperature T^+ and the quantity ΔT_m reaches 72°C for solutions of KH_2PO_4 (KDP). However, the inverse dependence $T_c = f(T^+)$ is observed for some salts with small anions (F^-, OH^-). For example, the temperature T_c of the onset of crystallization of the NH_4F solutions increases with an increase in the temperature T^+. In this case, after the dissolution and holding of solutions in a superheated state at T^+, their additional holding in the supercooled state at T^- for 10 h allows us to construct the continuation of curve *2* in the range of the metastable state (from T_0 = 48 °C to T^- = 40 °C). This boundary of the metastability is also non-monotonic, and the maximum supercooling of the NH_4F solution reaches 48.0–13.8 = 34.2 °C. Then, all salts are divided into three parts according to values of ΔT: 1) All solutions of the first group (I) have an maximum ΔT_m ~ 80-110 °C. Owing to high stability of the supersaturated solutions the crystals of this group can be easily grown from pure solutions by different methods, including accelerated ones. The crystals of group (I) are moderate piezoelectrics and, or ferroelastics. There are crystals of nitrates, iodates, phosphates, sulfates, polyborates, acetates and others among these salts. 2) The solutions of the second group (II) have moderate ΔT_m ~30-79 °C. In pure solutions of these salts it is observed usually the growth of imperfect crystals, having many solution inclusions, non-perfect faces, twins. The perfect crystals of this salts group can be grown only in multi-component solutions, which contain certain macro- and micro-constituents. The crystals of group (II) can be many point of symmetry. Crystals with the highest acentric properties are arranged in taxon II-A. 3) The solutions of the III type have the least values of ΔT_m (6-29 °C). Owing to low stability of supersaturated solutions the perfect crystals of this salts group can be grown only at precise temperature stabilization ~ 0.01-0.001 °C, or also from multi-component solutions. The crystals with weak acentric properties, or paraelastic crystals are preferentially in this group. These crystals are cubic (chlorides, bromides, iodides, perchlorates, perrhenates), rhombic (chlorates, perchlorates, nitrates, fluorides, sulfates, selenates), trigonal (chlorates), tetragonl (hydroxides, perrhenates), hexagonal (perchlorates, nitrates), monoclinic (iodides, nitrates, carbonates, oxalates). So, if we can predict, or estimate salts SP and ΔT_m for different solutions, than we can divide all set of electrolytes into 9 taxons according to values of {lg(SP) - ΔT_m}, Fig. 1. Then we can a priory design of the perfect crystal growth technology from aqueous solutions for novel promising piezoelectric, ferroelectric and others materials, particularly for organic and biological crystals [3, 4].

[1] Kidyarov B.I. Physics of the Solid State. 2009. V.51. P.1435.
[2] Sangwal K. J. of Crystal Growth. 1989. V.97. P.393.
[3] Kidyarov B.I. Mechanism, kinetics of crystals formation and nonlinear crystals growth for opto- electronics. Doctoral thesis. Novosibirsk. 2011. 196 p. (In Russian).
[4] Tsekova D.S. Bulgarian Chemical Communications. 2012. V.44. № 3. P.267.

STRUCTURAL AND PHYSICAL MICRO-SCALE STAGES OF CRYSTAL GENESIS IN LIQUID PHASE

Kidyarov B.I.
A.V. Rzhanov Institute of Semiconductor Physics, SB RAS, Novosibirsk, Russia
kidyarov@isp.nsc.ru

The knowledge of the nano-scale stages of crystal nucleation mechanism is very important for understanding of crystal growth peculiarities of large crystals because the certain stages of these processes are the same in nano-, and micro -scale [**1**]. The «disorder-order» structural transformation from liquid-to-solid phase (from chaos, dynamic short-ordering to long-range 3D-ordering) can not pass in a moment, but one must undergo some successive structural and physical micro-scale stages [**1-2**]. So we must develop a theoretical concept of transformation from disordered structures to three-dimensional ordered structures, to conceptually substantiate the possibility of the stepwise character of crystal genesis. The first taxonomy of the nucleation processes must take into account the nature of simples, and complex substances: metals, semiconductors, dielectrics, and then the existence of 32 groups of crystal point symmetry, which divided into 11 affined groups of «structure-property» relation [**1**]. The main groups are non-centrosymmetric crystals (ferroelectric, non-polar piezoelectric), centrosymmetric crystals (ferroelastic, paraelastic) [**3**]. Besides, the condensed phase can be liquid crystalline, amorphous (glass-like), quasi-crystalline, plastic crystalline [**1**]. At formation and growth of the small cluster (sub-embryo), its nature, electronic and crystalline structure change interrupted, because the relation of surface tension to tension of internal atoms change consequently, but the diverse way at different temperatures for various «classic» and «quantum» substances [**4**].

The work of the formation of stable crystal nucleus with radius ***r*** from precursor cluster, or energetic nucleation barrier ***ΔG(r)***, is the sum of its surface ***(σ·S)*** and volume ***(ΔH·υ)*** energy [5]. In case of any restructuring of this cluster the dimensional dependence of surface tension ***σ(r)*** will have some extremum (Fig.-a), which, respectively, results in a two-barrier form of ***ΔG(r)*** reflecting here a two-stage nucleation process (Fig.-b) [**5**]. The possibility of cluster structure transformation also results from the thermodynamic perturbation theory (Fig. -a) [**6**]. In case of a two-barrier form ΔG(r), there are two critical radii of nucleus, which corresponding to parabolas maximums (Fig.-b). So, physical cause of a break (zigzag) function σ(r), and origin of a two-barrier form ΔG(r) is a phase transition in nano-nucleus at first critical radii r_{k1} [**1, 7**]. At two-barrier form ΔG(r) any kinetic characteristics of non-steady state nucleation are essentially changed: a time lag of nucleation, the nucleation rate, and their dependence on melt (solution) supercooling [**1, 7**]. The type of structural transformation of precursor cluster resulting in a two-barrier formation of stable nucleus can be different [**1**]. In published works we find data concerning the same transitions from amorphous to crystal state [**8**], from ferroelectric phase to para-phase [**9**], from acentric metal nucleus to acentric semiconductor nucleus [10], from meso-phase nucleus to crystalline nucleus [**11**]. The author of [**7**] reports a two-stage nucleation of proteins according to the scheme "solution – dense liquid precursors – crystal nuclei". In the frames of general crystallization theory [**12**] the above-mentioned facts allow distinguishing a stage of «mesophase» formation. Outside the shell of these clusters is a fractal, probably with a nematic type of ordering, whereas inside the sphere of the clusters is characterised mainly by a smectic type of self-assembling with gradual change of its order as the crystalline nucleus «ripens». In other words, mesophase is the product of the first crystal genesis stage which is an assembly of precursor clusters of liquid-crystal type, potentially able to evolve into stable crystallization centers [**12**]. The crystalline center of the precursor must be objectively surrounded by a semi-ordered inner shell with the volume of some more Brave cells supporting the structural ordering of crystal core and carrying the self-structuring algorithm from it to the outer liquid-crystal shell of nucleus [**12**]. Thus, the origin of crystalline core in liquid-crystal

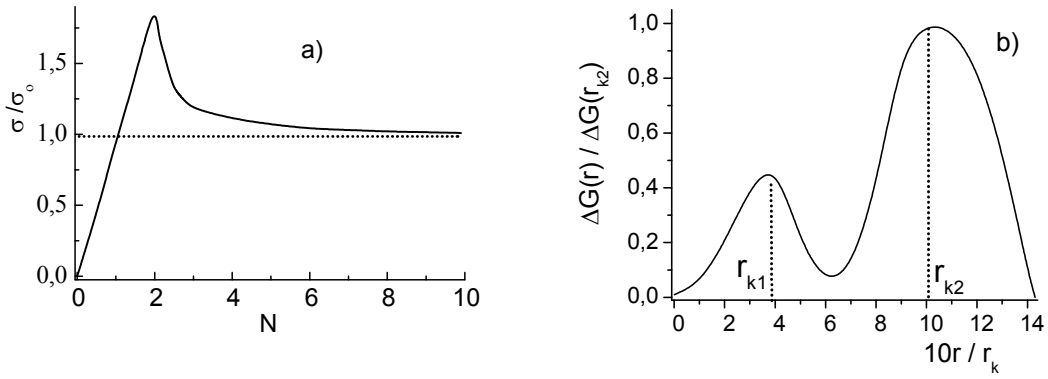

Figure 1. Features of *σ(r)* and *ΔG(r)* dependences at two-barrier nucleation: a) *σ(r)* dependence in case of precursor's restructuring; b) *ΔG(r)* dependence at two-barrier nucleation.

precursors somewhat changes the character of surface arrangement of nuclei and, hence, the value of their surface tension. It is this fact that is responsible for overcoming of the first nucleation barrier, r_{k1}, following from the above-mentioned phenomenology and formal thermodynamics (Fig.-b). It is obvious that with the growing number of crystal-forming components in nucleus, its crystal core will grow by way of gradual, from center to periphery, ordering of inner shell structure. After the crystalline core achieves a particular size, its stability to temperature (or concentration) fluctuations of medium increases and growth process becomes irreversible (overcoming of the second nucleation barrier, r_{k2}) (Fig. -b). The other case of the possible stepwise character of crystalgenesis is a nucleation process near a boundary of the metastable «fluid – fluid» phase transition [**13-14**].

[1] Kidyarov B.I. Mechanism, kinetics of crystals formation and nonlinear crystals growth for optoelectronics. Doctoral thesis. Novosibirsk. 2011. 196 p. (In Russian).
[2] Tsvetkov E.G. J. Cryst. Growth. 2005. V.275, P.e53.
[3] Kidyarov. B.I., Atuchin V.V. Ferroelectrics. 2010. – V.397. №1. - P.159.
[4] Magomedov M.N. Russ. Thermo -physics of High Temperatures.2005. V.43. P.870. (In Russian).
[5] Kidyarov B.I. Journal of the Structural Chemistry. New York: Springer. 2004. V.45. Suppl. P.31.
[6] Samsonov V.M., Bazulev A.N., Sdobnyakov N.Yu., in: Proceedings of the 10-th Russian conference on thermo-physical properties of substances. Kazan' State Technical University Publishers. Kazan'. 2002. P.267. (In Russian).
[7] Vekilov P.G. Nanoscale. 2010. V.2. P.671.
[8] Faupel F., Frank W., Macht M-P.et al.. Rev. Modern Phys. 2003. V.75. P.237.
[9] Astakhov M.V., Stel'mukh I.V., Kapustin M.G. Inorg. materials. 1996. V.32. № 10. P.1250. (In Russian).
[10] Petrosyan V.I., Stenin S.I., Skripkina P.A., Vasin O.I. Microelectronika. 1973. V.2. №3. P.1003
[11] Patashinskii A.Z., Mitus' A.Ya. Journal of the experimental and theoretical physics. 1981. V.80. № 4. P.1554.
[12] Tsvetkov E.G., Kidyarov B.I. Zapiski Rossiyskogo mineralogicheskogo obshchestva. 2007. V.136. Special issue. P.66. (In Russian).
[13] Ganesh P., Widom M. Physical review letters. (USA). 2009. V.102. – P.075701 (4).
[14] Xu Limei, Buldyrev S.V., Stanley H.E., Franzese G. Phys. Rev. Lett. (USA). 2012. V.109, № 9. – P.095702 (5).

SYNTHETIC ANALOGUES AND VARIATIES OF MINERALS –PRODUCTS OF HYDROTHERMAL CRYSTALLIZATION IN BORATE-PHOSPHATE SYSTEMS

Kiriukhina G.V., Yakubovich O.V., Dimitrova O.V.

Lomonosov Moscow State University, Moscow, Russia
g-biralo@yandex.ru

Products of hydrothermal crystallization in borate-phosphate systems with alkali *A* (Li, Na, K, Rb, Cs) and transition *M* (Mn, Fe, Co, Ni, Cu, Zn, and V) metals in presence of Cl^-, F^-, CO_3^{2-} mineralizers have been studied by X-ray spectral analysis and by X-ray diffraction. Crystals were synthesized in a PTFE-lined stainless steel autoclave at a temperature of 553 K and a pressure of 100 bar, over a period of 18 days per one experiment. Main components of the system were varying within P_2O_5 : B_2O_3 : MO/M_2O_3 = 1 : 1 : 1, 2 : 1 : 1 and 1 : 2 : 1; mineralizers' concentration was equal to 10%.

We identified 19 phases from 21 experiments; these are synthetic analogues and varieties of minerals: lithiophosphate Li_3PO_4, santite $K[B_5O_6(OH)_4](H_2O)_2$, gaspéite $NiCO_3$, berlinite $AlPO_4$, Li-boracite $Li_4B_7O_{12}Cl$, Zn-beryllonite $NaZnPO_4$, Ni-containing spherocobaltite $(Co,Ni)CO_3$, Co-maricite $NaCoPO_4$ and Mn/Co-maricite $Na(Mn,Co)PO_4$, borate-sodalite $Zn_4O(BO_2)_6$, Rb-elpasolite $Rb_2Na(AlF_6)$. The phases crystallized in our experiments that have at the moment no mineral analogues are: $KZnPO_4$ with structure type related to tridymite, RbCl with structure type of halite, $Zn_3(PO_4)_2 \cdot H_2O$, $KZn_4(PO_4)_3$, $(Co,Mn)_7[HPO_4]_4[PO_4]_2$ and $(Co,Ni)_7[HPO_4]_4[PO_4]_2$, $Na_5Cu_3[PO_4]_2[PO_4HPO_4]$, $Na_2Ni_3(PO_4)_2(OH)_2$, RbV_3O_8 and CuB_2O_4.

The following conclusions can be made basing on the results of our investigation:

1. The majority of synthesized phases belongs to the phosphate chemical class (10 phases); the number of synthesized borates is only 4. This fact shows higher activity of phosphorus compared to the activity of boron under using conditions of temperature, pressure, type and concentration of mineralizers.
2. Absence of borophosphates or of borate-phosphates among the products of crystallization correlates with the fact that natural borophosphates are exotic minerals having extremely rare occurrence; they are presented by two phases only, namely borate-phosphate seamanite $Mn^{2+}_3[B(OH)_4](PO_4)(OH)_2$ and borophosphate luneburgite $Mg_3[B_2(OH)_6](PO_4)_2 \cdot 6H_2O$. It is worth mentioning that under using conditions phosphate and borate representatives may be formed in one experiment (for example, santite $K[B_5O_6(OH)_4](H_2O)_2$ and $KZn_4(PO_4)_3$), but without formation of the mixed borate-phosphate phases.
3. The influence of mineralizers manifests itself mostly indirectly. High solubility of borate acid promotes its migration and makes possible its presence in natural phosphate systems as a mineralizer keeping alkalinity of the solution close to neutral. In some cases volatile elements Cl and F were incorporated as main components into synthesized crystals with formation of chlorides, fluorides or borates (RbCl, Rb-elpasolite $Rb_2Na(AlF_6)$, Li-boracite $Li_4B_7O_{12}Cl$). Two synthesized carbonates – analogues of the minerals gaspeite $NiCO_3$ and spherocobaltite $(Co,Ni)CO_3$ – were formed only in chlorine free experiments. This fact may be explained by the higher activity of Cl^--ions as mineralizers comparing to the CO_3^{2-}-ions.
4. Alkali cations under using experimental conditions on one hand can form their own phases (lithiophosphate Li_3PO_4, santite $K[B_5O_6(OH)_4](H_2O)_2$, Li-boracite $Li_4B_7O_{12}Cl$, Rb-elpasolite $Rb_2Na(AlF_6)$, RbCl), or may be incorporated in crystals coupled with transition metal cations ($NaZnPO_4$, $NaCoPO_4$, $Na(Mn,Co)PO_4$, $KZnPO_4$, $KZn_4(PO_4)_3$, $Na_5Cu_3[PO_4]_2[PO_4HPO_4]$, $Na_2Ni_3(PO_4)_2(OH)_2$, RbV_3O_8), on the other hand. They may also influence indirectly, by controlling the alkalinity of the system; in this case phosphates, borates and carbonates without alkaline cations in their composition crystallize.

The crystal structures of Rb-elpasolite $Rb_2Na(AlF_6)$ and $Na_2Ni_3(PO_4)_2(OH)_2$ have been studied by X-ray diffraction analysis (Xcalibur_S_CCD diffractometer). Rb-elpasolite $Rb_2Na(AlF_6)$ (fig.1): a = 8.3087(1) Å, sp. gr. $Fm\bar{3}m$, Z = 4, R = 0.0188, [1]; $Na_2Ni_3(PO_4)_2(OH)_2$ (fig.2): a = 14.259(5), b = 5.695(2), c = 4.933(1) Å, β = 104.28(3)°, sp. gr. $C2/m$, Z = 2, R = 0.026.

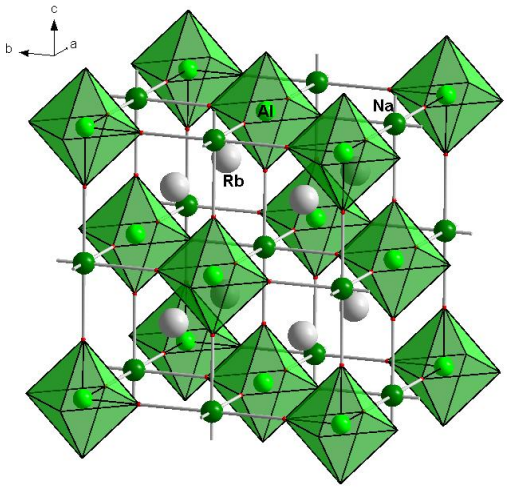

Figure 1: Axonometric projection of the Rb_2NaAlF_6 crystal structure.

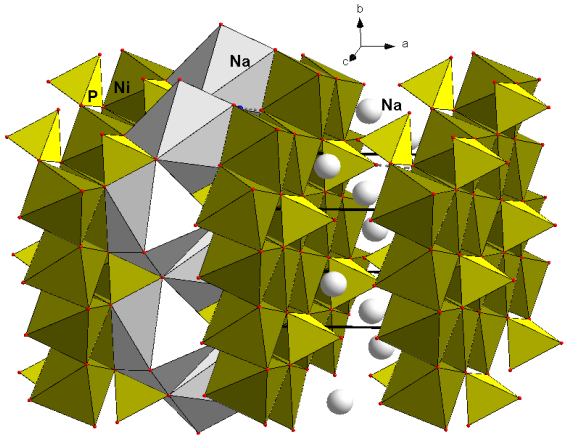

Figure 2: Axonometric projection of the $Na_2Ni_3(OH)_2(PO_4)_2$ crystal structure.

References:

[1] Yakubovich O.V., Kiriukhina G.V., Dimitrova O.V. (2013) Crystal structure of Rb-elpasolite Rb_2NaAlF_6. Crystallogr Rep 58:3:400–403

STUDY OF TETRADYMITE-TYPE COMPOUNDS FOR TOPOLOGICAL INSULATORS

Kokh K.A. [1,2], ***Golyashov V.A.*** [2,3], ***Atuchin V.V.*** [3], ***Tereshchenko O.E.*** [2,3]

[1]*Sobolev Institute of Geology and Mineralogy, SB RAS, Novosibirsk, Russia*
[2]*Novosibirsk State University, Novosibirsk, Russia*
[3]*Rzhanov Institute of Semiconductor Physics, SB RAS, Novosibirsk, Russia*
k.a.kokh@gmail.com

The group of tetradymite (Bi_2Te_2S) is represented by a broad range of chalcogenide minerals with a common formulae $(Bi,Sb)_2(Te,Se,S)_3$. The industry produced analogues of these compounds are considered among the best thermoelectric materials operating near room temperature **[1]**. During the last 5 decades a large amount of research was focused on the study of Seebeck coefficient as a function of doping agent, its concentration, crystalline size etc. in order to increase the performance of thermoelectric devices. Another issue was to check the type of conductivity provided by a given impurity since it is necessary to have separate blocks of *n*- and *p*- type elements.

In 2007 it was shown that not only films but also bulk crystals are able to have the properties of topological insulators (3D TI) **[2]**. The essence of the properties lies in the new electronic state which enables the crystal to conduct spin-polarized electrons along its surface. On the other hand the bulk volume should remain insulated. In 2009 the existence of 3D TI was claimed among some members of tetradymite group **[3]**. These properties are highly interesting both for fundamental physics and applied material science **[4]**.

The crystal structure of tetradimyte compounds (R-3m) is composed of sandwiches interlayered by hexagonal lattices of anions and cations. For instance for Bi_2Se_3 and Bi_2Te_3 the sandwich is a quintuple of Te(Se)-Bi-Te(Se)-Bi-Te(Se). In turn, the sandwiches are coupled by Van der Waals bonding which provides a remarkable perfect cleavage along {0001} (Fig. 1). And it is that surface that has the properties of 3D TI, so no polishing or additional treatment of the samples is required. From theoretical point of view, this surface should be atomically flat and hence, chemically stable because the covalent bonds of boundary layers in the sandwiches are oriented into quintuple layers. However, exposure of the freshly cleaved surface to air was proved to result in the partial oxidation. **[5,6]** The breakdown of the surface structure and formation of intrinsic oxides observed on the (0001) of Bi_2Se_3 andBi_2Te_3 crystals can be responsible for the change of sign in surface conductivity with time **[7]** and even for deterioration of the topological surface states properties **[5]**.

Another issue of 3D TI materials is a presence of intrinsic carriers which hamper the study and application of the specific surface states. The tetradymite materials are hard to be grown with stoichiometric composition. Therefore lattice defects provide metallic behavior of the bulk. Overcoming of this problem was predicted by means of p-n junction which should result in the compensation of intrinsic carriers with different signs **[8]**. Experimental attempts concerning bulk crystals were reported only for the system Bi-Te-Se up to date. The first work has shown positive to negative transition of Hall coefficient with temperature in the Bridgman solidified $Bi_2Te_2Se_{0.995}$ melt **[9]**, while another team has correlated a presence of p- and n- type phases in room-temperature Bi_2Te_2Se crystal with the decay of solid solution **[10]**.

In this report we present our progress on the preparation and study of some tetradymite compounds. High purity (4N) elementary components were used in the growth experiment. The charge with chosen composition was fused in a quartz ampoule sealed at residual pressure $\sim 10^{-4}$ bar. Recrystallization of the obtained ingots was performed using the vertical variant of the Bridgman method with a rotating heat field **[11]**. The grown crystals consisted of one or several large single crystalline blocks (Fig. 1a,b,c). For some compositions a slow cooling of as-

synthesized melt with a ramp 1K/hour was enough to obtain single crystalline samples (Fig. 1d,e).

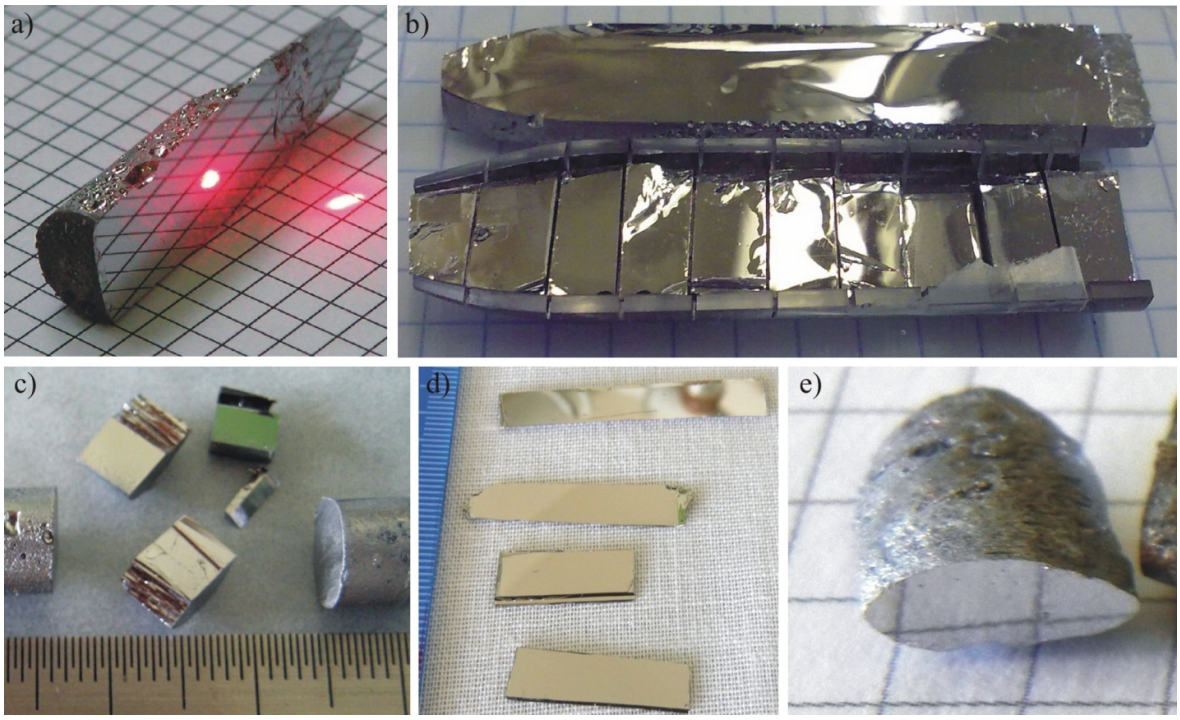

Figure 1. Bridgman grown crystals of Bi_2Se_3, Bi_2Te_3 and Bi_2Te_2Se and single crystalline samples obtained by slow-cooling of the melt: (d) - Bi_2Se_3, (e) - Bi_2Te_3.

Study of surface degradation has shown that cleavage planes of tetradymite compounds have very high chemical stability. The reason for that is assumed to be a perfect crystallographic quality of the samples which was confirmed by RHEED and AFM study **[12]**. It was proven by XPS that first signs of oxidation do not appear even after 1 month of sample collecting at the air atmosphere. The most outstanding resistance was demonstrated by Bi_2Se_3 which started to oxidize just after Ar bombardment and following exposure to NO_2+O_2 agent **[13]**.

In order to obtain p-n junction in the as-grown crystals of topological insulators it is proposed to use natural segregation of the components during quazi-equilibrium crystallization of solid solution. According to this approach we report the procedure and theoretical explanation of reproducible growth of Bi_2Te_3 single crystals with p- and n- conductivity in the beginning and final parts, correspondingly. Due to orientation of cleavage plane {0001} along the growth axis the samples with p/n junctions were obtained. The electrophysic measurements have shown high charge mobility for this region – more than $6 \cdot 10^4$ cm^2/Vs at T=4 K.

The crystals with complex composition were found to be more promising since isostructural compounds have almost absolute intermixing. Therefore it is possible to tune electrical properties of a sample in the right way. The instant example is Bi_2Te_2Se crystal which was proven to be more effective in spin polarization than binary members Bi_2Te_3 and Bi_2Se_3 **[14]**.

Acknowledgements: RFBR #12-02-00226-a.

References:

[1] X.A. Yan, B. Poudel, Y. Ma et al. // Nano Letters 2010,10, 3373.
[2] J.E. Moore, L. Ballents // Phys.Rev.B 2007, 75, 121306.
[3] J. Zaanen, Science, 2009, 323, 888.

[4] F.Xiu, L. He, Y. Wang et al. // Nature Nanotechnology 2011, 6, 216.
[5] D. Kong, J. J. Cha, K. Lai et al. // ACS Nano 2011, 5, 4698.
[6] H. Bando, K. Koizumi, Y. Oikawa et al. // J. Phys. Condens. Matter 2000, 12, 5607.
[7] A.A. Taskin, Z. Ren, S. Sasaki et al. // Phys. Rev. Lett. 2011, 107, 016801.
[8] J. Wang, X. Chen, B.-F. Zhu, and S.-C. Zhang // Phys. Rev. B 2012, 85, 235131.
[9] Sh. Jia, H. Ji, E. Climent-Pascual et al. // Phys. Rev. B 2011, 84, 235206.
[10] J.-Li Mi, M. Bremholm, M. Bianchi et al. // Advanced materials 2013, 25, 889.
[11] K.A. Kokh, B.G. Nenashev, A.E. Kokh and G.Yu. Shvedenkov // J. Cryst. Growth 2005, 275, e2129.
[12] V.V. Atuchin, V.A. Golyashov, K.A. Kokh et al. // Crys.Gr&Design 2011, 11, 5507.
[13] V.A. Golyashov, K.A. Kokh, S.V. Makarenko et al. // J Appl. Phys. 2012, 112, 113702.
[14] K. Miyamoto, A. Kimura, T. Okuda et al. // Phys. Rev. Let. 2012, 109, 166802.

BRIDGMAN GROWTH AND REAL DEFECT STRUCTURE OF GaSe

Kokh K.A. [1,2], ***Atuchin V.V.*** [3], ***Gavrilova T.A.*** [3], ***Kozhukhov A.*** [3], ***Maximovskiy E.A.*** [4], ***Pokrovsky L.D.*** [3]

[1] *Sobolev Institute of Geology and Mineralogy SB RAS, Novosibirsk, Russia*
[2] *Novosibirsk State University, Novosibirsk, Russia*
[3] *Rzhanov Institute of Semiconductor Physics SB RAS, Novosibirsk, Russia*
[4] *Nikolaev Institute of Inorganic Chemistry SB RAS, Novosibirsk, Russia*
k.a.kokh@gmail.com

Gallium selenide, GaSe, is a well-known nonlinear optical crystal widely used for frequency conversion over visible, IR and THz spectral ranges. During last decade, the breakthrough application of GaSe for terahertz (THz) generation over extremely wide spectral range under the pump by near-IR coherent sources was reported. Most recently, efficient THz generation from two collinearly propagating CO_2 laser pulses was demonstrated that resulted by significant improvement of the frequency conversion efficiency of CO_2 laser within mid-IR (second, third and forth harmonic generation) GaSe possesses layered crystal structure with high cleavage properties.

Initially, 120-150 g of polycrystalline material was obtained in single-zone horizontal furnace using high purity (99.9999%) gallium (Ga) and selenium (Se). The synthesis was performed in sealed quartz ampoules by direct fusion of the elements and following homogenization for 1 day at 1000˚C.

The crystals used in this study were grown by the conventional Bridgman technique in evacuated quartz ampoules 18 mm in diameter. The temperature gradient at the crystallization front was 10 deg/cm and the crystal pulling rate - 6 mm/day. The samples 20–22 μm, 70–80 μm, ~ 0.3–0.5 mm, and 3 mm in thickness were cleaved from the grown ingots parallel to (001) and were studied without any additional treatment and polishing.

Micromorphology of cleaved GaSe(001) surface has been observed by AFM with Solver P-47H device in noncontact mode. SEM explorations were implemented using LEO 1430 and JEOL JSM 6700F devices. Structural properties were evaluated by TEM analysis. As it was shown by AFM observation, the cleaved GaSe(001) surface is almost entirely atomically flat with as low rms parameter as ~0.06 nm for an area of 5×5 μm^2. In several scans, a hillock-type formations were detected with bottom diameter of ~200 nm and height of ~20-35 nm. The hillocks were also detected in high-resolution SEM patterns. The Ga/Se ratio estimated by local chemical composition analysis was as low as 0.55-0.84 that indicates drastic depletion of the hillock material by gallium.

Acknowledgements: This study is supported by SB RAS (Project 46.13) and Ministry of Education and Science of the Russian Federation (Contract 16.518.11.7091).

SYNTHESIS AND CRYSTAL STRUCTURE OF $Pb_2(VO_2)(SeO_3)_2Cl$

Kovrugin V. [1,2], ***Colmont M.*** [1], ***Mentré O.*** [1], ***Siidra O.*** [2], ***Krivovichev S.V.*** [2]

[1] *Unité de Catalise et de Chemie du Solide, Université Lille 1, Villeneuve d'ASCQ Cédex, France*
[2] *Geological Faculty, Department of Crystallography, St. Petersburg State University, St. Petersburg, Russia*
kovrugin_vm@hotmail.com

Selenium-containing lead compounds are of special interest since of their geochemical and mineralogical abundance. During the last decade there has been a surge of research activity in the study of PbO–M_xO_y–SeO_2 (M = Cu^{2+}, Ni^{2+}, Fe^{3+}, V^{5+} ; x = 1, 2, y = 1,3,5) ternary system. Special attention was paid to selenium-containing lead compounds as promising non-centrosymmetric (NCS) polar materials with interesting physical properties. Here, we report on the synthesis, characterization, and structure of novel lead vanadate selenite chloride.

Crystals of $Pb_2(VO_2)(SeO_3)_2Cl$ (**I**) were obtained by the hydrothermal techniques from aqueous solution of lead(II) chloride, vanadium(V) oxide, and selenic acid with the ratio of reactants 3:2:25. The reaction was performed in 23 mL Teflon-lined Parr reaction vessel heated in Thermo Scientific mechanical convection oven up to 200 °C and hold at this temperature over 48 hours. Afterward the vessel was cooled to room temperature at a rate 2.4 degree/hour. Products were recovered and filtered, and consisted of red-brown prismatic crystals of **I** up to 300 μm in maximal dimension, as well as fine-grained yellow-brown powder.

Crystals selected for data collection were examined under an optical microscope, glued onto tapered glass fibers, and placed on a Bruker X8 four-circle diffractometer equipped with an APEX II CCD detector and monochromated Mo$K\alpha$ radiation. The structure of **I** was solved by direct methods and refined using least–squares techniques. The compound is monoclinic, $P2_1$, a = 8.342(3) Å, b = 5.318(2) Å, c = 10.724(4) Å, β = 111.702(15) °, V = 442.0(3) $Å^3$, R_1 = 0.0757 for 1054 unique reflections with $|F_o| \geq 4\sigma_F$.

One crystallographically unique V^{5+} cation forms distorted VO_6 octahedra in the crystal structure of **I.** V−O distances vary in the range of 1.593−2.119 Å. Two Se^{4+} cations demonstrate typical SeO_3 trigonal pyramidal arrangement, with Se−O distances in the range of 1.623-1.732 Å. The structure of **I** contains also two symmetrically distinct Pb^{2+} cations. Both lead cations are surrounded by common O atoms with SeO_3 and VO_6 groups, and Cl atoms. All Pb-O and Pb-Cl bonds ≤ 3.5 Å were considered. The Pb(1) site is coordinated by two Cl atoms (<Pb(1)–Cl> = 2.972 Å), and six O atoms (<Pb(1)–O> = 2.742 Å). Highly distorted coordination of Pb(2) site consists of one Cl atom (Pb(2)–Cl(1) = 3.056 Å), and nine O atoms (<Pb(2)–O> = 2.833 Å). Generally both Pb^{2+} cations demonstrate short and strong Pb-O bonds in one coordination hemisphere and long weaker Pb-Cl bonds in another. This coordination is typical for divalent lead with stereochemically active lone electron pair.

The VO_6 octahedron shares four equatorial vertices with two adjacent VO_6 octahedra and two adjacent SeO_3 pyramids. Only one of its apical vertices is shared with SeO_3 pyramid. The second VO_6 apical vertex is non-shared. VO_6 octahedra and SeO_3 trigonal pyramids polymerize by sharing common O atoms to form $[(VO_2)(SeO_3)_2]^{3-}$ chains parallel to the b axis. Thus the structure of **I** is based on 1D chains linked by Pb^{2+} cations and Cl^- anions. The structure of chains in **I** can be considered as a derivative from 'vanadium bronzes'.

This work was supported by the French Ministry of Research and High Education MESR, the Russian Foundation for Basic Research RFBR (grant 12-05-31349), the French National Research Agency ANR (grant ANR 2011 JS08 003 01) and the Agency Campus France.

THE INFLUENCE OF GROWTH CONDITIONS ON THE OPTICAL CHARACTERIZATION OF LANTHANUM – GALLIUM TANTALATE CRYSTALS

Kozlova N.S. [1], ***Buzanov O.A.***[2], ***Didenko I.S.***[1], ***Kozlova A.P.***[1], ***Siminel N.A.***[1]

[1]*National University of Science and Technology "MISIS", Moscow, Russia*
[2]*Company Fomos-Materials, Moscow, Russia*
kozlova_nina@mail.ru

Lanthanum – gallium tantalate crystals $La_3Ta_{0.5}Ga_{5.5}O_{14}$ (langatate) are widely used as active element of sensors based on the direct piezoelectric effect and are regarded as a perspective laser material. Langatate is LGS-type crystals which have the $Ca_3Ga_2Ge_4O_{14}$ type structure with the P321 space group. One of the investigation issues of langatate is crystal coloration which depends on the presence of color centers. It is necessary to understand the mechanism and nature of color centers formation in crystals to have influence on formation processes. Growth conditions and heat treatment are factors of great.

In this study, we performed experiments with langatate crystals produced by the company Fomos-Materials. The samples of polar cut and thickness of 2 mm were used in the experiment. The crystals were grown by the Czochralski method in iridium crucibles in the Ar atmosphere and in the mixture of argon and oxygen (Ar +(2%)O_2) and (Ar +(~0,5%) O_2). Crystals grown in the Ar atmosphere are almost colorless, while those grown in the (Ar+O_2) atmosphere are of bright orange color (Fig. 1).

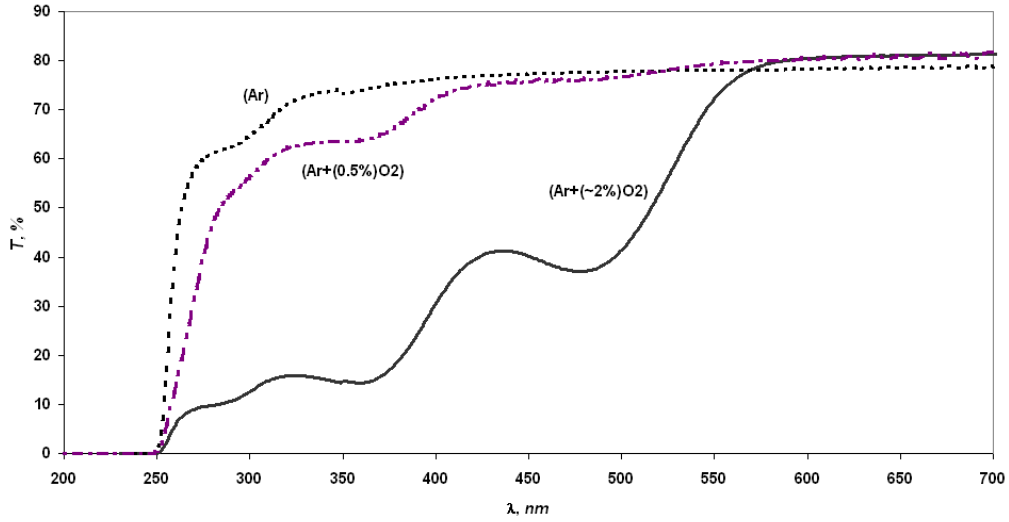

Figure 1. Optical spectra of as-grown crystals obtained in different atmospheres

Presence of point defects in structure and processes of recharge have an influence on color centers formation. It leads to generation of optical active localized states. Formation processes might be activated with additional postgrowth treatment particularly with annealing.

Isothermal annealing was carried out at temperatures from 500 ^{0}C to 1000 ^{0}C with an increment of 100 ^{0}C, each sample was held within 4 hours at only one temperature in the air and at 1000 ^{o}C in the vacuum.

All samples were investigated with methods of optical spectroscopy, optical microscopy, atomic force microscopy, X-ray photoelectron spectroscopy before and after annealing. Optical transmission and diffused reflection spectra were measured with spectrophotometer “Cary 5000 UV-VIS-NIR” and attachment “DRA 2500” for diffused reflection measurements in the

wavelength range 230-3000 nm. A strong effect of the annealing temperature on the state of defects in langatate structure and crystal surfaces has been revealed. It depends on the growth atmosphere.

Increased absorption is observed on specific absorption bands at wavelengths 280 nm, 360 nm and 480 nm. Consecutive decrease of transmission coefficient is accompanied by temperature rise.

Measurement by means of optical microscopy demonstrated the fact that annealing leads to significant change of one of the crystal surfaces. Optical transmission spectra give integral characteristic measurements whereas diffused reflection spectra allow of investigating each of both surfaces separately. Analysis of these spectra shows differences between diffused reflection coefficients of positive and negative surfaces of the samples. It might be connected with unequal structure changing of surfaces.

The surfaces of samples were researched by means of X-ray photoelectron spectrometer PHI 5500 ESCA. The results showed a trend toward reduction of the concentration ratio of Ga to La in the samples annealed at 1000 ^{o}C.

The obtained results are the evidence of isothermal annealing having a profound effect on optical properties and surfaces states of polar cuts of $La_3Ta_{0.5}Ga_{5.5}O_{14}$ crystals. Dependence of surface state on their polarity and the growth atmosphere is observed. Anisotropy of absorption centres was observed in all investigated samples.

Results of the first obtained luminescent properties of langatate single crystals grown in different atmospheres are investigated (Fig.2). The luminescence was excited with second and third harmonic of YAG:Nd^{3+} laser with energy of 2mJ. Wide emission spectra were observed with a maximum at ~450 nm (Fig. 2a) and ~750 nm (Fig. 2b). With increasing of the oxygen concentration in the growth atmosphere the luminescent intensity decreases. It indicates the activization of the oxygen centres formation.

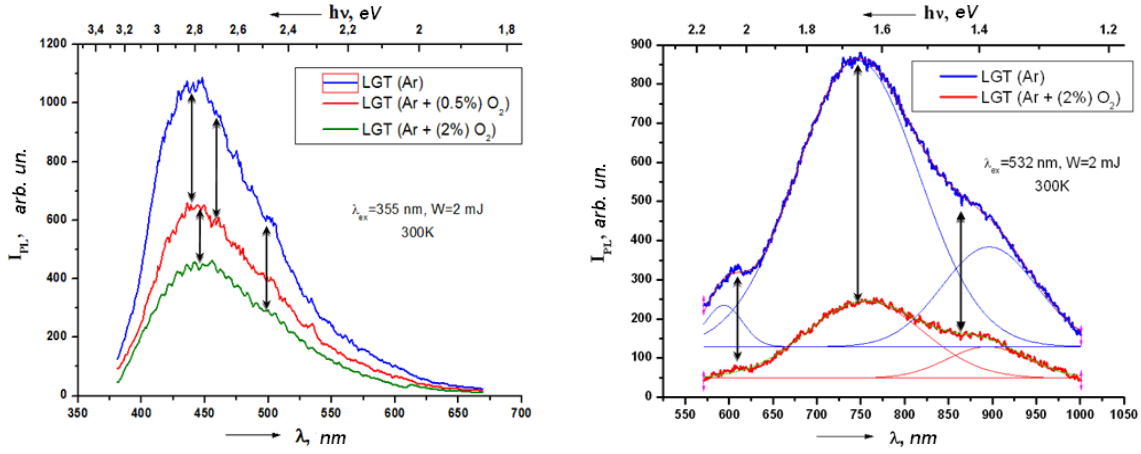

a b

Figure 2. The luminescence spectra of crystals at different excitation wavelengths λ_{ex}=355 nm (a) and λ_{ex}=532 nm (b)

A significant effect of the growth atmosphere and the annealing temperature on optical and luminescent characteristics of langatate crystals is revealed.

CRYSTAL GROWTH FROM MULTICOMPONENT BORATE SYSTEMS

Maltsev V.V., Leonyuk N.I., Koporulina E.V.
Department of Crystallography and Crystal Chemistry,
Moscow State University, Moscow, Russia
maltsev@geol.msu.ru

As a result of investigating the phase diagrams of borate systems and mineralogical field study, numerous high temperature borates and their structural derivatives have been synthesized and found in Nature **[1]**. About 40 of them are minerals. The structures were investigated and the structure types have been established by X-ray diffraction studies for, at least, four hundreds of anhydrous borates. Predominant among these structures are isolated BO_3 triangles (about 65%). Of the rest, almost one-half is represented by framework structures containing three-dimensional B_nO_m polyanions. In this case, BO_3 and BO_4 groups join by sharing common O atoms. Then, it is followed by insular (pyroborates and ring metaborates), network and chain-forming structures**.** Several hundreds of these compounds and their structural derivatives can be considered as possible candidates to guide the search for new crystalline materials with unique properties.

Generally, the stability of numerous structural types of technologically promising borates in multicomponent systems mostly depends on the delocalization of formal charges of the B_nO_m anions as a result of their polymerization. On the other hand, it leads to high viscosity of their melts and restricts crystal growth process. Ortho- and oxyorthoborates with discrete BO_3^{3-} anions are the most stable compounds of this class of inorganic materials. For this reason, $RAl_3(BO_3)_4$ and $Ca_4RO(BO_3)_3$ crystals can be grown over 1100°C at the normal pressure. Of them, however, $RAl_3(BO_3)_4$ tends to decompose, in part, into RBO_3 and the aluminium aluminoborate having two-dimensional (2D) polyanion $Al_3BO_9^{6-}$ in which AlO_4 tetrahedra and BO_3 triangles joined by sharing common corner O atoms. It implies that this mixed polyanion with four-fold coordinated Al atoms has a rather high thermodynamic stability at enhanced temperatures.

The proposed report is aimed at synthesizing new highly efficient single crystals and glass-crystalline nano-structures from multicomponent oxide melts tending to form a wide variety of phases exhibiting diverse compositions and structures that, for a number of reasons, are not realized in nature. This work is mainly focused on studying the crystal genesis in borate systems pursuing optimization of growth conditions for (Er,Yb):$RAl_3(BO_3)_4$ (R=Y or lanthanide) single crystals and fabrication of glass-crystalline nano-composites.

Precise methods have been developed for investigation of phase relationships in the fields of existing liquids in complex borate systems. Particular attention is paid to the crystal growth technology of new rare earth borate material $YAl_3(BO_3)_4$ (YAB) co-doped with Yb^{3+} and Er^{3+} which demonstrates efficient CW, Q-switched and ultra fast diode-pumped solid state and waveguide lasers emitting in the 1.5-1.6 μm spectral for applications in medicine and telecommunications **[2]**.

Appropriate potassium molybdate flux systems are suggested for these unique materials. In particular, for $RAl_3(BO_3)_4$ borates, $K_2Mo_3O_{10}$ is preferred. This is one of the $K_2Mo_nO_{3n+1}$ polymolybdates (n = 2, 3, 4, 6, 8), whose melting temperatures do not exceed 650°C. The region of primary YAB crystallization was revealed for 17 and 20 wt % of YAB cross sections in the YAB-$K_2Mo_3O_{10}$-B_2O_3-Y_2O_3 pseudo-quaternary system (Fig.1). Phase relationships and Er:$Yb_xY1_{-x}Al_3(BO_3)_4$ solubility in the $K_2Mo_3O_{10}$-B_2O_3-Y_2O_3 complex fluxes have been refined in the temperature range of 1150-900°C. In this case the x value was varying from 0 to 0.2, but the Er admixture was up to 1 at.%. Additions of ytterbium and erbium to the system leads to increasing saturation temperature of high-temperature solutions (about 5-10°C, depending on the flux composition).

Solubility diagrams of $Yb_xY_{1-x}Al_3(BO_3)_4$ were studied in the range of x = 0.05–0.15. The main attention is focused on comparison of primary fields of YAB crystallization, and their

solubilities (tys) depending on the flux composition. Since the regions of single-phase YAB and crystallization do not exist at their concentration above 20 wt % in the temperature range of 1150-1050°C, these crystals were obtained only at lower nutrient concentrations. As a result, (Er,Yb):*R*AB single crystals with optical quality and the size up to 20x10x10 mm have been grown on the seeds. The segregation coefficients of the Er and Yb are close to unit as a consequence of minor difference in the sizes of *R*-cations.

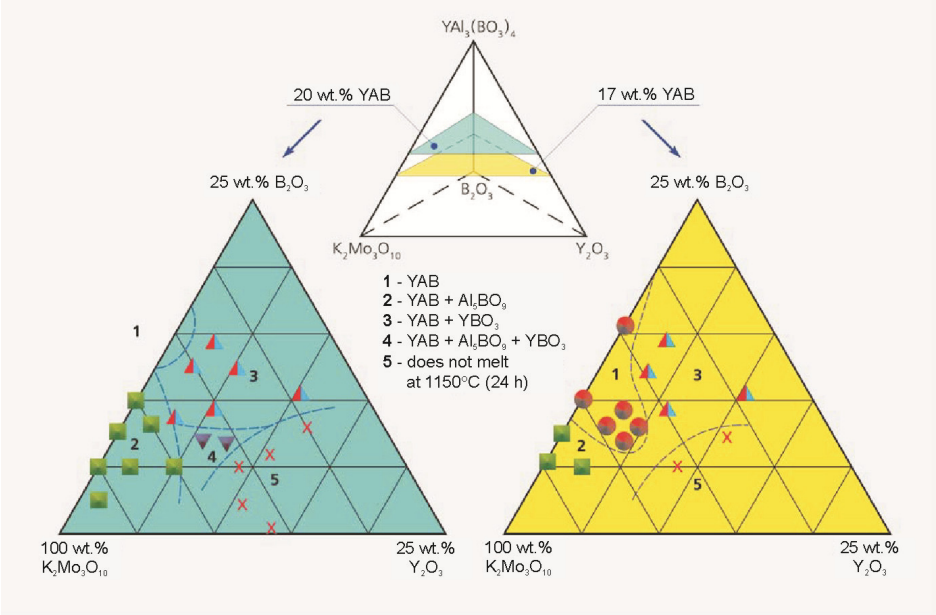

Figure 1. Schematic comparison of single-phase YAB crystallization from $K_2Mo_3O_{10}$ based fluxed melts in the temperature range of 1150-900°C, as their projections to cross sections at 900°C.

The most acceptable solvents for crystal growth of a new spin gap 2D cuprate-borate $SrCu_2(BO_3)_2$ are also suggested. The phase formation in the SrO-CuO-B_2O_3-Li_2O and SrO-CuO-B_2O_3-Na_2O systems in the field of existing melts was analyzed taking into account the regularities obtained from the viewpoint of crystal chemistry. It was determined that the most acceptable solvents for flux growth of $SrCu_2(BO_3)_2$ crystals are $LiBO_2$ and $Na_2B_4O_7$. The structures of latter compounds contain B-O polymers, which are rather easy destroyed at liquid/solid boundary during crystallization process.

In conclusion, crystallization of other borate materials, including formation of glass-crystalline nano-composites, is discussed as well. Increase in concentration of B_2O_3 in complex borate melts leads to decreasing crystallization temperature and the replacement, in a step-by-step, of orthoborates by pyroborates (M'M"B_2O_6 where M'=K,Rb,Cs and M"=Nb,Ta) with isolated B_2O_5 pyroborate dimers, metaborates (BaB_2O_4, or BBO) having discrete B_3O_6 metaborate rings and 1D&2D boron-oxygen polyanions. Finally, in crystallization process of polyborates ($Li_2B_4O_7$, LiB_3O_5, CsB_3O_5, SrB_4O_7), there are substantial restrictions to transport very large B_nO_m polymers from the melts into the crystal structure that practically has the same polyanion configurations with covalent boron-oxygen bonds (over 500 kJ/mole). In this connection, the role of various cations as catalysts is analyzed.

The mixed 3D compounds *M*'$_2Al_2B_2O_7$ (*M*'=Na or K) and *M*"$_2Al_2B_2O_7$ (*M*"=Ca,Sr,Ba) having non-linear optical potential can also be fallen into categories of high temperature aluminoborates, even if potassium aluminoborate crystals can be grown at moderate temperatures. Additionally, $Sr_2Be_2B_2O_7$, $KBe_2BO_3F_2$ and other "toxic" NLO crystals are within the limits of this group.

This research was supported in part by the RFBR grants 12-05-90010-Bel_a, 12-05-00912_a and 13-05-90450-Ukr_a.

[1] N.I. Leonyuk, L.I. Leonyuk. Crystallochemistry of Anhydrous Borates. Moscow: MSU Press, 1983, 215 p. (in Russian).

[2] A.A. Lagatsky, V.E. Kisel, A.E. Troshin, et al. Optics Letters **33** (2008) 83.

EVOLUTION OF STRUCTURAL COMPLEXITY DURING FORMATION OF Mg-Be-Al SILICATES (EXPERIMENT AND INTERPRETATION)

***Mikhailov M.A.*[1], *Krivovichev S.V.*[2], *Mamontova S.G.*[1], *Demina T.V.*[1], *Bogdanova L.A.*[1], *Belozerova O.Yu.*[1], *Demina O.I.*[1]**

[1] *Vinogradov Institute of Geochemistry SB RAS, Irkutsk, Russia*

[2] *Faculty of Geology, St. Petersburg State University, St. Petersburg, Russia*

mikmik@igc.irk.ru

The problem of the evolution of complex systems has many sides and its quantitative description is important for both theory and practice **[1, 2].** From the viewpoint of the crystallogenesis, it is interesting to follow changes of structure types (ST) with changing of the thermodynamic parameters of the reaction environment. Smirnova and Belov **[3]** pointed out to the evolution of crystalline solids in the course of the evolution of the Universe "... from the simplest STs with high symmetry ... to the highly organized multi-component STs with lower symmetry ...". Goldsmith **[4]** proposed the principle of simplexity, which states that structurally simple phases form more *easily* than the phases with complex structures. Recently introduced quantitative information-based measures of structural complexity of crystals **[5-7]** allow to investigate evolution of complexity in terms of bits of information that are accumulated (or dissipated) by the system. In this contribution, we apply these measures to the study of evolution of the multi-phase system in the course of crystallization of beryllian indialite (ideal formula $2MgO•BeO•Al_2O_3•6SiO_2$).

The following basic principles have been used in order to calculate structural information amount of multi-phase system:

(1) Structural information amount of a non-crystalline phase (whether liquid or X-ray amorphous) is considered as 0 bits (despite the fact that it still may possess some degree of atomic ordering).

(2) Information contents of separate crystalline phases, $I_{G,total}$, are calculated according to the following formula: $I_{G,total} = \Sigma p_i \log_2 p_i$ [bits/unit-cell = bits/u.c.], where $p_i = m_i/v$, m_i – multiplicity of the ith crystallographic orbit (Wyckoff site) in the structure; v – total number of atoms in the unit cell. Summation proceeds over all crystallographic orbits in the structure.

The $I_{G,total}$ parameter is unique for a given crystal structure and is a characteristic of distribution of atoms over crystallographic orbits. It is important that the value of $I_{G,total}$ is given for a single unit cell, i.e. information is considered as an *extensive* parameter of a crystalline solid. In this work, the following $I_{G,total}$ values **[7]** have been used: mullite – 36.000, forsterite and chrysoberyl – 70.606, enstatite – 265.754, cristobalite - 5.510, tridymite - 17.510, quartz and quartz-phase structure (PSQu) - 8.265, petalite-phase structure (PSP) - 104.000 , bromellite - 4.000, beryllian indialite (BI) and beryl – 120.175, mullite – 36.000, cordierite – 201.763. IG_{total} spinel - 19.303 bits/u.c. (as in the isotypic hercynite and ganite)

(3) Information content of a n-phase system, I_Σ, is calculated according to the following formula: $I_\Sigma = k_1 \times {}^{[1]}I_{G,total} + k_2 \times {}^{[2]}I_{G,total} + ... + k_n \times {}^{[n]}I_{G,total}$, where k_i – relative amount of the ith phase in the system [$\Sigma k_i = 1$], and ${}^{[i]}I_{G,total}$ is the structural information amount of the ith phase.

We have studied evolution of the I_Σ parameter of the phase portraits ([8]; phase associations) during evolution of melts with the compositions $Mg_2BeAl_2Si_6O_{18}$, $Mg_{1,824}BeAl_{2,334}Si_{5,833}O_{18}$ and $Mg_{1.81}Be_{1.09}Al_{2.27}Si_{5.84}O_{18}$, as well as temperature-dependent evolution of the I_Σ values of associations that form in the course of solid-state reactions (SSRs) from the two initial mixtures with the general compositions $Mg_2BeAl_2Si_6O_{18}$ и $Mg_{1.81}Be_{1.09}Al_{2.27}Si_{5.84}O_{18}$). It can be seen (Fig. 1, curves 8-10) that, for SSRs, increasing temperature is associated with the increasing I_Σ parameter (information amount in the system), which manifests increasing complexity of the system in the course of chemical reactions. The use of xerogel as a starting charge (curve 10) results in changing of the complexity behaviour

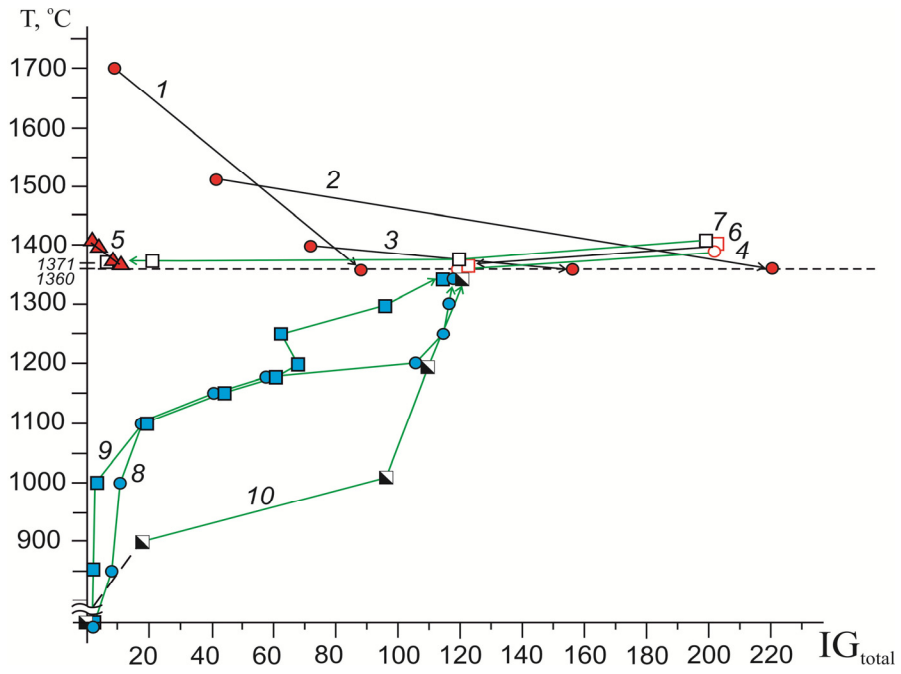

Figure 1. Behaviour of the I_Σ values in the course of different crystallization processes (arrows indicate direction of the system evolution). Curves 8-10: air atmosphere. Growth from melt: 1-3,5,6 –Ar atmosphere (1-3- $\Delta T^{melt/crystal}$ = 80-180°/cm; 5.6 - $\Delta T^{melt/crystal}$ = 32°/cm); 4, 7 – air atmosphere, $\Delta T^{melt/crystal}$ = 5°/cm. T_{melt} = 1360 and 1371°C for stoichiometric and non-stoichiometric Be-indialite, respectively. The same type of symbol (circle, square, triangle) indicates the same type of initial mixture.

compared to the mixture of crystalline phases (corundum and periclase) with x-ray amorphous components (SiO_2 and BeO) as initial charge (curves 8 and 9).

There are two groups of experiments with different types of the evolution of the I_Σ parameter. During spontaneous crystallization from melt with compositions $Mg_2BeAl_2Si_6O_{18}$ (curves 1-3; different overheating temperature) and $Mg_{1.824}BeAl_{2.334}Si_{5.833}O_{18}$ (curve 5), phase portraits of metastable compounds that form in the system are more complex that their predecessors. In the second group (curves 4, 6 and 7), we have used a seed crystal of cordierite ($I_{G,total}$ = 201.763 bits/u.c.), which is overgrown by beryllian indialite (curves 4 and 6) or beryllian indialite is replaced by mixture of phases with stuffed quartz- and petalite-type frameworks (curve 7).

In our contribution, we shall discuss the phase sequences described above and the regularities observed.

This work was supported by the Russian Foundation for Basic Research (№ 11-05-00712).

References: **[1]** Regularities of development of complex systems (evolution of supramolecular and nonequilibrium phenomena). 1980, Nauka, 344 p. **[2]** Yushkin N.P. // ZVMO, 1982, vol. 4, p. 432-442. **[3]** Smirnova N.L., Belov N.V. // History and Methodology of Natural Sciences, 1979. p. 94-102. **[4]** Goldsmith J.R // J. Geology, 1953, v. 61, p. 439-451. **[5]** Krivovichev S.V. // Acta Crystallogr. 2012. Vol. A68. P. 393-398. **[6]** Krivovichev S.V. // Micropor. Mesopor. Mater. 2013. Vol. 171. P. 223-229. **[7]** Krivovichev S.V. // Mineral. Mag. 2013. Vol. 25. P. 275-326. **[8]** Mikhailov, MA / Proc. Russia. soveshch. "Modern problems of geochemistry", Irkutsk, 2012, p. 288-291.

GROWTH OF $NaBaYb(BO_3)_2$ CRYSTALS FROM MELT SOLUTIONS

Nabeeva T.N., Kokh A.E., Kononova N.G., Kokh D.A.

Sobolev Institute of Geology and Mineralogy, SB RAS, Novosibirsk, Russia
svetlyakovatn@gmail.com

Compounds of simple and complex orthoborates of rare-earth elements (REEs) are of interest as laser matrices and promising materials for nonlinear optics. The series of complex REE borates with alkali metals, for example, $RNa_3(BO_3)_2$ (R = Y, La, Nd, Gd) **[1, 2]** and alkali-earth elements of $R_2Ba_3(BO_3)_4$ (R = La, Pr, Gd) type **[3]** are of particular interest owing to the luminescent properties and low concentration quenching of REE ions **[4]**.

In our earlier study of phase formation in the systems R_2O_3-BaO-Na_2O-B_2O_3 (R=Sc, Y) we have established new complex compounds $NaBaSc(BO_3)_2$ и $NaBaY(BO_3)_2$ containing alkali and alkali-earth cations **[5]**. Further investigations in this series resulted in the discovery of new ytterbium-bearing borate: $NaBaYb(BO_3)_2$ **[6]**. The X-ray patterns of crystal samples of $NaBaYb(BO_3)_2$, $NaBaR(BO_3)_2$ (R = Sc, Y) are similar in the arrangement of reflexes and their relative intensity, which suggests that the compounds are isostuctural (space group R-3). In the structure of compounds $NaBaM(BO_3)_2$ (M = Yb, Sc, Y) BO_3 – triangles are arranged in layers. Ba2+ cations are coordinated by six layered O atoms and three atoms from the neighboring layer. Na+ is shifted from the surface of layer and has a one-sided ditrigonal coordination. M^{3+} cations are located between the coupled Ba- и Na-layers in octahedral coordination **[7]**. The parameters of the unit cell for the new compound $NaBaYb(BO_3)_2$: a = 5,3369(3), c = 35,526(2) Å, Z=4 were determined using the XSA technique.

Yb^{3+} cation has a great number of radiative transitions, the efficiency of which depends on the hosting crystal matrix as well **[8]**. To study the generation characteristics of Yb^{3+} cations, it is necessary to grow a crystal of high optical quality and proper size.

The aim of this work is to obtain high-quality $NaBaYb(BO_3)_2$ crystals. In order to grow the crystals from melt solution, we used the procedure of spontaneous crystallization on a platinum loop. The solvent was chosen experimentally, using the data of solubility curve study and the calculated values of output crystal coefficients. We have analyzed two eutectic compositions of the system BaO–Na_2O–B_2O_3: 0.56 BaB_2O_4-0.44 $NaBO_2$, 0.56 $NaBO_2$-0.44 BaNaBO3; and the eutectic of the system BaB_2O_4-NaF (0,39 BaB_2O_4). The results obtained evidence that the optimal solvent for growing $NaBaYb(BO_3)_2$ crystals is eutectic 0.56 BaB_2O_4-0.44 $NaBO_2$. Fig. 1 shows the photo of the spontaneously grown druse of $NaBaYb(BO_3)_2$ crystals synthesized using the chosen flux. The temperature range of crystallization was 905-880ºC, and the rate of temperature decreasing was 2 deg/day. The grown crystals do not dissolve in water and diluted mineral acids and have good cleavage on (0001).

The work was financially supported by project Nb.12-05-31028mol-a from the Russian Foundation for Basic Research.

References:

[1] Mascetti J., Vlasse M., Fouassier C. // J. Solid State Chem. 1981. V. 39. P. 288.
[2] Zhang Y., Chen X.L., Liang J.K. et al. // J. Alloys Compounds. 2002. V. 333. P. 72/
[3] Palkina K.K., Kuznetsov V.G., Dzhurinskii B.F. et al. // Russ. Inorg. Chem. 1972. V. 17. P. 341.
[4] Blasse G., Bril A. // J. Inorg Nucl. Chem. 1967. V. 29. P. 266.
[5] Svetlyakova T., Kononova N., Kokh A. et al. // Russ. Inorg. Chem. 2011. V. 56. P. 117.
[6] Svetlyakova T., Kokh A., Kononova N. et al. // Cryst. Reports. 2013/ V. 58. P. 54.
[7] Seryotkin Yu., Bakakin V., Kokh A. et al. // J. Solid State Chem. 2010. V. 183. P. 1200.
[8] Krupke W.F. // IEEE J. Quantum Electron. 2000. V. 6. P. 1287.

Figure 1. Photo of the druse of spontaneous $NaBaYb(BO_3)_2$ crystals. A square is 2.5x2.5 mm^2 in size.

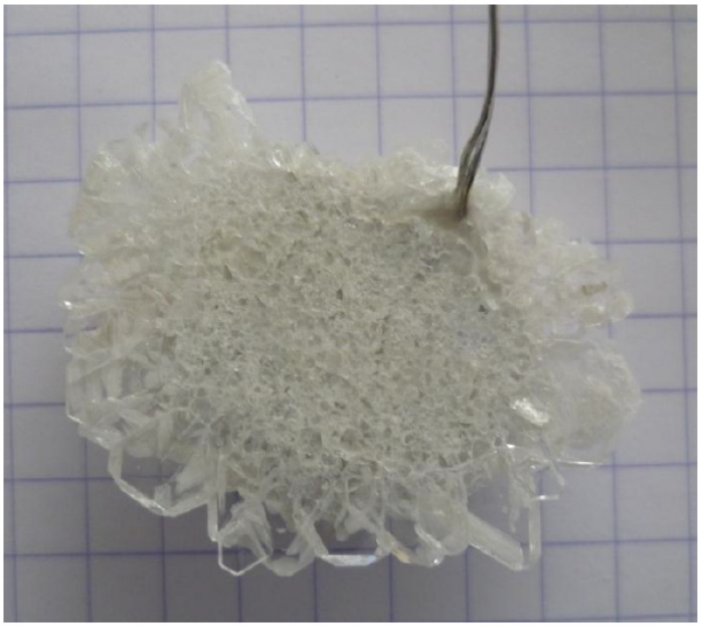

IMPURITIES DISTRIBUTION IN CHARACTERISTIC OF MULTICRYSTALLINE SILICON GROWTH MODE

Presnjakov R.V.

Vinogradov Institute of Geochemistry SB RAS, Irkutsk, Russia
ropr@igc.irk.ru

At present multicrystalline silicon (mc-Si) is the basic material for solar cells [1]. The basic problem of solar energy, is the price of raw silicon (Fig.1).

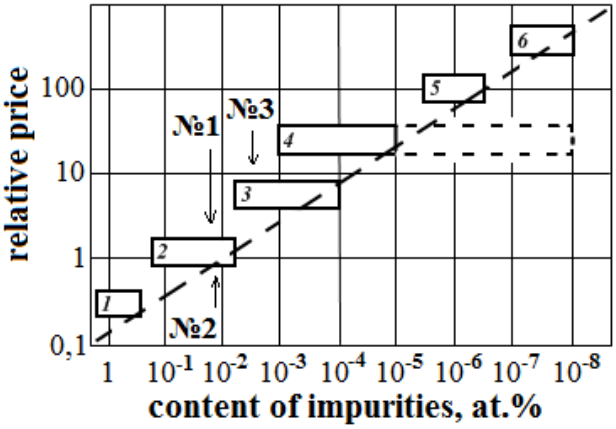

Figure 1. № 1-3 - silicon used in the present work for the growing of mc-Si. 1 – metallurgical grade silicon, 2 – basic purity of refined metallurgical silicon (HP1), 3 - high purity of refined metallurgical silicon (HP2), 4 - terrestrial solar grade silicon, 5 – monocrystalline silicon, 6 – semiconductor grade silicon [2].

From this point of view, the most promising is the refined metallurgical silicon. One key issue is knowing the limit of impurities concentrations to obtain a material with established properties. During the directional solidification requires final cleaning of silicon impurities with efficiency, determined its equilibrium distribution coefficient (k_0), and the formation of macro- and microstructure of the ingot. The value of the effective distribution coefficient of impurities due to the characteristics of the growth process, which determine the features of heat and mass transfer. In the equation of Burton-Prim-Slichter (1) for the stationary distribution of impurities in the melt is expressed through the convection-diffusion parameter Vδ/D, called the Peclet number.

$$k_{eff} = \frac{k_0}{k_0 + (1 - k_0)e^{-(V\delta / D)}} \quad (1)$$

Ingots on the basis of HP1-Si and HP2-Si have been grown under optimum conditions. This means: 1) rotation of the crucible melt-crystal at a rate sufficient to equalize the thermal field, 2) moving the crucible of molten crystal at a low speed, which prevents concentration supercooling at the solid-liquid interface. Using the method of ICP MS in different sections on the growth axis ingots were identified impurity concentration of Fe, Ti, Ni, Co, V, Cr, Mn. Calculation of effective distribution coefficients of these elements in the ingot approximation Pfann (2) shows reduction of their values (Table 1) at increasing concentrations of impurities in the initial charging (C_0):

$$C = C_0 k_{eff} (1 - f)^{k_{eff} - 1} \quad (2),$$

where f - fraction of crystallized silicon.

Table 1. Effective distribution coefficients of impurities in ingots from refined metallurgical silicon of compositions № 1-3.

	Fe		Ni		V		Ti		Cr		Mn		Co	
	k_{eff}	Δ	k_{eff}	Δ	k_{eff}	Δ	k_{eff}	Δ	k_{eff}	Δ	k_{eff}	Δ	k_{eff}	Δ
№1	0,06	9	0,15	10	0,0015	5,9	0,15	10,8	0,04	8,2	0,03	8	0,0003	3,6
№2	0,08	9,3	0,18	10,2	0,003	6,6	0,08	10,1	-	-	0,06	8,8	0,0012	5
№3	0,2	10,3	0,3	11,1	0,008	7,6	-	-	0,12	9,4	0,16	9,8	0,0010	4,8

Impurity profiles are significantly different from the distribution of Pfann, showing the influence of transient phenomena characteristic of the initial and final stages of crystallization due to the finite amount of Si. Moreover, the values of Peclet numbers shown in Tables. 1, much larger than 1. This shows that in this system remains a diffusion heat and mass transfer under the dominant influence of natural convection [3]. Consequently, analysis of the distribution obtained based on the approximation that describes the convective transfer of the substance, it is not valid. The report presents the results of the analysis of experimental impurity profiles in ingots on the model Favier by numerical solutions of the diffusion equation with a moving boundary [4].

Hall effect measurements carried out on rectangular samples of the crystals obtained before and after heat treatment [5]. The samples were cut in the lower ($f < 0,2$) and upper ($f > 0,8$) parts of the ingots. It is shown that an increase in total impurities is no reduction in the Hall mobility of the charge carriers in mc-Si below the values typical of the currently produced mc-Si p-type conductivity [6]. Found that samples with the same conductivity Hall mobility of carriers mc-Si based HP1-Si is more resistant to high temperature annealing (1200^0C) than samples mc-Si based HP2-Si.

References:

[1] Schreiber D. Solar PV markets and industry today and tomorrow global vision. // 2011 // www.eupd-research.com.

[2] Dietl J., Helmreich D., Sirtl E. “Solar” silicon / Crystals, Growth, Properties and Application. B. 5. Springer Verlag. – 1981. - P. 43-107.

[3] Nepomnjashhih A.I., Presnjakov R.V., Antonov P.V., Berdnikov V.S. Vlijanie rezhima vyrashhivanija na makrostrukturu slitka mul'tikristallicheskogo kremnija. // Izvestija vysshih uchebnyh zavedenij. Prikladnaja himija i biotehnologija. - 2012. - №. 1(2). - S. 28-34.

[4] J.J. Favier. Macrosegregation – I. Unified analysis during non-steady state solidification. // Acta Metallurgica. – 1981. - V. 29. - Is. 1. – P. 197-204.

[5] Wu H., Ma W, Chen X., Jiang ., Mei X., Zhang C., Wu X. Effect of thermal annealing on defects of upgraded metallurgical grade silicon. // Transactions of Nonferrous Metals Society of China. - 2011. - V. 21. - Is. 6. - P. 1340-1347.

[6] Martinuzzi S., Perichaud I., Palais O. Segregation phenomena in large-size cast multicrystalline Si ingots. // Solar energy materials and solar cells. – 2007. – V. 91. - Is. 13. – P. 1172-1175.

ANALYSIS OF BROADENING OF X-RAY DIFFRACTION MAIMA IN CASE OF HETEROGENOUS CRYSTALS

Pyankova L.A., Punin Yu.O., Shtukenberg A.G., Komissarov A.A.

Inc. "Scientific Instruments", SPbGU, Saint-Petersburg, Russia
lyuba@pyankova.ru

The main goal of this work is to elaborate a method to measure sizes of coherent scattering regions (CSR) and mosaicity in heterophase crystals as a function of impurity type and concentration. As an example we considered heterophase $NH_4Cl:Me^{2+}$ crystals (crystals with "anomalous isomorphism") consisting of NH_4Cl matrix and oriented syntactic intergrowths with three types of guest phases **[1]**. For such crystals simple approximation of diffraction maxima profiles by the Gaussian function cannot provide correct sizes of CSR. More sophisticated mathematical models are expected to provide better result. However direct verification of calculated parameters such as physical broadening and average block sizes is hardly possible now. For example, very powerful and popular method of electron probe microanalysis is almost inapplicable due to NH_4Cl decomposition in high vacuum. Correctness of the data obtained can be verified only by indirect techniques such as atomic force microscopy (AFM) **[2]**.

The crystals of $NH_4Cl:Me^{2+}$ (Me = Mn, Cu) were grown in Petri dishes from supersaturated water-formamide solutions containing $MeCl_2$ and NH_4Cl (T = 20°C) for 3 - 4 days without stirring. Water to formamide weight ratio was 1:1. Twenty five heterophase crystals were studied at room temperature (T = 20°C) with X-ray diffractometer DIFREY (Inc. "Scientific Instruments"), software package Difract. Experimental conditions: sharp-focused X-ray tube BSV-30, $Cr_{K\alpha}$ (0.22897 nm) radiation, bent position sensitive detector with the angular range of simultaneous data collection of 20°, capillary collimator 0.5 mm, exposure time 300 sec. The studied crystal face was aligned with the plane of the diffactometer stage. The face was coated by α-Al_2O_3 powder to calibrate detector and correct for angular misalignment of the sample. An ammonium chloride crystal grown from water-formamide solution without Me^{2+} impurities and characterized by minimal half-widths of diffraction maxima was used as a standard to account for instrumental broadening of reflections. The average sizes of CSR, D_{CSR}, were calculated from the broadening of X-ray diffraction reflections by Selyakov-Sherrer method **[3]**. More accurately, analysis of CSR size was done using Selivanov-Smyslov method applicable to the systems where particles do not have internal microstrain and their shapes are close to spherical. The broadening of reflections was determined using the method of approximation and the CSR sizes were modeled assuming the lognormal distribution of crystallites.

Analysis of X-ray diffraction maxima obtained from (100) face of $NH_4Cl:Me^{2+}$ have shown that syntactic intergrowths of guest phases are preferably oriented in the crystal structure of the host phase. Their mutual orientations obey to the crystallographic similarities of corresponding crystal planes **[1]**. The microblock sizes in ammonium chloride crystals without impurities are much bigger than corresponding sizes in crystals with manganese impurity, ~1500 nm and 30 – 200 nm, respectively. These results agree well with the AFM data **[2]**.

The standard Selyakov-Sherrer formula does not show any correlation between crystal imperfection and impurity concentration (Fig. 1).

However, the Selivanov-Smyslov method with lognormal distribution of CSR sizes and approximation of the diffraction maxima by Cauchy and Gauss functions shows a clear trend (Fig. 1). Despite high degree of imperfection at the macroscale (cracking, twinning, non-crystallographic branching), which has to mask all possible trends, increasing in impurity concentration results in decreasing of CSR sizes. Moreover, increasing of impurity concentration in NH_4Cl:Mn crystals leads to the higher degree of misorientation of microblocks (Fig. 2) and increased number of macroblocks.

Variations of CSR sizes calculated for five different crystals formed in one growth run are 20%. Measurements carried out for ten different points of the same crystal give smaller variations attaining 6%. It is worth noting that the minimal physical broadening is observed in the crystal core, which is characterized by the minimal anomalous birefringence (higher degree of perfections).

Thus, heterophase crystals and solid solutions are characterized by the same rules of defect arrangement: there is clear and strong correlation between defect distributions at different scales. This conclusion is supported by calculations of CSR sizes and macroblock mosaicity.

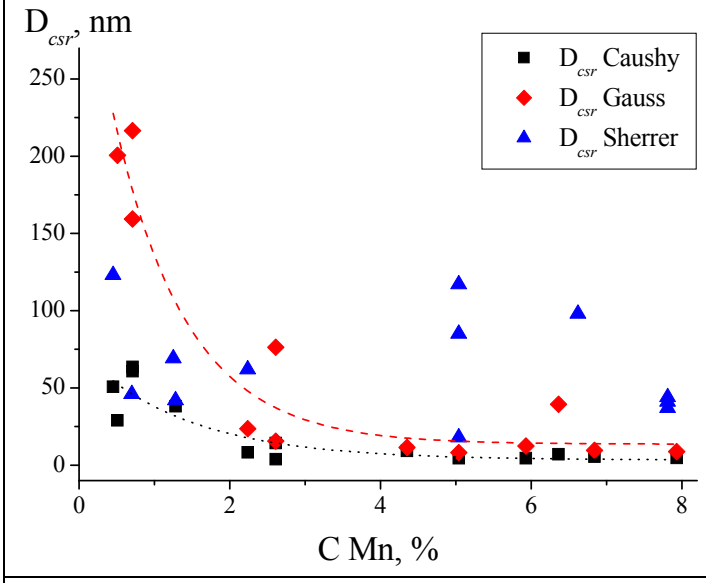

Figure 1. The size of CSR obtained from three different models as a function of impurity concentration.

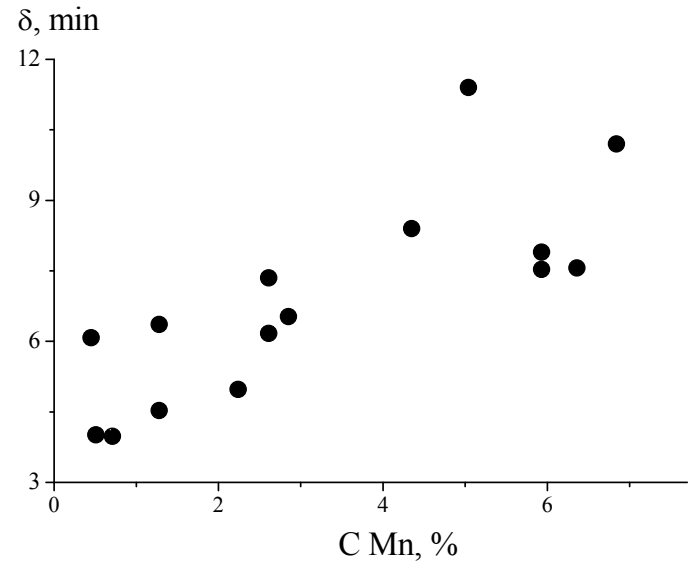

Figure 2. The average degree of misorientation of microblocks as a function of impurity concentration in the crystal.

References:

[1] Pyankova L. A., Shtukenberg A. G., Punin Yu. O. Anomalous isomorphism and mixed crystals in the systems NH_4Cl:(Cu,Mn) // Crystal Growth & Design, 2012, 12, p. 5283−5291.

[2] Pyankova L. A., Bocharov, S. N., Shtukenberg A. G., Punin Yu. O. Bakhvalov, A. S., Franke, V. D. Complex study of syntactic intergrowth distribution in heterophase NH_4Cl:(Mn^{2+},Cu^{2+}) crystals // Vestnik SPbGU, Ser. 7, N 1, 2011, p. 45-54 (in Russian).

[3] Ryaboshapka, K. P. Physics of X-ray scattering by deformed crystals. Kiev, Naukova Dumka, 1993. 408 p (in Russian).

SCINTILLATION MATERIAL BASED ON ALKALI-HALIDE COMPOUNDS

Rusakov A.I.

A.P. Vinogradov Institute of Geochemistry SB RAS, Irkutsk, Russia
rusakov@igc.irk.ru

The scintillation method is used for the registration of ionizing radiation. Scintillation detectors are materials in which the particles absorpb photons of ionizing radiation and transform them to the light flash called scintillation. This glow accurately describes intensity and type of ionizing radiation. With the ability to convert the energy of ionizing radiation into light signals, scintillators are widely used everywhere, where a detection of elementary particles or electromagnetic radiation is hard.

From the previous studies we know that the halogen compounds are large compared to the glow oxides. Among the alkali-halide crystals, the most effective scintillator by the values of glow and the decay time of the scintillation crystals are NaI(Tl). Now activated NaI crystals can also be used at low temperatures in the dark matter detectors **[1]**.

The aim of this work was to obtain a non-activated crystals of NaI and CsI in the vertical Bridgman method embodiment of a multi-zone growth vessel. Growth vessel of this type allows one to create any configuration of the temperature field over the entire height of the furnace.

Due to the high water absorbancy, a great attention was paid to the preparation of raw materials. The salts of NaI and CsI are kept under vacuum for 12 - 16 hours at a temperature from 100^{o}C to 450^{o}C. The prepared materials were sealed under a vacuum of 10^{-5} - 10^{-4} mm Hg. The growth experiments were performed in the artificial quartz ampoule. The crystal growth rate was 2 mm / h at a temperature gradient of 10^{o} - 15^{o}C in 1 cm. Grown crystals are of sufficient purity and transparency.

In the last few years a lot of effort to find new scintillator materials was applied **[2]**. This work serves as a basis for the synthesis and investigation of new promising scintillation materials especially in the ternary systems (such as: BaBrI, BaClI, BaClBr activated Eu^{2+}).

References:

[1] Bernabei R. et. al. Dark matter search // Riv. Nuovo Chim. –2003. -V.26. –P.1
[2] S.E. Derenzo et. al., IEEE Transactions on Nuclear Science 55 (2008) 1458–1463.

SYNTHESIS OF FINE-CRYSTALLINE TOURMALINE IN SUPERCRITICAL FLUIDS

Setkova T.V. [1], ***Balitsky V.S.*** [1], ***Vereshchagin O.S.*** [2], ***Kalinin G.M.*** [1], ***Shapovalov Yu.B.*** [1]

[1] *Institute of Experimental Mineralogy RAS, Chernogolovka, Russia*
[2] *Crystallography Department, Saint-Petersburg State University, Saint-Petersburg, Russia*
setkova@iem.ac.ru

Recently there is a growing tendency for developing of technology of new nano- and fine-crystalline materials for production of ceramics, filters, sieves etc. in a world science and engineering. The tourmaline is characterized by valuable pyro and piezoelectric properties. For this reason, synthesis of fine-crystalline tourmaline has practical interest for production of piezoelectric ceramics and textures. In a first half of the last century, tourmaline was used in various radio- and acoustic devices (for location of surface ships and submarines, as well as measurement of pressure at powerful explosions). Due to development of industrial growth of quartz single crystals, which is widely used now in piezotechnics, acousto-electronics, optics and other fields of science and technology, the interest in tourmaline material has fallen over time. However, the main benefit of tourmaline in comparison with quartz is a high piezoelectric constant and a larger value of frequency coefficient. In addition, the technology of producing ceramics has a number of extra advantages in comparison with single crystal growth technology. Considerably more bulky details including a predicted shape can be obtained from ceramics.

Previous work on the tourmaline synthesis **[1-3]** has a practical and scientific interest in for study of structural and crystal-chemical features of minerals of tourmaline group. We have demonstrated a possibility of growth of tourmaline single crystals on a seed in boron, boron-fluoride, boron-chloride, boron-chlorine-fluoride hydrothermal fluids also previously **[4-6]**. Fine-crystalline tourmaline of spontaneous nucleation with size 5-500 micrometers was formed in many those experiments along with single crystal growth. The experimental study of physical and chemical conditions of crystallization of fine-crystalline tourmaline can help to solve some problems of its crystal chemistry and geochemistry, to determine the conditions of its formation in nature as well as to develop of synthesis methods of nano-sized and fine-crystalline tourmaline for production of piezoelectric ceramics and textures.

The experiments were performed in boric (H_3BO_3), boric– fluoride (H_3BO_3+NH_4F), boric–chloride–fluoride (H_3BO_3+AlF_3+NaCl), and boric–chloride (H_3BO_3 +NaCl+$CoCl_2 \cdot 6H_2O$) supercritical fluids at pressure of 100 MPa and at temperature of 400–650 °C. The studies were performed in titanium and chromium-nickel alloy autoclaves of 20, 50, and 200 cm^3 in volume. Different types of nutrient were used in the experiments: silicon and alumina oxide or mixture of quartz and corundum monocrystal bars. The nutrient was put on the bottom of an autoclave. Chemical reagents of H_3BO_3, NH_4F, and NaCl and CoCl2·6H2O were used to prepare solutions. Poorly water-soluble AlF3 was loaded directly into an autoclave in required proportions. An autoclave was filled with the solution, closed hermetically and placed in an electric furnace. The temperature was measured using standard chromel-alumel thermocouples attached to an autoclave walls with an accuracy of ±3 °C. Pressure was assigned by the autoclave filling factor and was estimated according to the PVT diagram for pure water or solutions close in composition. The duration of the runs was 15–30 days. The crystal morphological characteristics of the obtained crystals were investigated using of a binocular microscope (MBS-10) and SEM (Vega TS5130MM electron scanning microscope). Identification of phases was performed based on powder X-ray diagrams (survey by Bruker D8-advance).

Spontaneous nucleation of fine-crystalline tourmaline was observed in each sets (boric, boric-fluoride, boric-chloride) fluids. The most amount of crystals were formed only in run with boric-fluoride solution (H_3BO_3+NH_4F). Density of spontaneous crystallization was estimated with $\mathbf{m_f}$ factor that is equal to quotient of weight of fine-crystalline tourmaline to weight of

initial nutrient ratio. In boric-fluoride solution, the $\mathbf{m_f}$ factor was equal 80%. The composition of fine-crystalline tourmaline formed in boric-fluoride solution is characterized by high iron content (up to 7 wt.%) and crystals size from 10 to 100 μm. Crystals grow in quantity with increasing concentration of boric acid in the solution. At low boron content in the solution, topaz appeared as accessory phase in the experiment products. In runs with solution of 30 wt.% H_3BO_3 + 4 wt.% NH_4F pure Fe-bearing tourmaline crystals with no other mineral phases were obtained in the experiment products (Fig. 1).

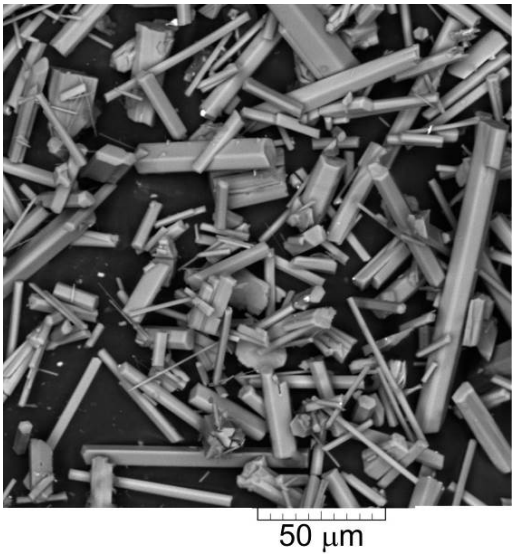

Figure 1. SEM image of fine-crystalline Fe-bearing tourmaline.

Optimal conditions and solution composition of fine-crystalline mass crystallization of tourmaline were established. Such kind of a fine-crystalline material can be used for developing methods for production of piezoelectric ceramics and textures.

This work was supported by RFBR (grant No 12-05-31030-mol_a) and Ministry of education and science of Russian Federation (Agreement No.8378).

References:

[1] London D., Ertl A., Hughes J.M., Morgan G.B. VI, Fritz E.A. & Harms B.S. (2006): Synthetic Ag-rich tourmaline: structure and chemistry. Am. Mineral. 91, 680-684

[2] London, D. (2011) Experimental synthesis and stability of tourmaline: a historical overview. Can. Mineral. 49, 117–136.

[3] Ertl A., Giester G, Thomas Ludwig, Hans-Peter Meyer, and George R. Rossman (2012) Synthetic B-rich olenite: Correlations of single-crystal structural data. Am. Mineral. 97, 1591-1597.

[4] Setkova T.V., Shapovalov Yu.B., Balitsky V.S. (2006) Experimental study of stability and opportunities of tourmaline synthesis in hydrothermal solutions. Abst. 11th EMPG. Bristol, UK. P. 67.

[5] Setkova T., Shapovalov, Yu., Balitsky, V. (2009) Experimental study of stability and crystallization peculiarities of tourmaline in hydrothermal conditions. Rep. RAS. 424, 1, 94-97.

[6] T. Setkova, Yu. Shapovalov, V. Balitsky. (2011) Growth of tourmaline single crystals containing transition metal elements in hydrothermal solutions. J. Crystal Growth, 318, 904-907.

SYNTHESIS AND CRYSTAL STRUCTURES OF NOVEL MICROPOROUS COPPER RUBIDIUM DIPHOSPHATES

***Shvanskaya L.V.*, Yakubovich O.V., Urusov V.S.**

Dept. of Geology, Moscow State University, Moscow, Russia,
lshvanskaya@mail.ru

Our day search of new microporous materials follows direction of getting stable phases based on open framework crystal structures. These kind of zeolite-like materials with transition metal atoms are promising not only as catalysts, sorbents, molecular sieves etc., but seem being technologically perspective due to their magnetic, electrochemical or photoluminescence properties **[1, 2]**.

Single crystals of the $Rb_2CuP_2O_7$(I) and $Rb_2Cu_3(P_2O_7)_2$(II) were obtained by solid-state/flux crystallization method. A powder mixture of Rb_2CO_3, CuO and $(NH_4)_2HPO_4$ in a molar ratio corresponding to Rb:Cu:P=2:1:2 (for I) and 4:3:6 (for II) was ground and heated progressively to 650°/750°C, isothermed for 48 hour and then slowly cooled. Transparent, blue, isometric (I) and platelet-like (II) crystals up to 0.1 mm in size were isolated mechanically or separated from the matrix flux by washing. The presence of Rb, Cu, P and O in the samples was confirmed with semi quantitative X-ray spectral analysis (a Jeol JSM-6480LV microscope equipped with an INCA-Wave 500 energy dispersive X-ray spectrometer).

The unit cell parameters and intensity data were measured on a four-circle Xcalibur-S diffractometer equipped with CCD detector, using Mo Kα (λ=0.71073Å) radiation (graphite monochromator) at 298 K. Collected reflection intensities were corrected for the Lorentz and polarization factors. Empirical correction for absorption was applied on the basis of the crystal shape. All calculations were performed with the SHELX program package **[3]**. Atomic scattering curves and anomalous dispersion corrections were taken from **[4]**. Selected crystallographic characteristics and structure refinement details are presented in Table 1.

Table 1. Crystal data for β-$Rb_2CuP_2O_7$ and $Rb_2Cu_3(P_2O_7)_2$

Compound	β-$Rb_2CuP_2O_7$	$Rb_2Cu_3(P_2O_7)_2$
Formula mass [g mol-1]	408.42	709.44
Symmetry, space group, Z	Monoclinic, *Cc*, 4	Monoclinic, $P2_1/c$, 2
Cell parameters [Å]	a = 7.0020(10)	a = 7.7119(2)
	b = 12.751(3)	b = 10.5245(2)
	c = 9.773(2)	c = 7.8034(2)
	β = 110.93(3)	β = 103.862(2)
Cell volume [Å]	815.0(3)	614.91(3)
D_x [g/sm^3]	3.329	3.832
μ [mm^{-1}]	14.934	13.607
h, k, l ranges	$-9 \le h \le 9$;	$-9 \le h \le 10$;
	$-17 \le k \le 17$;	$-13 \le k \le 13$;
	$-13 \le l \le 13$	$-10 \le l \le 10$
Number of reflections; measured / independent (N1) / with $I>2\sigma(I)$ (N2)	10989/2380/1902	11697/1403/1361
Number of parameters	109	106
R_1/wR_2 for N1	0.0490/0.0449	0.0319/0.0698
R_1/wR_2 for N2	0.0347/0.0433	0.0307/0.0693
S	0.865	1.138
Flack parameter	0.044(8)	-

The XRD investigation of two new copper rubidium diphosphates has shown that compound (I) represents a new modification of the $Rb_2CuP_2O_7$ with layered structure **[5]**. The second phase (II) is isotypic to the $Cs_2Cu_3(P_2O_7)_2$ **[6]**.

Their crystal structures (fig. 1) are based on mixed microporous three-dimensional frameworks built from diphosphate $[P_2O_7]$ groups and $[CuO_5]$ tetragonal pyramids (for I) and the triplets of highly distorted $[CuO_6]$ octahedra sharing edges (for II). The framework of (I) has a system of intersecting open channels, running along [001], [101], [110], and [100] directions. The 3D framework of (II) is denser and characterizes by one dimensional channels running along [001] direction. The rubidium ions positioned in the channels show CN8 (I) and CN 10 (II).

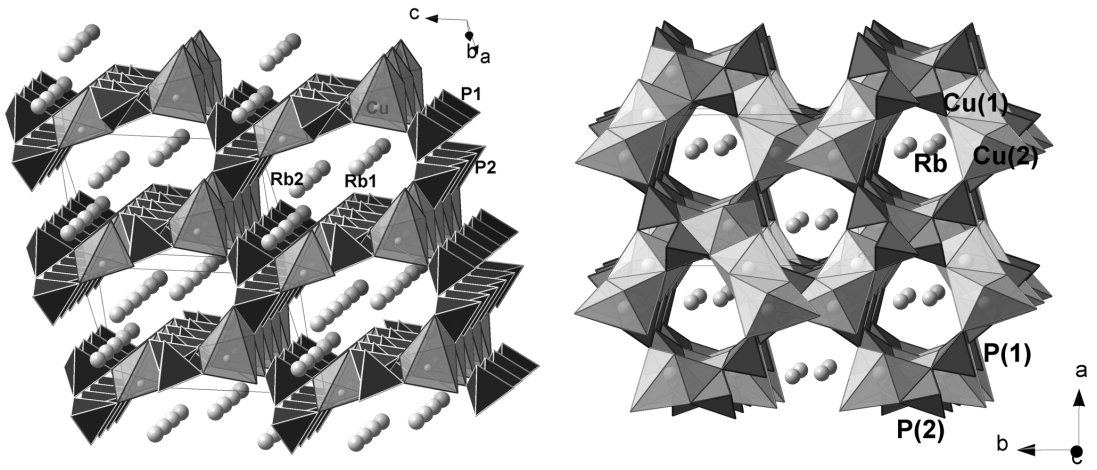

Figure 1. Crystal structures of β-$Rb_2CuP_2O_7$(left) and $Rb_2Cu_3(P_2O_7)_2$ (right): 3D copper-phosphorus framework with open channels occupied by rubidium cations.

Thus, two new copper rubidium diphosphates, $Rb_2CuP_2O_7$(I) and $Rb_2Cu_3(P_2O_7)_2$(II), have been obtained using solid-state and flux crystallization methods in the system Rb-Cu-P-O at 650^o and 750^o C, respectively. The system of open channels in the crystal structure of (I) is suitable for possible migration of alkali metal cations, what in combination of the acentric character of the structure assumes its valuable technological characteristics.

We are grateful to V.V. Mal'tsev for his help with the solid-phase synthesis, N.V. Zubkova and A.G. Ivanova for the help with the X-ray diffraction experiment, E.V.Guseva and V.O. Yapaskurt for the microprobe analysis of the crystals.

References:

[1] P. Barpanda, S. Nishimura, A. Yamada, Adv. Energy Mater. 2 (2012) 841-859.
[2] J. A. Armstrong, E. R. Williams, M. T. Weller, J. Am. Chem. Soc. 133 (2011) 8252-8263.
[3] G. M. Sheldrick, Acta Crystallogr., Sect. A. 64 (2008) 112–122
[4] E. Prince, International Tables for Crystallography, IUCr, 2004, Tables 4.2.6.8; 6.1.14.
[5] A.P. Chernyatieva, S.V. Krivovichev, and D.V. Spiridonova, Book of Abstracts V International Conference"Inorganic Materials" Dresden: Elsevier (2008) 3-143.
[6] K. G. S. Ranmohotti, X. Mo, M. K. Smith, S.-J. Hwu, Inorg. Chem. 45 (2006) 3665–3670.

INVESTIGATION OF PHASE EQUILIBRIA AND GROWTH OF BBO (β–BaB_2O_4) CRYSTALS IN Li, Ba // BO_2, F TERNARY RECIPROCAL SYSTEM

Simonova E.A. [1], ***Kononova N.G.*** [1], ***Fedorov P.P.*** [2], ***Kokh A.E.*** [1], ***Shevchenko V.S.*** [1]

[1] *V.S. Sobolev Institute of Geology and Mineralogy, SB RAS, Novosibirsk, Russia*
[2] *General Physics Institute, RAS, Moscow, Russia*
simonovakatherine1986@gmail.com

Introduction. Barium borate β–BaB_2O_4 (BBO) single crystals are widely used for laser frequency conversion in the UV / visible range. Due to the phase transition at 925°C, β–BaB_2O_4 crystals are commonly grown from high–temperature solutions by the top–seeded solution growth (TSSG) technique **[1]**.

In this work phase equilibria in the Li, Ba // BO_2, F ternary reciprocal system have been studied. LiF is considered the promising solvent for β–BaB_2O_4 crystal growth due to the essential viscosity reduction. Also, lithium ions should not enter isomorphically into the structure of barium borate because of crystallochemical characteristics. In the mentioned reciprocal system only boundary sections BaB_2O_4–$LiBO_2$ **[2]**, BaB_2O_4–BaF_2 **[3]**, BaF_2–LiF **[4]**, $LiBO_2$–LiF **[5]** have been investigated so far. The BaB_2O_4–LiF section was first studied by Bykov **[6]**.

Experimental procedures. We investigated phase equilibria in the Li, Ba // BO_2, F ternary reciprocal system using the modified visual polythermal analysis (VPA), differential thermal analysis (DTA), methods of spontaneous crystallization on a platinum loop, solid–state synthesis and X–ray powder diffraction analysis.

VPA allows one to determine the liquidus temperature. Experiments were carried out in a heating furnace with a highly symmetrical and stable heat field. A platinum crucible 40 mm in diameter and 60 mm in height filled with 20 g of melt was used. Ready melt was overheated and held for homogenization. Chips of spontaneous crystals, compositionally corresponding to the crystallization field of the given phase, were placed on the melt surface. If the melt temperature was above liquidus, chips dissolved, otherwise, they started growing. The temperature at which chips lay on the melt surface for several hours neither dissolving nor growing was considered as the equilibrium temperature.

For spontaneous crystallization a platinum rod with a loop was placed in the center of the melt surface. The temperature was decreased in steps (5 °C/h). Beginning from the moment when spontaneous crystals were found, the melt was cooled at 2 °C/day to form quality spontaneous crystals.

Solid–synthesized samples were prepared by stepped annealing of the mixture of starting reagents in a platinum crucible with periodic grinding. The proportion and amount of the reagents corresponded to the calculated composition and weight (5 g) of the final product.

All samples investigated by thermal analysis (DTA) were prepared through the solid–phase synthesis. The heating rate was 10 °C/min; the maximum heating temperature depends on the composition under investigation and was not higher than 1000 °C.

Phase equilibria in the Li, Ba // BO_2, F system. Boundary systems. The compounds BaB_2O_4, BaF_2, LiF, $LiBO_2$ melt at 1100, 1373, 870 and 845 °C, respectively. The eutectic coordinates for the BaB_2O_4–BaF_2 system *e1* are 760 °C, 41 mol % BaB_2O_4, 59 mol % BaF_2, for the LiF–BaF_2 system *e2* 827 °C, 64 mol % BaF_2, 36 mol % LiF, for the $LiBO_2$–LiF system *e3* 725 °C, 59 mol % $LiBO_2$, 41 mol % LiF, for the BaB_2O_4– $LiBO_2$ system *e4* 797 °C, 79 mol % $Li_2B_2O_4$, 21 mol % BaB_2O_4.

Diagonal section. The BaB_2O_4–LiF diagonal section in Li, Ba // BO_2, F ternary reciprocal system was studied. It has been found that BaB_2O_4–LiF system is not quasi–binary. The liquidus of the BaB_2O_4–$(LiF)_2$ section consists of the primary crystallization fields of the BaB_2O_4,

$Li_2Ba_4B_{10}O_{20}$ and LiF phases. The concentration interval from 82–75 mol % and 75–57mol % BaB_2O_4 corresponds to the primary crystallization of β–BaB_2O_4 and $Li_2Ba_4B_{10}O_{20}$ respectively.

BaB_2O_4 crystal growth in the BaB_2O_4–LiF section. The β–BaB_2O_4 crystal was grown by the top–seeded solution growth (TSSG) technique in a precise furnace with a heat field of 3–fold axis symmetry *L3* **[7]**. A high–temperature solution of 1 kg 65 mol % BaB_2O_4 – 35 mol. % LiF composition was melted in a platinum crucible (90 mm in diameter and 95 mm in height). A crystal was grown on a 5 × 5 mm^2 seed oriented along the optical axis. The growth procedure consisted in searching for equilibrium temperature through the seed touching the central area of the high–temperature solution. The cooling rate was 0.2–0.3 °C/day. Total temperature decrease was only 21.5 °C due to the very narrow crystallization area, but the yield coefficient was as high as 7.44 g/(kg·°C). The crystal was 60 mm in diameter and 25 mm in height, its weight was 160 g.

There are four invariant points in Li, Ba // BO_2, F ternary reciprocal system (except boundary sections). The BaB_2O_4–$LiBaF_3$, BaB_2O_4–(0.6 BaF_2–0.4 LiF), BaB_2O_4–(0.7 BaF_2–0.3 LiF) systems has been studied in detail and much broader crystallization area of BaB_2O_4 was found in Li, Ba // BO_2, F system. We suppose that the use of various compositions in this system is of great interest for the growth of large β–BaB_2O_4 crystals.

References:

[1] Fedorov P.P., Kokh A.E. and Kononova N.G. // Russ.Chem. Rev. 2002. V. 71. № 8. P. 651–671.

[2] Shilie Pan, Jared P. Smit, Courtney H. Lanier, Michael R. Marvel, Laurence D. Marks, and Kenneth R. Poeppelmeier. Optical floating zone growth of β–BaB_2O_4 from a $LiBa_2B_5O_{10}$–based solvent// Crystal growth & design. 2007. V. 7. № 8. pp. 1561–1564.

[3] Bekker T. B., Fedorov P. P., Kokh A. E. Phase formation in the BaB_2O_4–BaF_2 system // Crystallography Reports. 2012. V. 57. № 4. pp. 574–578.

[4] Bychkova N.A., Bergman A.G. – ZHOKH, 1956, V.26, P.639 (in Russian).

[5] Petit M.G., Jaeger M. – «C. r. Acad. Sci.», 1957, V. 244, № 13, P. 1734.

[6] Bykov A.B., Dozmarov V.V. Growth of β–BaB_2O_4 monocrystals from fluorine containing solution–melt // Crystallography. 1994. V. 39. №4. P. 720–724 (in Russian).

[7] Kokh A.E., Kononova N.G., Mokruchnikov P.W., J. Crystal Growth 216 (2000) 369.

GEOMETRICAL MODELING OF CRYSTAL REGENERATION

Thomas V.G. [1], ***Gavryushkin P. N.*** [1,2], ***and Fursenko D. A.*** [1]

[1] *V.S. Sobolev Institute of Geology and Mineralogy SB RAS, Novosibirsk, Russia,*
[**] *Novosibirsk State University, Novosibirsk, Russia*
vithomas@yandex.ru

The problems of crystal regeneration processes and the associated phenomena have been attracting attention of the crystallographers and other specialists in the field of crystal growth for over a century. However, despite the evident progress in this area (see **[1]** for the detailed discussion of findings made by early 80's), there are a number of relevant questions left out of consideration, including the following:

1. What could explain specific, macroscopically rough structure of the regeneration surfaces (i.e. surfaces that are not parallel to any other crystal faces under given conditions) of a crystal?
2. What is the nature of small faces that form subindividuals (i.e. individual convex areas) on the regeneration surface? Why are these often curved?
3. What are the driving forces of the geometrical competition between subindividuals on the regeneration surface – the process that is certain to be taking place during the regeneration surface growth?
4. What would explain changes in the advancement velocity of the regeneration surface front, given that the growing rate of the real faces remains constant?
5. Would it be possible for a face that appears on a curved smooth surface during its regeneration to grow faster than the contacting regeneration surface?

In order to answer these and other questions, we studied kinematics of the growth of the surfaces (both regeneration as well as parallel to possible faces) in potasium alum crystals [**2**]. Findings of this investigation suggested a model [**3**], according to which the microscopical protrusions and cavities of a macroscopically even surface are the genetic predecessors of the subindividuals. The model, however, does not give explanations for the appearance of these surface elements, which could be due to original physical treatment of a crystal (e.g., sawing and polishing), initial decoration of the surface defects, fluctuational perturbations on the growing surface, etc. Proposed model considers the regeneration process to begin with an immediate covering of each of the initial protrusions by a full set of possible faces. Subsequently, these faces of a newly created surface grow in parallel to themselves with a constant velocity, with rates equal to those observed under the experimental conditions for large seeds .

According to the model, changes in growing speed of the regeneration surface during its evolution, as well as decrease in the number of subindividuals that form the growing surface could be accounted for by the influence of two types of geometrical competition. The first one is the process of competition between faces within subindividuals; it consists in absorption of quickly growing faces by those growing more slowly. The second type is a competition between subindividuals; it leads to absorption of a subindividual by adjacent subindividuals. Driving forces for these competitions are the differences in size and curvatures of the surface roughnesses. These differences also account for variability in the sets of possible faces for each protrusion, which subsequently leads to the differences in the velocity of growth observed for the subindividuals.

The quantitative representation of the model was given in 2D approximation, i.e. within a single crystallographic zone. The initial surface roughnesses were approximated by contacting arcs of circles of a random radius R_i evenly distributed on the $[R_{\min}, R_{\max}]$ interval. The input parameters of the quantitative model include experimentally measured growing rates of the faces of possible crystallographic forms, and the estimates for $R_{\min}$ and $R_{\max}$. The latter have physical meaning and correlate with vertical (Rz) and horizontal (Sm) characteristics of the surface

roughnesses: $\mathrm{Rz} \equiv R_{\min}$, $\mathrm{Sm} = 2\sqrt{R_{\min} R_{\max}}$. Therefore, the real values for these estimates can also be checked experimentally. The comparison between numerical and real growth experiments has shown that even a 2D approximation of the model can describe the ongoing regeneration processes with reasonable quantitative agreement.

Applying this model to the problem of regenerating spheres evolution, allowed us to explain the appearance of flat round areas (germs of flat faces) on the regenerating surface of a sphere, which at first continue to develop tangentially, then begin to decrease in size, and eventually become completely absorbed by the adjacent regenerating surface. This was the same effect as we have observed in the regenerating crystals of potassium alum [**2**]. Interestingly, this effect has been observed by the founder of the sphere regeneration method, D. N. Artemiev [**4**]; this result, however, was later forgotten. The reason for this effect is the decrease of the rates of the regeneration surface growth due to geometrical competition process. The face continues to develop tangentially as long as its constant growing velocity is lower than the one of the adjacent regenerating surface (See Figure1). When the latter becomes lower than the face growing speed (time *t* on Figure 1), the face starts to diminish in size – up until it is completely absorbed by the regeneration surface. Numerical 2D modelling has shown that, apart from cube and octahedron, this process is typical for the faces of the absolute majority of crystallographic forms in potassium alum crystal spheres.

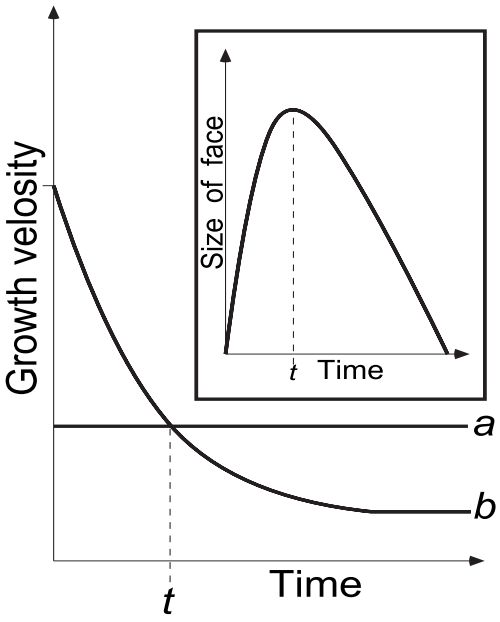

Figure 1. Illustration of the causes for face absorption by adjacent regeneration surface (see explanations in the text). *a* – growth velocity of a flat face, *b* – growth velocity of a regeneration surface, contacting with the flat face.

Furthermore, 2D modelling of sphere regeneration allowed us to explain the appearance of unusual morphological forms that resemble curved ridges [**2**], which appear as a result of an unsmooth joining of two growing fronts of the regenerated surface around the face after its absorption.

We are grateful to V.A. Kosyakov (Institute of Inorganic Chemistry, Siberian Branch, Russian Academy of Sciences, Novosibirsk, Russia) and to Yu.N. Pal'yanov, S.Z. Smirnov, and A.F. Khokhryakov (Institute of Geology and Mineralogy, Siberian Branch, Russian Academy of Sciences, Novosibirsk, Russia) for our fruitful discussions. This study was supported by the OOO Tairus (Novosibirsk, Russia) and RFBR grant № 13-05-00471. Project of IGM BR RUS №VII.66.1.2.

References:

[1] A. M. Askhabov. Regeneration of Crystals (Nauka, Moscow, 1979) [in Russian].
[2] P. N. Gavryushkin and V. G. Thomas. Crystallogr. Rep. 54 (2), pp.334-341 (2009).
[3] V. G. Thomas *et al*. Crystallogr. Rep. 57 (6), pp.848-859 (2012).
[4] D.N. Artemiev. The Method of Crystallization of Spheres ... (Petrograd, 1914) [in Russian].

SYNTHESIS AND THE STUDY OF GROWING CONDITIONS OF Co-BEARING TOURMALINE IN BORON -CHLORIDE HYDROTHERMAL SOLUTIONS

***Vereshchagin O.S.*[1], *Setkova T.V.*[2]**

[1] *Crystallography Department, Saint-Petersburg State University, Saint-Petersburg, Russia*
[2] *Institute of Experimental Mineralogy RAS, Chernogolovka, Russia*
oleg-vereschagin@yandex.ru

Tourmaline is the important borosilicate mineral with general formulae $X_{0-1}Y_3Z_6(T_6O_{18})(BO_3)_3V_3W$ **[1]**, where X=Ca, Na, K, [] (vacancy); Y=Li, Mg, Fe, Al, Co; Z=Mg, Al, Fe, Cr; T=Si, Al, B; V=OH, O;W=OH, F, O. The phenomenon of pyro-and piezoelectricity was first discovered and described in this mineral. Currently tourmaline found its application in various fields of science and technology: it used for producing new ceramics, which effects on water to be endowed with surface activity **[2]**, antibacterial composite materials **[3]**, synthetic textile fibers, etc. **[4]**. The goal of this work was to synthesize of Co-bearing tourmaline with various concentrations of cobalt and evaluate its stability depending on the crystallization conditions. Previously, it has been found that Co-containing tourmaline has the highest growth rate **[5]**. Statement of the problem also is explained by the low prevalence of Co-containing tourmaline in nature, as well as the fact that the natural samples are solid solutions of complex composition.

Synthesis experiments were carried out by the two techniques and in two temperature ranges. The first method was based on a standard hydrothermal method. Synthesis was carried out in an autoclave of 20 cm^3, made of a titanium alloy at a temperature of 400-450°C and a pressure of 100 MPa in the temperature gradient conditions **[6]**. The second series of experiments was carried out in gold capsules of 3 cm^3 in volume at a temperature of 650°C (no temperature gradient) and a pressure of 100 MPa by chamber method of Goerne **[7]** (cold-seal hydrothermal techniques). This method was based on the concentration gradient of solution components, which is created in a growth chamber. The temperature was measured with an accuracy of ± 3 º C. The pressure was managed by the filling factor of the autoclave and the capsule. The solutions of the chemical reagents H_3BO_3 (15 wt.% solution), NaCl (10 wt.% solution) and $CoCl_2 \cdot 6H_2O$ (5-60 wt.% solution) were used. The plate crystals of elbaite from Malhanskoe field (Baikal) were used as a seed; they were cut perpendicular to the optical axis. The seeds were suspended in top and bottom areas the autoclave on metal frames, in one vial was placed in a growth chamber primer. The charge consisting of a mixture of quartz crystals and fragments of corundum, placed at the bottom of the autoclave. Duration runs was from 10 to 30 days.

As a result of experimental studies the direct correlation between the content of cobalt in the overgrown layer of Co-bearing tourmaline and the initial concentration of cobalt chloride in the solution was found. Under otherwise equal (PT conditions C_{H3BO3}, C_{NaCl}) the growth on the seed, which was formed in 5 wt.% solution of $CoCl_2$ was of 0.2 mm thickness with the average cobalt content of 8.5 wt.%, in 10 wt. % solution of $CoCl_2$ - 0.35 mm and 9 wt. % CoO, in 20 wt. % solution of $CoCl_2$ - 1 mm and 12 wt. % CoO, in 30 wt. % solution of $CoCl_2$ - 1 mm and 13.5 wt. % CoO (Fig. 1). The average value of the content of cobalt in the overgrown layer for analysis and plotting were calculated because it is not distributed uniformly (the concentration decreases from the border to the periphery of the seed layer). Coloring of tourmaline crystals depends on the content of cobalt. The intensity of color is filled (from pale to intense crimson-burgundy) with increasing cobalt content.

The main purpose of this phase of work, in addition to producing of crystals of tourmaline containing various concentrations of cobalt, was to obtain single crystals of tourmaline with the highest possible content of the element. However, solutions with a concentration of crystalline cobalt chloride more than 40 wt. % $CoCl_2$ at temperatures 400/450°C were not succeed: there were no overgrowth on a seed; instead, there were faceted rhombic crystals formed boracite

cobalt ($Co_6B_{14}O_{26}Cl_2$) on the surface of the seed and the charge. The formation of cobalt boracite occurs at higher concentrations of cobalt chloride solution (60 wt. % or higher) in experiments at 650°C. It was observed earlier by IE Voskresenskaya **[8]** that tourmaline crystallized simultaneously with boracites at 750°C and a pressure of 200 MPa in solutions with a concentration of 80 wt.% of crystalline chlorides of 3d elements. This indicates a shift in the field of education boracite to the higher concentration of cobalt chloride in the initial solution with increasing temperature.

The overgrowth observed with only one hand of monohedron, when tourmaline grown in autoclaves (T = 400/450°C). The overgrowth of tourmaline observed with both faces of monohedron and on a hexagonal prism in synthesis in golden capsules (T = 650°C) (Fig. 2). Thus, increasing the crystallization temperature of tourmaline increases the growth rate of the positive and negative sides of monohedron and hexagonal prism.

This work was supported by the Russian Foundation for Basic Research (projects 06–05–64900–a, 09-05-00769-a and 12-05-31030-mol-a).

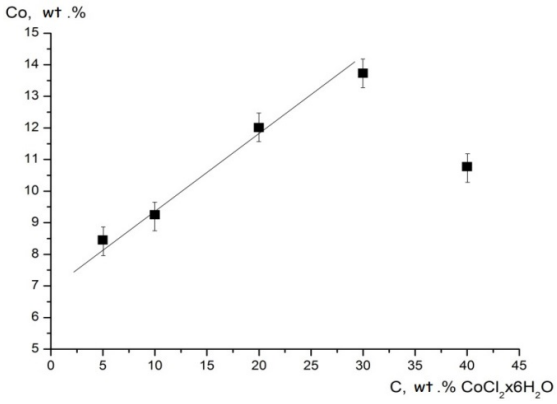

Figure 1. Dependence of the content of cobalt in the overgrown layer of Co-tourmaline on the initial concentration of cobalt chloride in the solution.

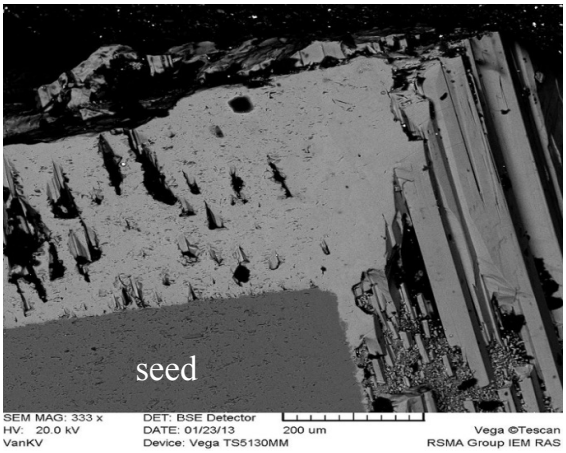

Figure 2. Overgrowth of Co-tourmaline on monohedron face and on face of hexagonal prism.

References:

[1] Henry, D. J., Dutrow, B.L. // Am. Mineral. 2001. 86. 1130.
[2] Nakamura, T.& Kubo, T. / Ferroelectrics, 1992, 137, 13-31.
[3] Ruan, D. et al. // J. of Polymer Science: Part B, 2004, 42, 367–373.
[4] Ying Wang et al.// Colloid Polym Sci, 2006, 284: 1465–1470.
[5] Setkova, T., Shapovalov, Yu., Balitsk,y V. // J. Crystal Growth, 2011. V.318, P. 904–907.
[6] Setkova, T., Shapovalov, Yu., Balitsky, V. // Rep. RAS, 2009, 424, 1, 94-97.
[7] Von Goerne, G., Franz, G., Wirth, R. // Europ. J. Miner. 1999. V. 11. P. 1061.
[8] Voskresenskaya, I. E., Barsukova, M. L. In Hydrothermal synthesis of crystals. Nauka, 1968.

A SECTOR-ZONE IN SODIUM CHLORATE-BROMATE CRYSTALS GROWN IN AREA OF KINETIC ANOMALIES

Vikharev A.E.*, *Bocharov S.N.
Saint-Petersburg State University, Saint-Petersburg, Russia
alexvikev@gmail.com

In geology and geochemistry zone and sectorial distribution of a chemical composition in bulk of a crystal are using for reconstruction of conditions of mineral formation. At mineralogical reconstructions it is supposed that dependence of growth rate on temperature is described by simple dependences linear or exponential. Detailed kinetic measurements show that growth rate in dependence on temperature characterized by strongly nonmonotonous changes **[1-4]**. Such phenomenon is known as "kinetic anomalies". Kinetic anomalies investigation of mixed crystal growth showed that their chemical composition also changes nonmonotonical with temperature **[5]**. It was supposed that such nonmonotonic changes of chemical composition will result in zone or sector-zone formation in bulk of crystal **[6]**.

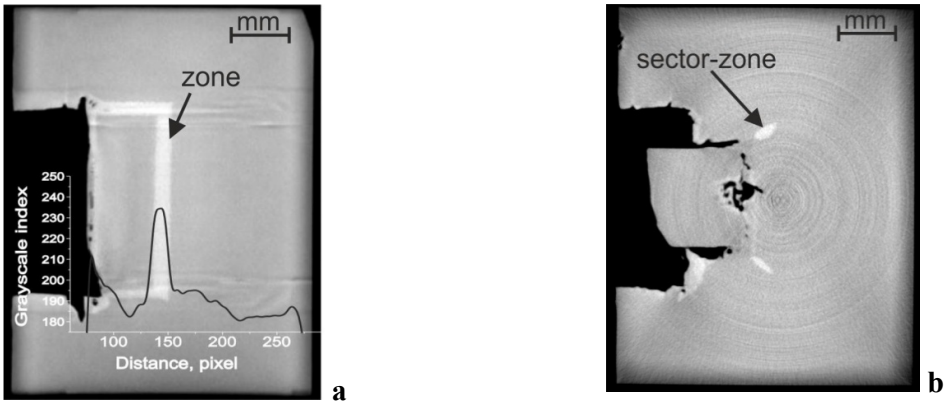

Figure 1. Microtomography slices for $Na(Cl,Br)O_3$ crystal grown in kinetic anomalies areas; cursors show sector-zone (b) and zone (a) which is saturated by sodium bromate.

For experimental check of this assumption we used sodium chlorate-bromate model system. This system characterized by contrast physical properties (density – 2.49, 3.49 g/cm^2, unit cell - 6.575 Å (ICDD PDF 5610), 6.706 Å (ICDD PDF 430647) for sodium chlorate and bromate respectively) that give us possibility to find chemical composition changes even at low concentration of bromate compound in grown crystal. Crystals for investigation have been received by three different methods. The first one (combined method) is combination of temperature gradient (temperature decrease from bottom to top of crystallizer) and temperature decrease methods. Other two is spontaneous crystallization and constant supercooling method (microcrystallization). Last two of them were used for comparison of chemical composition distribution at crystals grown in different conditions.

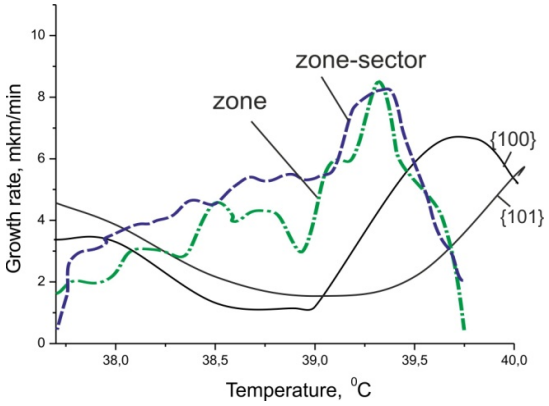

Figure 2. Comparison of grayscale index profile (the dotted line) with growth rate (the solid line).

Received crystals have been investigated by x-ray microtomography method. This method is based on different absorption of x-ray beam by parts of different chemical composition. That gives us possibility to reconstruct distribution of X-Ray density at sample volume by recalculation of absorption coefficient range to range of grayscale index.

All crystals grown by combined method show zone or sector-zone distribution of grayscale index. It is clearly seen on figure 1(a) where zone correlate to maxima on grayscale index profile. The same distribution exists for sector-zone figure 1(b).

The crystals grown by spontaneous crystallization and microcrystallization methods show random changes in chemical composition.

Received grayscale index for zone and sector-zone were compared with growth rate cube and rhombic dodecahedron faces (fig. 2). This comparison shows that growth rate {101} lower than {100} in this temperature area (39-40 ^{0}C) thus rhombic dodecahedron faces are shown in crystal. From this point {101} faces can form like sector-zone as we can see at figure 1 (b) and sector-zone can formed with temperature monotonic decrease as well as zone.

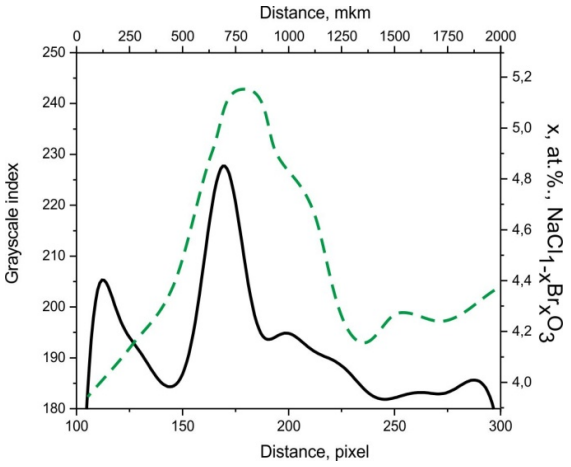

Figure 3. Comparison of theoretical changes of chemical composition (the dotted line) with grayscale index profile (the solid line).

Received profiles of grayscale index distribution were compared with theoretical chemical composition changes (fig. 3). This comparison shows that grayscale profile and line of theoretical changes of composition are matched by means of extrema amount and their localization in bulk of crystal. On figure 3 there is a match on 750 mkm (upper scale), 1000 mkm (wing of peak) and around 1500 mkm. Such matches are observed for all crystal grown by combined method. In the same time peaks intensities differ in case where more than one zone.

Received data show that chemical composition can change nonmonotonic with zone and sector-zone formation even in case of monotonic temperature decrease at growth process due to kinetic anomalies influence.

The study was partially supported by Russian Foundation for Basic Research, project No. 12-05-00876-a and 13-05-12053-ofi_m.

References:

[1] V. V. Sipyagin, “Some anomalies of NaClO3 и KClO3 faces growth rate in dependence on temperature at constant supersaturation”, Kristallografiya, 12 (4), 678, 1967. [Sov. Phys. Crystallogr. 12, 590 (1967)].

[2] V.V. Sipyagin, A.A. Chernov, “Anomalies of crystal growth rate from aqueous solution of KNO3, NaNO2, NaNO3, NaClO4 and Seignette's salt”, Kristallografiya, 17 (5), 1003, 1972. [Sov. Phys. Crystallogr. 17, 881 (1972)].

[3] A.A. Chernov, V.V. Sipyagin, Current Topics in Materials Science, 5, 281, 1980.

[4] S.N. Bocharov, A.E. Glikin, “Kinetic anomalies of crystal growth: extension of methodical approaches and interpretations”, Crystallography Reports, 1, 147–153, 2008.

[5] Bocharov S. N., Gille P., Glikin A. E.. Kinetic anomalies of mixed crystal growth and their effect on the crystal isomorphic composition // Cryst. Res. Technol. 2009. V. 44. N. 1. P. 13.

[6] S.N. Bocharov, “Anomalies of growth rate and variations of isomorphic composition on the example of NaClO3-NaBrO3 model system”,Proceedings of RMS, 3, 122-131, 2010. [in Russian].

THE INFLUENCE OF GLASS OBTAINING ATMOSPHERE COMPOSITION ON NUCLEATION AND GROWS OF THE SPHERULITES IN $SrO \cdot 2B_2O_3$ GLASSES

Zaitsev A.I., Cherepakhin A.V., Zamkov A.V.

L.V.Kirensky Institute of Physics SB RAS, Krasnoyarsk, Russia
az@iph.krasn.ru

Strontium diborate composition falls in the glass formation range of $SrO \cdot 2B_2O_3$ system. The process of crystallization of this glass is quite complicated, with the possibility of simultaneous and independent appearance of up to four different crystalline compositions on the glass surface: stable crystals of α-SrB_4O_7 and metastable crystalline forms – crystals of β-SrB_4O_7, $Sr_4B_{14}O_{25}$, and spherulites, presumably a mixture of crystalline phases of unknown composition **[1]**. In all these cases, the nucleation is heterogeneous, which determines not only the strong effect that the surface state has on the nucleation rate, but also the type of crystals appearing on the surface in a certain area. As it was previously shown **[1]**, only spherulites form on the walls of the platinum and glass carbon crucibles during all crystallization process.

The influence of glass obtaining atmosphere composition on nucleation rate (V_{nucl}) and growth rate (V_g) of the spherulites in the platinum crucible has been studied. To obtain the SBO glasses, transparent α-SBO single crystals without cracks and inclusions have been used.

The spherulites were formed on interface glass – platinum only.

In the glass obtained in pure Ar atmosphere V_{nucl} of spherulites (normalized by area and time of annealing) increases with the annealing temperature (T_{ann}), reaching a maximum at 665 ^oC, and then decreases as the temperature is further raised. If glass is obtained in the atmosphere with addition of 20% O_2, V_{nucl} of spherulites was found to be two orders of magnitude lower, while position of the V_{nucl} maximum remains at the same temperature.

Measurements of nucleation rate vs. O_2 concentration in the glass obtaining atmosphere were conducted at T_{ann}=665^oC. Measured dependence is shown in Figure 1. At low O_2 concentrations (about 0.3%) V_{nucl} decreases by an order of magnitude and reaches minimum around 2.5% V_{nucl}. Then V_{nucl} slowly increases until O_2 concentration hits 7.5%, and smoothly drops to near zero at 20% O_2.

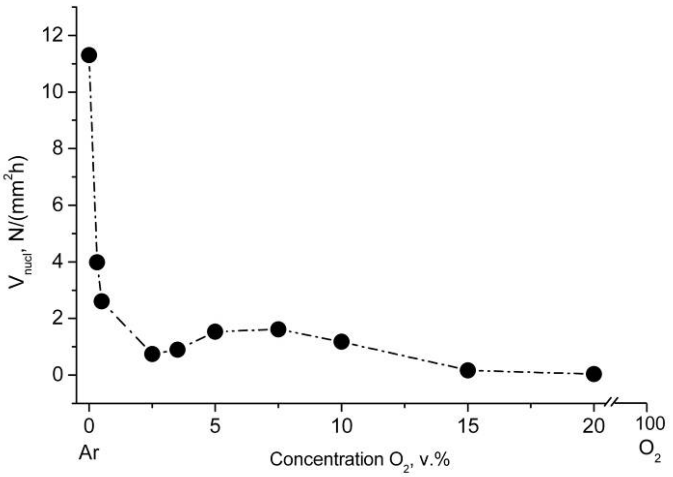

Figure 1. Dependence of the spherulites V_{nucl} on oxygen concentration in the glass obtaining atmosphere.

Measurements of spherulites V_g vs. temperature in the glass obtained in the pure Ar atmosphere and in the atmosphere with O_2 admixtures (up to 80 vol. %) have been made. The dependence of spherulites V_g in the pure Ar is submitted to Arrhenius law (Fig. 2). Using the data in figure 2, growth activation energy of spherulites in this case was calculated to be around 640 kJ/mol. The spherulites V_g shows a weak dependence on oxygen content in the glass preparing atmosphere.

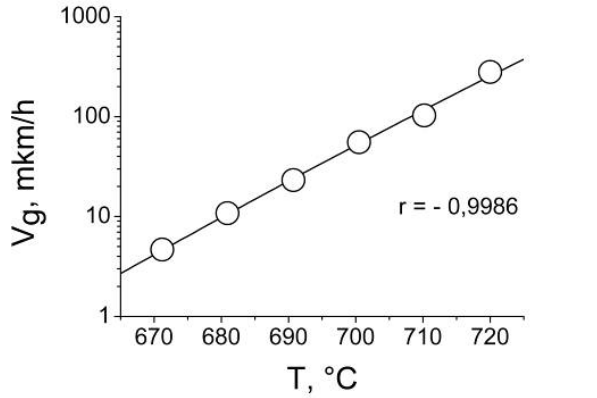

Figure 2. Dependence of spherulites growth rate V_g on the temperature with pure Ar as the glass obtaining atmosphere.

This study is supported by SB RAS Project 103, by Grant of the President of the Russian Federation for the support of leading scientific schools SS-4828.2012.2 and by RFBR Grant 11-02-00596-a.

References:

[1] Zaitsev A.I., Zamkov A.V., Koroleva N.S., Molokeev M.S., Cherepakhin A.V. Phase formation upon crystallization of $SrO{\cdot}2B_2O_3$ glasses // Crystallography Reports. - 2011. - V. 56, No. 1. - pp. 44–51.

THE ROLE OF COMPLEXING AND CVT-REACTIONS IN THE MATURATION OF SULFIDE MINERALS IN THE NATURAL-LIKE CONDITIONS AT MODERATE PRESSURES

Zavrazhnov A.Yu., Kosyakov A.V., Naumov A.V., Sergeeva A.V.

Voronezh State University, Voronezh, Russia
alzavr08@rambler.ru

In the present paper the different ways of the maturation of some binary sulfide phases (minerals) – pyrite, marcasite, vaesite and chalcocite – at low-temperature hydrothermal and low-pressure chemical vapor-transporting (CVT) synthesis are under consideration. It is shown that low-temperature hydrothermal synthesis of these sulfides proceeds through the stages of formation and destruction of the dissolved complex compounds. As the most important ligands we consider polytionide ($S_xO_6^{2-}$), cyanide (CN^-), thiocyanide(NCS^-) ions as well as thiocarbamide ($SC(NH_2)_2$). A comparison between the synthesis of sulfides using the technique of the pyrolysis metal complexes (for example, thiocarbamide compounds) and the mineral maturation in natural hydrothermal conditions is discussed **[1]**. The possibility of CVT – synthesis of the desired modification of sulfide compounds (for instance, marcasite or pyrite) is under consideration also.

This work was supported by Russian Foundation for Basic Research, pr. 13-03-01013.

References:

[1]. A.V. Sergeeva, A.V. Naumov, V.N. Semenov and Yu.V. Sokolov / Phase composition and the microstructure of In_3S_4 and $CuInS_2$ – films, deposited on silicon using the method of aerosol pyrolysis // J. Inorg. Materials (Russia) **43**, No 10, (1997), p. 1-5.

SESSION 3

Bio- and organogenic minerals and materials

PHYSICOCHEMICAL STUDY OF SILICON-SUBSTITUTED HYDROXYAPATITE

Berdinskaya M., Golovanova O.

Omsk State University, Omsk, Russia
filchenkomarija @rambler.ru

Materials based on hydroxyapatite $Ca_{10}(PO_4)_6(OH)_2$ (HA) are analog of the mineral component of bone and are considered as the most perspective for replacement of bone defects.

The bioactivity of the materials is defined by their chemical composition, crystal morphology and surface properties. The main method of data management features is the chemical modification of calcium orthophosphate. In view of the fact that silicon plays an important role in physiological processes of growth and reconstruction of bone and cartilage development of various methods for the synthesis of silicon-substituted hydroxyapatite (Si-HA) is a relevant physicochemical problem **[1]**. To achieve a higher biological response of the body in the recovery of damaged bone hydroxyapatite chemical modification should be carried out in conditions close to physiological. Information about the possibility of synthesis of silicon-substituted hydroxyapatite in these conditions is absent.

The purpose of the study - the synthesis of silicon-substituted hydroxyapatite of the model solution of extracellular fluid human physical and chemical investigation of the samples.

As starting components «Simulated Body Fluid» (SBF) using solutions of $CaCl_2$, $MgCl_2$, K_2HPO_4 , $NaHCO_3$, Na_2SO_4 , NaCl. The sources of silicate groups was selected Na_2SiO_3. The concentration of silicate ions was varied in the range of 0.5 ÷ 5.0%. Ratio Ca / P = 1.67. The pH for this system was 7.40. Upon completion of the synthesis time (48 hours) in the liquid over a deposit was determined by chemical analysis of the residual concentration of phosphate ions, silicate ions and calcium ions. Solid phases were studied by FTIR spectroscopy, XRD, thermal analysis, BET.

Chemical analysis of the liquid over a deposit indicate that all the solid phase is a silicon-substituted hydroxyapatite (Table 1).

Table 1. The concentration of silicate ions in the solid phase, the solid phase composition.

The initial concentration, %	Concentration in the solid phase, M	Ca/P	Composition of solids
0.5	$6.26 \cdot 10^{-5}$	2.48	Excess calcium hydroxyapatite
1.0	$3.06 \cdot 10^{-5}$	2.42	
1.5	$5.45 \cdot 10^{-4}$	2.30	
2.5	$9.32 \cdot 10^{-4}$	2.31	
5.0	$5.74 \cdot 10^{-3}$	2.30	

The increase of sodium silicate in the initial solutions, increases the amount of silicon, which became part of hydroxyapatite.

XRD showed that the received connections have a diffraction pattern at which there are all reflections, the reference for hydroxyapatite. We calculated the lattice parameters for the sample with the original content Si 0.5%: a = 9.466 ± 0.007, with a = 6.885 ± 0.007 Å. These data exceed the lattice parameters of unmodified HA a = 9,4302, a = 6,8911 Å **[2]**, confirming the substitution of different sizes orthophosphate ion silicate ion. Violations of the crystal structure (defects and vacancies) increase the degree of resorption of the biomaterial based on Si-HA.

The FTIR spectrum of the compounds are present all the bands characteristic of calcium hydroxylapatite, as well as bands at 1650, 1410-1570 (ν_3), 880, 873 (ν_2) cm^{-1}, corresponding to the vibrations of the carbonate groups (Fig. 1).

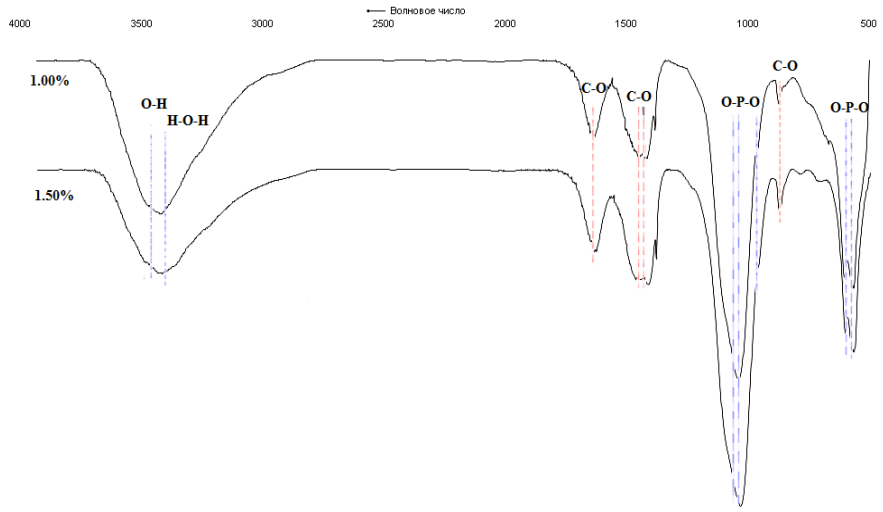

Figure 1. FTIR spectrum of samples with an initial concentration of Si 1.0 and 1.5%.

Occurrence is confirmed into the structure of the silicon-substituted hydroxyapatite, SO_3^{2-} groups of atmospheric air and the synthesis of one of the components - $NaHCO_3$, due to the need to compensate the excess of negative charges generated by substitution of triply charged ions to phosphate ions quadruply silicate.

When calcinating silicon - substituted hydroxyapatite decays in some stages. The mass loss for the samples with C Si = 0.5, 2.5, 5.0% was 15.11, 14.79 and 23.08%, respectively. Increasing the temperature to 600 ° C leads to a loss of water, increase to 980 ° C corresponds to the release of CO_2. The resulting residue has a clear infrared spectrum of the crystalline calcium hydroxylapatite.

Based on the obtained measurement data porosity adsorption of nitrogen (77.4 K), it can be said that the introduction of a greater amount (wt.%) of silicon in the pore volume increases (Table 2). High porosity leads to an increase in surface area and solubility - the most important characteristics of the biomaterial.

Table 2. Texture data samples.

The initial concentration Si, %	0.5	2.5	5.0
S , m^2/g	115	120	163
Pore diameter, Å	139	145	-

Thus, chemical methods, thermal, XRD analysis and IR spectroscopy indicated that in the «Simulated Body Fluid» HA possible modification silicate ions. The resulting samples are phase silicon-substituted hydroxyapatite, which has the required level of chemical properties and the ability to integrate with bone tissue.

This work was supported by the Russian Foundation for Basic Research (№ 12-03-98011-r_sibir_a and № 13-05-90432-Ukr_f_a).

References:

[1] Sventskaya N., Beletskiy B., The role of silicon in the silicate Implants // synopsis.
[2] Dorozhkin S., Calcium orthophosphates // Journal of Material Science. 2007, 42: 1061-1095.

METASOMATIC CRYSTAL GENESIS CONNECTED WITH THE ACTIVITY OF MICROORGANISMS

Frank-Kamenetskaya O.V.*, *Vlasov D.Yu.

Saint Petersburg State University, Saint Petersburg, Russia
ofrank-kam@mail.ru

The research of destructive metasomatic crystal genesis on the surface of carbonate rocks in urban environment in natural and biomimetic systems has been carried out using the modern mineralogical and biological methods.

The samples of oxalic and sulfur patina from the surface of marble and limestone monuments exposed in different climatic conditions (Saint Petersburg, Russia; Sevastopol and nearby areas, Crimea, Ukraine) were studied. Thus calcium oxalate (whewellite $Ca(C_2O_4)•H_2O$ and weddellite $Ca(C_2O_4)•(2+x)H_2O$), $x \leq 0.5$) rich patina and biofilms containing both oxalates and gypsum were found for the first time in these regions. A comparative analysis of microorganisms (fungi, lichens) from different rocks has been made. Besides the series of simulation experiments have been carried out: to study the metasomatic transformation of calcite into gypsum; to research the influence inorganic gypsum patina contaminants and the metabolism products of patina inhabiting fungi on this transformation and on the gypsum solubility and crystal habit; to study the morphogenetic characteristics of calcium oxalate crystals forming under the influence of fungi and the influence of a number of factors on acid production activity of fungi.

On the base of obtained data the role of microorganisms in metasomatic crystallization processes was refined and the biogenic and ecological aspects of these processes wereclarified. It was shown that calcium oxalate crystallization is initiated by microorganisms which produce oxalic acid (lichens from genera of Lecanora and Caloplaca, fungi Penicillium spp., Aspergillus niger) [1]. The acidophilic activity of fungi is affected by the calcium carbonate substratum, and concentration and distribution of carbohydrates and heavy metals on the rock surface [2]. The crystallization of calcium oxalate hydrates starts by formation of almost ideal dipyramidal and dipyramidal-prismatic crystals of weddellite at pH values < 5 [3, 4]. Morphology and size of the biomimetic tetragonal weddellite crystals are closely related to the weddellite crystals observed in the oxalic patina on the surface of marble and limestone monuments in Tauric Chersonesos (Ukraine, Crimea) (Fig.1) .

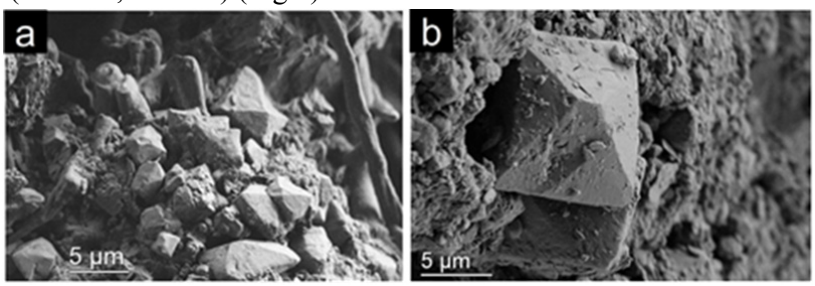

Figure 1. SEM images of natural tetragonal weddelite crystals observed on the surface of marble monuments in Tauric Chersonesos (Ukraine, Crimea).

At lower pH values also biomimetic calcium oxalate monohydrate, whewellite, forms as spherulite-like intergrowth of lamellar individuals on the hyphae of fungal mycelium on the culture. The gypsum patina formation is initiated mainly by sulphur dioxide which is common in urban atmosphere. The morphological features of the gypsum crystals developed on the surface of the carbonate rocks in urban environment (Fig.2) indicate that the processes of growth and dissolution replace each other, which is typical for metasomatic crystallization [4,5]. The degree of carbonatic rocks sulphation and the size of gypsum crystals depend on the local conditions, fissuring and porosity of the rock, structure/texture peculiarities and mineral composition of carbonate bedrock. A complicated relief of the monument promotes the moisture accumulation on the rock surface. For

this reason, the high artistic monuments with a complex relief (made of homogeneous Carrara marble) as well as the monuments made of highly porous travertine suffer most from the sulphation.

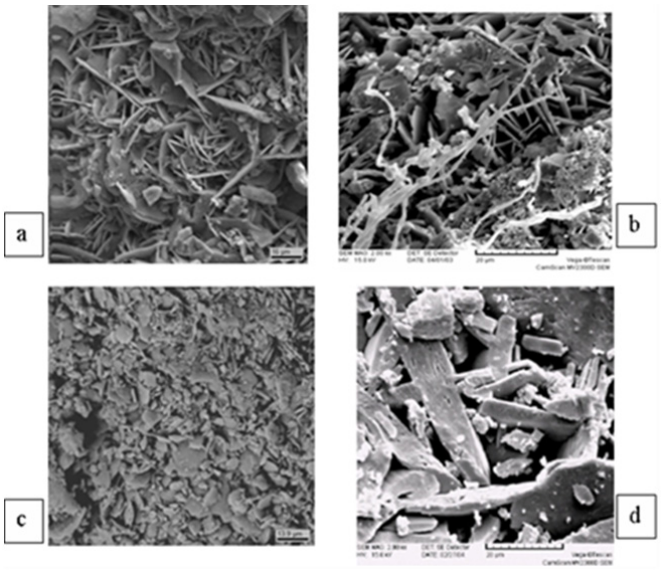

Figure 2. SEM images of sulphated patina. Gypsum crystals on the surface of different carbonate rock: Carrara compact marble (a), Ruskeala heterogeneous marble (b), stratified Putilovskii limestone (c), porous Pudostskii travertine (d). Saint Petersburg, Russia.

Dissolution, nucleation and growth of gupsum crystals take place in the presence of a numerous microorganisms such as bacteria, microfungi, algae and lichens. Three main stages of the gypsum-rich patina formation on the surface of carbonate rock monuments in the presence of microorganisms were noticed. 1. The initial stage when a thin biofilm is formed on the rock surface. Tiny gypsum crystals occur beneath the biofilm. 2. The intermediate stage is characterized by formation of numerous large gypsum crystals. Thin biofilms formed by microfungi, algae and other microorganisms occur between gypsum crystals. 3. The intensive stage is reached as soon as a layer of gypsum crystals is formed. The microbial community develops beneath this gypsum layer.

Acidophilic activity of microorganisms is one of the primary factors defining the processes of metasomatic crystallisation not only calcium oxalates, but also and gypsum.

The results of this research can be the scientific basis for the development of new methods of stone monuments preservation.

This study was supported by Russian Foundation for Basic Research (projects 09-05-01062-a). The authors are grateful to the M. S. Zelenskaya, E.V. Rosseeva, K.V. Sazanova and A.V. Rousakov for their active collaboration in this work.

References:

[1] Rousakov A.V., Frank-Kamenetskaya O.V., Zelenskaya M.S., Vlasov D.Yu., Gimelbrand D.E., Knauf I.V., Plotkina J.V. (2010). The first find of calcium oxalates in biofilms on the surface of archeological monuments of Tauric Chersonesos limestone (Crimea, Ukraine) // Russian Mineralogical Society Notes (in Russian).

[2] Barinova K.V., Vlasov D.Yu., Schiparev S.M., Zelenskaya M.S., Rusakov A.V., Frank-Kamenetskaya O.V. (2010). Production of organic acids by micromycetes from the rock substrates // Mycology and Phythopathology 44 (2). P. 137-142 (in Russian).

[3] Rosseeva E., Zelenskaya M., Sazanova K., Rusakov A., Frank- Kamenetskaya O., Vlasov D., Kniep R. (2013). Metasomatic Crystallization of Calcium Oxalate Hydrates by Interaction of Calcite Marble with Fungus Aspergillus Niger. Crystal Growth & Design (in press).

[4] Frank-Kamenetskaya O.V., Vlasov D.Yu., Shilova O.A. (2012) Biogenic crystals genesis on a carbonate rock monument surface: the main factors and mechanisms, the development of nanotechnological ways of inhibition. In Minerals as Advanced Materials II. Krivovichev S.V. Ed.; Springer: Heidelberg New York. P. 401-413.

[5] Frank-Kamenetskaya O.V., Vlasov D.Yu., Zelenskaya M.S., Knauf I.V., Timasheva M.A. (2009). Decaying of the marble and limestone monuments in the urban environment. Case studies from Saint Petersburg, Russia» // Studia Universitatis Babes-Bolyai Geologia 54 (2). P. 17-22.

STUDY OF DISPERSION COMPOSITION OF BIPHASIC SYSTEMS BRUSHITE – HYDROXYAPATITE

Galashova S.A., Golovanova O.A., Lobov I.A.

Omsk State University, Omsk, Russia
galashovasa@mail.ru

Since ancient times people various methods attempt restore the lost section of hard tissues. Nowadays there is a sufficient amount of synthetic composites, compositions and forms of biomaterials for the treatment and recovery parts of the human body. However, despite this success, research in this area should not lose their relevance in view of the complexity of natural analogue - bone properties that you want to achieve.

The purpose of research – determination of the dispersion composition of synthetic calcium phosphates by atomic force microscopy.

The paper studied the system of «brushite - hydroxyapatite». Phase of brushite and hydroxyapatite synthesized by chemical deposition on the following reactions (1, 2):

$$20Ca(NO_3)_2 + 12(NH)_2HPO_4 + 34\ NaOH = 2Ca_{10}(PO_4)_6(OH)_2 + 15NH_4NO_3 + 34NaNO_3 + 3H_2O, \quad (1)$$

$$Ca(NO_3)_2 + (NH_4)_2HPO_4 + 2H_2O \rightarrow CaHPO_4 \cdot 2H_2O \downarrow + 2NH_4NO_3. \quad (2)$$

Biphasic systems were prepared by mechanical mixing in a specific ratio, composition of the resulting mixtures is shown in Table 1.

Table 1. Composition of biphasic systems

GA, % mass	100	90	80	70	60	50	40	30	20	10	0
Brushite, % massc	0	10	20	30	40	50	60	70	80	90	100

The linear dimensions of the particles of calcium phosphate in aqueous suspension was determined by atomic force microscopy. Pre-conditions have been investigated for measuring particle sizes, namely, was picked material of the substrate - glass, solvent - water, the concentration of calcium phosphate in suspension - 0,1 mass. %, scan mode - semi-contact. Substrates with drops were left at room temperature until completely dry.

Next, the surface was scanned drops. For high-resolution images used an atomic force microscope Solver Pro (semi-contact scan mode, probe NSG01 with a radius of curvature 10 nm). Imaging was performed using a software package Image Analysis 2.1.2.

Fig. 1 shows AFM images of the surface drops suspension of biphasic systems. It was found that increasing the concentration of hydroxyapatite in the system is modified geometric shapes and sizes of the particles. The geometry of the particles changes with trapezoidal flat plate (corresponding to phase brushite) to the spherical shape, indicating that the transition from brushite to hydroxyapatite. Size of the particle also decreases with increasing concentration of hydroxyapatite (Fig. 2). Also with increasing concentrations of hydroxyapatite observed gluing particles and forming of aggregation. Established size of precipitation particles are shown in Fig. 2.

Dispersion composition is heterogeneous at a ratio of hydroxyapatite 60% - brushite 40%, this system can be divided into 3 fractions following ranges: 0,03-0,05 mkm, 0,05-0,07 mkm,

0,07-0,09 mkm. In the system hydroxyapatite 100% observed fractionation: individual crystallites and aggregates.

Thus, we have shown the possibility of determining the dispersion composition of synthetic calcium phosphates by atomic force microscopy.

This work was supported by the Russian Foundation for Basic Research (№ 12-03-98011-r_sibir_a and № 13-05-90432-Ukr_f_a).

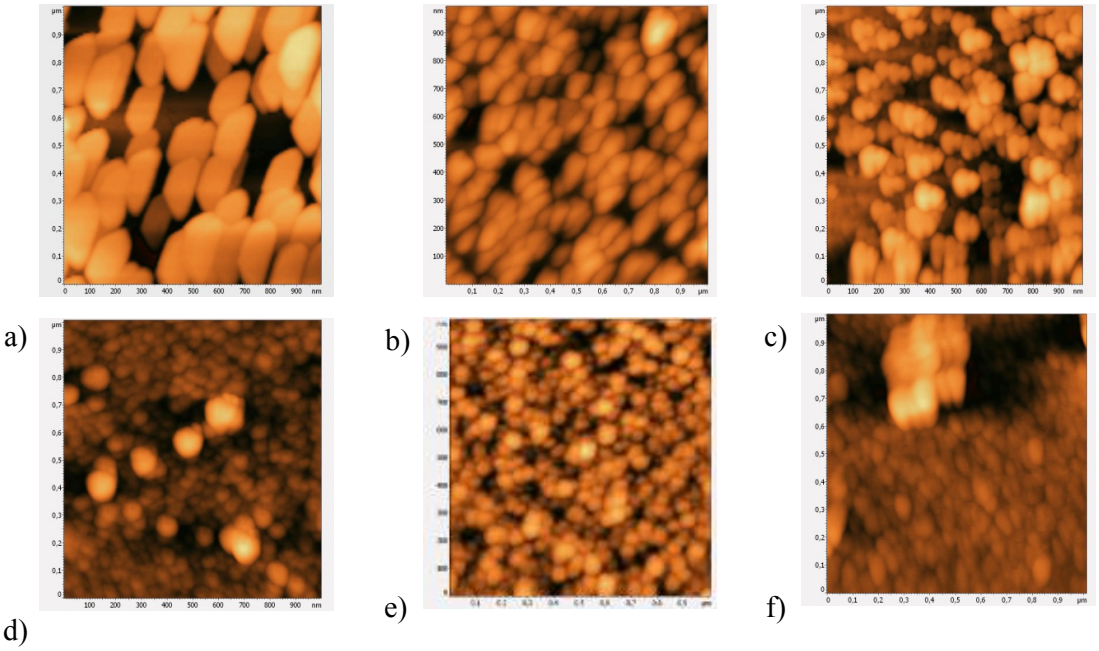

Figure 1. AFM images of biphasic systems: a) brushite 100%, b) system hydroxyapatite 20% - brushite 80%, c) system hydroxyapatite 40% - brushite 60%, d) system hydroxyapatite 60% - brushite 40%, e) system hydroxyapatite 80% - brushite 20%, f)

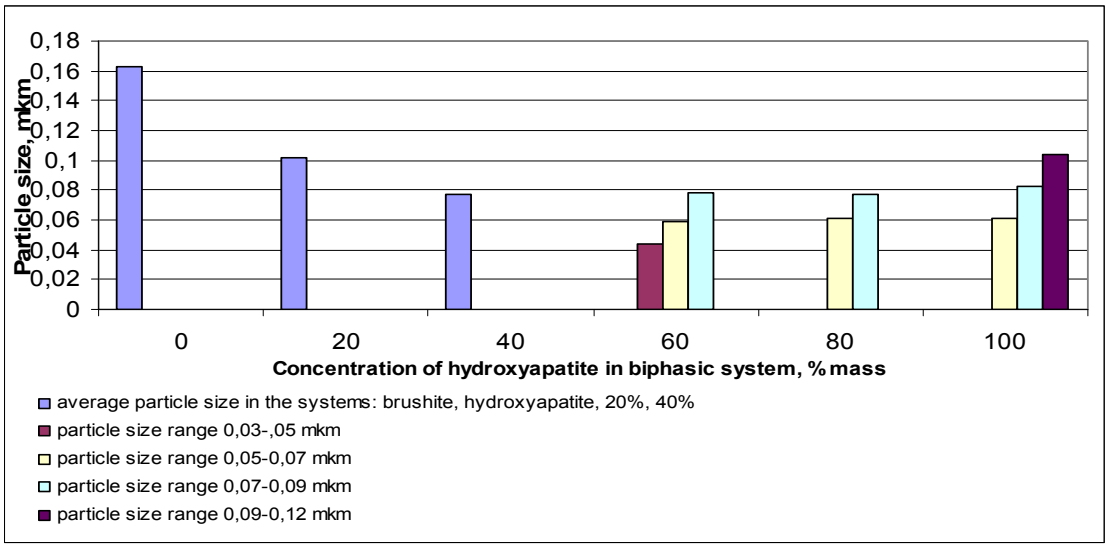

Figure 2. The results of determination of size of the particles

THERMODYNAMIC REGULARITIES IN CRYSTALLIZATION OF PROTOTYPES OF BIOLOGICAL LIQUIDS

Golovanova O.A.

F.M. Dostoevsky Omsk State University. Omsk, Russia
golovanoa2000@mail.ru

Methods of modeling allow to reveal features of processes of emergence of new growths in a human body and action of the systems regulating their growth. At the same time studying of formation of a number of minerals in not to peculiar environment for them with accurately regulated conditions of a human body different (sometimes very significantly) from conditions of the abiogenous environment, expands idea of genesis of minerals and promotes development of the general theory of mineralogenesis.

Methods of thermodynamic modeling received broad distribution in geochemical researches for the description of processes of mineralogenesis with participation of mainly diluted solutions. The solution of a task includes use of the corresponding criterion answering to a condition of stable equilibrium of system, and thermodynamic a reasonable choice of association of minerals which can potentially be in balance with environment for this limited area of conditions. Change of standard energy of Gibbs at formation of a deposit is connected with work of solubility of slightly soluble connection by the equation:

$$\Delta G^0_{(M_pX_q),T} = -RT\ln\frac{1}{K_s^{\,0}} = RT\ln K_s^{\,0} \quad (1)$$

where – $\Delta G^0_{(M_pX_q),T}$ Gibbs's standard energy, kJ/mol; R – universal gas constant (J / моль·К); T – temperature, K.

One of ways of graphic representation of balance the sediment ↔ rastvor in system in which formation of almost insoluble connection from water solution proceeds, is construction of "stability fields" (fig1). The principle of creation of similar charts consists in establishment of functional dependence of the minimum concentration of the cation which is a part of a deposit which needs to be created for receiving supersaturation on this phase, from pH solution and concentration of anion: $pC_{M^{q+}} = f\left(pC_{X^{p-}}, pH\right)$

During the carried-out thermodynamic calculations conditions and possibility of formation of almost insoluble connections in hypothetical solution of sediment-forming ions are revealed. On the basis of the constructed charts of stability for a series of phosphates of calcium and magnesium, and also calcium oxalate, areas at which formation of these phases from solutions most thermodynamic is probable are defined.

Thermodynamic calculation reflects possibility of formation of phases only proceeding from data on their thermodynamic stability in a standard condition and doesn't consider, in particular, the kinetic factors having impact on process of formation of a solid phase in actual practice.

When carrying out model experiments analogs of phosphatic minerals were received, and also distinctions in the conditions of their education are revealed. The analysis of the obtained data showed that size pH solution has the most essential impact on structure of a being formed solid phase. Thus the variation of initial concentration of components of solution, in the range of values, characteristic for biological liquid, brings in the basic to quantitative, instead of to high-quality changes of structure of a deposit.

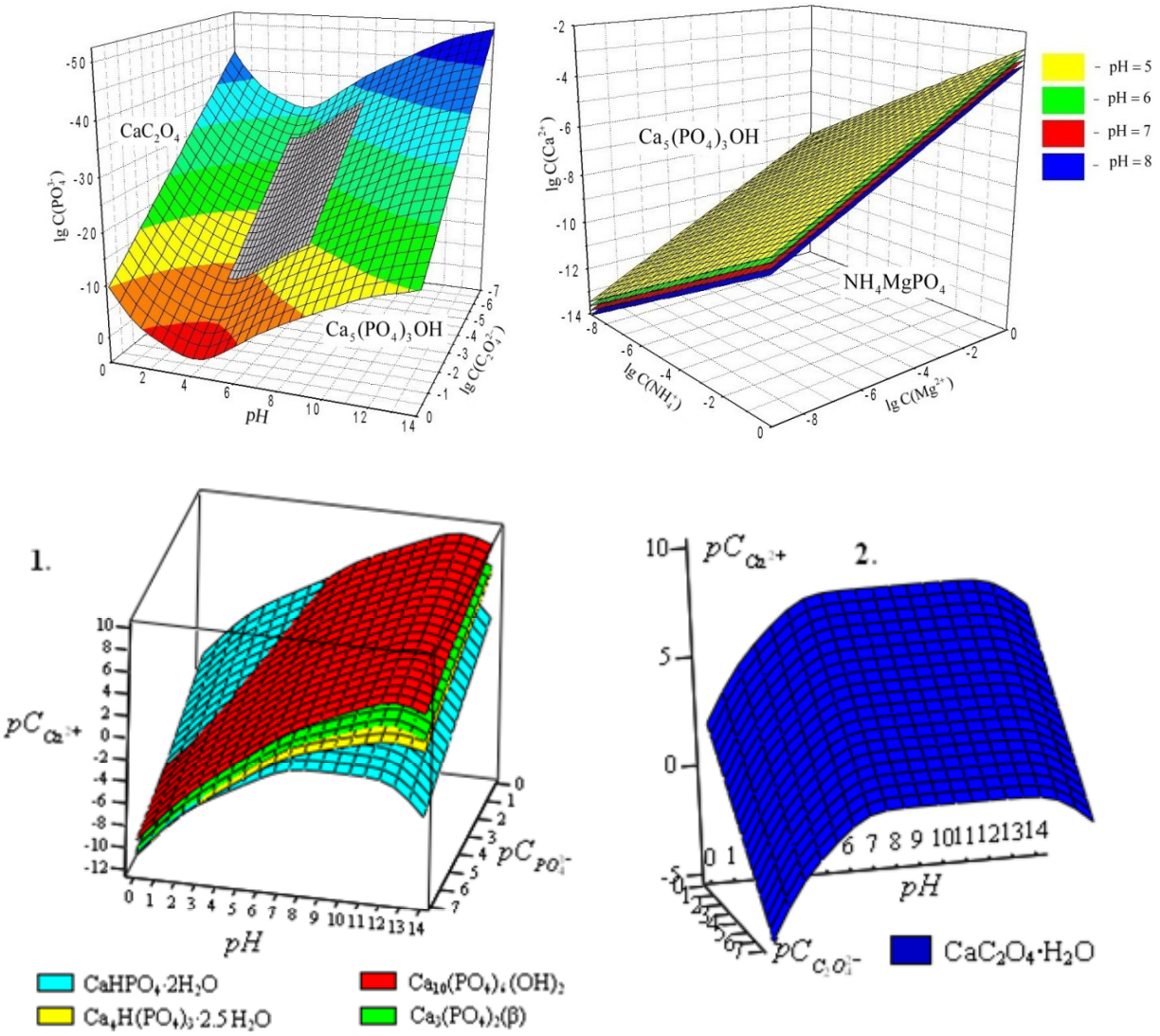

Figure 1. Stability field of the insoluble compounds.

This work was supported by the Russian Foundation for Basic Research (№ 12-03-98011-r_sibir_a and № 13-05-90432-Ukr_f_a).

TO THE QUESTION OF THE OXALATE RENAL STONES FORMATION CONDITIONS

Izatulina A.R., PuninYu.O., Shtukenberg A.G.

St.Petersburg State University, Geology Dept., St.Petersburg, Russia
alina.izatulina@mail.ru

Most part of the human urinary system stones consists of calcium oxalates both stable monohydrate (whewellite, $CaC_2O_4 \cdot H_2O$) and metastable dihydrate (weddellite, $CaC_2O_4 \cdot (2+x)H_2O$) and the amount of calcium oxalate stones is from 45 to 80% depending on the region. Physiological liquid (urine) several times supersaturated for calcium oxalate under the normal conditions, thus the calcium oxalate renal stones could be formed in the organism of any healthy person, but actually does not. Despite the fact that the formation of pathogenic biominerals dicussed in many papers, so far there is no experimental basis for the theory to explain the formation of any pathogenic minerals in the body.

The results of the calcium oxalate renal stones internal structure investigation (whewellite spherulitic aggregates, correlation between whewellite and weddellite, thin rhythmic zoning of whewellite renal stones after the organic substance impurity, weddellite dendrite structures) show the essentially nonstationary processes of calcium oxalate phases crystallization. Repeated nucleation acts of whewellite spherulites, periodic alternation of whewellite and weddellite phases reflect changes in the composition of physiological solution caused by external factors related to the activity of the organism. Fine zoning of the whewellite units – is a consequence of self-oscillation growing processes. This zoning is characterized by periodic and chaotic components, and could be described using fractal statistics from 2 to 5 parameters. Within stone segments with more complex and simpler dynamics of formation are localized. Last ones call for the description of one less parameter. The impurity poisoning of the spherulites surface is proposed as a mechanism of self-oscillations, leading to the hysteresis of growth rates and periodic growth stops with deposition of organic matter.

Features of the stones internal structure are determined by the processes of nucleation, oxalate crystallization kinetics, whewellite and weddellite phase stability that has been studied in model systems in terms of variation of temperature and concentrations of inorganic and organic components of the solution. The results showed that the inhibition of nucleation and crystal growth processes of calcium oxalate monohydrate in physiological solution at its conventional amino acid composition is caused by adsorption of amino acids on the surface of the stone. Crystallization of whewellite starts with the concentration of oxalate ions raises up to the values of oxalatourea desease. Addition of organic substance (ovalbumin, gelatin, protein-containing media) or microorganisms (bacteria and viruses) in the oxalatourea desease conditions facilitates crystallization of whewellite and leads to the simultaneous formation of weddellite with a variable amount of water, that causes the different weddellite stability. Addition of magnesium ions, sodium ions and carbonate ions to a solution leads to the co-crystallization of whewellite and weddellite.

This work was supported by RFBR (grant 12-05-31415). XRD studies were performed at the X-ray Diffraction Centre of St.Petersburg State University.

PREPARATION OF BIOACTIVE CALCIUM PHOSPHATE COATING ON TITANIUM

Izmailov R.R., Golovanova O.A.

Omsk F.M. Dostoevsky State University, Omsk, Russia
izmailov_87@mail.ru

One of the actual problems of modern science (chemistry, physics, medicine) is the synthesis and study of bioactive substances for medical use. Most effective among coatings with bioactive properties are calcium phosphates coatings. In this paper we identified adhesion characteristics of carbonate hydroxylapatite (CHA) on titanium, using the measurement of contact angle and surface tension of CHA suspensions. Found that surface tension and contact angle increase with the growth of carbonate hydroxylapatite concentration. In our opinion, this fact may be related to the partial dissolution of calcium phosphate and formation of inorganic surface inactive substances. At a concentration of CHA in a suspension of more than 10%, the surface of titanium alloy is not wetted. One of the main and important characteristics of the coating is ratio of the energy of adhesion (W_a) and cohesion (W_c). This ratio may be obtained from the Young–Dupré equation:

$$\frac{W_a}{\sigma_{01}} = 1 + \cos\Theta, \quad (1) \qquad \frac{W_a}{2\sigma_{01}} = \frac{1+\cos\Theta}{2}, \quad (2)$$

$$W_c = 2\sigma_{01}, \quad (3) \qquad \frac{W_a}{W_c} = \frac{1+\cos\Theta}{2}. \quad (4)$$

In this case, it was found that the growth of the CHA concentration of suspension causes decrease of the adhesion energy which characterizes the interaction of the dispersed system with a titanium surface.

So with a doubling of the amount of carbonate hydroxylapatite the adhesion energy decreases of 0.7 and more (fig. 1).

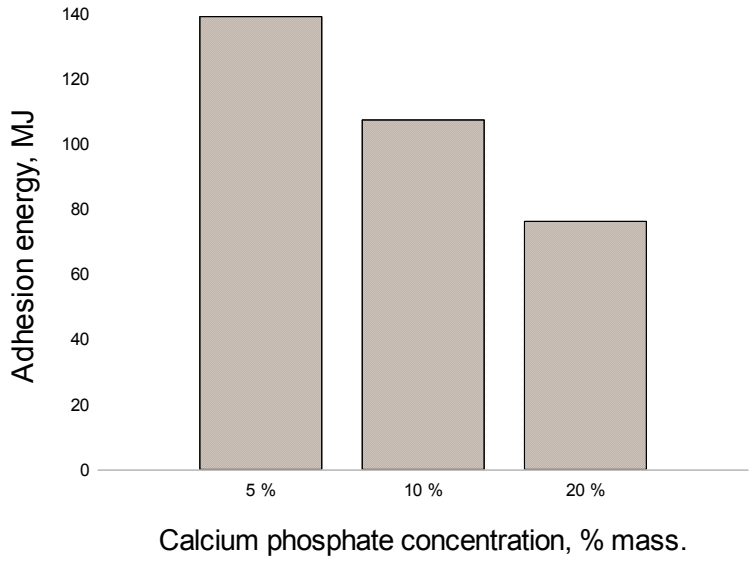

Figure 1. Dependence of the adhesion energy of calcium phosphate concentration

Also, there is an increase the cohesive energy, which characterizes the interaction in the dispersion system. In our opinion, this fact may be explained by the formation of the thick coating.The degree of wetting is determined by a balance between adhesive and cohesive energies, in addition, when its ratio is close to 1 and then there is wet, etc. Found that at the concentration of calcium phosphate over 10% there is a transition to a nonwettability.

As a result of research the adhesion characteristics that allow to control the quality of the bioactive calcium phosphate coatings on titanium alloys obtained by using the thermodynamic parameters.

This work was partially supported by the Russian Foundation for Basic Research (№ 12-03-98011-r_sibir_a)

STUDY OF THE CALCIUM OXALATE CRYSTALLIZATION BY OPTICAL MICROSCOPY

***Korolkov V.V.*, Golovanova O.A., Panova T.V., Obrezanova I.P.**

F.M. Dostoevsky Omsk State University. Omsk, Russia
v.v.korolkov@chemomsu.ru

Study of crystallization of compounds that enter into the composition of physiogenic and pathogenic organic-mineral aggregates (OMA) is important and actual field of modern researches. One of the main components of OMA is calcium oxalate which has a large significance in its formation [**1, 2**]. It is found in the stones of the urinary system, the salivary stones and in other pathogenic mineralization. High prevalence of oxalate stones in the urinary system explains the increased interest in the study of the crystallization of calcium oxalate in the conditions close to the environment that exists in the human body. However, the causes and mechanisms of pathogenic aggregates not fully understood and require further study.

Purpose of work is the study of the calcium oxalate crystallization and determination of the size and number of crystals by stereometric metallography.

The process of crystallization has been studied at 37°C and various values of supersaturation (γ = 40, 50, 60). Selection of these values of supersaturation justified in previous work [**3**]. Calcium oxalate supersaturation was produced by a chemical reaction

$$Ca^{2+} + C_2O_4^{2-} \rightarrow CaC_2O_4,$$

which has been implemented by mixing the stock solutions of the stoichiometric composition of the soluble compounds.

All series of experiments were conducted with constant stirring and at certain time intervals samples were taken and applied to a microscope slide.

Practical method of metallography was used to investigate the parameters of the crystal structure of calcium oxalate. Thus method for determination of the size of the linear sections of microparticles (characterizes the particle diameter) and a method of estimating the number of the cutting lines and the sizes of sections of the microparticles [**4**] were implemented on an optical microscope Neophot-2. The lengths of the chords were determined taking into account the increase of the linear structure of the image.

In addition, for a given system the fraction of calcium oxalate monohydrate increases with the growth of initial supersaturation. At the same time, a large number of calcium oxalate dihydrate crystals formed at high supersaturation. This fact contradicts modern concepts and thermodynamic calculations of formation of pathogenic phases. Thus, carrying out research proves the difficulty of crystallization processes of calcium oxalate and necessity of further research.

This work was supported by the Russian Foundation for Basic Research (№ 12-03-98011-r_sibir_a and № 13-05-90432-Ukr_f_a).

References:

[**1**] Tiktinsky O.L., Alexandrov V.P. Urolithiasis. 2000. 384 p.
[**2**] Golovanova O.A. Pathogenic minerals in the human body. 2007. 395 p.
[**3**] Golovanova O.A., Efimova A.V., Lakman A.V., Panova T.V. The application of optical microscopy to study the crystallization of calcium oxalate monohydrate J. Izvestiya vuzov. Seriya «Khimiya i khimicheskaya tekhnologiya», 2008. 51, №. 9, P. 34-38.
[**4**] Saltykov S.A. Stereometric metallography. 1976. 256 p.

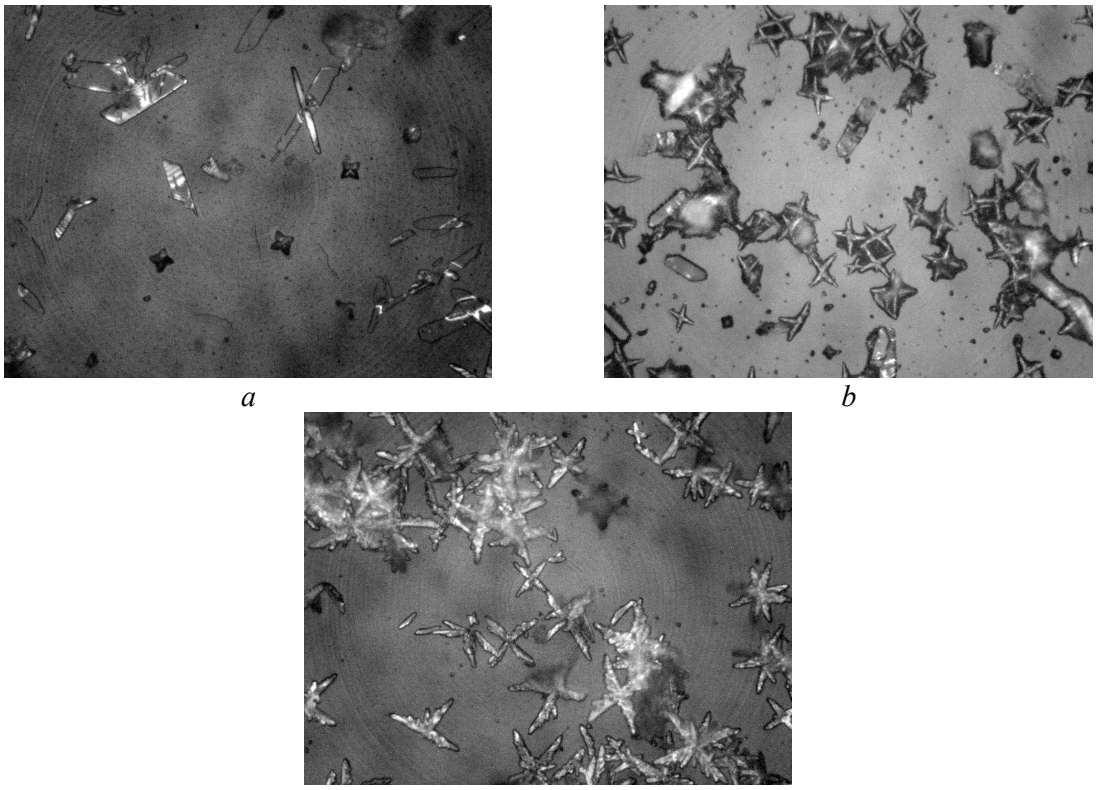

a *b*

c

Figure 1. The results of optical microscope at different supersaturations: *a* – 40; *b* – 50; *c* – 60

SOLID SOLUTIONS IN ORGANIC SYSTEMS: IDENTIFICATION, VERIFICATION AND PHASE DIAGRAMS

***Lorenz H.*[1], Kotelnikova E.N. [2], Taratin N.V.[2], Binev D.[1], Seidel-Morgenstern A. [1]**

[1] *Max-Planck-Institut für Dynamik komplexer technischer Systeme, Magdeburg, Germany*
[2] *St. Petersburg State University, Crystallography Department St. Petersburg, Russia*
lorenz@mpi-magdeburg.mpg.de

The purification potential of crystallization is determined by thermodynamic and kinetic factors. Kinetic effects include the incorporation of impurities into the crystal in 3-dimensional faults as liquid inclusions or mother liquor remained in the crop whether adsorbed on the crystal surface or entrapped between crystals. These factors can be partially influenced by the crystallization conditions (e.g. growth rate) and optimized downstream processes. On the other hand, the extent of purification is thermodynamically limited by miscibility of the target compound and the impurity at solid state that can be complete (continuous series of mixed crystals) or finite.

For organic systems miscibility in solid state is not that frequent as known from inorganic metallic and mineral systems; literature references state an occurrence of such cases of about 15% [1]. Examples are summarized in [2, 3] also comprising chiral systems. However, the number of phase diagrams showing the presence of solid solutions and specifying the boarders of miscibility is rather rare. Also, in practice partial miscibility occurring in a system is not recognized, which might be attributed to low levels of miscibility (that are hardly detectable) or difficulties to attain equilibrated samples due to the low mobility of (rather complex) molecules in solid state. However, the knowledge of miscibility at solid state in a system is of crucial relevance, since it limits the purification potential of a single crystallization step and thus, determines the crystallization technique applicable.

In this context, in the lecture mainly results of joint studies of the two groups involved are presented. They refer to the investigation of several chiral and diastereomeric systems, such as malic acid, a mandelic acid derivative and amino acids, and focus on recognition/identification of the occurrence of solid solutions in the particular system and the determination of the corresponding phase diagrams in connection with crystal structure features of the solid phases in the system.

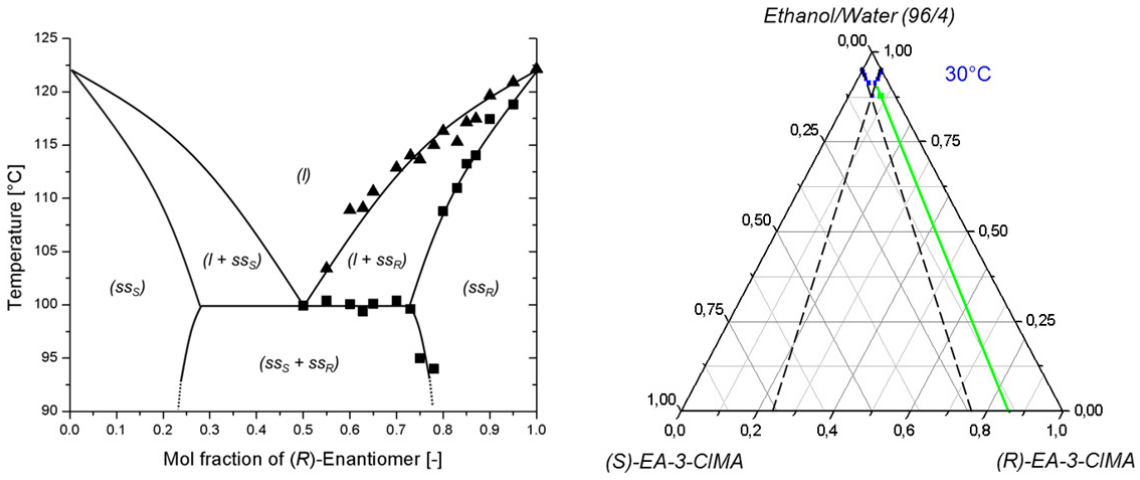

Figure 1: Melt phase diagram [4] (left) and ternary solubility phase diagram (right) of (S)- and (R)-enantiomers of the ethanolamine salt of 3-chloromandelic acid (EA-3-ClMA).

With regard to solid-liquid equilibria, both melt and solution equilibria in a solvent were studied. Exemplarily, in Figure 1 the binary melt and ternary solubility phase diagrams of a chiral system investigated are shown.

Main methods applied here were Differential Scanning Calorimetry (DSC), X-ray Powder Diffraction and High Performance Liquid Chromatography (HPLC), the latter particularly for analysis of compositions of solutions and mixed crystals.

Obviously, the nature (stereoisomeric composition and crystal structure) of the precipitated solid phase will be different for the enantiomer, corresponding solid solutions, the racemic compound and a eutectic mixture (enantiomers and/or solid solutions). A reliable identification of phases may be carried out by X-ray methods such as Powder Diffraction, High Temperature Powder Diffraction and Single Crystal X-ray Diffraction. In this lecture special attention is drawn to the possibilities of these methods.

For example, the unit cell parameters in the composition range from the pure (enantiomer) component to the equimolar (racemic) mixture could be calculated based on powder diffraction data. Such approach facilitates not only the identification of different polymorphs of enantiomers and their double compounds, but also the determination of the limits of solid solutions in enantiomeric and diastereomeric systems [4]. Exemplarily, in Figure 2 the dependence of the cell parameter *c* on the composition in the chiral system of the ethanolamine salt of 3-chloromandelic acid is shown. The observed trend of the parameter *c* is in a good agreement with the results obtained from phase diagram studies as depicted in Figure 1. Areas with varying and constant parameter values correspond to the single-phase domains (solid solutions) and two-phase domains (eutectic mixture of solid solutions) in the binary phase diagram, respectively.

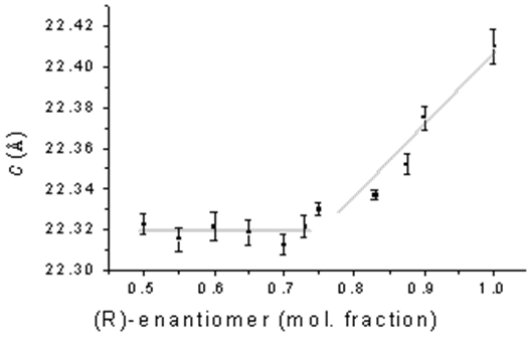

Figure 2: Dependence of cell parameter *c* on composition in the binary system of (S)- and (R)-enantiomers of EA-3-ClMA. Compositions from the racemate (*left*) to the (R)-enantiomer (*right*) are shown.

High Temperature X-ray Powder Diffraction was found to be a useful method in the *in situ* investigation of thermal deformations and phase transitions in enantiomeric and diastereomeric systems. Thermal phase transitions were studied in the chiral system of malic acid [5] and the diastereomeric system of threonin. Further, Single Crystal X-ray Diffraction was used for refinement of crystal structures of the (S)-enantiomer of EA-3-ClMA [4] and a (R,S)-solid solution of threonine diastereomers .

References:

[1] Matsuoka, M. in: Garside, J., Davey, R.J., Jones, A.G. (eds): Advances in Industrial Crystallization, Butterworth-Heinemann, Oxford, 1991.

[2] Kitaigorodskii, A.I.: Molekülkristalle, Akademie-Verlag, Berlin, 1979.

[3] Jacques, J., Collet, A., Wilen, S. H.: Enantiomers, Racemates, and Resolutions, Krieger, Malabar, 1994.

[4] Taratin, N.V., Lorenz, H., Kotelnikova, E.N., Glikin, A.E., Galland, A., Dupray, V., Coquerel, G., Seidel-Morgenstern A.: Cryst. Growth Des. 12 (2012), pp. 5882-5888.

[5] Isakov, A.I., Kotelnikova, E.N., Kryuchkova, L.Yu., Lorenz, H.: Proceedings 19th Int. Workshop on Industrial Crystallization (BIWIC 2012), Tianjin (China), pp. 615-622.

THE DETAILS OF CALCIUM PHOSPATE CRYSTALLIZATION ON BONE SAMPLES FROM PROTOTYPE OF BIOLOGICAL FLUID

Malovskaya E.A., Golovanova O.A., Panova T.V.

F. M. Dostoevsky Omsk State University, Omsk, Russia
katovi@mail.ru

Currently, due to the increasing number of bone diseases focus more on creating biocomposite materials. Large perspective experimental and clinical applications have synthetic materials based on calcium phosphates, which have high biocompatibility with respect to the bone tissue in humans and able to perform by virtue of its inertia matrix function along which the neoformation of bone structures [1].

Also of interest to the study of these compounds is the fact that calcium phosphates are part of the majority of pathogenic biological minerals, the causes and mechanism of formation, which has not yet been identified [2]. It should be noted that in recent years an increasing number of diseases associated with formation of the data units in humans.

So an important direction is the study of the crystallization process of the prototypes of biological liquids. This direction is much research, but mainly being crystallisation from aqueous solutions.

The aim of this work is to study the features of the crystallization of calcium phosphates of the prototypes of biological liquids on bone samples.

To simulate the process of crystallization on bone samples was placed a series of experiments. For this purpose, the basic values of the concentration range of the inorganic components and the pH of the intercellular and liquid synovial average healthy adult humans [3]. The choice of initial reagents and their ratio in the solution were determined in such a way that the concentration of ions and ionic strength of the solution were as close as possible to the given parameters of the simulated system.

The material of the study is a collection of "normal" and coxarthrosis affected femoral heads of the Omsk Region residents aged 30 - 79 years.

The results of determination of ions in solutions of different saturations are shown in the following table 1.

Table 1. The chemical analysis of supernatant liquid.

Intercellular liquid	**$[Ca^{2+}]$, mmol/l**	**$[PO_4^{3-}]$, mmol/l**	**pH**	**Synovial liquid**	**$[Ca^{2+}]$, mmol/l**	**$[PO_4^{3-}]$, mmol/l**	**pH**
S=30				S=30			
1 week	3,00	2,27	6,62	1 week	3,09	2,42	6,83
2 week	2,86	1,82	6,99	2 week	3,02	1,51	6,92
3 week	3,02	1,16	7,12	3 week	3,38	2,52	7,39
S=50				S=50			
1 week	2,96	2,02	6,75	1 week	3,31	3,78	7,32
2 week	2,88	1,82	7,01	2 week	3,38	2,17	7,84
3 week	2,95	1,16	7,10	3 week	3,50	2,62	7,84
S=70				S=70			
1 week	2,50	1,92	6,08	1 week	3,33	3,78	7,22
2 week	2,86	1,82	6,93	2 week	3,10	2,32	7,25
3 week	3,04	1,16	7,26	3 week	3,49	2,83	7,68

Analyzing the data can be noted that in the case of all the processes the intercellular liquid flow more smoothly, as ionic strength is small. In the solution decreases with time the content of phosphate ions and the medium made of alkaline.

In synovial liquid mixed processes. This may be due to various reasons:

- ion strength of the solution is more than twice than in the intercellular liquid;
- there are processes of salting-out of the bone tissue and bone matrix contains as various ions, it is possible their impact on the hydrolysis of HA and OCP.

The precipitate formed on the bone samples were analyzed using the optical microscopy.

Found that the supersaturation of the solution does not affect the formation of products, but only affects the rate of formation of precipitate.

In the case of interstitial liquid does not matter what time of experience hydroxyapatite is formed (Fig. 1).

In an environment of synovial liquid on the surface of the bone samples formed octacalcium phosphate and hydroxyapatite (Fig. 2). The latter is a thermodynamically metastable polymorph of hydroxylapatite.

The difference in the products produced on the surface of bone and synovial environment intercellular fluids can be explained by differences in the carbonate and sulfate ions. [4]

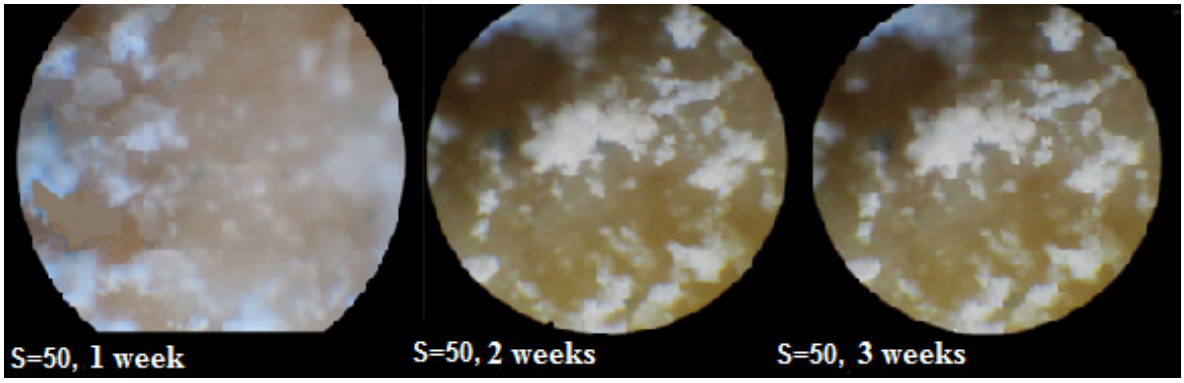

Figure 1. Optical microscopy results of precipitation obtained by crystallization from the extracellular liquid.

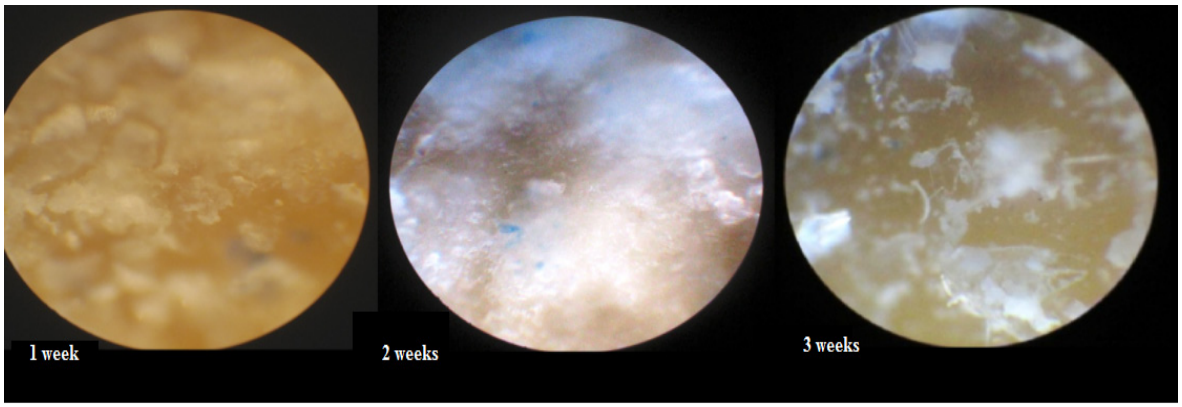

Figure 2. Optical microscopy results of precipitation obtained by crystallization from the synovial liquid.

Thus, the possibility of crystallization of calcium phosphate bone samples of the prototypes of biological liquid. In the extracellular liquid formed carbonate hydroxyapatite, and synovial - octacalcium phosphate and hydroxyapatite.

References:

[1] S.V. Barinov, Russian Chemical Reviews, 79, 1 (2010) 15-32.
[2] O. A. Golovanov Pathogenic minerals in the human body. Omsk, 2007.
[3] Human Anatomy: Textbook. / Ed. L. L. Kolesnikova, S.S. Mikhailov. M. GEOTAR-MED, 2004. 816.
[4] Jalota S., Bhaduri S.B., Tas A.C. In vitro testing of calcium phosphate (HA, TCP, and biphasic HA-TCP) whiskers // Journal of Biomedical Materials. - 2006. - Part A. - V. 78. - P. 481 – 490.

INFLUENCE OF BACTERIA AND VIRUSES ON THE URINARY PHOSPHATE PHASE PRECIPITATION

Nikolaev A.M.[1], Kus'mina M.A.[1],
Frank-Kamenetskaya O.V.[1] Malyshev V.V.[2]

[1]Saint Petersburg State University, Saint Petersburg, Russia
[2]S.M.Kirov military medical academy, Saint Petersburg, Russia
e-mail: ofrank-kam@mail.ru

Disappointing ecological environment in the modern megalopolises leads to the increasing number of the pathogen stones diseases in the human organism. So the investigation of the pathogen crystallization mechanisms becomes increasingly actual during last 10-15 years. All existing theories of pathogen mineral formation aren't completely experimentally and theoretically proved. Moreover bacterial theory [1-3] is the least developed

In the present work the study of influence of bacteria which can exist in the human urinary system during the inflammation, on the uralite phase formation was carried out.

Biomemetic synthesis of the main mineral phases of renal stones was carried out in the presence of the bacteria: Escherichia E.coli ("e"), Klebsiella pneumoniae ("kl"), Pseudomonas aeruginosa ("ps") and Staphylococcus Ahrens ("s"). To provide the survival of the pathogens two types of organic substrate were added to the solutions: beef extract broth (MPB-series) and Muller Hinton broth (MH-series). Synthesizes were carried out by isotherm precipitation in the solutions simulating human urine inorganic composition. Initial pH of the solutions varied from 5.77 to 7.46. PO_4-ion concentration was set either 13 or 33 mmol/l (these concentrations are taken from the maximum and minimum composition of the normal human urine).

Main phases that precipitate from the model urinary solutions are brushite $CaH[PO4]•2H_2O$ (as thin plate-like crystals), hydroxylapatite $Ca_5[PO_4]_3(OH)$ and struvite $(NH_4)Mg(PO_4)•6H_2O$ (large prismatic crystals). Octacalcium phosphate $Ca_8(HPO_4)_2(PO_4)_4•5H_2O$ (as powder or in the spherolites) and whitlockite $Ca_{18}Mg_2H_2(PO_4)_{14}$ are less frequent among precipitated phases.

Initial pH in the series with the minimum urinary components concentrations varied from 5.77 to 7.05. Crystal precipitates were obtained in the most experiments. pH ratio in the solutions of MH-series decreased on 0.48 – 1.33. Crystals of brushite were obtained in the wide interval of pH (5.3 – 6.2). Also, struvite was detected in the experiments, where pH was over than 5.8. In some rare cases whitlockite precipitated as well in the solutions with the 6.0 pH ratio. In the solutions of MPB-series in some experiments pH ratio decreased on 0.04 – 0.31, meanwhile in others it increased on 0.03 – 0.26. Precipitates were observed only in the experiments with pH ratio more than 6.4. Brushite was observed in the experiments with the pH ratio more than 6.4, apatite – with the pH ratio more than 6.5. Struvite becomes the main phase in the solutions with pH more than 6.85. Whitlockite presence was detected in the 6.6 – 7.0 pH interval. In the similar system (but without organic substrate and bacteria added) brushite is the main phase in such conditions. Octocalcium phosphate appears with pH more than 6.5, and hydroxylapatite appears only with pH more than 6.8. Thus, organic substrate and bacteria move the border of the hydroxyapatite's phase stability into the lower pH area.

Initial pH in the series with the maximum urinary components concentrations varied from 6.00 to 7.46. Crystal precipitates were obtained in the most experiments. In the solutions of MH-series pH ratio decreased on 0.16 – 0.7, in some rare cases it increased on 0.06 – 0.17. Crystals of brushite were obtained with the solution pH more than 5.74. Also, struvite was detected in the experiments, where pH was in the 6.3 – 6.5 interval. In the 6.8 – 7.0 pH interval co-precipitation of brushite and hydroxylapatite is observed. In the solutions with the pH ratio more than 7.0 struvite is the main component of precipitate. In the solutions of MPB-series in some experiments pH ratio decreased on 0.03 – 0.35, but usually it increased on 0.03 – 0.49. Brushite

crystallization was observed in the solutions with pH more than 5.97. Brushite and struvite precipitate in the approximately equal quantities in the solutions with pH more than 6.44 and up to 7.2. Struvite is the practically only precipitate in the solutions with the pH ratio more than 7.2. In the similar system (but without organic substrate and bacteria added) brushite is the main phase in such conditions and struvite appears only after increasing of the pH ratio up to 7.0/ So organic substrate and bacteria move the area of the struvite crystallization into the lower pH area.

In general, the presence of the organic substrate and bacteria in urine-like solutions leads to the pH ratio changing and also significantly influence on the phase composition of the renal stones, moving crystallization areas of hydroxylapatite and struvite into the lover pH areas. The result changing of the pH ratio in the solution is the summary of the bacteria influence (which usually decrease it) and influence of the crystallization processes (which always decrease it)..

The work was supported by RFBR (projects 10-05-00881-a, 11-05- 90425-Ukr_f _a, 12-05-31415-мол-а, 13-05-90432 Ukr_f _a).

The authors are grateful to the A.R Isatulina and Yu.O. Punin for active collaboration in this work.

References:

[1] Каткова В.И. Мочевые камни: минералогия и генезис. Изд. Коми научного центра УрОРАН, Сыктывкар, 1996

[2] Bouropoulos C, Vagenas N, Klepetsanis P, et al., Cryst. Res. Technol. 39, 699 (2004).

[3] Petrova E.V.,Gvozdev N.V., and Rashkovich L.N., J. Optoelectron. Adv. Mater. 6(1), 261 (2004).

COMPOSITION AND SPATIAL DISTRIBUTION OF DISPERSED ORGANIC MATTER IN BRECCIA ORE OF VORONTSOVSKOE DEPOSIT

Rovnushkin M.Yu. [1], *Azovskova O.B.*[1] *Koryakova O.V.* [2]

[1] *Institute of Geology and Geochemistry, UB RAS, Yekaterinburg, Russia*
[2] *Institute of Organic Synthesis, UB RAS, Yekaterinburg, Russia*
rovn@list.ru

Over the recent decades mineralised gold reserves in many countries have grown thanks to discovery and exploration of a particular type of mineralisations known as "Carlin". After discovery in early 1960's of Carlin gold deposit in Nevada (USA) a number of similar deposits have also been discovered along a 60 km long and 5-8 km wide NW trend controlled by a system of deep seated faults (Carlin-trend). Similar, Carlin-type, deposits also exist in canada, China, in central Asia and in a number of other countries.

Deposits of this type occur in similar geotectonic environments and have similar ore composition. Distinctive features of ores of Carlin-type deposits are low-temperature antimony-arsenic-mercury mineralisation, very particular metasomatism and geochemical range of mineralisation, as well as high gold-silver ratio, ultrafine, submicroscopic size of gold particles etc. One of the features of deposits of this type is the presence of dispersed organic matter (DOM) within ore bodies.

Most authors believe that one of the typical Carlin-type mineralisations is the Vorontsovskoye gold deposit in the Northern Urals where mineralisation is located within zones of brecciation of mramorized limestone with heterogenous cement and, partially, overlying igneous-sedimentary rock. There is a distinctive structural control (varydirectional faults, thrust zone). Gold in the ore is either associated with sulphides (predominantly pyrite, arsenopyrite) or it is free and finely dispersed.

Organic matter (OM) within the deposit occurs in various rock formations, however the most OM is present within the cement of brecciated carbonate ore [1, 2]. We studied cement of carbonate breccia from various stratigraphic levels in the deposit. Samples were collected from core in exploration holes, from benches and sides of the existing opencast mine – mostly from within ore bodies. This resulted in new data on the OM composition and its distribution within the ore.

Structure of brecciated ore cement is microgranular, inequigranular, mineral phases cannot be identified visually (and often under microscope as well); clastic material in the breccia partially consists of marmorized limestone, with fragment size ranging from few millimetres to several centimetres. Breccia cement structure often has clear lamination, with alternating sulphide-rich layers and predominantly carbonate layers. Dispersed organic matter in the breccia is finely dispersed, often forms irregular clots up to 0.3 mm across.

X-ray phase analysis (diffractometer XRD-7000) and thermal analysis (derivatograph Diamond TG/DTA) demonstrate multicomponent composition of the breccia cement, with dominant proportion of carbonates – calcite and dolomite (from 5% to 80%). Sulphides in the cement vary from few per cent to 30%, and they are normally represented by pyrite and arsenopyrite and, to a lesser extent, chalcopyrite. Common among other minerals are quartz, chlorite, kaolinite, serpentine, light-coloured mica, and hydromica.

Our studies and previous research [1] suggests that there are no free carbon phases (graphite, carbon matter) in the DOM of Vorontsovskoye deposit. No solid bitumen of anthraxolite or kerite range have been found either. Thermal analysis puts organic matter in all samples within the same type of lower-middle kerite, with the degree of alteration which is comparable to regional epigenetic alteration i.e. practically absent. Total C_{org} in the analysed samples does not exceed 1% weight, while the amount of soluble bitumen (chloroform extract, Soxhlet extractor) varies from 32 mg/kg to 450 mg/kg.

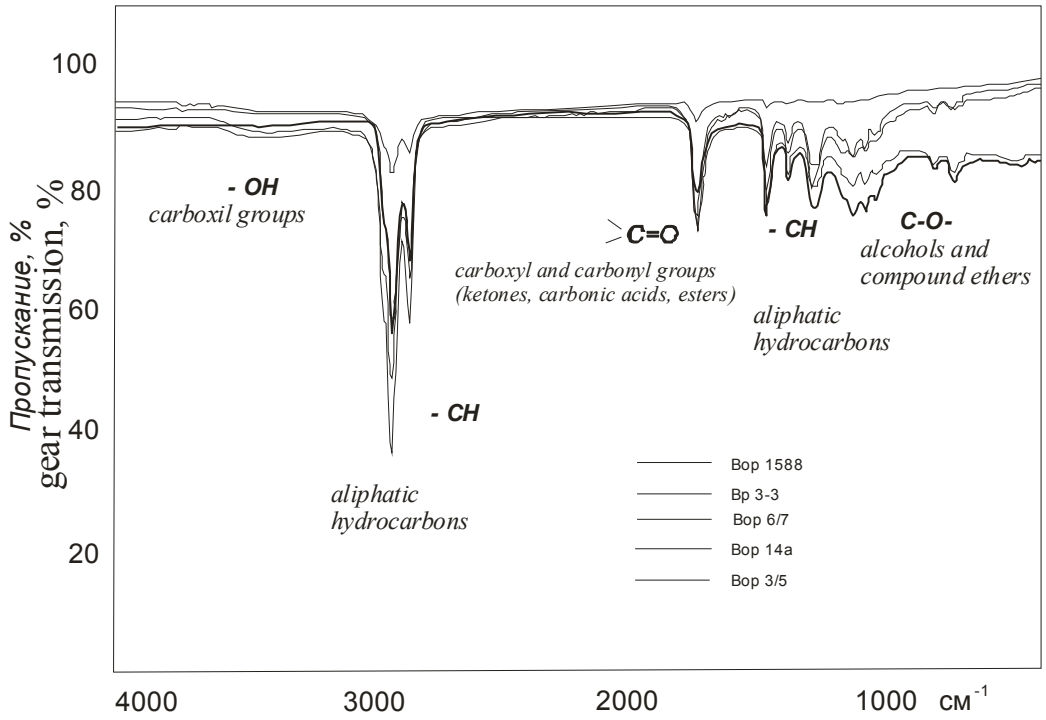

Figure 1. Composition of organic matter in ore breccia of Vorontsovskoye deposit based on IR-spectrometry data. Northern Quarry. Hor.+120m.

The results of IR-spectrometry (spectrometer «Nikolet 6700») reflect the composition of soluble bitumen (Fig. 1). Band amplitude indicates relative content of particular typical groups in each sample. Dominant are aliphatic hydrocarbons (bands 2800-3000 and 1300-1500 cm^{-1}), there are alcohols and compound ethers (bands 1000-1300 cm^{-1}), while the presence of carboxyl groups (bands 3300-3400 cm^{-1}) probably indicates the presence of higher organic acids and a number of other complex compounds. Analysis of IR-spectroscopy data indicates that aliphatic hydrocarbons dominate in all samples, and variation in bitumoid composition is mainly defined by the presence of various acid-containing complexes.

Studies of flat polished thin sections under SEM JSM-6390LV identified diverse shapes of organic matter – rounded, irregular-isometric, elongated; with size normally not more than 50 μm. No expressed association of OM with sulphidised areas was identified. Luminescent microscopy was used for identification and description of the DOM morphology in flat polished thin sections. They were studied using OI-18 lamp with SVD-120A quartz-mercury bulb in combination with Olimpus BX-51, optical microscope equipped with Infinity Lumenare camera. It was established that microinclusions of OM quite clearly show themselves under UV light with wavelength λ = 365millimicron ((UFS-3 filter) with practically no afterglow. No positive effect of pretreatment by organic solvent (chloroform) on colour or intensity of the luminescence was identified). Luminescence microscopy allows to outline dispersed organic matter within the rock more accurately, to establish its shape and size. It was observed that most OM inclusions are spatially associated with grain contacts or with microdeformations in rock (Fig. 2).

In a number of foreign articles on mineralogy of Carlin-type deposits dispersed organic matter is referred to as one of the ore components, its possible relationship with gold mineralisation is pointed out [Radtke, 1985; Radtke, Scheiner, 1970; Li, Peters, 1998; Almrdia et al., 2010 etc.]. On the other hand, practically no one has established any clear quantitative relationships between ore components and concentrations of organic carbon and composition of DOM. Our current results do not give any confident indication of presence or absence of relationship between OM and gold mineralisation, but they provide sufficient grounds to suggest

some connection between carbonisation and the latest low-temperature mineralisation and metasomatism.

The research supported by program of UB RAS, project № 13-05-96039.

References:

[1] E.V. Rakhov Organic Matter in Ore-Bearing Breccia of Vorontsovskoye Gold Deposit in the Northern Urals. // Annals-1997. Yekaterinburg: IofG&G RAS, Urals Branch, 1998, pp. 67-68.

[2] O.B. Azovskova, M.Yu. Rovnushkin, O.V. Koryakova, M.Yu. Yanchenko Organic Matter in Ore and Surrounding Rock of Vorontsovskoye Deposit // Annals 2010. Yekaterinburg: IofG&G RAS, Urals Branch, 2011, pp. 46-51

[3] M.Yu. Rovnushkin, O.B. Azovskova Organic Matter in Brecciated Ore of Vorontsovskoye Deposit. // "Metallogeny of Ancient and Modern Oceans – 2012 Hydrothermal Fields and Ore". Proceedings of XVIII Youth Research School. Miass, 2012, pp 190-194.

[4] M.Yu. Rovnushkin, O.B. Azovskova, S.P. Glavatskikh Electron Microscopy Potential for Studying Organic Matter in Ore) // Annals 2011. Yekaterinburg: IofG&G RAS, Urals Branch, 2012, pp. 252-254.

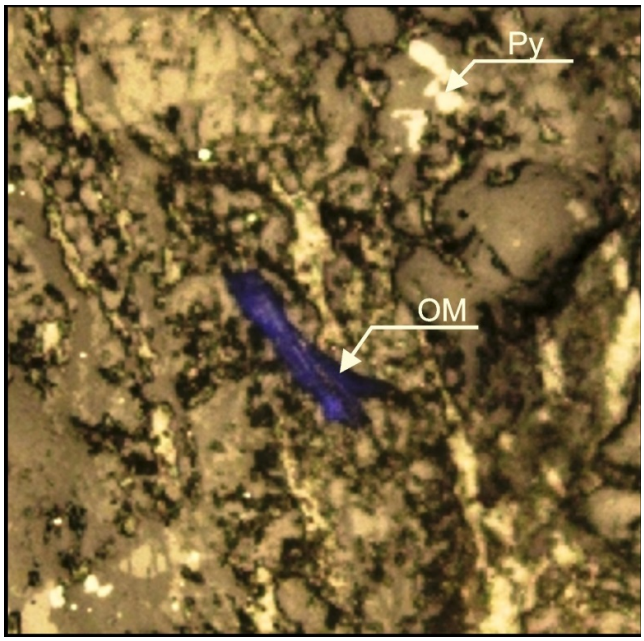

Figure 2. Identification of 80 micron OM in microfracture zone. Sample Vor-62/7, UV+reflected light,

THE STUDY OF THE CRYSTALLIZATION PROCESS OF THE PROTOTYPES OF HUMAN BLOOD PLASMA

Solodyankina A.A.*, *Golovanova O.A.

Omsk State University, Omsk, Russia
a.a.solodyankina@chemomsu.ru

Crystallization processes of sparingly soluble compounds have always attracted the attention of researchers. The interest aroused by the fact that these compounds are part of the pathogenic minerals. They are diseases the human organism and are also used in the synthesis of advanced biomaterials.

The second most common disease of arterial vessels is arteriosclerosis. [1] This disease is associated with the formation of calcium salts deposits in the vessels.

Therefore, the study of the crystallization of insoluble compounds in human body for the purpose of disease prevention is a perspective area of research.

The main purpose - study the character of crystallization of the prototypes human plasma under conditions close to physiological.

It is known that the plasma comprises about 55% of blood volume. The blood plasma contains 90-92% water and 8-10% of dry matter primarily proteins and salts [2].

Many substances dissolved in the plasma. They are low molecular organic compounds (urea, uric acid, amino acids, etc.), they are very large and complex structure of protein molecules, partially ionized inorganic salts.

Several solutions with different initial supersaturation were made for studying the crystallization of solution, modeling the composition of blood plasma. Correction of pH to physiological values was performed by adding 30% NaOH solution or HCl (conc.). Visual method was used to determine the induction period. Investigation the crystallization kinetics carrying out with using conductometric and photometric methods. Residual concentration of calcium ions was detected with potentiometric method. Type microcrystallisation the resulting solutions was defined by optical microscopy.

Analysis of the results showed that the pH of mixed solutions decreases with increasing supersaturation. In our opinion this is associated with sedimentation and decrease amount of Ca^{2+}. Three areas with different types of pH change can be distinguished on the curves: 3-15 supersaturation, supersaturation 15-30 and 30-90. By the study influence of supersaturation on the test solutions by conductometric and photometric method similar dependence was obtained (Fig. 1).

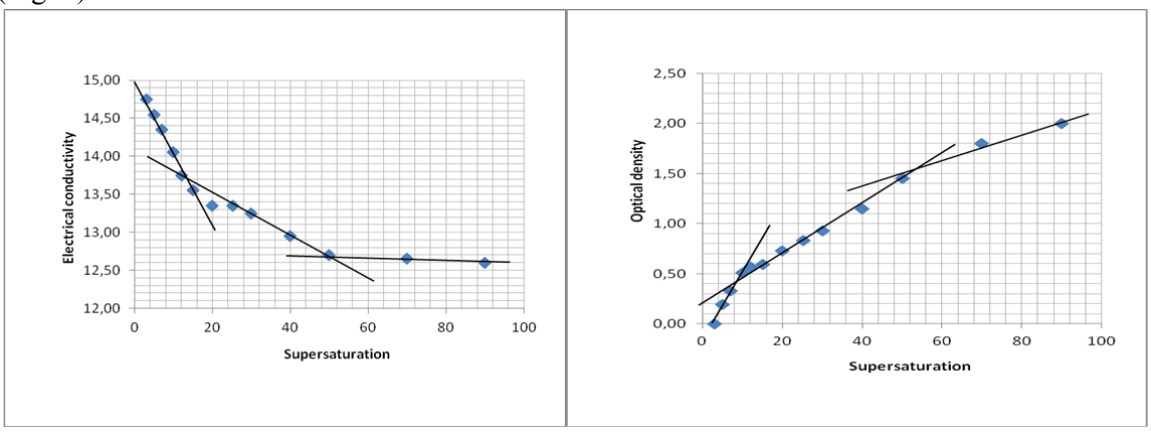

a b

Figure 1. Dependence of the electrical conductivity (a) and optical density (b) according to supersaturation.

General reaction order (n = 1,6) and the rate constants for different supersaturation was calculated according to the obtained values of induction periods (Fig. 2).

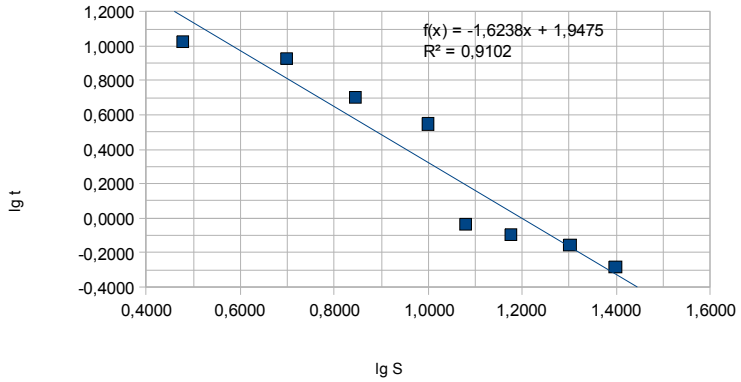

Figure 2. Logarithmic dependence of time from supersaturation.

The results of optical microscopy provided the above data. In the micrographs, conglutination observed with increasing supersaturation. This is typical for dominance of aggregation processes (Fig. 3).

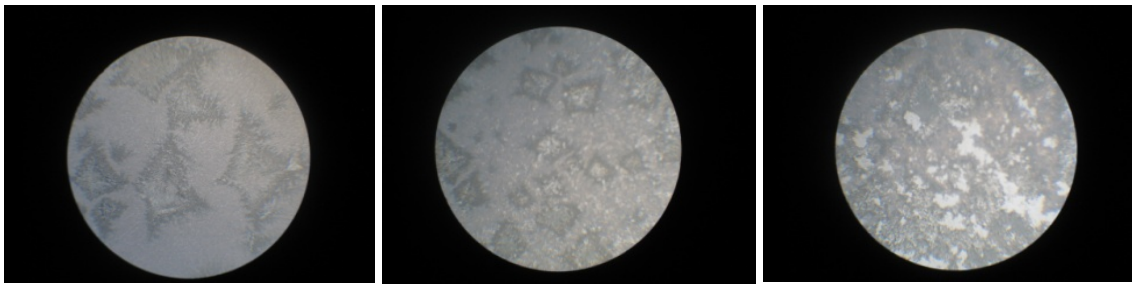

a b c

Figure 3. The results of the optical microscope (a - supersaturation 5, b - supersaturation 20, c – supersaturation 40).

Thus, during the research was established the dependence pH, conductivity and optical density model solutions from the degree of supersaturation of the systems, types microcrystallisation; was calculated the order and the constants the crystallization of insoluble compounds.

References:

[1] http://www.who.int/ru/index.html

[2] Human Physiology. Ed. V. Pokrovsky, Korot'ko G.F. Moscow: Medicine, 1997. Vol. 1, 448 p.

SEPARATION OF SOLID OLUTIONS VIA A COUNTER-CURRENT CRYSTALLIZATION PROCESS

Temmel E. [1], ***Seidel-Morgenstern A.***[1,2], ***Lorenz H.***[1]

[1]*Max Planck Institute for Dynamics of Complex Technical Systems, Magdeburg, Germany*
[2]*Otto von Guericke University Magdeburg, Chair of Chemical Process Engineering, Magdeburg, Germany*
temmel@mpi-magdeburg.mpg.de

The occurrence of complete or partial solid solutions in solution crystallization limits the applicability of commonly used crystallization processes and complicates separation tasks. Due to the particular solid-liquid equilibria (SLE) it is not possible to purify these mixtures within one crystallization step. Furthermore, many examples of complete or partial miscibility in the solid state are published for organic and inorganic systems **[1, 2]** but up to now no efficient crystallization based separation process was identified for such substances.
Generally fractional crystallization can be applied **[1, 3, 4]** because it is possible to separate systems forming solid solutions with repeated dissolution and crystallization procedures. This principle can be realized by exploiting a cascade of batch crystallizers. Furthermore, it was shown that a counter-current between the solid and liquid phase in such a process would lead to optimal process performance in terms of yield and productivity. Nevertheless, the realization and automation of the transport of the solid phases between the separation stages is difficult and requires a huge instrumental effort.

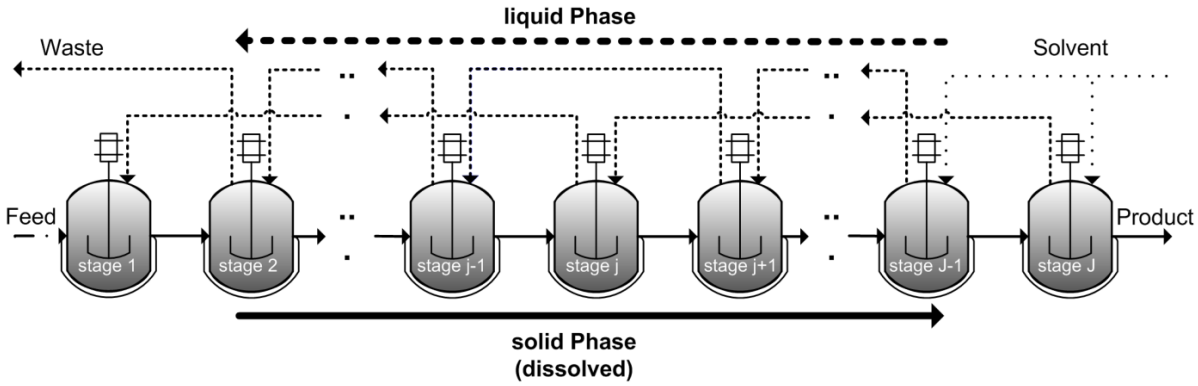

Figure 1: Configuration of a counter-current crystallization cascade. Due to the specific operation and connection between the stages it is possible to avoid the transport of solid phases can be avoided.

Recently an automatic counter-current crystallization cascade (Figure 1) was developed by the HAPILA Gera GmbH (Germany) **[5]**. In this plant exclusively liquid phases are transported. The solid phase is dissolved after the crystallization to avoid the expensive transport of the crystalline phases in the solid state. Hence, an efficient multi stage counter-current process can be realized and automated easily.

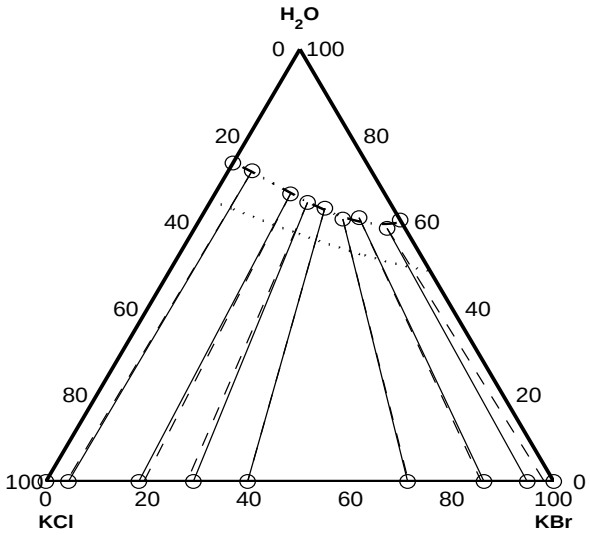

Figure 2: Ternary phase diagram of the system KCl / KBr / H_2O with isotherms for 30°C and 80°C and conodes indicated.

In the contribution the measured SLE of two different systems forming complete solid solutions will be shown (e.g. Figure 2). This data was subsequently implemented into a recently developed multi-stage equilibrium model to design and follow purification experiments for the two substance mixtures. Therefore, the required mathematical framework will be explained and the model validation by a manually operated counter-current crystallization in a rotary evaporator will be presented. Subsequently, the counter-current crystallization cascade is described and discussed on the basis of the process scheme and the verified model. Finally, this plant was used to run a semi-automatic separation experiment where the comparison of theoretical and experimental results will be given. To show the wide range of application opportunities for this process also a partial solid-solution forming system was theoretically investigated in a simulation study.

References:

[1] Mullin, J. W., Crystallization, Boston, Butterworth-Heinemann (1997)
[2] Dejewska, D.; Szymański, T., Cryst. Res. Technol., 1998, 33, 757-765
[3] Lin, S. W; Ng, K. M.; Wibowo, C., Comput. & Chem. Eng., 2008, 32, 956–970
[4] Balawejder, M.; Galan, K. ; Elsner, M. P.; Seidel-Morgenstern, A.; Piatkowski, W.; Antos, D., Chem. Eng. Sci., 2011, 66, 5638–5647
[5] HAPILA GmbH, Patent, DE 10 2008 023 833 A1, 2009

CALCIUM PHOSPHATE MINERALIZATION IN HUMAN ORGANISM

Titov A.T. [1], ***Larionov P.M.*** [2], ***Zaikovskii V.I.*** [3], ***Ivanova A.S.***

[1] *V.S. Sobolev Institute of Geology and Mineralogy SB RAS, Novosibirsk, Russia,*
[2] *Institute of Traumatology and Orthopedy, Novosibirsk, Russia*
[3] *Institute of catalysis of SB RAS, Novosibirsk, Russia*
titov@igm.nsc.ru

Mineralization of organic tissues is a necessary requirement for the existence of humans and animals. The inorganic part of bone tissue, teeth and pathologic formations is usually represented by calcium phosphate. It is known that the major mineral of bone tissue and many solid pathologic deposits in humans and animals is hydroxyapatite (HA) $Ca_{10}(PO_4)_6(OH)_2$. The most commonly accepted hypothesis is the formation of primary calcific deposits on the aorta and cardiac valves by the membrane mechanism similar to bone mineralization (Anderson 1983). Here the role blood is limited to transport of Ca and P ions. Acid phosphates formation: octacalcium phosphate (OCP)-Ca_8H_2 $(PO_4)_6 \cdot 5H_2O$ or dicalcium phosphate digidrate (DCPD-brushit) $CaHPO_4 \cdot 2H_2O$ is assumed to be more preferable as precursor phases that undergo transformation into the most stable one hydroxyapatite (Tomasic 2001). In the present paper we prove the alternative mechanism assuming that HAP forms in the blood plasma without participation of any intermediate phases. It is assumed that participates in the tissue mineralization, whereas the formation of more acid calcium phosphates results from secondary transformations.

In the present work, we used intraoperative material: mineralised aortal and mitral heart valves taken from patients with acquired valvular defects of rheumatic and septic genesis. Mineralized bioprostheses (pig) were obtained in reoperations aimed at revalving. The macroscopic and histological analysis of the valves was carried out. In addition, blood was sampled from patients with heart valve mineralization. The dry residue of blood plasma was examined. For comparison, we carried out a similar analysis of the donors blood.

Modeling experiments were carried out under adjustable conditions (T=37ºC, pH=7.4) with respect to the ionic composition of the main elements (Ca, P, Mg and NaCl) in aqueous solutions close to their contents in the blood plasma. The basic blood protein albumin was used. As the modeling protein the serum bovine albumin served.

Methods of local structural and chemical analysis were used in the work: transmission electron microscopy high resolution (HREM), electron diffraction, scanning electron microscopy (SEM) and X-ray spectra microprobe analysis with energy dispersion (EDX). We also used X-ray diffraction

According to the data of TEM, the aggregates of heart valve calcificates are composed of primary particles differing in size, morphology and structural ordering. The major part of HAP of the valves is composed of nanocrystals 10-100 nm in size similar to bone apatite with the c axis in the crystal plane. Relatively large grains are usually composed of off-oriented blocks 5 to 20 nm in size. In separate mineralised valves, microcrystals of lamellar and prismatic habits were observed in the vicinity of hydroxyapatite. Often they grow from a common centre forming spherical inclusions up to 60 μm in diameter. The values of Ca/P ratio obtained in comparison with the reference apatite are within the range 0.95 to 1 for different measurements, which better corresponds to brushite. X-ray diffraction studies also revealed reflexions characteristic of brushite, with the corresponding interplanar spacings: 7.57; 4.24; 3.05; 2.92; 2.62; 2.60. The formation of brushite requires higher concentrations of calcium and phosphorus, and lower pH in comparison with hydroxyapatite. It follows from the results of our work that more acidic calcium phosphates (brushite) are formed after hydroxyapatite

mineralization as a result of secondary processes leading to a decrease in pH in tissue fluids (tissue degradation or bacterial infection).

Investigation of mineralised cusps of bioprostheses by means of SEM and TEM showed that the mineral deposits on the cusps of bioprostheses substantially differ in structure and chemical composition from the calcificate of natural valves. Massive calcificate is represented mainly by calcium phosphate and a small amount of iron phosphate. The Ca/P ratio for calcium phosphate corresponds to calcium-deficient hydroxyapatite (<1.67). For different bioprostheses and for different parts of a bioprosthesis, the Ca/P ratio varies from 1.43 to 1.60. Hydroxyapatite is represented in all the samples by nanocrystals of needle-like shape up to 200 nm long and about 5-10 nm wide, with the typical contrast in TEM images: a light central line and dark edges. Direction c is located in the nanocrysal plane along the direction of predominant growth. It is noteworthy that the crystals similar to these ones in morphology, structure and chemical composition were obtained by us by means of the controllable synthesis (T=37°C, pH=7.4), when the concentrations of calcium and phosphorus in the aqueous solution correspond to their concentrations in the blood of a healthy adult (Ca=1.3mM, P=1.5mM), but magnesium is absent or its concentration is two times lower (Mg = 0.4mM) than the lower boundary of the normal level.

It is noteworthy that the crystals similar to these ones in morphology, structure and chemical composition were obtained by us by means of the controllable synthesis (T=37°C, pH=7.4), when the concentrations of calcium and phosphorus in the aqueous solution correspond to their concentrations in the blood of a healthy adult (Ca=1.3mM, P=1.5mM), but magnesium is absent or its concentration is two times lower (Mg = 0.4mM) than the lower boundary of the normal level. An increase in magnesium content to 0.8mM causes the formation of thin-lamellate microcrystals which are similar in their morphology to the corresponding crystals comprising the calcificate of natural heart valves.

We have discovered the hydroxyapatite crystals (10-70nm) which are structurally and morphologically similar to the bone apatite and fine fraction of the cardiac valve calcification (Titov 2001). They have been found both in the solid residue of the blood plasma of the patients with calcinosis, and in the blood of healthy donors.

A physicochemical model of bone and pathological mineralization is proposed on the basis of the experimental material. The model considers extracellular formation of calcium phosphate in blood plasma as one of the possible mechanisms of physiological and pathological mineralization of tissues in an organism. One of the basic arguments in favour of this consideration is nanocrystalline HAP discovered by us in the blood plasma of healthy donors. It was concluded also that the blood protein promote the formation of HAP nanocrystals. Extracellular mineralization plays an important part in the mineralization process in a human organism. The matrix of a growing bone consumes albumin from blood [4]. A special role of albumin may be assumed not only for the formation of hydroxyapatite nanocrystals in blood but also for its participation as a structural element in bone mineralization process. Spontaneous precipitation of hydroxyapatite in blood is capable of producing a large mass of hydroxyapatite nanocrystals that may participate also in pathological mineralization of hearth and aorta valves. The penetration of HAP nanocrystals formed in blood to collagen fibres followed by precipitation may promote impairment of endothelium and tissue degradation, which is observed in many studies dealing with the mineralization of the natural heart valves and their bioprostheses.

[1] Anderson H.C. 1983. Calcific diseases. A concept. Arch. Pathol.Lab. Med.107: 7, 341-348.
[2] Tomasic B.B. 2001. Physicochemical principles of cardiovascular calcification. Z. Cardiol. 90:3, III/68-III80.
[3] Titov A.T., Larionov P.M., Shchukin V.S.et al. 2000. Possible formation of hydrohyapatite in blood. Doklady Biochemistry. 373: Julu-August.132.
[4] Owen M., Triffitt J.T. 1976. Extravascular albumin in bone tissue. J. Physiol..257: 293-307.

FEATURES OF MICROCRYSTALLIZATION OF STUDENT-BADMINTON PLAYERS SALIVA

Ulyankin E.B*, Popenko Y.A, Golovanova O.A, Turmanidze V.G.

Omsk State University, Omsk, Russia
battlepochtol@gmail.com

The saliva of the person can be a source of information on the general condition of an organism. On composition and structural properties of a saliva possibly identification of organism deviations an as a whole. It is known that recovery processes — the most important link of athlete efficiency. Search of simple available methods the express – diagnostics of a human body condition before physical activity for the purpose of carrying out recovery actions is important.

Work purpose: choice of effective indicators of a condition of a human body on the example of amateur athletes group on the saliva analysis before and after training.

Research methods: As material of research - the saliva of the persons who are engaged in badminton aged from 17-24 years. Two groups were distinguished from amateur athletes: 1) people with a good state of health — group "N", 2) people with slight violation (myopia) — group "C". For receiving comparable results saliva collected on an empty stomach, in a sterile test tube with densely being closed stopper, previously a mouth rinsed with the distilled water. Tests of oral liquid were selected before and after training. Microcrystallization of saliva is carried out on a method of an open drop. The assessment of microcrystallization of saliva is made on a 5-point scale. If less than a point, the general condition of an organism is worse.

Microcrystallization is influenced significantly by concentration of calcium in saliva, which was defined by complexion-meter titration.

The error of these methods makes no more than 10%.

Results of research: Among the examined 13 samples of oral liquid of group "N" and 20 samples of group "C" the essential difference in concentration of ions of calcium (tab. 1) (twice) and a microcrystallization average rating (pic. 1) is observed. The analysis of the received photos of microcrystallization showed that more accurate picture of microcrystallization at group "H"

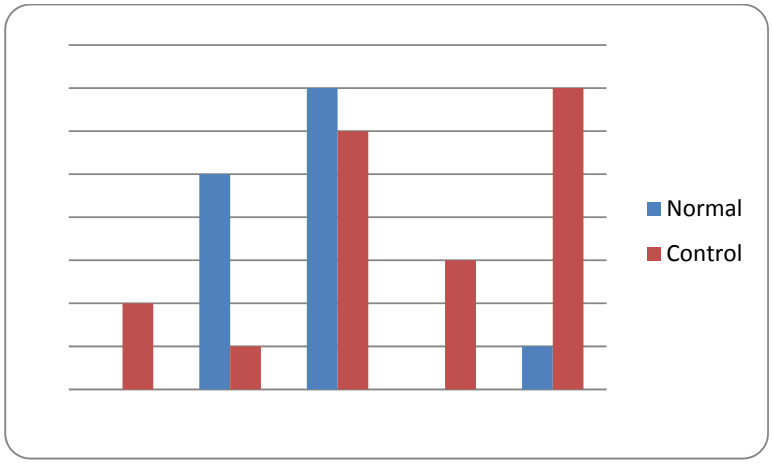

Figure. 1. Microcrystallization results of examined samples

So the offered technique of microcrystallization and analysis of saliva's electrolytic structure allow watching dynamics of health's physical state changes at amateur athletes and other groups of people.

Table 1. Concentration of ions of calcium in examined samples.

	C(Ca2+), g/l															
Normal	0,06	0,06	0,05	0,06	0,05	0,06	0,06	0,04	0,07	0,07	0,05	0,07	0,08	0,04	Average	0,06
Control	0,03	0,03	0,02	0,04	0,02	0,04	0,02	0,03	0,03	0,02	0,04	0,04	0,02	0,02		0,03

5 points 2 points 0 points

Figure 2. Microcrystallization examples of examined samples of oral liquid.

STUDY OF SOLUBILITY OF SILICON-SUBSTITUTED HYDROXYAPATITE

Zayts A.V., Berdinskaya M.V., Golovanova O.A.
Omsk State University, Omsk, Russia
a.v.zayts@chemomsu.ru

Materials based on hydroxyapatite $Ca_{10}(PO_4)_6(OH)_2$ used frequently in modern medicine because it is a synthetic analogue of bone and biologically compatible with the human body. One major disadvantage of unsubstituted hydroxyapatite is low rate of resorption by the body in contact with interstitial fluid [1]. Silicon-substituted hydroxyapatites (Si-HA) have the best characteristic of resorption, this is explained by silicic component which changes the effective surface charge of material. This is connected to a specific location of silicate ions relative phosphate ions in the crystal lattice of Si-HA [2].

Purpose of the research–study solubility of silicon-substituted hydroxyapatite synthesized from a model solution of human extracellular liquid at different conditions.

Samples of silicon-substituted hydroxyapatite with a concentration of silicate ions 0.5; 1.0; 1.5; 2.5; 5.0% were selected as starting objects of study. Dissolution was carried out at constant stirring for 40 minutes at temperatures 20°C, 50°Cand 80°C. 0.01 M hydrochloric acid solution and 0.9% sodium chloride solution was used as the solvent. Resorption rate was determined by adjusting the pH and concentration of ions of Ca, the pH and pCa was determined by potentiometric method.After dissolution, the remaining sediment was filtered off, dried and weighed. In the liquid phase, the residual concentration of phosphate and silicate ions was determined by photocolorimetry.

Samples containing 1.0 and 1.5% of silicate ions are have the best characteristics of resorption. This was noted in the study of the dissolution curves of silicon-substituted hydroxyapatite (Fig. 1). In this case, a further increase concentration of silicate ions does not affect on the nature of the dissolution process.

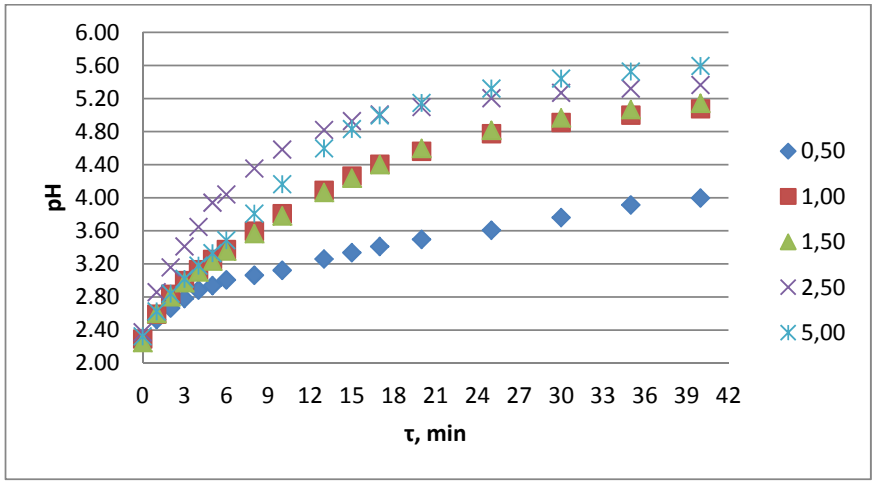

Figure 1.Study of solubility in hydrochloric acid.

Samples with concentration of silicate ions 0.5 and 5.0% were taken to further study the dissolution.

Graph of dissolution (fig. 2) show that the dissolution rate significantly increases with increasing temperature of process. The rate of resorption of Si-HA with Si = 0.5% at 20 ^{0} C is reached complete dissolution, and at 50 ^{0} C to the velocity characteristic of Si-C HA with Si = 5%. The rate of dissolution study phase at a temperature of 80° C coincide.

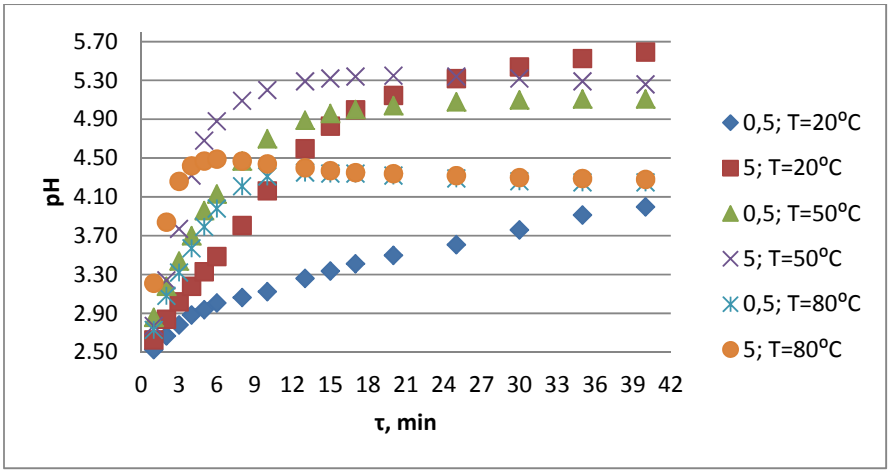

Figure 2. Study of solubility in hydrochloric acid solution at different temperatures.

A similar experiment was carried out in isotonic environment at various temperatures. The dependences of pH from temperature was obtained (Fig. 3). They are show that the dissolution is complicated process, perhaps due to the reactions of hydrolysis. Found that complete dissolution of Si-HA occurs in the first minutes of the experiment and the temperature rise promotes the growth rate of resorption.

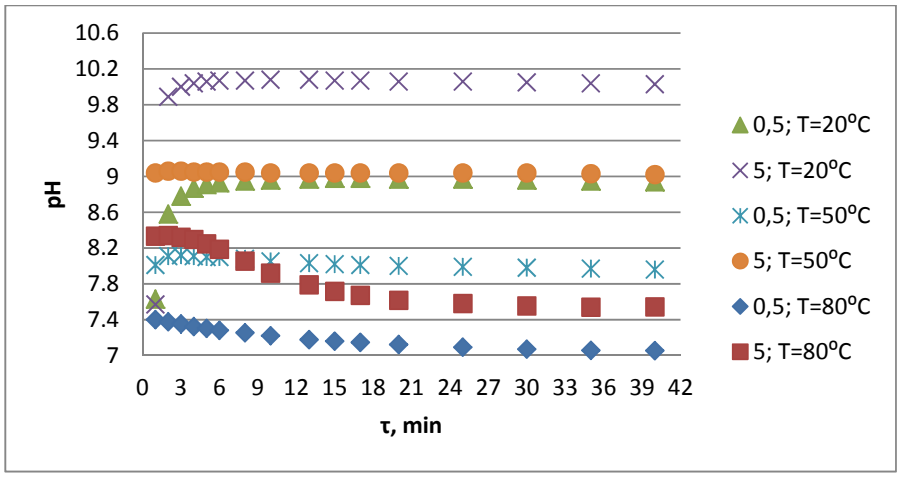

Figure 3. Study of solubility in physiological saline at different temperatures.

Thus, the dissolution of silicon-substituted hydroxyapatite in different solvents and at different temperatures has been investigated. Found that samples Si-HA with concentration of Si 1.0 and 1.5% in hydrochloric isotonic solution have the best characteristics of resorption.

This work was supported by the Russian Foundation for Basic Research (№ 12-03-98011-r_sibir_a and № 13-05-90432-Ukr_f_a).

References:

[1] Trubitcin MA, Gabruk NG, Oleinikova II, Le Van Thuan, Doan Van Dat Synthesis of Modified nanogidroksiapatitov by precipitation from solution and the study of their bioresorbable / / Scientific Statement, Belgorod State University, "Natural Science" - 2012 - Issue 18 - № 3, p. 180-185.

[2] Bielecki BI, Svente NV The role of silicon in the silicate Implants / / Abstracts – 2011.

SESSION 4

Crystallogenesis of minerals

INVESTIGATIONS OF THE STRUCTURAL FEATURES OF FERRO-SPINELS SYNTHESIZED BY RADIATION-THERMAL METHOD

Ancharova U.V. [1], ***Mikhailenko M.A.*** [1], ***Tolochko B.P.*** [1] ***Sharafutdinov M.R.***[1], ***Shtarklev E.A.***[2], ***Eliseev V.S.***[2], ***Vlasov A.Yu.*** [2], ***Korobeinikov M.V.***[2]

[1] *Institute of Solid State Chemistry and Mechanochemistry SB RAS, Novosibirsk, Russia*
[2] *Budker Institute of Nuclear Physics SB RAS, Novosibirsk, Russia*
ancharova@gmail.com

Electron beams allows to obtain new effects in high temperature chemistry of solid state. A stimulated influence of irradiation at comparable temperature conditions may be a subject of technological interest considering that increase of reaction rate **[1]**. Presumably, the use of initial oxides in nanoparticle form (obtained also by radiation-thermal method) allows additional increase of the reaction rate and may modify the ceramics properties.

Structural features of manganese-zinc and nickel-zinc ferrites were studied. The samples were synthesized by three different ways:

1. Standard ceramic thermal synthesis with preliminary mechanical activation of the reactants;
2. Radiation-thermal sintering of mechano-activated oxide mixtures;
3. Radiation-thermal synthesis of the reaction mixture prepared from nano-sized reactants powders.

The nanoparticles are synthesized from the initial oxides by radiation-thermal method.

It is shown that the use of electron beam for ferro-spinels' synthesis can raise the reaction rate and to reduce the sintering temperature.

This work was carried out with the involvement of equipment belonging to the shared research center "SSTRC" and supported by the Ministry of Education and Science of the Russian Federation.

References:

[1] N.Z. Lyakhov, V.V. Boldyrev, A.P. Voronin, O.S. Gribkov, LG. Bochkarev, S. V. Rusakov, V. L. Auslender // Journal of Thermal Analyais, Vol. 43(1995) 21-31.

ENHANCING THE SORPTION PROPERTIES OF VERMICULITE OWING TO ADDITIVES AND MECHANICAL ACTIVATION

Assilov A.B. [1], ***Kerimbek S.*** [1], ***Balgysheva B.D.*** [1], ***Kuanysheva G.S.*** [1], ***Shevchenko V.S.*** [2], ***Urakaev F.Kh.*** [2]

[1] *al-Farabi Kazakh National University, Almaty, Kazakhstan*
[2] *Sobolev Institute of Geology and Mineralogy SB RAS, Novosibirsk, Russia*
asylov.alybek@live.kaznu.kz

Mechanical activation of vermiculite with NaH_2PO_4 was investigated. It was found that in the system of vermiculite−NaH_2PO_4 formed aqua−phosphate glass with high sorption properties.

Currently, the search for new natural inorganic sorbents with high capacity and selectivity, radiation stability, environmental safety, and low cost is becoming increasingly important. Vermiculite is a mineral class of layered silicates group hydromicas was expressed by average $Mg_x(Mg, Fe)_{3-x}[AlSi_3O_{10}]\cdot(OH)_2\cdot 4H_2O$, which fully meets the above criteria **[1]**.

Vermiculites from Cherry Mountain (Southern Urals, Russia, Fig. 1) and Kazakhstan were used as starting materials. Vermiculite from Kazakhstan has a composition presented in the table below:

SiO_2	Al_2O_3	CaO	MgO	K_2O	Na_2O	Fe_2O_3	MnO	TiO_2	P_2O_5	SO_3
42.3	0.11	5.2	25.1	4.67	0.06	8.44	<0.01	1.8	1.31	0.07

Fig. 1. Museum sample (IGM SB RAS).

Fig. 2. Preparation of the starting samples.

Large flakes of the natural vermiculite were crushed and homogenized (including additives) using a steel one-ball vibratory mill (Fig. 2).

To obtain a sorbent mixture of vermiculite and sodium dihydrogen phosphate at different ratios (1:1, 2:1, 3:1, 4:1, respectively) were subjected to mechanical activation (MA) in a planetary mill Pulverissette 6. MA products studied by XRD (Fig. 3), derivatography, DTA, DSC (Inserts), IR spectroscopy. According to the sorption studies, MA effects on vermiculite laced with salt NaH_2PO_4 increases the capacity of the sorbent for cations Mn^{2+}. The best balance

of vermiculite and sodium dihydrogen phosphate is 4:1, in which the degree of adsorption is 98%. The degree of sorption MA vermiculite without adding NaH_2PO_4 is lower and consist 80%.

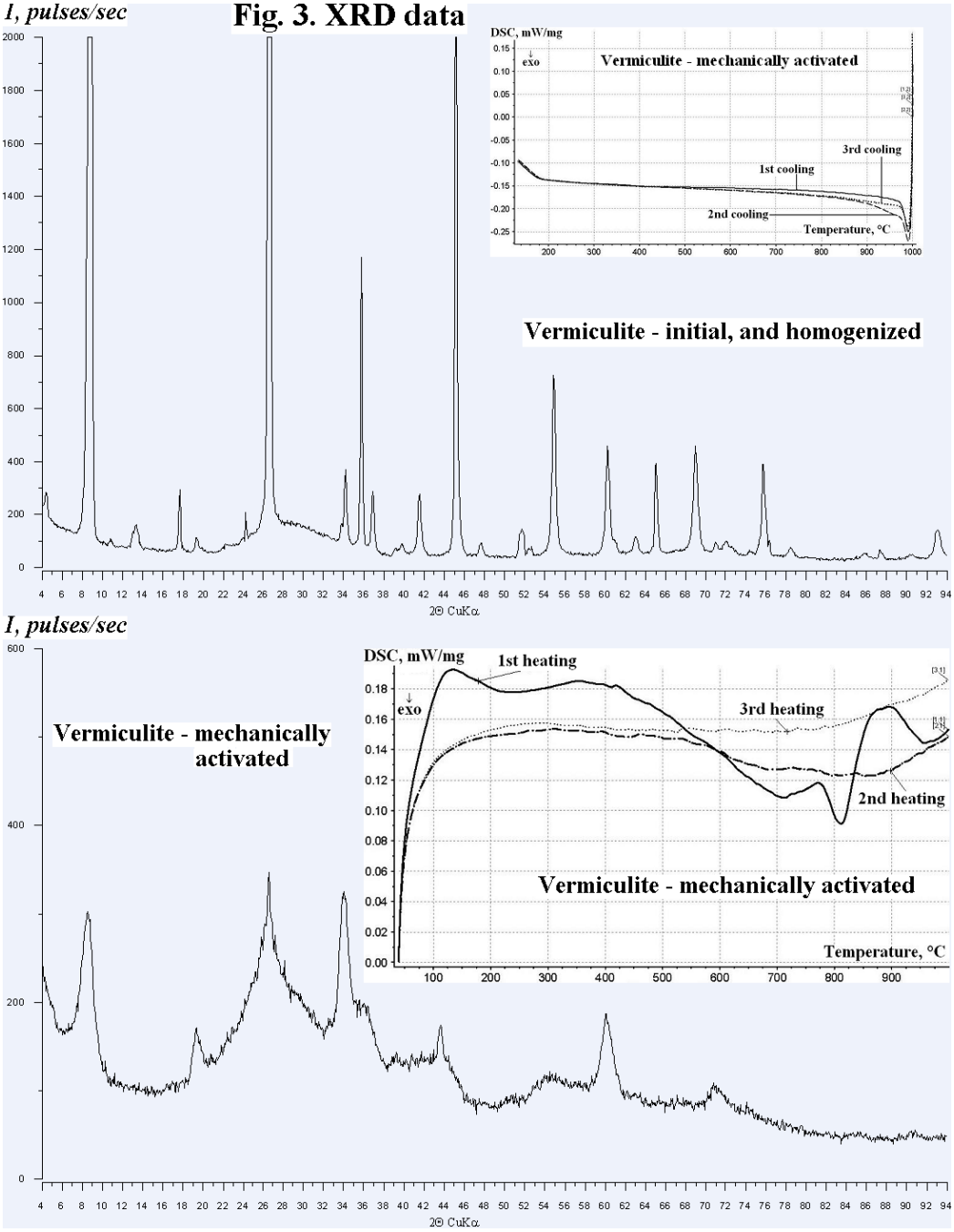

IR spectroscopy showed a change in the structure of vermiculite after mechanochemical activation, associated with the formation of a new amorphous phase, new bands are observed in the region of 1633-1641 cm^{-1} relevant $H_2PO_4^{-1}$.

Increasing the sorption properties of vermiculite after MA with the addition of sodium dihydrogen phosphate, can be explained by the formation of aqua-phosphate glasses. Aqua-phosphate glasses are new sorption centers in the structure of vermiculite.

[1] L.A. Perez-Maqueda, et al. *Journal of Thermal Analysis and Calorimetry*. 2012. Vol. 107. Iss. 2. P. 431-438.

COMPREHENSIVE STUDY OF MECHANICAL ACTIVATION OF GLAUCONITE AND GLAUCONITE SAND TO OBTAIN SORBENTS

Assilov A.B. [1], ***Kerimbek S.*** [1], ***Balgysheva B.D.*** [1], ***Kuanysheva G.S.*** [1], ***Shevchenko V.S.*** [2], ***Urakaev F.Kh.*** [2]

[1] *al-Farabi Kazakh National University, Almaty, Kazakhstan*
[2] *Sobolev Institute of Geology and Mineralogy SB RAS, Novosibirsk, Russia*
asylov.alybek@live.kaznu.kz

Glauconite is the water complex potassium-aluminum silicate, mineral hydromica subclass group of phyllosilicates and intermittent composition expressed by the formula averaged $K_{<1}(Fe^{3+},Fe^{2+},Al,Mg)_{2\text{-}3}[Si_3(Si,\ Al)O_{10}][OH]_2 \cdot nH_2O$ and has high sorption properties **[1]**. Influence of mechanical activation (MA) on the structure and properties of glauconite studied quite poorly. MA method can be modified to obtain sorbents based on glauconite sands.

Glauconite from Maardu deposit (Estonia, Fig. 1) and glauconite sand of Sokolov-Sarybay deposit (waste ore-dressing, Kazakhstan) were used as starting materials. Glauconite sand from Kazakhstan has a composition presented in the table below (PRDA is a percentage reduction during annealing):

SiO_2	Al_2O_3	CaO	MgO	K_2O	Na_2O	Fe_2O_3	MnO	TiO_2	H_2O	PRDA
46.70	13.77	12.00	3.13	2.44	1.84	4.89	0.08	0.70	1.40	12.64

Glauconite sand additives NaH_2PO_4 was treated in an agate one-ball (diameter 7 cm) vibratory mill for preparation starting homogenized samples. MA of the sample was carried out by a planetary mill Pulverissette 6 at different conditions of MA using hard WC accessories (Fig. 2).

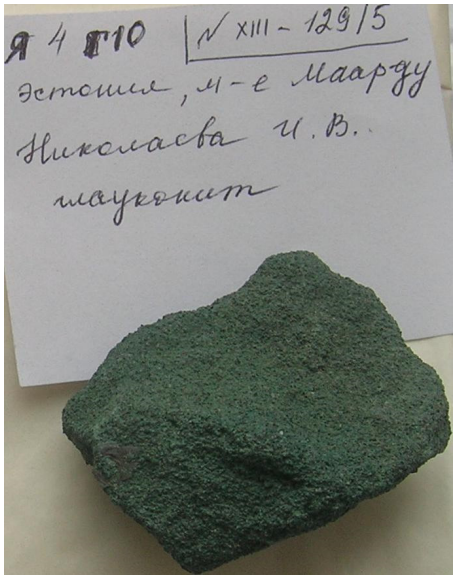

Fig. 1. Museum sample (IGM SB RAS).

Fig. 2. Museum glauconite after MA.

MA products studied by XRD (Fig. 3), derivatography (in N_2), DTA, DSC (in Ar, Insert), IR spectroscopy. According to the results of MA samples derivatography the TG curve after a smooth slide that characterizes the loss of adsorption, crystallization and constitutional water again sought up, which is possible only in the interaction of the samples with nitrogen. Intensity weight gain depends on the initial ratio and NaH_2PO_4 glauconite sand in the mixture. Maximum weight gain was observed for the sample with the highest content NaH_2PO_4. In the thermograms of samples glauconite sand without the addition of NaH_2PO_4, a similar phenomenon was not

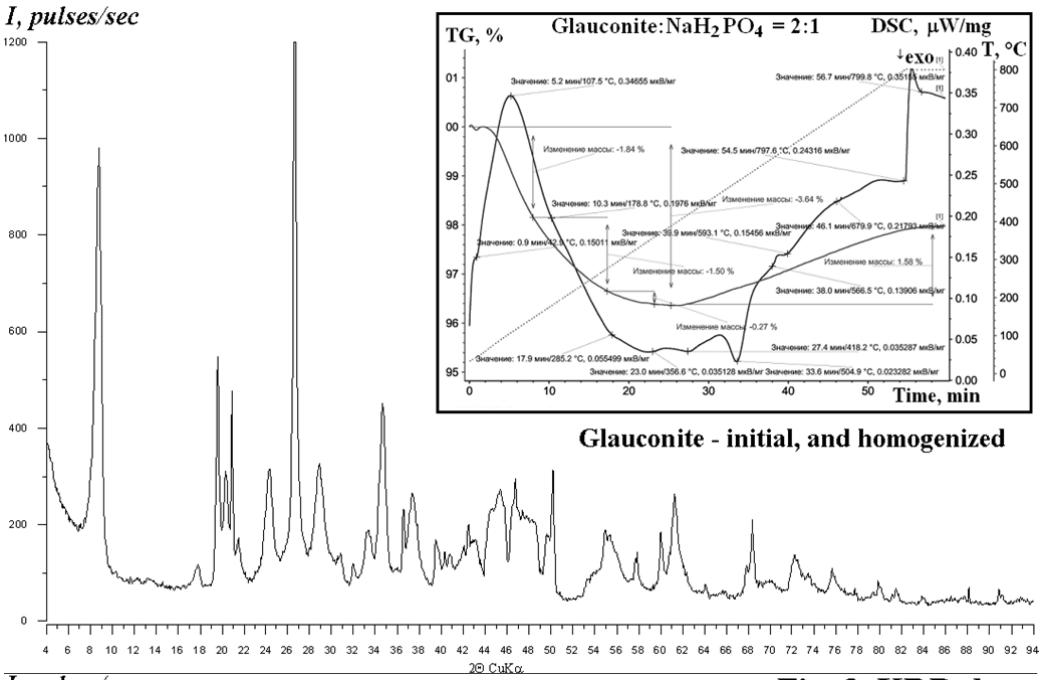

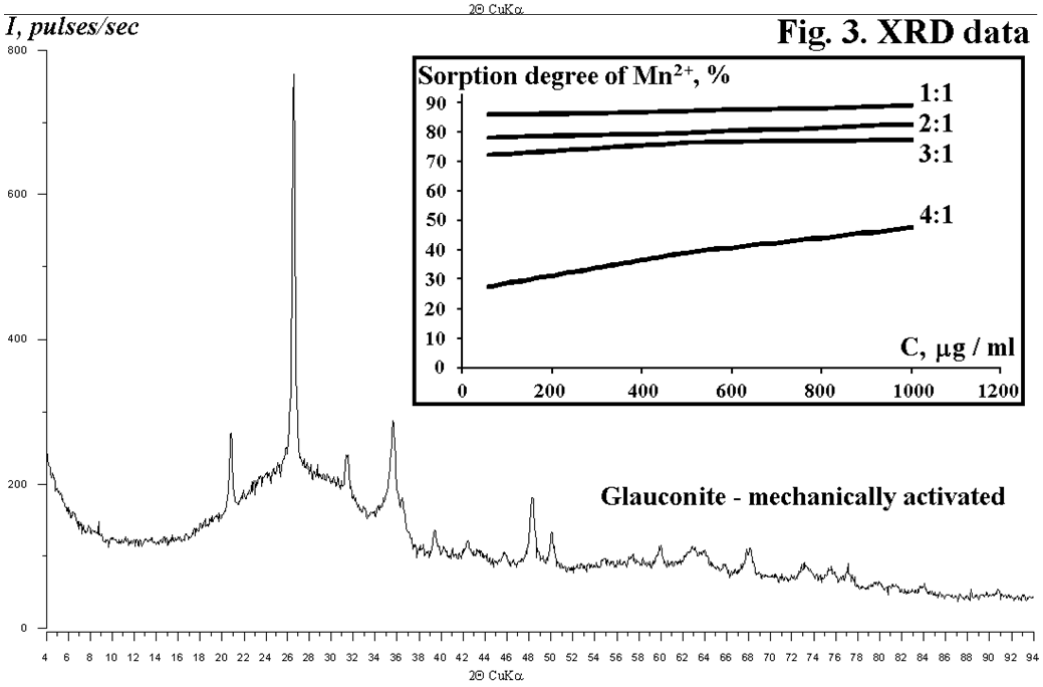

Fig. 3. XRD data

observed. The increase in weight when TG well explained by the sorption of nitrogen on the surface of the MA glauconite sand. Sorption capacity of sorbents studied in static and constant stirring of the model solutions with concentrations of manganese sulfate 60−1000 µg/dm^3.

The concentrations of manganese ions in the initial and equilibrium solutions was determined by atomic absorption spectrometry. These sorption studies have shown that the maximum capacity in relation to the manganese ion has a sorbent with a ratio of glauconite sand: NaH_2PO_4 = 1:1 (Insert). The maximum degree of sorption of a sorbent reaches 89.2 %. The degree of adsorption increases with the concentration of Mn^{2+} in the original solution.

[1] Drits V.A. Problemy opredeleniya real'noy struktury glaukonitov i rodstvennykh tonkodispersnykh silikatov (Problems of Determining the Real Structure of Glauconites and Related Fine Silicates). - Moscow: Khimiya, 1993, 200 pp.

THE RESULTS OF MICROSCOPIC STUDIES OF GOLD DEPOSIT SOUTHERN ASHALY (KAZAKHSTAN)

Baibatsh A., Dyussembayeva K., Kassenova A.

K. Satpayev Kazakh National Technical University, Kazakhstan
baibatsha48@mail.ru

Gold deposits in black shale stratas are characterized by significant resource potential for the noble metals **[1, 2]**. In the CIS countries known by such large fields as Bakyrchik (Kazakhstan), Sukhoi Log, Natalkinskoye, Nezhdaninskoye (Russia), Muruntau (Uzbekistan), Kumtor (Kyrgyzstan).

Large deposits of Bakyrchik in Kazakhstan are still not executed, because of the difficulties of its enrichment of ores (the presence of carbonaceous matter, arsenic as a harmful impurity, finding the gold in pyrite and arsenopyrite in an invisible form).

Figure 2 shows a structural position, geological soning and gold mineralization of western-Kalbinsky belt **[3]**. The Southern Ashaly is the part of Akzhal-Daubaisky ore region and is timed to the Ashaly-Daubaisky ore field.

The Southern Ashaly deposit is located in the south-western part of the Kalba range (East Kazakhstan region) in the south-eastern part of Ashaly-Daubaisky ore field. The total area of the ore field is estimated at about 50 km2 and incorporates Daubaisky group of the fields and Ashalinsky. There are about 20 ore occurences and small-scale gold deposits in the field.

The host rocks for the ore bodies of the deposit are terrigenous formation of the middle carboniferous of the Bukon suite. The block rocks that holds the deposit is restricted from west and east by faults northeastern direction - it is Baiburinsky and Dolinnoye faults. The distance between these structures in the plan is about 1000-1200 m.

The main factors which control placement of the ore bodies on the deposit is lithologic-and – stratigraphic (ore bodies are confined to the upper shale assise of the Bukon suite, the most differentiated in composition of part of its geological record, represented fine-laminated carbonaceous shales, siltstones and sandstones), and structural (localization of ore bodies is controlled by fault zones that transect the lamination and schistosity at an acute or steeper angles).

Ore bodies in relation to lamination of the rocks are mostly take the obliquely cutting position close to substratified. This includes, first of all, to the largest and most rich in content of gold ore body № 3 and accompanying it ore bodies - 2, 4, 5, 6 and 7. Other leading the body number 1, tending to the shale assise, which is controlled by the cross-section of relative to lamination of the crushing and crumpling zone, which has the north-western direction. The largest ore bodies (№ 1, 2 and 3) are presented by ribbon-like bodies which have steeply dipping and sub-lateral west-north-western strike.

Gold-sulfide Southern Ashaly belongs to the deposits which are localized in the carbonaceous terrigenous (black shale) stratas, confined to areas of infolded and post infolded tectonic deformation **[4, 5]**.

In the Southern Ashaly the host rocks and ores composing the main ore bodies № 1 and 3 were studied by microscopically. The results of microscopic study of thin rock section show that the gold mineralization is associated with small intrusions of plagiogranites and zones of plagiogranite porphyry dykes. It is located in the hydrothermal-metasomatic altered volcanic and sedimentary rocks (aleuritic tuffsandstone, tuff breccia) and sericite-carbonaceous shales. There are carbon-sericite, quartz-sericite, carbonate-quartz metasomatic associations in the deposit.

Carbonaceous formations are represented by the oxidized (carbonates) and reclaimed (disperse carbonaceous particles and anthraxolite) forms.

The main ore-forming minerals are pyrite and arsenopyrite, which form the an uneven fine disseminations in silicified, carbonatized and sericitized host rocks, and also encountered in thin

quartz and quartz-carbonate veinlets. It is noted the presence of subordinate amount of chalcopyrite, chalcosine, tetrahedrite ore and carbonaceous matter and rutile. The amount of sulfides reaches 5-8% in total. Pyrite is the main sulphide among them. In arsenopyrite gold is extremely rare. The particles of gold in pyrite have been viewed and pictures are taken on a microprobe JCXA-733 because of their poor visibility in the light microscope (finely dispersed particles). There are two types of gold mineralization: 1) is a richer in beresitizated plagiogranites and plagigranite-porphyries and 2) in hydrothermally altered tuff sandstones, tuff breccia and carbonaceous shales.

Gold in thin aggregative pyrite II is generally in the form of point, barely any visible in the light microscope inclusions 1-2 microns in size. In different places of thin aggregative pyrite II found about 35 gold grains. Their size is from 1 micron or less and up to 6 microns. Often there are grains of gold in pyrite along the border with arsenopyrite and even moving in arsenopyrite. Below are pictures of gold, made by light microscopy and micro-probe in different modes - compo and back-scattered electrons (*Figure 1*).

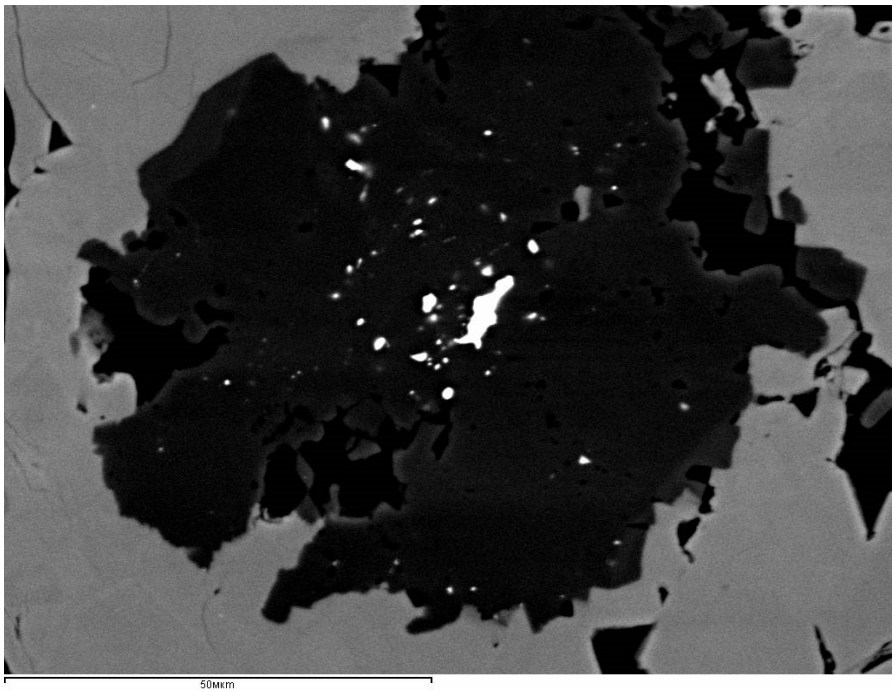

Figure 1. The micro-sized grains of gold (white) in the thin aggregative pyrite II (black). Gray – arsenopyrite.

References:

[1] Konstantinov M.M. Auriferous province in the world. Scientific World, 2006. - 358 p.
[2] Muruntau gold deposit. Tashkent: FAN Acad. of the Republic of Uzbekistan, 1998. 540 p.
[3] Raphailovich M.S., Mizernaya M.A., Dyachkov B.A. The large deposits of gold in the black shale strata: the conditions of formation, signs of similarity. - Almaty, 2011. – 272 p.
[4] Narseev V.A., Gostev Y.V., Zakharov A.V. and others. Bakyrchik (geology, geo- chemistry, mineralization). M. TsNIGRI, 2001. - 174 p.
[5] Zhautikov T.M. Gold-bearing carbonaceous-terrigenous Bakyrchik-Suzdalsky carbon made metallogenic complex //Deep structure and mineral resources of Kazakhstan. Metallogeny, Volume II. Almaty, 2002. - P. 180-186.

CRYSTALLOGENESIS OF ZEOLITES: HOW TOPOLOGICALLY IDENTICAL FRAMEWORKS CORRELATE WITH VARIOUS WATER-CATION ASSEMBLAGES

Bakakin V.V. [1], ***Seryotkin Yu.V.*** [2]
[1] *A.V. Nikolaev Institute of Inorganic Chemistry, SB RAS, Novosibirsk, Russia*
[2] *V.S. Sobolev Institute of Geology and Mineralogy, SB RAS, Novosibirsk, Russia*
bakakin@niic.nsc.ru

In the structures of zeolites with the general formula $|M_n(H_2O)_x|\cdot[(T,T')_mO_{2m}]$, two subsystems can be distinguished: the framework and extraframework ones consisting of $(T,T')O_4$ tetrahedra and water-cation assemblages (**WCA**), respectively. This is an important crystallogenetic problem to estimate the relationships and interrelations between those.

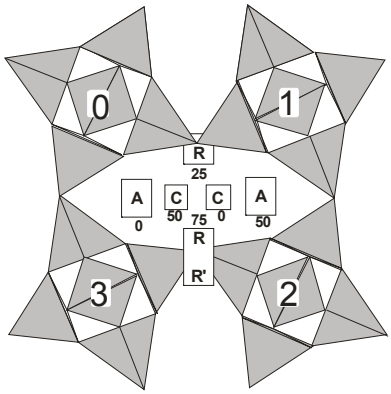

Fig. 1. Basic extraframework positions in the channels of NAT framework.

The frameworks of the given topologic type form frequently with involving essentially different WCA. At a high lability of WCA, as opposed to rigid organic molecules, for instance, the formation process should be recognized as structure-directing rather than templating one. Natrolite-type zeolites and zeolite-like heteroframework minerals of the hilairite group were considered as models.

The flexible narrow-porous framework of natrolite compounds (NAT) is built of the rigid T_5O_{10} chains joined together on four levels (Fig. 1). The subsystem of the extraframework cations and H_2O molecules can be outlined by the set of three basic positions. The medium-sized cations, e.g. Na^+ and Ca^{2+}, are located on two levels nearby the channel **c**enter (**C**-positions). **R**-positions nearby the vertical 8-member **r**ings are populated either by H_2O molecules or by K^+ cations. They are supported for the framework. H_2O molecules can occupy also additional **A**-positions. A general positional formula for the compounds of NAT-topology can be presented as $|\mathbf{C_2R_2A_2}|\cdot[T_5O_{10}]$. The real versions of its filling depend both on the composition of extraframework atoms and T^{4+}/T^{3+} ratio (see Table 1).

Table reports the examples of filling the $|\mathbf{C_2R_2A_2}|$ positions – from the complete population of all six positions to $|R_2\square_4|$. Fundamental differences are due to the framework charge, firstly, i.e., the number of the extraframework cations and, secondly, to their sizes (with inversion in the population of the positions of different sorts).

In zeolite-like hilairite minerals $Na_2[Zr(Si_3O_9)]\cdot 3H_2O$, there is a rigid framework of helical Si_3O_9 chains and (M^{4+}, M^{3+}) octahedra. Its cavities involve the assemblages of alkaline and alkaline-earth cations and H_2O molecules. The general positional formula is $|A_2B_3C_6|\cdot[M_2(Si_3O_9)_2]$, where A = Na, K, Ca, Ba; B = Na, Ca; C = H_2O, K; and M = Zr, Ti, Sn, TR (rare-earth element). The filling of the eleven-site extraframework $|A_2B_3C_6|$ subsystem (Fig. 2 and Table 2) varies from 11 to 4. In anhydrous K_4 form, the large K^+ cations occupy half the cation A positions, and also half those and half the "aqueous" C positions, the remaining positions being vacant. Of curiosity is the case of the cation-deficient calciohilairite, obviously, genetically transformational mineral according to A. P. Khomyakov [1].

The both considered groups of compounds show the similar regularities of agreement between narrow-porous frameworks with essentially different water-cation assemblages upon formation of minerals. Thus, their functions are comparable in structure-forming processes.

This work was supported by Russian Foundation for Basic Research, grant # 13-05-00457.

[1] Khomyakov A.P. Mineralogy of hyperagpaitic alkaline rocks. Moscow, Nauka, 1990. 196 p.
[2] Pekov I.V., Chukanov N.V., Kononkova N.N., Pushcharovskii D.Yu. Rare-metal «zeolites» of hilairite group. In "New data about minerals", № 38, Moscow, 2003. P. 20–33.

[3] Lin Z., Ferreira A., Rocha J. Synthesis and structural characterization of novel tin and titanium potassium silicates $K_4M_2Si_6O_{18}$. J. Solid State Chem. (2003) 175, 258–263.

Table 1. Different WCA in compounds with NAT topology frameworks.

	Si/Al ≈ 1.5	1.0 ≤ Si/Al < 1.5
	M ≤ 2	**M ≤ 2**
Na,Ca	natrolite $\|Na_2^C(H_2O)_2^R\|[Al_2Si_3O_{10}]$ scolecite $\|(Ca\ \square)^C(H_2O)_2^R(H_2O)^A\|[Al_2Si_3O_{10}]$ *super-hydrated natrolite** $\|Na_2^C(H_2O)_2^R(H_2O)_2^A\|[Al_2Si_3O_{10}]$	gonnardite $\|(Na_{1.65}Ca_{0.35})^C(H_2O)_2^R(H_2O)_{0.7}^A[Al_{2.35}Si_{2.65}O_{10}]$ paranatrolite $\|Na_{1.65}Ca_{0.35})^C(H_2O)_{1.2}^R(H_2O)_2^A\|[Al_{2.35}Si_{2.65}O_{10}]$ high-Ca paranatrolite $\|(Na_{1.2}Ca_{0.5}\square_{0.3})^C(H_2O)_{1.7}^R(H_2O)_{1.7}^A\|[Al_{2.2}Si_{2.8}O_{10}]$
	M = 2	**M > 2**
Na,K		K-rich paranatrolite $\|Na_2^CK_{0.3}^R(H_2O)_{1.3}^R(H_2O)_{1.7}^A\|[Al_{2.3}Si_{2.7}O_{10}]$
Inversion of M and H_2O positions		
K(Rb)	*K-substituted natrolite** $\|K_2^R(H_2O)_2^C\|[Al_2Si_3O_{10}]$	*K-substituted gonnardite** $\|K_2^RK_{0.3}^C(H_2O)_{0.6}^R(H_2O)_{1.7}^C\|[Al_{2.3}Si_{2.7}O_{10}]$
	Rb-GaGe-natrolite $\|Rb_2^R\|[Ga_2Ge_3O_{10}]$ K-GaSi-natrolite $\|K_2^R(H_2O)_{1.6}^C\|[Ga_2Si_3O_{10}]$	K-GaSi-gonnardite (PST-1) $\|K_{1.7}^RK_{0.5}^C(H_2O)_{1.0}^R(H_2O)_{1.5}^C\|[Ga_{2.2}Si_{2.8}O_{10}]$

* modified phases are marked by italic.

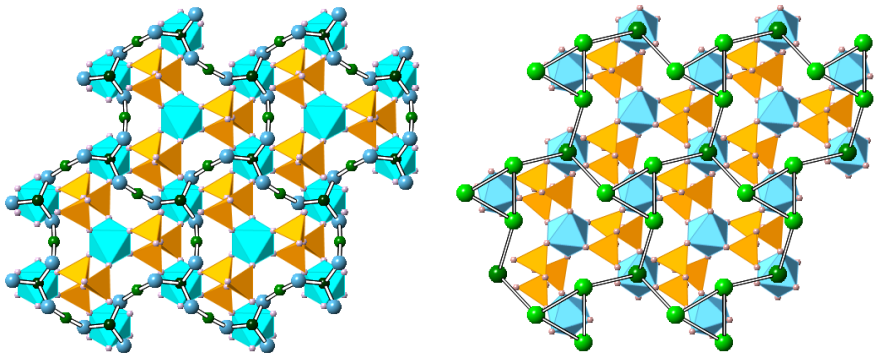

a b

Figure 2. $|Na_5(H_2O)_6|$ (a) and $|K_4|$ (b) extraframework nets in hilairite-type structure.

Table 2 . Different WCA in compounds with frameworks of hilairite topology [2].

Mineral	Idealized formula	Water-cation associates
sazykinaite-(Y)	$\|Na_5(H_2O)_6\|\cdot[YZr(Si_3O_9)_2]^{5-}$	$\{Na_2^ANa_3^B(H_2O)_6^C\}$ corrugated net
pyatenkoite-(Y)	$\|Na_5(H_2O)_6\|\cdot[YTi(Si_3O_9)_2]^{5-}$	$\{Na_2^ANa_3^B(H_2O)_6^C\}$ corrugated net
hilairite	$\|Na_4(H_2O)_6\|\cdot[Zr_2(Si_3O_9)_2]^{4-}$	$\{Na_{1.6}^ANa_{2.4}^B\square^{(A,B)}(H_2O)_6^C\}$ corrugated net with 1/5 vacancies in (A,B)-positions
calciohilairite	$\|Ca_2(H_2O)_6\|\cdot[Zr_2(Si_3O_9)_2]^{4-}$	$\{Ca^A(H_2O)_3^C\}_2$ islands as net fragments; $\square_3^B$
komkovite	$\|Ba_2(H_2O)_5\|\cdot[Zr_2(Si_3O_9)_2]^{4-}$	$\{Ba^A(H_2O)_{2.5}^C\square_{0.5}^C\}_2$ islands as net fragments; $\square_3^B$
cation-deficient calciohilairite	$\|Ca_{0.67}Na_{0.67}(H_2O)_6\|\cdot[Zr_2(Si_3O_9H)_2]^{4-}$	$\{(Ca,Na)_{1.33}^{(A,B)}\square_{3.67}^{(A,B)}(H_2O)_6^C\}$ island fragments of net with 2/3 (A,B)-vacancies
potassium titanium silicate (Ti-AV-11) [3]	$\|K_4\|\cdot[Ti_2(Si_3O_9)_2]^{4-}$	$K^AK_3^C$ corrugated net; net stacking forms a cation framework

CHEMICALLY INDUCED TWINNING AND ITS RELATION TO CRYSTAL GROWTH AND POLYTYPISM IN THE SPINEL − CHRYSOBERYL SYSTEM

Daneu N., Drev S., Rečnik A.
Department for Nanostructured Materials, Jožef Stefan Institute, Ljubljana, Slovenia; nina.daneu@ijs.si

Growth defects, for example, (*i*) twin, (*ii*) antiphase or (*iii*) inversion boundaries, are chemically induced structural faults that form in the nucleation stage and have a powerful influence on further crystal growth. They form as a result of structurally confined 2D chemical reaction between the host and dopant element, which triggers formation of the faulted structure. During the nucleation stage, dopant atoms are chemisorbed to the specific low-index crystallographic planes of hosting crystal in a highly ordered manner, forming a 2D structure that contains structural and chemical elements of the binary phase (polytype) that exists between the major phase and the dopant. The growth of these chemically induced defects takes place below the formation temperature of the binary phase and may be considered as a preparatory stage of the binary phase formation. Under favorable conditions crystals with transformation faults grow anisotropically and exaggeratedly along the direction of the inherent fault plane, thus they are more successful during growth compared to any normal crystals. Transformational growth-type defects are important indicators of geochemical and thermodynamic changes during crystal nucleation and growth. By identification of the dopant that is responsible for the formation of a specific type of 2D defect in a certain mineral, we retrieve a valuable information about the fault nucleation conditions that allow controlled reproduction of *e.g.* twinned crystals.

In natural minerals we often find different chemical elements segregated to growth defects, such as twin boundaries, which are present in initial stages of crystal growth. Identification of the element that actually triggered the formation of 2D defect is thus a difficult task. For chemical and structural characterization of chemically induced defects at the atomic scale we use combination of diffraction, imaging and analytical transmission electron microscopy (TEM) techniques. Besides conventional TEM techniques, we developed new methods for precise structural and chemical characterization of interfaces. One of these is concentric-electron-probe (CEP) analysis for highly accurate and precise analysis of interface chemistry at sub-nanometer scale using EDS or EELS analysis [1]. In our past studies we investigated different types of chemically-induced defects (twin, antiphase and inversion boundaries) in different synthetic and natural materials, such as: in different perovskites, sphalerite, zincite, pyrite, bixbyite, rutile and spinel. Here we present our investigations of twinning in natural and synthetic spinel and its relation to the formation of taaffeite-type modulated structures.

For study of naturally occurring twins of $MgAl_2O_4$ spinel we used contact twins from the Mogok metamorphic belt in Myanmar [2]. The translational state observed on these twins is described by a 180° rotation around [111]-axis in oxygen sub-lattice. This operation produces a local *hcp* stacking, which is the basic structural element of twinning. Chemical composition of the twin boundary was determined from a series of CEP/EDS analyses recorded on the twin boundary at nanometer scale. We have shown that elements, such as Si, Ti, Cr and V appear to be segregated in the vicinity of the twin boundary. From the Al/Mg ratio we found that Mg atoms that shall be occupying the boundary tetrahedral sites are missing. Such an abrupt change in chemistry is a strong indication of chemical triggers for twin boundaries. Using a combination of other electron microscopy methods (HRTEM, HAADF-STEM) we obtained an indirect evidence that the boundary tetrahedral sites are occupied by Be^{2+} instead of Mg^{2+}. This replacement is further supported by Pauling's principle of electroneutrality (Mg^{2+} replaced by isovalent Be^{2+}), structural correlation between spinel ($MgAl_2O_4$) and chrysoberyl ($BeAl_2O_4$) and the existence of taaffeite-type ($Be_xMg_yAl_{2(x+y)}O_{4(x+y)}$) series.

Recently we experimentally confirmed our hypothesis that the addition of BeO triggers twinning in $MgAl_2O_4$. Sintering $MgAl_2O_4$ with the addition of BeO simple and complex {111}

twins in spinel were synthesized [3]. These results showed that twinning in $MgAl_2O_4$ is in fact chemically induced by the presence of beryllium, which triggers the formation of local *hcp* stacking at twin boundary. The formation of chemically-induced twins in spinel has a dramatic influence on crystal growth; with twinned crystals being about 5 times larger compared to normal (untwined) crystals. Additions of BeO not only cause abundant {111} twinning of spinel, but also complex epitaxial overgrowths of $BeMg_3Al_8O_{16}$ taaffeite and related modulated phases on spinel crystals at higher BeO additions.

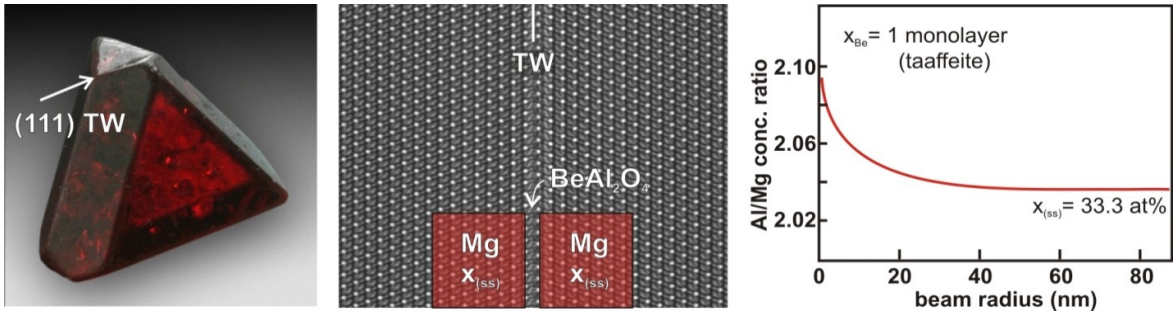

Figure 1. Left: A (111) spinel twin from Mogok (Myanmar) which was used for the atomic-sclae analysis of the twin boundary. Middle: HRTEM image of the twin boundary along the [1-10] zone axis. Boundary magnesium cations are replaced by beryllium cations, which trigger the local *hcp* stacking. Right: Results of the CEP/EDS analysis, where the depletion of one layer of Mg atoms at the twin boundary was determined.

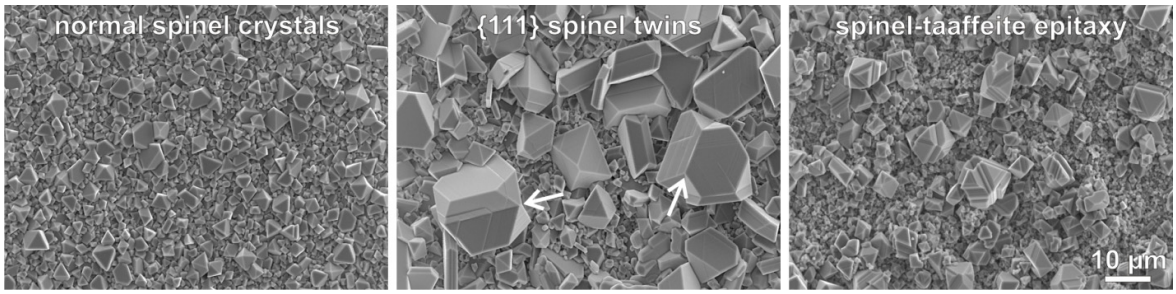

Figure 2. Left: As-synthesized normal $MgAl_2O_4$ spinel crystals (octahedrons). Middle: The addition of BeO triggers the formation of simple and complex {111} twins in spinels and these are about five times larger compared to the normal crystals. Right: Epitaxial overgrowths of $BeMg_3Al_8O_{16}$ taaffeite on spinel at even higher BeO additions.

Financial support of the Slovenian Research Agency under the project J1-4167: 'Twinning, epitaxies and phase transformations in minerals' and PR-4365 grant are gratefully acknowledged.

References:

[1] Rečnik A, Daneu N, Walther T and Mader W. Structure and chemistry of basal-plane inversion boundaries in antimony oxide-doped zinc oxide. *J Am Ceram Soc*, 2001, 84: 2657-2668.

[2] Daneu N, Rečnik A, Yamazaki T and Dolenec T. Structure and chemistry of (111) twin boundaries in $MgAl_2O_4$ spinel crystals from Mogok. *Phys Chem Miner*, 2007, 34: 233–247.

[3] Drev S, Rečnik A and Daneu N. Twinning and epitaxial growth of taaffeite-type modulated structures in BeO-doped $MgAl_2O_4$. *CrystEngComm*, 2013, 15: 2640-2647.

STUDY OF CARBONACEOUS MATERIAL FROM THE DEEP FAULT ZONES

***Danilova Yu.V.*[1], *Shumilova T.G.* [2]**

[1]*Institute of Earth Crust SB RAS; Irkutsk,Russia*
[2] *IG Komi SC UrB RAS; Syktyvkar, Russia*
e-mail: jdan@crust.irk.ru

Study of the carbonaceous material (CM) structural state by means of the transmission electron microscopy along with electron diffraction and Raman spectroscopy has been performed.

Carbonaceous material from high-carbon veins of ultrabasic rocks within the Ospinsk-Kitoi rock unit, from coaly carbonate-silicate shale of ospinskaya sequence enclosing ultrabasic rocks complex, veins of carbon-bearing apocarbonaceous metasomatites from the Tunka fault and coaly shale of carbonate-silicate toltinskaya sequence being a part of the Tunka terrane (Eastern Sayan) have been studied **[1]**.

On the data of the transmission electron microscopy and electron diffraction of monomineral specimens of carbonaceous material, the presence of reflections characteristic of the graphite crystalline structure has been distinguished. Particles exhibit a monocrystalline pattern of electron diffraction with interplate distances being essentially less than the standard values of hexagonal graphite (Table 1). Apart from monocrystalline particles of submicron size, particles of distinguishable size on the order of 50-500 nm in different sections have been analyzed. Structural parameters of particles in veins of high-carbon metasomatites from the

Table 1. Data for electron diffraction of the graphite particles

Experimental data									Characteristics from data of JCPDS (International Centre for Diffraction Data)	
I, point	d, nm	I, point	d, nm	I, point	d, nm	I, point	d, nm	Error, nm	d, nm	hkl
1		2		3		4				
6	0.208	10	0.205	10	0.204	10	0.206	0.0008	0.213	100
6	0.122	5	0.123	2	0.121	2	0.121	0.0003	0.123	110
10	0.113	-	-	-	-	-	-	0.0003	0.115	112
-	-	4	0.103	4	0.103	4	0.103	0.0003	0.105	201
5		6		7		8				
4	0.331	1	0.333	-	-	-	-	0.0007	0.335	002
10	0.207	10	0.207	10	0.208	10	0.202	0.0003	0.213	100
10	0.121	6	0.121	10	0.121	10	0.121	0.0001	0.123	110
8	0.114	2	0.114	2	0.113	-	-	0.0006	0.115	112
2	0.104	4	0.104	6	0.104	6	0.104	0.0006	0.105	201
9		10		11		12				
2	0.328	2	0.325	6	0.338	8	0.338	0.0007	0.335	002
6	0.195	10	0.198	10	0.209	10	0.207	0.0003	0.213	100
10	0.119	-	-	8	0.121	10	0.121	0.0001	0.123	110
-	-	6	0.117	-	-	-	-	0.0006	0.115	112
-	-	2	0.101	6	0.104	6	0.104	0.0006	0.105	201

Note. Particles of graphite: 1-4 – from veins of high-carbon apocarbonaceous metasomatites within the Tunka fault; 5-8 – from coaly shale of silicate-carbonate toltinskaya sequence; 9, 10 – from veins of high-carbon ultrabasic rocks within the Ospinsk-Kitoi rock unit; 11-12 – from coaly carbonate-silicate shale of ospinskaya sequence.

Ospinsk-Kitoi rock unit are characterized by most minimal values d_{002}=0.325÷0.328 nm, d_{100}=0.195÷0.198 nm, d_{201}=0.101 nm, d_{110}=0.119 nm, d_{112}=0.117 nm.

Detailed examination carried out using the Raman spectroscopy revealed more perfect forms of spectra for CM from veins of carbon-bearing metasomatites within the fault zones.

Thus, CM from high-carbon apocarbonaceous metasomatites of the Tunka fault exhibit clearly manifested bands of graphite – D (1346-1353 cm^{-1}) and G at the standard position of graphite1580 cm^{-1}. Width of G band on its half-height ($FWHM_G$) for all studied CM particles is 16 – 40 cm^{-1}. The most perfect "graphitic" form of spectrum may be observed in samples from central parts of high-carbon veins (Fig. a: spectrum 3 – center of vein; spectrum 2 – marginal part of vein). Size of L_a crystallites calculated by analogy with data from paper **[2]** is 3 – 15 nm for the majority of examined particles and only for single graphitic particles it is about 0.1 μm.

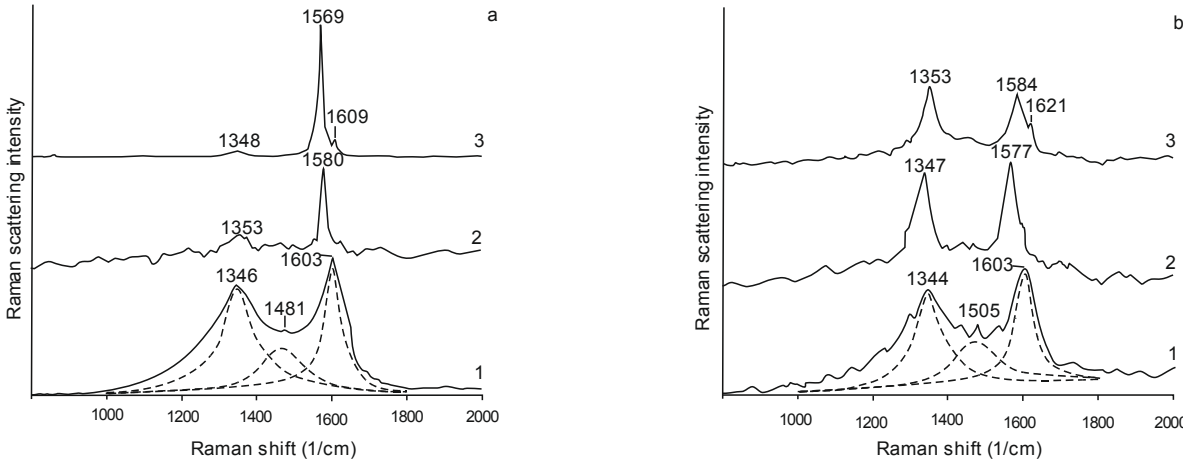

Figure 1. Raman spectra of CM from veins of apocarbonaceous metasomatites of the Tunka Fault and coaly shale of silicate-carbonate toltinskaya sequence (a);from veins of high-carbon ultrabasic rocks of Ospinsk-Kitoi rock unit and coaly carbonate-silicate shale of ospinskaya sequence (b). Degree of structural perfection of CM increases on spectra from bottom to top.

In comparison with them the CM of coaly shale of silicate-carbonate toltinskaya sequence is characterized by essentially broadened D and G bands with main G band in the range of 1603^{-1} cm and mathematically calculated an additional band in the range of 1481 cm^{-1} (Fig. a, spectrum 1). According to traditional interpretation of Raman spectra, this band at 1500 cm^{-1} is assigned to interplane defects and is due to amorphous carbon **[3]**. $FWHM_G$ can reach 100 cm^{-1}. Size of L_a crystallites for this group of samples does not exceed 1 – 3 nm.

Raman spectra of CM in high-carbon veins in ultrabasic rocks from the Ospinsk-Kitoi rock unit are characterized by the D and G bands both being broadened and intensive (Fig. b, spectra 3, 2). $FWHM_G$ varies over a wide range (from 27 cm^{-1} to 66 cm^{-1}). On the right of the main G peak an additional shoulder appears sometimes in the range of 1620 cm^{-1}. Its presence is attributed to interlayer defects as well as to increase of structural ordering of material during the graphitization process and with small size of crystallites **[3]**. Size of L_a crystallites for this sample group is 2 – 10 nm.

Carbonaceous material of coaly carbonate-silicate shale from ospinskaya sequence enclosing ultrabasic rock complex differs from metasomatic CM from veins of ultrabasic rocks. Their Raman spectra are imperfect and characterized by intensive and wide G band at 1600 cm^{-1} with $FWHM_G$ up to 60 cm^{-1} (Fig. a, spectrum 1). The D and G bands are intensive and wide. The additional D band is present in the range of 1500 cm^{-1}. Size of L_a crystallites is not beyond of 1 – 2 nm.

Analysis of structural parameters suggested that carbonaceous material in samples is generally presented by graphite of different degree of ordering with nanodimensioned crystallites. Poorly ordered and roentgeno-amorphous graphite-like CM and crystallites of graphite up to 0.1 μm are rare. Carbonaceous material of enclosing coaly carbonate-silicate shale is poorly ordered and soot-like. Size of crystallites for these samples is not more than 1 – 3 nm **[2, 4]**.

Degree of the carbonaceous material ordering in the carbon-bearing metasomatites veins from the deep fault zones is higher in comparison with carbonaceous material from enclosing metamorphic complexes.

This research is supported by SB RAS (Grant 89), program for Basic Reseach of UrB RAS (Grant 12-C-5-1035) and RFBR (Grant 13-05-00206).

References:

[1] Boos R. G. Paleozoic of the Tunka bald mountains within the East Sayan (stratigraphy, metamorphism, formations). Novosibirsk: Nauka, 1991, 144 pp. (in Russian).

[2] Wopenka B., Pasteris J.D. Structural characterization of kerogens to granulite-facies graphite: Applicability of Raman microprobe spectroscopy // American mineralogist, 1993. V. 78. P. 533-557.

[3] Beyssac O., Goffe B., Chopin C. and Rouzaud J.N. Raman spectra of carbonaceous material in metasediments: a new geothermometer // J. Metamorphic Geology, 2002 V. 20, N. 9. P. 859-871.

[4] Ferrari A. C., Robertson J. Raman spectroscopy of amorphous, nanostructured, diamond-like carbon, and nanodiamond // Phil. Trans. R. Soc. Lond. A., 2004. V. 362. P. 2477–2512.

DOES SOLUBILITY PLAY A ROLE IN CRYSTALLIZATION?

García-Ruiz, J.M. [1], ***Kimura, Y.*** [2], ***Otálora, F.*** [1]

[1] *Laboratorio de Estudios Cristalográficos, Instituto Andaluz de Ciencias de la Tierra, CSIC-Universidad de Granada, Granada, Spain*
[2] *Department of Earth and Planetary Materials Science, Tohoku University, Sendai, Japan*
juanma.garciaruiz@gmail.com

The birth of crystals is one of the most intriguing problems in today science. We are teaching our students that crystals form when the concentration of a solution exceeds the solubility, i.e. when the mother solution from which the crystal form is supersaturated. We also teach them that the crystals we observe are those that did reach a critical size and become stable for further growth. Thus, when a compound may crystallize in more than one crystal structure, each one with its own solubility, the Ostwald "law" of stages states that the precipitation sequence of polymorphs starts with the less stable phase and ends with the more stable one [1]. Recent experimental results [2] demonstrate a) that crystalline nuclei form at equilibrium and even within undersaturated solutions, thus suggesting the existence of density fluctuations in the solution with amplitude large enough to trigger crystallization; and b) that different polymorphs form simultaneously independently of their respective solubility values, thus proving that the creation of crystalline nuclei of different polymorphs is not dictated by supersaturation.

We discuss in this communication the idea that the arrangement of the molecules or ions arising from a maximal local concentration is merely the result of a compromise between the disorder of the accumulation, i.e. the rate at which molecules or ions cluster in a single point, and the degree of structural order of the different polymorphic configurations [3]. The concomitant formation of polymorphs at the earliest stages of nucleation provides an explanation to the formation of metastable phases as precursors well below equilibrium solubility [4]. The lifetime of the nuclei with different structural arrangements depends on their respective surface properties, thus explaining the exclusive detection of the stable phase at micron or larger scale and the "rule" proposed by Ostwald more than a century ago.

This work was supported by the Tohoku University GCOE program for "Global Education and Research Center for Earth and Planetary Dynamics", by a Grant-in-Aid for challenging Exploratory Research from KAKENHI (25610068) and by the Consolider Project "Factoría de Cristalización" of the Spanish Ministry of Economy and Innovation, MICINN

References:

[1] W. Ostwald, W., 1897. Z. Phys. Chem. 22: 289–330.
[2] Kimura, Y., Niinomi, H., Tsukamoto, K., García-Ruiz, J.M., 2013. Submitted.
[3] J.M. García-Ruiz, J.M., Amorós, J.L., 1980. Estudios Geológicos 36:193-200
[4] Van Driessche, A. E. S., Benning, L.G., Rodriguez-Blanco, J. D., Ossorio, M., Bots, P., García-Ruiz, J.M., 2012. Science, 336: 69-72.

GROWTH AND CHARACTERIZATION OF LOPEZITE CRYSTALS

Gets V.A. [1], ***Chepkasov S.Yu.*** [2], ***Khomyakov M.N.*** [3]

[1] *V.S. Sobolev Institute of Geology and Mineralogy SB RAS, Novosibirsk, Russia*
[2] *Novosibirsk State University, Novosibirsk, Russia*
[3] *Institute of Laser Physics, SB RAS, Novosibirsk, Russia*
gva45@mail.ru

Lopezite is a rare red chromate mineral with chemical formula: $K_2Cr_2O_7$. It crystallizes in the triclinic crystal system. Space group: $P\bar{1}$. Cell parameters are: a = 0,7445 nm, b = 1,3367 nm, c = 0,7376 nm, α = 90,75°, β = 96,21°, γ = 97,96°.

The aim of this work is to investigate the optical properties of $K_2Cr_2O_7$ crystals, because this mineral is easily obtained synthetically.

$K_2Cr_2O_7$ crystals for the study were grown from seed in an unstirred aqueous solution. Prior to atomic force microscopy (AFM) observation, the crystals were quickly removed from the solution and dried immediately with water-absorbing paper to preserve the as-grown faces as good as possible.

AFM is one of the most powerful techniques for observing and investigating the microstructure of the interface. A Nikon optical microscope was used to observe the morphology of the grown crystals. The transmission spectra were measured at room temperature with Shimadzu UV-3600 spectrophotometer.

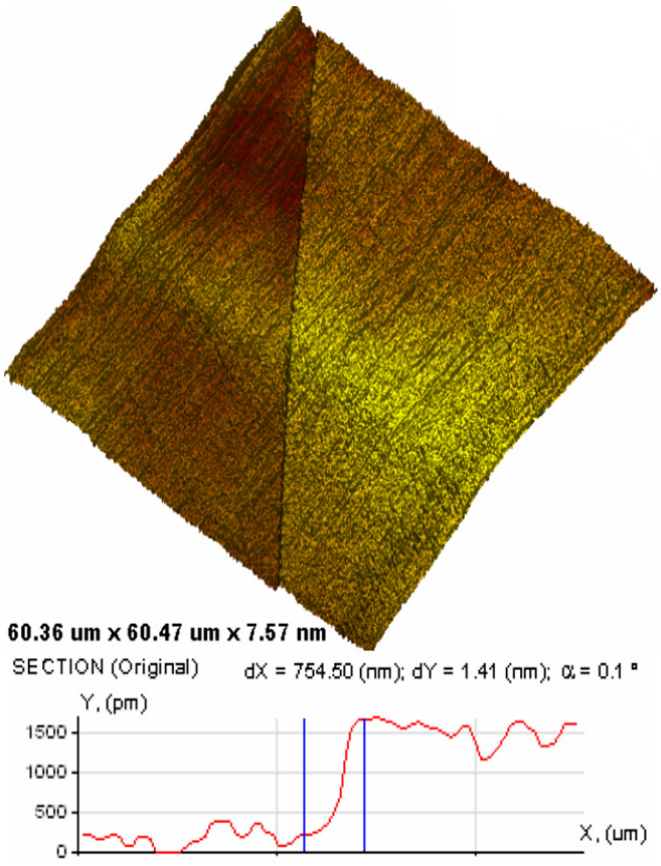

The face forms that frequently occur on triclinic lopezite are {001}, {101}, {100}, $\{10\bar{1}\}$, $\{0\bar{1}1\}$, {010}, {011}.

A (001) face of a synthetic lopezite crystal was examined by AFM, using a Nanoscan 3D. The height of the lowest observed steps on the {001} $K_2Cr_2O_7$ surfaces is 1,4 nm, which coincides with the elementary step heights d = 1,34 nm as predicted by Bravais-Friedel-Donnay-Harker laws and Hartman-Perdor theory. The results of our work are in good agreement with **[1].**

The short-wave edge of the transparency region is located at 564 nm in lopezite and at 541 nm in its aqueous solution. Respectively, $K_2Cr_2O_7$ crystals are transparent in the range of 564–3000 nm, its aqueous solution is transparent in the range of 541-1350 nm.

References:

[1] Borc J. *et al*., Surface science 489, 174 (2001).

COMPARISON OF EQUILIBRIUM AND IDEAL CRYSTAL FORM

Ivanov O.K.

The Urals Institute of Mineral Products, Ekaterinburg, Russia
okivanov@gmail.com

A key problem of crystallogenesis is a correlation berween the crystal form and their inner structure. There are three approaches. The first, a classical one, based on the Brave principle in the last formulating of I.I. Shafranovsky [12] is: "It is generally known that the crystal form is, first of all, a function of an inner structure, and an influence of crystalloforming medium can leave its imprint only in certain and quite limited boundaries". Though in "which boundaries" and in what in particular - is not pointed. A.G. Bulakh specified that such definition refers only to ideal crystals. The second approach based upon the experimental data on the crystal growth, says:"the role of the structure can have only a subordinated meaning' [2], though, which,in particular, is also not specified. An analytical approach used by A.S. Povarennikh [10] led him to a conclusion that "correlation between the individual appearance and structure is not synonimous and is determined by crystallization conditions…" *Such a scatter of* conclusions *stimulates searches of proofs , influence of these or those factors upon the crystal appearance.* The comparison of the crystal elongations, being formed in different, on degree of equilibrium, conditions of crystallization showed [3-6, 8] that:

1. The crystalline structure of a mineral behaves passively and at usual non-equilibrium conditions of crystallization does not influence or weakly influences upon the crystal appearance and habit
2. The crystal appearance and habit is determined by physical, chemical, symmetry peculiarities of the medium of crystallization, as well as by the conditions (speed, degree of supercooling or supersaturation) of crystallization

It was suggested that at the near-equilibrium crystallization the crystal appearance and habit would correspond to its inner structure. It led to the necessity of establishment of the equilibrium crystal form and specification of the notions of "equilibrium" and 'ideal' crystals [7], which, according to the last data, are being formulated like this:

"An ideal crystal is a crystal having an ideal inner structure, a form corresponding to the form of the mineral elementary cell (connection) and flat mirror faces".

"An equilibrium, or, to be more exact, near-equilibrium crystal, is a real crystal, being formed in geologically near-equilibrium conditions".

The analysis of the habit variation and the crystal facing from ultra non-equilibrium to near-equilibrium conditions ofcrystallization , established on geological data, demonstrated [9], that "crystallographically (geologically) the near-equilibrium crystal forms of middle crystal systems have thebipyramidal form (for the tetragonal – tetragonal, for the hexagonal – hexagonal, for the rhombohedronal – the form ofrhomdohedrons)". With all these it was assumed that the development of flatted crystals of apophillite, calcite, apatite, beryl is, quite possible, caused by adsorbtional processes".

Hence, logically the question arises on the reason of formation of the crystal bipyramidal forms of middle crystal systems, though their structures as often as not are rather different.

For this purpose it was carried out a comparison of the near-equilibrium crystal form with an elementary cell of the same crystals, or- that is the same – with the ideal crystal form. As an example we can cite the data only on the zircon crystals.

The comparison of the near-equilibrium crystal form of a number of typical minerals with the ideal crystal form shows that, in all the cases we have a considerable lack of coincidence of the expected elements of the form.

For the crystals of tetragonal and hexagonal crystal systems there coincide the crystal elongations or the correlations of the main parameters of a cell and crystal, as well as the forms of section perpendicular to the axis C, - that is the main peculiarities of the structure.

Crystal signs	Near equilibrium zircon crystal	Ideal crystal or zircon elementary cell
Crystal form	Tetragonal bipyramid	Tetragonal prizm
Lengthening	0.9	0.9
Face	{111}	{110},{001}, {100}
Habit	Tetragonal-bipyramidal	Tetragonal-short-prizmatic

For the same crystal systems crystal forms, habits and crystal facings – that are the main form particularities – do not coincide.

The reason for such difference is ,evidently, that even at equilibrium, or, to be more exact, at near-equilibrium conditions of crystallization , the crystal form reflects not so much the structure peculiarities, but is energetically more profitable under the conditions of near-equilibrium crystallization the elements of form, habit and facing.

From the results obtained it follows that the inner structure does not determine just the form, habit and facing of the near-equilibrium crystals, hence the rule of Brave has a limited significance.

Since, on E.S. Fyodorov, [11], all the crystal systems are reduced to the tetragonal and hexagonal ones, the described relations should be characteristic of the rest crystal systems as well.

References:

[1] Bulakh A.G. Mineralogy with the crystallography basis. M.;/Nedra, 1989. 351p.

[2] Glikin A.I., Glazov A.I. Problems of genetic interpretation of the crystal form. Zap.AMS,1979. Iss. 5. P.536-551.

[3] Ivanov O.K. Evaluation of equilibrium-nonequilibrium degree during the magmatic mineral-formation // The Uralian mineralogical school – 2009. Materials of all-Russian scient. conf. Ekaterinburg, 2009. P.105-109

[4] Ivanov O.K. Orthomagmate petrogenic mineral appearance (elongation) in dependence on the factors of crystallization. The Ural geol. j. 2010.N.5.P.24-45.

[5] Ivanov. O.K. An influence of mineral structure upon its appearance in orthomagmatic rocks.// The Ural. geol. j. 2011. N.1 (79). P.33-45.

[6] Ivanov O.K. Zircon: Dependence of the crystal appearance upon the composition of source rocks, the associated with them properties and conditions of crystallization. // The Ural geol. j. 2012. N.85. P.21-47.

[7] Ivanov O.K. Elemantary, ideal and real (equilibrium and nonequilibrium) crystals. Typing. // The Ural geol. j. 2012. N.4 (88). P. 43-47.

[8] The crystalline structure influence upon the crystal appearance and habit. //Crystalline and solid noncrystalline state of mineral substances; problems of structuring, regulating and evolution. Mater. of Mineral. conf. Siktivkar. IG of Komi Sc. C. of UB RAS.2012. P.28-30

[9] Ivanov O.K. The crystal near-equilibrium forms of middle symmetry. // The Ural geol. J. 2013. N.3 (93). P. 57-79.

[10] Povarennikh A.S. About dependence of the mineral individual appearance and conditions of ctrystallization // Morphology, properties and genesis of minerals. Kiev: Naukova Dumka,1965.

[11] Fyodorov E.S. One of the most general laws of crystallography. // Izvestiya of Imper. AS, 1903. V.18, N.4. P.1-6.

[12] Shafranovsky I.I. Some notes on the problem of genetic interpretation of the crystal form.// Zap. of AMS. 1979, Iss.5. P.119-124.

M-FENILENDIAMINE AS CRYSTAL-FORMED AGENT AT ZEOLITE SYNTHESIS WITH THE FAUJASITE FRAMEWORK

Kazantseva L.K. [1], ***Seryotkin Yu.V.*** [1,2], ***Goryainov S.V.*** [1]

[1] *Sobolev Institute of Geology and Mineralogy SB RAS, Novosibirsk, Russia*
[2]*Novosibirsk State University, Novosibirsk, Russia*
kazantseva@igm.nsc.ru

Crystals commonly reach sizes of 1-10 μm under sol-gel hydrothermal synthesis of NaX or NaY zeolites (FAU type). Large crystals of NaX zeolites up to 100 μm were grown from aluminosilicate gels with the addition of triethanolamine (TEA) for the first time in **[1].** The use of other amine-bearning compounds did not result in the creation of larger FAU type crystals. In subsequent investigation, large NaX zeolites were produced only from TEA-containing gels **[2].** The effect of TEA on enlargement of crystals is explained by the formation of intermediate complex $[N(C_2H_4O_3)_3–Al(OH)_4]^-$, resulting in the undersaturation of the reaction solution with the active growth element $[Al(OH)_4]^-$. As a consequence, the heterogeneous crystal nucleation of zeolites is suppressed, and the initially formed crystals are enlarged. Unfortunately, the crystals do not always attain such dimensions despite observing all the parameters of synthesis **[2].** The aim of this work was to study the effect of amine-bearing compound with different composition at zeolite synthesis with faujasite framework.

Zeolites were synthesized at 90°C from an aluminosilicate gel precursor with a mole composition $2.4Na_2O/1.43SiO_2/1.0Al_2O_3/330H_2O$ corresponding NaX zeolite composition. Triethanolamine – $(CH_2OHCH_2)_3N$ and m-fenilendiamine (MFDA) – $(C_6H_4(NH_2)_2$ were used as amine-bearning compounds. The concentration of amine-bearning compounds into aluminosilicate gels was: TEA – 1.5 M is commonly used in the synthesis of large NaX zeolites **[3],** and MFDA – 0.5; 1.0; 2.0; 3.0 M.

Depending on the addition of the differing additives or on the concentration of MFDA, a different dimensions and phase composition of the synthesis zeolite crystals to the equal initial aluminosilicate gels were observed. Enlargement of zeolete crystals was ensured by the following variation of the gel composition: gel without additives < gel+1.5M TEA < gel+1.0M MFDA (fig.1)

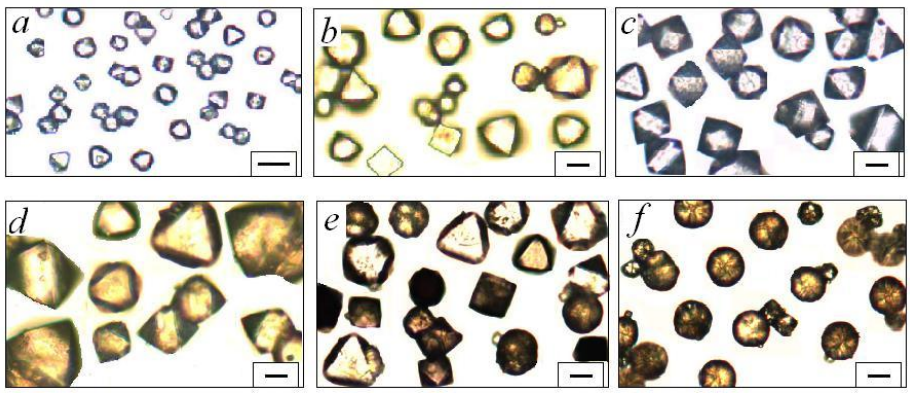

Figure 1. Microimage of zeolites grown from aluminosilicate gels with a mole composition $2.4Na_2O/1.43SiO_2/1.0Al_2O_3/330H_2O$: *a* – gel without additives; *b* – gel+1.5M TEA; *c* – gel+0.5M MFDA; *d* – гель+1.0M MFDA ; *e* – gel+2,0M MFDA; *f* – gel+3.0M MFDA. Scale is equal 10 μm.

The crystalline phase grown in a gel without additives was 7-8 μm with low size dispersion (fig.1a). According to the X-ray phase analysis data, the crystalline phase corresponded to well-crystallized pure NaX zeolites (fig.2a).

NaX zeolites grown in a gel with additive of TEA reached 35 μm with high size dispersion. Besides NaX zeolites, crystallization product is included a spherical phase and NaA zeolites (LTA types) (fig.1b).

Well-crystallized pure NaX zeolites up to 40 μm were synthesized from a gel with additive of 0.5M MFDA (fig.1c). The enlargement of MFDA additive up to 1.0M lead to synthesis of 50-60 μm zeolites with the faujasite framework (fig.1 e). Accoding to X-ray phase analysis data, this is NaY zeolites (fig.2b).

The enlargement of MFDA additive to 2.0M leads to the decrease of NaY zeolite size and crystallization product can include a spherical phase (fig.2e). At 3.0M MFDA additive in a gel only a spherical phase was synthesized (fig.2f).

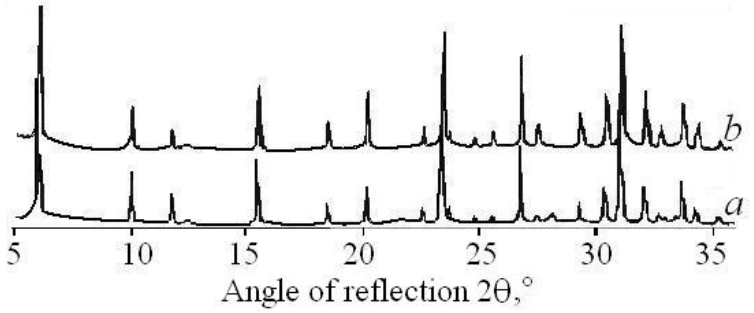

Figure 2. Powder diffraction profiles: (*a*) – NaX zeolites synthesized from a gel without additives and from a gel + 0.5M MFDA; b – NaY zeolites synthesized from a gel + 1.0 M MFDA.

Enlargement of zeolite crystals with the faujasite framework on the addition of amine-bearing compound – m-fenilendiamine is confirmed that, like TEA, it is formed intermediate complex $[MFDA–Al(OH)_4]^-$. The latter substance decrease the degree of supersaturation of reaction solution by active $[Al(OH)_4]^-$ and the initially formed crystals are enlarged.

Synthesis of NaY zeolites from aluminosilicate gels corresponding NaX zeolites composition but with adding 1.0 M MFDA is explained by more stability of intermediate complex than with adding TEA. Crystallization system is began more siliceous that is corresponded condition of NaY zeolite synthesis. Besides, m-fenilendiamine can be trapped into the zeolite cages as template agent.

This work is supported by the Russian Foundation for Basic Research, grant no. 11-05-01121-a.

References:

[1] Charnell J.F. // J. of Crystal Growth, 1971. № 8. P. 291.
[2] Schmitz W., Kornatowski J., and Finger G. // Cryst. Res. Technol., 1988. № 23. P. 25.
[3] Warzywoda J., Bac N., Jansen J.C., and Jr A.S. // J. of Crystal Growth, 2000. № 220. P. 140.

TEXTURAL CHARACTERISTICS OF METAMORPHIC ZIRCON AND CHEMICAL CHANGE

Kiliç A.D.*, *Ateş C.

Fırat Üniversitesi, Jeoloji Mühendisliği Bölümü, Elazığ, Türkiye
adkilic@firat.edu.tr

Zircon ($ZrSiO_4$) in situ gneissic rocks in the subduction zone high temperature metamorphites were mineralogically characterized by inductively coupled plasma mass spectrometry (ICP-MS), X-ray powder diffraction and Cathodoluminescence (CL) analyses, which show that the zircon grains have developed two textures. These textures are oscillatory zoning and porous. Mineral assemblages of gneiss consist of K-feldspate+ quartz+ biotite +chlorite + apatite+ zircon+ opaque minerals and mineral assemblages of biotite schist consist of biotite+ quartz+ muscovite (chlorite)+ plagioclase (albite)+ apatite+ zircon+ opaque minerals. Zircons from granitic gneisses and amphibolite schists were mineralogically and texturally characterized by inductively Couples Plasma Mass Spectrometry (ICP-MS) and Cathodoluminecans (CL) metods. These zircons show a variable degree of metamictization. Zircons have textural and chemical variety, which presents characteristic of metamict behavior and are usually made visible by inward-penetrating, irregularly curved, cauliflower like. In the zircons, which are homogeneously luminescent or inclusion rich and porous domains. Metamict grains are characterized by higher CL. Some grains are colorless to light brown and CL-weak, rounded core that is featureless or shows a faint growth, patchy zonation. Chemical analyses show that it loses variable amounts of Zr, Hf, U, Th and REE. Radiation damaged zircons understanding the processes that produced these internal textures is essential U-Pb age obtained from these space. Among the inclusions in these grains we can find thorite, xenotime and K-feldspar. These observations suggest that variety of zircons is probably associated with fluids and metamorphism conditions in the moderate to high temperatures.

CRYSTALLINITY INDEX IDENTIFICATION OF QUARZITES THROUGH X-RAY DIFFRACTION METHOD

Korovkin M.V. [1], ***Ananeva L.G.*** [1], ***Nebera T.S.*** [2], ***Razva O.S.*** [1]

[1] *National Research Tomsk Polytechnic University, Tomsk, Russia*
[2] *National Research Tomsk State University, Tomsk, Russia*
mvk@tpu.ru

Due to such characteristics as abundance, high-purity and cheapness, quartz rocks, such as quartzites and quartz sand, are becoming more and more perspective sources in different industrial areas. An excellent example is Antonovsk quartzite deposit clusters in Western Siberia, Russia [1,2]. The quartzite origin pertains to sedimentary- metamorphic deposits and is the product of lithification under conditions of the early metagenesis of quartz-hydromica-sericite facies [3]. As a result of the metamorphism of biogenic siliceous thickness, amorphous silica is crystallized forming crystalline α-quartz phase.

It is assumed that the estimated degree of silica thickness and the identification of the purest quartzite varieties could be determined by the Ki crystallinity index in X-ray diffraction patterns which was first proposed by Murata & Norman [4].

Quartzite samplings from different ore bodies of open-pit "Sopka-248" are transformed into finely-crushed samples and further compressed into a "tablet". Measurements were carried out on the diffractometer X»Pert PRO. X-ray diffraction patterns indicated increments of 0.02 in the range of 5-70 degrees; 2θ at rotation 30 rpm and exposure of 0.1 sec. The peak intensity of 2θ = 67,74^{O} at multiplet peak within 67^{O}…69^{O} (Fig. 1) was used to calculate the "crystallinity index". The peak intensity values of 2θ = 67,74^{O} are used in the following formula 10 Kci = F a / b, proposed Murata & Norman. Calculated values for crystallinity index different quartzite types presented in Table 1.

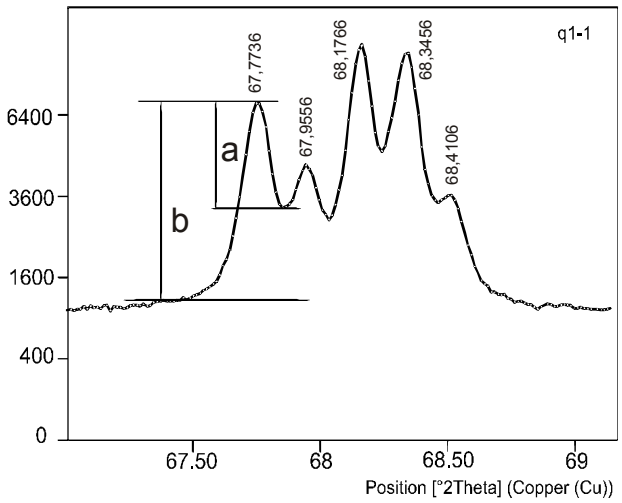

Figure 1. Multiplet peak within 67^{O}…69^{O} on the X-ray diffraction pattern to calculate crystallinity quartzite index according to Murata & Norman method

Microcrystalline quartzite deposit "Sopka-248", a relatively highly- pure deposit, is characterized by the calculated crystallinity index values within 1.90 ... 2.28. Quartzites change their chemical composition and color, while their crystallinity index increases up to 3.16 ….4.40 relative to depth increase and from the central zones to the periphery of the ore bodies. It is assumed that quartzite crystallinity degree increase is associated with superimposed metamorphic processes, resulting in the formation of crystalline α-quartz phase. In local areas, especially in increased crushed zones, initial chemically pure quartzites under the impact of supergene processes degrade, while their crystallinity degree increase up to 5.6 in some areas.

These values reflect some relative crystallinity index values representing the degree of quartzite conversion. The crystallinity index estimates in accordance to Murata & Norman method [4] applying the multiplet peak of 2θ = 67,74^{O} verify the results obtained by IR spectroscopy [5, 6].

Table 1. Estimated value of quartzite crystallinity index in deposit "Sopka-248"

Quartzite sample	Crystallinity index K_{ci}
White quartzite	1,9
Grey quartzite with iron oxide spots	3,5
Grayish quartzite with clay matter spots	4,0
Black quartzite	4,0
Grey quartzite with Mnspots	4,4
Jasperoid brownish- red quartzite with black veins	0

It should be noted that the calculated values of quartzite crystallinity index according to proposed method are quite relative and can be used in the comparative analysis within one ore deposit. The bond between quartz micro-grain sizes and crystallinity index has not been established yet. This estimation could be a genetic feature and used further in metallurgical sampling in view of the fact that most samples indicated the lowest crystallinity index values.

References:

[1]. Ananiev Y.S., Ananieva L.G., Dolgov I.V., Korobeinikov A.F., Korovkin M.V. (2001) Prospecting, estimation and enrichment of quartzite sources for high technology// TPU Izvestja, V.304, No 1., pp. 123-130 (only in Russian).

[2]. Ananieva L.G., Korovkin M.V. (2003). Mineralogist-geochemical study of quartzite from Antonovsk deposit clusters // TPU Izvestja, V.306, No 3., pp. 50-55 (only in Russian).

[3]. Korovkin, M.V., Ananieva L.G. Estimation of quartzite metamorphism degree in Antonovsk deposit clusters to the mineralogical data, (2012), Mineralogy, geochemistry and mineral resources of Asia. Tomsk: Tomsk CSTI - branch FGBU "CEA" Russian Ministry of Energy, Issue 2. pp. 139-144 (only in Russian).

[4]. Murata K.J., Norman II M.B. An index of crystallinity for quartz // American Journal of Science. – 1976. – V. 276. – Pp. 1120–1130.

[5]. Korovkin M.V., Ananieva. L.G., Antsiferova A.A. Assessment of quartzite crystallinity index by FT-IR. In: Broekmans MATM (editor): Proceedings of the 10th International Congress for Applied Mineralogy (ICAM), Trondheim, Norway. – 2011- Pp. 403-410.

[6]. Korovkin M.V., Ananieva. L.G., Antsiferova A.A. (2012) Transformation of quartzite by infrared spectroscopy //TPU Izvestja, V.320, No 1., pp. 47-54 (only in Russian).

ATOMIC RESOLUTION TOPOGRAPHY IMAGES OF GRAPHITE, GOLD, N-TYPE SILICON WAFER AND CADMIUM OXIDE FILMS USING STM

Mustafa F.A.

Laser Physics Department/College of Science for Women, Babylon University, Iraq
albassam1799@yahoo.co.uk

Morphological surface images of atomic resolution in 3-dimension, lateral images color map, line graph, 3-Dimension view scan forward shaded map , 3-Dimension view lateral and 3-Dimension back of graphite, gold, n-type silicon wafer and cadmium oxide films using scanning tunneling microscopy(STM) are investigated. The images of surface graphite appear a regular geometrical distribution with hexagonal arrangement atoms about 0.25Å of planer distance with 0.34nm. But the gold surface appears with the dissociation of atoms and great density of electrons. While the n-type silicon wafer reveal to stacking rows and show a line defect(dislocations) produce from inserting an extra atoms as result to impurities. Also the dissociation molecular oxygen on cadmium and its site are clear with island-like. It was applied to the study of cadmium oxide films deposited on holder surfaces. The simulated images reproduce the main features of experimental observations, as a powerful and direct imaging methods coincidence with theoretical tunneling quantum model.In the lattice model of graphite, figure 1 (a) shows topography scan of graphite profiles and (b) 3-Dimension view scan forward can be observed. It can see that there are two different positions of carbon atoms in the graphite hexagonal crystal lattice. An atom with a neighboring in the plane below (gray) and one without a neighbor in the lattice below(white). It is way more difficult to obtain good images of gold. Atomic structures are difficult to observe, because the electrons on the surface are much more homogeneously distributed than the graphite as shown in figure 2. The contrast on the image is due to variations in charge density. But, with some training, the mono-atomic gold steps of topography, line fit map and graph can be observed

Three-dimensional representation of a scanning tunneling microscopy image of the silicon atoms at the edge of the silicon wafers. We see a pattern consisting of bright, dark and more bright spots with very few numbers (doped silicon), and first be aware that bright spots show topographic high spots. An atom with neighboring atom in the plane below (dark)and without a neighboring in the lattice below(white) with tetragonal bonds. If silicon atoms in the row have line defect (dislocation) that produce from inserting an extra atoms , the row as line fit as shown in figure 3(a). The deflection about the regular lattice sites, the graph can be observed in figure 3(b). 3- Dimension the lateral view structure refers to stacking row of atoms in y-line.

The surface morphologies of CdO films showed a grain growth with mixture of island- like and granular grain shapes. The grain boundaries (planer defects) tend to be loosely bound. The Images of the polycrystalline structure of the film as shown in figure 4, describes irregular positions of CdO molecules as a result of deposited film type . It consists of point defects (vacancy, self interstitial, extra atom, substitutional atom). So it is difficult to description the aggregate of atoms in many positions. The aim of the research is to provide a three-dimensional profile of the conductor and semiconductor surfaces which is very useful for characterizing surface roughness, observing surface defects, coincidence theoretical tunneling quantum model, and determining the size and conformation of molecules and aggregates on the surface.

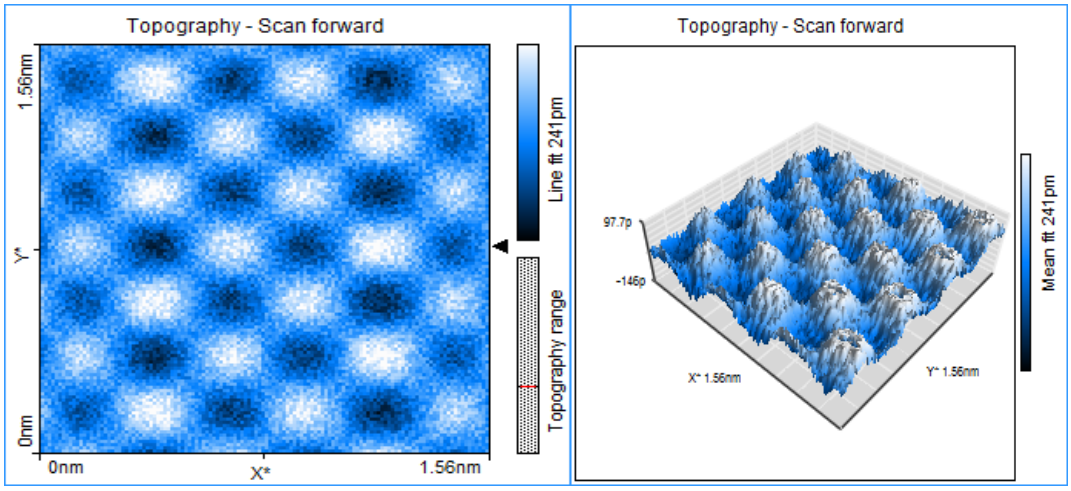

Figure 1. (a) Topography scan of graphite profiles(b) 3-Dimension view scan forward

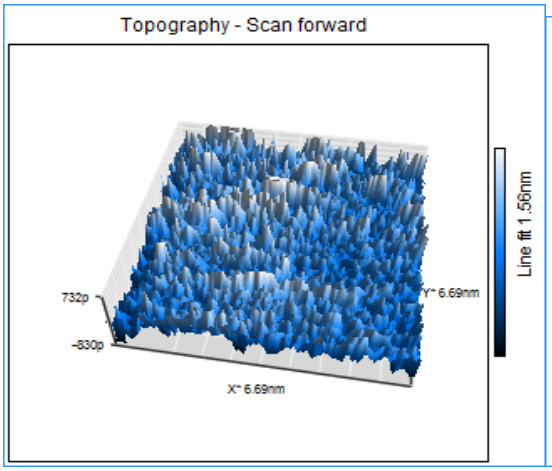

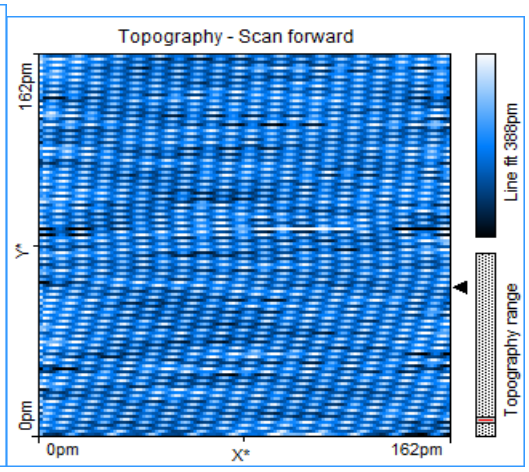

Figure 2. 3-Dimension view scan forward(gold) Figure 3. (a)Topography scan of Si wafer

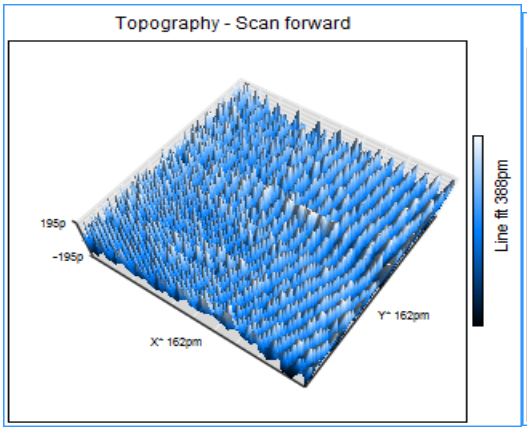

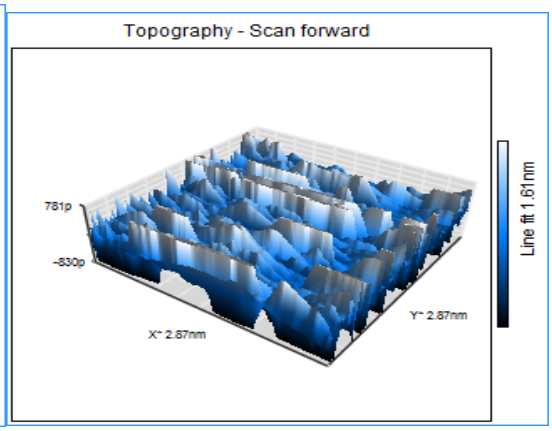

(b) 3-Dimension view scan forward Si wafer Figure 4. 3- Dimension view lateral(CdO film)

SURFACE AND BULK INHOMOGENEITY OF MIXED CRYSTALS ON EXAMPLE OF (K,Rb)$HC_8H_4O_4$ ISOMORPHIC SERIES

Pankova Yu.A., Kryuchkova L.Yu., Glikin A.E.

Crystallography Department of Geological Faculty, Saint-Petersburg State University, Saint-Petersburg, Russia
yulika1314@gmail.com

It is common knowledge that most of minerals and synthetic compounds are solid solutions. Mechanisms of formation of such crystals differ a lot from crystallization of compounds of a fixed composition. The subject of this work is an investigation of spatial inhomogeneity of mixed crystals at micro and macro levels.

The isomorphic series potassium acid phthalate – rubidium acid phthalate ($KHC_8H_4O_4$–$RbHC_8H_4O_4$, or KAP–RbAP) is characterized by continuous isomorphism. KAP–RbAP–H_2O work system was chosen mainly as a model to illuminate basic processes with the help of the crystals that can be grown easily. The precipitation of crystal ensembles was caused by spontaneous crystallization from aqueous solutions with different component ratios (KAP/RbAP): 100/0, 70/30, 50/50, 30/70, 0/100 wt %. Also the experiments on replacement of mixed crystals in solutions with different composition were held. Received crystals were investigated by means of optical microscopy, atomic-force microscopy, scanning electron microscopy and computer X-ray micro- and nanotomography.

The computer X-ray microtomography (mCT) method enables to study density distribution and as a result distribution of isomorphic composition in a bulk. The end members of that isomorphic series are characterized with significant difference between densities (1,064 g/cm^3), that is why it is convenient to study these isomorphic crystals by mCT. Microtomographic patterns of (K,Rb)$HC_8H_4O_4$–crystals were obtained ex situ with the microtomograph SkyScan 1174 and nanotomograph SkyScan 2011. Crystals of the end members of isomorphic series (K,Rb)$HC_8H_4O_4$ are homogeneous. But an inhomogeneity of mixed crystals is clearly observed. It is caused by heterogeneous distribution of isomorphic components. At the cross-sections it is possible to separate less dense inner zone, which is enriched with less soluble K-component, and denser outer zone, which is enriched with more soluble Rb-component. The borders of the zones are fuzzy. The pictures of both orthogonal cross-sections are the same. Except macro inhomogeneity there is micro inhomogeneity too. This is a micromosaic structure that is built by irregular shaped domains of different isomorphic composition. The size of domains is about 10 μm. They commensurate with the micro objects on the crystal surface (protuberances and etching pits). Bulk inhomogeneity seems to be a usual feature of mixed crystals. This corresponds with a spontaneous appearance and transformations on a surface of protuberances of various isomorphic compositions.

Investigations of surface morphology of mixed crystals were held by the *atomic-force microscopy (AFM)* (probe nanolaboratory Ntegra Prima NT-MDT) in the contact or semicontact mode. On the growth surface of the end members of (K,Rb)$HC_8H_4O_4$ isomorphic series separate steps and echelons of steps distinguished. They have straight or smoothly bending edges. The surfaces of mixed crystals are characterized with extreme inhomogeneity. There are areas of growth (protuberances) and dissolution (etching pits). Protuberances occur to be a continuation of steps. Than more protuberances are formed than steps become more bending. Some of protuberances are faceted (an evidence of growth) and some of them have a roundish shape (an evidence of dissolving) [3]. Along with these different habit of protuberances allows to see the difference in the chemical composition. Elongation of habit corresponds to the increase of the Rb-component content in the case of the (K,Rb)$HC_8H_4O_4$ isomorphic series [1].

Features of mixed crystals formation has been investigated in Crystallogenesis Laboratory of Crystallography Dept. of St. Petersburg State University since the 1980s. Experimental data

confirmed the metasomatic origin of some unusual peculiarities [4]. Over 150 isomorphic systems were studied [1, 4]. Experiments on exchange reactions between crystals of the end members of $(K,Rb)HC_8H_4O_4$ isomorphic series and solutions with different KAP/RbAP ratios were conducted before [2]. In this work we conducted the reaction vice versa. Interaction between crystals of both substances (RbAP and KAP) as well as their solid solutions (in ratios of components 30/70, 50/50 and 70/3 wt %) and aqueous solutions saturated with either KAP or RbAP has been studied. Observation of the pseudomorph morphology and monitoring of the replacement reactions were conducted at room temperature with help of preparations described for analogous investigations before [4] and similar to those used in petrographic study. It made possible to observe movement of the reaction front toward the crystal center and changes in macroscopic relief at the sample selvages.

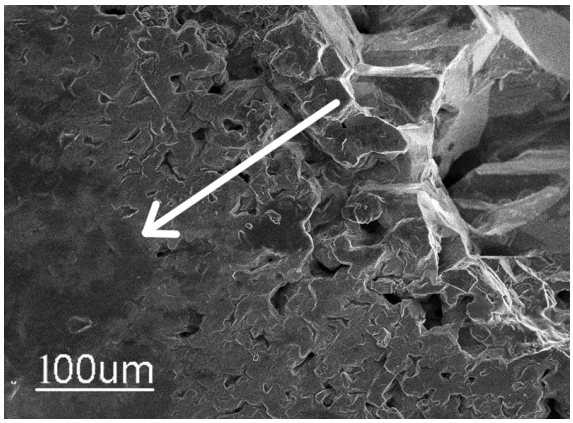

Figure 1. Mixed crystal of KAP/RbAP in ratios 50/50 wt % replaced in solution of KAP for 8 days. An arrow shows the movement of the reaction front from the periphery toward the crystal center.

All the processes were observed in situ by means of *optical microscopy* (Digital microscope Leica DVM 5000). The first stage of interaction was formation of defect zone with porous texture. And the second stage was formation of epitaxial excrescences on the surface of the pores and the crystal. Both of stages occur simultaneously (AFM data). Such mechanism of isomorphic replacement between a crystal and solution was explained a shift mechanism of replacement from volume-deficit toward volume-excess is caused by a considerable convexity of the solubility isotherms in the concentration diagrams for mixed solutions of the model system [2].

The same results were received as already replaced crystals ex situ by means of *scanning electron microscopy* (Hitachi S 3400N). The defect porous outer zone and the massive part of the unsubstituted protocrystal and winding boundary between them are clearly distinguished (fig. 1). A porous texture of outer zone is formed by lots of intruded inclusions of irregular shape. The monicrystallinity of formed pseudomorphous is preserved.

Crystals of $(K,Rb)HC_8H_4O_4$ isomorphic series obtained by the method of mass precipitation are characterized macro inhomogeneity (zonality) and micro inhomogeneity (micromosaic structure). The surface of mixed crystals features with heterogeneous relief. We connect it with a different composition of relevant areas. During the process of their formation mixed crystals are permanently in disequilibrium with solution. It causes to local metasomatic exchange of components between a crystal and solution and as a result of that processes inhomogeneous structure of the mixed crystals is formed.

This work is supported by the Russian Fund of Basic Research (grants 12-05-00876, 13-05-12053) and the "Geomodel" Resource Centre.

References:

[1] A.E. Glikin. Polymineral-Metasomatic Crystallogenesis // Saint-Petersburg, "Journal NEVA" Edition (2004) 320. (Russ.)

[2] A.E. Glikin, S.I. Kovalev, E.B. Rudneva, L.Yu. Kryuchkova, A.E. Voloshin. *Journal of Crystal Growth* 255 (1-2) (2003) 150-162.

[3] A.E. Glikin, L.Yu. Kryuchkova, L.Yu. Plotkina, M.Yu. Sinai, P. Gille, J. Schneider and R. Stark. *Zapiski VMO* (Special issue) (2007) 7-35.

[4] A.E. Glikin, M.Yu. Sinai. *Zapiski VMO* 112 (6) (1983) 742-748. (Russ.)

DEVELOPMENT OF FUNDAMENTALS ON CRYSTALLOGENETIC MECHANISM OF ISOMORPHISM

Petrova E.V. [1,2], ***Bogdashkina D.V.***[2], ***Glikin A.E.***[3]

[1] *University of Houston, Houston, TX, USA*
[2] *Moscow State University, Moscow, Russia*
[3] *St. Petersburg State University, St. Petersburg, Russia*
elena.petrova.biocryst@gmail.com

We performed ex-situ AFM experiments on the growth of isomorphic crystal systems from solution as related to surface processes at nanolevel and its theoretical description. The crystal formation of mixable isomorphic components KCl-KBr has been studied while varying supersaturation and ratio of components. We placed a seed KCl crystal in mixed KCl-KBr solutions. Then we dried the crystal surface by compressed air and scanned 15×15 μm^2 areas of the (100) face to observe morphological changes after interaction with mixed solution. The ratio KBr/KCl was varied around 0.5, 1, 2, and 3; concentration of the components were measured as g/100 g H_2O. Supercooling ΔT was equal to 5 and 10°C. To trace the growth process as a function of time we employed 1, 5, and 10 seconds expositions.

The typical images illustrated that the flat (100) face of KCl crystal lost stability and split to separate square blocks, which could have the same or different orientations with respect to the original face. There were growth sources in the middle of those square blocks. We analyzed ratio and product of molar concentration of potassium cations and mixed anions. Ions Cl^- and Br^- were considered as equivalent building units at kinks of the growth steps. The crystal surface lost the stability both at greater supercooling and increased molar concentrations of solution components. A ratio of the components can be examined by introduction of the activity coefficients of the species.

These studies have demonstrated the necessity in development of new methods and broadening of the genetic factors, which are related to kinetics, morphology and composition of the formed crystal compound.

We thankfully acknowledge funding support provided by Russian Foundation for Basic Research, grant 11-05-90707-mob_st.

NATURAL NANOSTRUCTURED GRAPHITE: MORPHOLOGY, STRUCTURE, CHARACTERIZATION, FORMATION MODELS

Ryabov V.V. [1], ***Ponomarchuk V.A.*** [1,2], ***Titov A.T.*** [1,2], ***Moroz T.N.*** [1], ***Semenova D.V.*** [1]

[1] *Novosibirsk, IGM SB RAS,* [2] *Novosibirsk State University, Novosibirsk, Russia*
trap@igm.nsc.ru

Understanding of the fundamental properties of carbon has increased significantly over the past few decades. Graphene (2D - dimension), nanotubes (1D - dimension), fullerene (0D - dimension) were added to the already well-known allotrope of carbon - diamond, graphite, lonsdaleite, carbines. Nanotubes and fullerene firstly were obtained experimentally [1, 2, 3]. Currently, various methods, including plasma, laser, spark arc, are used for synthesis of nanotubes and fullerenes. General conditions of the synthesis are: 1) temperature is about 400-2000°C; 2) the presence of carbonaceous materials, preferably gases; 3) the presence of catalysts, mainly transition elements, as well as Pt, Cu; 4) the pressure equal to or lower than atmospheric; 5) a relatively short time of synthesis from minutes to ten hours, and, - that it is important to emphasize, - 6) strict control of the synthesis conditions. In the earth interior the only first three conditions of the synthesis may realize, but there are few reports in the literature about findings of natural carbon nanotubes, microtubes (fullerene is not considered in this report) and other nanostructuring formations in magmatic rocks [**4**]. Natural carbon nanotubes, microtubes are much rarer than diamonds. In this regard, the question arises - what explains their uniqueness and what the nature of physical and chemical conditions of their formation in comparison with the synthetic ones.

The present report provides the detailed comparison of the morphological characteristics of synthetic (published data) and natural sp2 - hybridized carbon nanostructuring formations.

The object of our study was the aggregates of micro- and nanostructuring carbon of different morphology, found in a globular graphite leicogabbro of Pt-lowsulfide ores of Verhnetalnahskaya intrusion (Norilsk region) [**5, 6**]. Structural and morphological features of these aggregates were briefly described in publications [**7,8**]. In this report, the SEM images of the original natural "sp2 material" in comparison with morphologically similar, synthetically-grown carbon nanostructures (published data) are discussed.

Paired SEM images of morphologically similar carbon structures are shown in figures 1 and 2. Pictures of “natural” SEM images are highlighted by a dotted frame, and SEM images of synthetic structures are marked by literary source.

Study of natural carbon formations by different methods has shown the following: 1) nanostructured graphite is a complex of hybrid nanostructures and morphologically different from the classical forms of graphite formed during metamorphism and mineralization; 2) reflections on the X-ray diffraction spectra coincide with the reflections typical for graphite (oral communication of doctor Seryotkin Y.V.); 3) according to Raman spectroscopy, the position of the bands (around 1360, ~ 1580, ~ 1620, ~ 2700 cm-1), peak half-heights resolution and it’s intensity ratio is roughly close to those of the graphite, it is important to note that in some cases these characteristics reach the parameters of highly oriented pyrolytic graphite (HOPG); 4) according to the energy dispersive analyzer data, carbon content is not below 85%, 5) microelement analysis of nanostructured graphite has shown the presence of Fe, Ni, Cu, Ge, Pt, that may act as catalysts; 6) isotopic composition of carbon is within narrow interval that is evidence of homogeneity of the carbon source.

Physical-chemical regularities of the formation of synthetic carbon nanostructures (nanotubes, nanocones, nanorods, onion-like structures, graphene, etc.) is still under intense debate, but some of well-established conclusions can be used for specifying the model of formation of natural nanostructured graphite. In particular, based on petrographic data, the

formation process is discrete and multi-pulsed, but the high temperature, presence of hydrocarbons and element-catalysts are prerequisite.

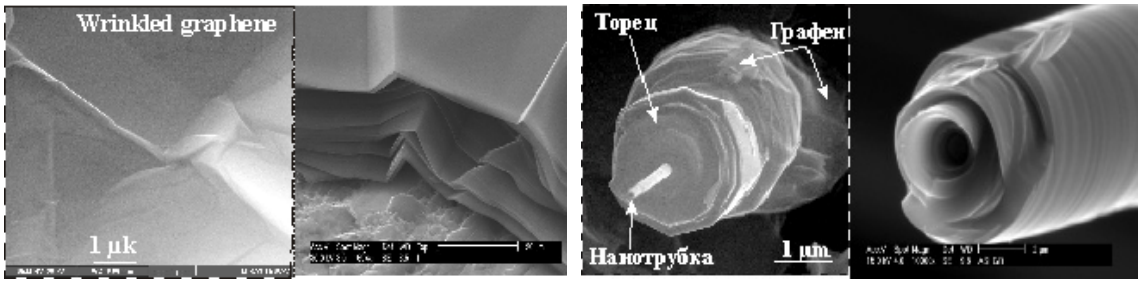

Figure 1. SEM images: left pair: folds in graphene layers, right pair - end of microtubes.

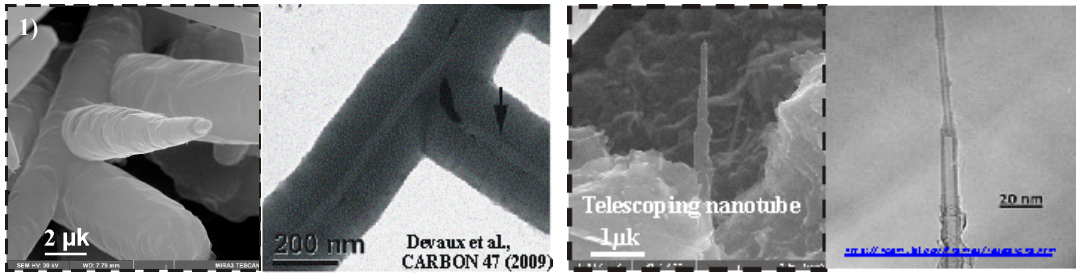

Figure 2. SEM images: left pair: T-junction, right pair: telescope nanotubes.

References:

[**1**] Iijima, S., Nature, 1991, no. 354 (6348), pp. 56–58.

[**2**] Kroto, H.W., Heath, J.R., O'Brien, S.C., et al., Nature, 1985, vol. 318, no. 14, pp. 162–163.

[**3**] Radushkevich, L.V. and Luk'yanovich, V.M., Zh. Fiz.Khim., 1952, no. 26, pp. 88–95.

[**4**]. Jasczak, J.A., Dimovski, S., Hackney, S.A., et al., Canad. Mineralogist, 2007, vol. 45, pp. 379–389.

[**5**] Ryabov, V.V., Shevko, A.Ya., and Gora, M.P., Magmaticheskie obrazovaniya Noril'skogo raiona (Magmatic Buildups of Norilsk District), vol. 2: Atlas magmaticheskikh porod (Atlas of Magmatic Rocks), Novosibirsk: Nonparel', 2000.

[**6**] Ryabov, V.V., Shevko, A.Ya., Gora, M.P. Trap Magmatism and Ore Formation in the Siberian Noril'sk Region. 2014 (в печати).

[**7**] Ryabov, V.V., Ponomarchuk, V.A., Titov, A.T., and Semenova, D.V., Dokl. Ross. Akad. Nauk, 2012,

[**8**] Ponomarchuk V. A. Kolmogorov Y. P., Ryabov V. V., et al., SR XRF Study of Natural Micro- and Nanostructured Carbon from Igneous Rocks Bulletin of the Russian Academy of Sciences. Physics, 2013, Vol. 77, No. 2, pp. 203–206.

STRUCTURAL EVOLUTION OF ZEOLITE-LIKE ZIRCONOSILICATES AT HIGH PRESSURE

Seryotkin Yu.V. [1], ***Bakakin V.V.*** [2], ***Pekov I.V.*** [3]

[1] *V.S. Sobolev Institute of Geology and Mineralogy, SB RAS, Novosibirsk, Russia*
[2] *A.V. Nikolaev Institute of Inorganic Chemistry, SB RAS, Novosibirsk, Russia*
[3] *Moscow State University, Moscow, Russia*
bakakin@niic.nsc.ru

The high-pressure structural evolution of zirconosilicates such as catapleite, hilairite, and elpidite (Table) was studied using X-ray single-crystal diffraction (Oxford Diffraction Xcalibur Gemini diffractometer) and a Boeler-Almax diamond-anvil cell. A 4 : 1 methanol/ethanol mixture was used as pressure-transmissing medium.

	Chemical composition, unit cell parameters (Å)	Space group	P_{max} (GPa)
Catapleite	$Na_{1.4}Ca_{0.3}(H_2O)_2[ZrSi_3O_9]$, Z = 32 *a*=25.6848(9), *b*=20.0802(6), *c*=14.8237(6)	*Fdd*2	4.04
Hilairite	$Na_{1.8}(H_2O)_3[ZrSi_3O_9H_{0.2}]$, Z = 6 *a*=10.5665(2), *c*=15.9109(4)	*R*3	4.73
Elpidite	$Na_{1.7}Ca_{0.15}(H_2O)_3[ZrSi_6O_{15}]$, Z = 4 *a*=7.13201(19), *b*=14.6787(4), *c*=14.6297(3)	*Pbcm*	4.95

The pressure trends of the unit cell parameters of catapleite and hilairite are close to linear; the compression of the structure is isometric. Over the studied pressure ranges, no anomalies in the structure evolution of catapleite were detected. As for hilairite, the increasing pooper of diffraction data is observed above 3.8 GPa. The unit cell parameters measured at 1.68 GPa during unloading were much lower than those in the direct course (Fig. 1). Clearly the structure of hilairite has undergone irreversible changes associated with the bond breakage in the framework.

The compression of elpidite up to 1.2 GPa is isometric, the unit cell parameters varying almost linearly. At higher pressure elpidite undergoes the second-order phase transition with doubling the *a*-parameter. The compression of the structure along *a* and *c* above the transition accelerates through turns of the SiO_4 tetrahedra and thus the band distortions. At pressure above 3 GPa the unit cell parameters are observed to be departed from orthorhombicity resulting in the selection of new coordinate directions of the monoclinic unit cell.

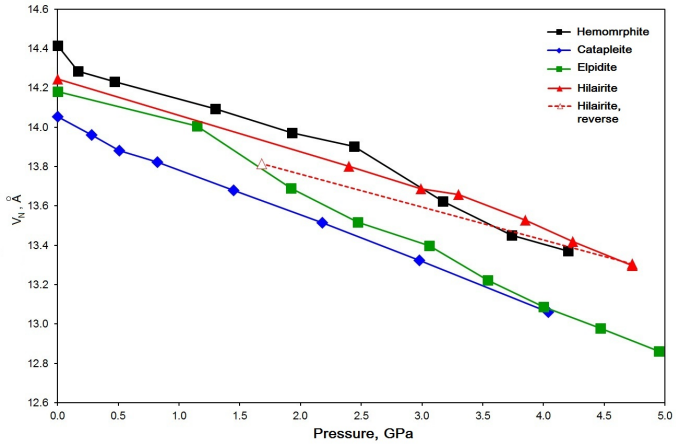

Figure 1. Normalized volume V_N of heteroframework compounds vs. pressure

A comparative crystal chemical analysis requires usage of uniform characteristics which have to be brought to the unified scale. The authors of the project propose one such characteristic, the so-called normalized volume V_N, i.e. the volume for one atom of the compound [1]. Figure 1 shows the pressure dependence of V_N for zirconosilicates studied as well as for hemimorphite $Zn_4Si_2O_7(OH)_2 \cdot H_2O$ [2]. Catapleite with the least V_N value under normal conditions, when compressed, undergoes only isometric compression with no structure transformations, at least in

the pressure range studied. In principle, the lesser normalized volume may be thought of as evidence of the greater stability of the given structure to the elevated pressure [1]. Hilairite and elpidite have the close V_N values under normal conditions while they behave differently when compressed. Elpidite undergoes two phase transitions to gain the greater capacity for compression after each transition (Fig. 1). Finally, after the second transition, the $V_N(P)$ dependence falls on the compression curve of catapleite, and right there perturbations with elpidite end. Hilairite holds noticeably greater normalized volume over the whole pressure range, resulting in drastic reconstruction with irreversible changes of the structure. The zincosilicate hemimorphite behaves somewhat similarly (Fig. 1) undergoing two phase transitions.

There is no doubt that such distinct behavior of zirconosilicates is due to their structure features. In the framework of catapleite, the stories of the Zr octahedra alternate with those of the hard ring radicals $[Si_3O_9]$ to give hardness to the whole Zr,Si framework (Fig. 2). The extraframework $Na_2(H_2O)_2$ component is located in the Zr story with the corrugated net configuration.

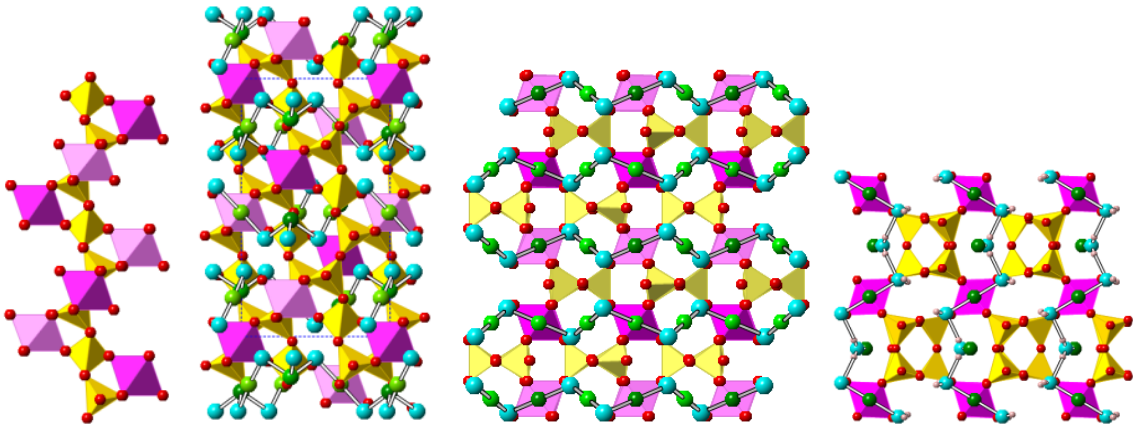

hilairite $Na_2(H_2O)_3[ZrSi_3O_9]^{\infty}$ chain | catapleite $Na_2(H_2O)_2[ZrSi_3O_9]$ ring | elpidite $Na_2(H_2O)_3[ZrS_6O_{15}]^{\infty}$ band

Figure 2. Three heteroframework zirconosilicates from a view point with Zr octahedra in a similar edge orientation.

In hilairite, the oxygen-silicon framework part involves the Si_3O_9 chains which seemingly have to be rather versatile by definition. However, in this case each two adjacent tetrahedra of the chains are tightened by the edge of the Zr octahedron (at the left of Fig. 2) resulting in the mixed construction to consist of the hard triple ring links (Si–O–Si–O–Zr–O) with the 132–140º angles on the oxygen atoms. Owing to this, hilairite has the minimal compressibility of all the compounds studied and its increase is possible only through a radical structure rebuilding.

In the structure of elpidite, the basic joint circuit of the oxygen-silicon radicals with Zr is the same as that in the structure of catapleite. Changing the triple rings to the bands, however, has eliminated the reason of the heteroframework hardness. In addition, changing the story circuit for the two-story bands alongside with the appearance of the extra H_2O molecule gave rise to the reorientation of the Na, H_2O-component.

The relative hardness/flexibility of the heteroframework following the Si–O–Si and Si–O–Zr angle values as a criterion results from the structure of oxygen-silicon radicals and mechanism of joining with Zr. Phase transformations with retention of the framework topology are typical of a flexible construction alone.

This work was supported by Russian Foundation for Basic Research, grant # 13-05-00457.

References:
[1] Bakakin V.V., Seryotkin Yu.V. J. Struct. Chemistry, 2009, 50 (Suppl.), S116–S123.
[2] Seryotkin Yu.V., Bakakin V.V. Phys. Chem. Minerals, 2011, 38, 679–684.

Mineral	hilairite	catapleite	$[elpidite]^{\infty}$
Si_3O-radical and its behavior	chain **hard because of Zr blocking**	triple ring **very hard**	doubled band **with flexibility resource**
Mechanism of joining with Zr	**very hard**	**flexible**	**flexible**
Characteristics of heteroframework	**very hard**	**hard**	**flexible**
Pressure behavior	Isometric compression with evidence of disruption above 3.85 GPa	Only isometric compression over the range up to 4 GPa	Two phase transitions, at 1.2 and 4.95 GPa

SYNTHESIS AND CRYSTAL STRUCTURE OF PETROVSKAITE AgAuS. A FINE FOUR-FOLD INTERPENETRATING 3D $(Au,Ag)^{[2]}$-NETWORKS.

Seryotkin Yu.V., Bakakin V.V., Pal'yanova G.A., Kokh K.A.

V.S. Sobolev Institute of Geology and Mineralogy, SB RAS, Novosibirsk, Russia, bakakin@niic.nsc.ru

Mineral petrovskaite AgAuS discovered by Nesterenko et al. [1] has been described as monoclinic with unit cell parametes a = 4.94, b = 6,67, c = 7.22 Å, β = 95.68°, space group $P2/m$, but the structure is unknown so far. We have synthesized petrovskaite directly from stoichiometric mixture of Au, Ag, and S using ampoule technique described elsewhere [2].

Synthesized crystals are of low quality. On the base of single-crystal X-ray diffraction data, the structural model with space group $R\bar{3}m$ is suggested. Then the structure was refined by the Rietveld method using powder diffraction pattern. The unit cell parameters are a = 13.4235(3), c = 9.0873(4) Å, V = 1418.07(6) $Å^3$, Z = 24. This hexagonal lattice and above-mentioned monoclinic lattice are related with the transformations as: $\vec{a}_h = \vec{b}_m$, $\vec{b}_h = \vec{a}_m - \vec{b}_m/2 + \vec{c}_m/2$, $\vec{c}_h = \vec{a}_m/2 - \vec{c}_m/2$.

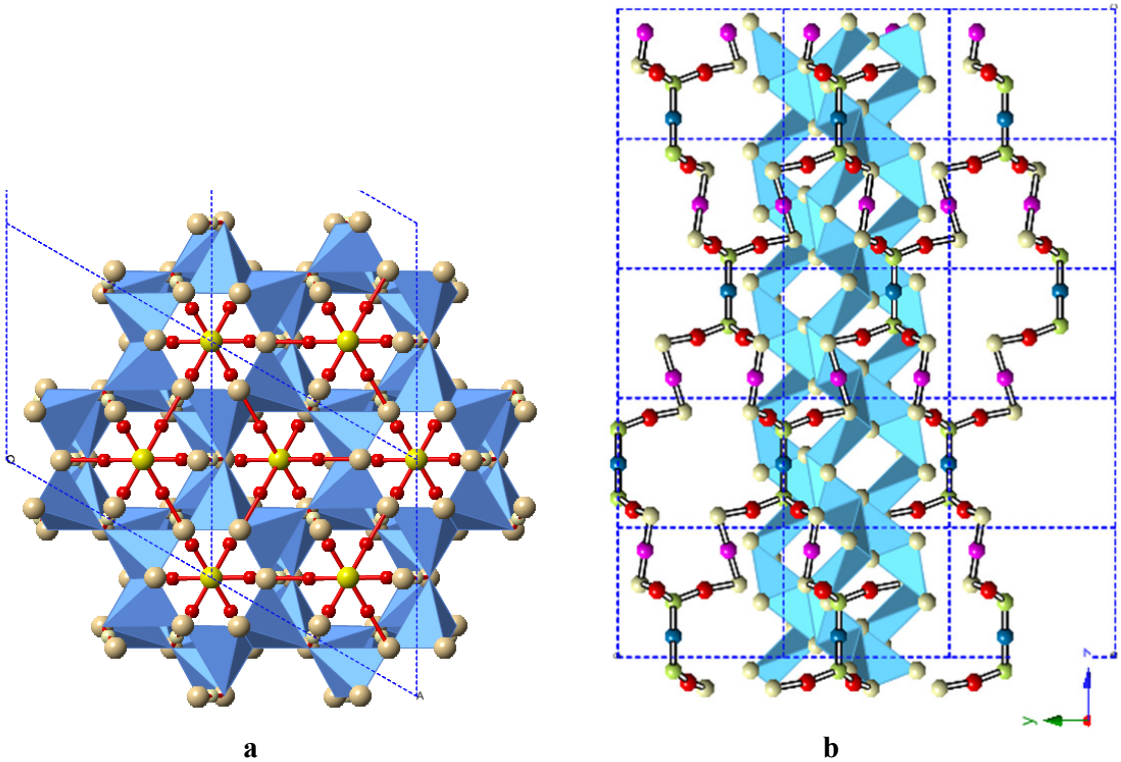

a **b**

Figure 1. Crystal structure of AgAuS. **a** – Projection along the c axis. AgS_4-tetrahedra framework is in blue, $[Au_8^{[2]}Ag_2^{[2]}S_8]_3$ skeletons is shown with ball-stick. **b** – Projection along the b axis. One of four interpenetrating $[Au_8^{[2]}Ag_2^{[2]}S_8]_3$ skeletons that enlace tube formed by six $Ag^{[4]}{}_3$–ribbons. Three other skeletons are omitted for clarity.

In the AgAuS structure, 48 cations per unit cell are distributed over four sites. One position is of 18 multiplicity and is occupied with Ag^+ in tetrahedral coordination by S^{2-}. Three sites are arranged in linear coordination with S^{2-}. One of them is of 18 multiplicity and occupied with

Au^+, other one is of 9 multiplicity occupied statistically with 6 Au^+ and $3Ag^+$, and the last one is of 3 multiplicity occupied only with Ag^+. Thus, all 24 Au^+ occupy their sites in the structure in the linear coordination with respect to chalcogen anion, typical for Au cations. Of 24 «chameleon-like» Ag^+ cations, 18 are in their typical distorted tetrahedra, and 6 are involved in the linear motif general for Au^+ as well.

The lattice of the S^{2-} is a strongly distorted body-centered cubic packing. It may be subdivided into vacant irregular tetrahedra, or sphenoids [3,4]. The sphenoids are partly occupied with Ag^+. The linearly coordinated $(Au,Ag)^+$ are located on the edges of the vacant sphenoids. In structures with rhombohedral subcells it is convenient to describe the basal columns along the 3-fold symmetry axis, which is composed of skew trigonal prisms with three sphenoids in each prism. Two such prisms form a c-translation of ≈ 9 Å. A half of the sphenoids that form the prisms are occupied by Ag^+, and the rest half is vacant. The channel is formed with six prismatic columns and contains a network system of $(Au,Ag)^+$ cations, which are coordinated linearly and are located on the edges of the sphenoids. The systems located in adjacent channels are linked into 3D skeletons, which possess remarkable feature. They are four-fold interpenetrating $(Au,Ag)^{[2]}$-networks (Fig. b). Translation for a separate network is $c' = 4c$.

Crystal-chemical formula for petrovskaite is $Ag_{24}^{[4]}[Au_8^{[2]}Ag_2^{[2]}S_8]_4$. Comparative analysis of structures for Au-Ag chalcogenides is discussed with the emphasis on crystal genesis.

This work was supported by the Russian Foundation for Basic Research (grant # 11-05-00504).

References:

[1] Nesterenko G.V. et al. Petrovskaite AuAg(S,Se), a new Se-containing Au–Ag sulfide. Zapiski VMO, (1984) No. 5, 602–607.

[2] Pal'yanova G.A., Kokh K.A., Seryotkin Yu.V. Formation of gold and silver sulfides in the system Ag–Au–S. Geologiya i Geofizika (2011) 52 (4), 568–576.

[3] Bakakin V.V. Crystal Structures of Gold, Silver, and Sodium Chalcogenides: Sphenoidal Interpretation. Crystallography Reports (2011) Vol. 56, No. 6, 970–979.

[4] Seryotkin Yu.V., Bakakin V.V., Pal'yanova G.A., Kokh K.A. Sythesis and crystal structure of the trigonal silver(I) dithioaurate(I), Ag_3AuS_2. Crystal growth & design (2011), 11, 1062–1066.

Si-RICH NATURAL ANALOG OF $Ca_4Ti_2Fe_2O_{11}$ IN LARNITE-GEHLENITE ROCK FROM HATRURIM BASIN, ISRAEL

Sharygin V.V. [1], ***Wirth R.*** [2], ***Sokol E.V.*** [1], ***Nigmatulina E.N.*** [1], ***Karmanov N.S.*** [1]

[1] *V.S. Sobolev Institute of Geology and Mineralogy SB RAS, Novosibirsk, Russia*
[2] *Helmholtz Centre Potsdam, GFZ German Research Centre for Geosciences, Potsdam, Germany*
sharygin@igm.nsc.ru

Experimental studies in the system perovskite-brownmillerite

The synthetic compounds of the $CaTiO_3$-$CaFe_2O_5$ series have been studied intensely since 1960-70s due to specific properties of oxygen-deficient Fe-rich perovskites: superconductivity, oxygen ionic conductivity, electronic conductivity. Numerous compounds with the generalized formula $CaTi_{1-2x}Fe_{2x}O_{3-x}$ ($0 \leq x \leq 0.5$) were synthesized within the system **[1]**. However, only four orthorhombic compounds are fully ordered in oxygen vacancies and seem to be most stable: $CaTiO_3$ (x=0), $Ca_4Ti_2Fe_2O_{11}$ (x=0.25), $Ca_3TiFe_2O_8$ (x=0.33) and $Ca_2Fe_2O_5$ (x=0.5) **[1-6]**. According to the phase diagram $CaTiO_3$–$CaFeO_{2.5}$ (Fig. 1) the coexistence of perovskite and brownmillerite is impossible in any associations, because phases $Ca_3TiFe_2O_8$ and $Ca_4Ti_2Fe_2O_{11}$ are more stable in energy than the perovskite + brownmillerite paragenesis. The intermediate phases $Ca_4Ti_2Fe_2O_{11}$ and $Ca_3TiFe_2O_8$ should be stoichiometric in composition without vacancies of cations and oxygen. Any deviations in Ti content should lead to the appearance of nanoscale intergrowths/domains of $Ca_4Ti_2Fe_2O_{11}$ + Fe-perovskite, $Ca_3TiFe_2O_8$ + $Ca_4Ti_2Fe_2O_{11}$ or $Ca_3TiFe_2O_8$ + $Ca_2Fe_2O_5$.

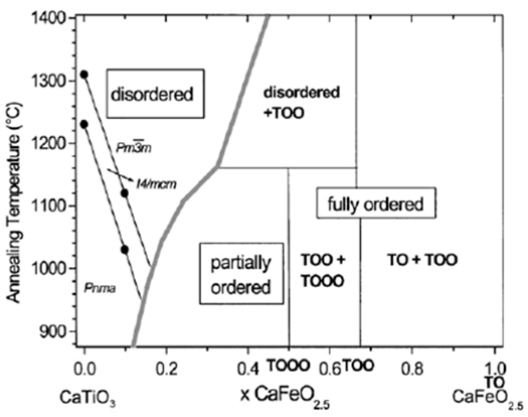

Figure 1. Phase diagram for the system $CaTiO_3$-$CaFeO_{2.5}$ [2-3]. *TO, TOO* and *TOOO* indicate the sequence of tetrahedral *(T)* and octahedral *(O)* layers in the ordered structures. *TO* – $Ca_2Fe_2O_5$; *TOO* – $Ca_3TiFe_2O_8$; *TOOO* – $Ca_4Ti_2Fe_2O_{11}$. *Pnma, I4/mcm, Pm3m* – fields of Fe-perovskite with cubic, orthorhombic and tetragonal symmetry.

At present natural analogs of these intermediate phases are found. Shulamitite $Ca_3TiFeAlO_8$, a natural Al-rich analog of synthetic $Ca_3TiFe_2O_8$, was described as a new mineral in combustion metamorphic larnite rocks at Hatrurim Basin, Israel **[7-8]**. Natural $Ca_3TiFe_2O_8$ is also found in metacarbonate rocks from some natural and anthropogenic occurrences, but not yet approved as new mineral species **[8-9]**. Here we provide first information about natural $Ca_4Ti_2Fe_2O_{11}$, which is a potential new mineral.

Occurrence of natural $Ca_4Ti_2Fe_2O_{11}$

This phase was recently found in larnite-gehlenite fine-grained rock at Hatrurim Basin, Israel. The primary mineral paragenesis represents larnite, gehlenite, magnesioferrite, $Ca_4Ti_2Fe_2O_{11}$, fluorapatite and unidentified Ca-P-silicate (nagelschmidtite ?). Retrograde phases are hydrogarnet, portlandite, calcite, hashemite, ettringite, afwillite and other hydrated Ca-silicates. The $Ca_4Ti_2Fe_2O_{11}$ phase forms subhedral grains (up to 20 μm) and is the sole member of the perovskite-brownmillerite series in the rock (Fig. 2). Its contents in the rock is <5 vol.%.

Chemical composition

According to elemental maps and microprobe data the individual grains of natural $Ca_4Ti_2Fe_2O_{11}$ are homogeneous in composition (Table 1). However, compositions of discrete grains vary essentially in TiO_2 (26-35 wt.%), Fe_2O_3tot (16-23 wt.%) and SiO_2 (3-7 wt.%) what suggests the possible presence of nanoscale intergrowths or domains. In contrast with synthetic compound, the natural phase is rich in SiO_2 and Al_2O_3, and probably in FeO. The incorporation of Si in the structure assumes two variants of formula: $Ca_4Ti_2Fe^{3+}(Si_xFe^{3+}_{1-x})O_{11+x}$ or $Ca_4Ti_2Fe^{3+}_{1-x}Fe^{2+}_x(Si_xFe^{3+}_{1-x})O_{11}$, where $x \leq 0.5$

Table 1. Chemical composition and unit cell parameters for natural and synthetic $Ca_4Ti_2Fe_2O_{11}$.

wt.%	1	2	3	4		1	2	3	4
SiO_2	4.92	5.21	4.53		Si	0.436	0.460	0.400	
TiO_2	29.49	29.51	30.14	29.38	Al	0.202	0.223	0.200	
ZrO_2	0.69	0.71			$^{IV}Fe^{3+}$	0.362	0.317	0.400	1.000
Nb_2O_5	0.04	0.03			Ti	1.967	1.959	2.000	2.000
Cr_2O_3	0.08	0.09			Zr+Nb	0.032	0.032		
Al_2O_3	1.93	2.14	1.92		Cr	0.006	0.006		
Fe_2O_3	19.57	19.29	21.09	29.37	$^{VI}Fe^{2+}$	0.391	0.419	0.400	
MnO	0.05	0.04			$^{VI}Fe^{3+}$	0.553	0.545	0.600	1.000
CaO	42.44	42.51	42.31	41.25	Mn	0.004	0.003		
SrO	0.25	0.24			Ca	4.032	4.021	4.000	4.000
UO_2	0.17	0.13			Sr	0.013	0.012		
Sum	99.63	99.90	100.00	100.00	U	0.003	0.003		
a, Å		5.254		5.437(1)					
b, Å		30.302		30.22(1)					
c, Å		5.488		5.489(1)					
Space group		*Pnma* ?		*Pnma*					
Source		our		**[5-6]**					

1-2 – Hatrurim Basin: 1 – average for all grains of natural phase (n=37); 2 – grain used for HRTEM (n=2); 3 – ideal composition $Ca_4Ti_2Fe^{3+}_{0.6}Fe^{2+}_{0.4}(Al_{0.2}Si_{0.4}Fe^{3+}_{0.4})O_{11}$; 4 – synthetic $Ca_4Ti_2Fe_2O_{11}$. Fe^{3+} and Fe^{2+} are calculated from charge balance for formula based on 8 cations and 11 oxygens.

HRTEM study

The complex study of a FIB-milled foil has shown that natural $Ca_4Ti_2Fe_2O_{11}$ phase from Hatrurim Basin are homogeneous and does not contain any oriented ingrowths of silicates or domains of other perovskite-type structures. Thus, Si is an isomorphic component, which stabilizes the crystal structure of this phase at variable Ti and Fe^{3+} contents. Moreover, obtained data allow calculating unit cell parameters for the Hatrurim phase (Table 1), which are very similar to those for synthetic $Ca_4Ti_2Fe_2O_{11}$ **[5-6]**.

This work was supported by the Russian Foundation for Basic Research (grant 12-05-00057).

References:

[1] Grenier *et al.* (1981) Structure and Bonding **47**, 1-25.
[2] Becerro *et al.* (1999) Phase Trans. **69**, 133–146.
[3] Becerro *et al.* (2002) J. Solid State Chem. **167**, 459-471.

[4] Rodrígues-Carvajal *et al.* (1989) Mat. Res. Bull. **24**, 423-430.
[5] Gonzáles-Calbet & Valet-Regí (1987) J. Solid State Chem. **68**, 266-272.
[6] Hovmöller *et al.* (1988) J. Solid State Chem. **77**, 316-321.
[7] Sharygin *et al.* (2008) Russ. Geol. Geophys. **49** (10), 709-726.
[8] Sharygin *et al.* (2013) Eur. J. Mineral. **25**, 97-111.
[9] Galuskin *et al.* (2008) Am. Mineral. **93**, 1903-1910.

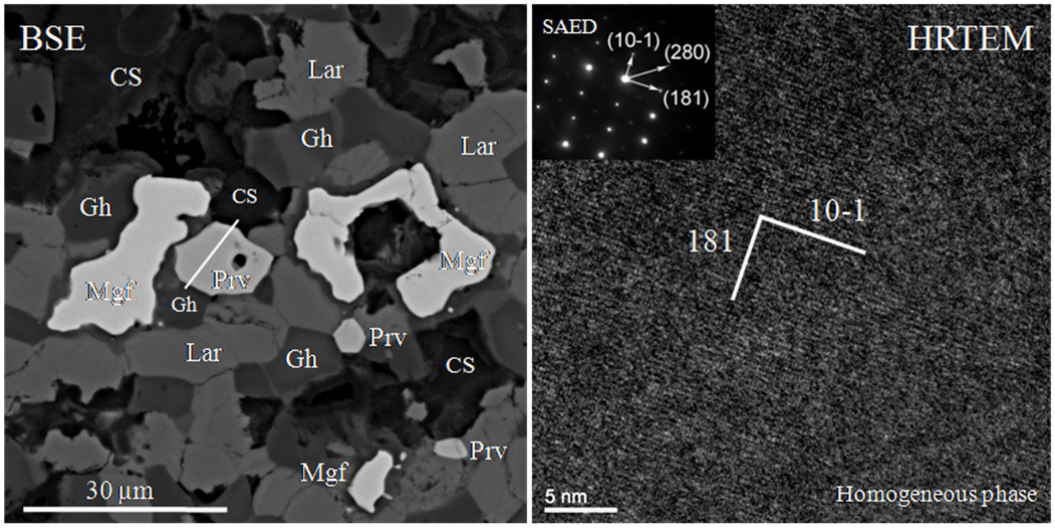

Figure 2. BSE and HRTEM images for the $Ca_4Ti_2Fe_2O_{11}$ phase from larnite-gehlenite rock, sample W-11-3, Hatrurim Basin. Symbols: Lar – larnite; Gh – gehlenite; Mgf – magnesioferrite; Prv - $Ca_4Ti_2Fe_2O_{11}$; CS – hydrated Ca-silicates. Line on the BSE image means position of FIB-milled foil for HRTEM.

METHANE-DERIVED MG-CALCITES AND ARAGONITES FROM THE NE BLACK SEA: MINERALOGICAL AND GEOCHEMICAL EVIDENCE

Shnyukov E.F. [1]***, Korzhova S.A.*** [2]***, Sokol E.V.*** [2]***, Kozmenko O.A.*** [2]

[1] *Department of Marine Geology and Sedimentary Ore-Formation Kiev, Ukraine*
[2] *VS Sobolev Institute of Geology and Mineralogy SB RAS, Novosibirsk, Russia*
sa_novikova@inbox.ru

In cold seep marine environments, methane contained in ascending fluids is oxidized as CO_2 by a microbial consortium of sulfate reducing bacteria and methanotrophic archea. The CO_2 released during the process of anaerobic oxidation of methane (AOM) is then mostly precipitated as authigenic carbonates. They are archives of the AOM process, with their mineralogy, geochemistry, and isotopic compositions bearing a record of the composition and origin of the fluids they have precipitated from. Their main characteristic is very low $\delta^{13}C$ (down to –62‰ PDB), which relies on the methane source of carbon [1]. In the NE Black Sea, various types of AOM-related carbonate deposits occur in several areas along the shelf/slope of the Crimea Peninsula to be buried in loose, gas-saturated bottom sediments. In the oxic zone (at the 60 m water depth), carbonate precipitates are mostly small and pancake-shaped. At the water depths 110-190 m, carbonates form plates and irregular small chimneys. In the anoxic zone below 230 m, the precipitates are tall chimneys up to 1m high that are penetrated by active seepage [2, 3].

We have studied a unique buildup of methane-derived authigenic carbonates (MDAC) grown free into below the chemocline. It is a 1.5 meter high tower, with the diameters 40 cm on the top and 15 cm at the base, and with a distinct central channel. It was sampled under 1600 m of water on the slope of the submarine Lomonosov rise (station 5390; 44° 27.4' N; 32° 48.6' E) during 56th trip of R/V *Professor Vodyanitskiy*. ^{14}C contents give the apparent radiocarbon ages of 9050-7540 ± 180 a BP where gaseous methane discharged into the water column, and so indicate the minimum ages of carbon derived from a fossil hydrocarbon source. The top of this tower-like MDAC edifice is covered by pink and orange microbial mats [4]. The walls of the buildup are 1-4 cm thick and layered. The mineralogy consists mainly of micritic and rarely spherulitic high-Mg-calcite. Aragonite exists as sporadic prismatic crystals within a Mg-calcite matrix or spherulites at the top of the buildup. The carbonate matrix often contains pyrite framboids, organic matter, and *Emiliania huxleyi* coccoliths, as well as minor gypsum and barite. The contribution of detrital silicate material is negligible. Norsetite $BaMg(CO_3)_2$ was mentioned by [4]. Both spherulites and foliated acute rhombohedrons of Mg-calcite are typical of the outer zones of the edifice. Within the intermediate (recrystallized ?) zones, Mg-calcite occurs as obtuse rhombohedrons with curved faces (3-10 μm-sized). $MgCO_3$ contents in calcites vary from 9 to 13 mol.%. The impurities are 0.13-0.28 wt.% SrO, 0.13-0.26 wt.% Na_2O, and 0.06-0.29 wt. % MnO. The early calcites have higher BaO enrichment than the late ones (0.07-0.20 wt.% against ≤ 0.09 wt.%).

The $\delta^{13}C$ values of the seep carbonates lower than –33.0 ‰ PDB indicate that the precipitates are predominantly methane-derived. The $\delta^{13}C$ values are the lowest (–46.5 ‰ PDB) in a late spherulitic aragonite, whereas the coexisting Mg-calcite has higher ^{13}C from –41.5 to –40.0 ‰ PDB. Micritic Mg-calcite from the buildup root has $\delta^{13}C$ between –38.2 and –36.6 ‰ PDB (in the central portion), with –33.0 ‰ PDB the heaviest. The pink mat covering the buildup has high ^{12}C enrichment being depleted in ^{13}C ($\delta^{13}C$ about –71 ‰ PDB) [4]. The $\delta^{18}O$ values in methane-derived carbonates of a narrow range from +31.1 to +32.3 ‰ (SMOW) show seawater to have been the main source of oxygen during the buildup formation. The predominance of Mg-calcite in the deep-sea carbonate buildup of the Crimean slope in the anoxic water column (at the depth of 1600 m) is evidence of an environment where sulphate is rapidly converted into sulphide upon AOM: $CH_4 + SO_4^{2-} \rightarrow HCO_3^- + HS^- + H_2O$ (1) and $Ca^{2+} + Mg^{2+} + 2HCO_3^- \rightarrow$

$(Ca,Mg)CO_3$ (↓) + CO_2 + H_2O (2). Precipitation of aragonite may evidence of lower rates of the sulphate-dependent AOM reaction and a higher steady-state sulphate concentration [3].

The MDA carbonates are of two groups according to their REE+Y signatures (Fig. 1). Inasmuch as Mg-calcite and aragonite coexist on a small spatial scale, we could analyze monomineral fractions in two cases only, and in four cases that was a micritic aggregate of Mg-calcite with minor or trace aragonite (KM1-KM4).

The carbonates of the first group inherit high Sr enrichment (up to 1800 ppm), Ce/Ce* depletion, and Y/Ho ratios between 30 and 44. They show HREE enrichment over LREE indicating seawater as a predominant REE+Y source during precipitation of primary carbonates (Fig. 1a). These features are especially prominent in late aragonite spherulites from the buildup top but are more poorly pronounced in micritic carbonates from the upper part of its root. Late (recrystallized ?) Mg-calcite has lost its HREE enrichment, as well as other seawater signatures. The REE+Y shale-normalized patterns become flat (Fig. 1b). The same features are observed in carbonates sampled at the contact of the buildup roots with the underlying plagiogranite (KM2, KM3). Some authigenic carbonates are characterized by a pronounced positive Eu anomaly they may possibly have inherited from the igneous rocks of the Lomonosov submarine pluton.

The results highlight the potential of seep carbonates as sensitive tracers of both chemophysical factors and AOM environments, namely the metabolism of a microbial consortium.

The study was supported by grant 12-05-90403 from the Russian Foundation for Basic Research. It was carried out as part of joint research project of the NAS Ukraine and SB RAS N 1 (2013).

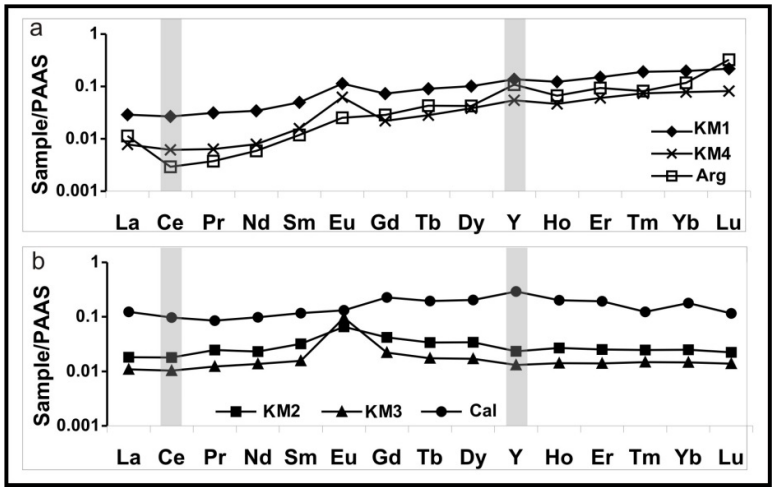

Figure 1. Shale-normalized REE+Y patterns of Holocene seep carbonates from the Crimea Peninsula slope. Calcite (Cal), aragonite (Arg), micritic aggregate of Mg-calcite with minor or trace aragonite (KM1-KM4).

References:

[1] Pierre C., Fouquet Y. Authigenic carbonates from methane seeps of the Congo deep-sea fan // Geo-Marine Letters, 2007, v.27, p. 249-257.

[2] Shnyukov E.F., Sobolevskiy Y.V., Kutniy V.A. Unusual carbonate buildups at the continental slope of the north-western Black Sea: an apparent consequence of the degassing of sediments // Lithology and Minerals, 1995, v.5, p. 461 – 541. (in Russian).

[3] Reitner J., Peckmann J., Reimer A., Schumann G., Thiel V. Methane-derived carbonate build-ups and associated microbial communities at cold seeps on the lower Crimean shelf (Black Sea) // Facies, 2005, v.51, p. 66–79.

[4] Shnyukov E.F., Kutniy V.A. Carbonates derived from gas seeps in the Black Sea battom. Geofizicheskii Zhurnal, 2003, v.25(2), p. 90-99. (in Russian).

MODERN VIEW TO MINERALOGY OF NATIVE CARBON

Shumilova T.G.

Institute of Geology of Komi Scientific Center UB RAS, Syktyvkar, Russia
shumilova@geo.komisc.ru

Diamond and graphite are the most widely known and actively studied carbon natural phases. At the same time carbon owing to features of an electronic structure of its atom is characterized by possible different electronic states such as sp^3, sp^2, sp^1 and intermediate configurations. The last is a reason of the wide variety of carbon phases and substances **[1]**. During the last decade the information about native carbon mineralogy was developed essentially underlining complicated character of natural carbon. Here we describe the modern data in the field of carbon mineralogy.

The important point concern to carbon nanostructures studies. Among natural carbon nanoparticles and nanostructured substances the study of natural fullerene, fullerene-like particles and diamond-lonsdaleite composites were studied by Buseck (1992; 2002), Becker (2000), Kovalevski (2005) and others. As the published data on carbon substances of handled and native origin are quite wide by present some generalization in the field of nanostructural studies at atomic resolution was provided, which summarized the data and proposed a new intermediate type of nanostructures by Shumilova et al. (2008).

By the next point it is need to take attention to findings of new carbon phases in a single-crystalline form. Among them we would like to list natural lonsdaleite demonstrating possible hexagonal diamond existing as independent single crystal substance **[2]** and single crystals of α-carbyne **[3]**.

In 2008 a new carbon intermediate state between diamond and graphite was discovered which was named as diaphite **[4, 5]**. The state was experimentally produced by photoinduced conversion of carbon atom hybridization. By the process interlayer bonds within graphite structure are appeared forming nanometer-sized sp^3 clusters. At the detailed study of natural carbon substances from Kumdykol diamond deposit (Kazakhstan) we have found natural diaphite particles and analyzed its microscopic and spectroscopic characteristics **[6]**.

The most new phase presented by amorphous optically transparent diamond-like carbon was met by us within diamond-containing carbonatites of Chagatai complex (Uzbekistan) and Kosyusky complex (Timan, Russia), which were written by Shumilova et al. (2012, 2013).

The mineralogy of native carbon and experimental synthesis products keeps a lot of secrets and opens with time a new basic knowledge about carbon statement in nature and lab conditions.

Acknowledgements to the grant of UB RAS Program #12-C-5-1035 for financial support.

[1] Shumilova T. G. *Mineralogy of Native Carbon* (Ural. Otd. Ross. Akad. Nauk, Yekaterinburg, 2003) (In Russian).

[2] Shumilova T. G., Mayer E., Isaenko S. I. Natural Monocrystalline Lonsdaleite. Doklady Earth Sciences, 2011a, Vol. 441, Part 1, pp. 1552–1554.

[3] Shumilova T. G., Danilova Yu. V., Gorbunov M. V., Isaenko S. I. Natural Monocrystalline α-Carbyne. Doklady Earth Sciences, 2011b, Vol. 436, Part 1, pp. 152–154.

[4] Nasu K., Sp^3 domain in graphite by visible light and photoinduced phase transitions, Eur. Phys. J. B (2010) [16 p].

[5] Nishioka K., Nasu K., Photoinduced sp^3 Nanosize Domain with Frozen Shear Displacement in Graphite, ACTA PHYSICA POLONICA, A 2 (2012) 350-354.

[6] Shumilova T., Mayer J., Isaenko S., Heidelmann M., Herwartz C., Wagner D. Lonsdaleite of a new genetic type and natural diaphite. European Mineralogical Conference. Vol. 1, EMC2012.

CRYSTALLOGENETIC MODELS AND NATURAL OBJECTS (AN EXAMPLE OF METASOMATIC REPLACEMENTS IN ZIRCON CRYSTALS)

Sinai M.Yu. [1], ***Kaulina T. V.*** [2]
[1] *St. Petersburg, Hertzen University, St. Petersburg, Russia*
[2] *GI KSC RAS, Apatity, Murmansk region, Russia*
kaulina@geoksc.apatity.ru

The experimental studies on low-temperature modeling of monocrystal replacement for many years have been conducted at St. Petersburg State University under the guidance of Professor A.E. Glikin. These studies revealed a number of specific processes, which are a combination of dissolution and growth forms of crystals. These forms are genetically linked and are in different proportions, determined by the system deviation from equilibrium. These experimentally obtained effects may be the basis for the interpretation of natural processes.

Natural zircon crystals from various geological environments often show complex secondary textures visible by cathodoluminescence and backscattered electron imaging: inward-penetrating, irregularly curved or inclusion-rich, porous domains, which cut across primary growth zones (Fig 1). According to modern data, these textures are formed in zircon crystals in presence of hydrothermal solutions and fluids by two processes: diffusion-reaction (in zircon with structural damage caused by self-irradiation) and a coupled dissolution-reprecipitation (in zircons with undamaged structure) (**[1]** and reference therein). In the first case, the initial zircon does not dissolve and new zircon matter is not supplied. Solid phase diffusion is facilitated by occurrence of permeable metamict domains in zircon and ion exchange proceeds between zircon and a fluid. Hydrous phases spread inward and catalyze rearrangement of the matter (Fig 1a). Mechanism of dissolution–reprecipitation results in the formation of similar morphological patterns in unaltered zircon with sufficiently high U, Th, and Y contents in solid solutions transformed in the course of alteration into mineral inclusions of uraninite, thorianite, etc. **[1]**. Zircon reacts with aqueous fluid and dissolution–reprecipitation leads to the formation of chemically purer zircon with lower concentration of impurities in comparison with primary zircon. The difference in solubility is the driving force of replacement. Some domains of the primary zircon are retained unchanged, while new mixed and “pure” domains are formed (Fig 1b).

Data of experimental low-temperature modeling of monocrystal replacement are involved to explain the mechanism of secondary textures formation in zircon crystals and to reconstruct the conditions of zircon alteration and re-equilibration. Such analogies are possible, because similar crystallogenetic mechanisms proceed at different temperatures. The morphological similarity of artificial and natural objects gives grounds for discussion and comparison of their formation mechanisms. At the same time, it is necessary to bear in mind the convergence of morphological attributes related to different processes. Poly and monocrystalline classes are distinguished among the products of replacement obtained in experiments with water–salt systems. In all cases, salting out is the driving force of replacement, when dissolution of a crystal of a replaced component results in oversaturation relative to another component and induces its crystallization. Polycrystalline products are formed in systems with singular eutonic points and in the absence of isomorphism between components, whereas monocrystalline products arise in systems of isomorphic components without singular points.

Comparison of the morphology of altered zircons with the experimentally obtained replacement products makes it possible to judge about their formation. In our opinion, the replacement mechanisms within zircon are reduced to the two types of processes mentioned above. The transformation of metamict zircon is characterized by the appearance of polycrystalline products of replacement: dissolution of amorphous domains and precipitation of a new zircon matter in the form of tiny crystals (Fig 1a). The transformation of crystalline zircon is characterized by monocrystalline replacement, by dissolution of the primary zircon and

crystallization of a new zircon matter differing in composition of isomorphic admixtures (Fig 1b). Let us consider in more detail the formation of products similar in morphology to the zircon crystals with specific internal structure. These products have been obtained in modeling systems with isomorphic components $MgSO_4$–$NiSO_4$–H_2O, $CoSO_4$–$FeSO_4$–H_2O, $(NH_4)_2Co(SO_4)_2$–$(NH_4)_2Ni(SO_4)_2$–H_2O, etc. The replacement of $MgSO_4 \cdot 7H_2O$, $CoSO_4 \cdot 7H2O$, $(NH_4)_2Co(SO_4)_2 \cdot 6H_2O$ crystals in the corresponding solutions gives rise to the formation of monocrystalline products of mixed composition $(Mg,Ni)SO_4 \cdot 7H_2O$, $(Co,Fe)SO_4 \cdot 7H_2O$, $(NH_4)_2(Co,Ni)(SO_4)_2 \cdot 6H_2O$. A characteristic example of the structure of replaced object is shown in Fig. 1c. The inner spongy zone and overgrowing monocrystalline zone are seen. The inner zone is a relic of the primary crystal. The newly formed zone not only has the shape of a protocrystal but also retains its structure, i.e., a monocrystalline pseudomorph. Pores arise as a result of the difference between volumes of the phases: the volume of a new phase is smaller than the volume of the primary phase. Inheritance of the structure of the primary mineral is caused by synchronous growth and dissolution. The microsites of the surface in disequilibrium with solution dissolve, whereas oversaturation is achieved in other domains and they grow. The monocrystalline shell that forms around the spongy zone due to saturation is the youngest and indirectly indicates monocrystalline character of replacement. As was established in experiments, the inclusions can be filled with residual solution and syngenetic or postgenetic crystalline phases **[2]**. When the system deviates from equilibrium, e.g., at a temperature gradient, the replacement may develop against the background of growth or dissolution of objects **[3]**. Fluctuations in temperature result

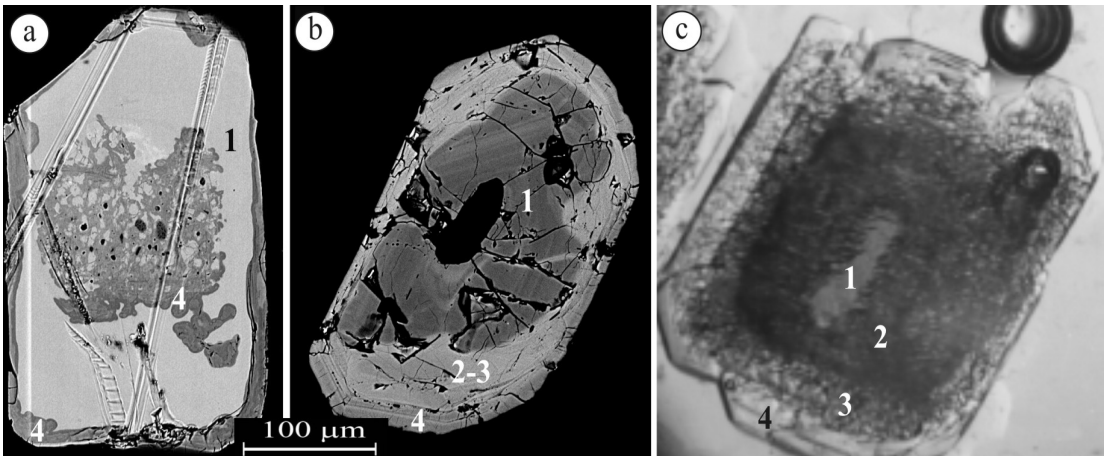

Figure 1. Replacement of metamict zircon (a), nonmetamict zircon (b), of $CoSO_4 \cdot 7H_2O$ crystal (c). Zones: 1- relic of primary crystal, 2- inner replaced zone, 3- outer replaced zone, 4- zone of overgrowth (monocrystalline shell).

in aggregation and enlargement of inclusions and, as a limit, in the disappearance of the spongy zone and formation of a monocrystalline shell (Fig. 4c). Thus, the internal structure of the studied zircon crystals can be explained in terms of isomorphic substitution. Porous spongy zones, several zones with inclusions varying in number and size, tortuous boundaries between zones, and monocrystalline shell around porous core are considered to be morphological features of monocrystalline replacement.

We are grateful to our supervisor and teacher Glikin A.E. The bright memory of him.

References:

[1] Geisler T., Schaltegger U., Tomaschek F. Elements. 2007. No. 3. P. 43-50.
[2] Glikin A.E. Polymineral metasomatic genesis of crystals. St. Petersburg: Neva. 2004. 318 p.
[3] Kryuchkova L.Yu., Glikin A.E., Voloshin A.E., Kovalev S.I. ZRMO. 2002. V. 131. N. 3, P. 62–77.

DISTRIBUTION OF REE IN MINERALS FROM UHP ROCKS FROM KOKCHETAV MASSIF, NORTHERN KAZAKHSTAN

Sitnikova E., Ragozin A.L.

V.S. Sobolev Institute Geology and Mineralogy, SB RAS, Novosibirsk, Russia
ragoz@igm.nsc.ru

The geochemical features of banded UHP metamorphic rock garnet-biotite gneiss with layer of feldspar-pyroxene rock - Fig. 1a from Kumdy-Kol district (Kokchetav Massif, Northern Kazakhstan) have been examined in this study. This rock was collected at underground gallery from diamondiferous region but it does not contain diamond only some graphite. Major composition of minerals was detected by EPMA. REE concentrations in rock-forming garnet, mica, and plagioclase were examined by LA-ICP-MS techniques. Selected grains of minerals (0.1–3 mm) have clear area without inclusions, color zonation or cracks.

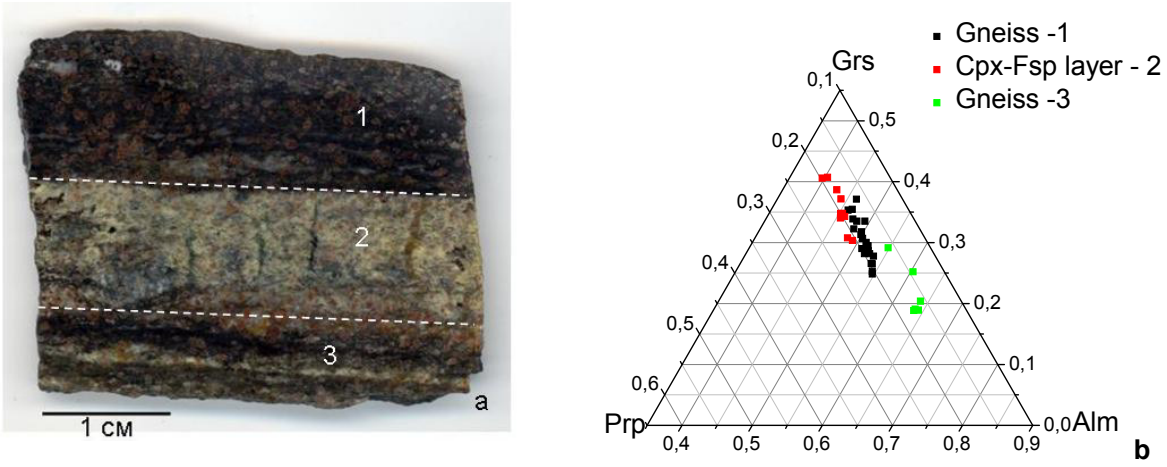

Figure 1. a) Banded garnet-biotite gneiss with layer of feldspar-pyroxene rock. b) Composition of garnets in different layers of rock.

Obtained data indicate that all garnets characterized by $Alm_{0.46-0.64}Grs_{0.37-0.19}Prp_{0.21-0.11}$ components and have a Mn impurity. Mn content in garnets in gneissic layers is varying from 1.7 to 2 wt% (Fig. 1b). In feldspar-pyroxene layer Mn content in garnets are higher and vary from 3.7 to 4.5 wt%. Most garnets have compositional zonation with increasing Alm component from core to rim. Micas in gneiss layers are phengite (Si 3.2-3.4 p.f.u.) and biotite, also it was estimated secondary chlorite. The presence of phengitic mica in gneisses indicates its UHP origin [**1**]. Polycrystalline aggregate of quartz in garnets surrounded by radial cracks are characterized by cloudy extinction that suggest that it was originally coesite. Pyroxene in feldspar-pyroxene rocks is augite-diopside with Mn impurity 0.9–1.6 wt%. The absence of K impurity in pyroxene is the main reason testifying its overlaid nature. Temperature estimates indicate that gneissic layers have been formed at temperature near 680-790°C **[2]** at 4GPa. This calculation for feldspar-pyroxene layer is impossible because garnet and pyroxene were not equilibrated.

REE patterns of garnets from different layers of studied rock have similar character. Distribution of LREE is depleted, from Gd to Yb distribution are almost flat (Fig. 2). La/Yb_N in garnets from all layers varies from 0.001 to 0.054.

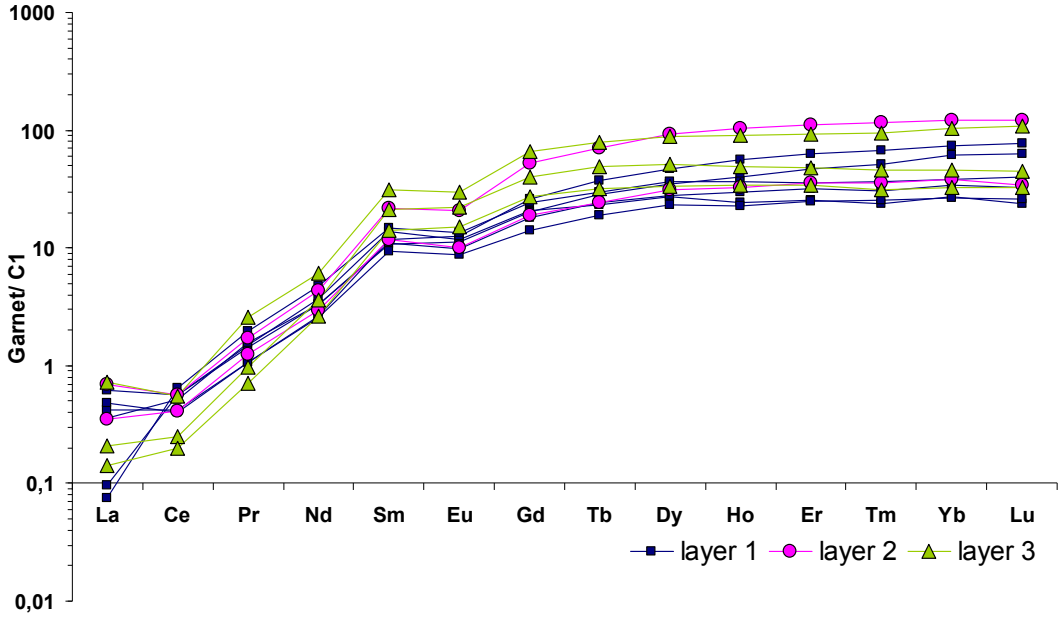

Figure 2. Chondrite normalized distribution of REE in garnets from different layers.

LA-ICP-MS data enabled us to evaluate the characteristics of melts in equilibrium with rock forming garnets. Calculated concentration of REE using the experimental data **[3, 4]** in the melts coexisting with garnets show that concentrations of LREE are 10 times higher than C1 and HREE are at same level **[5].** All garnets of studied rock have minor compositional variations. The REE patterns of garnets are identical in all layers and this is corresponding to their restitic nature. An overlaid nature of pyroxene in feldspar-pyroxene layer may indicate that this rock have finally been formed at P-T conditions lower then peak UHP metamorphism to which the diamond formation period relates [**1**].

We would like to thank Shatsky V.S. for providing samples and comments.

References:

[1] Shatsky V. S., Sobolev N. V., Vavilov M. A. 1995 Diamond- bearing metamorphic rocks of the Kokchetav Massif (Northern Kazakhstan). // In Coleman RG, Wang X (ads) / Ultrahigh pressure metamorphism. Cambridge Univ Press, Cambridge. pp. 427-455.

[2] Dasgupta S., Sengupta P., Guha D., Fukuoka M. 1991 A refined garnet – biotite FE – Mg exchange geotermometer and its application in amphibolites and granulites // Contribution to mineralogy and petrology v. 109, pp. 130-137.

[3] Stalder R., Foley S.F., Brey G.P., Horn I. 1998Mineral-aqueous fluid partitioning of trace elements at 900–1200°C and 3.0–5.7 GPa: new experimental data for garnet, clinopyroxene, and rutile, and implications for mantle metasomatism // Geochimica et Cosmochimica Acta, v.62, pp. 1781-1801

[4] Rubatto D., Hermann J. 2007 Experimental zircon/melt and zircon/garnet trace element partitioning and implications for the geochronology of crustal rocks // Chemical Geology, v. 241, pp. 38-61

[5] McDonough, W. F., and Sun, S.-S. The composition of the Earth // Chemical Geology, 1995, v. 120, pp. 223-253.

AN ULTRAHIGH-TEMPERATURE α-Ca_2SiO_4 POLYMORPH DOPED WITH PHOSPHORUS AND ALKALIS: THE FIRST FINDING IN NATURE

Sokol E.V. [1], ***Seryotkin Yu.V.***[1,2], ***Kokh S.N.***[1]
[1] *VS Sobolev Institute of Geology and Mineralogy SB RAS, Novosibirsk, Russia*
[2]*Novosibirsk State University, Novosibirsk, Russia*
sokol@igm.nsc.ru

Dicalcium orthosilicate (Ca_2SiO_4) has at least five polymorphs. The structures of α'_H, α'_L and β-forms are derived from that of the high-temperature pure α–Ca_2SiO_4 and/or α–Ca_2SiO_4 solid solutions (ss) by progressive decreases in symmetry. The phase transitions α–α'_H and β-γ are reconstructive, while α'_H– α'_L and α'_L–β are displacive [1, 2]. The crystal structure of α-Ca_2SiO_4 at 1545°C has been described with space groups $P6_3/mmc$ [3]. The α'_H-Ca_2SiO_4 (*Pnma*) and α'_L-Ca_2SiO_4 ($P2_1/cn$ or $Pna2_1$) modifications are orthorhombic. Calcio-olivine γ–Ca_2SiO_4 (*Pbnm*) is the only Ca_2SiO_4 modification thermodynamically stable under ambient conditions, but it is extremely rare in nature [4, 5]. There is, however, a naturally occurring mineral of larnite, common to high-temperature – low-pressure contact zones and xenoliths, which is analog of the monoclinic β-Ca_2SiO_4 ($P2_1/n$) modification, metastable under ambient conditions [6]. Both pure α'_H-Ca_2SiO_4 (T=1177-1425°C) and α-Ca_2SiO_4 (T=1425-2150°C) phases are hard to retain at ambient temperature, and they have never been found in nature. α′-Ca_2SiO_4 (ss) has been reported from Marble Canyon skarns, USA [4] and from combustion metamorphic rocks of the Hatrurim Fm., Israel [7, 8]. The α-to-α'_H transition is the first-order transformation realized as nucleation and growth processes. The α'_H-phase occurs as six sets of crossing lamellae related by twining within the parent α-Ca_2SiO_4 (ss) crystal. Both pure and doped α'_H phase, rapidly inverts on cooling to the β-Ca_2SiO_4 phase passing through the α'_L-phase. The $\alpha'_L \leftrightarrow \beta$ inversion is athermal martensitic transformation [1, 9, 10]. High-temperature Ca_2SiO_4 forms are usually stabilized by dopants Ba, Sr, P (± Na, K), Fe, Al, and B, which effectively depress the transition rate of α-Ca_2SiO_4 (ss)→α'_H→α'_L and the transformation temperature of α'_L→β. The temperature intervals which high-temperature Ca_2SiO_4 (ss) modifications can tolerate are much larger than those for pure Ca_2SiO_4 [1, 2]. The α'_H phase existing in equilibrium with α-Ca_2SiO_4 (ss) at 1280°C forms at the maximum rate around 1100°C regardless of its chemical composition [1].

Gross [7] discovered a Ca_2SiO_4 (ss) modification of $Ca_{1.89}Na_{0.03}K_{0.03}(Si_{0.79}P_{0.2})O_4$ with P enrichment (8.27 wt% P_2O_5) in ultrahigh-temperature combustion metamorphic rocks of the Hatrurim basin, Israel, and identified the mineral as nagelschmidtite. It was a host phase for a set of β-Ca_2SiO_4 intersecting lamellae. However, the true $Ca_7(SiO_4)_3(PO_4)_2$ nagelschmidtite contains 19 wt% P_2O_5 , and the phase Gross [7] studied is α–Ca_2SiO_4 (ss) rather than nagelschmidtite.

We have found large (100-250 μm) grains of yellowish and transparent α-Ca_2SiO_4 (ss) with typical intersecting lamellar textures in a garnet-rich paralava sample (YV-402) collected by Dr. Ye. Vapnik in the south of the Hatrurim basin. The rock contains (in wt%) 30.89 SiO_2, 0.83 TiO_2, 11.00 Al_2O_3, 5.77 Fe_2O_3, 0.72 FeO, 0.02 MnO, 1.16 MgO, 41.44 CaO, 0.68 Na_2O, 0.42 K_2O, and 2.45 P_2O_5, 0.94 H_2O, 0.97 CO_2. The mineral assemblage consists of (vol.%) ~ 40 α-Ca_2SiO_4 (ss), ~ 30 gehlenite-rich melilite (ss), 15 rankinite, and 10 Ti-andradite. Minor phases (~ 5 vol.%) are perovskite, $Ca_2Fe_4O_7$, and Cr-spinel. Ti-andradite, melilite, and occasionally rankinite contain tubular inclusions of cloudy α-Ca_2SiO_4 (ss). Two types of symmetry-related domain structures of β-form are set in a α-Ca_2SiO_4 (ss) matrix. The striations intersect at an angle of 60° or 120° in cross-sections perpendicular to the c_α-axis of the host. In other sections, lamellae cross at 23, 15˚ and 27˚. The orientation relationship between the host α-Ca_2SiO_4 (ss) and the β-form lamellae is $\{11\bar{2}0\}_\alpha \parallel \{100\}_\beta$ and $<0001>_\alpha \parallel <010>_\beta$ [11]. Most β-lamellae show {100} twining.

Generally, the sample shows a marked compositional heterogeneity of both α- and β-Ca_2SiO_4 (ss). The calcium content decreases as P, Na, and K increase (Fig.). The cationic vacancies become more numerous as P increases (up to 0.21 apfu) but remain within 5%. Five grains with maximal P contents ($Ca_{1.79}Na_{0.06}K_{0.06}[P_{0.20}Si_{0.80}O_4]$) mainly composed of homogeneous α-Ca_2SiO_4 (ss) have been studied with single-crystal XRD. The examined grains are hexagonal and show superstructures with N=8 along the a-axis while the metrics holds along z: a = 43.4323(17), c = 6.8251(3) Å, V = 11149.8(7) $Å^3$. The selected space group $P6_3$ is not centrosymmetric unlike $P6_3/mmc$ in pure α-Ca_2SiO_4. The symmetry reduction of α-Ca_2SiO_4 (ss) may result from the ordering of SiO_4- and PO_4-tetrahedrons. Earlier the space groups $P6_3/mc$, $P6_2c$ or $P6_3/mcc$ were inferred for high-temperature Ca_2SiO_4 (ss) with 0.175-0.4 apfu P [9]. On cooling α–Ca_2SiO_4 (ss) shows incommensurate phases, hexagonal phases with modulations, and/or superstructures [1, 9]. The incommensurate orthorhombic phases doped with P, Na, Al, Fe, K and Ba commonly show one-dimensional modulation along the a- (N=3; 3.87, 3.96 and 4.09) or c-axis (N=3) of the α–phase cell. The modulation may reflect different ordering degrees of tetrahedral atoms and cation vacancies in the $(Ca_{2-x/2}\square_{x/2})(Si_{1-x}P_x)O_4$ structure. Because temperatures of α'_L–to-β transition are 610˚C for pure Ca_2SiO_4 and 160˚C for Ca_2SiO_4 (ss), the α′–to-β transformation should be completed during cooling [1, 9, 10]. The main course of α–Ca_2SiO_4 (ss) retention in natural rocks seems to be quenching typical of combustion metamorphic events.

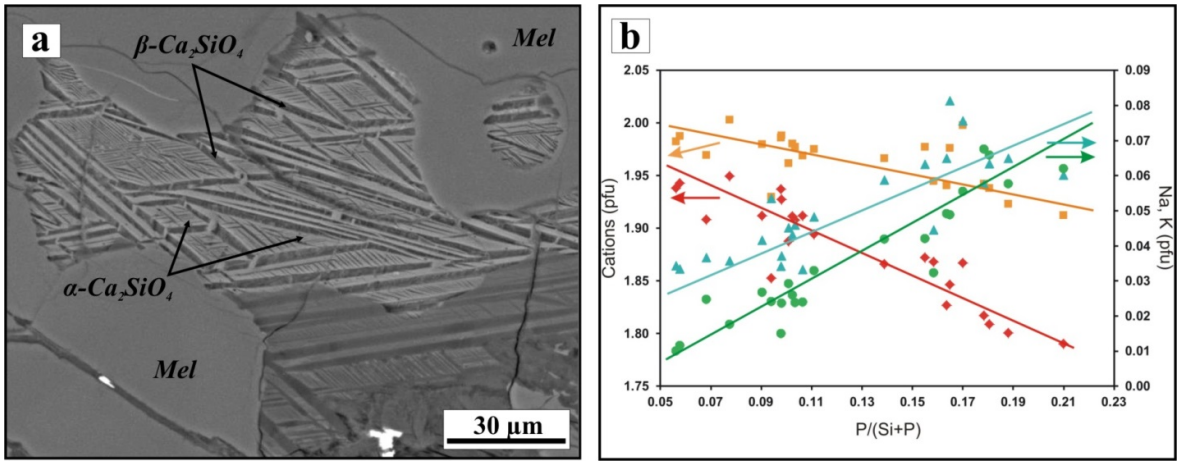

Figure 1. A. Morphological features of the α- and β-Ca_2SiO_4 in paralava. β-Ca_2SiO_4 lamellae in P, Na, K-doped α-Ca_2SiO_4 matrix. BSE image. *Mel* = melilite.
B. Ca, Na, K and Σ (Ca, Na, K) vs. P/(Si+P) contents of doped α-Ca_2SiO_4. (orange square is Ca + Na +K; red diamond is Ca; blue triangular is Na; green circle is K.

The study was supported by grant 12-05-00057 from the Russian Foundation for Basic Research.

References:

[1] Fukuda K., J. Ceram. Soc. Japan, 2001, 109 (3), 43-48. [2] Taylor H.F.W., Cement Chemistry, Tomas Telford Services, London, 1997. [3] Mumme R J et al., Neues Jahrbuch für Mineralogie. Abhandlungen, 1995, 169 (1), 35-68. [4] Bridge T.E. Am. Mineral., 1966, 51, 1766-1774. [5] Gobechiya E.R. et al., Crystallography Reports, 2008, 53(3), 404-408. [6] Grapes R. Pyrometamorphism, Springer, Berlin, 2011. [7] Gross S. The mineralogy of the Hatrurim Formation, Israel, Geol. Surv. Isr. Bull., 1970, 70, 80. [8] Kokh et al., European Mineralogical Conference, 2012, 142. [9] Fukuda K. et al., J. Ceram. Soc. Japan, 1997, 105 (2), 117-121. [10] Fukuda K. et al., Cem. Concr. Res. 1998, 28, 1105-1108. [11] Fukuda K. and Maki I., Cem. Concr. Res. 1989, 19, 913-918.

MINERALOGY AND CRYSTAL CHEMISTRY OF ENDOGENIC CARBONATES FROM CALCITE-DOLOMITE SERIES OF SALINE LAKES SEDIMENTS

Solotchina E.P. [1], ***Sklyarov E.V.*** [2], ***Solotchin P.A.*** [1]

[1] *V.S. Sobolev Institute of Geology and Mineralogy, SB RAS, Novosibirsk, Russia*
[2] *Institute of the Earth's Crust, SB RAS, Irkutsk, Russia*
solot@igm.nsc.ru

We present the results of mineralogical and crystallochemical studies of the endogenic carbonates from bottom sediments of shallow saline lakes at Baikal region. The objects of studying are Holocene evaporite sections of three closed lakes with carbonate type of sedimentation –Verchnee Beloe, Bol'shoe Alginskoe and Kiran. They are located in western Transbaikalia - the region with prevailing of arid and semi-arid climate conditions. The main methods of investigations are: X-ray diffraction analysis (ARL X'TRA, Cu K_α radiation) and IR-spectroscopy; additional methods are scanning electron microscopy, SR XFA, analysis of stable isotopes ($\delta^{18}O$ and $\delta^{13}C$) and others.

The assemblage of endogenic carbonate minerals of the lacustrine sediments consists of Mg-calcites with different Mg contents and excess-Ca dolomites. By the chemical composition and the position of main analytical peaks on X-ray patterns as well as position of absorption bands on IR spectra Mg-calcites and excess-Ca dolomites are situated between $CaCO_3$ and stoichiometric dolomite ($CaMg[CO_3]_2$). Natural low-temperature Mg-calcites are poorly crystallized; the crystallites are smaller than 10 μm. Their detailed study encounters difficulties because of the lack of single crystals of required quality and size.

Carbonate mineralogy was considered on the basis of the position of the most intense reflection (*hk* =104) in the trigonal varieties in the range of angles of 28.5–32.5º (2Θº Cu*K*α) (Fig. 1). The interplanar spacing d_{104} varies from 3.036Å (calcite) to 2.887Å (stoichiometric dolomite) and serves as a measure of the Mg content of these carbonates. For a detailed description of the Mg-calcites, we divided them into three groups: (1) low-Mg calcites (LMC) with $MgCO_3$ < 4–5 mol.% (3.036 Å > d_{104} > 3.02 Å); (2) intermediate-Mg calcites (IMC) with 5–18 mol.% $MgCO_3$ (3.02 Å > d_{104} >2.98 Å); and (3) high-Mg calcites (HMC) with 18–43 mol.% $MgCO_3$ (2.98 Å > d_{104} > 2.90 Å). The excess-Ca dolomites, in which excess of $CaCO_3$ can amount to 7 mol.% as compared with the stoichiometric dolomite, are characterized by d_{104} of 2.90 to 2.887Å. On the high-resolution X-ray patterns of the studied samples, the peaks corresponding to d_{104} of carbonate minerals look like two maxima of varying intensity: (1) LMC and IMC and (2) HMC and excess-Ca dolomites (Fig. 1). The conventional boundary between them is located at 30º 2Θ Cu*K*α (d_{104}=2.98 Å). These broadened diffraction peaks are of intricate shape, and each of them is a superposition of several peaks of carbonate phases with different contents of Mg in the structure. Decomposition of complex XRD-profiles of carbonates into individual peaks by the Pearson function VII provided the whole set of existing carbonate minerals in each sample **[1]**. The model approach allowed us to determine the position of the maximum, integral intensity of the analytical peak of each phase and to obtain their quantitative ratios with a high accuracy. The concentration of $MgCO_3$ in Mg-calcite structure was determined by the calibration plots of dependence between the d_{104} and $MgCO_3$ content (mol.%) **[2].**

At present, Mg-calcites are regarded as mixed crystals varying from true solid solutions (low-Mg calcites) to mixed-layered structures (high-Mg calcites) in the series calcite-dolomite and characterized by different stabilities **[3]**. These structures are sequences of calcite and magnesite layers alternating with different degrees of ordering and forming nanosized domains. Mixed-layer structure of excess-Ca dolomite **[4]** is more similar to the structure of high-Mg calcite than to that of dolomite *sensu stricto*, this mixed crystal is the end-member of the series of anhydrous Ca–Mg carbonates including low-Mg calcite, intermediate-Mg calcite, high-Mg calcite, and excess-Ca dolomite. Moreover, stoichiometric and nonstoichiometric dolomites are,

most likely, of different genesis. Stoichiometric dolomite is extremely rare in Holocene and modern sediments of continental water basins, even when the waters are oversaturated with $CaMg(CO_3)_2$ **[5]**. Our investigations have shown that the excess-Ca dolomites are a permanent component of saline lakes sediments just as Mg-calcites. We have established that the lacustrine Mg-calcites do not form a continuous series from low-Mg to high-Mg varieties: there is a break between Mg-calcites containing <18 mol.% $MgCO_3$ and >30 mol.% $MgCO_3$ (a blank space on the XRD spectra near 2Θ Cu$K\alpha$ = 30º). We suppose that the break in the series of Mg-calcites is probably due to the transition from true solid solutions ($MgCO_3$ < 18 mol.%) to layered "domain" crystals, which are regular in their utmost form.

It is known, that sedimentation of carbonates of the calcite–dolomite series is determined by a number of factors: Mg/Ca ratio, total carbonate alkalinity, salinity, pH value, temperature, and organic productivity of the water **[6]**. These factors are controlled by the lake water balance depending mainly on the regional climate. Based on the studies performed, we obtained a carbonate record carrying the information about the stratigraphic distribution of Mg-calcites and Ca-dolomites in sedimentary sections. Juxtaposing the carbonate record with the data of lithological analysis, determined stable isotopes ($\delta^{18}O$ and $\delta^{13}C$), and distribution of some geochemical indicators of climatic changes, we reconstructed the intricate evolution of lakes, which was controlled by the regional climate **[1].**

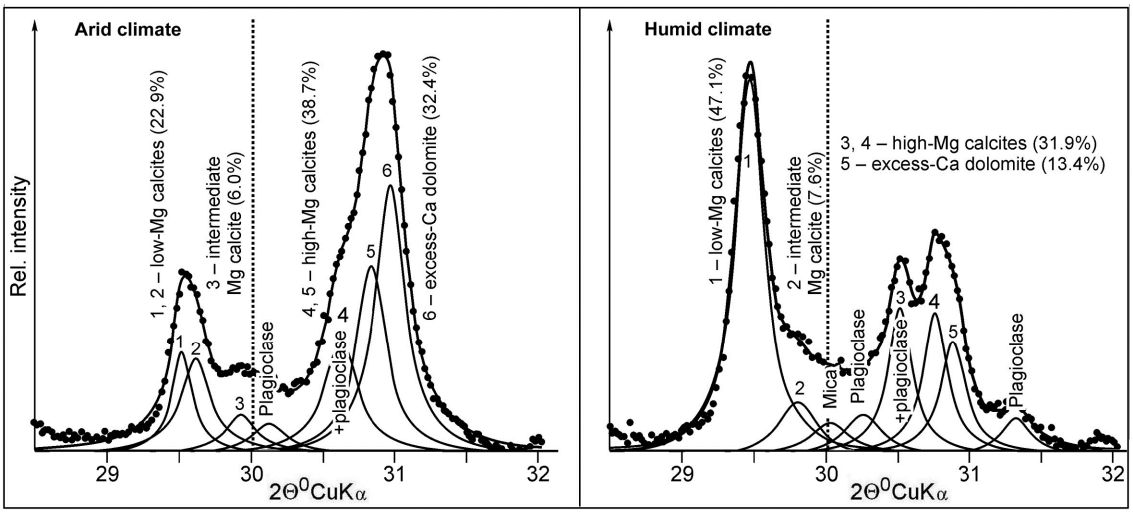

Figure 1. Results of modeling of experimental XRD profiles of carbonates in the range of d_{104} peaks. The total modeled profiles (solid line) are in agreement with the experimental ones (dotted line). The diffraction peaks of individual phases are described by Pearson VII function. The total content of carbonates in the sample is taken equal to 100%.

This study was supported by RFBR, grant No 11-05-00816a and by SB RAS, integration projects No 4-16 and No 52-5.

References:

[1] Solotchina, E.P., Sklyarov, E.V., Solotchin, P.A., et al., 2012. Russ. Geol. Geophys. 53, 1351-1365.

[2] Goldsmith, J.R., Graf, D.L., 1958. Am. Mineral. 43, 84–101.

[3] Deelman, C., 2011. Low-temperature formation of dolomite and magnesite. Open-access e-book, 512, http://www.jcdeelman.demon.nl/dolomite/bookprospectus.html.

[4] Drits, V.A., McCarty, D.K., Sakharov, B., Milliken, K.L., 2005. Canadian Miner. 43, 1255-1290.

[5] Last, W.M., 1990. Earth Sci. Rev. 27, 221–263.

[6] Nechiporenko, G.O., Bondarenko, G.P., 1988. The formation conditions of marine carbonates (on experimental data). Nauka, Moscow. 132. [in Russian].

FORMATION OF MULTIPHASE MINERAL ASSOCIATIONS AND SELECTION OF COMPONENTS BY GROWING CRYSTALS: INTERDEPENDENT PROBLEMS OF CRYSTAL GENESIS STUDIED BY A.E.GLIKIN AND RELATED TO SUPERFICIAL NANOSTRUCTURES

Tauson V.L. [1], ***Lipko S.V.*** [1], ***Arsentev K.Yu.*** [2], ***Smagunov N.V.*** [1]

[1] *Vinogradov Institute of Geochemistry SB RAS, Irkutsk, Russia*
[2] *Limnological Institute SB RAS, Irkutsk, Russia*
vltauson@igc.irk.ru

A number of natural associations of crystalline mineral substances, especially mineral micro-parageneses, cannot exist in terms of the laws of Gibbs thermodynamics because they contradict the Phase Rule. This might be one of the possible reasons to redirecting the physicochemical modeling from concrete processes and reactions, and their equilibrium constants, to the procedure of minimization of the thermodynamic potentials of multisystems. Such approach does not appeal to the condition of equality of chemical potentials of each component in all coexisting phases under the equilibrium and therefore, does not require the Rule fulfillment. However, it gives no possibility to understanding the reasons for its non-compliance as well. The problem becomes not so sharp when the concepts of real crystals and generalized chemical potentials are introduced to consideration **[1]**. Nevertheless, if accounting for the standard treatments, in the majority of cases everyone appeals to the non-equilibrium conditions of the formation of mineral associations.

Consider a mineral paragenesis containing several minerals with a common component (e.g. sulfur in sulfide minerals). Under the gradient of certain intensive parameter (say, temperature), the crystallization of a mineral association proceeds under the regime of supersaturation determined by the solubility of the most soluble phase of a given association. This supersaturation is constant but not equal for each mineral. In the micro-heterogeneous system where the phases have an excess energy due to highly developed surface, the more soluble minerals with smaller crystals would grow slowly, and finally, make room for the less soluble phases. However, this is not the case for a lot of mineral parageneses and unexpectedly, all crystals of such associations have nearly the same size. The crystal sizes of equilibrium forms of coexisting phases in micro- and nano-associations obey definite relations **[2]**.

The problem under investigation is akin to that considered by A.E.Glikin in respect to the regulation mechanism of the component selection by growing mixed crystals. His three fundamental principles are the following **[3]**: (1) various ensembles of particles characterized by certain statistical distribution by composition are deposited at the surface of growing crystal; (2) only “native” ensembles consisting of particles that satisfy special conditions survive; (3) the remaining ensembles being “alien” dissolve and initiate the salting-out of the “native” ones. This idea looks absolutely clear and well-justified. However, the question remains how the system can recognize the “native” and “alien” ensembles? If there is a pure statistical selection, the growth of the crystal face by the attachment of “native” ensembles and its poisoning with “alien” ones seem to be equally probable.

We have studied the crystal surfaces of the pyrite-pyrrhotite-magnetite association obtained in the hydrothermal thermogradient experiments by the methods of atomic force microscopy and scanning electron microscopy combined with energy-dispersive spectrometry. The data obtained allowed to conclude that the distributing function, i.e., the property to recognizing the “native” and “alien” clusters and complexes may be taken over by the nanophases forming as a result of chemical modification of the surface of growing crystal. Under the crystal growth process, the supersaturated hydrothermal solution incoming to the interphase boundary has a higher chemical potential of crystallizing component than it needs for the formation of the stable matrix crystal under given conditions. The supersaturated solution reaches a metastable equilibrium with

superficial nanophase which has a higher chemical potential as compared to the bulk phase attaining the stable equilibrium with the saturated solution under the same conditions **[4]**. The chemical over-potential is realized in the surface nonautonomous phase as an alteration from the matrix phase (the mother phase, after A.I.Rusanov) in structure, stoichiometry, chemical composition or ordering degree. Let us suppose that the incompatible element is present in the growth medium. It might be thermodynamically more preferable for such element to form the superficial nanophase or to be incorporated into the structure of such phase instead of its chemosorption. After the superficial phase attains certain critical size, the diffusive interrelation of its inner layers adjoining to the bulk matrix and supersaturated fluid should be disturbed. These layers lose their local stability supported by the excess chemical potential and transform to the stable bulk phase by the mechanism of solid state transformation.

Therefore, the nanophases occupying the superficial layers of growing crystals may be responsible for the regulation of interrelation between the crystal and the growth medium because of the selective interaction of such phases with elementary growth units - clusters and complexes - and decrease the probability of their "irregular" discharge. Absorbing incompatible elements, these phases act as the filters for impurities poisoning the growth surface. Permanently transforming to the crystal volume by the mechanism of solid state transformation, the nanophases escape such elements onto the imperfect places of their conjugation with matrix where they form separate (autonomous) phases up to several microns in size.

The above bears a direct relation to the "forbidden" mineral parageneses. To take an example, consider the ore bodies represented by pyrite containing gold in chemically bound state in mineral structure or in surface nonautonomous phase. Let it be much more by mass than Au in native form. Thus, the solubility of Au-containing pyrite but not the solubility of Au(0) buffer the Au activity in the coexisting solution (fluid). The phase having a minor mass should be either dissolved and thereafter enters pyrite until its saturation with Au^{+} or covered by sulfide or oxysulfide film capable to achieve the equilibrium with Au-containing pyrite phase. In fact, between two superficial phases – oxysulfide-like on native Au and pyrrhotite-like on pyrite **[5]** – the metastable forced equilibrium could be attained **[6]**. Such phases were really observed both on natural and experimental samples **[5,7]**. The relative stability of such systems is possibly due to the fulfillment of the principle of continuity of phase formation at coexisting mineral surfaces **[8]** which allows such phases to accommodate to one another under the change of physicochemical conditions.

This work was supported by the Russian Foundation for Basic Research under grants Nos. 12-05-00144, 13-05-00308, 12-05-98957_r_Siberia and the Siberian Branch of Russian Academy of Sciences (project ONZ-5.1).

References:

[1] V.L.Tauson & M.G. Abramovich (1988) Physicochemical Transformations of Real Crystals in Mineral Systems. Novosibirsk, Nauka, 272 p.
[2] V.L.Tauson, M.G.Abramovich., V.V Akimov & V.A. Scherbakov (1993). Geochim. Cosmochim. Acta, **57,** N 4, p.815-821
[3] A.E.Glikin (2007). Proc.Russian Mineral. Soc., **136**, N 2, p. 1-6.
[4] E.I.Akhumov (1987). Z. Neorg. Khimii, **32**, N 1, p. 248-250.
[5] V.L.Tauson & S.V.Lipko (2013). In: Pyrite: Synthesis, Characterization and Uses. N.Whitley & P.T.Vinsen, Eds. Nova Sci. Pub., NY, Chapter 1, p. 1-40.
[6] V.L.Tauson & V.V.Akimov (1997) Geochim. Cosmochim. Acta, **61**, N 23, p. 4935-4943.
[7] V.L.Tauson, S.V.Lipko, Yu.V.Shchegolkov (2009) Crystal. Reports, **54**, N 7, p.1219–1227.
[8] V.L.Tauson (2009) Doklady Earth Sci., **425A**, N 3, p. 471-475.

OPTICAL AND GEMOLOGICAL PROPERTIES OF FACETED SYNTHETIC VINSDIAM™ DIAMONDS

Vins V.G. [1], ***Yelisseyev A.P.*** [2], ***Lebedev I.K.*** [1]

[1] *VinsDiam, Ltd., Novosibirsk, Russia,*
[2] *Institute of Geology and Mineralogy, SB RAS, Novosibirsk, Russia*
vgvins@gmail.com

Approximately one hundred synthetic diamonds were studied by optical spectroscopy. The diamonds were grown by *VinsDiam Ltd.* in a high-pressure BARS apparatus using the temperature gradient method. The diamonds ranged from 2 to 5 carats; the size of some samples reached 8 mm. Around 40% of all samples were yellow. These diamonds revealed bands due to donor and paired nitrogen (C and A centers, respectively) in their absorption spectra. The content of C centers (N_C) did not exceed 100 ppm. The samples with $N_C \leq 50$ ppm showed the intensity ratio of two major IR absorption bands, μ_{1130}/μ_{1344}, to be $1 \div 1.2$, which indicated that the samples were of high structural perfection.

The color of the samples was graded by gemologists after the samples had been cut into round brilliants (R57). The cut diamonds varied from 0.9 to 1.1 carats. Depending on the content of C centers, the samples were graded as follows: Fancy Yellow with $4 \leq N_C \leq 8$ ppm; Fancy Intense Yellow with $8 \leq N_C \leq 15$ ppm; and Fancy Vivid Yellow with $15 \leq N_C \leq 25$ ppm. Samples with higher N_C content had an orange tint in their color which turned to brown at even higher N_C concentrations. The color of a sample with $N_C = 90$ ppm was graded Fancy Brown-Yellow.

The yellow color of some samples was changed to pink and red by electron irradiation (3 MeV/10^{18}cm^{-2}) followed by annealing at 900°C for 120 min. The spectra of the color-enhanced samples showed dominating bands at 637 and 575 nm associated with negatively charged and neutral NV centers, respectively. It was determined that the relative intensities of the bands depended on the N_C concentration. The 575 nm band was dominant in the samples with $N_C \leq 5$ ppm. Such samples were pink. The 637 band was dominant in the samples with $N_C \geq 5$ ppm. The color of such samples was red.

Colorless and near-colorless type IIa samples grown in the systems with nitrogen getters were of particular interest. Nitrogen concentration in type IIa diamonds does not exceed 2 ppm. The concentration was impossible to measure in most of our type IIa samples because they showed no absorption in the one-phonon region of the IR spectrum and at long wavelengths; a sharp edge at 225 nm was observed in the UV region. Cut R57 type IIa samples ranged from 1.1 to 1.2 carats. Their color was graded E; the clarity being VVS1. Some samples even withstood the "magnet test". They were inert to a strong Nd-Fe-B magnet, which indicates the absence of metallic inclusions. Luminescence was observed in a broad band upon UV excitation. The band peak and intensity (I) depended both on the nitrogen concentration and the wavelength of the exciting radiation. Thus, at $\lambda_{excitation.} = 250$ nm and $N_C < 1$ppm, the band peak of medium intensity was at 450-460 nm. At $\lambda_{excitation.} = 360$ nm and $N_C \sim 2$ ppm, the band peak of weak intensity was at 480-490 nm. All crystals revealed intensive long phosphorescence upon UV and X-rays excitation at LNT, the spectral distribution of which coincided with that of PL. The phosphorescence duration reduced more than ten times at RT, which could serve as a serious identification criterion of HPHT grown type IIa diamonds.

About 30% of all studied samples were light-to-dark blue type IIb diamonds. The blue color of these samples was attributed to uncompensated boron ions. Their IR absorption spectra revealed bands at 2460, 2802, 2936 cm^{-1}, the most intensive being the one at 2802 cm^{-1}. The continuous absorption which began at 2985 cm^{-1} of the IR region decreased towards the UV region, causing the blue color of the samples. An asymmetric band with a peak at 1290 cm^{-1} was observed in the one-phonon region. The intensity of the band, μ_{1290}, was correlated to the sample color. In particular, the following correlations were determined for round brilliant (R57) samples

from 1.3 to 1.5 carats in size: very light blue - $\mu_{1290} = 0.1 – 0.2$ cm^{-1}, light blue - $\mu_{1290} = 0.2 – 0.5$ cm^{-1}, medium blue - 0.5 – 0.8 cm^{-1}, intense blue – 0.8 – 1.1 cm^{-1}, vivid blue – 1.1 – 1.5 cm^{-1}, deep blue - 1.5 – 2.0 cm^{-1}, dark blue – over 2.0 cm^{-1}.

The study of optical and gemological properties of the diamonds will be continued as larger VinsDiam™ diamonds are produced. Identification criteria will be determined.

Fe-Ca GARNETS OF MAKSYUTOV COMPLEX (SOUTHERN URAL)

Zvorygina A.A. [1], ***Valizer P.M.*** [2], ***Rusin A.I.*** [1]

[1] *Zavaritskii Institute of Geology and Geochemistry, UB RAS, 620075, Ekaterinburg, Russia*
[2] *Lenin Ilmensky State Nature Reserve, UB RAS, Miass, Russia*
Anj1789@rambler.ru

Garnet is the major rock-forming mineral UHP-HP rock associations. The pyrope-almandine with a high content of calcium component and pyrope-grossular are characteristic for eclogite, grospydites and calc-silicate rocks containing diamond and coesite [1–3, 7].

In Maksyutov eclogite glaucofaneschist complex iron-calcium garnets: zoned grossular-almandine (c), pyrope-grossular almandine (r), almandine-grossular (c), pyrope-almandine-grossular (r) and non-homogeneous almandine-grossular (Table 1, Fig. 1) were defined. They are set in the periphery of the body jadeite and diopside-jadeite eclogite spatially aligned with the UHP ultramafic units I and garnet-pyroxene and lavsonit-containing rocks which associated with antigorit-serpentinites mafic-ultramafic unit.

Garnet $Alm_{40–45}Grs_{51–55}$ (c)–$Py_{25–27}Alm_{30–35}Grs_{35–40}$ developed in the chlorite rim of jadeite eclogite bodies. In association with it is present ($Jd_{8–12}$, F = 11%) diopside, (F = 13–17%) clinozoisite and (F = 17%) chlorite. Zonal $Grs_{34–44}Alm_{46-53}$ (c)–$Grs_{22-26}Py_{29-33}Alm_{42-46}$) grossular-almandine–grossular-pyrope-almandine in association with (Jd_{38-48}, Aug_{52-62}, F = 12-17%) omphacite, (F = 1.4% and F = 13–15%) zoisite-clinozoisite, (Si = 3.34–3.37 pfu, Na = 0.02–0.03 pfu, F = 28%) phengite compose the rims of diopside-jadeite eclogite bodies. The grains of garnet contain of K-feldspar, biotite, barite inclusions, omphacite is replaced by diopside and tremolite.

Table 1. Representative microprobe analyzes of Fe-Ca garnets.

№	зерно	SiO_2	TiO_2	Al_2O_3	FeO	MnO	MgO	CaO	Na_2O	K_2O	Σ
1	c	38.4	0.14	21.5	19.2	0.93	1.38	18.4	0.00	0.00	100.0
	i	39.1	0.04	22.2	17.9	0.92	5.26	14.6	0.00	0.00	100.0
	r	39.9	0.07	22.0	16.0	0.64	7.08	14.1	0.00	0.00	100.0
2	c	38.5	0.00	22.1	18.3	1.05	1.36	18.7	0.00	0.00	100.0
	r	39.1	0.00	22.7	18.3	1.30	5.37	13.1	0.00	0.00	100.0
3	c	37.1	0.21	20.6	25.6	2.87	1.79	11.7	0.00	0.00	100.0
	r	38.9	0.00	21.8	21.3	0.12	8.58	9.2	0.00	0.00	100.0
4	i	36.5	0.30	19.6	26.9	0.70	1.71	13.9	0.00	0.00	100.0
	r	38.3	0.08	21.7	24.1	0.23	5.82	9.5	0.00	0.00	100.0
5	c	38.2	0.14	21.8	21.0	1.74	0.88	16.1	0.00	0.00	100.0
	r	38.3	0.23	22.0	20.1	1.13	1.24	16.9	0.00	0.00	100.0
6	c	37.9	0.10	21.0	21.2	0.65	0.61	18.5	0.00	0.00	100.0
	r	38.2	0.16	20.8	18.4	0.62	1.18	20.6	0.00	0.00	100.0
7	c	38.1	0.16	21.0	16.9	2.67	0.57	20.5	0.00	0.00	100.0
	r	38.0	0.12	22.1	14.0	0.58	1.54	23.6	0.00	0.00	100.0

Note. 1–2 – garnet-diopside-clinozoisite-chlorite rock, edging the boudin of jadeite-grossular eclogite, sample m-08, near the village Karayanovo; 3–4 – garnet-omphacite-diopside-zoisite rock, semple 25-1, 25-5, 25-10, near the village Utarbaevo; 5–6 – garnet-diopside-omphacite-klinozoissite rock, sample. 13/12, 1854-12, 23/12, the area of the village Utarbaevo-Karayanovo; 7 – garnet-chlorite-pumpellyite rock. Areas of grain: c – center, i – mean, r – edge.

Almandine-grossular ($Alm_{41–47}Grs_{45–51}$ (c) - $Alm_{37–41}Grs_{53–56}$) with low pyrope (Py_{3-5}) and variations from 1.5 to 8.5 mol. % of spessartine component characteristic for the garnet-clinopyroxene rocks. Clinopyroxene is presented by individual grains of diopside (Jd_{12}, C_2O_3 =

0.1–0.5 wt.%, F = 12–36%), omphacite ($Jd_{40-49}Aug_{54-64}$) or its zoned grains. Clinopyroxene occurs as inclusions in crystals of garnet and in the matrix of the rock. Almandite-grossulyaria with a high content of calcium ($Alm_{35}Grs_{57}$ (c)–$Alm_{29}Grs_{65}$ (r)) developed in association with calcium pumpellyite (F = 54-62%) and magnesia chlorite (F = 25-30%).

It is believed that the Fe-Ca garnets unlike Mg-Ca garnets should crystallize at lower *P-T* parameters. To determine the *P–T* conditions of metamorphism we have used Gt-Cpx thermometer [5], for associations with phengite – program «*PT* H*P*–UH*P* basic rocks" [5] and took into account the experimental data on Ca-garnet (Grs_{60}), lawsonite/zoisite, pumpellyite [4, 6].

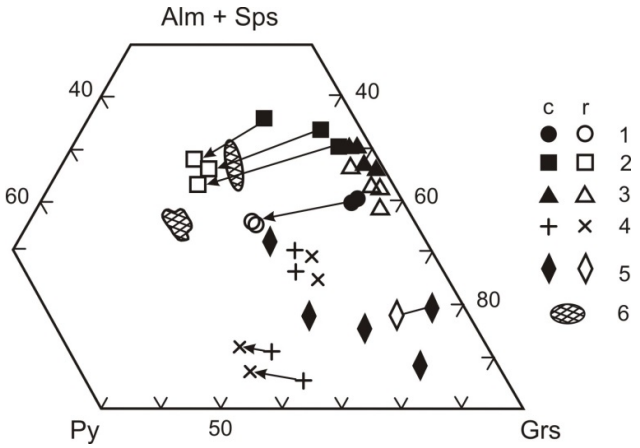

Figure 1. Component composition of Ca-Fe garnet from Maksyutov complex.

1 – from garnet-diopside-chlorite rocks, 2 – from garnet-omphacite-diopside-zoisite rocks, 3 – from garnet-clinopyroxene rocks, 4 – from calc-silicate metamorphic rocks of the Kokchetav massif [3, 7], 5 – from grospydites and kyanite eclogite [1, 2], 6 – from eclogite of Dora Maira and Rongcheng County massives [4].

By Gt-Cpx thermometer at *P* = 25 kbar was calculated temperature: 1. 424–451°C by Alm-Grs_{47-52} (F = 89–91%)–low-ferriginous Di (F = 11-17%) or Omp (Jd = 40, F = 13-15%); 2. 547–577°C by Alm-Grs_{46-54} (F = 92-94%)– ferriginous (F = 35-36%) Di or Omp (Jd_{40}); 3. 647–730°C by $Py_{26-31}Grs_{24-37}$ (F = 59-66%) low-ferriginous (F = 11-16%) Di and Omp (Jd_{40}).

By Gt-Cpx-Ph thermobarometer *P-T* parameters of metamorphism for Alm-Grs + Di + Ph, Alm-Grs + Di-Omp + Ph and Py-Alm-Grs + Omp + Ph agree with 22 kbar–490°C, 29 kbar–650°C and 26-29 kbar–700-730°C, respectively.
U - Pb (SHRIMP - II) dating of zircons with clearly expressed oscillate zoning (824 ± 11, 560 ± 10, 474 ± 7, 444 ± 12 Ma), suggests that the crystallization of jadeite eclogite and diopside-grossular rocks associated with meta-ultrabasites, occurred prior to the opening of the Ural paleoocean.

The study was conducted with the financial support of the Ural Branch of the Russian Academy of Sciences (Project 12-H-5-2035, 12-C-5 1011).

References:

[1] Sobolev, N.V. Paragenetic types of garnets. Moscow, "Nauka", 1964, 218 p.
[2] Sobolev, N.V. Deep inclusions in kimberlites and the problem of the composition of the upper mantle. Novosibirsk, "Nauka", 1974. 264 p.
[3] Shatsky, V.S., Ragozin A.L., Sobolev, N.V. Some aspects of the metamorphic evolution UHP calc-silicate rocks of the Kokchetav massif // Geology and Geophysics, 2006, V. 47 (1), p. 105–118.
[4] Makamura D., Banno S. // Contrib Mineral Petrol, 1997, v. 130, p. 93–102.
[5] Ravna E.J., Paquin J. //EMU Notes in Mineralogy, 2003, v. 5 (8), p. 229–259.
[6] Schmidt M.W., Poli S. Earth Planet. Sci. Lett., 1994, v.124, p. 105 – 118.
[7] Sobolev NV, Shchertl HP, Valley JW et al. Contrib. Mineral. Petrol, 2011, v 162, p. 1079–1092.

SESSION 5

High-pressure mineralogy and crystallogenesis

HIGH-PRESSURE STRUCTURE BEHAVIOR OF LABUNTSOVITE-FE UP TO 23 GPA

Aksenov S.M. [1], ***Bykova E.A.*** [2], ***Rastsvetaeva R.K.*** [1], ***Makarova I.P.*** [1], ***Kurnosov A.***, ***Dubrovinskaia N.*** [2], ***Dubrovinsky L.*** [2]

[1] *Shubnikov Institute of Crystallography RAS, Moscow, Russia*
[2] *Universität Bayreuth, Bayreuth, Germany*
aks.crys@gmail.com

Specific "zeolitic" properties of microporous framework heterosilicates depend on the configuration of the channels. Ion-exchange properties of microporous titanosilicates are of great interest taking into account their capability to accumulate some radioactive species. However, there are no investigations of these materials under high-pressure.

A labuntsovite-group (LG) minerals with generalize formula (Z=1) $A_4B_4C_{4-x}[D_x(H_2O)_{2x}][M_8(O,OH)_8[Si_4O_{12}]_4 \cdot 8H_2O$ (A = Na, Ca; B = K, Na, H_3O; C = K, Ca, Sr, H_3O, H_2O, OH; D = Fe^{2+}, Mn, Zn, Mg; M = Ti, Nb, Fe^{3+}, Fe^{2+} and x = 0 – 2) are characterized by a framework consisting of chains of $(Ti,Nb)O_6$-octahedra with shared trans-vertices. The chains are linked by tetrahedral four-member rings $[Si_4O_{12}]$, forming a three-dimensional framework that contains cavities in the form of channels and cages which are usually occupied by H_2O molecules and extra-framework large alkali and alkali-earth metal cations (Fig. 1). These characteristic features of labuntsovite and related minerals make them similar to zeolite-type minerals. High-pressure structural investigation of these minerals allow a significant insight into the nature of ion-exchange properties of microporous heterosilicates.

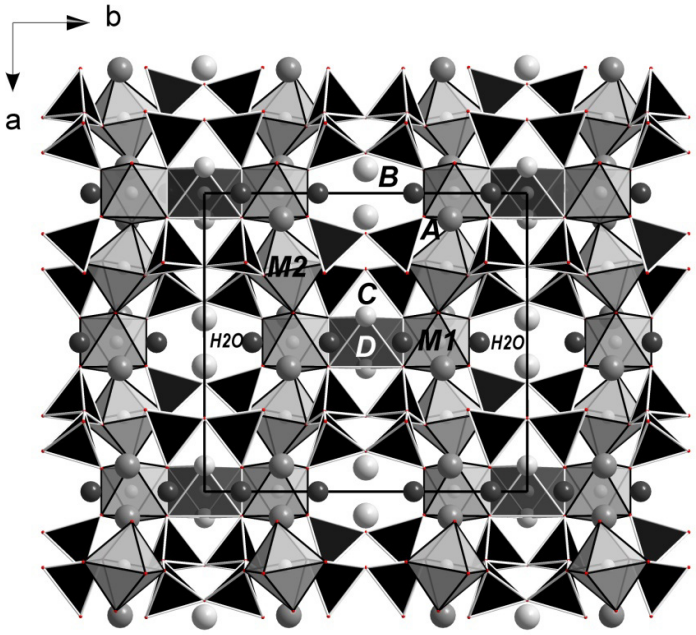

Figure 1. Crystal structure of the labuntsovite-group minerals.

The crystal structure of the natural labuntsovite-Fe with the idealized formula $Na_2K_2Ba_{0.7}Fe_{0.5}Ti_4(Si_4O_{12})_2(OH,O)_4 \cdot 5H_2O$ (space group $C2/m$, Z=2) was refined previously at ambient conditions. The unit cell parameters were found to be a=14.234(2) Å, b=13.7742(7) Å, c=7.7741(8) Å, β=116.787(17)°; R=3.89% for 758 independent reflections with $|F_{obs}| > 3\sigma$.

Now we present the *in-situ* single crystal X-ray diffraction study of the labuntsovite-Fe conducted in a diamond anvil cell. Measurements were carried out at the ID09 beam line at ESRF. Ne was used as a pressure transmitting medium and the pressure was determined by the ruby fluorescence method. The data were collected on compression up to 22.5 GPa with a step of ~ 2.5 GPa. Data treatment was performed with the CrysAlis RED software.

Figure 2a shows the pressure dependence of the unit cell volume of labuntsovite-Fe. The fit of experimental data with the 3rd order Birch-Murnaghan equation of state resulted in the bulk modulus K = 72(2) GPa and K′= 3.7(2) with V_0= 1363(2) Å^3. The linear compressibility is represented in the relative change of the unit cell parameters. It is clearly seen in Figure 2b that the compressibility of the material along the *c* direction is considerably larger than that along *a* and *b* directions.

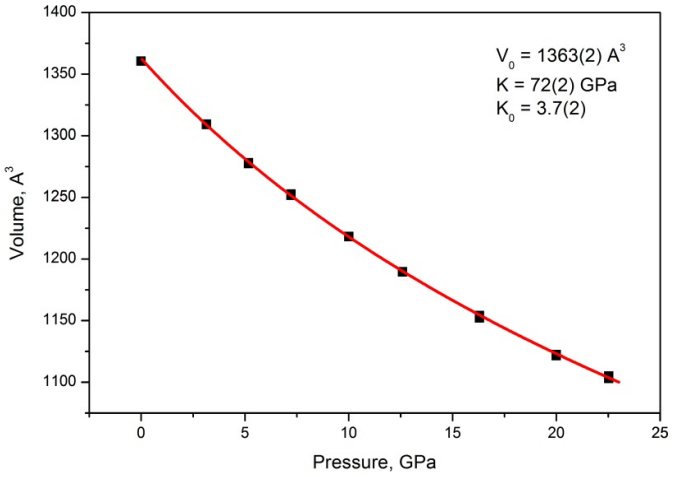

a

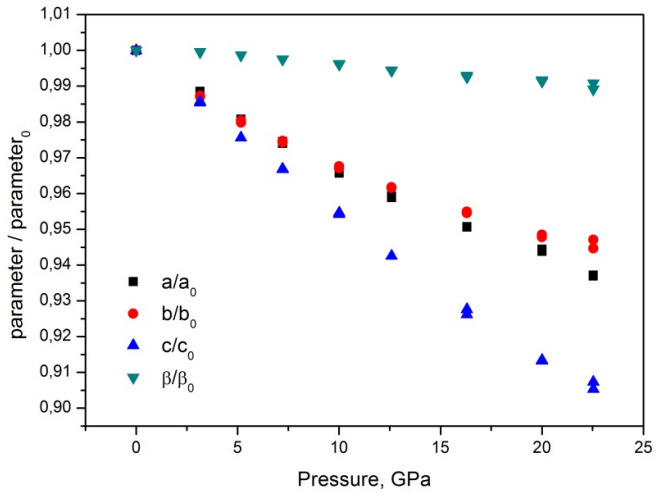

b

Figure 2. The volume and linear compressibility of labuntsovite-Fe. (a) The unit-cell volume as a function of pressure; (b) the relative unit-cell parameters as a function of pressure.

EFFECT OF NaCl ON MELTING PERIDOTITE: EXPERIMENTS AT 6 GPA

Butvina V.G.*, *Safonov O.G.

Institute of Experimental Mineralogy RAS, Chernogolovka, Moscow district, Russia
butvina@iem.ac.ru

At the conditions of diamond and kimberlite melts stability, KCl and NaCl are important constituents of complex carbonate-silicate, carbonatite and carbonate-chloride fluid-melts, whose inclusions are known in diamonds world-wide (e.g. **[1]**). In depths 45 - 75 km, alkali chlorides participate in aqueous-carbonic fluids, that is supported by findings of Cl-bearing apatites, amphiboles and micas, as well as brine inclusions in minerals of spinel peridotites nodules **[2-5]**. Despite these data, experimental data on interaction of the chloride-bearing fluids with peridotites are extremely scarce. In the most cases, conclusions on influence of chlorides on phase relations in upper-mantle assemblages are based on extrapolation of results of experiments at pressures below 2 GPa and in the systems unrelated to peridotite (e.g. **[6]**). Experiments by Chu et al. **[7]** on melting of Mg_2SiO_4+$MgSiO_3$ at presence of the H_2O+KCl fluid at 5 GPa show, that solidus temperature of this assemblage increases with increasing of KCl content in the fluid, that is related to reduction of the H_2O activity with addition of salts **[8]**. These experiments were conducted in model system, which did not contain such important components as Al_2O_3, CaO, Na_2O. Presence of such components can have a significant influence on interaction of peridotites with brine fluids. For example, Al has strong affinity to alkalis destabilizing Al-rich silicate minerals. Previously, we have shown experimentally **[9]** that the H_2O-KCl fluids destabilize the assemblage of orthopyroxene with Al-bearing phases (garnet, spinel, amphibole), but do not affect clinopyroxene and olivine. As a result of these reaction, the clinopyroxene-olivine-phlogopite assemblage forms, whose solidus temperature decreases. Thus, the effect of chemical interaction of chlorides and silicate minerals predominates over the effect of the reduction of the H_2O activity. The effect of NaCl, apparently, is related to stability of pargasite amphibole. However, at pressures above 3 GPa, where amphibole is unstable, the NaCl effect on phase relationships in H_2O-bearing peridotite is less obvious.

In order to study the effect of NaCl on the Al_2O_3, CaO, Na_2O-rich H_2O-bearing peridotite transformation at pressures above 3 GPa, we have conducted the experiments on interaction of model peridotite $Fo_{57}En_{17}Prp_{14}Di_{12}$ with the H_2O-NaCl fluid at 6 GPa and 1050-1450^{O}C. Starting materials were mixtures of oxides, $Mg(OH)_2$ and jadeite (mg): SiO_2 (37.04); Al_2O_3 (3.66); CaO (3.62); $Mg(OH)_2$ (48.30); MgO (4.14), $NaAlSi_2O_6$ (3.24). NaCl added at 8 wt. %, that corresponds to mole fraction of X_{NaCl} = NaCl/(NaCl+H_2O) in the fluid 0.05. The present experiments were performed using Pt capsules of 0.02 mm of the wall thickness.

In absence of NaCl in the fluid, the assemblage Fo+Opx+Cpx+Grt was observed in the solidus of the model peridotite, while melting began at about 1200-1300^{0}C. Clinopyroxene shows the increase of jadeite content with increasing temperature. Addition of NaCl reduces melting temperature down to 1050-1100^{0}C. Amount of orthopyroxene and garnet in solidus decreases, the Al content in orthopyroxene decreases, and the jadeite content of clinopyroxene increases in presence of NaCl. These relationships can be described by the following reactions:

(1) 1/4 Mg-Ts + 7/4 En + 1/2 NaCl + 1/4 H_2O = Fo + 1/2 Jd + 1/2 HCl,
(2) 1/4Prp + 5/4 En + 1/2 NaCl + 1/4 H_2O = Fo + 1/2 Jd + 1/2 HCl
(3) 1/4 Grs + 11/4 En + 1/2 NaCl + 1/4 H_2O = Fo + 3/4 Di +1/2 Jd + 1/2 HCl

(where Mg-Ts – Mg- Tschemack molecule, $MgAl_2SiO_6$ in orthopyroxene, En – enstatite, Fo – forsterite, Prp – pyrope, Grs – grossular, Di – diopside, Jd – jadeite). These reactions show the destabilization of Grt-Opx association in the presence of the H_2O-NaCl fluid.

Thus, an addition NaCl in the H_2O-peridotite system does not influence on phase assemblages. However, changing of mineral compositions, mostly increase of the jadeite content in clinopyroxene, results in the decrease of melting temperature. Present experiments further

support our conclusion **[9]** that the effect of interaction of alkali chlorides with silicates in complex peridotite assemblages overpowers the effect of the reduced H_2O activity in the brine fluid **[7]**.

Support: MD – 222.2012.5, RFBR 13-05-00353, 12-05-31017_mol_a.

References:

[1] *Weiss Y., Kessel R., Griffin W.L., Kiflawi I., Klein-BenDavid O., Bell D.R., Harris J.W., Navon O.* A new model for evolution of diamond-forming fluids: evidence from microinclusion-bearing diamonds from Kankan, Guinea // Lithos. 2009. V. 112. P. 660-674.

[2] *Andersen T., O'Reilly S.Y., Griffin W.L.* The trapped fluid phase in upper mantle xenoliths from Victoria, Australia: implications for mantle metasomatism // Contribution to Mineralogy and Petrology. 1984. V. 88. P. 72-85.

[3] *Ionov D.A., Bushlyakov I.N., Kovalenko V.I.* Minerals-halogen concentrators in the upper mantle: F and Cl contents in mantle phlogopites, amphibole and apatite from the Shavaryn-Tsaram volcano, Mongolia //"Deep-seated xenolithes and lithosphere structure". Moscow. Science. 1987. P. 117-127.

[4] *Agrinier P., Mével C., Bosch D., Javoy M.* Metasomatic hydrous fluids in amphibole peridotites from Zabargad Island (Red Sea) // Earth Planetary Science Letters. 1993. V.120. P. 187–205.

[5] *Frezzotti M.-L., Ferrando S., Peccerillo A., Petrelli M., Tecce F., Perucchi A.* Chlorine-rich metasomatic H_2O–CO_2 fluids in amphibole-bearing peridotites from Injibara (Lake Tana region, Ethiopian plateau): Nature and evolution of volatiles in the mantle of a region of continental flood basalts // Geochimica et Cosmochimica Acta. 2010. V. 74. P. 3023-3039.

[6] *Stalder R., Kronz A., Simon K.* Hydrogen incorporation in enstatite in the system MgO–SiO_2–H_2O–NaCl // Contribution to Mineralogy and Petrology. 2008. V. 156. P. 653-659.

[7] *Chu L., Enggist A., Luth R.W.* Effect of KCl on melting of Mg_2SiO_4-$MgSiO_3$-H_2O system at 5 GPa // Contribution to Mineralogy and Petrology. 2011. V. 162. P. 565-571.

[8] *Aranovich L.Y., Newton R.C.* H_2O activity in concentrated KCl and KCl-NaCl solutions at high temperatures and pressures measured by the brucite-periclase equilibrium // Contribution to Mineralogy and Petrology. 1997. V. 127. P. 261-271.

[9] *Safonov O.G, Butvina V.G.* (2013) Interaction of the model peridotite with the fluid H_2O-KCl: experiment at pressure 1.9 GPa and its application to the upper mantle metasomatism. Petrology (in press).

NOVEL HIGH-PRESSURE PHASES OF $TiPO_4$

Bykov M. [1], ***van Smaalen S.*** [1], ***Bykova E.*** [1,2], ***Dubrovinsky L.*** [2], ***Liermann H.-P.*** [3]
[1] *Laboratory of Crystallography, University of Bayreuth, Bayreuth, Germany*
[2] *Bayerisches Geoinstitut, University of Bayreuth, Bayreuth, Germany*
[3] *Photon Sciences, FS-PE, DESY, Hamburg, Germany*
maxim.bykov@uni-bayreuth.de

$TiPO_4$ belongs to the $CrVO_4$ type materials, which crystal structure and physicochemical properties have been intensively studied over the last years. The building blocks of the structure are TiO_6 octahedra sharing their edges, thus forming TiO_4 ribbon chains. These ribbons are interconnected by sharing corners with PO_4 tetrahedra (Fig. 1). Being quasi-one-dimensional compound $TiPO_4$ exhibits interesting magnetic properties, and undergoes a phase transition upon cooling towards a dimerized spin-Peierls (SP) state **[1]**.

Recent high-pressure investigations of another Ti-containing SP compound TiOCl suggested the possibility of pressure-induced SP dimerization in the vicinity of 15 GPa. However, our studies of isostructural *M*OCl (*M* = Cr, Fe) showed that structural phase transitions take place in the same pressure region, and are unrelated to the transition metal atom. Thus, the phase diagram of TiOCl is complicated due to the nontrivial coupling of several mechanisms. In case of $TiPO_4$ we were motivated to detect a pure SP phase transition separated from structural phase transitions on the pressure scale.

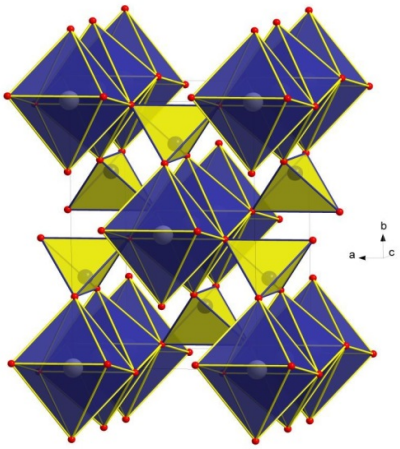

Figure 1. Crystal structure of $TiPO_4$ at ambient conditions.

In addition to the magnetic properties, phosphates crystallizing in the $CrVO_4$-type structure are interesting because their structure is intermediate between quartz-like structures with only fourfold coordinated cations, and structures containing only sixfold coordinated cations. Crystal chemistry arguments predict that, under compression, these phosphates will undergo phase transitions to crystal structures where sixfold coordinated phosphorus can be achieved **[2, 3]**. Therefore, the high-pressure studies of $CrVO_4$ family are attractive from the structural systematics point of view.

High-pressure single-crystal X-ray diffraction study of $TiPO_4$ was performed at beamline P02.2 (DESY, Hamburg). A high-quality single crystal was placed into a BX90 diamond anvil cell along with ruby spheres for pressure determination and loaded with Ne as a pressure-transmitting medium. We have detected the phase transition towards a dimerized phase already at 7 GPa. This phase is analogous to the SP phase at low temperatures, and it is stable up to 45 GPa, whereupon it transforms to denser high-pressure phases, which were not predicted for $CrVO_4$ structures. It appeared to be that $TiPO_4$ is a peculiar member of $CrVO_4$ family, where the interplay between magnetic and structural effects leads to novel high-pressure phases, and its behavior gives rise to the high-pressure systematics of SP compounds.

In this contribution we will present the detailed discussion of the sequence of the phase transitions, similarities and differences of phase diagrams of TiOCl and $TiPO_4$ and discrepancies between predicted and observed phases. The treatment of incomplete high-pressure data for the analysis of high-pressure superstructures with the use of the superspace formalism will be discussed.

[1] J.M. Law *et al.,* Phys. Rev. B **83**, 180414(R) (2011).
[2] S. López-Moreno and D. Errandonea, Phys. Rev. B **86**, 104112 (2012).
[3] J. Pellicer-Porres *et al*. Nature Materials **6**, 698 (2007).

NOVEL HIGH-PRESSURE Fe_2O_3 POLYMORPH

Bykova E. [1,2], ***Bykov M.*** [2], ***Prakapenka V.*** [3], ***Konôpková Z.*** [4], ***Liermann H.-P.*** [4], ***Dubrovinskaia N.*** [2], ***Dubrovinsky L.*** [1]

[1] *Bavarian Research Institute of Experimental Chemistry and Geophysics, University of Bayreuth, Bayreuth, Germany*
[2] *Laboratory of Crystallography / Material Physics and Technology, Department of Physics, University of Bayreuth, Bayreuth, Germany*
[3] *GSECARS, ID-13D, APS, Argonne, USA*
[4] *P02.2 ECB, Petra III, Hamburg, Germany*
knilav@gmail.com

High pressure behavior of iron sesquioxide, Fe_2O_3, has been a long-standing subject of research due to its high importance in understanding Earth interiors. Moreover the compound is interesting from a physical point of view since at the pressures from 40 to 60 GPa it undergoes series of transformations with a diverse origin: structural transformation to an orthorhombic phase with large volume discontinuity (~10%) **[1]**; drop in the resistivity **[2]**; spin crossover of Fe^{3+} **[3]**; and disappearance of the ordered magnetic state **[2]**. The enigmatic crystal structure of the "orthorhombic phase" being able to shed light on the physics of the observed pressure-induced phenomena remained controversial for a long time. Perovskite and Rh_2O_3-II structural types have been proposed as candidates and both were based on Mössbauer data supplemented with powder X-ray diffraction (XRD) **[2,4]**. Recent single crystal XRD studies unambiguously established that compression to 40 GPa and laser heating to 2300 K yields in formation Rh_2O_3-II structural type phase, however the volume discontinuity was shown to be rather small (1.5 %) **[5]**. The crystal structure of the phase(s) observed on compression at ambient temperature above 50 GPa is still under the question since only powder XRD data were available so far, while Mössbauer and Raman spectroscopies studies cannot provide definitive structural information.

A reconstructive phase transition was reported to occur during a laser heating of Fe_2O_3 compressed at or above 70 GPa **[6–8]**. Powder diffraction pattern was indexed with $CaIrO_3$ type structure, however no crystallographic data were provided so far. It is noteworthy that $CaIrO_3$ structural type is possessed by high pressure modification of $(Mg,Al)(Si,Fe)O_3$ perovskite known as a post-perovskite while the transition perovskite – post-perovskite is responsible for an abrupt increase of density in D'' layer, the lowest part of the mantle **[9]**.

An uncertainty in the crystal structure of Fe_2O_3 at 40—60 GPa pressure region and absence of crystallographic data for post-perovskite Fe_2O_3 phase encouraged us to perform a series of high-pressure and high-temperature XRD experiments on single crystals, since the powder XRD data have limitations both in accurate unit cell determination and in a structure solution and refinement. High-quality single crystals of Fe_2O_3 were placed inside diamond anvil cells, compressed up to 71 GPa, heated with the laser afterward and finally decompressed while single crystal XRD was measured concurrently.

We report finding of a novel high-pressure polymorph of Fe_2O_3 by means of the in situ high pressure single crystal XRD. The transition occurs under compression of the hematite to ~54 GPa yielding in the about 10 % of volume reduction. The phase crystallizes in a double perovskite structural type (space group $P2_1/n$, a= 4.588(3), b = 4.945(2), c = 6.679(7) Å and β = 91.31(9)°) related by a distortion with the perovskite structure. No phase transition to the orthorhombic Rh_2O_3-II has been observed upon compression at ambient temperature up to at least 71 GPa. Laser heating to ~2100±100 K at pressures above 70 GPa promotes a transition to *Cmcm* $CaIrO_3$-type phase. Decompression experiments show that the *Cmcm* phase transforms back to the hematite between ~25 and 15 GPa.

References:

[1] J. S. Olsen, C. S. G. Cousins, L. Gerward, et al. (1991) *Phys. Scripta*, **43**, 327.
[2] M. P. Pasternak, G. K. Rozenberg, G. Y. Machavariani, et al. (1999) *Phys. Rev. Lett.*, **82**, 4663.
[3] J. Badro, G. Fiquet, V. Struzhkin, et al. (2002) *Phys. Rev. Lett.*, **89**, 205504.
[4] G. Rozenberg, L. Dubrovinsky, M. P. Pasternak, et al. (2002) *Phys. Rev. B*, **65**, 064112.
[5] L. Dubrovinsky, T. Boffa-Ballaran, K. Glazyrin, et al. (2010) *High Press. Res.*, **30**, 620.
[6] S. Ono, T. Kikegawa, and Y. Ohishi (2004) *J. Phys. Chem. Solids*, **65**, 1527.
[7] S. Ono and Y. Ohishi (2005) *J. Phys. Chem. Solids*, **66**, 1714.
[8] S.-H. Shim, A. Bengtson, D. Morgan, et al. (2010) *PNAS*, **106**, 5508.
[9] M. Murakami, K. Hirose, K. Kawamura, et al. (2004) *Science*, **304**, 855.

ON THE INTERACTION OF PYROPE GARNET AND KIMBERLITE MELT AT HIGH P-T PARAMETERS (THE EXPERIMENTAL STUDY)

Chepurov A.A.

V.S. Sobolev Institute of Geology and Mineralogy SB RAS, Novosibirsk, Russia
achepurov@igm.nsc.ru

The pyrope garnet is a mantle mineral that encloses information about the composition of the Earth's depths and also of the interaction with transporting material. Study of the conservation conditions of pyrope garnets during their transportation to the surface is an interesting and important problem. The current work describes the experimental study of stability of the pyrope garnets in the kimberlite melt at high P-T parameters.

The experiments have been carried out using a multiple-anvil high pressure apparatus of the "split-sphere" type (BARS) at pressure 4 GPa and temperatures interval 1200-1400 ^{o}C. The duration of experiments was from 1 to 22 hours. In details, the experimental procedure used is described in the work **[1]**. For this study the samples of kimberlite from the Yakutian deposits (the Nurbinskaya and Udachnaya pipes) were selected. The composition of the both kimberlites are following: SiO_2 – 32.08 and 25.26; TiO_2 – 0.47 and 1.82; Al_2O_3 – 3.71 and 2.97; Cr_2O_3 – 0.00 and 0.00; FeO+Fe_2O_3 – 6.91 and 11.47; MnO – 0.14 and 0.17; MgO – 31.05 and 28.75; CaO – 7.63 and 13.95; Na_2O – 0.47 and 2.43; K_2O – 1.74 and 1.21; P_2O_5 – 0.31 and 0.54; loss – 16.18 and 11.77; total – 100.68 and 100.34, respectively. The samples of pyrope garnet grains with the size of 0.5-3 mm were extracted from the xenolith of garnet peridotite from the Udachnaya pipe.

After the experiments the pyrope grains were extracted from the samples. On the outer surface of the grains the reaction zone with the width of about 50 μm has been detected. It was determined that this zone consists mostly of garnet, which composition is enriched with CaO (up to 17 wt. %). It was analyzed that the CaO content in the initial pyrope grains have increased after the experiments. The mass of kimberlite after the experiments has consisted mostly of olivine with garnet, spinel, perovskite, rutile and carbonate. The composition of the newly formed garnet from the mass is characterized with a high CaO content (22-24 wt. %).

The current study has demonstrated that in the model system that corresponds to natural kimberlite (by the quantity ratio of the main petrogenic components) at P-T parameters of the experiments the crystallization of pyrope-grossular garnet with CaO content up to 24 wt. % occurs. It is known, that such a high content of the grossular component is typical for the rarely find in nature garnets of the vehrlite paragenesis **[2]**. It was also shown, that during the interaction between the natural pyrope and the newly formed calcium rich garnet the tendency of smoothing between their compositions is taken place. As a result, in the garnet from the reaction zone the content of CaO decreases to 17 wt. %.

The author thanks N.S. Tychkov for the samples of pyrope garnets provided for this study. The work has been performed according to the scientific program of the laboratory № 449 of the IGM SB RAS.

References:

[1] Zhimulev E.I., Chepurov A.I., Sinyakova E.F., Sonin V.M., Chepurov A.A. and Pokhilenko N.P. Geochemistry International, 2012, V. 50, № 3, P. 205-216.

[2] Sobolev N.V. Deep-seated inclusions in kimberlites and the problem of the composition of the upper mantle // Novosibirsk, Nauka, 1974, 264p.

REVISED AND UPDATED EQUATION OF STATE OF hcp-Fe

Dorogokupets P.I. [1], ***Sokolova T.S.*** [1], ***Litasov K.D.*** [2,3]
[1] *Institute of the Earth's Crust, SB RAS, Irkutsk, Russia*
[2] *V.S. Sobolev Institute of Geology and Mineralogy SB RAS, Novosibirsk, Russia*
[3] *Novosibirsk State University, Novosibirsk, Russia*
e-mail: dor@crust.irk.ru

The equation of state of hcp-Fe **[1]** was calculated with consideration of the ruby scale and the room-temperature isotherm of tungsten **[2]**, shock wave data **[3]** and *ab initio* modeling **[4]**. Recent PVT measurements **[5,6]** can be used to obtain a new equation of state of hcp-Fe using a pressure scales from **[7]** and the equation of state of B2-KCl based on measurements of **[8]**. The equation of state of B2-KCl obtained on base of the Vinet-Einstein model **[9]** and yielded following parameters: V_0 = 2.282 cm^3/mol **[8]** (62.36 Å^3), K_{T0} = 172 GPa **[8]**, K' = 5.92, Θ_{Eo} = 160 K, γ_0 = 1.268, β = 0.742, γ_∞ = 0, a_0 = 61.2 × 10^{-6} K^{-1}, m = –0.261. Table 1 present calculated PVT properties of B2-KCl.

Table 1. PVT properties of B2-KCl.

$x=V/V_0$	Temperature (K)				
	298.15	1000	2000	3000	4000
1	0.000	1.332	3.220	5.086	6.927
0.8	7.285	8.686	10.675	12.635	14.563
0.6	36.063	37.554	39.676	41.757	43.793
0.4	174.493	176.108	178.420	180.665	182.835

The equation of state of hcp-Fe is evaluated using the formalism from **[7]**. Room-temperature parameters are V_0 = 6.763 cm^3/mol (11.23 Å^3), K_0 = 160 GPa, K' = 5.55 (Vinet EoS). The volume dependence of characteristic temperatures is determined from $\Theta = \Theta_0 x^{1/6-\delta} K_0^{-1/2}\left(K_T - 2tP/3\right)^{1/2}$, where δ = 0.991, t = 2.661. The volume dependence of the Grüneisen parameters is obtained from: $\gamma = \frac{K'/2 - 1/6 - t/3\left(1 - P/3K_T\right)}{1 - 2tP/3K_T} + \delta$. The pressure ($P$), isothermal modulus ($K_T$) and K' depend on the volume on room-temperature isotherm in these equations. The rest of the fitting parameters are as follows: Θ_{10} = 346 K, Θ_{20} = 237 K, e_0 = 20E–6 K^{-1}, g = 0.166. The volume dependence of the Grüneisen parameter can be approximated by the Altshuler equation: $\gamma = 2.712*(2.712–1.651)*x^{1.467}$. Tables 2 and 3 present thermodynamic properties at different T and P, and pressure depending on T and x for hcp-Fe. Fig. 1 presents the differences between observed and calculated pressures for hcp-Fe.

Table 2. Thermodynamic properties of hcp-Fe.

P	T	$x=V/V_0$	αE-6	S	C_P	C_V	K_T	K_S	γ_{th}	ΔG
GPa	K		K^{-1}		J mol^{-1} K^{-1}		GPa			kJ mol^{-1}
0	298.15	1.00000	57.67	27.10	24.22	23.15	160.00	167.42	2.696	0.000
0	500	1.01251	64.84	40.28	26.67	24.52	149.49	162.61	2.707	-6.893
0	1800	1.13770	132.41	80.83	43.45	25.83	72.56	122.05	2.862	-89.118
0	298.15	0.74906	13.78	11.89	18.19	18.02	602.97	608.75	2.335	569.595
100	298	0.75146	17.23	22.61	22.79	22.34	594.84	606.79	2.332	566.060
100	1800	0.77082	20.82	55.31	27.81	25.59	543.76	590.76	2.306	511.624
100	3000	0.79116	22.62	70.12	30.40	26.32	496.86	573.91	2.285	435.746
100	4000	0.80993	24.31	79.18	32.76	26.84	457.61	558.63	2.270	360.938
200	298.15	0.65864	7.22	7.16	14.23	14.16	975.60	980.25	2.214	1042.518
200	298	0.65985	10.41	16.29	20.56	20.33	967.77	978.92	2.213	1040.127
200	1800	0.67063	13.29	47.35	26.71	25.39	918.69	966.62	2.181	995.328
200	3000	0.68171	13.99	61.45	28.58	26.21	874.34	953.35	2.152	929.428
200	4000	0.69150	14.54	69.87	30.06	26.75	837.55	941.26	2.129	863.603

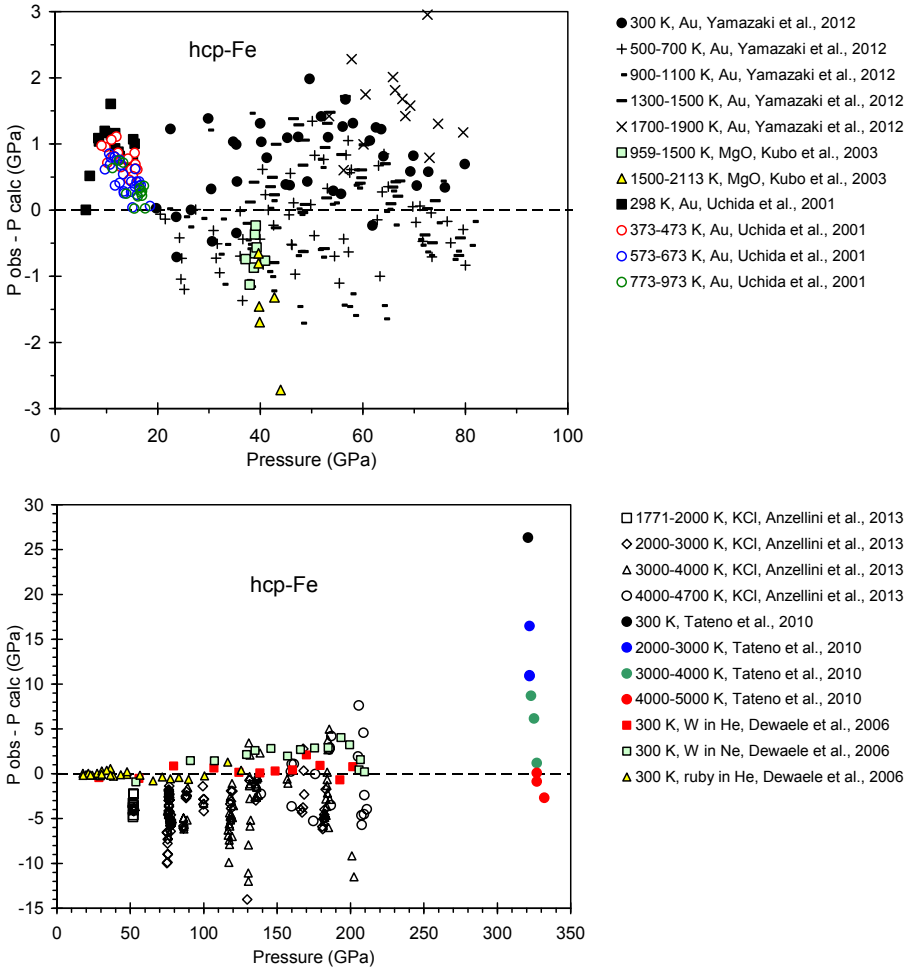

Figure 1. Differences between observed and calculated pressure for hcp-Fe.

Table 3. PVT properties of hcp-Fe.

$x=V/V_0$	Temperature (K)					
	298.15	1000	2000	3000	4000	5000
1	0.000	6.858	16.844	26.866	36.907	46.962
0.9	22.490	29.555	39.996	50.495	61.018	71.559
0.8	65.122	72.401	83.452	94.602	105.788	116.998
0.7	146.676	154.083	165.909	177.920	189.991	202.096
0.6	307.551	314.809	327.562	340.694	353.938	367.238

This work was supported by IP SB RAS No 97, RFBR (No 12-05-00758) and Ministry of Education and Science RF No MD-500.2013.5.

[1] Dewaele A., Loubeyre P., Occelli F., et al., 2006. Phys. Rev. Letters, 97: 215504.
[2] Dorogokupets P.I., Oganov A.R., 2007. Phys. Rev. B, 75: 024115.
[3] Brown J. M., Fritz J. N., Hixson R. S., 2000. J. Appl. Phys., 88: 5496.
[4] Alfe D., Price G. D., Gillan M. J., 2001. Phys. Rev. B, 64: 045123.
[5] Yamazaki D., Ito E., Yoshino T., et al., 2012. Geophys. Res. Lett., 39: L20308.
[6] Anzellini S., Dewaele A., Mezouar M., et a., 2013. Science, 340: 464–466.
[7] Sokolova T.S., Dorogokupets P.I., Litasov K.D., 2013. Russ. Geol. Geoph., 54: 181–199.
[8] Dewaele A., Belonoshko A.B., Garbarino G., et al., 2012. Phys. Rev. B, 85: 214105.
[9] Dorogokupets P.I., 2010. Phys. Chem. Miner., 37: 677–684.

SYNTHESIS OF Na-BEARING MAJORITIC GARNETS IN ALUMOSILICATE MELTS AT 7.0 AND 8.5 GPa

Dymshits A.M. [1,2], ***Bobrov A.V.***[3], ***Litvin Yu.A.***[4]

[1] *V.S. Sobolev Institute of Geology and Mineralogy SB RAS, Novosibirsk, Russia*
[2] *Novosibirsk State University, Novosibirsk, Russia*
[3] *Moscow State University, Moscow, Russia*
[4] *Institute of Experimental Mineralogy, RAS, Chernogolovka, Russia*
a.dymshits@gmail.com

In this study we obtained the first results on the synthesis of Na-bearing majoritic garnets in the model system **pyrope–grossular–$Na_2MgSi_5O_{12}$** (*Prp*-*Grs*-Na-*maj*) more precisely reflects the composition of garnet from natural eclogite. Phase relations were investigated at 7 GPa by analysis of three binary sections: pyrope−$Na_2MgSi_5O_{12}$ **[1]** pyrope−grossular and grossular–$Na_2MgSi_5O_{12}$ (Fig. 1).

Prp-Grs system. Significant solubility between the components was established in the pyrope–grossular system in comparison to the same compositions at 3 GPa **[2]**. Immiscibility gap is set in a range of compositions from 50 to 65 mol. % *Prp*. Liquidus garnet together with clinopyroxene in the system was obtained at temperature about1600°C due to the reaction:

$Mg_3Al_2Si_3O_{12}$(*Prp*) + $Ca_3Al_2Si_3O_{12}$(*Grs*) = $CaMgSi_2O_6$(*Di*) + $2CaAl_2SiO_6$(Ca-*Ts*) + $Mg_2Si_2O_6$(*En*).

The formation of clinopyroxene solid solutions are associated with increased Al solubility in diopside (Ca-Ts molecule) with temperature. Lowering the temperature in the system leads to a narrowing of the *Cpx* + *L* field and expanding the fields of garnets.

Grs-Na-maj system. Orthopyroxene is the liquidus mineral within the compositional range of >50 mol % Na-*maj*. The increase of $Na_2MgSi_5O_{12}$ content up to 70 mol % results in the appearance of the association *Opx* + *Cs* + *L*. *Opx* in experiments has an enstatitic composition with low (up to 10 mol %) content of jadeitic component. The *prp*-Na-*maj* solid solutions demonstrate a wider stability field of liquidus majoritic garnets, whereas mixing of *Grs* with Na-*maj* results in significant spreading of an enstatitic pyroxene field. We selected the section $Prp_{30}Grs_{20}$Na-maj_{50} to check and confirm the location of cotectic lines. Na-majoritic pyrope and grossular garnets form liquidus fields that border the liquidus fields of *Opx* and separated by the liquidus field of *Cpx*. *Opx* have essentially enstatitic composition and *Cpx* are mostly jadeitic. All garnets obtained in experiments are characterized by high concentration of Si (3.025–3.037 f.u.) and Na admixture (up to 0.33 wt % Na_2O).

Thus experiments confirmed the compatibility of Na-maj with sodium-rich silicate melts. The formation of Na-bearing majoritic garnet and its composition are controlled by several factors, among which, in addition to melt composition, are pressure and temperature. Increase of pressure leads to the growth of sodium content in garnet. Meanwhile, decrease of temperature relatively to liquidus values resulted successive increase of sodium content, so that the highest sodium concentrations were observed at the solidus of the systems. The first results of the study of multicomponent system pyrope−grossular−$Na_2MgSi_5O_{12}$ system allow us to transform experimentally established regularities on crystallization of natural eclogitic garnets under high pressure conditions with confidence. Distinct correlation between Na and Si contents in synthesized garnets allows us to consider a scheme of heterovalent isomorphism like Mg + Al → Na + Si resulting from appearance of $Na_2MgSi_5O_{12}$ end-member as a mechanism of their formation.

This work was supported by OPTEK LLC (Russia) and Ministry of education and science of Russian Federation, project No 14.B37.21.0457. It is partially supported by IP SB RAS No 97 and RFBR (12-05-31351 mol_a).

References:

[1] Bobrov A., Litvin Yu., Bindi L., Dymshits A. 2008. Contribution to Mineralogy and Petrology. 156. P. 243–257.

[2] Surkov N.V., Gartvich Yu.A. 2000. Petrology. 8. (1). 95-107.

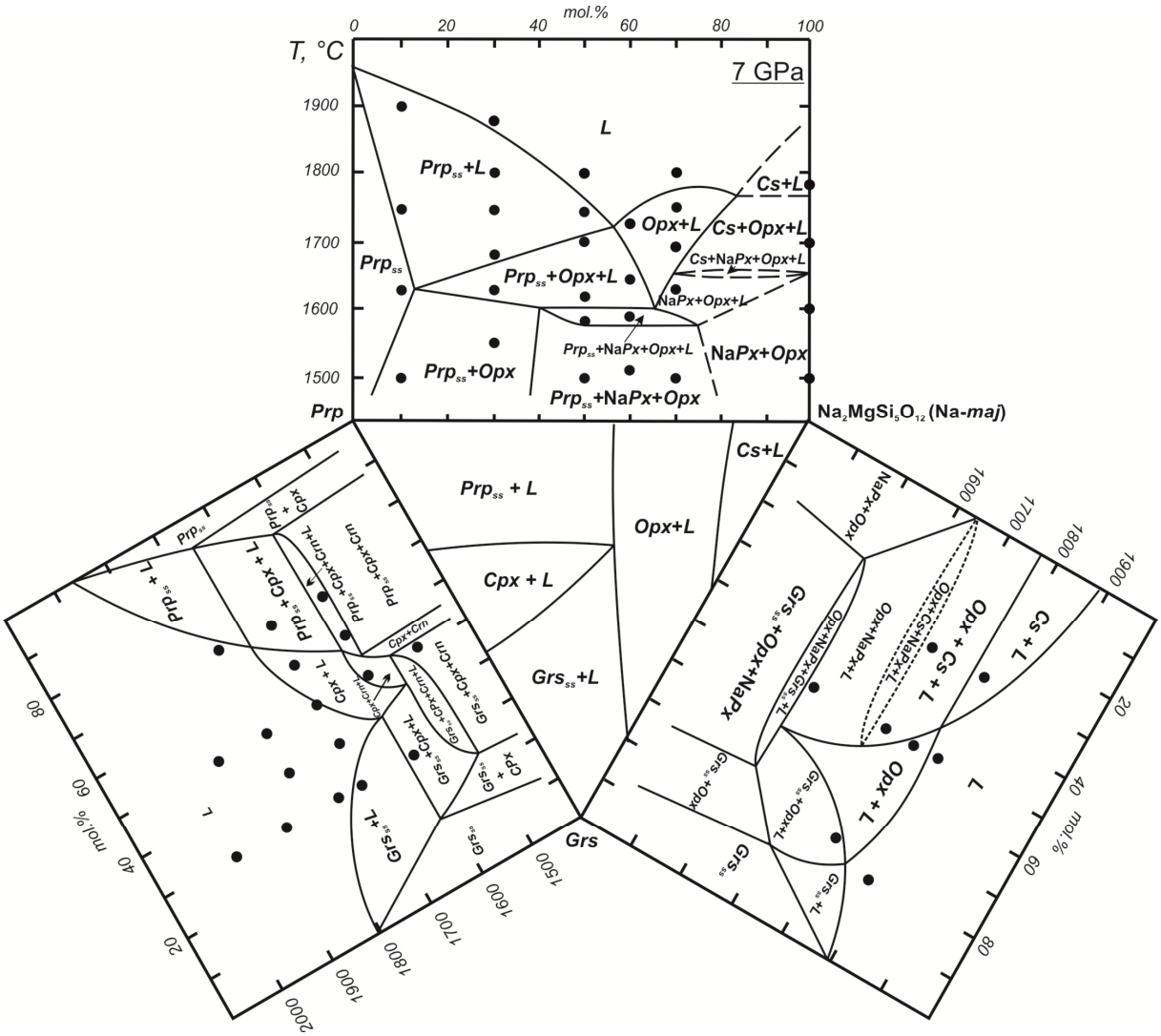

Figure 1. Ternary phase diagram of the system pyrope–grossular–$Na_2MgSi_5O_{12}$ at 7 GPa. Central part illustrates the cotectic lines of the system.

PRELIMINARY RESULTS ON CRYSTAL CHEMISTRY AND PHASE TRANSITIONS OF ALKALI AND DOUBLE ALKALI CARBONATES

Gavryushkin P.N. [1,2], ***Shatskiy A.*** [1,2], ***Litasov K.D.*** [1,2], ***Seryotkin Y.V.*** [1,2], ***Likhacheva A.Y.*** [1], ***Kuribayashi T.*** [3], ***Sharygin I.S.*** [1,2], ***Borzdov Y.M.*** [1], ***Pal'yanov Y.N.*** [1,2], ***Higo Y.*** [4], ***Funakoshi K.*** [4], ***Ohtani E.*** [3]

[1] *V.S. Sobolev Institute of Geology and Mineralogy SB RAS, Novosibirsk, Russia*
[2] *Novosibirsk State University, Novosibirsk, Russia*
[3] *Department of Earth and Planetary Material Science, Tohoku University, Sendai, Japan*
[4] *SPring-8, Japan Synchrotron Radiation Research Institute, Kouto, Hyogo, Japan*
p.gavryushkin@gmail.com

Increasing interest to alkali carbonate phases is explained by their recent finding in the inclusions in deep-seated minerals, including diamonds. Alkali carbonate phases are important for determination of melting in experimental studies of carbonate-bearing systems at high-pressure. Previous investigations in the systems with low-alkali contents have failed to determine true solidi in carbonated systems [**1**]. Most recent experimental studies of carbonated peridotite, eclogite and sediments indicate major control of melting from alkali-bearing carbonates [**2,3**], which previously were not identified. We performed phase diagram studies of the following carbonate systems K-Mg, K-Ca, Na-Ca, Na-Mg, K-CaMg, and Na-CaMg at pressures up to 6 GPa and 900-1400°C. The stability of various double carbonates was confirmed and new high pressure polymorphs were identified. The determination of crystal structures and elastic parameters of new carbonate phases is important for further thermodynamic description of Earth's mantle assemblages.

In this work our attention were predominantly focused on high pressure polymorph of the following carbonates: Na_2CO_3, K_2CO_3, $K_2Mg(CO_3)_3$, $Na_2Mg(CO_3)_3$ $Na_2Ca_3(CO_3)_4$, and $K_2Ca_3(CO_3)_4$.

The experiments were carried out using large volume multianvil apparatuses at Tohoku University (Sendai, Japan) and IGM SB RAS (Novosibirsk, Russia). The *in situ* X-ray diffraction experiments were conducted at the SPring-8 synchrotron radiation facility (Japan), using a Kawai-type multi-anvil apparatuses, "SPEED-MkII," and "SPEED-1500" installed at a bending magnet beam line BL04B1. An energy-dispersive X-ray diffraction technique was used for the *in situ* measurements. The single crystal diffraction experiments were carried out on Oxford Diffraction Xcalibur Gemini R Ultra diffractometer (graphite-monochromatized Mo*K*α radiation).

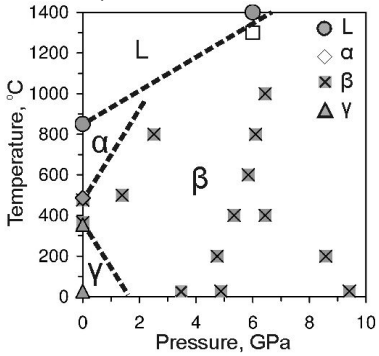

Figure 1. Pressure-temperature phase diagram of Na_2CO_3

Several temperature-induced phase transitions in Na_2CO_3 were established experimentally by means of *in situ* X-Ray studies at ambient pressure (Fig.1). As can be seen, the temperature range for the β-Na_2CO_3 stability field expands with pressure significantly from 150 ºC up to 1000 °C or more at 6 GPa. γ-Na_2CO_3 was observed only under ambient conditions after decompression. β-Na_2CO_3 does not transform to α-Na_2CO_3 at least up to 800ºC at 2.5 GPa and up to 1000°C at 6.4 GPa. We did not observe any pressure-induced phase transitions in β-Na_2CO_3 up to 11.7 GPa at 27 ºC and up to 15.2 GPa at 1200 ºC, which is consistent with theoretical prediction in [**4**]. Very preliminary lattice parameters of β-Na_2CO_3 determined by autoindexing are following a=8.554(2), b=5.2055(3), c=6.463(1), β=100.24°(1), α=γ=90° (P=3.41(13) GPa, T=27°C) [**5**].

According to the results, high pressure polymorphs of K- double carbonates are unquenchable. In contrast, the high pressure polymorphs of Na- double carbonates are quenchable.

$K_2Mg(CO_3)_3$ polymorph stable at ambient conditions is isostructural to $Na_2Mg(CO_3)_3$ [**6**]. According to present XRD *in-situ* experiments new phase of K-Mg carbonate is stable in the pressure range from 1 to 6.5 GPa [**7**]. Preliminary unit cell dimensions of new polymorph were obtained as follows: a=9.0235(7), b=8.0148(8), c=5.1259(6), α=β=γ=90° (1.1GPa, 27°C). The unit-cell volume of this phase is nearly 10% less than that of lower-pressure polymorph.

$K_2Ca_3(CO_3)_4$ is a new high-pressure phase. Three plausible models of unit cell parameters were determined. We choose one with the highest M20, F20 figure of merit and based on the systematical absences define 4 possible space groups: $P2_1/m$,P2/m, P2/c, $P2_1/c$. Unit cell parameters were calculated to be: a=4.8265(5), b=18.158(2), c=4.3610(4), and β=96.978(6). The new phase was observed at pressure-temperature interval of 0.9 - 6.72 GPa, 27 - 1000°C.

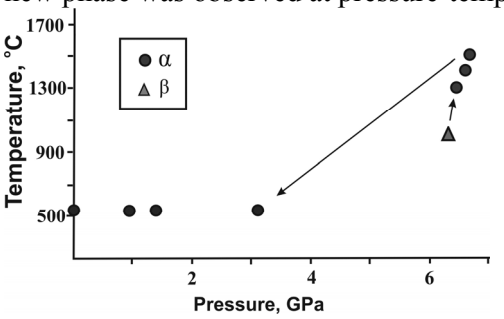

Fig.2. Pressure-temperature phase diagram of $Na_2Ca_3(CO_3)_4$

The analysis of XRD patterns of $Na_2Ca_3(CO_3)_4$ phases gives the following results. The reactants interact with each other and form β-$Na_2Ca_3(CO_3)_4$ at pressure between 4.5 and 6.3 GPa and temperature between 300 K and 773 K (Fig.1, 2). β-$Na_2Ca_3(CO_3)_4$ transforms into α-$Na_2Ca_3(CO_3)_4$ at temperature between 773 K and 1073 K (P ≈ 6.3 GPa) The following decreasing the temperature to 300 K and pressure to 4.5 GPa does not lead to the back transformation into β-$Na_2Ca_3(CO_3)_4$, α-$Na_2Ca_3(CO_3)_4$ is stable down to 273 K and 0 GPa (Fig.2). Both modifications α-$Na_2Ca_3(CO_3)_4$ and β-$Na_2Ca_3(CO_3)_4$ have not been described earlier. The single crystals of α-$Na_2Ca_3(CO_3)_4$ were picked from the product of experiment and were studied also using laboratory diffractometer. According to systematic absences possible space groups are following $P2_1/n11$, $P2_1mn$, Pmnm, a=7.43582(19), b=8.1961(2), c=31.4425(8), α=90.032(2), β=89.923(2), γ=90.003(2). Three important findings can be emphasized: (i) the *c* axis is unusually long, (ii) the *β* angle is close, but not identical to 90° and (iii) the full set of systematic absences doesn't satisfy to any space group. The first fact can be the sign of superstructure of *β*-$Na_2Ca_3(CO_3)_4$ compare to *α*-$Na_2Ca_3(CO_3)_4$, the second and third – the signs of pseudomerohedral twinning. The one more confirmation of twinning are difficulties arising at the stage of structure solution. Both superstructure and polysynthetic twinning can be results of the polymorphic transition from α- to β-modification, which take place in the process of synthesis.

This study was supported by the Global Center-of-Excellence program at Tohoku University, the Ministry of Education and Science of Russia (project No. 14.B37.21.0601) and by the Russian Foundation for Basic Research (project Nos. 12-05-01167 and 12-05-33008).

References:

[**1**] Ghosh, S., Ohtani, E., Litasov, K.D., Terasaki, H. (2009) Chemical Geology, 262, 17–28.
[**2**] Litasov, K.D., Goncharov A.F., Hemley R.J. (2011) Earth and Planetary Science Letters, 309, 318–323.
[**3**] Grassi D., Schmidt M.W. (2011) Journal of Petrology, 52, 4, 765-789.
[**4**] Cancarevic, Z., Schon, J.C., Jansen, M. (2006) Zeitschrift für anorganische und allgemeine Chemie, 632(8-9), 1437-1448.
[**5**] Shatskiy, A., Gavryushkin, P.N., Sharygin, I.S., Litasov, K.D., et al. (2013) The system Na_2CO_3–$MgCO_3$ at 6 GPa and 900–1400ºC, American Mineralogist, in press.
[**6**] Hesse, K.-F., Simons, B. (1982) Zeitschrift fur Kristallographie 161, 289-292
[**7**] Shatskiy, A., Sharygin, I. S., Gavryushkin P. N., Litasov, K. D. et al. (2013) The system K_2CO_3–$MgCO_3$ at 6 GPa and 900–1450°C, American Mineralogist, in press.

MULTIPLE MANTLE METASOMATISM BENEATH THE SANGILEN HIGHLAND: EVIDENCE FROM CAMPTONITIC COMPOSITE (WATER-BEARING PYROXENITES/SP LHERZOLITES) XENOLITHS

Gibsher A.A., Malkovets V.G., Kuzmin D.V., Pokhilenko N.P.

V.S. Sobolev Institute of Geology and Mineralogy SB RAS, Novosibirsk, Russia
n.gibsher@gmail.com

Mantle metasomatism and partial melting are the main processes that change the composition of the lithospheric mantle. Metasomatic enrichment in mantle xenoliths and peridotite massifs is evident from the presence of newly formed, mainly hydrous minerals (modal metasomatism), as well as from enrichment of peridotitic minerals in incompatible elements (cryptic metasomatism). The suite of deep xenoliths brought up to the surface by Late Ordovician lamprophyric dykes of the Agardag alkaline basalt complex contains several composite xenoliths exhibiting veining in spinel peridotites; the veins are composed of hydrous minerals (amphibole and phlogopite) ± clinopyroxene. Here we discuss detailed mineralogy of four composite mantle xenoliths. The study designed to define the thickness of metasomatic zones around veins in the peridotite matrix and major features of the metasomatic alteration of peridotitic minerals.

The studied composite xenoliths are Cpx-Phlog (5H759), Amph-Phlog (5H760), and Amph veins (5H767 and 5H789), crosscutting the spinel facies peridotites. Mineral assemblages change in peridotites away from the contact with veins (Fig. 1a). Peridotites at the contact with the Phlog-bearing veins (5H759 and 5H760) were transformed to wherlites. The variations of the chemical composition of vein and peridotite minerals are shown in Fig.1 b-h. Peridotites at the contact with Phlog-bearing veins reveal the metasomatic enrichment profiles, whereas no profiles have been found at the contact with Amph-bearing veins. The most striking feature of peridotite metasomatic changes at the contact with Phlog-bearing veins (5H759 and 5H760) – is the enrichment in iron (Fig. 1 c, e, g) and titanium (Fig. 1 f) in the rather narrow zone - 16 mm away from the contact. The peridotites at the contact with Amph-bearing veins do not reveal any enrichment close to the vein boundaries. Rather the overall chemistry of the peridotite demonstrates the high enrichment in iron (Fig. 1 c, e, g).

Based on the mineralogical and chemical composition of veins and character of metasomatic enrichment of peridotites at the contact with veins of different composition we identify at least two stages of metasomatic enrichment of the lithospheric mantle beneath the west Sangilen. The last stage was related to the formation of the Phlog-bearing vein network. The time of their formation closely preceded the camptonite intrusion that is evidenced from the surviving of the metasomatic enrichment profiles at the contact with this kind of veins (5H759 and 5H760). The earlier stage of the peridotite metasomatic enrichment was related to the formation of the Amph-bearing veins. Samples 5H767 and 5H789 do not reveal any gradients of peridotite minerals chemical composition away from the vein contact.

Parental melts of the Phlog-bearing veins are the alkaline silica-undersaturated melts, enriched in Ti and K, volatiles, such as H_2O, Cl, F, CO_2, P_2O_5, and incompatible elements, and probably related to the host camptonites. Amph-bearing veins crystallized from mildly alkaline transitional basaltic melts (iron-rich, with lower titanium and potassium contents), and probably have older age in comparison with the Phlog-bearing veins. The significant iron enrichment of peridotites at the contact with Amph-bearing veins could be formed by reaction of host refractory peridotites with evolved (Mg numbers 0.6–0.7) silicate melts at high melt/rock ratios, which replace olivine with orthopyroxene and decrease Mg numbers.

This work was supported by the Grant of the President of the Russian Federation, project No MK-2689.2013.5 and RFBR (No 12–05–00487, 12–05–33035, 13–05–01051).

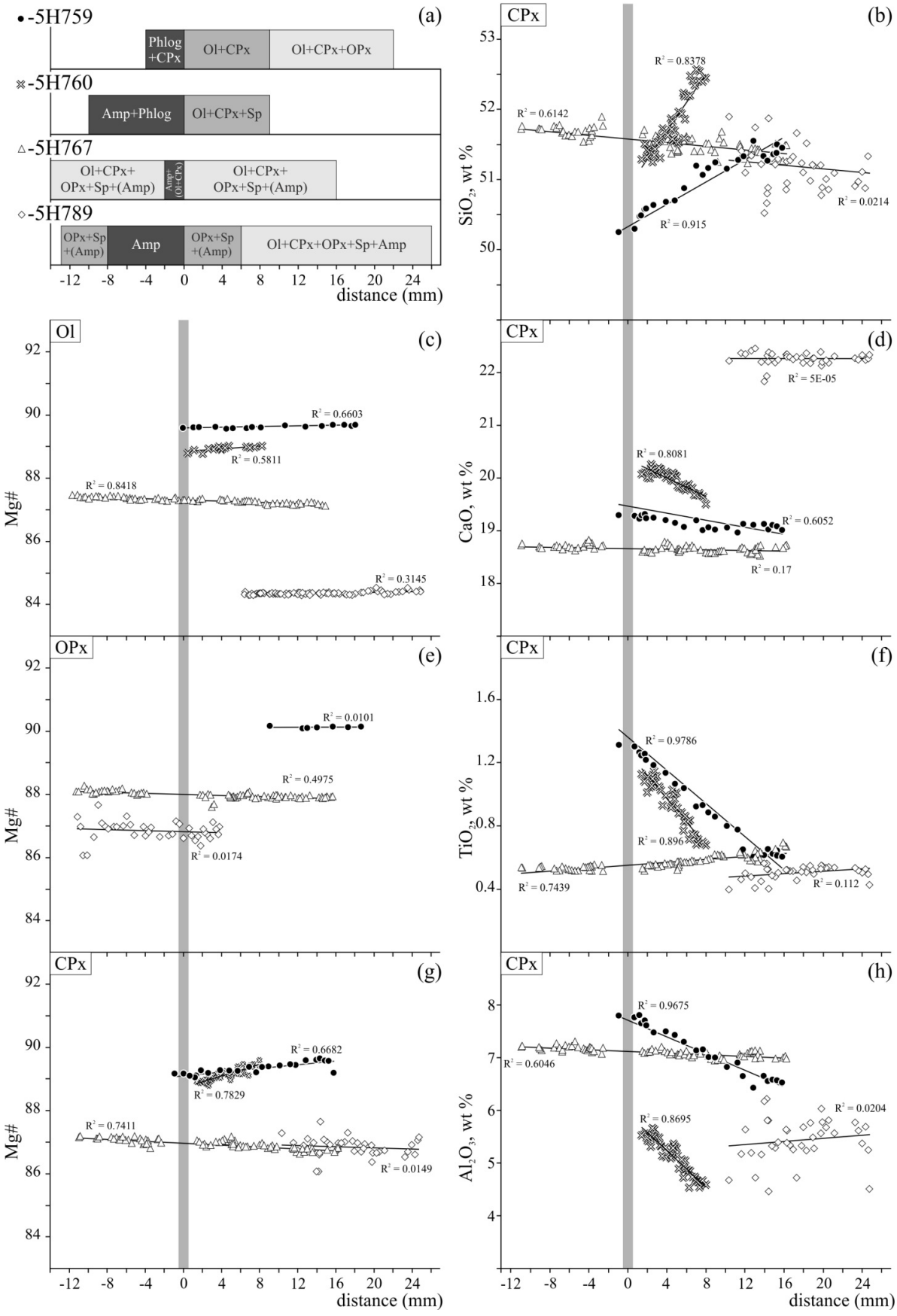
-5H759
-5H760
-5H767
-5H789
Phlog +CPx
Ol+CPx
Ol+CPx+OPx
Amp+Phlog
Ol+CPx+Sp
Ol+CPx+ OPx+Sp+(Amp)
Amp (Ol+CPx)
Ol+CPx+ OPx+Sp+(Amp)
OPx+Sp +(Amp)
Amp
OPx+Sp +(Amp)
Ol+CPx+OPx+Sp+Amp
distance (mm)
(a)
(b)
(c)
(d)
(e)
(f)
(g)
(h)
Ol
CPx
OPx
Mg#
SiO2, wt %
CaO, wt %
TiO2, wt %
Al2O3, wt %
R2 = 0.8378
R2 = 0.6142
R2 = 0.0214
R2 = 0.915
R2 = 5E-05
R2 = 0.8081
R2 = 0.6052
R2 = 0.17
R2 = 0.9786
R2 = 0.896
R2 = 0.7439
R2 = 0.112
R2 = 0.9675
R2 = 0.6046
R2 = 0.8695
R2 = 0.0204
R2 = 0.6603
R2 = 0.5811
R2 = 0.8418
R2 = 0.3145
R2 = 0.0101
R2 = 0.4975
R2 = 0.0174
R2 = 0.6682
R2 = 0.7829
R2 = 0.7411
R2 = 0.0149

STABILITY OF COMPLEX THORIUM FLUORIDES AT HIGH PRESSURES

Grzechnik A. [1], ***Friese K.*** [2]

[1] *Institute of Crystallography, RWTH Aachen University, Germany*
[2] *Jülich Center for Neutron Science, Germany*
grzechnik@xtal.rwth-aachen.de

The first crystallographic studies of actinide fluorides were performed during the Manhattan Project [**1-4**]. The interest in these materials, especially in the thorium fluorides, has now been revived since they could be used as core coolants with solid fuels, liquid fuel in a molten salt reactor, or solvents for spent nuclear solid fuel. The safety requirements regarding modern nuclear power generation and nuclear waste storage have extensively been discussed in a series of recent analyses [**5-7**]. Several of the known compounds have been structurally re-examined [**8-11**] and several novel materials have been synthesized [**12-16**] in the last few years. The fact that stable complex thorium fluorides could be easily grown using various methods encourages further explorations of the systems containing thorium and fluorine.

The coordination numbers of the Th atoms in fluorides are either 8 or 9 [**17**]. In the first case, the ThF_8 polyhedra are square antiprisms, dodecahedra, or bicapped trigonal prisms. In the latter, they are tricapped trigonal prisms. We are interested in the structural features and stabilities of solid complex thorium fluorides with different polyhedra around the Th atoms and distinct polyhedral connectivities. Our work on their structures is performed not only at atmospheric conditions but also at high pressures using single-crystal x-ray diffraction in diamond anvil cells on laboratory diffractometers and at synchrotron facilities.

The results of our studies [**8-11**] indicate that the materials with low-dimensional structures built of chains or layers of face- or edge-sharing Th-F polyhedra are structurally stable at least to about 10 GPa at room temperature. This observation suggests that, in general, moderate high pressure has no effect on the coordination polyhedra around the Th atoms and the topology of the structure of complex thorium fluorides. The bulk compressibility of the thorium fluorides entirely depends on the alkali metal present in the structure.

Currently, we have been involved in the structural studies of framework fluorides containing thorium and tetravalent lanthanides [**18**]. Our preliminary observations suggest that there is no influence of the thorium and lanthanide substitutions on the bulk moduli of these materials.

We would like to thank Jean-Yves Gesland, Christopher C. Underwood, and Joseph W. Kolis for a collaboration.

References:

[1] W.H. Zachariasen, *J. Am. Chem. Soc*., 1948, **70**, 2147.
[2] W.H. Zachariasen, *Acta Crystallogr*., 1948, **1**, 265.
[3] W.H. Zachariasen, *Acta Crystallogr*., 1949, **2**, 388.
[4] W.H. Zachariasen, *Acta Crystallogr*., 1949, **2**, 390.
[5] N. Cooper et al., E*nviron. Sci. Technol*., 2011, **45**, 6237.
[6] S.F. Ashley et al., *Nature*, 2012, **492**, 31.
[7] M. Mitchell Waldrop, *Nature*, 2012, **492**, 26.
[8] A. Grzechnik, M. Fechtelkord, W. Morgenroth, J.M. Posse, K. Friese, *J. Phys.: Condens. Matter*, 2007, **19**, 266219.
[9] A. Grzechnik, W. Morgenroth, K. Friese, *J. Solid State Chem*., 2008, **181**, 971.
[10] K. Friese, W. Morgenroth, J.M. Posse, A. Grzechnik, *Dalton Trans*., 2011, **40**, 1902.
[11] A. Grzechnik, C.C. Underwood, J.W. Kolis, K. Friese, *J. Fluorine Chem*., 2013, **150**, 8.
[12] M. Mann, J. Kolis, *J. Chem. Crystallogr*., 2010, **40**, 337.

[13] C.C. Underwood, M. Mann, C.D. McMillen, J.W. Kollis, *Inorg. Chem*., 2011, **50**, 11825.
[14] C.C. Underwood, C.D. McMillen, J.W. Kolis, *J. Chem. Crystallogr*., 2012, **42**, 606.
[15] J. Strizinger, C.D. McMillen, J.W. Kolis, *J. Chem. Crystalogr*., 2012, **42**, 366.
[16] C.C. Underwood, M. Mann, C.D. McMillen, J.D. Musgraves, J.W. Kolis, *Solid State Sci*., 2012, **14**, 574.
[17] A.F. Wells, *Structural Inorganic Chemistry*, 5th Edition, Oxford University Press, Oxford, 1984.
[18] A. Grzechnik, C.C. Underwood, J.W. Kolis, K. Friese, to be published.

HIGH PRESSURE BEHAVIOUR OF THREE-MEMBERED [Si_3O_9]-RINGS IN THE CYCLOSILICATES BENITOITE $BaTiSi_3O_9$, WADEITE $K_2ZrSi_3O_9$ AND REALTED COMPOUNDS

***Hejny C.*[1], *Miletich R.*[2], *Kahlenberg V.*[1], *Pippinger T.*[2], *Jasser, A.*[3], *Schouwink P.*[4], *Niederwieser N.*[1], *Jessacher M.*[1]**

[1] *Mineralogy and Petrography, University of Innsbruck, Innsbruck, Austria*
[2] *Mineralogy and Crystallography, University of Vienna, Vienna, Austria*
[3] *Institute for Geosciences,University of Heidelberg, Heidelberg, Germany*
[4] *Laboratoire de Cristallographie de l'Université de Genève, Genève, Switzerland*
clivia.hejny@uibk.ac.at

The ring like structural units of cyclosilicate structures are in the focus of a systematic study to investigate their elastic behavior and nonlinear anomalies. For this aim in-situ investigations of $BaTiSi_3O_9$, $K_2ZrSi_3O_9$ and $K_2SiSi_3O_9$ by means of single-crystal diffraction and Raman spectroscopy have been carried out using diamond-anvil cell techniques. For $BaTiSi_3O_9$, benitoite, the state mineral of California, a well-priced gemstone with strong pleochroism and a use-oriented fluorescent material, a second-order phase transition from *P*-6*c*2 at ambient pressure (AP) to *P*31*c,* with $a_{HP} \sim a_{AP}\sqrt{3}$, at pressures above 4.24(3) GPa has recently been investigated and shown to be accompanied by a significant softening of the *c*-axis, and hence a significantly anisotropic change of the compressibility **[1]**.

The mineral wadeite $K_2ZrSi_3O_9$ and isostructural synthetic $K_2SiSi_3O_9$, $P6_3/m$ **[2-5]**, host the same type of three-membered rings of SiO_4 with internal symmetry 3/m as found in benitoite. However, the connection via octahedra ($Ti^{[6]}$ in benitoit, $Zr^{[6]}$ in wadeite, $Si^{[6]}$ in $K_2SiSi_3O_9$) to form an octahedral-tetrahedral framework with potassium in nine-fold coordination is different from the one known from benitoite. Synthetic $K_2SiSi_3O_9$ does not show a phase transition up to 10.4GPa **[6]**, but similarly to the case of benitoite single crystal diffraction experiments of wadeite $K_2ZrSi_3O_9$ show additional Bragg peaks, that increase in intensity with (a) increasing pressure (HP form) and (b) with decreasing temperature (LT form), hence giving rise to $a_{HP} \sim a_{LT} \sim 2a_{AP}$ (Fig. 1). In the course of tracking down the pressure and temperature of the likely phase transition, it was found that these additional ($^h/_2{}^k/_2 l$) reflections are actually present at ambient conditions, although extremely weak. The true structure of natural $K_2ZrSi_3O_9$ was solved from a dataset collected at 173°K in space group $P2_1/c$ with a = 13.820(6), c = 10.1781(4) Å and shows a very similar distortion of the triple ring unit as found for the HP polymorph of benitoite (Fig. 2).

References:

[1] Hejny C., Miletich R., Jasser A., Schouwink P., Crichton W., Kahlenberg V., 2012. Amer Mineral. **98**: 1749-1763.
[2] Henshaw D.E., 1955. Amer. Mineral. **40**:775-775.
[3] Blinov V.A., Shumyatskaya N.G., Voronkov A.A., Ilyukhin V.V., Belov N.V., 1977. Kristallografiya **22**: 59-65.
[4] Kinomura N., Kume S., Koizumi M. 1975. Mineral. Mag. **40**:401-404.
[5] Swanson D.K., and Prewitt C.T. 1983. Amer. Mineral. **68**: 581-585.
[6] Chang L., Chen Z., Liu X., Wang H., 2013 Phys. Chem. Mineral. **40**: 29-40.

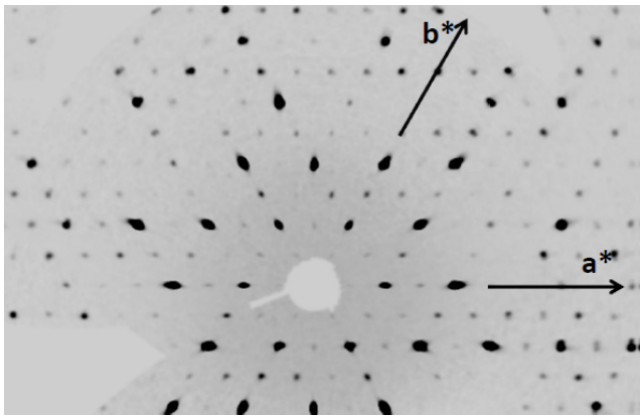

Figure 1. Reconstructed *hk*1 reciprocal layer of wadeite $K_2ZrSi_3O_9$ measured at 173 °K showing weak reflections at ($^{h}/_{2}$ $^{k}/_{2}$ l) for an indexation of the strong reflections according to the $P6_3/m$ structure with a = 6.910(6), c = 5.089(1) Å.

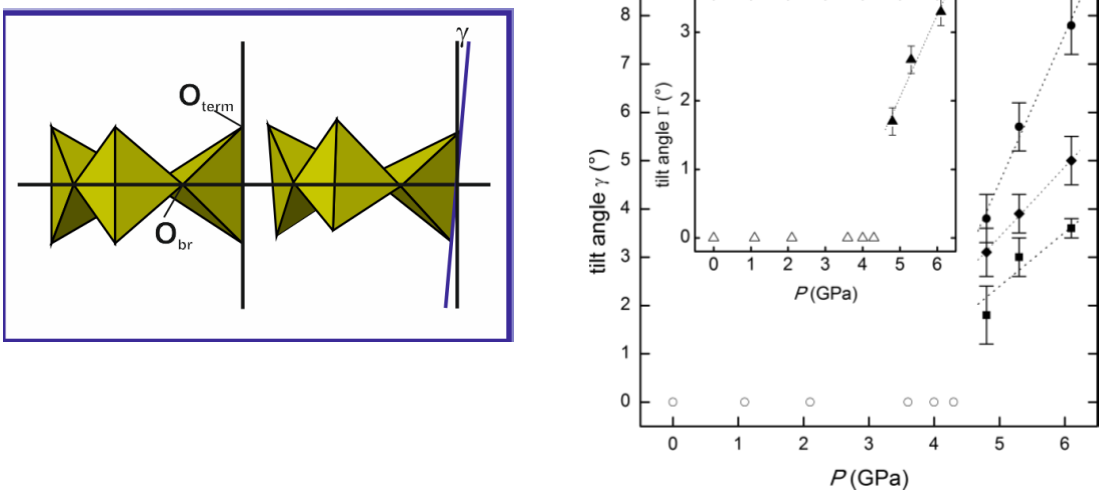

Figure 2. Tilt angle γ of the SiO_4 tetrahedra in benitoite with increasing pressure.

THREE DIMENSIONAL VISUALIZATION OF RESIDUAL PRESSURE AROUND INCLUSIONS IN SAPPHIRE

Kagi H. [1], ***Kamegata N.*** [1], ***Fuetes J.*** [1], ***Noguchi N.*** [1], ***Abduriyim A.*** [2]

[1] *Graduate School of Science, University of Tokyo, Hongo, Tokyo, Japan*
[2] *Gemological Institute of America*
kagi@eqchem.s.u-tokyo.ac.jp

Mantle derived minerals can tell us much information about processes within the deep Earth. It is important to determine the original depth of these mineral samples. Kagi et al. 2009 showed that three-dimensional Raman mapping observations can be used to visualize the distribution of residual pressure around inclusions in diamond, which has provided information about the depth of diamond formation. Corundum is the second hardest mineral after diamond and is expected to also show substantial residual pressure around inclusions.

Samples were collected from New South Wales, Australia as well as Chanaburi, Thailand and are associated with alkali basalts. It is possible to distinguish between corundum crystals formed from various settings, such as metamorphic versus igneous settings, based on trace element analyses. However, distinguishing between crystals of different geographic locality and similar geologic settings is not yet possible using nondestructive methods. Based on current geochemical observations, there are two models for the formation of igneous corundum crystals. Guo et al. 1996 proposed that these crystals formed in the middle crust by a hybrid reaction between carbonatite melt and silicic magma. Alternatively, Sutherland et al. 1998 suggested that they may form directly from volatile-rich felsic melts generated at lower crustal conditions. By using 3D mapping techniques, it may be possible to evaluate the P-T history of the host rock as well as differentiate between gems from different localities.

The fluorescence spectrum of corundum has two peaks associated with the excitation of Cr^{3+} impurities in its structure, R1 and R2. Because the R2 line is insensitive to differential stress, the residual pressure can be calculated based on the peak shift of the R2 line using a pressure calibration curve.

The samples were excited using 514.5 nm emission of Ar-ion laser with a diameter of 2 micron. Measurements were taken every 5 to 10 micrometers around albite, zircon, and rutile inclusions using a point-by-point mapping illumination system. The R2 and R1 lines of the fluorescence spectra were fitted by Lorentzian functions after subtraction of background. In order to account for peak oscillations caused by changes in room temperature, real-time calibration of the fluorescence spectra energy axes were performed by neon emission lines as discussed in Odake et al. 2008.

Over 25 two- and three-dimensional maps of various inclusions have been created so far. The maximum residual pressure for each map ranges from 0.1 GPa to 0.51 GPa. In many of these samples, stress distribution can be explained by differences in elastic constants between the host and inclusion. For example, our results show one slice of a 3D map around a zircon inclusion. In this case, the c-axis of the corundum and the c-axis of the zircon are nearly parallel. With decreasing temperature and pressure, the c-axis is expected to have higher residual pressure due to differences in linear thermal expansion coefficients and bulk moduli between the host and inclusion. It is clear that the c- axis has the highest residual pressure, as expected. Another notable observation is that the maximum residual pressure surrounding zircons correlates with length of the crystal along the c-axis. Two distinct trends between residual pressure and length are observed. This may be due to many factors including the relative orientation of the host and inclusion or the presence of cracks surrounding the inclusion. It could also be due to the different geographic localities. However, more measurements need to be taken to confirm.

Previous methods to determine original depth, such as those used by Barron 2005 and Izraeli et al. 1999, which assume isotropic elastic properties in inclusion and diamond, cannot be used in these corundum-inclusion pairs. Our results show that relative orientation of corundum and inclusions must be accounted for in future calculations of P-T history.

THE ESTIMATION OF EQUILIBRIUM DEGREE BETWEEN MINERALS FROM DEEP-SEATED XENOLITHS IN YAKUTIAN KIMBERLITES

Kalashnikova T.V. [1], ***Solov'eva L.V.*** [2], ***Kostrovitsky S.I.*** [1]

**Vinogradov Institute of Geochemistry SB RAC, Irkutsk, Russia*
***Institute of Earth Crust SB RAC, Irkutsk, Russia*
Kalashnikova@igc.irk.ru

The deep-seated xenoliths rising by kimberlite melts are supposed to represent the lithosphere mantle matter beneath the region. The P-T crystallization estimating for mantle rocks is very important because the mineral equilibrium is necessary information. One of eguilibrium indicator is trace element ratio between garnet and clinopyroxene as main trace element concentrators. If the crystallization was equilibrated in case of melt crystallisation, the Grt/Cpx ratio would close to the ratio of distribution coefficient for trace element in garnet and clinopyroxene ($D_{Grt\text{-}melt}/D_{Cpx\text{-}melt}$) for certain melt. The metamorphic or metasomatic recrystalline mineral paragenesis would also to been equilibrated.

In this article the xenolith collection from two kimberlite pipes was investigated. The Udachnaya pipe is located in the Siberian craton centre, the Obnajennaya pipe is located in the north-east in Kuoika kimberlite field. The deformed peridotites consist about 60% in Udachnaya pipe and are absent in the Obnajennaya pipe [1]. These deformed peridotites were treated by dynamometamorphism recrystallization reflected in porphyroclasts of garnet, clinopyroxene, orthopyroxene, olivine and recrystallization of fine-grained olivine matrix. The metasomatic treatment by asthenospheric melts resulted to the mineral composition change [2, 3]. On the basis of porphyroclast size and modal mineral composition the rocks were distinguished as large-porphyric and fine-porphyric types [2]. In the Obnjennaya pipe the content of Grt pyroxenites is about 40% and coarse-grained high-Cpx lherzolites containing Sp and Sp-Grt are about 27% [1]. The spinel facies rocks are minor in the Udachnaya pipe (less than 10%). In the Obnajennaya pipe the Sp, Sp-Grt, Grt lherzolites, Ol-websterites and pyroxenites form united series with continuous transition of petrographic features and mineral compositions [4]. In this series the deformation traces, exsolution structures and spinel displacement to garnet are wide-spread indicating the gradual cooling at stressing and possible sinking to lower levels.

The calculating element ratio between Grt and Cpx ($D_{Grt/Cpx}$) is presented in Figure 1. $D_{Grt/Cpx}$ for basalt and carbonatite melts were also plotted by more common literature data. It should be noted that peridotites from both pipes approach to basalt melt. Nevertheless, the Ti maximum is showed for the Udachaya pipe and minimum for the Obnajennaya pipe. The minimum for titanium characterize the carbonatite melt as well as the maximum for hafnium observed for Obnajennaya lherzolites-websterites. Maximum for zirconium characterized the basalt melt and are observed for Udachnaya peridotites. On the whole, deformed lherzolites from the Udachanaya pipe and lherzolite – Ol-websterite – pyroxenite series from Obnajennaya pipe have similar $D_{Grt/Cpx}$. The coarse- grained peridotites from the Udachnaya demonstrate more wide range of the coeffients, that may be interpreted by mantle metasomatism during kimberlite-forming cycle [5]. According to estimating of P-T crystallization conditions, the series from Obnajennaya was formed on depth from 50 to 120 km; the deformed peridotites from Udachnaya were crystallisated lower (180-230 km). The influence of plume basalt melts (CFB type) is supposed for Udachnaya deformed peridotites [2]. In rocks from Obnajennaya the small Eu anomaly is observed and oxygen isotope composition is essentially higher than middle-mantle value [6], indicating the sea water influence. The Obnajennaya rock series is supposed to crystallize in basite melt sources in supersubduction zone under the influence of subduction fluids.

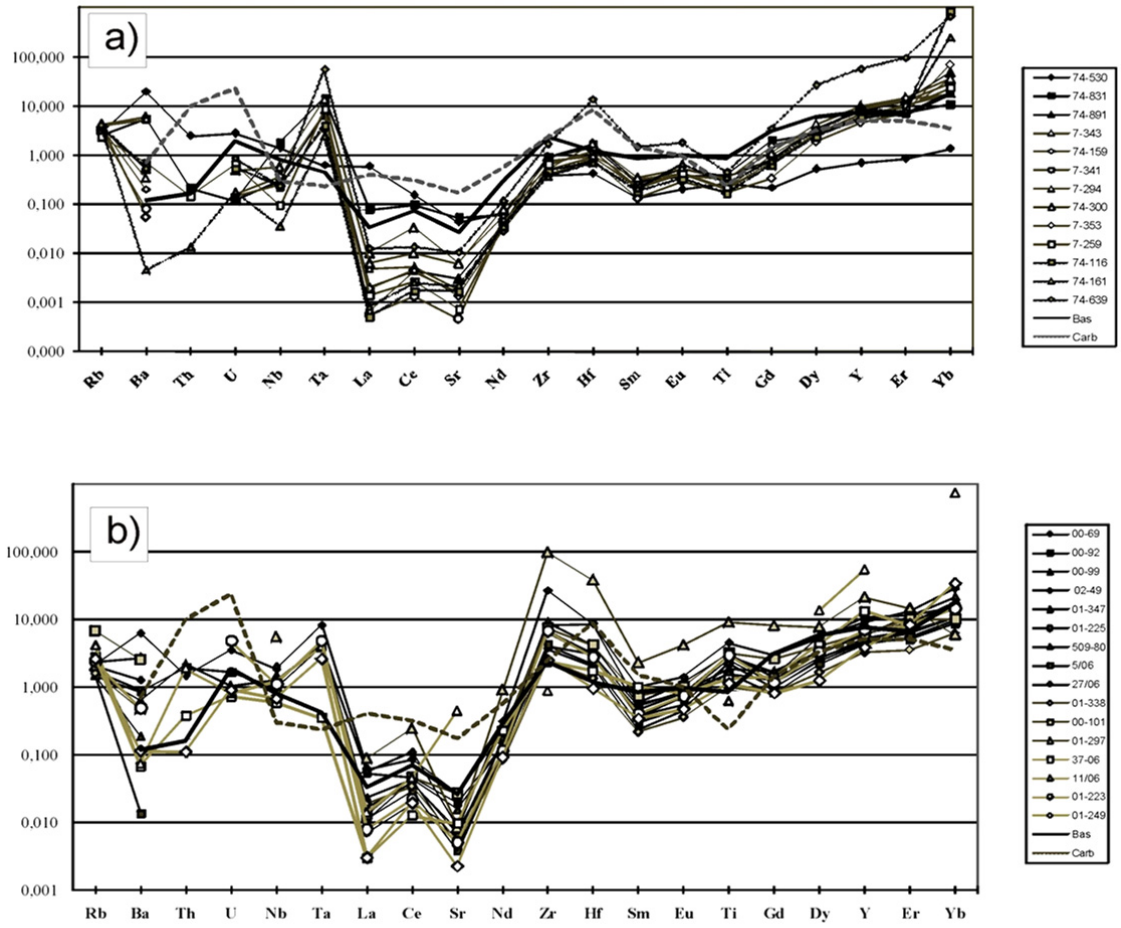

Figure 1. The trace element concentration ratio between garnet and clinopyroxene ($D_{Grt/Cpx}$) in comparison with the same for basalt melt (Bas - thick black line) and carbonatite melt (Carb – thick grey dashed line). a) – Obnajennaya pipe. The filled black signs – Sp- and Sp-Grt lherzolites; empty signs – Ol-websterites; grey signs – pyroxenites. b) - Udachnaya pipe. The filled black signs – large-porphyric lherzolites; empty signs – fine-porphyric lherzolites; grey signs – coarse-grained lherzolites.

References:

[1] Ukhanov A.V., Ryabchikov I.D., Khar'kiv A.D. Lithospheric mantle of Yakutian kimberlite province (in Russian). - Nauka, Moscow. 1988.

[2] Solov'eva L.V., Egorov K.N., Lavrent'ev Yu.G., Korolyuk V.N., Kostrovitskii S.I., Suvorova L.F. Russian Geology and Geophysics. 2008. V. 49. № 4. P. 207-224.

[3] Agashev A.M., Ionov D.A., Pokhilenko N.P., Golovin A.V., Cherepanova Yu., Sharygin I.S. Lithos. 2013. V. 160-161. P. 201-215.

[4] Solov'eva L.V., Vladimirov B.M. et al. Kimberlite and kimberlite – similar rocks: matter of upper mantle beneath ancient platforms (In Russian) - Nauka, Novosibirsk. 1994.

[5] Solov'eva L.V. Doklady Earth Sciences. 2007. V. 413. № 1. P. 238-243.

[6] Taylor L.A., Spetsius Z.V., Uhizly R., Spicuzza M., Wally D.U. Russian Geology and Geophysics. 2005. V. 46. №12. P. 1198-1206.

ABSORPTION AND GASKET-SHADOWING CORRECTION FOR A DIAMOND-ANVIL CELL

Kazmierczak M.*, *Katrusiak A.

Department of Materials Chemistry, Faculty of Chemistry, Adam Mickiewicz University, Poznan, Poland
katran@amu.edu.pl

The diamond-anvil cell is now routinely applied for structural studies on single and powder samples by x-ray diffraction. The quality of so determined structures directly depend on the quality and correctness of the diffractometric data.

Primary and incident beams passing through the Diamond Anvil Cell (DAC) [1-2] are weakened by absorption of sample and DAC and shadowed by the opaque gasket. This affects intensities of collected reflexes. The method used in our experiments is based on geometrical representation of the system including directions of beams [3], shape of chamber and shape of crystal sample [4].

This study was supported by the TEAM grant No 2009-4/6 from the Foundation for Polish Science.

References:

[1] Jamieson, J. C., Lawson, A. W. & Nachtrieb, N. D. (1959). Rev. Sci.Instrum. 30, 1016–1019.
[2] Weir, C. E., Lippincott, E. R., van Valkenburg, A. & Bunting, E. N.(1959). J. Res. Natl Bur. Stand. Technol. 63A, 55–62.
[3] Katrusiak, A., *Z. Kristallogr.* **216** (2001) 646-647.
[4] Katrusiak, A., *Z. Kristallogr.* **219** (2004) 461-467.

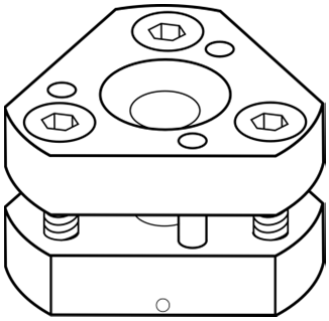

Figure 1. Diamond Anvil Cell.

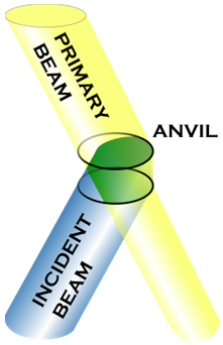

Figure 2. Gasket-shadowing effect for the sample volume available for x-ray radiation.

SHOCK-INDUCED SYNTHESIS OF HIGH-PRESSURE ALUMINIUM NITRIDE WITH ROCKSALT STRUCTURE

Keller K. [1], ***Schlothauer T.*** [1], ***Heide G.*** [1], ***Kroke E.*** [2]

[1] *Freiberg High-Pressure Research Centre (FHP), Freiberg/ Germany and TU Bergakademie Freiberg, Institute of Mineralogy, Freiberg/ Germany*
[2] *TU Bergakademie Freiberg, Institute of Inorganic Chemistry, Freiberg/ Germany*
kevin.keller@mineral.tu-freiberg.de

Aluminium nitride is a ceramic material with a high thermal conductivity, a small thermal expansion coefficient and good mechanical properties. Moreover AlN is a wide-bandgap semiconductor (E_g = 6.2eV) and therefore used as a substrate material for high-power electronic applications **[1]**. At pressure from 14-23 GPa the wurtzitic aluminium nitride (w) undergoes a phase transition to the rocksalt structure (rs) at static experiments **[2-4]**. The high-pressure phase of aluminium nitride with rocksalt-structure (rs-AlN) arouse some interest in the last two decades because of its potential use as a hard material, heat sink in high-power electronics and as an optoelectronic material **[5]**. However, only a few reports on the synthesis and the properties of the rs-AlN are known.

Currently rs-AlN was successfully synthesized from w-AlN in the gram-range with shock waves using the flyer-plate method with subsequently sample recovery **[6]**. A 80mm metal plate was accelerated to several km/s by the detonation of an high explosive, striking a steel container with the AlN sample powder. To obtain good conditions a flat shock wave was produced with a special plane-wave-generator (see Fig. 1). For several sample conditions (high-pressure and high-temperature) impedance and reflection method were applied. Samples were characterised using XRD, SEM, (HR)TEM, solid-state NMR and FT-IR spectroscopy.

The fine greyish powder, which can be gathered from the recovery container, shows a phase mixture of the high-pressure rs-AlN-phase, w-AlN, corundum and several AlON-phases because of the high oxygen content of the starting powder. We observe a sluggish phase transition caused by the kinetic barrier, so that a large overpressure is needed. Though the transition is activated by the temperature raise during compaction, a temperature-driven re-conversion to w-AlN was observed as an opposed process. Therefore the experimental design and parameters have to been chosen carefully. By mixing the w-AlN with a metal powder and using the impedance method for single shock loading, the post-shock-temperature can be controlled much better and samples can be cooled faster. As a consequence an almost completely conversion to rs-AlN can be achieved neglecting the oxygen-bearing impurities.

The phase transition to rs-AlN could be observed in all cases only when using nanocrystalline AlN powder (<25 nm), while for more coarse powders no rs-AlN was found in the synthesis products. Hence a crystallite-size dependent stabilisation mechanism is proposed. For a better understanding of the transition and stabilisation mechanisms further investigations are necessary.

This work was performed within the Cluster of Excellence 'Structure Design of Novel High-Performance Materials via Atomic Design and Defect Engineering' (ADDE) that is financially supported by the European Union (European regional development fund) and by the Ministry of Science and Art of Saxony (SMWK).

References:

[1] W. Werdecker, F. Aldinger: Aluminum Nitride-An Alternative Ceramic Substrate for High Power Applications in Microcircuits. *IEEE Trans. Compon., Hybrids., Manuf. Technol.* **7** (1984), 399-404 .

[2] I. Gorczyca, N.E. Christensen, P. Perlin, P. I. Grzegory, J. Jun, M. Bockowski: High pressure phase transition in aluminium nitride. *Solid State Commun.* **79** (1991), 1033-1034.

[3] M. Ueno, A. Onodera, O. Shimomura, K. Takemura: X-ray observation of the structural phase transition of aluminum nitride under high pressure. *Phys. Rev. B* ***45*** (1992), 10123-10126.

[4] Q. Xia, H. Xia, A.L. Ruoff: Pressure-induced rocksalt phase of aluminum nitride: A metastable structure at ambient condition. *J. Appl. Phys*. **73** (1993), 8198-8200.

[5] H. Vollstädt, H. Recht: Verfahren zur Herstellung von kubischem Aluminiumnitrid. *Patent DD0000002929O3A5* (1991).

[6] K. Keller, T. Schlothauer, M. Schwarz, G. Heide, E. Kroke: Shock wave synthesis of aluminium nitride with rocksalt structrure. *High Pressure Res.* **32** (2012), 23-29.

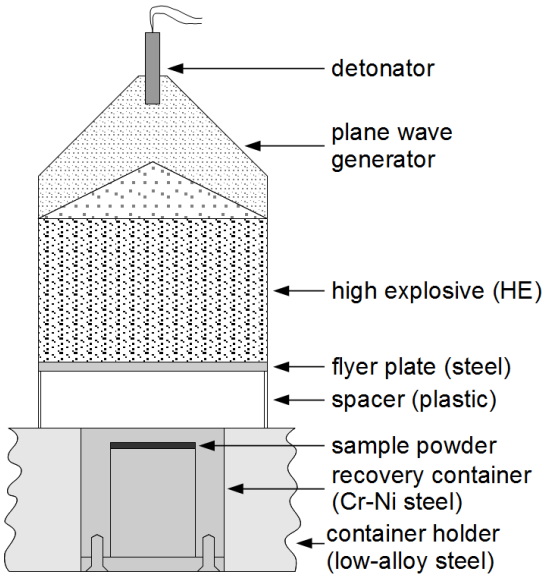

Figure 1: Experimental Set-up for shock wave synthesis with the flyer-plate method.

SINGLE-CRYSTAL ELASTIC PROPERTIES OF $(Mg,Fe)SiO_3$ – PEROVSKITES AT HIGH PRESSURE

***Kurnosov A.*, Trots D.M., Boffa Ballaran T., Frost D.J.**

[1] *Bayerisches Geoinstitut, Universität Bayreuth, Bayreuth, Germany.*
alexander.kurnosov@uni-bayreuth.de

Perovskite structured $MgSiO_3$ is widely accepted to be the dominant phase in the Earth's lower mantle where it coexists with ferropericlase. An understanding of the plausible chemical variation of $MgSiO_3$-perovskite (enrichment with Fe/Al) in addition to the consequent effects on density and elastic properties is important in order to understand the origin of seismic velocity anomalies in the lower mantle reported in a number of studies **[1-3]**.

In this study two differently oriented single-crystals of magnesium silicate perovskite containing 4 mol% of the $Fe^{2+}SiO_3$ component [$(Mg,Fe)SiO_3$] and two single crystals of pure $MgSiO_3$ perovskite have been studied by means of Brillouin spectroscopy and X-ray diffraction in-situ in diamond anvil cells. Helium or neon was used as the pressure transmitting medium and experiments were performed in the pressure range from 2 to 31 GPa for iron-containing samples and from ambient to 15 GPa for iron free perovskite. Ruby pressure markers were used to obtain similar pressure conditions in both diamond anvil cells. The Brillouin spectra were measured in symmetric platelet geometry for each crystal at different orientations in the plane of the platelet. The data at each pressure were fitted for two crystals with similar chemical composition simultaneously in order to reduce correlations of Cij constants. Using the data from two crystals with different non-specific orientations we were able to obtain all 9 independent Cij elastic constants for orthorhombic symmetry at 8 different pressure points for $(Mg,Fe)SiO_3$ and 4 pressure point for $MgSiO_3$. The orientation matrix and cell parameters for each crystal at every pressure point were refined using in-situ x-ray diffraction measurements. From sample densities obtained from x-ray diffraction data and simultaneous measurements of the adiabatic bulk modulus obtained from Brillouin measurements, it was possible to calculate the absolute pressure for all our experimental points. This approach allowed the elastic properties of $(Mg,Fe)SiO_3$-perovskite to be determined as a function of primary pressure, i.e. without resort to a secondary pressure standard. This consequently provides a more reliable data set to be compared with seismic data for the lower mantle. Equations of state and structural evolution for both compositions were determined using synchrotron single crystal x-ray diffraction data up to 75 GPa.

This work was supported by ERC advanced Grant no. 227893 ''DEEP'' funded through the EU 7th Framework Programme.

References:

[**1**] Ni et al., 2005, Geophys. J. Int. 161: 283–294.
[**2**] Masters et al., 2000, AGU Monograph Series, 117: 63–87.
[**3**] Garnero et al., 2005, The Geological Society of America Special Paper, 430: 79–101.

STRUCTURE DEFORMATIONS AT HIGH PRESSURE: FEW EXAMPLES FROM DIFFRACTION EXPERIMENTS AT SIBERIAN SYNCHROTRON RADIATION CENTRE (SSTCR)

Likhacheva A.Yu. [1], ***Seryotkin Yu.V.*** [1,2], ***Manakov A.Yu.*** [3], ***Rashchenko S.V.*** [1,2], ***Litasov K.D.*** [1,2], ***Ancharov A.I.*** [4,5]

[1] *Sobolev Institute of Geology and Mineralogy SibD RAS, Novosibirsk, Russia*
[2] *Novosibirsk State University, Novosibirsk, Russia*
[3] *Nikolaev Institute of Inorganic Chemistry SibD RAS, Novosibirsk, Russia*
[4] *Institute of Solid State Chemistry SibD RAS, Novosibirsk, Russia*
[5] *Budker Institute of Nuclear Physics SiDb RAS, Novosibirsk, Russia*
alih@igm.nsc.ru

Here we report some results of the high-pressure powder diffraction experiments performed at the 4th beamline of the VEPP-3 storage ring of the Siberian Synchrotron Centre using diamond anvil cell. They are mainly focused on the structural variations in microporous silicates driven by the mobility of water as the external fluid compound. Depending on the structure topology, a different response to the high water pressure is observed. The most striking example - the over-hydration effect in fibrous zeolites (scolecite $Ca[Al_2Si_3O_{10}]*3H_2O$, thomsonite $NaCa_2[Al_5Si_5O_{20}]*6H_2O$) with flexible framework; it consists in the framework expansion due to a pressure-induced penetration of additional H_2O molecules into the channels. Unlike fibrous zeolites, large-pore zeolites such as NaA ($Na_{12}[Al_{12}Si_{12}O_{48}]*27H_2O$) do not exhibit appreciable structure deformation upon pressure-induced over-hydration; instead, a decrease of the volume compressibility is observed. The over-hydration was shown to result in a significant increase of the diffusion mobility of H_2O molecules [**1**] and anomalous increase of ionic conductivity in zeolites [**2**], and thereby it provides large opportunities for various applications of this phenomenon.

Apart from zeolites, the pressure-induced excess hydration can be observed in other microporous minerals, for example, in cordierite $(Mg,Fe)_2[Al_4Si_5O_{18}]*n(H_2O,CO_2)$. A distinct decrease of compressibility in the range of 4-5 GPa (Fig.1) is caused by the addition of about 60% of the initial water content into the cordierite channels through a stepwise filling of the H_2O position inside the 6-membered rings. This prevents their contraction and even causes their slight enlargement along *a* direction, apparently related to the orientation of H-bonds. This results in anisotropic deformation of the unit cell and the increase of *a* parameter in the H*P* phase at 4.9 GPa, as well as the decrease of linear compressibility along *a* upon further compression up to 6 GPa.

A counter example of contraction of a framework structure depleted of the H_2O molecules, which prevent the deformation of structure cavities, is given by the phase transition in dehydrated analcime $Na[AlSi_2O_6]*[]$ observed at 0.6 GPa. The migration of a half of cations in empty H_2O positions inside the channels leads to trigonalization of the aluminosilicate framework (Fig.2). The decrease of mean aperture of the structure-forming 6- and 8-membered rings through tetrahedral tilting leads to a 7.5 % volume contraction.

The interest to naphthalene as a model aromatic molecular compound was stimulated by its importance in natural environment (interstellar space, comets and planets) and the lack of the high-pressure structure data at $P > 2$ GPa. The anisotropic compression of naphthalene structure, determined by directional character of intermolecular interactions and asphericity of the $C_{10}H_8$ molecules, is preserved up to 6 GPa. The structure refinements confirm the compression mechanism found previously [**3**], i.e. 'tightening' of the herringbone structural motif, to be preserved on the whole up to 6 GPa. Though no appreciable anomalies in the high-pressure dependences of the unit cell parameters and volume are observed, a small but distinct deviation

from a regular contraction of the intermolecular distances between the herringbone layers was detected at 3 GPa. This is apparently related with spectroscopic and optical anomalies observed previously in naphthalene in the region of 3-4 GPa [**3**].

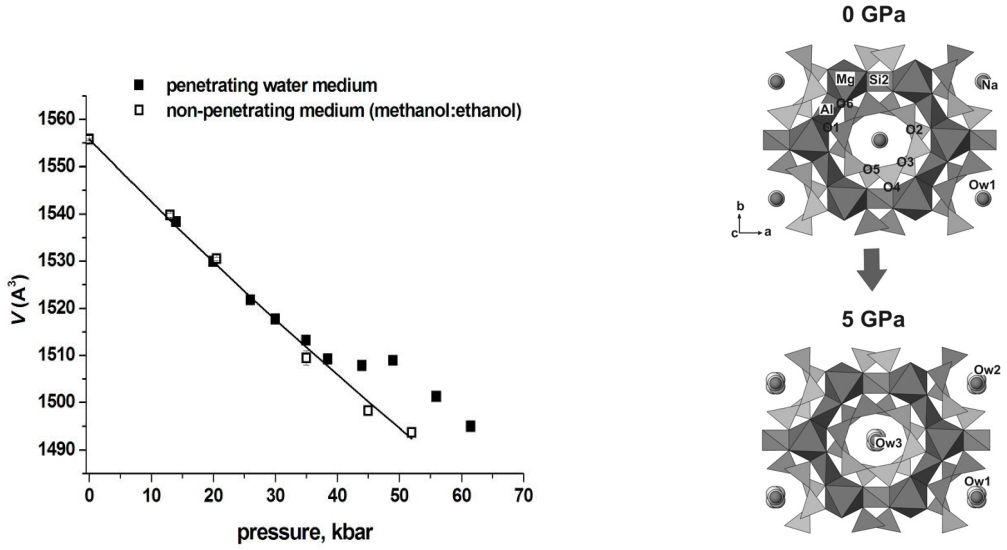

Figure 1. The *V*/*P* curve of cordierite (on the left): the deviation from regular compression is associated with excess hydration of cordierite compressed in water medium. The corresponding structure change is shown on the right.

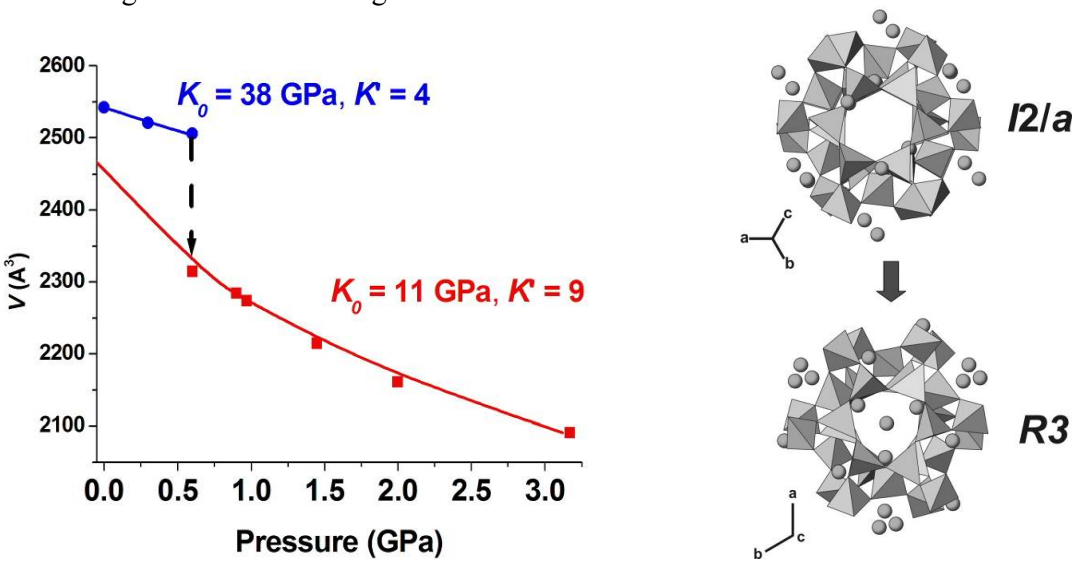

Figure 2. The volume discontinuity on the *V*/*P* curve of dehydrated analcime observed at compression in methanol:ethanol (on the left) and corresponding change of the structure (on the right).

This work is supported by the Ministry of Education and Science of the Russian Federation, and RFBR (grants # 12-05-00841, 13-05-00185). The work was carried out involving the equipment belonging to the SSTRC.

[**1**] Moroz, N.K.; Kholopov, E.V.; Belitsky, I.A.; Fursenko, B.A. (2001) *Micropor. Mesopor. Mater.* **42**, 113-119.
[**2**] Secco, R.A.; Goryainov, S.V.; Huang, Y. (2005**)** *Phys. Stat. Sol. B*. **242**, R73-R75.
[**3**] Fabbiani, F. P. A.; Allan, D. R.; Parsons, S.; Pulham, C. R. (2006) *Acta Cryst*. **B62**, 826–842.

HIGH-TEMPERATURE – HIGH PRESSURE BEHAVIOR OF MOLECULAR CRYSTALS: *IN SITU* SYNCHROTRON DIFFRACTION STUDY OF NAPHTHALENE TO 13 GPA AND 773 K

***Likhacheva A.Yu.*[1], *Rashchenko S.V.*[1,2], *Chanyshev A.D.*[1,2], *Litasov K.D.* [1,2]**

[1]*Sobolev Institute of Geology and Mineralogy SB RAS, Novosibirsk, Russia*
[2]*Novosibirsk State University, Novosibirsk, Russia,*
rashchenko@igm.nsc.ru

At the ambient pressure conditions naphthalene has a large thermal expansion coefficient ($\alpha \sim 10^{-4}$ K^{-1}) **[1]**, however, the thermal contribution to the volume compression at a sufficiently high pressure is unknown. The elastic behavior of solid naphthalene was studied by *in situ* synchrotron powder diffraction up to 13 GPa and 773 K. High-pressure diffraction patterns of solid naphthalene were measured using a membrane diamond anvil cell (EasyLab). Temperatures up to 773 K were obtained by a resistive heating of the cell. Angle-dispersive X-ray diffraction patterns were measured at the 4th beamline of the VEPP-3 storage ring of Siberian Synchrotron and Teraherz Radiation Center (Novosibirsk), with monochromatic beam (λ = 0.3685 Å) and image plate detector **[2]**.

The high-pressure X-ray diffraction data for solid naphthalene show the anisotropic compression to be preserved, on the whole, up to 13 GPa. If V0 is fixed at 361 $Å^3$ the Vinet equation of state (EOS) fitting of the volume data for the pressure range of 0-13 GPa (298 K) gives K_0 = 8.4 (4) GPa and K' = 7.2 (3). Our high-temperature diffraction experiments revealed the nearly zero temperature effect onto the compression behavior of naphthalene at $P \geq 3$ GPa within the temperature range of 298-773 K. Such behavior is apparently a specific feature of the high-pressure behavior of molecular crystals like naphthalene and benzene, and seems to reflect weak intermolecular interactions in their structures. The diffraction experiment shows the initial monoclinic phase of naphthalene with the space group $P2_1/c$ ($P2_1/a$) to be stable up to at least 773 K in the pressure range of 3-15 GPa and to about 20 GPa at 298 K. The data are reasonably consistent with theoretical predictions for EOS of naphthalene in **[3]**.

This work is supported by the Ministry of Education and Science of the Russian Federation, Russian Foundation for Basic Research (grants 12-05-00841 and 12-05-33008) and BP research grant to AC. The work was carried out involving the equipment belonging to the SSTRC.

References:

[1] Franco, O., Reck, G., Orgzall, I., Schulz, B., 2002. Journal of Physics and Chemistry of Solids, 63(10): 1805-1813.
[2] Ancharov, A.I., Manakov, A.Y., Mezentsev, N.A., Tolochko, B.P., Sheromov, M.A., Tsukanov, V.M., 2001. Nuclear Instruments & Methods in Physics Research A, 470(1-2): 80-83.
[3] Inerbaev, T.M., Litasov, K.D., Likhacheva, A.Yu., this volume.
[4] Akella J., Kennedy, G.C., 1970. The Journal of Chemical Physics, 52: 970.
[5] Vaidya, S.N., Kennedy, G.C., 1971. Journal of Chemical Physics 55: 987.

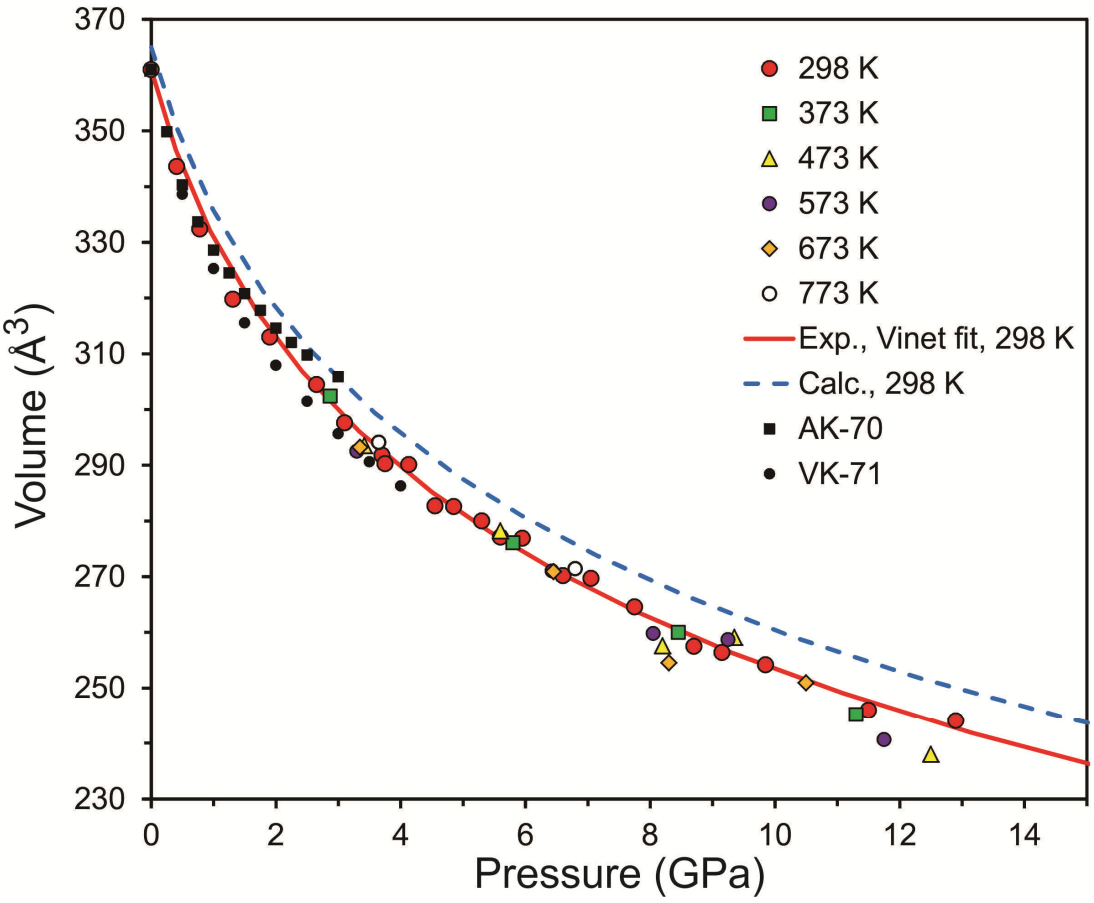

Figure 1. *P-V-T* data for naphthalene measured using in situ X-ray diffraction. Calc – data of the first principles computation **[3]**. Previous data are from AK-70 **[4]** and VK-71 **[5]**.

THERMODYNAMIC ANALYSIS AND CALIBRATION OF Fe-FeO AND Ni-NiO OXYGEN BUFFERS TO 130 GPa

Litasov K.D. [1,2]***, Danilov B.S.*** [3]***, Dorogokupets P.I.*** [3]

[1] *V.S. Sobolev Institute of Geology and Mineralogy SB RAS, Novosibirsk, Russia*
[2] *Novosibirsk State University, Novosibirsk, Russia*
[3] *Institute of the Earth's Crust, SB RAS, Irkutsk, Russia*
klitasov@igm.nsc.ru

The redox state of the Earth's interior is critical parameter for melting, crystallization, material transport, and therefore for global geodynamics. Drastic change of the oxidation state caused by crystal chemistry or compositional changes in the mantle minerals can initiate voluminous magmatism and this effect can be comparable with the addition of volatiles or increasing temperature.

In high pressure and high temperature experimental and natural environments, the oxygen fugacity is frequently characterized via metal-oxide buffers (such as Fe-FeO, Ni-NiO, Re-ReO_2). Therefore, it is important to characterize these buffers at high pressures via equations of state for constituent solid phases and subsequent estimation of fO_2 via relation: x/2 RT ln fO_2 = DG (MO_X) – DG(M), where M is metal and M + x/2O_2 = MOx.

Recently, Campbell et al **[1]** calibrated Fe-FeO and Ni-NiO buffers to pressures of about 100 GPa using simultaneous measurements of oxide and metal in multianvil and diamond anvil experiments. Although useful, this approach has significant source of uncertainty arisen from possible solubility of oxygen and may be other components in the cell in the pure metal and minor impurities can significantly affect its unit cell volume. Besides, metals have high pressure modifications and their thermodynamic properties, such as zero-pressure heat capacity and enthalpy of formation can be poorly determined. Finally, it was not clear which zero-pressure thermodynamics was used for the calibration. The approach of simultaneous thermodynamic analysis of thermochemical, elasticity, high-pressure, and shock compression data proposed in [2,3] is very useful to test new calibrations of metal-metal oxide buffers in **[1]** and create consistent dataset for fO_2 calculation to very high pressures.

In this work we used high-pressure and thermodynamic data from **[1,4-5, etc.]** new thermodynamic analysis for Fe metal EOS **[6]** to constrain fO_2 for Fe-FeO (iron-wustite) and Ni-NiO (NNO) buffers to pressures above 100 GPa. The results of the calculations are presented in Fig.1. The variations in buffer positions are different from that in **[1]** for 1-2 log units at highest pressures (Fig.2). This indicates general reliability of buffer calibrations proposed by Campbell et al. **[1]**. Further improvement may be connected with better specification of Ni EOS at high pressures, which is not yet studied in details.

This work was supported by the Ministry of education and science of Russian Federation, project No 14.B37.21.0457 and RF President Grant No MD-500.2013.5. It is partially supported by IP SB RAS No 97.

References:

[1] Campbell, A.J., Danielson, L., Righter, K., Seagle, C.T., Wang, Y., Prakapenka, V.B., 2009. Earth and Planetary Science Letters, 286: 556-564.
[2] Dorogokupets, P.I., Dewaele, A., 2007. High Pressure Research, 27: 431-446.
[3] Sokolova, T.S., Dorogokupets, P.I., Litasov, K.D., 2013. Russian Geology and Geophysics, 54: 181–199.
[4] Holland, T.J.B., Powell, R., 2011. Journal of Metamorphic Geology, 29: 333-383.

[5] Fischer, R.A., Campbell, A.J., Shofner, G.A., Lord, O.T., Dera, P., Prakapenka, V.B., 2011. Earth and Planetary Science Letters 304: 496-502.
[6] Dorogokupets et al., This volume.

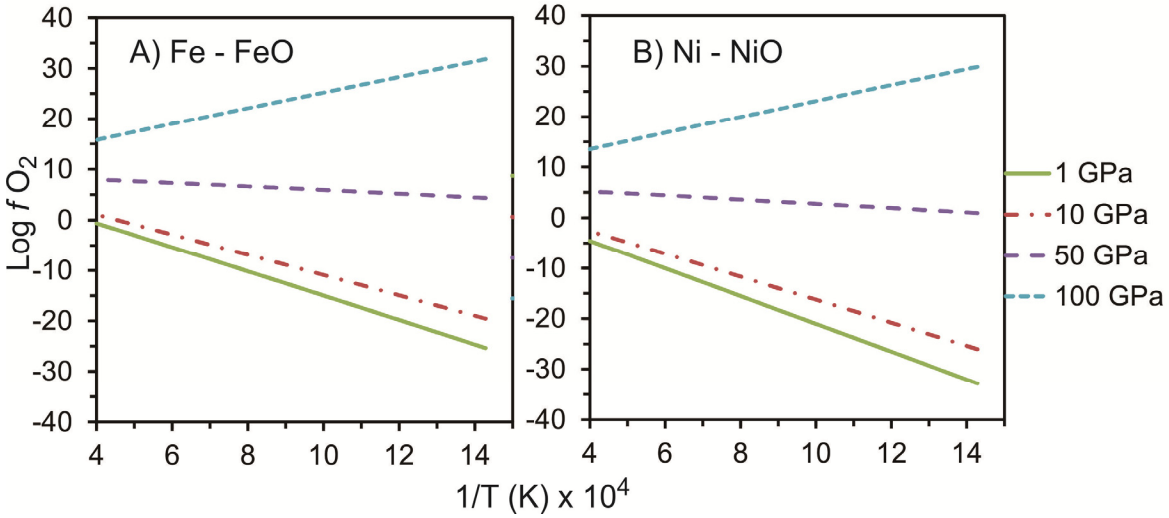

Figure 1. The Fe-FeO (IW) and Ni-NiO (NNO) oxygen buffers at high pressures.

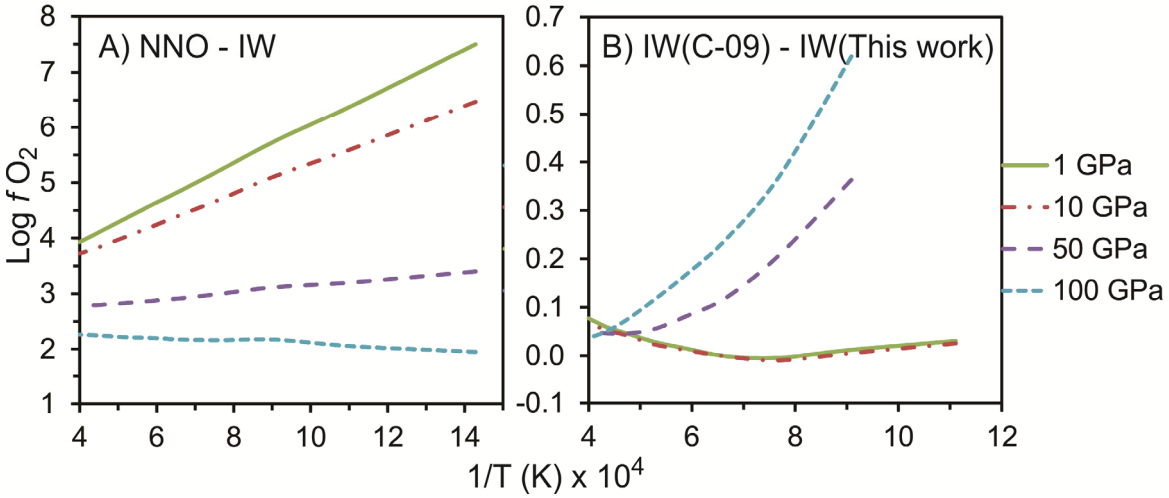

Figure 2. Comparison between IW and NNO buffers in this work (A) and between IW buffers calculated in this work and in Campbell et al. (2009) (C-09).

GEOCHEMISTRY OF MEGACRYSTALLINE PYROPE PERIDOTITES FROM THE UDACHNAYA PIPE, SIBERIAN CRATON

Malkovets V.G., Pokhilenko L.N., Pokhilenko N.P.

V.S. Sobolev Institute of Geology and Mineralogy SB RAS, Novosibirsk, Russia
vladimir.malkovets@gmail.com

Udachnaya kimberlite pipe brought up to the surface very wide range of uniquely fresh mantle xenoliths. One of the most interesting group of xenoliths are megacrystalline pyrope harzburgite-dunite which consist primarily of ultracoarse olivine (up to 10 cm) and subcalcic Cr-pyrope. Some of them may also contain diamond, orthopyroxene and chromite. The chemical composition of their constituent minerals is very similar to the diamond inclusion minerals found in Udachnaya kimberlite. Based on this argumentation it was proposed that harzburgite-dunite xenoliths with high chromium subcalcic pyrope represent fragments of the host rocks of Siberian diamonds **[1-3]**.

In the present communication we describe and discuss the concentrations of rare earth elements (REE), Ti, and Sr determined in individual crystals of sub-calcic pyropes from the new collection of uniquely fresh megacrystalline pyrope harzburgite-dunite xenoliths from Udachnaya pipe.

Pyrope composition vary in a wide range on Cr_2O_3 - CaO plot: Cr_2O_3 1.5-15.1 wt.% and CaO 0.86-7.58 wt.% **[4]**. Based on study of more then 500 peridotitic pyrope inclusions in worldwide kimebrlites Stachel and Harris defined a low-Ti (<0.04 wt.% TiO_2) group which is least undergone by mantle metasomatism processes **[5]**. Harzburgite-dunitic and lherzolitic pyropes from Udachnaya megacrystalline peridotites show a large range in TiO_2 content, up to 0.4 and 1.24 wt.%, respectively. Among them 37 pyropes of harzburgite-dunite pyropes belongs to the low-Ti (<0.04 wt.% TiO_2) group **[4]**.

Trace elements have been determined in pyropes from 25 samples. All the studied pyropes display sinusoidal REE_N patterns. They vary from strongly sinusoidal, typical for harzburgite-dunite pyropes, to mildly sinusoidal or "normal" patterns (positive slope from $LREE_N$ to $MREE_N$ and almost flat from $MREE_N$ to $HREE_N$) typical for lherzolitic pyropes. The most of distribution REE_N patterns for garnets of megacrystalline dunites have the peaks at the LREE and MREE showing increased Ce, Pr, Nd, Sm concentrations.

The core to rim variation of the REE, and Sr have been studied for four pyrope grains from three samples. Five spots across the pyrope grains have been analysed for each grain. All the grains display marked heterogeneities for Sr and $LREE_N$ with gradual core to rim increasing in concentrations. The Sr contents vary from 1 ppm in the core to 8 ppm at the rims without concomitant enrichment in Ca and Ti. The presence of the Sr heterogeneity indicates the relatively young metasomatic event, probably several millions years before the formation of the Udachnaya kimberlite pipe.

The heterogeneous distribution of Sr had been also reported for the sub-calcic pyrope inclusion in peridotitic diamond from the Mir kimberlite pipe, Yakutia **[6]**. The highest Sr content was found at the pyrope rim - 535 ppm relative to around 2 ppm at the core. These authors calculated that the time required to homogenize the 100 micron pyrope inclusion would be less than 7×10^4 yr at 1000^oC.

One of the sample shows striking evidence of the recent interaction with a carbonatitic melt. Orthopyroxene grains are replaced by clinopyroxene along cracks and grain boundaries. The low Ca pyrope (Cr_2O_3 10.33 wt.%; CaO 1.34 wt.%) have a discontinuous rim around 10 micron width of wherlitic composition (Cr_2O_3 11.47 wt.%; CaO 23.77 wt.%). The olivine shows evidence of the newly formed high Fo (96,16) olivine in a thin cracks of big olivine crystals (Fo = 91.96). The formation of the high Fo olivine along the cracks also accompany with the crystallization of djerfisherite sulfide and montichellite. The crystallization of montichellite

indicates the low pressure environment of this reaction. The presence of both djerfisherite and monticheIlite evidence for that this carbonatitic melt was related to the host Udachnaya kimberlite.

Our new data on geochemistry of sub-calcic pyropes from xenoliths of megacrystalline harzburgite-dunites shows significant heterogeneities in trace element composition of all studied pyrope grains. This imply that this rocks experienced relatively recent multiple metasomatic events. The observed mineralogical and geochemical heterogeneities require very careful consideration of any isotope studies for these unique samples.

This work was supported by the Grant of the President of the Russian Federation, project No MK-2689.2013.5 and RFBR (No 12–05–00487, 12–05–33035, 13–05–01051).

References:

[1] Pokhilenko, N.P., Sobolev, N.V., Lavrent'ev Yu.G., 1977. In: Extended Abstracts of the 2nd Intern. Kimberlite Conf. Santa Fe, USA. Ext. Abstr. № 71.

[2] Sobolev, N.V., Pokhilenko, N.P., Efimova, E.S., 1984. Geologiya i Geofizika, 25: 63–80.

[3] Pokhilenko, N.P., Pearson, D.G., Boyd, F.R., Sobolev, N.V., 1991. Annual Report Dir. Geophys. Lab. Carn. Inst. Wahington, USA: 1-18.

[4] Pokhilenko, L.N., Malkovets, V.G., Pokhilenko, N.P., Korolyuk, V.N., Kuzmin D.V., This volume.

[5] Stachel T., Harris, J.W., 2008. Ore Geology Reviews, 34: 5-32.

[6] Shimizu, N, Sobolev, N.V., 1995. Nature, 375: 394-397.

ORTHORHOMBIC, MONOCLINIC, TRICLINIC – SURPRISES ON THE HIGH-PRESSURE CRYSTALLOGRAPHY OF CORDIERITE

Miletich R. [1], ***Scheidl K.*** [1], ***Diego Gatta G.*** [2], ***Effenberger H.*** [1], ***Lotti P.*** [2], ***Merlini M.*** [2,3], ***Schuster B.*** [4], ***Trautmann C.*** [4]

[1] *Institut für Mineralogie und Kristallographie der Universität Wien, Austria*
[2] *Dipartimento di Scienze della Terra, Università degli Studi di Milano, Italy*
[3] *European Synchrotron Radiation Facility ESRF, Grenoble, France*
[4] *GSI Helmholtzzentrum für Schwerionenforschung, Darmstadt, Germany*
ronald.miletich-pawliczek@univie.ac.at

The high-pressure behavior of cordierite, $[(Mg,Fe)_2Al_4Si_5O_{18}](H_2O,CO_2)_n$, was investigated by means of in-situ single-crystal diffraction at high-pressure conditions using diamond-anvil cells. X-ray diffraction (XRD) was carried out to determine precise lattice parameters and to gather information on structural changes and comprise selected samples with different content of volatiles (H_2O, CO_2) but also sample crystals alterated by relativistic heavy ion irradiation (up to $\phi = 5\times10^{13}$ $^{197}Au/cm^2$) [1]. Series of static compression in diamond-anvil cells were conducted with various formally penetrating and non-penetrating pressure media (H_2O, argon, 4:1-methanol-ethanol) in order to determine isothermal equations of state (EOSs) and to track down possible elastic anomalies and structural phase transitions. In addition, the measurement of XRD intensities was used to monitor the structural evolution, in particular changes related to the sites of the intercalated extra-framework molecules inside the structural channels.

The measurement of lattice parameter revealed for naturally un-irradiated cordierite no over-hydration phenomena, while samples being partially dehydrated by irradiation treatment reveal subtle irregularities between 4 and 5 GPa in accordance with [2]. Apart from the accompanying positive volume evolution due to pressure-induced over-hydration, all *P*-*V* data between 1 to 7 GPa suggest an unexpected and anomalous linear volume decrease with d*K*/d*P* around 0 or being even negative for individual axis. Bulk moduli are apparently independent on the type of volatiles as long as the channels are saturated with intercalated CO_2 or H_2O and values of $K_{0,T=298}$ are similar corresponding to 131±1 GPa. Irradiated samples reveal a significantly larger compressibility ($K_0 \approx 115\pm2$ GPa). The compressional behavior of the main axial directions is anisotropic with $\beta_a^{-1} \approx \beta_b^{-1} > \beta_c^{-1}$ for an initial pressure regime up to ~3 GPa. At pressures above ~4 GPa, the compression of the *a* and *b*-axis starts to differ significantly, with the *b*-axis showing elastic softening as indicated by negative values for $\partial(\beta_b^{-1})/\partial P$ ($\partial(\beta_b^{-1})/\partial P = -4.3\pm0.9$, $\partial(\beta_c^{-1})/\partial P = -1.2\pm0.8$).

The observed elastic anomaly clearly indicates the structural instability and reveals the precursor effect of the impending ferroelastic phase transition at pressures around ~6.9 GPa. The transformation could be observed on all samples and appears to be independent on the variations in the amount and nature of the channel population. The transition involves a significant volume discontinuity (-6.9%), which suggests the structural transition to be first order in character and to be similar to that in beryl [3]. Unit cell parameter (*a*=15.566(2), *b*= 9.625(4), *c*= 9.085(5)Å; α= 90.36(4), β= 85.90(2), γ= 89.16(2)°, *V*= 1357.5(1.1)Å^3 at 7.84 GPa) suggest triclinic metrics with a pseudo-monoclinic *C*-centered lattice. Monoclinic pseudo-orthorhombic unit cells with β≈ 90.3°, as initially evidenced for pressurized irradiated crystals and the sample being in the over-hydration regime, could not be verified by the structure investigations. Results of single-crystal XRD investigations will be presented and shed light on the elastic properties, anomalies and the mechanisms of structural transformation from a crystallographic point of view.

References:

[1] Miletich et al. (2010) J. Solid State Chem. 183, 2372-2381
[2] Likhacheva et al. (2013) American Mineralogist 98, 181-186
[3] Prencipe et al. (2011) Phys. Chem. Minerals 38, 223-239.

MICROTEXTURE AND FORMATION MECHANISM OF POLYCRYSTALLINE DIAMOND OBTAINED BY DIRECT CONVERSION FROM GRAPHITE

***Ohfuji H.*[1], *Isobe F.*[1], *Irifune T.*[1], *Sumiya H.*[2]**
[1] *Geodynamics Research Center, Ehime University, Japan*
[2] *Electronics and Materials R&D Laboratories, Sumitomo Electric Industries, LTD, Japan*
ohfuji@sci.ehime-u.ac.jp

High-pressure synthesis of diamond has been extensively studied for several decades and widely applied for various industrial and scientific purposes. A major breakthrough was achieved in 2003 with the synthesis of nano-polycrystalline diamond (NPD) by the direct conversion of graphite under high pressure and temperature **[1, 2]**. It has high optical transparency, ultra-high hardness exceeding that of single crystalline diamond and no anisotropy of hardness (i.e. no cleavages). Due to these excellent properties, NPD has recently been used for various scientific and industrial applications **[3-5]**. The distinct hardness and fracture toughness of NPD are mainly attributed to its unique microtexture composed of a mixture of granular and lamellar crystals. Our recent study demonstrates that the microtexture of NPD is largely dependent on the crystallinity of the graphite starting sources and the unique microtextures (granular and lamellar textures) are derived from the heterogeneity in grain (crystallite) size of the starting graphite **[6]**. The former texture is produced by diffusion-controlled nucleation and growth of nano diamonds, which initiate at lattice defects and crystal surfaces (terminations) of nanocrystalline graphite particles, while the latter is formed as a result of the martensitic transformation of relatively large graphite flakes. A clear correlation between the crystallite size of the initial graphite sources and the grain size of granular nano-diamonds in the NPDs synthesized was also shown. These facts suggest that the average grain size as well as the relative abundance of lamellar crystals in NPD can potentially be controlled by carefully choosing graphite sources based on their crystallinity. Since the hardness and fracture toughness of NPD seem to depend largely on its microtexture **[7]**, our study is an important step to improve those physical properties toward more advanced applications of NPD.

Based on these data, we have been further exploring the synthesis of polycrystalline diamonds with more distinct texture and property from various types of graphite starting materials by using both multianvil and diamond anvil high pressure apparatuses. When using low crystalline carbon sources such as finely-milled graphite, glassy carbon and amorphous carbon, the products consist exclusively of very fine particles (less than 10-30nm) of cubic diamond. In particular, the product synthesized at relatively low temperature (~1400K) shows neither distinctive grain boundaries nor diamond lattice fringes in the (HR)TEM images, indicating that this material lacks long-range order of diamond structure and seems to be amorphous-like. On the other hand, when using highly crystalline graphite the products obtained are composed purely of layered crystals of a mixture of hexagonal and cubic diamonds as a result of martensitic transformation from graphite.

This work was supported by Grant-in Aid for Young Scientists (B) (#20740255) from Ministry of Education, Science and Culture, Japan and also supported partly by Grant-in-Aid for Specially Promoted Research ("2001005, Representative: T. Irifune) from Japan Society for the Promotion of Science.

[1] Irifune T. et al. 2003. Nature. 421. 559-600.
[2] Sumiya H. et al. 2004. Journal of Material Sicences. 39. 445-450.
[3] Kunimoto T., Irifune T. 2010. Journal of Physics: Conference Series. 215. 012190.
[4] Nakamoto Y. et al. 2007. Japanese Journal of Applied Physics. 46. L640-641.
[5] Sumiya H. et al. 2008. Review of Scientific Instruments. 79. 056102.
[6] Ohfuji H. et al. 2012. Physics and Chemistry of Minerals. 39. 543-552.
[7] Sumiya H., Irifune T. 2007. Journal of Materials Research. 22. 2345-2351.

AUROPHILIC INTERACTIONS UNDER HIGH PRESSURE

Paliwoda D.*, *Wawrzyniak P.*, *Katrusiak A.

Department of Materials Chemistry, Faculty of Chemistry, Adam Mickiewicz University, Poznań, Poland

Since 1989, when for the first time the term "aurophilicity" was used, the chemistry of gold-gold interactions have been widely investigated due to the structure-property relations [1]. Several classes of multifunctional materials based on gold containing aggregates were reported recently. Highly luminescent materials with broad light-emitting spectrum can be also used as photochemical sensors. Moreover, strongly pressure-dependent luminescent behavior has been found in gold(I) diethyldithiocarbamate coordination polymer [2].

We have focused our attention on the synthesis and high-pressure structural studies of gold(I) diethyldithiocarbamate coordination polymer, following its spectroscopic studies. Gold(I) diethyldithiocarbamate forms orthorhombic crystals, space group *Fddd*, where the metal ions are connected into infinitive subtly wavy chains. A single orange crystal was glued to the cullet surface in the Diamond Anvil Cell (DAC) and several high-pressure measurements have been performed.

The structural evidence of shortening of gold(I)-gold(I) distances has been found, which to confirms the assumed reduction of HOMO-LUMO energy gap of neighboring gold(I) centers. It was established that the compression mode of aurophilic interactions strongly depends on the molecular and crystal environment.

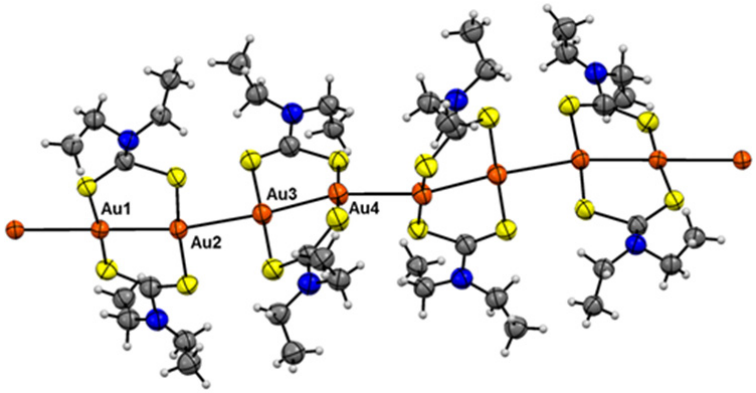

Figure 1. Chain interval of the gold(I) diethyldithiocarbamate coordination polymer.

This study was supported by TEAM Grant 2009-4/6 of the Foundation for Polish Science.

References:
[1] H. Schmidbaur, *Gold Bull.,* **33** (2000) 3-10.
[2] F. Baril-Robert, M. A. Radtke, C. Reber, *J.Phys. Chem C.,* **116** (2011) 2192-2197.

THE CLASSIFICATION OF REACTION RIMS AROUND GARNET OF MEGACRYSTALLINE HARZBURGITE-DUNITE FROM UDACHNAYA KIMBERLITE PIPE (YAKUTIA)

Pokhilenko L.N.

Sobolev Institute of Geology and Mineralogy, SB RAS, Novosibirsk, Russia
lu@igm.nsc.ru

As is well known, kelyphitic rims are a variety of secondary reaction rims around the pyrope grains in the garnet peridotites. They have a concentric-zonal structure and contain a number of minerals with hydroxyl group (amphibole, chlorite, serpentine, phlogopite) besides rhombic pyroxene and spinel; this is evidence that pyrope kelyphitisation has occurred in the melt with elevated amount of volatile components **[1]**. This paper considers the rims of 24 garnets from the fresh xenoliths of megacrystalline harzburgite-dunites. The observed rims were classified into some types.

1. "Usual" kelyphitic rims (rims1) – the rims between garnet and surrounded olivine. The rims thickness varies from the first microns to 400 microns. Gradual or abrupt enlargement of rims minerals in the direction from the garnet grain to the rim periphery is observed in the studied samples. Sodalite, calcite, potash feldspar, magnetite and sulfides (including djerfisherite) have been found in the rims besides typical minerals (opx, spinel, phlogopite and amphibole). We should take note of the frequent presence of high-Al-cpx in the garnet-rims of the most depleted mantle peridotites (17 from 24 samples). As we suppose, its presence or lack depend on the amount of Ca in garnet first of all. Pyroxenes from the rims around the garnets are enriched in alumina as compared to the rock forming pyroxenes (cpx from ga- and ga-sp-lherzolites, opx from 6 megacrystalline harzburgites) resulting in enhanced contents of Ca-Chermakite minal ($CaAl^{VI}Al^{IV}SiO_6$) in the clinopyroxene and Mg-Chermakite minal ($MgAl^{VI}Al^{IV}SiO_6$) in the orthopyroxene. Slight increase of the iron content was observed for clinopyroxenes and considerable one for orthopyroxenes from the rims. Both high alumina content and CaO entering into the orthopyroxene composition point to the high temperature of the formation of these pyroxenes. The compositions of cpx-opx of the garnet rims have been plotted on the scheme Ca in cpx – Ca in opx proposed by G.P. Brey for lherzolite paragenesis **[2]**. The chosen pyroxene pairs are in the high temperature part of the diagram and fall into the wide range of pressures (1-5 GPa). Pyroxenes with close compositions were observed in the areas of deep metasomatic treatment of eclogites **[3]**. Spinelides from the rims demonstrate lesser Cr content and slightly greater iron content as compared to the rock forming spinelides. Amphiboles of pargasite type among the minerals from the rims have been found in three samples under study. The total chemical composition of kelyphitic aggregate corresponds to garnet stoichiometry, but as compared to the garnet the decrease SiO_2, Al_2O_3 content and increase MgO content are observed and K_2O, Na_2O impurities appear.

2. Phlogopite borders of the rims1 (rims2). The continuous or interrupted phlogopite bands (up to 60 μm by thickness) are situated around the rims1 sometimes together with enlarged rims1 minerals of the same name. Phlogopite from the rims1 differs in morphology and composition from that of the rims2. Probably K was repeatedly added into the system. Pyroxenes and spinelides have lesser Al content than these minerals from the rims1, but greater one in comparison with the rock forming pyroxenes and spinelides. A small amount of jadeite in clinopyroxene of rims2 was detected in one sample. Sometimes the calcite aggregates fill the narrow cracks in phlogopite. In fact, the rims2 can be considered as the external part of rims1.

3. Phlogopite-spinel-magnetite rims (rims3) up to 350 μm by thickness are located between the garnet and adjacent kimerlite. They represent the intergrowing pieces of phlogopite, spinelide of variable composition, and possibly calcite and serpentine (in small quantities). Phlogopite dominates in inner zone (near the garnet) and magnetite prevails over others closer to kimberlite.

The rims3 were observed in two studied samples. Perovskite and barium sulfite have been found in the rims besides listed above minerals once.

4. Zonal phlogopite rims (rims4) were observed in two studied samples instead of the rims1+rims2. Thickness of the rims4 is about 60 microns. They present the aggregates of streaky phlogopite with variable composition (variations on MgO-FeO). The high Cr content was noted in every phlogopite kind of rims4 (Cr_2O_3 8-12 wt.%, when Cr_2O_3 in ga 9.8 wt.%).

5. «Pockets» into the garnets near the rims1 (rims5) have been noted in two samples. They have hemisphere shape and size about 20x10 microns. They are cryptocrystalline intergrowing pieces of phlogopite, calcite and chromespinelide.

Conclusions. The rims around the garnets of megacrystalline peridotites form as a result of heating with the active participation of deep fluids of wide range of compositions. Such transformation is a feature not only of ultrabasic garnets, but of basic ones as well. The variety of rim types suggests that the formation of rims is often a multi-stage and multivendor process. The mineral composition of the rims is defined not only by garnet composition but by the quality of the acting fluid. The time during which the rock experiences aggressive action before the removal to the surface is also an important factor. The presence of initial water in the rock also plays an important role. All types of the megacrystalline garnet rims contain the phlogopite with wide compositional variations. It is supposed that phlogopite is the main water-containing mineral for the garnet rims of given paragenesis. Amphibol, chlorite and serpentine occur far more frequently. Last two of them fill the cracks normally. Garnet kelyphitisation – reaction at the garnet-olivine boundary – ga+ol→sp+2px – varies in several cases. Thus alkaline water phases – phlogopite and amphibole form instead of pyroxenes (+rare phlogopite) at high fluid concentrations; calcite forms with the addition of CaO.

The work is supported by the RFBR grant 12-05-01043.

References:

[1] Geological dictionary, M: “Nedra”, 1978.

[2] Brey G.P. Fictive conductive geotherms beneath the Kaap-vaal craton. In: 5th Int Kimberlite Conf Brazil Ex- tended Abstr. CPRM Spec Publ 2/91. Brasilia. 1991. P. 23-25.

[3] Pokhilenko L.N., Agashev A.M. Classification peculiarities of mantle eclogites from Udachnaya-East pipe (Yakutia) (abstract). In: 30th International Conference on Ore potential of Alkaline, Kimberlite and Carbonatite Magmatism. Hurghada. Egypt. 7 – 13 September 2013.

NEW DATA ON MINERALOGY OF MEGACRYSTALLINE PERIDOTITES FROM THE UDACHNAYA PIPE, SIBERIAN CRATON

***Pokhilenko L.N.*, Malkovets V.G., Pokhilenko N.P., KorolyukV.N., Kuzmin D.V.**

V.S. Sobolev Institute of Geology and Mineralogy SB RAS, Novosibirsk, Russia
lu@igm.nsc.ru

Udachnaya kimberlite pipe brought up to the surface very wide range of uniquely fresh mantle xenoliths. Diamond inclusions from individual kimberlite field or province tend to be dominated by either peridotitic or mafic (eclogitic or websteritic) parageneses. Intensive studies of diamond inclusions mineralogy in Siberian kimberlites define host rock ranging from highly depleted (harzburgitic) to relatively fertile (lherzolitic), but most populations are overwhelmingly harzburgitic. The key minerals of this paragenesis are Al-poor chromite, subcalcic Cr-pyrope, magnesian olivine and enstatite. Several previous investigations have identified harzburgite-dunite xenoliths with high chromium subcalcic pyrope which are believed to be fragments of the host rocks of Siberian diamonds. Subcalcic pyrope and Al-poor chromite are commonly regarded as the most reliable indicator minerals in diamond exploration.

Here we present the results of the mineralogical study of the new collection of 99 uniquely fresh megacrystalline pyrope harzburgite-dunite xenoliths from Udachnaya pipe. These rocks consist primarily of ultracoarse olivine (up to 10 cm) and subcalcic Cr-pyrope. Ten of them contain orthopyroxene, eight Al-poor chromite, and four emerald-green clinopyroxene.

Pyropes in the megacrystalline peridotites can be assigned to three parageneses based on their CaO and Cr_2O_3 contents: harzburgite-dunite (n=78), lherzolitic (n=20) and wherlitic (n=1). Pyrope composition vary in a wide range on Cr_2O_3 - CaO plot: Cr_2O_3 1.5-15.1 wt.% and CaO 0.86-7.58 wt.%. The Cr_2O_3, CaO, and TiO_2 contents in wherlitic pyrope are 5.8, 16.5 and 0.24 wt.% accordingly. Based on the study of more than 500 peridotitic pyrope inclusions in worldwide kimberlites Stachel and Harris (2008) defined a low-Ti (<0.04 wt.% TiO_2) group which is the least undergone by mantle metasomatism processes. Harzburgite-dunitic and lherzolitic pyropes from Udachnaya megacrystalline peridotites show a wide range in TiO_2 content, up to 0.4 and 1.24 wt.%, respectively (Fig. 1b). Among them 37 samples of harzburgite-dunite pyropes belong to the low-Ti (<0.04 wt.% TiO_2) group.

Most olivines in the megacrystalline peridotites have Fo content in the range 90.4 - 94.1 (n=99; average 92.67, median 92.74). The average Fo content of olivines in equilibrium with pyrope of harzburgite-dunite paragenesis is 92.82 (n=78), lherzolitic paragenesis - 92.2 (n=20), wherlitic paragenesis - 90.87 (n=1). The contents of trace elements in olivines of megacrystalline peridotites vary within the following ranges (wt.%): NiO 0.365-0.398, CaO 0.004-0.05, MnO 0.07-0.107, Cr_2O_3 0.005-0.077, TiO_2 0-0.012. The correlation between Ca, Cr and Fo content is shown in Fig. 1 a,b.

The chromites are rich in Cr_2O_3 63.2-65.8 wt.% and poor in Al_2O_3 4.4-5.6 wt.%, TiO_2 0.04-0.29 wt.% and $Fe^{3+}/(Fe^{3+}+Cr+Al)$ ratio (Fig 1 d, e and f).

Our new data on mineralogy of megacrystalline peridotites indicates the similarity of their chemical composition to the diamond inclusion minerals from the Udachnaya pipe.

High Cr_2O_3 and Mg# and low TiO_2, CaO in pyropes, TiO_2 and $Fe^{3+}/(Fe^{3+}+Cr+Al)$ ratio in chromites indicate that at least 50% of our samples do not show any indications of metasomatic modification of these rocks. Thus, the studied megacrystalline peridotites provide us unique information about the nature of the Archean lithospheric mantle of the Siberian craton. Unlike the tiny diamond inclusion minerals and single subcalcic pyropes from heavy concentrate, the megacrystalline peridotites provide us enough material for all kind of geochemical and isotopic studies.

This work was supported by the Grant of the President of the Russian Federation, project No MK-2689.2013.5 and RFBR (No 12–05–00487, 12–05–33035, 13–05–01051).

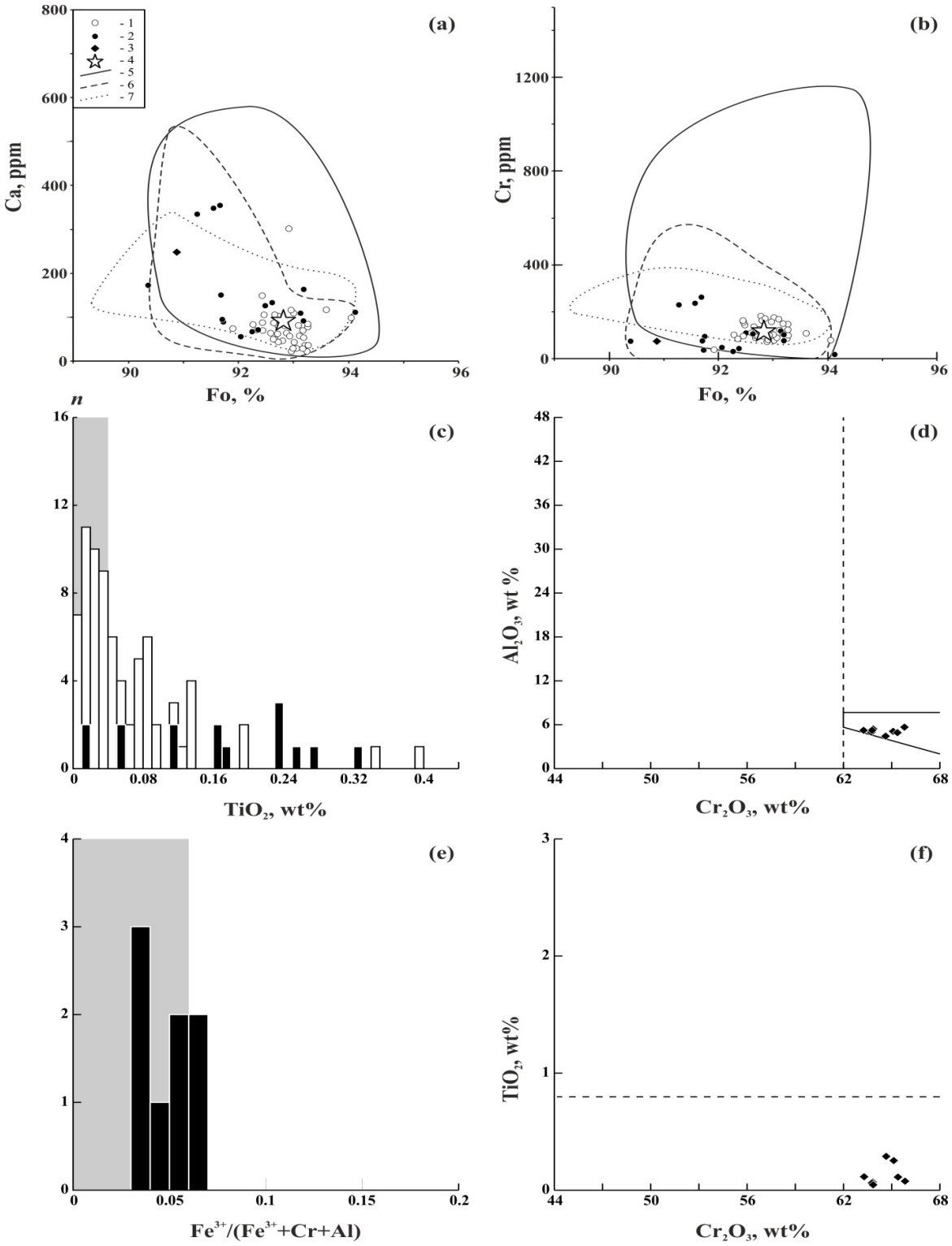
(a)
1
2
3
4
5
6
7
Ca, ppm
Fo, %
(b)
Cr, ppm
Fo, %
(c)
n
TiO2, wt%
(d)
Al2O3, wt %
Cr2O3, wt%
(e)
Fe3+/(Fe3++Cr+Al)
(f)
TiO2, wt%
Cr2O3, wt%

INCLUSIONS OF CRICHTONITE SERIES MINERALS IN PERIDOTITIC PYROPES FROM THE INTERNATIONALNAYA KIMBERLITE PIPE, YAKUTIA

***Rezvukhin D.I.*[1], *Malkovets V.G.*[2], *Kuzmin D.V.*[1], *Gibsher A.A.*[2], *Litasov K.D.*[1]**

[1]*V.S. Sobolev Institute of Geology and Mineralogy, Novosibirsk, Russia.*
[2]*Institute for the Studies of the Earth's Interior, Okayama University, Tottori, Japan*
fendstrat@mail.ru

Crichtonite series minerals (later – CSM) have rather complicated composition and structure. The general formula for the group is $AM_{21}O_{38}$, where site A takes cations with a large radius (Sr, Pb, REE, U, Ca, Na, K, Ba), and site M takes smaller cations (Ti, Fe, Cr, Al, Zr, Mg). The name of the mineral is defined by the dominant cation in A position: Sr for crichtonite, Ca - loverengite, Na - landauite, Pb - senaite, REE - davidite, Ba - lindsleyite, K – mathiasite **[1], [2], [3], [4].** This work aims to provide detailed information about mineralogical and compositional features of CSM as inclusions in pyropes from heavy mineral concentrate of the Internationalnaya kimberlite pype.

These inclusions are commonly presented as elongated, needle or blade-like structures with rounded or polygonal cross-section, sometimes laths and tablets. Typical diameter of needle cross-section ranges from 1 to 30 microns, although significantly larger inclusions are observed in sample INT-15. All inclusions are commonly black and opaque, even in thin sections. Needles of CSM often define a regular spatial arrangement in pyrope matrix in association with rutile. Such inclusions probably result from garnet exsolution, although complicated composition of these minerals must be a restrictive factor for such type of formation.

CSM have been revealed in peridotitic pyropes with Cr_2O_3 content ranging from 1 to 6 wt.%. The compositions of CSM are uniform in a single pyrope host, but variable among different pyrope crystals. Content of TiO_2 varies from ~53 to ~70 wt.%., Cr_2O_3 – from 6,5 to 19,2 wt.%. Cations in A position are dominantly Ba, Sr, La, Ce and Ca, but their content varies:

Ba (0,0 – 5,2 wt.%) – lindsleyite;
Sr (0,4 - 3,0 wt.%) – crichtonite;
La + Ce (0,4 - 2,9 wt.%) – davidite;
Ca (0,5 - 2,3 wt.%) – loveringite;

Despite of these variations, all analyzed minerals form probably one compositional trend that is lindsleyite – crichtonite – davidite – loveringite solid solution (Fig. 1). Such compositions correspond with analyzed CSM as inclusions in pyropes of Garnet Ridge **[5]**, but differ in terms of A cation position from CSM of metasomatic mantle associations **[e.g. 4]**, where CSM are commonly more alkali-rich, being presented as LIMA series (lindsleyite – mathiasite, Ba and K members, respectively).

Electron microprobe analyses of 44 inclusions give the following average formulae:

A = $Ba_{0,14}\ Sr_{0,23}\ Ca_{0,37}\ K_{0,05}\ Na_{0,14}\ REE_{0,16}$

B = $Ti_{13,89}\ Cr_{3,15}\ Al_{0,60}\ Zr_{0,32}\ Fe_{0,95}\ Mg_{1,77}\ V_{0,05}\ Mn_{0,04}\ Ni_{0,01}$

The distinctive feature of the CSM group is enrichment in incompatible and rare elements. In case of analyzed inclusions, members of LILE (Ba and Sr), HFSE (Zr, Ti) and REE (La, Ce) are revealed. The most incompatible are light ion lithophile elements (LILE).

CSM commonly originate during late stage of fluid-melt evolution, when crystallization phase is enriched in incompatible elements **[e.g. 6]**. Furthermore, CSM in mantle rocks reflect mantle metasormatism, with the metasomatic environment enriched in incompatible elements and volatiles **[e.g. 4, 7, 8]**. Thus, CSM are important storage site for rare elements in the upper mantle. The presence of such uncommon minerals as inclusions in pyrope strongly supports an assumption that pyrope crystallization in the lithoshperic mantle may occur from metasomatic fluid-melt phase.

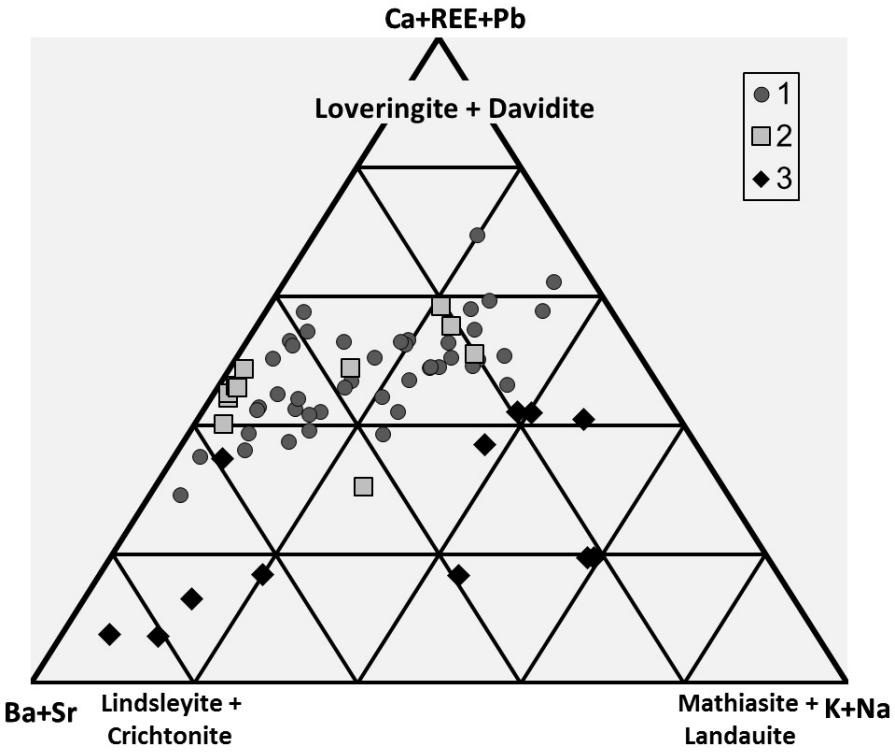

Figure 1. A recombined expression of CSM on the triangle diagram. 1 – CSM as inclusions in pyropes from kimberlite pipe Internationalnaya, 2 – CSM as inclusions in pyropes from Garnet Ridge [5], 3 – CSM from metasomatized peridotites and heavy mineral concentrate of South Africa kimberlites [4].

This work was supported by the Grant of the President of the Russian Federation, project No MK-2689.2013.5, Ministry of education and science of the Russian Federation, project No 14.B25.31.0032 and RFBR (No 12-05-31411, 12–05–00487, 12–05–33035, 13–05–01051).

References:

[1] Rouse RC, Peacor DR. The relationship between senaite, magnetoplumbite and davidite. // 1968. Am Mineral. Vol. 53. P 869-879

[2] Grey IE, Lloyd DJ, White JJS. The crystal structure of crichtonite and its relationship to senaite. // 1976. Am Mineral. Vol 61. P. 1203-1212

[3] Gatehouse BM, Grey IE, Campbell IH, Kelly P The crystal structure of loveringite - a new member of the crichtonite group // 1978. Am Mineral. Vol. 63. P. 28-36

[4] Haggerty SE, Smyth JR, Erlank AJ, Rickard RS, Danchin RV. Lindsleyite (Ba) and mathiasite (K): two new chromium titanates in the crichtonite series from the upper mantle // 1983. Am Mineral. Vol. 68, P. 494-505.

[5] Liping Wang, Essene EJ, Youxue Zhang. Mineral inclusions in pyrope crystals from Garnet Ridge, Arizona, USA: implications for processes in the upper mantle // 1999. Contrib Mineral Petrol. Vol. 135, p. 164-178.

[6] Lorand J-P, Cottin J-Y, Parodi GC. Occurrence and petrological significance of loveringite in the western Laouni layered complex, southern Hoggar, Algeria // 1987. Can Mineral 25: 683-693.

[7] Jones AP, Smith JV, Dawson JB. Mantle metasomatism in 14 veined peridotites from Bultfontein mine, South Africa // 1982. J Geol 90: 435-453.

[8] Haggerty SE. Oxide mineralogy of the upper mantle // 1991. In: Lindsley DH, Ribbe HP (eds) Oxide minerals: petrological and magnetic significance. (Reviews in Mineralogy, 25) Mineral Soc Am, Washington, DC, pp 355-416.

RUTILE INCLUSIONS IN KIMBERLITIC GARNETS OF SIBERIAN PLATFORM: MINERALOGY AND GENESIS

***Rezvukhin D.I.*[1], *Malkovets V.G.*[2], *Kuzmin D.V.*[1], *Gibsher A.A.*[2], *Litasov K.D.*[1]**

[1]*V.S. Sobolev Institute of Geology and Mineralogy, Novosibirsk, Russia*
[2]*Institute for the Studies of the Earth's Interior, Okayama University, Misasa, Tottori, Japan*
fendstrat@mail.ru

Rutile (TiO_2) is the most common naturally occurring titanium dioxide polymorph and is widely distributed as an accessory mineral in metamorphic rocks, but is also present in igneous rocks and mantle xenoliths. Rutile is a major host mineral for Nb, Ta and other HFSE, which are widely used as geochemical indicators of geological processes such as magma evolution and subduction-zone metamorphism. The investigation of rutiles in garnets of crustal and mantle origin is of particular importance because of direct chemical and genetic connection between inclusion and a host, and it is possible to compare compositional features of coexisting minerals, which is the key to reveal the genesis of pyrope in the lithospheric mantle. This work aims to provide detailed information about mineralogical and compositional features of rutiles as inclusions in garnets from heavy mineral concentrate of Internationalnaya and Mayskaya pipes, Yakutia.

Rutile is probably the most abundant type of inclusions in pyropes from the Internationalnaya pipe. It is commonly presented as elongated, needle or blade-like structures with rounded or polygonal cross-section, sometimes laths and tablets. The diameter of cross-section ranges from 1 to ~80 microns; length of needles is commonly hundreds of microns. Color ranges from orange (thin needles) to brown and black (thick inclusions), small inclusions are usually transparent. Needles of rutile (with CPX, apatite, minerals of crichtonite series) often define a regular spatial arrangement in pyrope matrix; the angle between crossing needles is ~ 71 degrees. It is believed, that such inclusions result of garnet exsolution **[1]**.

Rutile inclusions have been revealed in pyropes of peridotitic and eclogitic parageneses from the Internationalnaya pipe. The compositions of rutile are uniform in a single pyrope host, but variable among different pyrope crystals. These rutiles have been compared with rutiles from heavy mineral concentrate of this pipe, as well as with rutiles as inclusions in crustal garnets from the Mayskaya pipe. Compositional features of rutile vary among these groups (Fig. 1). Rutiles from peridotitic pyropes are often enriched in impurities, such as Cr and HFSE (Nb, Ta, Zr). Content of TiO_2 in such rutiles ranges from 71,6 to 98,2 wt. %, Nb_2O_5 - from 0 to 15,6 wt.%, Cr_2O_3 - from 0,6 to 9,7 мас. %. It is interesting to note two peridotitic samples: INT-5 and INT-335. Rutiles in pyrope INT-5 are strongly enriched in Cr, Nb and Ta - content of both Cr_2O_3 and Nb_2O_5 is up to 9,5 wt.%, while HFSE-sum Nb_2O_5+ Ta_2O_5 + ZrO_2 is equal to ~12 wt.%. Another example of uncommon composition is one rutile grain in pyrope INT-335. It is inhomogeneous from core towards rim, and the rim contains the highest amount of Nb_2O_5 among all analysed rutile inclusions – 15,6 wt.%. Contrary to inclusions in mantle pyropes, rutiles from crustal garnets of the Mayskaya pipe contain little amount of impurities (TiO_2 - from 96,3 to 99,3 wt. %, Nb_2O_5 – up to 0,3 wt. %, Cr_2O_3 – up to 0,4 wt.%). The same is true for rutiles from eclogitic garnets (Internationalnaya pipe), although eclogitic rutiles may contain significant amounts of Nb and other HFSE **[2]**. Analyzed rutiles from heavy mineral concentrate of Internationalnaya pipe tend to fairly clean composition, although several grains are Cr- and Nb-rich.

There is a relationship between Cr_2O_3 content in pyrope and in inclusion, and the positive trend is observed (Fig. 2). It is suggested that pyrope and rutile inclusions are in equilibrium in terms of Cr.

The problem of inclusion and pyrope genesis is the most difficult to solve. Regularly oriented thin rutile needles are believed to form as a result of exsolution processes. As for thick

rutiles, often enriched in impurities, we assume that their formation appeared simultaneously with pyrope from fluid-melt phase, enriched in incompatible elements. However, it is not possible to determine the actual origin of rutile grains, which possess features of both exsolution and metasomatic enrichment, as well as the origin of single thin needles without arrangement. However, inclusions of rutile in pyrope are not uncommon, and their presence is of particular interest. According to modern ideas, rutile does not occur in rocks of peridotitic paragenesis, so its presence in the form of inclusions in pyrope can serve as additional confirmation of the metasomatic origin of at least some pyropes in the lithospheric mantle.

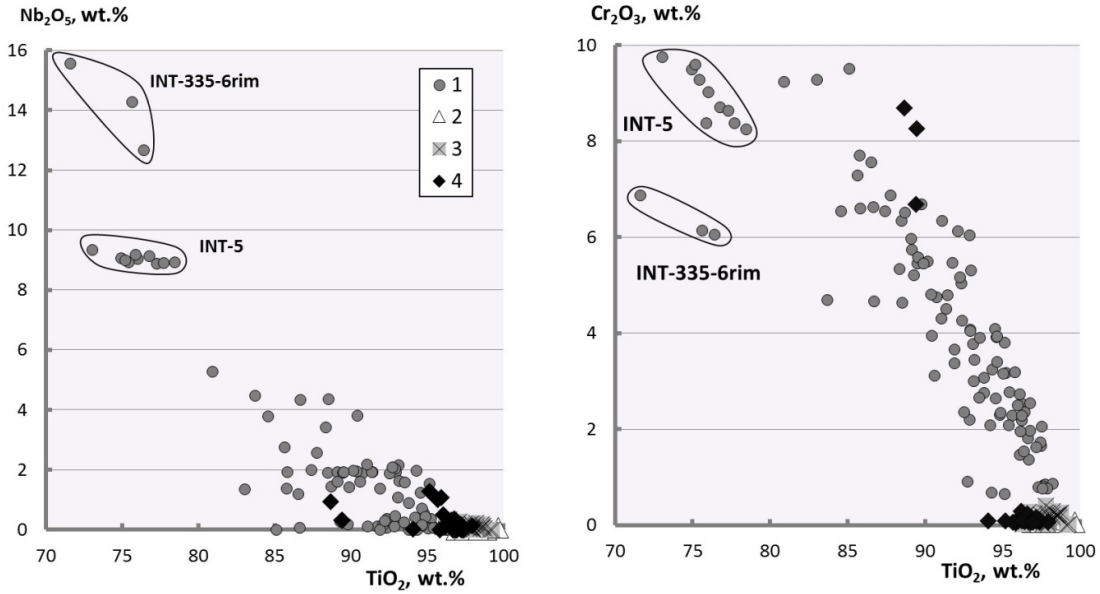

Figure 1. TiO_2 versus Nb_2O_5 (wt.%, left) and TiO_2 versus Cr_2O_3 (wt.%, right) for rutiles from kimberlitic pipes. 1 - rutile inclusions in peridotitic pyropes of the Internationalnaya pipe, 2 - rutile inclusions in eclogitic pyropes of the Internationalnaya pipe, 3 - rutile inclusions in crustal garnets of the Mayskaya pipe, 4 - rutile grains from heavy mineral concentrate of the Internationalnaya pipe

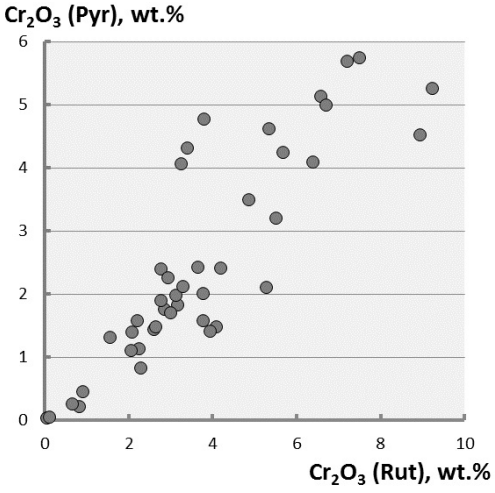

Figure 2. Cr_2O_3 (wt.%, rutile inclusion) versus Cr_2O_3 (wt.%, pyrope host) for samples from kimberlite pipe Internationalanaya. For several inclusions inside a host, the average content of Cr_2O_3 has been taken.

This work was supported by the Grant of the President of the Russian Federation, project No MK-2689.2013.5, Ministry of education and science of the Russian Federation, project No 14.B25.31.0032 and RFBR (No 12-05-31411, 12–05–00487, 12–05–33035, 13–05–01051).

References:

[1] Liping Wang, Essene EJ, Youxue Zhang. 1999. Contrib Mineral Petrol. Vol. 135, p. 164-178.
[2] Rudnick RL, Barth M, Horn I, McDonough WF. 2000. Science. Vol. 287, P. 278–281.

TRANSITION BETWEEN CARBONATE AND SILICATE MELTS IN THE SYSTEM PYROLITE-$CaCO_3$-KCl-NaCl AT 2-6 GPa

Safonov O.G.

Institute of Experimental Mineralogy, RAS, Chernogolovka, Moscow district, Russia
oleg@iem.ac.ru

Carbonate-bearing peridotites in the upper mantle are considered as a possible source for diversity of magmas, whose compositions vary from basaltic through silica-undersaturated nephelinitic and melilititic (including ultrapotassic kamafugites) to kimberlitic **[1-3]**. The major reasons for such wide variability of compositions of the melts appearing at partial melting of the carbonate-bearing peridotites are relations between decarbonation reactions with the peridotite-CO_2 solidi **[1]**, as well as influence of the volatile components (H_2O, F, Cl, P_2O_5) and alkalis. These components stabilize the near-solidus carbonate melts to lower temperatures and, thus, extend the intervals for transitions between carbonatite and silicate melts. Some of these components, for example KCl and NaCl, are able to form carbonate-salt liquids immiscible with both silicate and carbonate-silicate melts **[4, 5]**. The trends of gradual transitions between carbonatite and carbonate-silicate melts in the peridotite-carbonate-chloride systems at 5.5 GPa **[6]** allowed modeling of relations between chloride-bearing carbonatite melts preserved in the kimberlitic minerals (including diamonds) with kimberlites themselves. In order to investigate the influence of chlorides on the carbonate-silicate melt transitions at lower pressures, the experiments on melting of the model pyrolite MPY90 in presence of $CaCO_3$, KCl, NaCl at pressures 2, 4 and 6 GPa were performed. The composition of the starting model pyrolite (wt. %): SiO_2 – 44.74, TiO_2 – 0.17, Al_2O_3 – 4.37, Cr_2O_3 – 0.45, FeO – 7.55, MnO – 0.11, MgO – 38.57, CaO – 3.38, Na_2O – 0.4, NiO – 0.26. The experiments were performed for the mixture of 80 wt. % MPY90 and 20 wt. % $CaCO_3$+KCl+NaCl (2:1:1 by weight). The experiments were conducted using ½-inch piston-cylinder apparatus at the Research School on Earth Sciences at the Australian National University (Canberra, Australia).

A chloride-carbonate melt (L_{CC}) containing less than 10 wt. % SiO_2 was found to be stable at temperatures below 1000^OC. At 2 GPa, it coexists with *Ol*+*Cpx*+*Phl* (up to ~1100^OC) and *Ol*+*Cpx*+*Opx* (up to 1230^OC), whereas garnet joins these assemblages at 4 and 6 ГПа. Up to temperatures1250, 1370^OC and 1470^OC at 2, 4 and 6 GPa, respectively, phase relations are regulated by an equilibrium $Opx + L_{CC} = Cpx + Ol + CO_2$, which results in gradual dissolution of orthopyroxene. Above these temperatures, a carbonate-silicate melt (L_{CS}) with 35-37 wt. % SiO_2 immiscible with the chloride-carbonate liquid appears. Its formation within the temperature step of the experiments at 4 and 6 ГПа coincides with disappearance of orthopyroxene via reaction: $Opx + L_{CC} = Cpx + Ol + L_{CS}$. However, at 2 GPa orthopyroxene disappears before the incipience of L_{CS}, while L_{CC} becomes enriched in SiO_2. At higher temperatures, the assemblages $Ol+Cpx+L_{CC}+L_{CS}$ (2 GPa) and $Ol+Cpx+Grt+L_{CC}+L_{CS}$ (4 and 6 GPa) form, while olivine coexists with two liquids at liquidus of the system.

The SiO_2 content in the carbonate-silicate melts in the system pyrolite-$CaCO_3$-KCl-NaCl vary with temperature from 35-37 wt. % to 40-44 wt. %. The melts at 2 GPa are richer in SiO_2, but contains lower concentrations of K_2O+Na_2O (5-8 wt. %) and Cl (2.5-4.5 wt. %) in comparison to the melts produced at 4 GPa (7-9 wt. % K_2O+Na_2O, 4-8 wt. % Cl). The melts at 2 GPa show $K_2O/Na_2O < 1.0$, whereas this ratio in the melts at 4 GPa is 1.0-1.5. All melts are characterized by high CaO contents (11-15 wt. %), while the MgO content varies from 8 to 20 wt. % and directly depends on the degree of melting of the utrabasic constituents.

Thus, the transition of the carbonate-chloride melt to the carbonate-silicate melt in the system pyrolite-$CaCO_3$-KCl-NaCl at 2-6 GPa proceeds within the very narrow temperature interval ($<20^OC$). Comparison of the present data with the data on the chloride-free system peridotite KLB+CO_2 **[7]** indicates that chlorides notably affect both absolute temperatures and

temperature intervals of the transition from the carbonatite melt to the silicate melt. The transition is controlled by reactions of L_{CC} with orthopyroxene, which totally disappears as the carbonate-silicate melt forms. This indicates a principal role of orthopyroxene in formation and evolution of alkalic carbonate-bearing melts in the upper mantle. The important factor of the abrupt transition from the chloride-carbonate to the carbonate-silicate melt is liquid immiscibility, which results in a partial extraction of the carbonate constituent from the carbonate-silicate melt to the coexisting chloride-carbonate liquid. Compositions of the carbonate-silicate melts from the present experiments closely fit to compositions of kamafugites. The melts forming at 2 GPa show closer similarity to kamafugites, while the melts appearing at 4 and 6 GPa are more carbonate, chlorine and alkali-rich. The experiments support the model for formation of ultra-alkalic magmas via interaction of peridotites with the carbonate-salt liquids. The abrupt transition between the carbonate-chloride and silicate melts models a common bimodality of associations of carbonatites with alkalic magmas and substantiate a role of the liquid immiscibility in the formation of the carbonatite-kamafugite complexes.

The study is supported by the Russian Foundation for Basic Research (13-05-00353) and President Grant for Young Scientists (MD-222.2012.5).

References:

[1] Wyllie P.J., Huang W.L. Peridotite, kimberlite, and carbonatite explained in the system CaO-MgO-SiO_2-CO_2. Geology. 1975. V. 3, P. 621-624.

[2] Gudfinnsson G.H., Presnall D.C. Continuous gradation among primary carbonatitic, kimberlitic, melilititic, basaltic, picritic, and komatiitic melts in equilibrium with garnet lherzolite at 3-8 GPa. J. Petrol. 2005. V. 46. P. 1645-1659.

[3] Dasgupta R., Hirschmann M.M., Smith N.D. Partial melting experiments of peridotite+CO_2 at 3 GPa and genesis of alkali ocean island baslts. J. Petrol. 2007. V. 48. P. 2093-2124.

[4] Safonov O.G., Perchuk L.L., Litvin Yu.A. Melting relations in the chloride-carbonate-silicate systems at high-pressure and the model for formation of alkalic diamond-forming liquids in the upper mantle. Earth Planet Sci. Lett. 2007. V. 123. P. 112-128.

[5] Safonov O.G., Chertkova N.V., Perchuk L.L., Litvin Yu.A. Experimental model for alkalic chloride-rich liquids in the upper mantle. Lithos. 2009. V. 12S. P. 260-273.

[6] Safonov O.G., Kamenetsky V.S., Perchuk L.L. Links between carbonatite and kimberlite melts in chloride-carbonate-silicate systems: experiments and application to natural assemblages J. Petrol. 2011. V. 52. P. 1307-1331.

[7] Moore K.R., Wood B.J. The transition from carbonate to silicate melts in the CaO-MgO-SiO_2-CO_2 system. J. Petrol. 1998. V. 39. P. 1943-1951.

INFRARED SPECTROSCOPY ON SHOCK-WAVE SYNTHESIZED γ-$Si_3(N,O)_4$

Schlothauer T., Heide G.

TU Bergakademie Freiberg, Institute of Mineralogy, Freiberg and
Freiberg High Pressure Research Centre (FHP), Freiberg, Germany
thomas.schlothauer@mineral.tu-freiberg.de

The high-pressure phase of siliconnitride was first discovered in 1999 with static methods **[1]** and shows a high hardness and an excellent thermal stability up to 1230 K **[2]**. This interesting material was also synthesized with shock-wave methods with the impedance method (e.g. **[3]**) where the samples were leached with HNO_3 and purified with HF after experiment. Despite this chemical treatment is well estabilshed **[4]** the consequences for the high-pressure phases (HP-phases) remain unknown. Because the FHP Shock-Wave-Synthesis-Laboratory in Freiberg is currently able to synthesize high pressure phases in the gram-scale much better insights into structural properties, chemical composition and thermal behavior of the HP-phases are possible. Additionally to micromethods bulk sample analysis is feasible.

The synthesis conditions for the analyzed samples and its chemical compositions are given elsewhere **[5]**. For the IR-spectroscopy samples where measured with a NICOLET 380 FT-IR spectrometer in the transmitted light. ATR-measurements were not possible because the adsorption bands of the diamond anvils show a similar position to the most important spinel-structure related vibration bands.

Grain size effects, which are common in natural occuring samples **[6]** are absent due to the small crystallite size of the γ-$Si_3(N,O)_4$ (10-30 nm). A typical IR-spectra of pure g-silicon nitride with the assignment of the spinel related vibrations after Jeanloz [7] is shown in Fig. 1.

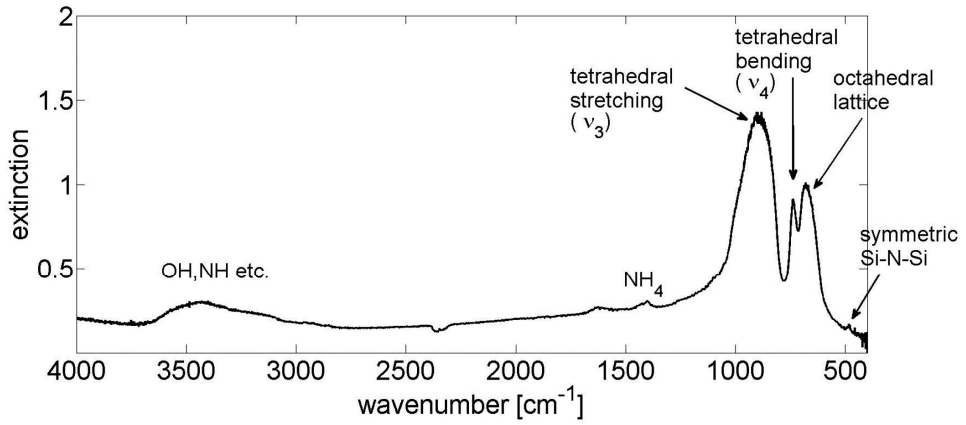

Figure 1. IR-spectrum (extinction) of pure γ-Si_3N_4 with description of the adsorption bands

After etching of oxygen rich samples with HF **[3]** the ratio between the main adsorption band (tetrahedral stretching at 858.6 cm^{-1}) and the tetrahedral bending (732.8 cm^{-1}) and the octahedral lattice vibrations (669.2 cm^{-1}) decrease strongly while the tetrahedral stretching itself sharpens (Fig. 2).

The peak positions of the spinel related vibrations remain unchanged. Furthermore the symmetric Si-N-Si-vibration at 418.2 cm^{-1} and the shoulder at 1071 cm^{-1} are absent after the etching. This vibrations are shifted slightly compared to the bands of amorphous Si_3N_4 **[8]** with approximately 500 cm^{-1} and 1000 cm^{-1}, while the tetrahedral stretching is shifted to 931 cm^{-1}.

This spectra indicates the simultaneous occurrence of silicon nitride and silicon oxide. Despite the fact that the XRD-measurements shows only the occurrence of one crystalline phase (γ-$Si_3(N,O)_4$) "low ordered areas" on the outer rim of the spinel-type nitrides are supposed.

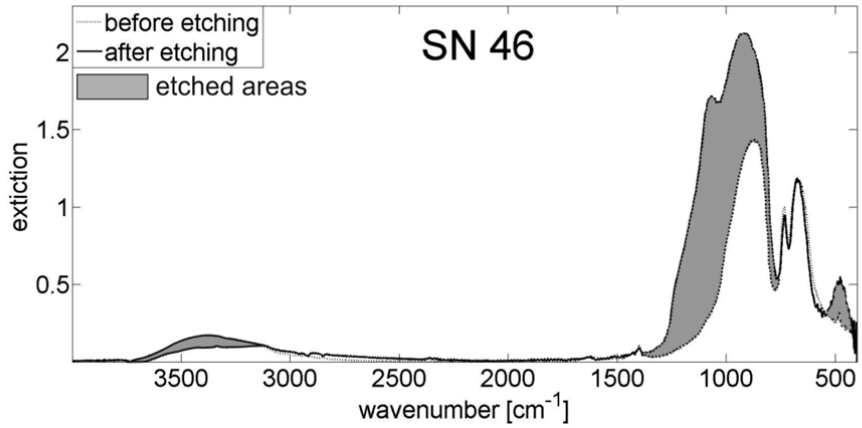

Figure 2. Comparison of the etched and unetched γ-$Si_3(N,O)_4$ with the solved areas, spectra normalized with the octahedral lattice vibration

Many thanks to the Dr. Erich-Krüger-Foundation for the generous financial support and the team of the shaft "Reiche Zeche" for her help to build up the new FHP shock-wave-synthesis laboratory.

References:

[1] A. Zerr, R. Riedel, G. Miehe, G. Serghiou, M. Schwarz, E. Kroke, H. Fueß, P. Kroll, R. Boehler, *Nature* **1999**, *400*, 340-342.
[2] J. Z. Jiang, F. Kragh, D. J. Frost, K. Ståhl, H. Lindelov, *J. Phys.: Condens. Matter* **2001**, *13*, L515.
[3] T. Sekine, H. He, T. Kobayashi, K. Kimoto, M. Mitomo, *Spinel Type Sialon, Spinel Type Silicon Oxinitride and Methods for producing their Powders*, *US 2002/0045529 A1* **2002**.
[4] T. Sekine, *Eur. J. Solid State Inorg. Chem.* **1997**, *34*, 823.
[5] T. Schlothauer, M. R. Schwarz, M. Ovidiu, E. Brendler, R. Moeckel, E. Kroke, G. Heide, in *Minerals as Advanced Materials II* (Ed.: S. V. Krivovichev), Springer Berlin Heidelberg. Berlin, Heidelberg **2012**, p. 375.
[6] Z. Xu, B. C. Cornilsen, D. C. Popco, W. D. Pennington, J. R. Wood, J.-Y. Hwang, *The Internet Journal of Vibrational Spectroscopy* **2004**, *5*.
[7] R. Jeanloz, *Phys. Chem. Mineral* **1980**, *5*, 327-341.
[8] N. Wada, S. Solin, J. Wong, S. Prochazka, *Journal of Non-Crystalline Solids* **1981**, *43*, 7.

PHASE RELATIONS IN ALKALI-ALKALINE EARTH CARBONATE SYSTEMS AT 6 GPA AND 900-1450ºC

Shatskiy A. [1,2], ***Borzdov Yu.M.*** [1], ***Litasov K.D.*** [1,2], ***Sharygin I.S.*** [1,2], ***Gavryushkin P.N.*** [1,2], ***Pal'yanov Yu.N.*** [1,2], ***Ohtani E.*** [3]

[1] *V.S. Sobolev Institute of Geology and Mineralogy SB RAS, Novosibirsk, Russia*
[2] *Novosibirsk State University, Novosibirsk, Russia*
[3] *Department of Earth and Planetary Material Science, Tohoku University, Sendai, Japan*
anton.antonshatskiy.shatskiy@gmail.com

Alkalis and carbonates play a key role in diamond formation, mantle metasomatism, and deep magma generation. Alkali-carbonates are common components of fluids/melts entrapped by mantle minerals such as diamond and olivine from kimberlite pipes. Numerous peridotitic mantle xenoliths from different localities display the petrographic and geochemical signatures of carbonatite metasomatism. Alkali carbonates would be essential components which control melting in subducting slab and upwelling mantle. Minor amount of alkalis (Na, K) and CO_2 drastically, by ~1000°C, reduces the solidus of lithospheric mantle and subducted rocks (peridotites, eclogites, and pelites). Melting at 3-24 GPa yields alkali-rich Ca-Mg carbonate melts. It's shown experimentally that proto-kimberlitic magma, which originates from more than 250 km depth, was essentially alkali-rich carbonatite melt. In this regard, it is essential to know melting phase relations in simple carbonate systems under mantle conditions.

In this study we conducted HP-HT experiments at 6 GPa and 900-1450ºC in binary K/Na_2CO_3-$Mg/Ca/FeCO_3$ and pseudo binary K/Na_2CO_3-$CaMgCO_3$ carbonate systems, using large volume multianvil apparatuses at Tohoku University (Sendai, Japan) and IGM SB RAS (Novosibirsk, Russia). Run duration ranged from 2 to 38 hs. Starting materials were loaded in graphite capsules and dried at 300ºC for 2-3 hs. Prior the experiment the cell assemblies were stored at 130ºC in vacuum. Recovered samples were mounted into petro-epoxy and polished in oil using sandpaper and diamond past. Benzine was used to remove oil. Samples were studied using SEM and EDS at Tohoku University (Sendai, Japan). EDS was calibrated using experimental samples with known composition and homogeneous texture (i.e. samples with complete melting or below solidus).

Based on obtained results we plotted phase diagrams for studied systems some of which are shown in Fig. 1 **[1-4]**.

This study was supported by the Global Center-of-Excellence program at Tohoku University, the Ministry of Education and Science of Russia (project No. 14.B37.21.0601) and by the Russian Foundation for Basic Research (project Nos. 12-05-01167 and 12-05-33008).

References:

[1] Shatskiy, A., Borzdov, Y.M., Gavryushkin, P.N., Litasov, K.D., Sharygin, I.S., Funakoshi, K., Palyanov, Y.N., and Ohtani, E. (2013a) The system K_2CO_3-$CaCO_3$ at 6 GPa and 900-1400 ºC. Geochimica et Cosmochinica Acta, submitted.

[2] Shatskiy, A., Gavryushkin, P.N., Sharygin, I.S., Litasov, K.D., Kupriyanov, I.N., Higo, Y., Borzdov, Y.M., Funakoshi, K., and Palyanov, Y.N. (2013b) The system Na_2CO_3-$MgCO_3$ at 6 GPa and 900-1400 ºC. American Mineralogist, in press.

[3] Shatskiy, A., Sharygin, I.S., Gavryushkin, P.N., Litasov, K.D., Borzdov, Y.M., Shcherbakova, A.V., Higo, Y., and Funakoshi, K. (2013c) The system K_2CO_3-$MgCO_3$ at 6 GPa and 900-1450 ºC. American Mineralogist, in press.

[4] Shatskiy, A., Sharygin, I.S., Litasov, K.D., Borzdov, Y.M., and Ohtani, E. (2013d) The system Na_2CO_3-$CaCO_3$ at 6 GPa and 900-1400 ºC. American Mineralogist, in press.

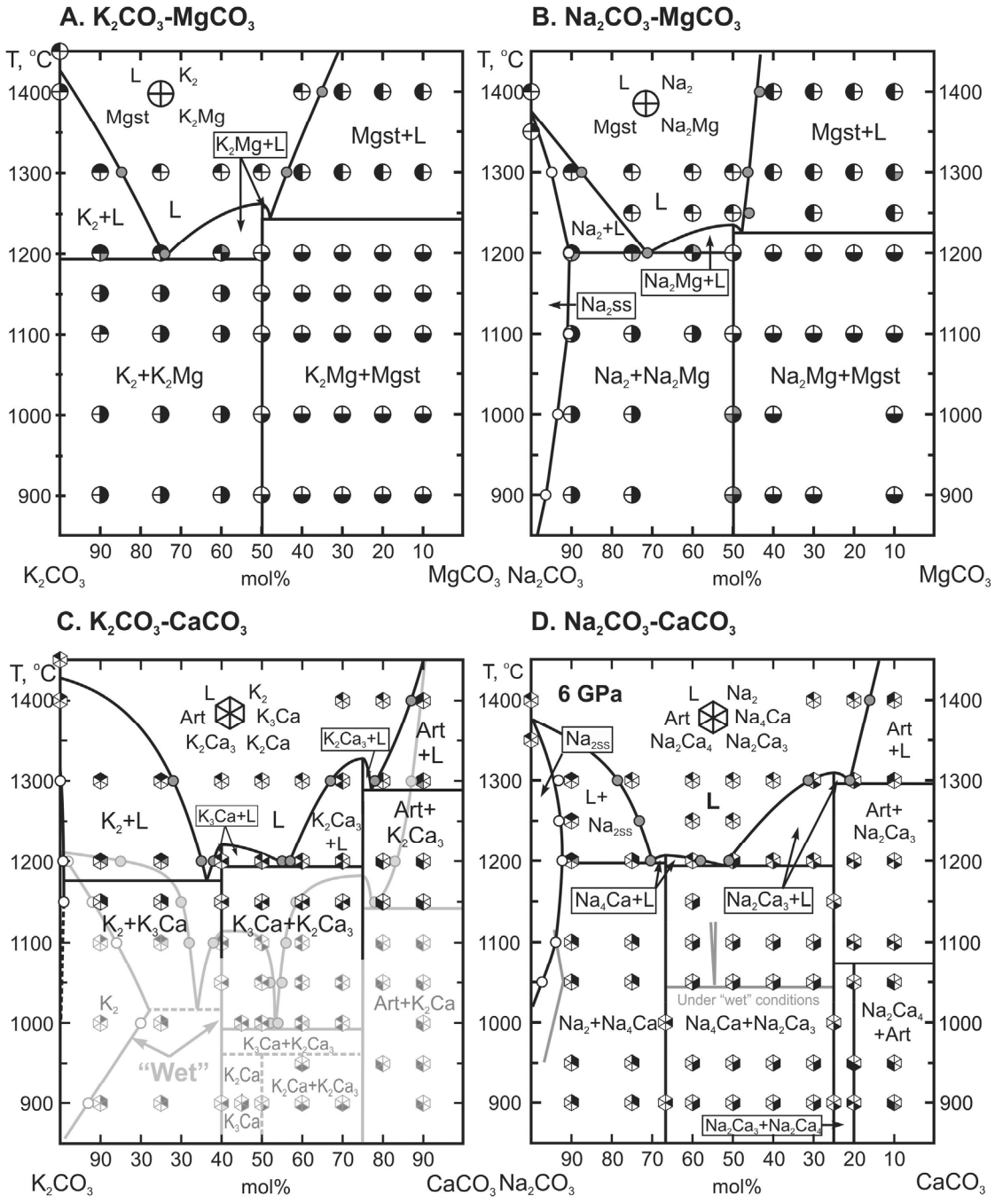

Figure 1. Phase relations at 6 GPa in binary carbonate systems.

H_2O STORAGE CAPACITY OF OLIVINE AS A KEY TO STUDY THE GENESIS OF KIMBERLITE MAGMA

Sokol A.G.*, *Kupriyanov I.N.*, *Palyanov Yu.N.

V.S. Sobolev Institute of Geology and Mineralogy, SB RAS, Novosibirsk, Russia
sokola@igm.nsc.ru

Melting experiments on kimberlite from the Udachnaya pipe have been performed at 6.3-7.5 GPa and 1300-1600°C using a split-sphere multianvil apparatus. Samples were prepared using finely powdered (to 10-50 μm) kimberlite (sample #UVS-01/01) pre-cleaned from olivine xenocrysts and xenoliths. The water content in kimberlite varied from 2.5 to 11.6 wt.% and the $CO_2/(CO_2+H_2O)$ molar ratio was from 0.61 to 0.23. The samples were placed in a graphite container inside a Pt capsule. The oxygen fugacity (fO_2) during the experiment was controlled by the equilibrium between graphite and water-bearing carbonate-silicate melt. At relatively low temperatures, fO_2 was close to the EMOG/D equilibrium, at higher temperatures, it shifted for approximately 1 log unit to more reduced conditions.

We have established the conditions of multiphase saturation of the Udachnaya kimberlite melt in experiments. This saturation appears near the kimberlite liquidus at 6.3 GPa and 6 to 8 wt.% H_2O and at 7.5 GPa with 6-10 wt.% H_2O. The kimberlite liquid obtained in these conditions is saturated with garnet wehrlite residue. Therefore, the Udachnaya kimberlite magma can have formed in subcratonic lithosphere or asthenosphere by partial melting of carbonated garnet wehrlite, with major controls of temperature (1450-1600°C) and input of aqueous fluids into the melting region.

The presence of clinopyroxene among the liquidus phases is due to the calcic nature and a high degree of silica undersaturation of the Udachnaya kimberlite. Olivine synthesized near the liquidus of water-rich kimberlite had its composition proximal to that of naturally occurring kimberlite-hosted olivine phenocrysts. The composition of garnet approaches that of Cr-poor megacrysts while the liquidus clinopyroxene is analogue to clinopyroxene megacrysts in kimberlite. The phases crystallized at lower melting degrees of kimberlite, from rather carbonatitic melt with relatively low water contents, are compositionally distinct from minerals of the megacryst/macrocryst suite.

The H_2O content in liquidus olivine, investigated in this study for the first time, is found to depend on the kimberlite bulk composition, its water content and pressure. Our results imply that the primary kimberlite magma should be rich in H_2O. It is found that water incorporates into olivines crystallized from kimberlite melt via two major mechanisms, in the form of the Ti-clinohumite-like defects and OH-clinohumite-like defects. Olivines with 120-170 ppm H_2O were experimentally synthesized at a pressure of 6.3 GPa, in equilibrium with melt compositionally close to the archetypical kimberlite containing as high as 6 wt.% of water. Olivine with 270-300 ppm H_2O was obtained using the same set up near liquidus of kimberlite only at a pressure of 7.5 GPa and 9.5-10.1 wt.% H_2O. We infer that olivine with 150-300 ppm H_2O, which is common to kimberlites, including the Udachnaya pipe, could very unlikely crystallize from anhydrous carbonated magma.

However, the specific mechanism of H_2O accumulation that provides the carbonatitic-to-kimberlitic magma transformation remains unclear. Understanding this mechanism will allow gaining more insights into the genesis of kimberlitic magma in the subcratonic uppermost mantle. Study of partitioning of H_2O between olivine and carbonate-silicate melts of the silicate-carbonate-chloride-H_2O system have been performed at 6.3 GPa and 1400°C. We have established, that water content of olivine depends on carbonate content of the melt and its saturation in equilibrium silicate phases. The H_2O storage capacity of olivine drastically decreases as the degree of melt carbonation reaches values corresponding to that of a kimberlitic

melt. As a result, the water partition coefficient $D^{perid/liq}_{H2O}$ becomes low enough for carbonated melt to extract water even from a peridotite source with ~100 ppm H_2O. So, dehydration melting peridotite source region should trigger by a sudden drop in H_2O storage capacity of NAM's when oxidized carbonated melts invade and metasomatize a reduced peridotite source region.

This study was supported by the Russian Foundation for Basic Research (No. 11-05-00429).

EQUATIONS OF STATE FOR MINERALS IN THE SYSTEM $MgSiO_3$-MgO

Sokolova T.S. [1], ***Dorogokupets P.I.*** [1], ***Danilov B.S.*** [1], ***Litasov K.D.*** [2,3]

[1] *Institute of the Earth's Crust, SB RAS, Irkutsk, Russia*
[2] *V.S. Sobolev Institute of Geology and Mineralogy SB RAS, Novosibirsk, Russia*
[3] *Novosibirsk State University, Novosibirsk, Russia*
dor@crust.irk.ru

We applied optimization model to approximate thermodynamics of high-pressure phases in system $MgSiO_3$-MgO using available experimental data from thermochemistry, dynamic and static compression, elasticity, and *P-V-T* measurements. The equations of state for forsterite, wadsleyite, ringwoodite, and Mg-perovskite were optimized using universal formalism developed for layered minerals **[1]**. Raw experimental P-V-T data were recalculated using our new pressure scales for Au and MgO, Table 1 and **[2]**). As an example Fig.1 shows comparison of calculated and measured pressures for Mg-perovskite, which show possible deviations in the experiments in diamond anvil cell up to 2-4 GPa (<4%). The obtained data were applied for calculation of the phase diagram in the $MgSiO_3$-MgO systems (Fig.2).

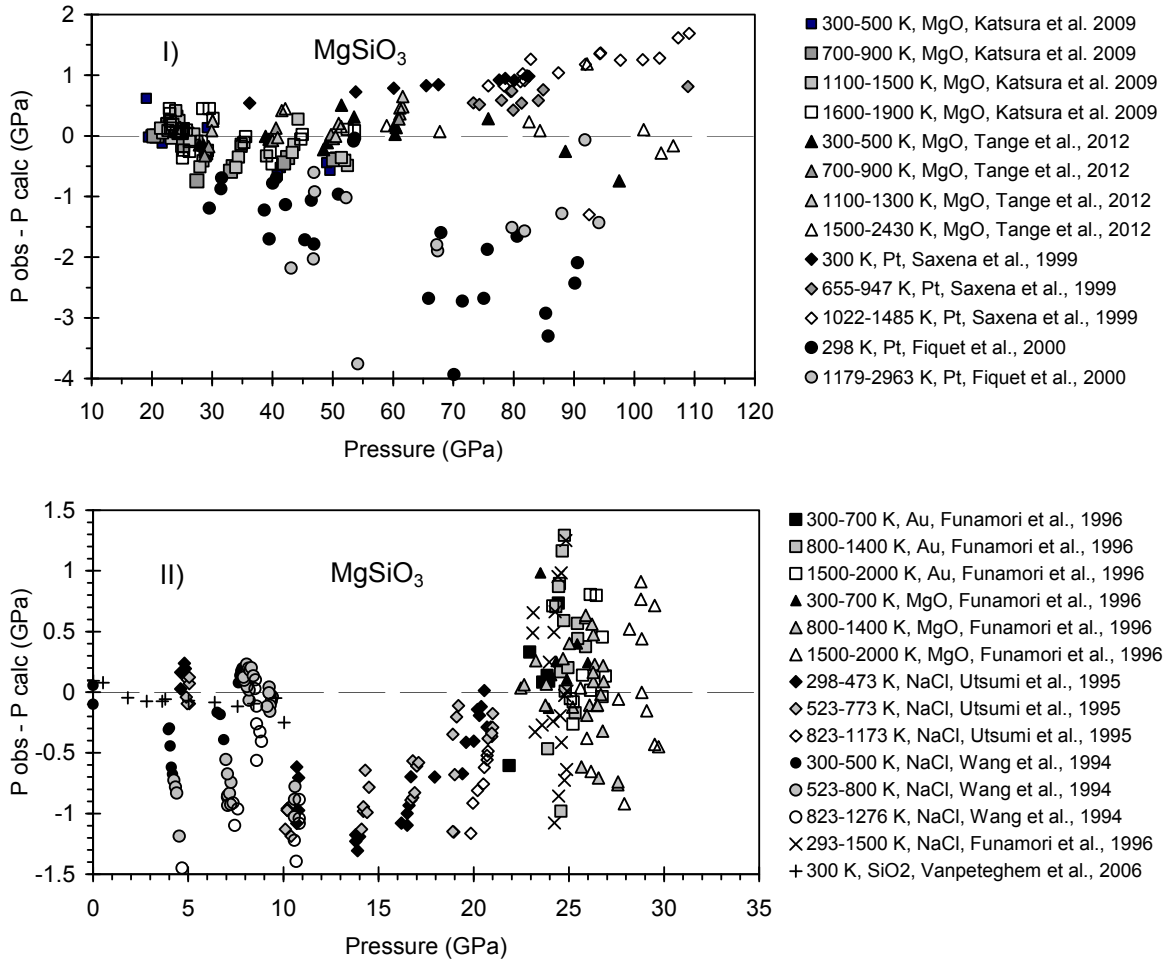

Figure 1. Differences between observed and calculated pressures for Mg-perovskite.

Table 1. Fitting parameters for pressure scales and studied minerals.

Parameters	Au, Gold	MgO, Periclase	α-Mg_2SiO_4, Forsterite	β-Mg_2SiO_4, Wadsleyite	γ-Mg_2SiO_4, Ringwoodite	$MgSiO_3$, Perovskite
U_0, kJ mol^{-1}	0	–609.571	–2206.635	–2173.130	–2157.600	–1164.000
V_0, cm^3 mol^{-1}	10.215	11.248	43.67	40.54	39.5	24.446
K_0, GPa	167.0	160.3	127.4	169.0	186.2	255.2
K'	5.9	4.25	4.0	3.95	3.95	4.13
k	2	5	5	5	5	5
Θ_{o1}, K	178.7	747	948	922	940	943
m_1	1.5	3	10.5	10.5	10.5	7.5
Θ_{o2}, K	83.3	399	347	391	411	417
m_2	1.5	3	10.5	10.5	10.5	7.5
γ_{o1}	2.94	1.53	0.46	0.54	0.98	1.49
β_1	5.06	2.115	2.43	2.53	1.33	2.37
$\gamma_{\infty 1}$	1.71	0.624	0	0	0	0
γ_{o2}	2.94	1.53	1.65	1.86	1.52	1.71
β_2	5.06	2.115	2.43	2.53	1.33	2.12
$\gamma_{\infty 2}$	1.71	0.624	0	0	0	0
a_0 (10^{-6}K^{-1})	–9.4	–15.9	–8.7	–6.9	–15.0	–
m	7.55	4.48	3.77	1.97	1.96	–
e_0 (10^{-6}K^{-1})	6.1	–	–	–	–	–
g	0.66	–	–	–	–	–

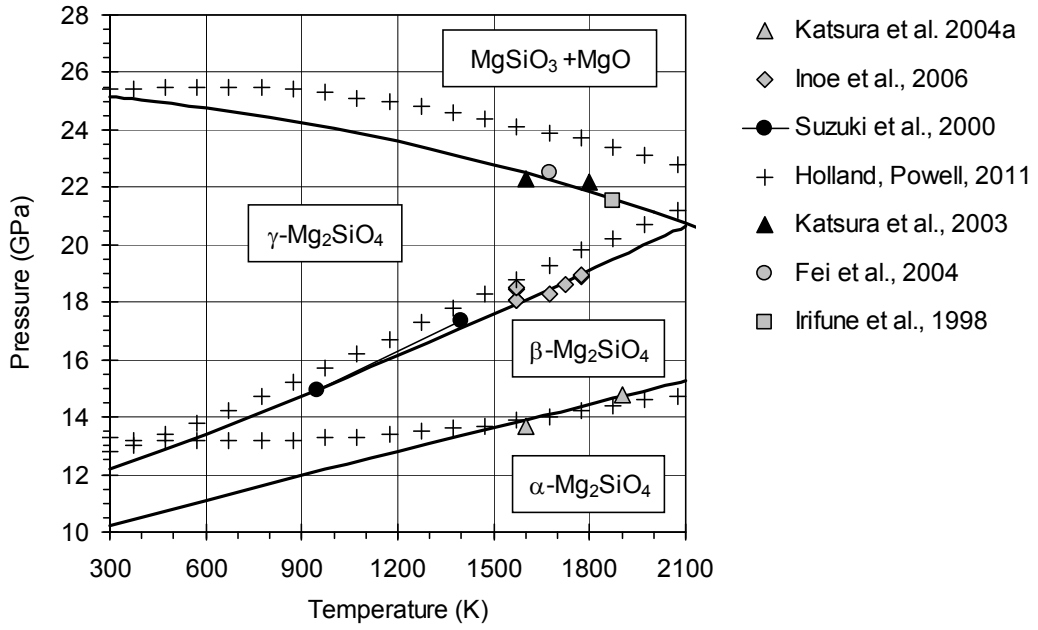

Figure 2. Phase diagram of the Mg_2SiO_4 system. Bold lines – this work. Crosses – using data from (Holland, Powell, 2011). Experimental data for forsterite-wadsleyite are after (Katsura et al., 2004), wadsleyite-ringwoodite (Suzuki et al., 2000; Inoe et al., 2006), and ringwoodite = Mg-perovskite + periclase (Katsura et al., 2003; Fei et al., 2004).

The work is supported by IP SB RAS No 97, RFBR (No 12-05-00758 and 12-05-33008) and Ministry of education and science of Russian Federation, No 14.B25.31.0032.

References:

[1] Sokolova T.S., Dorogokupets P.I., Litasov K.D., 2013. This volume.

[2] Sokolova T.S., Dorogokupets P.I., Litasov K.D., 2013. Russian Geology and Geophysics, 54: 181–199.

EQUATION OF STATE AND THERMODYNAMIC PROPERTIES OF GRAFITE

Sokolova T.S. [1], ***Dorogokupets P.I.*** [1], ***Litasov K.D.*** [2,3]

[1] *Institute of the Earth's Crust, SB RAS, Irkutsk, Russia*
[2] *V.S. Sobolev Institute of Geology and Mineralogy SB RAS, Novosibirsk, Russia*
[3] *Novosibirsk State University, Novosibirsk, Russia*
dor@crust.irk.ru

Graphite is layered mineral with a strong structural anisotropy in different crystallographic axes. Experimental data for diamond and graphite are summarized in a recent paper by H. Day **[1]**. The equation of state of the diamond has been obtained in our recent papers **[2, 3]**, but this formalism was found to be inappropriate for construction of the equations of state of layered minerals. The simplest approach to the equations of state of these minerals is as follows. The thermal part of the free energy is determined in the form with two Einstein parts with different dependences of characteristic temperatures on volume. In addition, for layered minerals the concept of pressure at infinite compression is not applicable. Thus, we replace the equation **[4]** for a more universal equation proposed in **[5]**, which allows to set the compressibility of minerals individually, without the introduction of the members of higher order.

The thermodynamic model is described in detail in **[2, 3]**, therefore here we note only principal modifications.

The pressure on the room-temperature isotherm is determined from the equation **[5]**:

$$P_r(V) = 3K_0 X^{-k}(1-X)\exp[\eta(1-X)], \quad (1)$$

where $X = (V/V_0)^{1/3}$, $\eta = 3K'/2 - k + 1/2$, k is additional parameter, which can be fitting.

The thermal part of Helmholtz free energy is expressed as:

$$F_{th}(V,T) = m_1 \mathrm{R}T\ln\left(1-\exp\frac{-\Theta_1}{T}\right) + m_2 \mathrm{R}T\ln\left(1-\exp\frac{-\Theta_2}{T}\right) - \frac{3}{2}n\mathrm{R}a_0 x^m T^2, \quad (2)$$

where Θ_1 and Θ_2 are characteristic temperatures with different dependence on volume, $x = V/V_0$, n is the number of atoms in the chemical formula of compound, $m_1 + m_2 = 3n$, a_0 represents the contribution of intrinsic anharmonicity in the Helmholtz free energy, m is the fitting parameter, R is the gas constant. The volume dependence of the Grüneisen parameter is expressed in the simplest form: $\gamma = \gamma_0 x^q$.

All links to the primary thermochemical, X-ray diffraction, and dilatometric data for graphite can be found in **[1]**. We performed simultaneous optimization of these data and obtained the following parameters for the equation of state of graphite: $V_0 = 5.3$ cm^{3}mol^{-1}, $K_0 = 36$ GPa, $K' = 8.5$, $k = 5$, $m_1 = 0.956$, $m_2 = 2.044$, $\Theta_{10} = 461$ K, $\Theta_{20} = 1704$ K, $\gamma_{10} = 0.736$, $\gamma_{20} = -0.049$, $q_1 = 0.22$, $q_2 = 0.105$, $a_0 = 15.6\text{E}{-6}$ K^{-1}, and $m = -0.078$. A comparison of the calculated and experimental thermodynamic functions of graphite is shown in Fig. 1. The calculated thermodynamic functions are in good agreement with the reference data, direct experimental measurements and theoretical calculations.

New calculated thermodynamic functions of graphite are presented in Table 1. They were tabulated against temperature at zero pressure, 10 and 20 GPa. The table presents the calculated coefficient of volumetric thermal expansion coefficient (α), entropy (S), heat capacity at constant pressure (C_P) and constant volume (C_V), isothermal (K_T) and adiabatic (K_S) bulk moduli, thermodynamic Grüneisen parameter ($\gamma_{th} = \alpha V K_T / C_V = \alpha V K_S / C_P$) and the Gibbs free energy increment relative to the standard state, which mainly coincides with the Gibbs energy increment from the known thermodynamic database **[6]**.

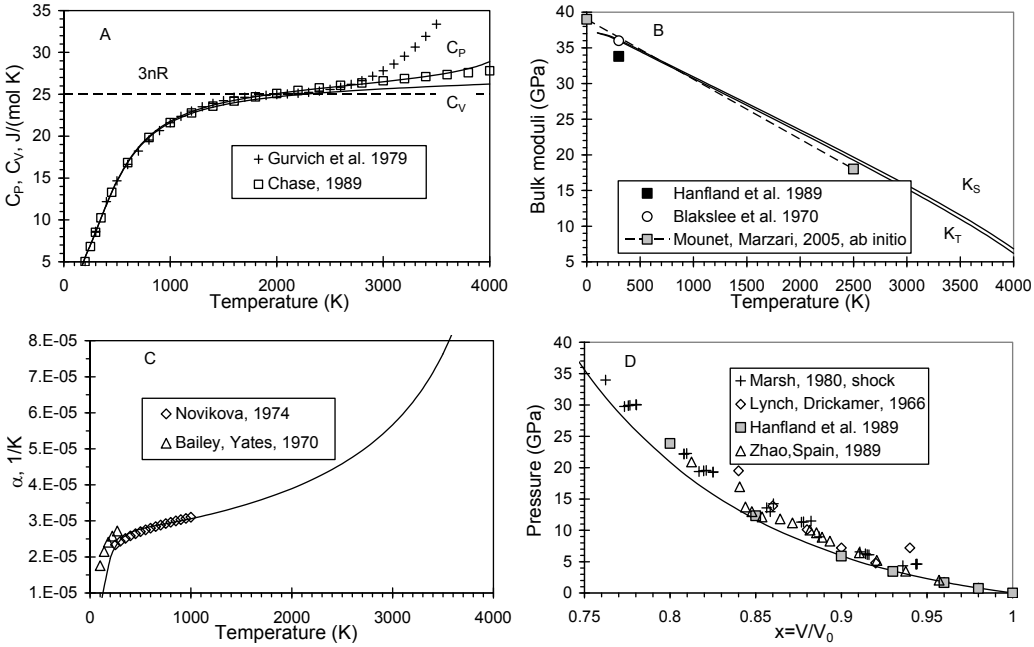

Figure 1. Thermodynamic functions of graphite. Solid lines are our calculation. A. Isobaric and isochoric heat capacity of graphite. B. Adiabatic and isothermal bulk moduli. C. Coefficient of volumetric thermal expansion. D. Calculated room-temperature isotherm, experimental measurements and shock wave data.

Table 1. Thermodynamic functions of graphite.

P	T	$x=V/V_0$	αE-6	S	C_P	C_V	K_T	K_S	γ_{th}	ΔG
GPa	K		K^{-1}	J mol^{-1} K^{-1}			GPa			kJ mol^{-1}
0	298.15	1	24.68	5.72	8.53	8.49	36.00	36.15	0.554	0.000
0	1000	1.0202	30.64	24.51	21.77	21.61	30.69	30.91	0.235	-10.954
0	2000	1.056	39.27	40.90	25.09	24.69	22.96	23.33	0.204	-44.414
0	4000	1.2155	185.09	59.29	30.02	26.21	4.31	4.94	0.196	-146.283
10	298.15	0.8616	8.78	5.05	8.26	8.25	108.32	108.46	0.526	48.591
10	1000	0.8676	10.18	23.71	21.68	21.63	103.93	104.17	0.225	38.176
10	2000	0.8767	10.60	39.98	24.81	24.71	97.76	98.16	0.195	5.574
10	4000	0.8964	11.72	57.78	26.48	26.25	85.63	86.35	0.182	-94.038
20	298.15	0.8013	5.72	4.74	8.13	8.12	171.43	171.58	0.513	92.518
20	1000	0.805	6.68	23.35	21.67	21.64	167.21	167.45	0.220	82.349
20	2000	0.8104	6.82	39.61	24.78	24.72	161.25	161.67	0.191	50.114
20	4000	0.8218	7.16	57.37	26.40	26.27	149.58	150.34	0.178	-48.715

The work is supported by IP SB RAS No 97, RFBR (No 12-05-00758 and 12-05-33008) and Ministry of education and science of Russian Federation, No 14.B25.31.0032.

References:

[1] Day H.W., 2012. Am. Mineral., 97: 52–62.
[2] Dorogokupets P.I., Sokolova T.S., Danilov B.S., Litasov K.D., 2012. Geodynamics and Tectonophysics, 3(2): 129–166. doi:10.5800/ GT-2012-3-2-0067.
[3] Sokolova T.S., Dorogokupets P.I., Litasov K.D., 2013. Russ. Geol. Geoph., 54: 181–199.
[4] Holzapfel W.B., 2010. High Pressure Research, 30: 372–394.
[5] Kunc K., Loa I., Syassen K., Phys. Rev. B, 68: 094107.
[6] Holland T.J.B., Powell R., 2011. J. Metamorphic Geology, 29: 333–383.

THE TWO-TYPE ZONALITY OF MAJOR AND TRACE ELEMENTS IN GARNETS FROM DEFORMED PERIDOTITES (UDACHNAYA PIPE, YAKUTIA)

Solov'eva L.V. [1], ***Kalashnikova T.V.*** [2], ***Suvorova L.F.*** [2], ***Kostrovitsky S.I.*** [2]

[1] *Institute of Earth Crust SB RAS, Irkutsk, Russia*
[2] *Vinogradov Institute of Geochemistry SB RAS, Irkutsk, Russia*
Solv777@crust.irk.ru

In this article the distribution of incompatible trace elements in different zones of garnet grains was investigated from deformed peridotites. The samples were represented by two unaltered lherzolite xenoliths from kimberlite Udachnaya pipe. The examinated lherzolites belong to two types of deformed peridotites in accordance with petrographic features, mineral and modal composition. The sample 00-69 is coarse-porphyric Grt lherzolite and presents probably the substance of asthenosphere or thermal boundary layer. While the sample 4-06 is referred to fine-porphyric type, it may be the lithosphere fragment trapped by asthenoshere melts [1]. The both xenoliths demonstrated similar P-T parameters according to different geothermobarometers (1200-1300C; 55-60 GPa) and crystallized very likely at near depth.

The distribution of incompatible trace elements is different in principle for garnet in these xenoliths. The first type (coarse-porphyric – sample 00-69) is characterized by normal REE distribution with various concentrations in different zones and sharp maxima of Zr+Hf and Ti in rims and Hf in cores. In fine-porphyric type (sample 4-06) sinusoidal REE distribution and minima for Zr+Hf and Ti are observed in cores. In rim zone distribution of incompatible elements is similar to garnet of coarse-porphyric type. It may be supposed that deformed fine-porphyric peridotites reserved relict lithosphere distribution. These rocks believed to be situated in lithosphere base, then got into percolation zone of plume asthenospheric melts. Probably, Middle-Paleozoic thermo-chemical Yakutian plume rising to Siberian craton lithosphere base realized mechanical and chemical erosion of lithosphere plate and involved lithosphere substance in the form of slaces and xenoliths into convective plastic asthenosphere and thermal boundary layer. As a whole, considered peculiarities of incompatible trace elements behavior in zonal Grt grains agree with the model of percolating melt with synchronous crystallization of megacryst association ("percolative fractional crystallization"- [2]).

In garnet rims of fine-porphyric type (sample 4-06) anomalous high concentration of K_2O and Na_2O are registered. At the same time the TiO_2 concentration is increasing. These zones don't differ from whole grain by optical features and microprobe image. It is supposed that in xenolith 4-06 garnet chemical composition was resulted of element diffusion from intergranular melt or fluid at grains boundary but not an account of melt crystallization. The high K_2O and TiO_2 concentration allow to hypothesize the penetration of mica or clinopyroxene nanodomens into garnet crystal matrix from kelyphite. It may be accounted for intensive plastic deformation and temperature increasing.

The received data for zonal trace element distribution in garnet grains indicate that substance trapped by kimberlite melts was unequilibrated and zonality was developed not long before kimberlite melt formation. The presence of relict "lithosphere" distribution in fine-porphyric garnet lherzolite points to thermal and chemical lithosphere erosion by hot plume and appearance of lithosphere-asthenosphere mixture under lithospheric plate during kimberlite-forming cycle. Thus, the melts developed in thermal boundary layer and asthenosphere included plume and mantle lithosphere substance. The plume matter replaced in fact the material earlier situating under lithosphere according to isotopic-geochemical investigation of megacrysts and deformed peridotites [3].

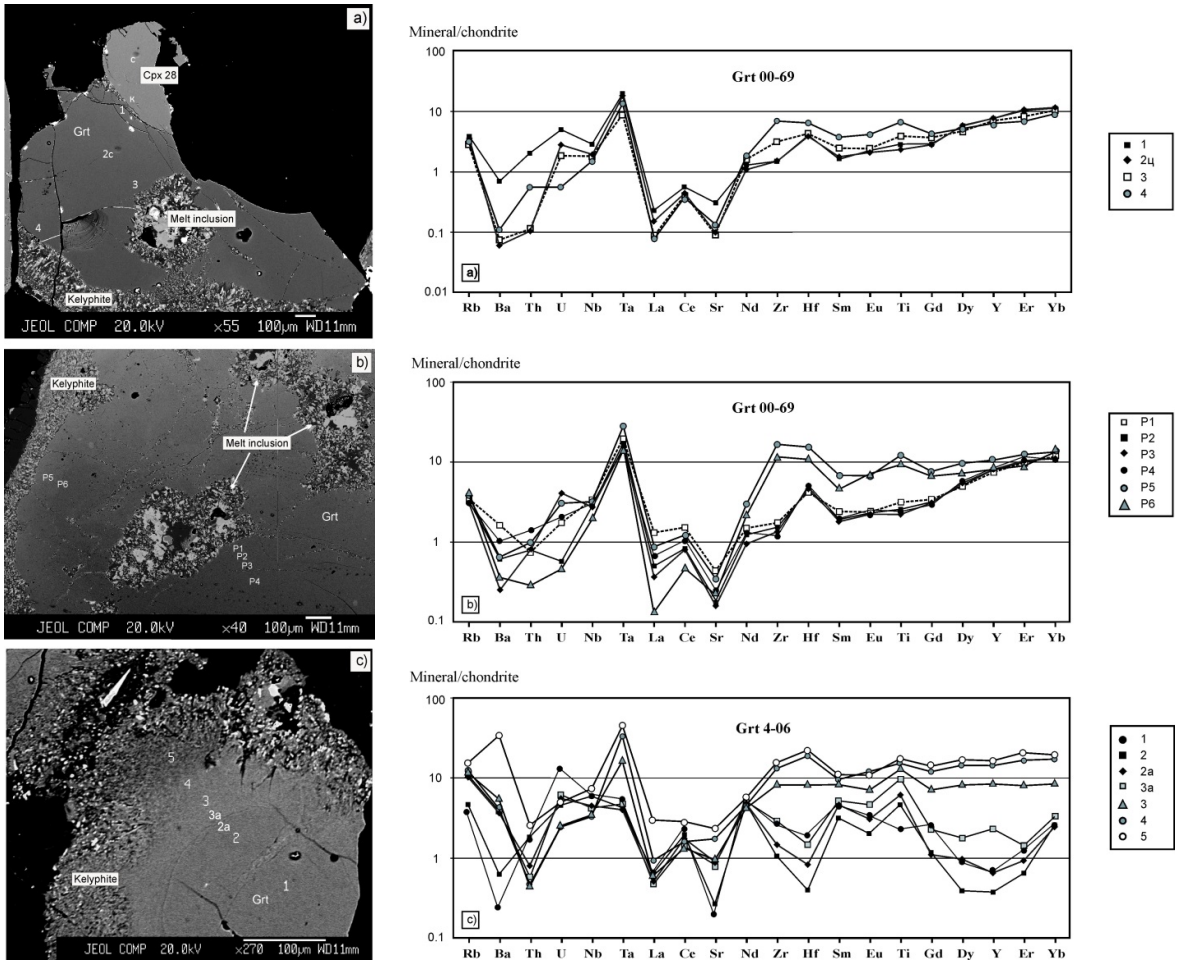

Figure 1. On the left - COMP photos of garnet grains.

a) – Sample 00-69 – the part of more large Grt grain, in centre – oval Cpx inclusion;

b) – Sample 00-69 – the part of another Grt grain with former melt inclusions;

c) – Sample 4-06 – the part of Grt grain.

On the right – C1 chondrite-normalized [4] trace elements concentrations in Grt grains (00-69 and 4-06). Line numbers correspond to analyses points on left photos.

References:

[1] Solov'eva L.V., Egorov K.N., Lavrent'ev Yu.G., Korolyuk V.N., Kostrovitsky S.I., Suvorova L.F. The genetic relationship of the deformed peridotites and garnet megacrysts from kimberlites with asthenospheric melts// Russian Geology and Geophysics. 2008. T. 49. № 4. C. 207-224.

[2] Harte B., Hunter R.H., Kinny P.D. Melt geometry, movement and crystallization, in relation to mantle dykes, veins and metasomatism. In: Philosophical Transaction of the Royal Society of London. Series A. 1993. V. 342. P. 1–21.

[3] Kostrovitsky S.I., Solov'eva L.V., Yakovlev D.A. et al. Kimberlite and megacryst assotiation – isotopic investigation (in Russian)// Petrology. 2013. V.21. № 2. P. 1-21.

[4] McDonough W.F., Sun S.-S. The composition of the Earth// Chemical Geology. 1995. V. 120. P. 223-253.

HP-HT EXPERIMENTS WITH SYNTHETIC $MgFe_2O_4$: DISTRIBUTION OF Fe^{3+} IN NATURAL SPINELS AS A POSSIBLE PARAMETER FOR GENETIC SUBDIVISION

Turkin A.I.
V.S. Sobolev Institute of Geology and Mineralogy, SB RAS, Novosibirsk, Russia
turkin@igm.nsc.ru

The distribution of cations A and B over octahedral (M) and tetrahedral (T) sites in a spinel is described by the inversion parameter *x*: $(A_{1-x}B_x)[A_xB_{2-x}]O_4$. At ambient pressure, as is well known, the inversion parameter changes with temperature, increasing for normal spinels and decreasing for inverse spinels. As for pressure increase at various temperatures, there are only sparse data on the relationship between the inversion parameter and pressure.

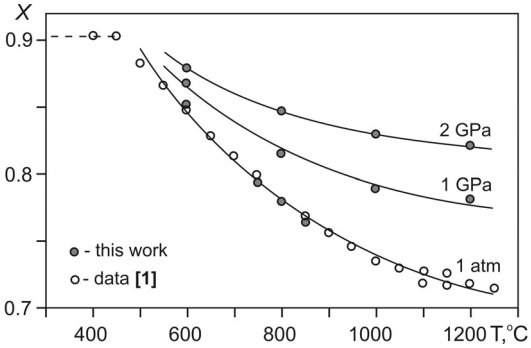

Figure 1. The inversion parameter in $MgFe_2O_4$. The dashed line is a guide for the eye to the "frozen" value of *x*.

The objective of the present study was to obtain experimental data on this relationship. Magnesioferrite $MgFe_2O_4$, an inverse spinel, has been chosen as the subject of this investigation because, on the one hand, it is a usual component of natural spinels. On the other hand, the relationship between its inversion parameter and temperature at room pressure has been carefully studied by O'Neill et al. **[1]**, and it was possible to compare the results. It has been found **[1]** that at ambient temperature the lattice parameter (α_o) is a function of the inversion parameter and is well fit by a straight line, which was then used in the present work to determine the inversion parameter from X-ray data.

The cation distribution in synthetic $MgFe_2O_4$ was investigated using a "piston-cylinder" apparatus at three pressures (1atm and 1 and 2 GPa) over a temperature range of 600 to 1200°C. The preparation of homogeneous stoichiometric magnesioferrite is described in **[2]**. Quenched samples were analyzed by X-ray powder diffraction. The inversion parameter was derived from the unit-cell parameter at ambient temperature using the relationship from **[1]**. More details of the experimental procedure and results were can be found elsewhere **[3]**. The calculated values of *x* for the samples, together with those reported in **[1]**, are shown in Fig.1. It is evident that the inversion parameter of magnesioferrite increases with pressure, being a smooth function of P-T conditions. The regular curve of *x*(T) for ambient pressure breaks near 450°C. The value of 0.9 is the low-temperature limit of *x*, which cannot increase further with decreasing temperature, because the cation migration has stopped. The cations are frozen-in at their sites to a greater degree. This is the reason why in situ high-pressure experiments at ambient temperature reveal no changes in the inversion parameter.

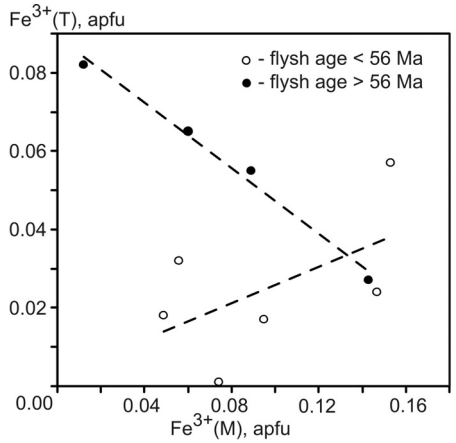

Figure 2. Spinels from flysch basins of southern Alps. Fe^{3+}(M) vs. Fe^{3+}(T) diagram plotted using analytical data **[4]**.

Since the positional distribution of Fe^{3+} in $MgFe_2O_4$ depends on P-T – two of the main rock forming parameters – it is interesting to analyze some known data on the cation position in natural spinels in terms of the Fe^{3+}(T) / Fe^{3+}(M) ratio. There are only few systematic studies in which the crystal chemistry of these minerals has been investigated in detail. In most cases, the structure was defined not by the inversion parameter but by cation-to-oxygen distances T-O and M-O or their

ratio - the so-called oxygen positional parameter u.

Lenaz and Princivalle **[4]** studied the crystal chemistry of chromian spinels from the flysch basins of some regions of the southeastern Alps with various tectonic settings in order to find structural differences. The authors separated the spinels into two groups using value of the parameter u. Additionally, this division was confirmed by age determination of flysch samples. The original diagram of Fe^{3+}(M) vs. Fe^{3+}(T) plotted using analytical data **[4]** also shows this grouping (Fig. 2).

Another example of the relation between the partitioning of Fe^{3+} in the spinel structure and the petrogenetic characteristics of host rocks was revealed in a close examination of data on the structure of spinels from two various types of xenoliths from the San Carlos Volcanic Field in Arizona **[5]**. Without considering the compositional and structural differences found by Uchida et al. **[5]** for spinels from Group I and II xenoliths, it is worthy of note that the Fe^{3+}(M) vs. Fe^{3+}(T) diagram also exhibits this subdivision (Fig. 3A).

Finally, Fig. 3B shows the points for spinels from xenoliths in the volcanic products of the Alban Hills (Roman Comagmatic Region) and from mantle xenoliths from Predazzo Area (Northern Italy). The initial data on the crystal chemistry for the diagram were presented by Carraro **[6]** and Lucchesi et al. **[7]**,. who were the first to perform a grouping of spinels from these areas. The cation-to-oxygen distances and the oxygen positional parameter were used as classification features. The grouping also manifests itself in a Fe^{3+}(M) vs. Fe^{3+}(T) diagram by the ascending and descending linear trends describing the two populations of spinels.

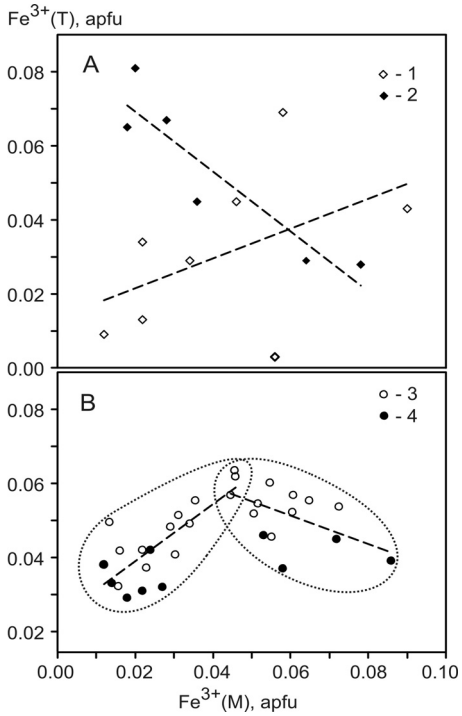

Figure 3. Fe^{3+}(M) vs. Fe^{3+}(T) diagrams for spinels from: A - various types (1 ,2) of mantle xenoliths from the San Carlos Volcanic Field; B – xenoliths in volcanic products of the Alban Hills, Roman Comagmatic Region (3) and mantle xenoliths from Predazzo Area, Northern Italy (4). Plotted using analytical data **[5, 6, 7]**. Outlined fields show the points with ascending and descending trends.

It is appropriate mention that a full structure refinement, including determination of site occupancies, bond distances, oxygen coordinates and so on, provides valuable information for mineralogists but it is a complex and laborious analytical procedure. There is a need for careful selection and preparation of samples for single crystal or powder X-ray study. Moreover, because of the complex chemistry of natural minerals, the calculation algorithm requires some simplifications and assumptions, which may be subjective. In this regard, the estimation of the iron position in crystal structure by Mössbauer spectroscopy is a simpler and more rapid procedure which may be used to analyze fast a large set of samples.

References:

[1] O'Neill H.St.C., Annersten H., Virgo D. Amer. Mineral.,1992, 77, N 7-8, 725-740.
[2] Turkin A.I., Drebushchak V.A. J. Crystal Growth, 2004, 265, N 1-2, 165-167.
[3] Turkin A.I., Drebushchak V.A. Amer. Mineral., 2005, 90, N 4, 764-767.
[4] Lenaz D., Princivalle F. Can. Mineral., 2005, 43, N 4, 1305-1314.
[5] Uchida H., Lavina B., Downs R.T., Chesley J. Amer. Mineral., 2005, 90,. N 11-12, 1900-1908.
[6] Carraro A. Eur. J. Mineral., 2003, 15, N 4, 681-688.
[7] Lucchesi S., Amoriello M., Della Giusta A. Eur. J. Mineral., 1998, 10, N 3, 473-482.

SESSION 6

Extraterrestrial mineralogy and crystallogenesis in space

STABBILIZATION OF RIBOSE BY INORGANIC IONS

***Furukawa Y.*, Horiuchi M., Nitta S., Kakegawa T.**

Tohoku University, Sendai, Japan
furukawa@m.tohoku.ac.jp

Ribose is an essential constituent for our life and considered as substantially important organic compound for the origin of life due to the ability of RNA for both the carrier of genetic information and enzymes **[1,2]**. The other components of RNA, phosphoric acid and nucleic acid bases, might have been available and more stably present on the early Earth as suggested in many geological and experimental studies as well as analyses of extraterrestrial objects **[3,4]**. Furthermore, ribose is the least stable in aldopentose, aldehyde-type carbohydrates contain five member carbons **[5,6]**. The substantial instability of ribose raises fundamental questions whether ribose could have been a constituent of primordial RNA and why ribose was selected as the constituent RNA sugar out of four aldopentoses: ribose, arabinose, lyxose, and xylose **[6]**.

Borate minerals or boron containing minerals can be found as evaporates in several lakes or as boron silicates even in Achaean rocks. Silicate minerals are more common and can be found in Hadean minerals. Therefore, borate and silicate ions must have been available in aquatic environments on the early Earth released from these minerals. Borate and silicate form complexes with carbohydrates and have been proposed as stabilizers of pentoses including ribose. Although the stabilization on pentoses by these ions has been demonstrated experimentally, their stabilization effects on each aldopentoses remain unclear because of the lack of suitable analytical technique.

In this study, we present the stabilization effects of silicate and borate ions on each aldopentose conducting incubation experiments of these aldopentoses in alkaline solutions. Borax, sodium tetra-borate ($Na_2B_4O_5(OH)_4 \cdot 8H_2O$), or sodium silicate ($Na_2SiO_4 \cdot 9H_2O$) was dissolved in water forming a 40 mM borate or silicate solution. An aldopentose (ribose, arabinose, lyxose, or xylose) was added in the solution to be 1 mM. Then, calcium hydroxide was added to the solution to buffer the pH level. The solution was incubated at a constant temperature with continuous starring. Aliquot of the incubation solution was collected each 90 minutes and analyzed with liquid chromatography-mass spectrometry for residual and produced aldopentoses in uncomplexed form. Incubations without borate and silicate are also conducted for comparison. The amounts of complexes of these ions and aldopentoses were also measured with mass spectrometry to compare the amounts and stabilization effects.

In the incubation experiments without borate and silicate, the concentration of ribose was quickly decreased compared with the other aldopentoses while arabinose kept the highest concentration. In the incubation experiments with borate, the decreasing rates of aldopentoses including ribose became lower depending on the concentration of borate. In the incubation experiments with silicate, the stabilities of aldopentoses except for arabinose were also increased. All kinds of aldopentose-borate 1:1 and 2:1 complexes were found. These amounts of 1:1 complex were apparently greater in ribose-borate complex while the amount of arabinose-borate complex were negligible amount. The aldopentose-silicate complex signals were below the detection limit of measurement. These results indicate that borate and silicate stabilize aldopentoses including ribose. This further suggests that ribose can be a primordial constituent when it was stabilized in borate- or silicate-rich environments like high-salinity lakes or in borate- or silicate-rich geofluids.

References:

[1] Benner, S. A., Ellington, A. D. & Tauer, A., *Proc. Natl. Acad. Sci.* **86**, 7054-7058 (1989).
[2] Bartel, D. P. & Szostak, J. W., *Science* **261**, 1411-1418 (1993).

[3] Callahan, M. P.*, et al., Proc Natl Acad Sci USA* **108**, 13995-13998 (2011).
[4] Pasek, M. A., *Proc. Natl. Acad. Sci.* 105, 853-858 (2008).
[5] El Khadem, H. S., Ennifar, S. & Isbell, H. S., *Carbohydr. Res.* **169**, 13-21 (1987).
[6] Larralde, R., Robertson, M. P. & Miller, S. L., *Proc. Natl. Acad. Sci.* **92**, 8158-8160 (1995).

MICROGRAVITY EXPERIMENT USING THE SOUNDING ROCKET S-520-28 FOR UNDERSTANDING A FORMATION PROCESS OF COSMIC DUST

Kimura Y. [1], ***Inatomi Y.*** [2], ***Takeuchi S.*** [2], ***Tsukamoto K.*** [1], ***Tanaka K.K.*** [3]
[1] *Department of Earth and Planetary Materials Science, Tohoku University, Sendai, Japan*
[2] *Institute of Space and Astronautical Science, Yoshinodai, Sagamihara, Kanagawa, Japan*
[3] *Institute of Low Temperature Science, Hokkaido University, Sapporo, Japan*
ykimura@m.tohoku.ac.jp

Nucleation theories have been used to understand the condensation sequence, number density and size of cosmic dust in a gas outflow of dying stars or a gas plume after shock wave heating in the primitive solar nebula **[1,2]**. However, it has been well known that nucleation rates obtained by classical nucleation theory (CNT) and by experiments have a large difference **[3,4]**. In addition, most of the physical parameters of nanometer sized particles are unknown, whereas the size of cosmic dust is typically less than 100 nm. Therefore, it is still not successful to explain the characters of cosmic dust by a nucleation theory. To determine the physical parameters of nanoparticles and evaluate nucleation theories, we constructed an in-situ observation system of temperature and concentration during homogeneous nucleation in vapor phase using interferometry **[5-7]**.

Nanoparticles are formed from a supercooled vapor after evaporation by electrical heating in a gas atmosphere. Using the new system, we succeeded to determine surface free energy and sticking probability of manganese nanoparticle from timescale for gas cooling and condensation temperature based on nucleation theories **[7]**. The surface free energy and sticking probability at ~1100 K were 1.6 J/m^2 and 0.4, respectively. In case of ground-based experiment, convection of gas atmosphere caused by thermal heating of an evaporation source generates heterogeneity of nucleation environment, such as temperature and concentration profiles. In addition, there is a possibility of that produced nuclei collides and then fused together to be a larger particle and decreasing number density after a stage of nucleation. This fusion growth is predominantly occurred in nanoparticles **[6]** and may be one of reasons of large differences of nucleation rates between experiments and theories. If we measure a size of resulting nanoparticles, sticking probability becomes apparently larger due to fusion growth. Very small sticking probability of zinc, ~10^{-5}, has been obtained by microgravity experiment **[8]** against sticking probabilities of close to unity obtained by ground based experiments.

If same kinds of experiments are performed in microgravity, evaporated vapor will diffuse uniformly and the temperature profile will become concentric around the evaporation source. As the result, nucleation will occur at the same condition, i.e., same supersaturation. Then, we can obtain physical properties of nanoparticles more precisely. Then we may be able to evaluate nucleation theories. Therefore,

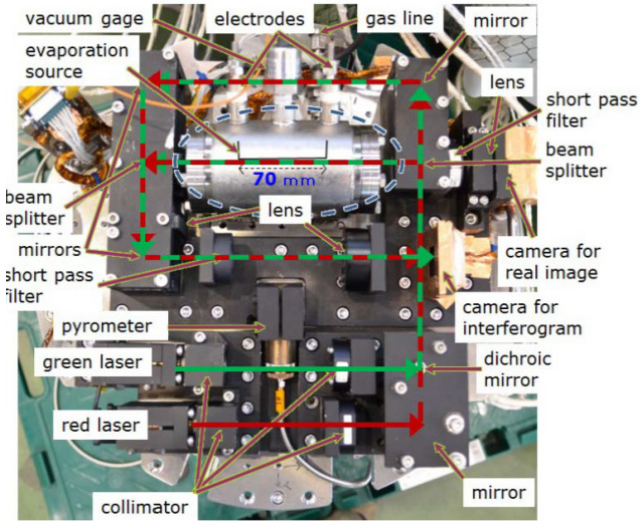

Figure 1. A photograph of the double wavelength Mach–Zehnder-type interferometer with an evaporation chamber indicated by a dotted circle. Red and green arrows show the optical path. The evaporation source, which is an iron wire (0.1 mm in diameter and 10 mm in length) wrapped around a tungsten wire (0.3 mm in diameter), prepared in the evaporation chamber has been drown by a black solid line.

we did a microgravity experiment using the sounding rocket S-520-28 launched on December 17th, 2012.

We prepared specially designed double wavelength Mach–Zehnder-type interferometers with an evaporation chamber and a camera recording system to fit the space and weight limitations of the rocket (Fig. 1). Three systems, named DUST 1 to 3, with same configuration except evaporation source and gas pressure in the chamber were installed into the nosecone of the rocket. The evaporation source and gas atmosphere of each system were tungsten and a gas mixture of oxygen (4.0×10^3 Pa) and argon (3.6×10^4 Pa) for DUST 1, iron and argon (2.0×10^4 Pa) for DUST 2, and iron and argon (4.0×10^4 Pa) for DUST 3. The working chamber was a stainless-steel cylinder with an internal diameter of 6.5 cm and a length of 15 cm, containing three viewports for optical observation and temperature measurement of the evaporation source by pyrometer, two ports for thermocouple, which measure a temperature at the end of the evaporation source and electrodes. The cylinder was evacuated through a valve by a combination of a turbo-molecular pump (50 L/s) and a scroll type dry vacuum pump. Because the refractive index of the argon buffer gas (>99.9999% purity) used in producing the nanoparticles is very low [$(n - 1)\mathrm{Ar} = 5.266 \times 10^{-5} \pm 0.016 \times 10^{-5}$ at 632.8 nm and 293.15 K for 2.0×10^4 Pa; **9]**, the evaporation source was prepared certainly parallel to the evaporation source and as long as possible to increase the column density, which is advantageous for the detection of tiny changes in the refractive index. With this experimental setup, we could detect a difference in refractive index of less than 1×10^{-6}, which, for example, corresponds to the difference in temperature from 298 K to 301 K for Ar gas at 2×10^4 Pa. Because the vapor pressure of metallic tungsten is quite low (10^{-5} Pa at 2508 K) compared with that of Fe (9.7×10^4 Pa at 2508 K), the partial pressure of metallic tungsten could be neglected during our experiments.

The experiments were run sequentially and automatically started from 100 s after launch of the rocket. Electrical heating of the evaporation sources were started at 105, 180 and 255 s for DUST 1-3, respectively. Evaporated vapor of tungsten oxide or iron was diffused, cooled and condensed in the gas atmosphere. The temperature and concentration at the nucleation site are determined from the changing of the refractive index, which is obtained from a movement of the fringes in the interferogram. Figure 2 shows an example image of interferogram after nucleation of iron nanoparticles for DUST 2 experiment. Here, we will show the first results of the microgravity experiment, such as supercooling, and the physical properties of the nanoparticles based on nucleation theories.

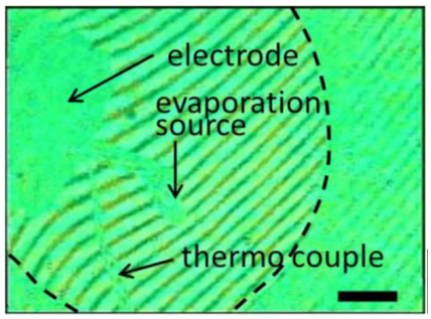

Figure 2. A still snapshot of *in-situ* observation of the interferogram during a microgravity experiment of DUST 2 using the sounding rocket S-520-28. Dotted circle indicates a nucleation front of iron nanoparticles. Diffuse fringes in the outside of the dotted circle are result of light scattering due to produced iron particles. The scale bar corresponds to 2 mm.

[1] T. Yamamoto, H. Hasegawa, *Prog. Theor. Phys.* **58**, 816 (1977).
[2] H. Miura, K. K. Tanaka, T. Yamamoto, T. Nakamoto, J. Yamada, K. Tsukamoto, J. Nozawa, *Astrophys. J.* **719**, 642 (2010).
[3] J. L. Schmitt, G. W. Adams, R. A. Zalabsky, *J. Chem. Phys.* **77**, 2089 (1982).
[4] G. W. Adams, J. L. Schmitt, R. A. Zalabsky, *J. Chem. Phys.* **81**, 5074 (1984).
[5] Y. Kimura, K. Tsukamoto, *J. Jpn. Soc. Microgravity Appl.* **28**, S9 (2011).
[6] Y. Kimura, H. Miura, K. Tsukamoto, C. Li, T. Maki, *J. Cryst. Growth* **316,** 196 (2011).
[7] Y. Kimura, K. K. Tanaka, H. Miura, K. Tsukamoto, *Crystal Growth & Design* **12**, 3278 (2012).
[8] B. P. Michael, J. A. Nuth III, L. U. Lilleleht, *Astrophys. J.* **590**, 579 (2003).
[9] Y. Clergent, C. Durou, M. Laurens, *J. Chem. Eng. Data* **44**, 197 (1999).

MICROTEXTURE AND FORMATION MECHANISM OF IMPACT DIAMONDS FROM THE POPIGAI CRATER, RUSSIA

***Ohfuji H.*[1], *Irifune T.*[1], *Litasov K.D.*[2], *Yamashita T.*[1], *Afanasiev V.P.*[2], *Pokhilenko N.P*[2].**

[1] *Geodynamics Research Center, Ehime University, Japan*
[2] *V.S. Sobolev Institute of Geology and Mineralogy SB RAS, Novosibirsk, Russia*
ohfuji@sci.ehime-u.ac.jp

Large meteoritic impact occasionally produces an extensive amount of diamond on the surface of the Earth **[1, 2]**. Popigai crater located in the north central Siberia is a typical example of such diamond-forming shock events and has recently been brought back into the spotlight due to its vast estimated reserves of the impact diamonds **[2-4]**. Authigenic impact diamonds occur in shocked graphite-bearing garnet-biotite gneisses that are found as inclusions in impact melt rocks, so-called tagamites and suevites. Popigai diamonds occur as irregular to tabular grains of 0.5-2 mm size (up to 10 mm) and usually show yellow, gray or black colors **[3]**. Electron microscopic (SEM and TEM) observations in previous studies described that they are polycrystalline aggregates of 0.1-1 μm grains and show a distinct preferred orientation along the [111], which is in a coaxial relation to the [001] of the original graphite source **[2-4]**. This crystallographic feature as well as the occasional coexistence of lonsdaleite, a metastable carbon polymorph, suggest the Martensitic phase transformation for the potential formation process of the impact diamonds from Popigai crater. However, the textural feature of the impact diamonds and its variation has not fully been examined. Here, we present the result of detailed microtextural observations of impact diamonds from the Popigai crater by transmission electron microscopy (TEM) and discuss the formation mechanism and condition in comparison with those of synthetic diamonds obtained by high pressure and high temperature experiments.

In total 10 diamond grains (7 transparent yellowish and 3 black samples) from the Popigai crater were studied. Each sample was first analyzed by a micro-focus XRD equipped with a Mo target and an IP detector. The results showed that transparent samples consist mostly of diamond and occasionally contain lonsdaleite, while black ones are a mixture of graphite, lonsdaleite and diamond, which are all in a coaxial relation as shown by 2D diffraction patterns. Each sample was then transferred to a focused ion beam (FIB) system to cut out TEM foil sections perpendicular to the surface (of the tabular grains). TEM observation revealed that although all the samples commonly possess layered structures and preferred orientation (mostly along [111] of diamond), there are varieties in crystallite (grain) size (down to 10-20 nm) and degree of preferred orientation. Taking into account the similarity in texture and preferred orientation feature between the Popigai diamonds and synthetic diamond, the variation is likely derived from the small difference in crystallinity of the starting graphite sources and perhaps more significantly from the difference in shock temperature.

According to the shock features recorded in the silicate minerals of the diamond-bearing impactites, the threshold pressure for the onset of the graphite-diamond transformation is estimated to be 34-36 GPa **[3]**. However, our recent experimental synthesis **[5]** demonstrated that a similar phase assembly (mostly diamond + traces of lonsdaleite) and microtexture can be produced at much lower pressures of 15-25 GPa at > 2000°C. The shock pressure as well as shock- and post-shock temperature accompanied with the formation of the Popigai crater might be needed to be reevaluated carefully to understand the real nature of the giant impact.

[1] Masaitis V.L. 1998. Meteoritics & Planetary Science. 33. 349-359.
[2] Langenhorst F., Shafranovsky G.I., et al. 1999. Geology. 27. 747-750.
[3] Deutsch A., Masaitis V.L., et al. 2000. Episodes. 23. 3-11.
[4] Koeberl C., Masaitis V.L., et al. 1997. Geology. 25. 967-970.
[5] Isobe F., Ohfuji H., et al. 2013. Journal of Nanomaterials. 2013. 380165.

MINERAL COMPOSITION OF THE CHELYABINSK LL5 CHONDRITE, RUSSIA

***Sharygin V.V.*, Karmanov N.S., Timina T.Yu., Tomilenko A.A., Podgornykh N.M.**
V.S. Sobolev Institute of Geology and Mineralogy SB RAS, Novosibirsk, Russia
sharygin@igm.nsc.ru

The entry in the Earth's atmosphere, further blasting and impact of the Chelyabinsk meteor body have been fixed at 9.20 hours (local time) on 15 February 2013. We studied small fragments (up to 5 g) collected in the areas of abundant meteorite shower (the Etkul region of the Chelyabinsk district, South Urals): between villages of Deputatskoe and Bereznyaki and between village of Emanzhelinka and settlement of Baturinsky (town of Emanzhelinsk). The Chelyabinsk meteorite was classified as an ordinary LL5 chondrite (S4, W0) [**1**]. It is very similar in mineral composition to other LL5 chondrites such as Salzwedel, Hautes Fagnes, Al Zarnkh and others **[2-7]**. All fragments of the Chelyabinsk meteorite consist of coarse- to fine-grained matrix, rare submillemetre chondrules and thin fusion crust (Fig. 1). Some fragments are brecciated.

Olivine ($Fo_{68-72}Fa_{28-31}Ln_{<0.5}$), orthopyroxene ($En_{70-74}Fs_{25-28}Wo_{1-2}$), Fe-Ni-metal, troilite, chromite and Na-rich plagioclase ($Ab_{77-86}An_{10-20}Or_{3-10}$) are major primary minerals in the inner part. Ilmenite, Cr-diopside ($Wo_{46-48}En_{43-45}Fs_{16-18}$, Cr_2O_3 – 0.6-0.8 wt%), chlorapatite $Ca_5(PO_4)_3Cl$ (Na_2O – 0.4-0.7; FeO – 0.2-1.1; Cl – 5.3-6.0; F – 0.0-1.1wt%), merrillite $Ca_9NaMg(PO_4)_7$ (MgO – 3.4-3.8; FeO – 0.8-1.5; Na_2O – 2.5-2.9 wt%) and feldspathic glass are minor. Coarse- to meduim-grained matrix mainly contains primary minerals (olivine, pyroxenes, etc.); some areas show fine recrystallization due to melting and further quenching with formation of skeletal crystals of Fe-rich olivine ($Fa_{29-46}Ln_{1-3}$), subcalcium pyroxene ($Wo_{22-42}En_{45-65}Fs_{13-22}$) and orthopyroxene in feldspathic glass (plagioclase). Metal-sulfide assemblage (up to 10 vol%) is represented by kamasite-taenite intergrowths ("plessite", Ni -15-25 wt%) or their individuals (Ni - 4.1-6.4 wt% in kamasite, Ni - 30.2-38.0 wt% in taenite) and troilite. Pentlandite (Fe – 43.6-45.0; Ni – 20.1-21.6; Cu - 1.0-1.5; S – 33.5-34.0 wt%) and native copper occur rarely. Variable compositions for kamasite and taenite are shown on BSE images and elemental maps, assuming their subsequent solid phase decay or recrystallization with decreasing of temperature.

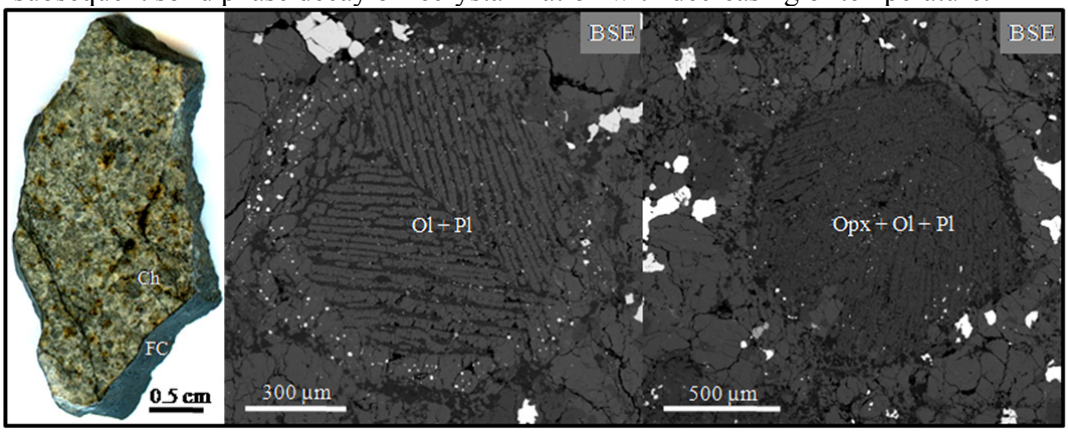

Figure 1. General view of a meteorite fragment and chondrules in it. Ch – chondules; FC – fusion crust; Ol – forsteritic olivine; Pl – albitic plagioclase; Opx – orthopyroxene.

Chondrules are different in mineralogy. Some of them show well-oriented "barred" texture and consist of olivine and Na-plagioclase (feldspathic glass) with minor chromite and chlorapatite (Fig. 1). Other phases (small metal-sulfide globules, Ca-silicates, orthopyroxene, etc.) mainly occur beyond of such chondrules or are localized in the outer parts of them. Other chondrules are similar in moda to the matrix and characterized by the predominance of orthopyroxene over olivine, but their oriented texture is less pronounced (Fig. 1).

Fusion crust (up to 1 mm) contains relics of primary minerals, mafic-ultramafic brown glass, abundant gas bubbles, new-formed minerals (zoned or skeletal crystals of silicates and

oxides) and Ni-rich metal-sulfide globules (Fig. 2). The central part of zoned spinel crystals is represented by chromite $FeCr_2O_4$, while outer part is magnetite $FeFe_2O_4$. Some skeletal aggregates of magnetite are rich in NiO. Some parts of fusion crust may bear wüstite (FeO – 92-96; CoO – 0.4-0.7; NiO – 0.7-2.1; MgO -0.9-1.2 wt%), which is located near metal-sulfide globules. New-formed crystals of olivine are zoned: the centre is forsterite (MgO – 30-36.7; FeO – 22.1-32.3 wt%); the rim is fayalite (MgO – 3.4-19.2; FeO – 43.4-65.3 wt%). Glass between zoned olivines is mafic-ultramafic in composition (wt%): SiO_2 – 41.3-41.5; Al_2O_3 – 3.5-3.8; FeO – 31.5-33.8; MgO – 3.5-3.9; CaO - 13.4-13.6; Na_2O – 1.5-2.5; K_2O – 0.3; Cr_2O_3 – 0.3. Dark brown glass in other parts of fusion crust (Fig. 2) is inhomogeneous and approaches olivine or orthopyroxene in the major oxides (wt%): SiO_2 – 40.8-43.5; Al_2O_3 – 2.1-2.8; Cr_2O_3 – 0.2-0.3; FeO – 21.7-27.1; MgO – 22.0-24.9; CaO – 1.8-2.5; Na_2O – 0.9-1.4; K_2O - 0.1-0.2; NiO – 0.3-1.1. Such variations seem to be caused by the amount and ratio of the main minerals (olivine, orthopyroxene, plagioclase, possibly Fe-Ni metal and troilite), which were involved in melting process on individual areas of the meteorite surface.

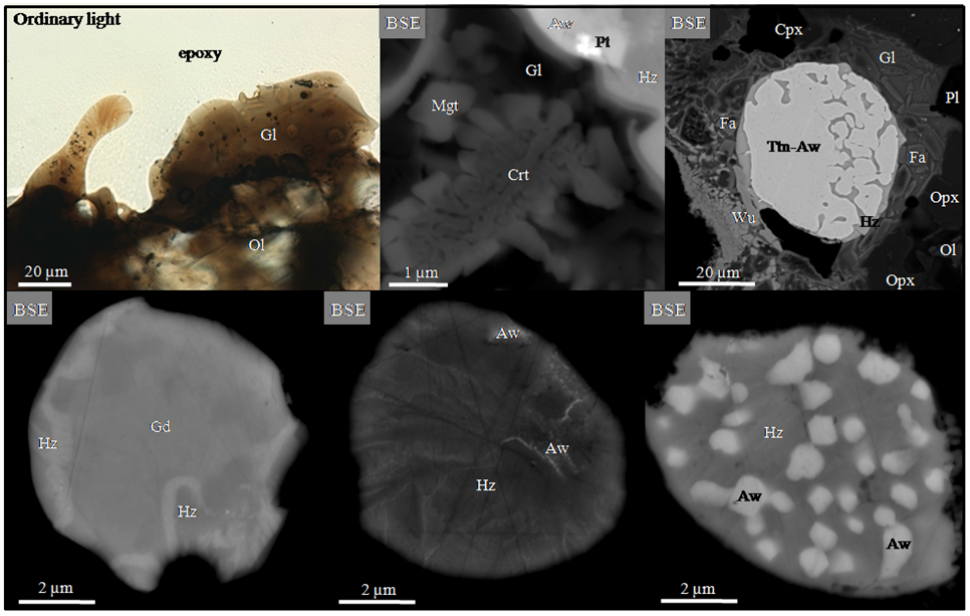

Figure 2. Glass, new-formed crystals and metal-sulfide globules in fusion crust of the Chelyabinsk meteorite. Gl – glass; Ol – forsteritic olivine; Crt – chromite; Mgt – magnetite; Hz – heazlewoodite; Pt – Os-Ir-Pt-Ni-alloy; Aw - awaruite; Ttn – tetrataenite; Fa – zoned forsterite-fayalite; Opx – orthopyroxene; Wu – wüstite; Gd – godlevskite.

Godlevskite- and heazlewoodite-rich metal-sulfide globules are most common in fusion crust of the meteorite (Fig. 2). In addition they may bear awaruite, tetrataenite, Cu-rich phases and rarely intermetallic alloy of Os-Ir-Pt-Ni. Globules with troilite and kamacite-taenite are scarce in fusion crust. BSE images and elemental maps for heazlewoodite and godlevskite phases indicate their solid decay transformation. This is strongly evidenced that heazlewoodite $(Fe_xNi_{1-x})_{3+y}S_2$ and godlevskite $Ni_{7+z}S_6$ solid solutions were first phases, which crystallized from new-formed sulfide-rich melt. According to the diagram Fe-Ni-S **[8]** these high-temperature phases should be inevitably transformed into stoichiometric heazlewoodite Ni_3S_2 or godlevskite Ni_9S_8 with temperature decreasing to form additional phases in the intergranular space.

[1] Anfilogov *et al.* (2013) *Lithosphere*, iss. **3**. **[2]** Matthes (1995) *Chem Erde-Geochem* **55**, 257-261. **[3]** Gismelseed *et al.* (2005) *Meteorit Planet Sci* **40**, 255-259. **[4]** Vandeginste *et al.* (2012) *Geol Belg* **15**, 96-104. **[5]** Graham *et al.* (1988) *Meteoritics* **23**, 321-323. **[6]** Reed & Chinner (1993) *Meteoritics* **28**, 421-421. **[7]** Gastineau-Lyons *et al.* (2002) *Meteorit Planet Sci* **37**, 75-89. **[8]** Kosyakov *et al.* (1996) *Geol Geofiz* **37**, 7-17.

CARBONACEOUS PHASES IN THE SURFACE LAYER OF INDIVIDUAL CHONDRULES OF SARATOV (L4) ORDINARY CHONDRITE: RAMAN RESULTS

Shiryaev A.A. [1]***, Fisenko A.V.*** [2]***, Averin A.A.*** [1]***, Verchovsky A.B.*** [3]***, Semjonova L.F.*** [2]

[1] *Institute of Physical Chemistry and Electrochemistry RAS, Moscow, Russia*
[2] *Vernadsky Institute of Geochemistry and Analytical Chemistry, Moscow, Russia*
[3] *Department of Physical Sciences, Open University, Walton Hall, Milton Keynes, UK*
shiryaev@phyche.ac.ru

Introduction. Nature of the phase Q is one of the most important problems of cosmochemistry. This phase contains the main fraction of trapped (primordial) heavy noble gazes (Ar, Kr and Xe) in meteorites. Numerous studies established that the phase Q makes less than 1 mass% and is resistant to HF+HCl treatment, but is almost completely destroyed during oxidizing treatment (e.g., HNO_3). The latter fact likely indicates that the phase Q is a carbonaceous substance. Therefore, investigation of noble gazes in various fractions of meteoritic material combined with study of associated carbon phases is one of the most promising approaches. Here we report some results of such complementary study of bulk material and of individual chondrules from Saratov (L4) chondrite.

Experimental methods. Noble gazes in bulk sample of Saratov meteorite were measured using multi-element isotope analyser "Finesse" in combination with stepped combustion. Separation of drop-like chondrules was performed by gentle step crushing of the meteorite down to ≤ 1.2 mm. Some chondrules (denoted as B) were treated with $K_2Cr_2O_7$ for 8 h at 80 °C. Individual chondrules of markedly different sizes (> 2 mm and <1 mm in diameter) were studied using Senterra Raman microscope in range 100-1700 cm^{-1} which allowed examination of carbon-related features and of mineralogy of silicate matrix. Excitation wavelength was 532 nm. Since on microscopic scale the chondrules are heterogeneous, many spectra were collected for each chondrule. The laser power was kept at low values (≤2 mW) to prevent sample damage. This value was selected based on test experiments on the same chondrules which showed negligible differences between spectra recorded at 0.2 and 2 mW. Stability of carbonaceous matter in chondrules under very similar conditions was earlier reported **[1, 2]**. In most cases fluorescence was weak and was neglected. After subtraction of linear background the "graphitic" range was analysed using components with Lorentzian shapes. In most cases decomposition into two bands (well-known G and D bands) a relatively weak band centered around 1550 cm^{-1} was required to achieve good fit of experimental spectra (fig. 1). The physics background of this additional weak band is discussed in literature (e.g. **[3]**) and may correspond to G-band of (semi)amorphous carbon.

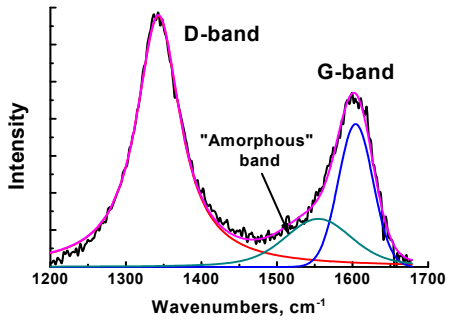

Figure 1. Typical Raman spectrum of carbonaceous phase in a chondrule. Example of spectral decomposition is shown.

Results and discussion. The main fractions of carbon and of noble gazes are released independently from each other during oxidation of bulk sample (fig 2). Most likely, oxidation of the phase Q results in peak of Ar release at 600°C with high $^{132}Xe/^{36}Ar$ ratio. Similarly high ratio observed at 900°C may indicate that the trapped gazes resides in two different carriers. Note that high $^{40}Ar/^{36}Ar$ ratio at 1200°C is due to radiogenic Ar from silicate minerals. According to Raman data olivine is the principal mineral phase of chondrules. A correlation between local mineralogy and carbon-related Raman features is likely present and partly explains observed scatter in position of the G-band and

I(D)/I(G) ratio between analysis spots on individual chondrules, but firm conclusions require more representative statistics.

Position of the G-band (1600-1608 cm^{-1}) suggests that carbon in surface layer of chondrules is mostly present as nanocrystalline graphite both in pristine and in acid-treated chondrules. In the same time, certain fraction of amorphous carbon is also present as indicated by clear contribution of broad "amorphous" band with position of maximum around 1540 cm^{-1}, i.e. close to G-band position of a-C.

Marked changes occur in position of the D-band after acid treatment: its position shifts to higher wavenumbers (from 1340 to 1350-1360 cm^{-1}) and FWHM increases, indicating growth of concentration of point defects (fig. 3). The intensity ratio I(D)/I(G), being a complex function of crystallite size, decreases in result of the acid treatment. Co-existence of carbons with various structure and perfection on microns scale stems also from examination of behavior of the "amorphous" band.

Conclusions. The results of this preliminary study of some fractions of Saratov (L4) meteorite show that (a) the main fraction of gazes of the phase Q during oxidation of the bulk sample is released at temperatures <700°C; (b) carbonaceous material in surface layers of small and large chondrules is largely similar, though considerable spot-to-spot variability is observed. Structure of the carbonaceous material is close to nanocrystalline graphite. After acid treatment mostly larger crystallites are preserved, but concentration of point defects increases.

This work is supported by RFBR grant 12-05-00208.

[1] Matsuda et al., *Geochim. Cosmochim. Acta*, 2010, 74, 5398-5409.
[2] Busemann et al., *Meteorit.Planet.Sci.*, 2007, 42, 1367-1416.
[3] Beny-Bassez and Rouzaud, *Scanning Electron Microscopy*, 1985, 119-132.

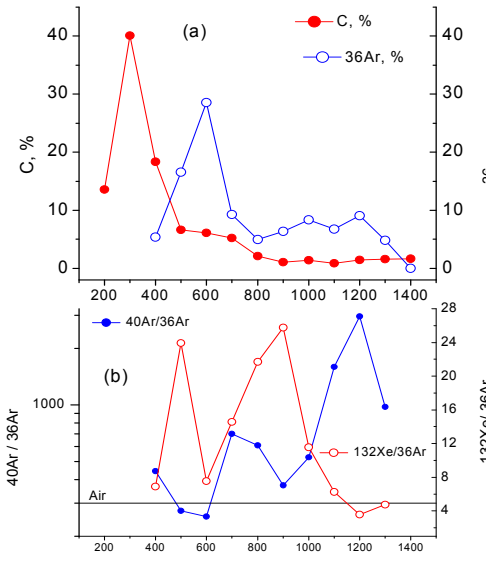

Figure 2. Gaz release from bulk sample of Saratov.

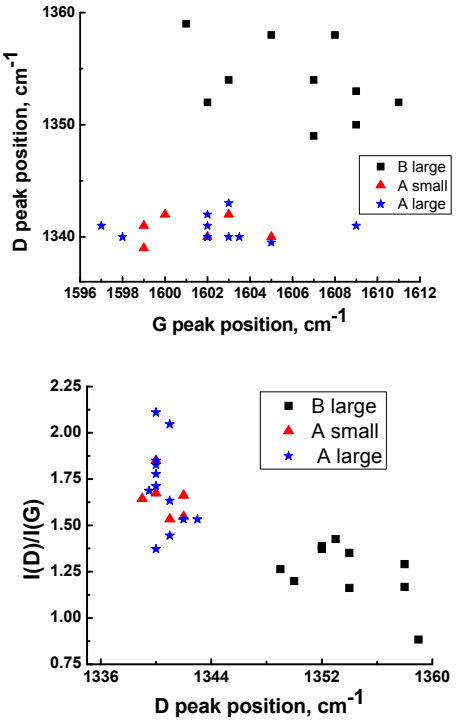

Figure 3. Structure-sensitive Raman features of carbon matter.

CRYSTALLIZATION 4.6 BILLIONS YEARS AGO

Tsukamoto K.

Graduate School of Science, Tohoku University, Sendai, Japan
Graduate School of Engineering, Osaka University, Osaka, Japan
ktsuka@m.tohoku.ac.jp

Crystallization of cosmic materials in the primitive solar system 4.6 billing years ago is an extremely large scaled crystallization. Chondrule, a mm sized silicate sphere formed before the formation of planets, is one of the good examples,

Notwithstanding the importance of chondrules, these have been believed from a few primitive crystal growth experiments to be formed very slowly in years at the temperatures near equilibrium of these constituting minerals, forsterite and enstatite. Since we have many experiences of crystallization in space environments, like in international space station, rockets and aircrafts, the idea of the extremely slow process did not fit to our understanding. We therefore started new in-situ observation of chondrule formation during levitating of high temperature melt droplets in air.

The levitation is the key for the understanding of crystallization of chondrules from the melt. Because of no contact of the melt with a holder or a holder, no heterogeneous nucleation, which is common nucleation and rapid compared to homogeneous nucleation, occurred and thus crystallization becomes very difficult. This results in the crystallization at the temperature of several hundreds degrees below the equilibrium temperature which we have never thought about. Such a large supercooling is defined as a hypercoolig regime in metallurgy with strange crystal growth behavior and effects of such difficult crystallization on the chondrule formation will be discussed.

STRUCTURE OF IMPACT DIAMONDS FROM THE POPIGAI ASTROBLEME INVESTIGATED BY OPTICAL SPECTROSCOPY

Yelisseyev A.P. [1], , *Afanasyev V.P.* [1], *Pokhilenko N.P.* [1], *Isakova A.* [1], *Meng G.S.* [2], *Lin Z.S.* [2], *Lin H.Q.* [3], *Rashchenko S.V.* [1], *Litasov K.D.* [1]

[1] *V.S.Sobolev Institute of Geology and Mineralogy, SB RAS, Novosibirsk, Russia*
[2]*BCCRD, Key Laboratory of Functional Crystals and Laser Technology, Technical Institute of Physics and Chemistry, CAS, Beijing, China*
[3]*Beijing Computational Science Research Center, Beijing, China*
eliseev.ap@mail.ru

Impact diamond is a new superhard carbon mineral, which formed in the place where an asteroid impacted the Earth. The P-T parameters at this moment were estimated to reach T~4000 °C and P~140 GPa which exceeds considerably those for the growth of kimberlite diamonds. The interest to impact diamonds is large because 1. it is a new nanostructured carbon material with an extremely high wear resistance (2 to 3 times higher in comparison with that for a usual kimberlite diamond) and 2. for the Popigai astrobleme there was a high carbon content in the breeds in the impact place and a great amount of impacts diamonds formed. It is very important to study in detail the structure of impact diamonds, to compare it with that of natural kimberlite and synthetic diamonds produced by different techniques in the laboratories. It is important also to estimate an opportunity of application of impact diamonds as well as of producing its synthetic analogues if necessary.

A set of structurally-sensitive non-destructive techniques were used to characterize the impact diamonds from the Popigai astrobleme: X-ray structure analysis (RSA), optical vibrational spectroscopy and absorption/luminescence spectroscopy. RSA shows a presence of both cubic (3C) and hexagonal (2H, lonsdaleite) diamond phases in transparent impact diamonds with the 2H input of about 30 %. Fundamental absorption edge for Popigai impact diamonds is shifted ~0.5 eV to lower energies in comparison with cubic structure, 3C diamonds (5.47 eV) supposedly as a result of the 2H input, in good agreement with ***ab initio*** calculations (E_g = 5.34 and 4.55 eV for 3C and 2H phases, respectively). Yellowish color of impact diamonds is due to Rayleigh light scattering on structural defects whereas graphite is responsible for grey to black coloring. In Raman spectra recorded at 514.5 nm excitation an intense signal near 1335 cm^{-1} dominates. It is similar to that in kimberlite 3C diamonds but considerably broadened (FWHM up to 30 cm^{-1}) and with a well-pronounced structure: the result of deformations in the lattice and the 2H input. The results of the first principles simulations for 3C and 2H diamonds were used for interpretation. In Raman spectra of dark impact diamonds there are signals from the amorphous, crystalline and disordered graphite with dominating sp^2-bonding. The sizes of graphite domains vary from 10 to 100 nm. Micro-Raman study shows also the inclusions of foreign noncarbon minerals such as quartz, magnetite, haematite. Their specific lines are somewhat shifted because of residual stresses in their lattice.

In the mid-IR region there is a multi-phonon absorption of 3C diamond in the 1800 to 4000 cm^{-1} range and some new bands at 969, 1102, 1225, 1330 cm^{-1} in the one-phonon region. Some of them are similar to those in polycrystalline nanostructured aggregates of 3C diamond and CVD diamond films. There is no nitrogen-related signal in the mid-IR absorption but luminescence spectroscopy showed the presence of nitrogen-vacancy centers with a different aggregation degree such as NV^-, NVN, N_3V. Some of the noncarbon inclusions demonstrate the Cr^{3+} luminescence.

This work was supported by the Russian Foundation for Basic Research (grant 13-05-00568a), Ministry of education and science of Russian Federation, No 14.B25.31.0032, National Natural Science Foundation of China, Nos 11174297 and 91022036 and National Basic Research Project of China, Nos 2010CB630701 and 2011CB922204.

LUMINESCENCE OF NANOSTRUCTURED SUPERHARD CARBON MATERIAL: IMPACT DIAMONDS FROM THE POPIGAI ASTROBLEME

Yelisseyev A.P. [1], ***Pustovarov V.*** [2], ***Sildos I.*** [3], ***Kiisk V.*** [3], ***Isakova A.*** [1], ***Afanasyev V.P.*** [1], ***Pokhilenko N.P.*** [1], ***Litasov K.D.*** [1]

[1] *V.S. Sobolev Institute of Geology and Mineralogy, SB RAS, Novosibirsk, Russia*
[2] *Ural Federal University, Yekaterinburg, Russia*
[3] *The University of Tartu, Tartu, Estonia*
eliseev.ap@mail.ru

Impact diamonds are a new nanostructured multiphase carbon mineral formed at extremal P and T –parameters in the shock process when an asteroid meets the Earth. According to electron microscopy and Raman scattering the sizes of crystalline pieces (blocks) vary from 10 to 100 nm. Luminescence analysis in different versions was used to study several tens of transparent impact diamonds from the Popigai astrobleme, each ~ 1.5 mm in size. They were mainly thin plates ~100 μm thick, of yellowish color with cubic, 3C and hexagonal, 2H diamonds as the dominating carbon phases. All crystals demonstrated an intense yellow photoluminescence at UV excitation. The transparency of impact diamonds varies to completely opaque (black colored) as the input of carbon phases with the sp^1, sp^2 hybritization increases.

The low-temperature luminescence spectra were recorded at the X-ray and optical (from the lamp, laser and synchrotron sources) excitation in the stationary and time-resolved regimes at 5, 80 and 300K. The X-rays and synchrotron radiation provide the band-to-band excitation, whereas the other sources produce the intra-center processes. The luminescence excitation spectra and PL temperature quenching and thermostimulated luminescence (TSL) curves were also studied. In PL spectra the broad bands with FWHM ~ hundreds nm dominate although sometimes there are also the relatively thin lines with FWHM~ 5 nm and their width does not change as crystal temperature decreases. The width of these zero-phonon lines (ZPL) is ~25 meV in impact diamonds whereas in kimberlite diamond single crystals it is ~ 0.5 meV (1 nm). It is a result of strong deformations and stresses in crystal lattice. On example of synthetic diamonds we observed that vibronic systems with a well-pronounced fine structure in the low-temperature absorption/luminescence spectra transform into broad bands of the Gauss shape as deformations increase and the vacancy-containing centers are the most sensitive in the diamond lattice.

Although nitrogen is not observed in the one-phonon absorption in the mid-IR we found nitrogen traces using the much more sensitive PL technique. In some impact diamonds we observed the vibronic systems with ZPLs at 638, 503 (system H3) and 415 nm (N3) related to nitrogen-vacancy centers with the structure NV, NVN (H3), N3V (N3), respectively. In PL decay for these centers there is usually a nanosecond component in accord with results for kimberlite diamond whereas there is also a long component with τ up to hundreds of μsec, which is a result of recombination processes with a charge transfer between the point defects. The presence of above-mentioned centers means that 1. There is some (<5 ppm) nitrogen in impact diamonds and 2. The formation conditions (T and maybe P) and the impurity aggregation degree vary considerably sample to sample. The lines in the 650 to 750 nm range are similar to those in 3C natural and synthetic diamonds and may be related to nickel-nitrogen-vacancy centers.

The temperature quenching of yellow PL in impact diamonds is described by the Mott law with the parameters E_T=0.1 eV, $\omega_0=1.4\times10^2$ sec^{-1} : PL decreases 3 to 4 times as temperature grows from 80 to 300 K and quenches completely to 500 K. In the TSL curves there is a set of peaks with the main components at 150, 280 and 380 K, which have no analogues in kimberlite diamonds; the kinetic parameters of corresponding traps were estimated.

This work was supported by the Russian Foundation for Basic Research (grant 13-05-00568a) and Ministry of education and science of Russian Federation, No 14.B25.31.0032.

SESSION 7

DEEP CARBON OBSERVATORY
Satellite symposium

"Deep carbon cycle:
Mineralogy and crystal chemistry of
carbon-bearing compounds"

STABILITY AND POLYMERIZATION OF POLYCYCLIC AROMATIC HYDROCARBONS AT HIGH PRESSURES AND TEMPERATURES

Chanyshev A.D. [1,2], ***Litasov K.D.*** [1,2], ***Shatskiy A.*** [1,2], ***Furukawa Y.*** [3], ***Ohtani E.*** [3]

[1]*Sobolev Institute of Geology and Mineralogy, Novosibirsk, Russia*
[2]*Novosibirsk State University, Novosibirsk, Russia*
[3]*Tohoku University, Sendai, Japan*
chanyshev_90@mail.ru

The origin of various deep-seated hydrocarbons was widely discussed in relation to the study of the C-O-H fluid. The estimation of fO_2 conditions in the deep mantle indicate that it can be in equilibrium with reduced fluids and absolute values of fO_2 in mantle rocks can be fluctuated near that for the iron-wustite buffer at the depth below 300 km [1]. Calculations of fluid compositions at these conditions in the simple C-O-H system indicate the dominant CH_4-H_2O mixture, with subordinate H_2, and heavier hydrocarbons [1]. However, some theoretical calculations of equations of state for a range of hydrocarbons indicate their possible increased stability in the deep mantle. According to estimations of [2] and [3] some heavy alkanes, alkenes, polycyclic aromatic hydrocarbons (PAH), as well as some C-N and C-S compounds can become stable in the mantle at the depths of 300-600 km and deeper. Study of natural samples, such as garnet, olivine and garnet from kimberlite pipes, has revealed hydrocarbons inclusions. The number of these hydrocarbons is limited and includes naphthalene, phenanthrene, pyrene, benzopyrene and benzoperylene [4]. Discovery of different PAHs in the Murchison meteorite also indicates importance of their study [5].

Experimental studies of reduced volatile species, such as hydrocarbons, and their phase relations with mantle silicates are extremely challenging and difficult. Recent high-pressure experiments reveal the limited temperature stability of several PAHs at pressure about 8 GPa [6]. Graphite and amorphous carbon were detected among experimental products. Behavior of polycyclic aromatic hydrocarbons at impact shock experiments were studied by Mimura and Toyama at pressures up to 30 GPa [7]. Polymers of starting materials were observed by gas chromatography. Anyway, these data are insufficient for full understanding of stability and chemical reactivity of PAHs at mantle conditions.

This research presents the results of stability and polymerization of different polycyclic aromatic hydrocarbons at pressures near 7 GPa and temperatures 773-1073 K. PAHs were selected according to abundance in natural samples [4] and meteorites [5]. The starting materials were from naphthalene ($C_{10}H_8$) to coronene ($C_{24}H_{12}$). The experiments were conducted in multianvil hydraulic presses. The decomposition parameters were detected by *in situ* X-ray diffraction at the SPring-8 (Japan). In the pressure range of 6-9 GPa selected PAHs become unstable at temperatures of 873-1073 K (Fig.1). At room temperature peaks were indexed according to published date (e.g. [8]). Laboratory multianvil experiments were performed in the Tohoku University at pressure about 7 GPa and fixed temperature. After experiments we analyzed products using matrix-assisted laser desorption/ionization method (MALDI). As a result, the formation of polymers of starting materials at 7 GPa and 773-873 K was determined. The polymers have atomic masses up to 5000 Da (Fig.2).

The determined P-T parameters for the PAHs stability field do not correspond to the upper mantle conditions; therefore PAHs in diamonds and other mantle minerals [4] would have secondary origin. Indeed, data for PAHs stability is important for near-surface geodynamics of small and large planetary bodies. Identified polymerization of PAHs at lower temperature also can play important role for study of the interstellar matter.

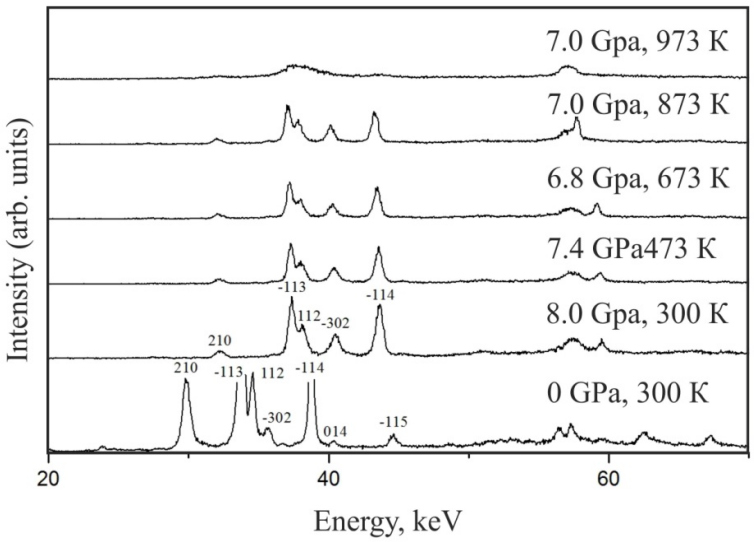

Figure 1. Changes of diffraction patterns of coronene at pressure near 7 GPa. Space group corresponds to $P2_1/a$ [8]. At 7 GPa and 973 K coronene is decomposed.

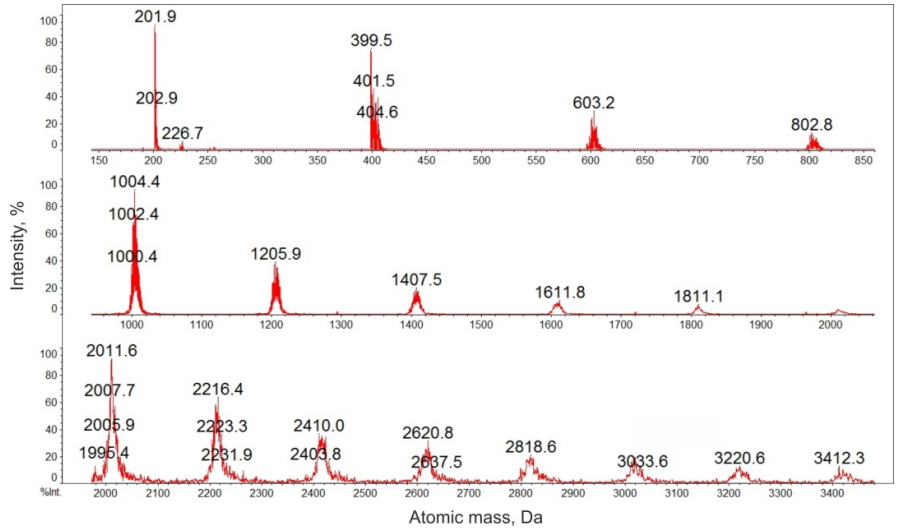

Figure 2. Strong polymerization of pyrene at 773 K and 7 GPa with formation of compounds with atomic masses to 5000 Da. The scale is relative to strongest peak of the selected interval.

The work is supported by RFBR No 12-05-00841, 12-05-33008 and research grant of "BP" for young scientists.

References:

[1] Frost D.J., McCammon C.A. // Annual Review of Earth and Planetary Sciences. 2008. V.36. P.389-420.
[2] Zubkov V.S. // Bulletin GeoIGU. Geochemical processes and minerals. 2000. P.10-28.
[3] Chekaluk, E.B., 1967. Oil of the Earth's upper mantle. Naukova Dumka, Kiev, 256 pp.
[4] Kulakova I.I., *et al.* // Doklady AN USSR. 1982. V.267. P.1458-1461.
[5] Oro J., Gibert J., Lichtenstein H., Wikstrom S., Flory D. // 1971.
[6] Davydov V., Rakhmanina A., Agafonov V., Narymbetov B., Boudou J.-P., Szwarc H. // Carbon. 2004. V.42. P.261-269.
[7] Mimura K., Toyama S. // Geochimica et Cosmochimica Acta. 2005. V.69. P.201-209.
[8] Echigo T., Kimata M., Maruoka T. // American Mineralogist. 2007. V.92. P.1262-1269.

3-D TOMOGRAPHY OF DIAMONDIFEROUS XENOLITHS FROM YAKUTIA

Howarth G.[1], Sobolev N.V.[2], Ketcham R.[3], Maisano J.[3], Logvinova A.M.[2], Taylor D.[1], Taylor L.[1]

[1] Earth & Planetary Sciences, Univ. of Tennessee, Knoxville, TN, USA
[2] V.S. Sobolev Institute of Geology and Mineralogy, SB RAS, Novosibirsk, Russia
[3] Jackson School of Geosciences, Univ. of Texas, Austin, TX, USA
ghowarth@utk.edu

Introduction: New innovations in three-dimensional (3-D), high-resolution X-ray computed tomography (HRXCT) of diamondiferous eclogite and peridotite xenoliths from Yakutia has successfully imaged diamonds (Ds) and their textural relationships with coexisting minerals. In total, some 20 diamondiferous xenoliths from the Mir and Udachnaya kimberlites have been processed ranging from 10 g to 8.8 kg. Ds (78; >1 mm), with a total weight of just over 5 carats and forming an ore grade of some 45,000 ct/ton, were found in one relatively small (4x5x6 cm) eclogite from Udachnaya. Another small (10.5 g) diamondiferous peridotite has >30,000 microdiamonds [1].

Using this new 3-D imaging technique, the Ds always appear to be associated with zones of secondary alteration of clinopyroxene (Cpx) and/or garnet (Gt) [Fig. 1a]. *The presence of Ds with secondary minerals is strong evidence that the Ds formed after the primary minerals of the xenoliths, in conjunction with episodes of metasomatic input(s) of carbon-rich fluids.* Rare dodecahedral Ds [Fig. 2b] within xenoliths, rather than typical octahedral morphologies [Fig. 2a], imply *in-situ* resorption, in these cases, unrelated to interaction with kimberlite magma transport. Metasomatic processes are also indicated by the non-systematic variations in Cpx inclusion chemistry in several Ds within the same xenolith. *The inclusions in the Ds can vary considerably in major- and trace-element chemistry within and between Ds, and do not always correspond to the minerals of the host xenolith, which usually have homogenous compositions* [2]. Sulfide inclusions in Ds [Fig. 1a] can be resolved by this X-ray imaging, due to their large attenuation contrast with Ds, and in sample U-65, inner inclusion-free and outer inclusion-rich zones of the Ds can be identified. This further implies D growth by multiple episodes of metasomatic fluids, in this case, initial growth from S-poor fluid and later growth from S-rich fluid.

A 3-D model is more representative of the sample than are thin-sections. Modal analyses of 5 thin sections from U-51 eclogite ranged from 25 to 40 vol% Gt, whereas the xenolith is actually 25.9 vol% Gt; most of the thin sections are poor representations of the complete xenolith. The 3-D image of the rock permits an effective mapping of all Ds and reveals D lineations along meta-somatic pathways [Fig.2b]. 3-D imaging permits for a systematic dissection of the xenolith.

X-ray tomography technique: High-resolution X-ray computed tomography (HRXCT) [3] permits the study of the entire volume of a xenolith in both 2-D and 3-D. This non-destructive technique can locate Ds and other minerals within the xenoliths and reveals their textural relationships. Subjecting an entire xenolith to this technique results in a complete series of 2-D slices, using a microfocal X-ray source and an image-intensifier detector system to measure the absorption of X-rays along thousands of different coplanar paths through the sample. These slices can be taken at intervals of <100 microns, and with further processing, a 3-D digital model that can be quantitatively analyzed for spatial and textural relationships can be created (Fig. 1b).

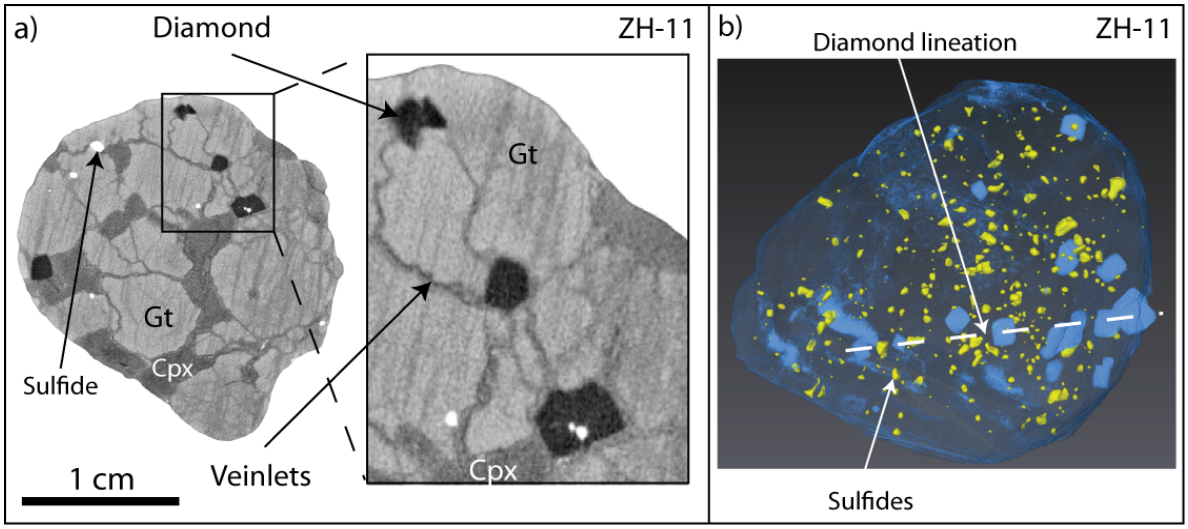

Figure 1. a) X-ray slice showing the ubiquitous occurrence of inter-connected cracks/veinlets between Ds and metasomatic pathways (Slice 573). b) 3-D rendered model showing multiple octahedral Ds in a lineation pathway. Ds (blue) and sulfides (yellow); Gt + Cpx invisible.

The 3-D HRXCT data were acquired in the plane containing the X-ray paths and divided into a matrix of cells or pixels (2048 x 2048); an X-ray attenuation value is derived for each cell in the matrix using standard tomographic techniques. Thereby, a 2-D image is produced that is a map of the values of the linear-attenuation coefficients for the input X-ray spectrum in a particular plane through the sample, in which different colors or levels of grey are assigned to different X-ray attenuation values [Figs 1 & 2]. The total attenuation depends upon the X-ray energy, mass density, and effective atomic number; proper selection of X-ray energies makes it possible to clearly distinguish diamonds from silicate, oxide, and sulfide minerals within the eclogite or peridotite specimens. Spatial relationships between diamonds and their surroundings can provide clues to the processes that control diamond formation. These relationships can be determined by rotating and viewing the model at different perspectives and orientations to look for any associations, possible D alignments, and secondary minerals.

Volume visualization software makes it possible to view any aspect of the 3-D model from any perspective. It is possible to render some of the model as transparent and display only one or two mineral phases at a time (Figure 1b). Then by rotating the model, it is possible to look for spatial relationships between different crystals of the same mineral or between different minerals. These visualizations are difficult to display as 2-D figures (Fig. 2), but an animation of the diamonds, garnets, clinopyroxenes, and alteration phases of eclogite xenoliths rotating in space can be most revealing.

This research was supported by the NSF Grant to LAT. EAR 1144337.

References:

[1] Logvinova, A. et al. (2013) A Unique Diamondiferous Peridotite Xenolith from Udachnaya: Evidence for Subduction. *DCO Abstract*, this vol.
[2] Taylor, L.A., Sobolev, N.V. et al. (2000) *Inter. Geol. Review 42*, 959-983.
[3] Ketcham, R.A. & Carlson, W.D. (2001) *Computers and Geosciences, 27*, 381-400.
[4] Liu, Y., Taylor, L.A., Sobolev, N.V. et al. (2009) *Lithos 112*, 1014-1024.

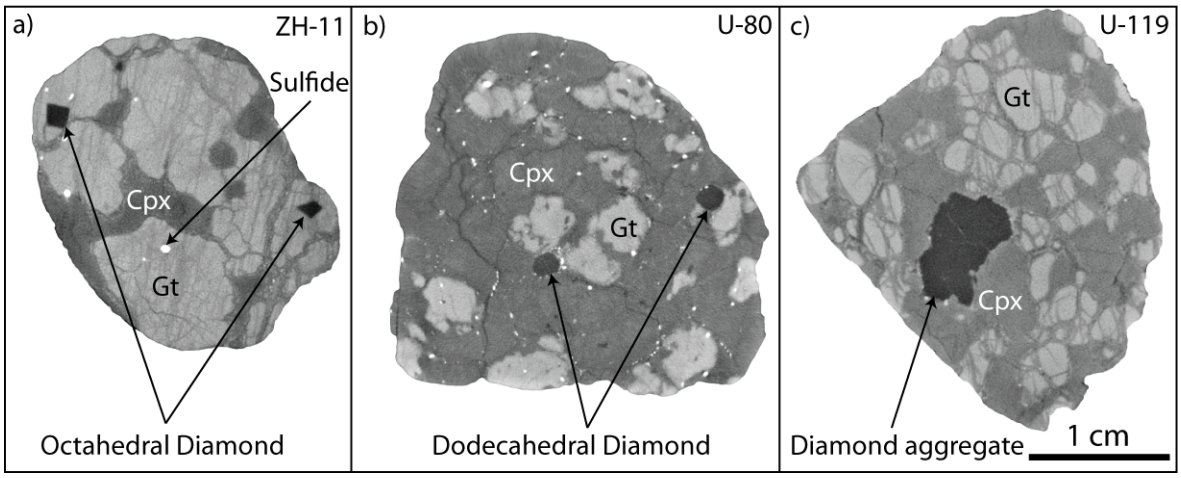

Figure 2. X-ray slices showing: a) octahedral Ds (black; slice 328); b) resorped dodecahedral Ds (slice 517); and c) diamond aggregates (slice 106). The white specks are sulfides.

EQUATION OF STATE OF NAPHTHALENE STUDIED BY FIRST PRINCIPLES CALCULATIONS

Inerbaev T.M. [1], ***Litasov K.D.*** [2,3], ***Likhacheva A.Y.*** [2]

[1] *LN Gumilyov Eurasian National University, Astana, Kazakhstan*
[2] *VS Sobolev Institute of Geology and Mineralogy SB RAS, Novosibirsk, Russia*
[3] *Novosibirsk State University, Novosibirsk, Russia*
klitasov@igm.nsc.ru

The high-pressure behaviour of hydrocarbons is widely discussed in relation to the nature of deep-seated C-O-H fluid and abiogenic origin of oil and gas deposits. Besides, hydrocarbons are important in planetary atmospheres and surface environments as well as in the interstellar space. The estimation of fO_2 conditions in the deep Earth's mantle indicate that it can be in equilibrium with reduced fluids and fO_2 in mantle rocks can be fluctuated near that for the iron-wustite buffer at the depth below 300 km. The calculations of fluid compositions at these conditions in the C-O-H system indicate the dominant CH_4-H_2O mixture. However, some thermodynamic calculations and high-pressure experiments predict that heavy hydrocarbons, such as alkanes, alkenes, polycyclic aromatic hydrocarbons (PAH), can become stable in the mantle fluids at 300-600 km and deeper. Indeed, high-pressure modelling of equations of state (EOS) for different hydrocarbons in solid and liquid state using experimental and theoretical approaches is extremely important for better understanding of deep Earth dynamics, as well this direction is also important to fundamental solid state chemistry. PAHs are important due to their presence in natural samples and meteorites. In this work the *P-V* and *P-V-T* EOSes of naphthalene were investigated using *ab initio* computations and compared with experimental data from *in situ* X-ray diffraction **[1]**.

Calculations are based on density functional theory (DFT) within the optPBE-vdW exchange–correlation functional **[2]** using a 600 eV plane-wave cut-off energy and 6x8x6 Monkshort-Pack K mesh. The crystal structure of $P2_1/a$ symmetry group experimentally determined at P=0.4 GPa was used for theoretical modeling **[3]**. The Helmholtz free energy of crystal was calculated using the lattice dynamics approach in the quasiharmonic approximation. In this way and third-order Vinet EOS we obtained V_0=373.8 A^3, K=7.3 GPa, and K'=8.2 for 298 K isotherm, which are fairly consistent with experimental data with slightly overestimated $_0$=361 A^3. Experimental data revealed K=8.4 GPa, and K'=7.2 **[1]**.We also obtained very low thermal expansion coefficients in accordance with the experiments. The extreme change of thermal expansion coefficient for PAH is observed between 0 and 1 GPa. The results for naphthalene EOS are shown in Figures 1-2.

The work is supported by RFBR No 12-05-00841, 12-05-33008.

References:

[1] Likhacheva A.Y., Rashchenko S.V., Chanyshev A.D., Inerbaev T.M., Litasov K.D., Kilin, D.S. Equation of state of solid naphthalene studied by in situ X-ray diffraction and first principles calculations, in prep.

[2] Klimeš, J.; Bowler, D.R., Michaelides, A. Journal of Physics: Condensed Matter 2010, 22, 022201.

[3] Fabbiani, F.P.A.; Allan, D.R.; Parsons, S.; Pulham, C.R. Acta Crystallographica Section B 2006, 62, 826-842.

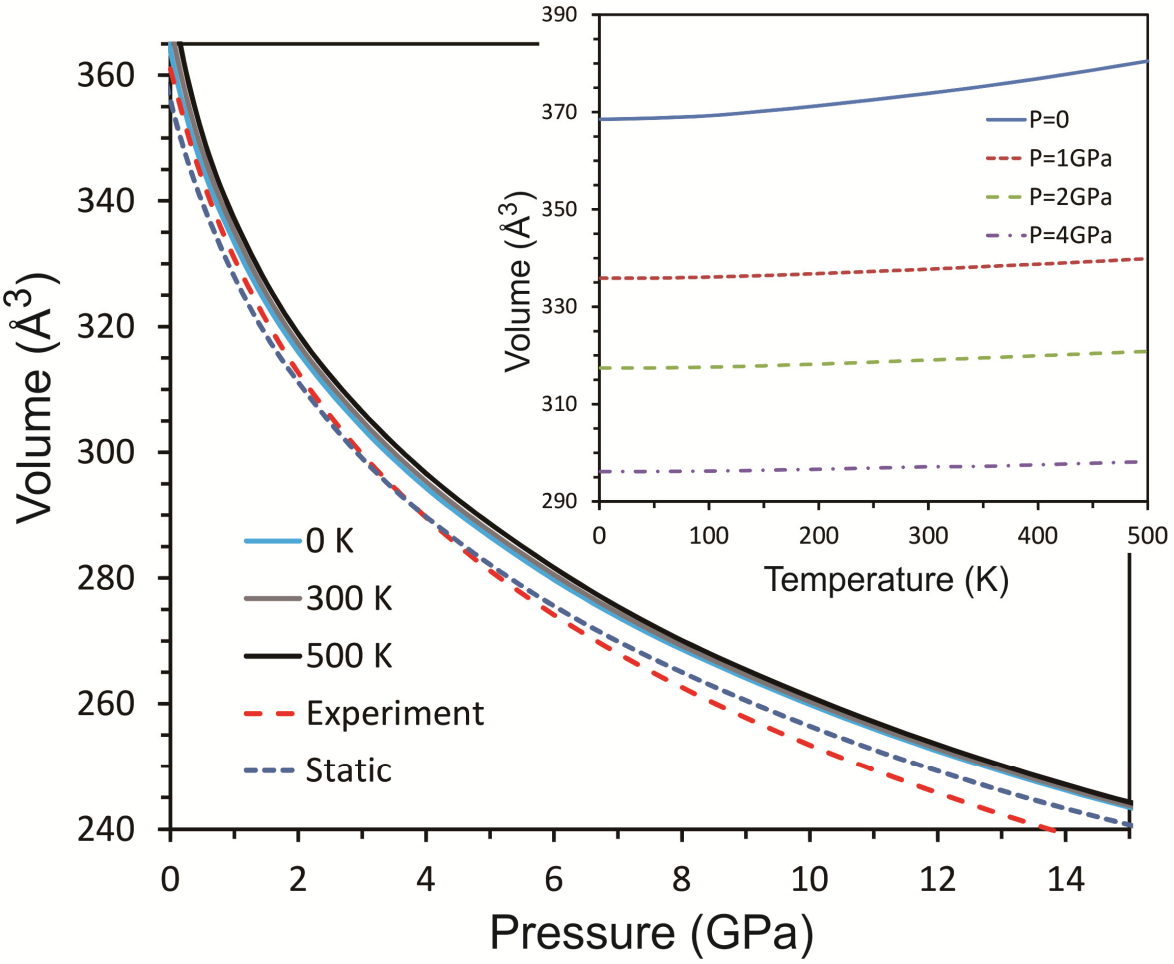

Figure 1. P-V-T relations of naphthalene from *ab initio* calculations. Static line corresponds to T=0 K without taking into consideration zero-point vibrations. Experimental curve is after **[1]**. Insert shows temperature dependence of volume at different pressures.

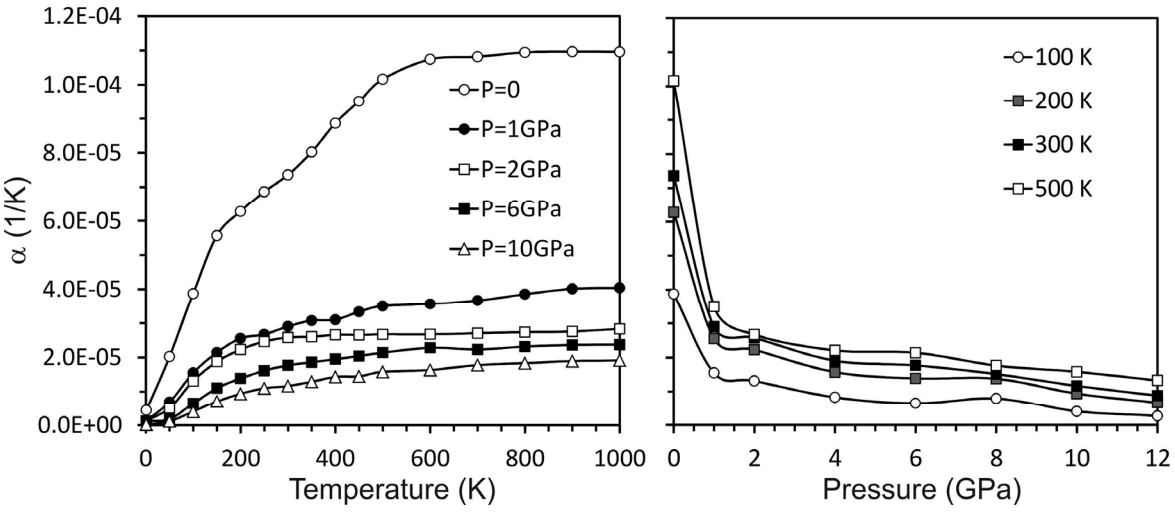

Figure 2. Thermal expansion coefficient of naphthalene from *ab initio* calculations.

STUDY OF MONOCRYSTALLINE LONSDALEITE BY RAMAN SPECTROSCOPY

Isaenko S.I.

Institute of Geology of Komi SC UB RAS, Syktyvkar, Russia
s.i.isaenko@gmail.com

The identification of lonsdaleite using Raman spectroscopy presently seems to be rather ambiguous. The position of diagnosis line of lonsdaleite in Raman spectra may be in range of 1315-1326 cm^{-1}. However, shift of three degenerate T_{2g}-mode of diamond (1332 cm^{-1} at room temperature) to short wavelength region of the spectrum may be due to laser heating at phase identification. For example, heating of diamond to 850-870 K during registration shifts the diagnostic line of diamond in Raman spectra from 1332 cm^{-1} to 1325 cm^{-1}, the largest shift occurs in nanocrystalline diamond. Ignoring the temperature shift may lead to erroneous interpretation of Raman spectra, incorrect detection of lonsdaleite phase in studied material. Therefore it is necessary to develop the instructional techniques that enable to distinguish Raman active modes of diamond and lonsdaleite.

For methodological adjustments of lonsdaleite micron-size particles diagnosis by Raman spectroscopy we have been carefully examined the samples, wherein previously using complex of methods we established lonsdaleite-containing and isolated single-crystal lonsdaleite particles of carbon mineralization of Kumdykol diamond deposit (Kazakhstan) **[1, 2]**. Raman spectra were registered by high resolution micro-spectrometer LabRam HR 800 (Horiba Jobin Yvon).

We used a dynamic scheme of Raman spectra registration at laser heating of the lonsdaleite particles. Initially a spectrum at a reduced power of the exciting radiation (1 mW) was registered and then a series of spectra with increased power (10 mW) was recorded with a minimum interval of time between registrations.

In dynamic mode more than thirty carbon particles of micrometer size has been studied. In their spectra with increasing laser power was observed either split of T_{2g}-mode (Figure 1a) or its conversion to an asymmetric form, which is expressed in appearance of the shoulder (Figure 1b). In some cases, the visible change in the spectrum is not detected (Figure 1c). The experimental spectra were decomposed onto components using the software LabSpec 5.36. The position of spectral components changes over time, and for different particles initial and final values are significantly different. After the initial shift to shorter wavelengths, spectral components with different velocities were shifted to longer wavelengths with a noticeable decrease in their half-width **[3]**.

Taking into account data obtained in dynamic mode for particles, among which previously have been detected monocrystalline lonsdaleite, lonsdaleite with cubic diamond it can be stated about three variety of substances identified by Raman spectroscopy.

Analysis of thermostimulated spectroscopic features allowed us to detect strong shift of A_{1g}-mode of lonsdaleite to shorter wavelengths (6-13 cm^{-1}) and to obtain experimental spectrum of monocrystalline lonsdaleite, demonstrating A_{1g}-mode splitting in form of a strip at 1319 cm^{-1} (FWHM 5.7 cm^{-1}) with shoulder at 1322 cm^{-1} (4.5 cm^{-1}). It was found, that in contrast to diamond, in dynamics lonsdaleite characterized by partial reverse of diagnostic line shift to longer wavelengths.

Thus, we have established the possibility of thermostimulated splitting of Raman active modes of diamond and lonsdaleite in tight intergrowths. The difference in behavior of these modes during laser heating can spectrally resolve lonsdaleite and diamond even if positions of their identification lines initially coincide.

The study was supported by the project of UB RAS # 12-U-5-1026.

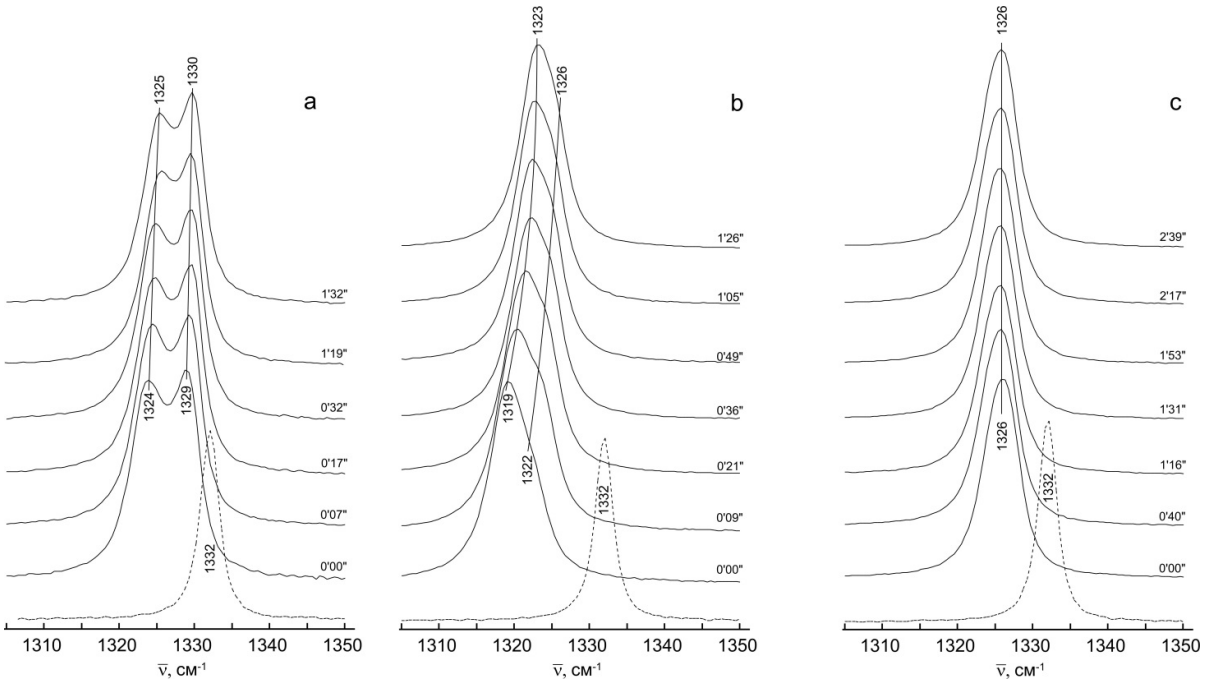

Figure 1. Raman spectra of the carbon particles in dynamics: a - diamond with lonsdaleite, b – lonsdalite, c - diamond. The dotted line - Raman spectrum of the particles in the laser power 1mW (line 1332 cm^{-1}). Solid lines are displayed spectra recorded at certain time intervals (indicated on the right time in the format min 's ") at 10 mW laser power. [3]

References:

[1] Shumilova T. G., Mayer E., Isaenko S. I. Monocrystalline lonsdaleite in regionally metamorphic metasomatically altered rocks // Mineralogical perspective: Proceedings of the International Mineralogical seminar. Syktyvkar: IG Komi Science Center, 2011. P. 162. (in Russian).

[2] Shumilova T. G., Mayer E. and Isaenko S. I. Natural Monocrystalline Lonsdaleite // Doklady Earth Sciences.Vol. 441, Part. 1, pp. 1552-1554. (Translated from Doklady Akademii Nauk, 2011, Vol. 441, No. 2, pp. 236–239).

[3] Isaenko S. I. Shumilova T.G. Thermostimulated splitting of raman active lonsdaleite modes // Vestnik Inst. of Geol. Komi SC UB RAS. No9. Syktyvkar, 2011. Pp. 29-33. (in Russian).

RARE ELEMENTS IN CARBONATE-SILICATE MEDIUM PARENTAL FOR DIAMONDS, BY EVIDENCE OF MANTLE GEOCHEMISTRY AND HIGH-PRESSURE EXPERIMENT

Kuzyura A.V.*, *Litvin Yu.A.

Institute of Experimental Mineralogy RAS, Chernogolovka, Russia
shushkanova@iem.ac.ru

Formation of carbonate-silicate parental medium for natural diamonds and syngenetic inclusions is a result of the upper mantle magmatic evolution marked by magmatic and metasomatic events. The chambers of diamond-and-inclusions parental melts could be originated when the upper mantle garnet lherzolite was affected by a chemically active "metasomatic agent» **[1]**. As a result, chemical composition of the parental melts has originally been composed by components as the mantle peridotite so the "metasomatic agent". Rare elements (RE) involving into the diamond-and-inclusions parental medium together with the mantle components, on the one hand, and the "metasomatic agent", on the other, can be identified from the RE geochemistry of mineral phases involved into the diamond-forming process. This became possible with the use of new experimental data on determination of the interphase partition coefficients (K_D^{RE}) of 21 representive rare elements in partially melted peridotite-eclogite-carbonatite diamond-forming system at 7.0 - 8.5 GPa **[2, 3]**. The experimental data demonstrate that rare elements partitioning is not altered significantly by changes in melt composition, with HREE concentrated in garnets predominantly. The contents of RE in the minerals of peridotite and eclogite parageneses included into diamonds as well as of diamond-bearing xenoliths of several kimberlite pipes were reported in **[4-6]**. Based on the experimental K_D^{RE}, the plausible concentrations of the RE in natural diamond-forming carbonatite melts of the mantle chambers were calculated and presented in the Fig. 1.

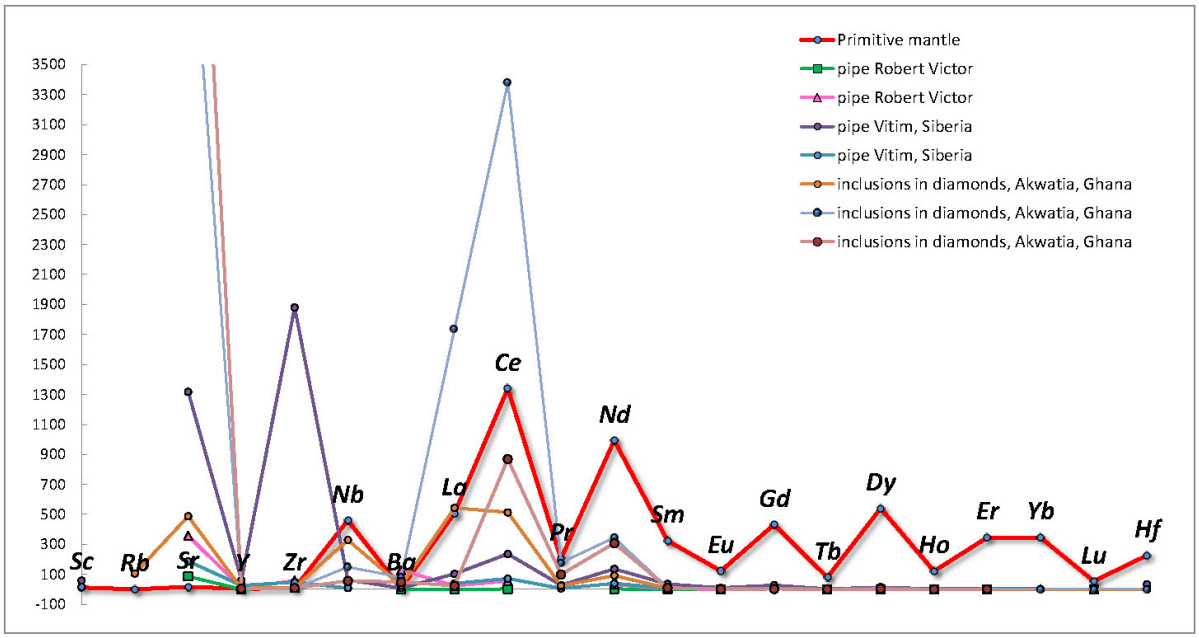

Figure 1. Model concentrations of RE in melts of parental media of xenoliths from kimberlite pipes, inclusions in diamonds for comparison to the primitive mantle **[7]**

It was found that the main contribution of RE in the parental melts is made by the mantle components. The diamond-and-inclusions parental melts are depleted by the medium (Sm, Eu, Gd) and heavy RE (Tb, Dy, Ho, Er, Yb, Lu, Hf), that in contrast to the primitive peridotite case.

Meanwhile, they are enriched in light (Sc, Rb, Sr, Ba, La, Ce, Pr, Nd) RE and Nb, but their content by 1-2 orders of magnitude is lower than for the primitive mantle peridotite. High Sr concentration in model melts can be concerned with the influence of "the metasomatic agent".

Support: Grants of the President ## MK-1386.2013.5, the Ministry of education and science of RF (agreements 8317, 8378) u RFBR 11-05-00401, 12-05-33044, 13-05-00835

References:

[1] Litvin Yu.A. (2011). Mantle origin of diamond-parent carbonatite megma: experimental approaches. Geophysical Research Abstracts, Vol. 13, EGU2011-3627, EGU General Assembly 2011, Vienna, Austria, 2-7 April 2011, CD.

[2] Kuzyura A.V., Wall F., Jeffries T. and Litvin Yu. A. (2010). Trace elements partitioning between garnet, clinopyroxene, and diamond-forming carbonate-silicate melt at 7 GPa. Mneralogical Magazine. V. 74(2), p. 227-239.

[3] Kuzyura A.V., Litvin Yu. A., Jeffries T., Vasiliev P. G., and Wall F. (2012). Experimental evidence on partitioning of trace elements in diamond-forming carbonatite, eclogite-carbonatite and peridotite-carbonatite systems at 7-8.5 GPa. Abstracts of 1 EMC.

[4] Harte B. & Kirkley M. B. (1997). Partitioning of trace elements between clinopyroxene and garnet: data from mantle eclogites. Chemical Geology, 136, 1–24.

[5] Ionov D. (2004). Chemical Variations in Peridotite Xenoliths from Vitim, Siberia: Inferences for REE and Hf Behaviour in the Garnet-Facies Upper Mantle. Joutnal of Petrology. V. 45(2), pp. 343-367.

[6] Stachel T. & Harris J., (1997). Diamond precipitation and mantle metasomatism – evidence from the trace element chemistry of silicate inclusions in diamonds from Akwatia, Ghana. Contributions to Mineralogy and Petrology, V. 129, № 2-3, pp 143-154.

[7] Lubetskaya T., Korenaga J. (2007). Chemical composition of Earth's primitive mantle and its variance: Implications for global geodynamics, J. Geophys. Res., 112, Art. No. B03212.

P-V-T EQUATION OF STATE AND THERMODYNAMIC PROPERTIES OF IRON CARBIDE Fe_3C TO 31 GPA AND 1473 K

Litasov K.D. [1,2], ***Sharygin I.S.*** [1], ***Dorogokupets P.I.*** [3], ***Shatskiy A.*** [1,2]
Gavryushkin P.N. [1,2], ***Sokolova T.S.*** [3], ***Ohtani E.*** [4], ***Li J.*** [5]

[1] *V.S. Sobolev Institute of Geology and Mineralogy SB RAS, Novosibirsk, Russia*
[2] *Novosibirsk State University, Novosibirsk, Russia*
[3] *Institute of the Earth's Crust, SB RAS, Irkutsk, Russia*
[4] *Department of Earth and Planetary Materials Science, Graduate School of Science, Tohoku University, Sendai, Japan*
[5] *Department of Geological Sciences, University of Michigan, Ann Arbor, MI, USA*
klitasov@igm.nsc.ru

Recent experimental and theoretical studies suggested preferential stability of Fe_3C over Fe_7C_3 at the condition of the Earth's inner core **[1-2]**. In this work we determined *P–V–T* equation of state of Fe_3C using multi-anvil technique and synchrotron radiation at pressures up to 31 GPa and temperatures up to 1473 K (Fig.1). Previous studies showed that Fe_3C remains in an orthorhombic structure with the space group *Pnma* to 250 GPa, but it undergoes ferromagnetic (FM) to paramagnetic (PM) and from PM to non-magnetic (NM) phases occurs at 6-8 and 22 or 55-60 GPa, respectively **[3-5]**. These transitions bring some uncertainties to the calculation of its thermoelastic and thermodynamic parameters. A fit of our *P–V–T* data to a Mie-Grüneisen-Debye equation of state produce the following thermoelastic parameters for the PM-phase of Fe_3C: V_0 = 154.6 (1) Å^3, K_{T0} =192 (3) GPa, K_T'=4.5 (1), γ_0 =2.09 (4), θ_0 = 490 (120) K, and q=–0.1 (3). Optimization of the *P-V-T* data for the PM phase along with existing reference data for thermal expansion and heat capacity using a Kunc-Einstein equation of state **[6-7]** yielded the following parameters: V_0 = 2.327 cm^3/mol (154.56 Å^3), K_{T0} = 190.8 GPa, K_T' = 4.68, Θ_{E10} = 305 K (which corresponds to θ_0 = 407 K), γ_0 = 2.10, e_0 = 9.2 × 10^{-5} K^{-1}, m = 4.3, and g = 0.66 with fixed parameters m_{E1} = 3n = 12, γ_∞ = 0, β = 0.3, and a_0 = 0. This formulation allows for calculations of any thermodynamic functions of Fe_3C versus T and V or versus T and P. Assuming carbon as the sole light element in the inner core, extrapolation of our equation of state of the NM phase of Fe_3C suggests that 3.3±0.9 wt.% C at 5000 K and 2.3±0.8 wt.% C at 7000 K matches the density at the inner core boundary (Fig.2).

This work was supported by the Ministry of education and science of Russian Federation, project Nos 14.B37.21.0457 and 14.B25.31.0032, RF President Grant No MD-500.2013.5 and conducted as a part of the Global Center-of-Excellence Program at Tohoku University. It is partially supported by IP SB RAS No 97 and RFBR (No 12-05-33008).

[1] Lord, O.T., Walter, M.J., Dasgupta, R., Walker, D., Clark, S.M., 2009. Earth and Planetary Science Letters, 284: 157-167.
[2] Takahashi, S., Ohtani, E., Sakai, T., Hirao, N., Ohishi, Y., 2012. Abst of G-COE symposium "Achievements of G-COE program for Earth and planetary dynamics", Sendai, Japan: 166.
[3] Gao, L., Chen, B., Wang, J., et al., 2008. Geophysical Research Letters, 35: L17306, doi:10.1029/2008gl034817.
[4] Ono, S., Mibe, K., 2010. Physics of the Earth and Planetary Interiors, 180: 1-6.
[5] Prescher, C., Dubrovinsky, L., McCammon, C., et al., 2012. Physical Review B, 85: 140402, doi: 10.1103/PhysRevB.85.140402.
[6] Sokolova, T.S., Dorogokupets, P.I., Litasov, K.D., 2013. Russian Geology and Geophysics, 54: 181-199.
[7] Litasov, K.D., Dorogokupets, P.I., Ohtani, E. et al., 2013. Journal of Applied Physics, 113: 093507.

[8] Sata, N., Hirose, K., Shen, G., et al., 2010. Journal of Geophysical Research-Solid Earth, 115: B09204, doi: 10.1029/2009jb006975.
[9] Seagle, C.T., Campbell, A.J., Heinz, D.L., Shen, G., Prakapenka, V.B., 2006. Journal of Geophysical Research, 111: B06209, doi:10.1029/2005jb004091.
[10] Dziewonski, A.M., Anderson, D.L., 1981. Physics of the Earth and Planetary Interiors, 25: 297-356.

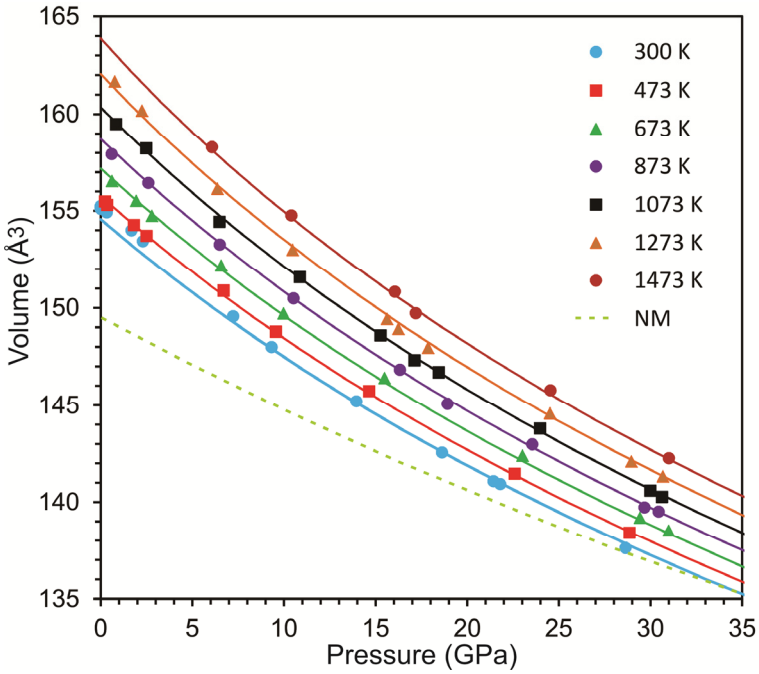

Figure 1. KE EOS fit to *P-V-T* data for Fe_3C. Solid lines are isothermal compression curves at 300, 473, 673, 873, 973, 1073, 1273, and 1473 K. The dashed line shows the compression curve of the NM phase of Fe_3C.

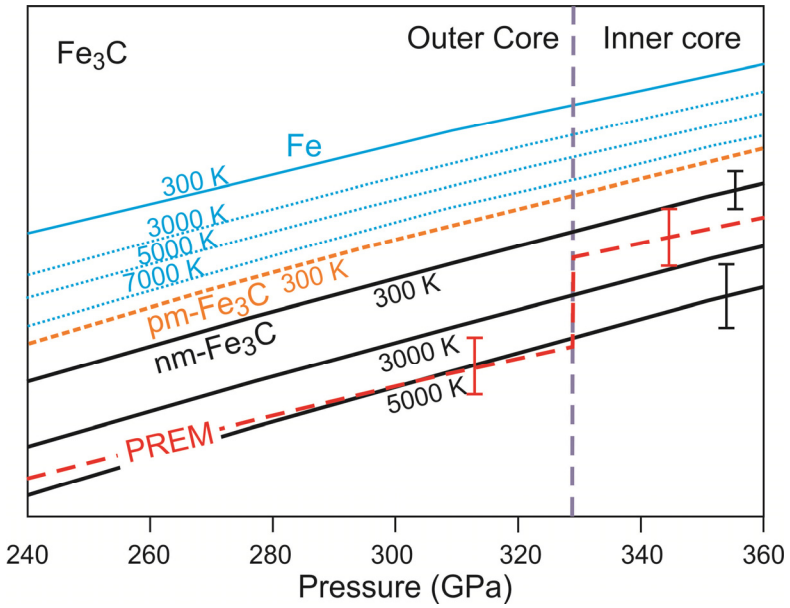

Figure 2. Calculated density of Fe_3C at Earth's core conditions. For NM-Fe_3C we used compressibility data from **[8]** and thermal parameters of PM phase from this work. Profiles for hcp-Fe are shown using parameters listed in **[9]**. The PREM profile is after **[10]**. The error bars for Fe_3C and PREM are shown.

CHEMISTRY OF CARBON-HYDROGEN FLUID UNDER HIGH PRESSURE AND TEMPERATURE

Lobanov S.S., [1,2] ***Chanyshev A.D.,*** [2,3] ***Litasov K.D.,*** [2,3] ***Goncharov A.F.*** [1,4]
[1] *Geophysical Laboratory, Carnegie Institution of Washington, Washington, DC, USA*
[2] *V.S. Sobolev Institute of Geology and Mineralogy SB RAS, Novosibirsk, Russia*
[3] *Novosibirsk State University, Novosibirks, Russia*
[4] *Key Laboratory of Materials Physics, Institute of Solid State Physics CAS, Hefei, China*
slobanov@ciw.edu

Competing phase transitions as well as chemical transformations in the carbon-hydrogen system under different thermodynamic conditions is of particular interest to a broad scientific community including material research, organic chemistry, geochemistry *etc.* [**1-3**] Methane, the simplest hydrocarbon, comprises roughly 1/3 of the icy mantles in the interiors of Uranus and Neptune (icy giants) [**4**], and therefore is of particular importance to planetary sciences as chemical reactions in 'hot ices' largely determine observed physical properties of these planets [**5, 6**]. Also, it is possible that hydrocarbons are involved in terrestrial C-O-H fluid cycle deep in Earth's mantle since redox conditions expected beneath the lithosphere shift the CO_2-H_2O equilibria to CH_4-H_2O [7**]**. Here we present the results of laser heated diamond anvil cell (LH DAC) experiments [**8**] on hydrocarbons chemical reactivity at pressures up to 50 GPa and temperatures up to 2000 K. Ethane (C_2H_6), and *n*-docosane ($C_{22}H_{46}$) were chosen as starting materials. Raman spectroscopy at high pressure [**9**] was used to probe C-H fluids under high temperatures and after quenching to room temperatures.

Positions of ethane and *n*-docosane melting lines under pressure were found by visual observations of fluid-solid interface at high temperature. The loci of the melting lines in the P-T space (Fig. 1) are within uncertainties of temperature measurements (± 200 K) from the recently determined CH_4 melting curve [**10**], implying that hydrocarbon high pressure solids resemble similarities in intermolecular bonding in molecular crystal lattice. Ethane and *n*-docosane molecular fluids remained intact below 1100-1900 K (Fig. 1) with C-H bond breakage being highly dependent on pressure. Heating of samples above the dashed line in Fig. 1 results in chemical transformations. Raman spectra of quenched products show a variety of features depending on temperature, pressure and starting composition.

Gradual decomposition of hydrocarbon molecule is evident with increasing temperature at pressures below 20 GPa (Fig. 2) as the intensity of C-C stretching vibration decrease, which is accompanied with graphite 'G' band rise. No molecular hydrogen was observed at pressures below 44 GPa and T<2000 K. These spectroscopic features are in agreement with the following reaction: $C_2H_{n+2} \rightarrow ((n+1)/2)\ CH_4 + ((n-1)/2)\ C$. Diverse reaction products are observed in quenched samples after LH DAC experiments at P > 20 GPa. Heating up to 2000 K at 34.2 GPa resulted in a number of significant changes in the Raman spectra (Fig. 3). Clear changes in the C-C stretching (780-1300 cm^{-1}) and C-H bending (1400-1600 cm^{-1}) regions are observed. We attribute these bands to the newly formed hydrocarbons containing C-C single bonds [**11**], i.e. elongation and/or branching of the hydrocarbon skeleton occurs. In addition, Raman signals at 1800 cm^{-1} and 1950 cm^{-1} are evident for the formation of hydrocarbons containing double carbon to carbon bonds (Fig. 3). A broad peak (or series of weak peaks) appeared upon heating in the 4350-4450 cm^{-1} frequency range. This feature can be attributed to the formation of C_2H_6-H_2 van der Waals compounds, similar to high pressure phases described in CH_4-H_2 system [**12**]. Consistently, molecular hydrogen rotational modes appear in low frequency region (Fig. 3). It is remarkable that we were able to synthesize free hydrogen at T~2000 K and pressures above 34 GPa. The production of unbounded hydrogen from ethane shows that the role of CH_4 in the C-H fluid at pressures above 20 GPa is continuously decreased.

Our results show that CH_4 dominate hydrocarbon fluid at pressures below 20 GPa in the whole studied temperature range. However, a crossover to complex hydrocarbon species occurs

at pressures above 20 GPa. The interpretation of Raman spectra of quenched reaction products synthesized at T~2000 K is uncertain. In general, P and T affect the average lifetimes of C-H and C-C bonds at extreme conditions. Temperature provides energy to overcome kinetic barriers for bond breakage, while stabilization of the bonds with pressure is more pronounced for C-C bond. The composition of C-H fluid is determined by the competition between C-C and C-H bonds. This competition can result in hydrocarbons with long C-C network. The role of double and triple carbon bonds at high pressure cannot be ruled out from this study. However, we deem unsaturated hydrocarbons appear on quenching from highly dissociated C-H fluid rather than being thermodynamically favored.

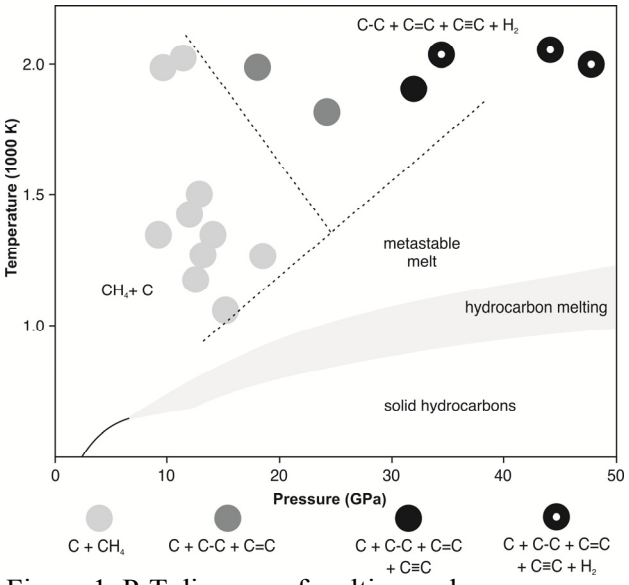

Figure 1. P-T diagram of melting and transformations in the C-H system

The work is supported by RFBR No 12-05-00841, 12-05-33008 and research grant of "BP" for young scientists.

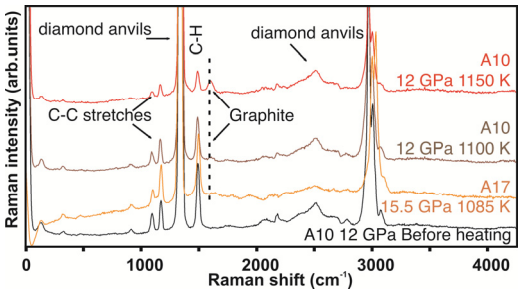

Figure 2. *In situ* Raman spectra of *n*-docosane at 12 GPa and its decomposition products.

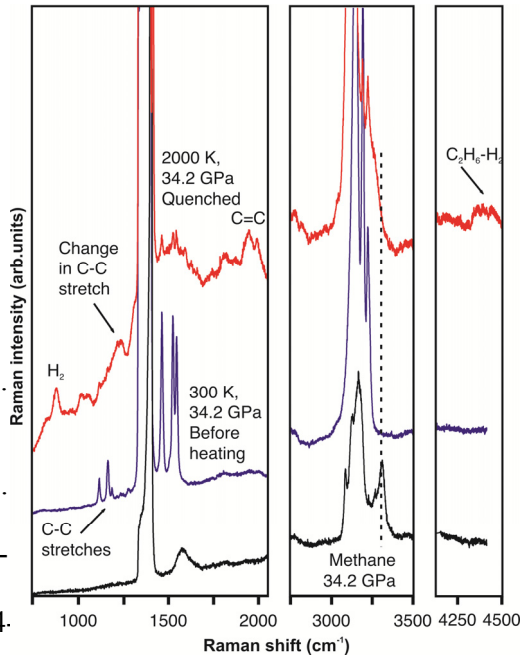

Figure 3. Raman spectra of ethane (blue line) and its reaction products (red line) produced after heating to 2000 K at 34 GPa. Methane Raman spectrum is shown for comparison.

1. Brazhkin, V.V. and A.G. Lyapin, Nat Mater, 2004. **3**(8): p. 497-500.
2. Gao, G.Y., et al., J Chem Phys, 2010. **133**(14).
3. Kenney, J.F., et al., P Natl Acad Sci USA, 2002. **99**(17): p. 10976-10981.
4. Hubbard, W.B., Science, 1981. **214**(4517): p. 145-149.
5. Cavazzoni, C., et al., Science, 1999. **283**(5398): p. 44.
6. Chau, R., S. Hamel, and W.J. Nellis, Nat. Commun., 2011. **2**: p. 203 doi:10.1038/ncomms1198.
7. Frost, D.J. and C.A. McCammon, Annu. Rev. Earth Planet. Sci., 2008. **36**: p. 389-420.
8. Subramanian, N., et al., Rev. Sci. Instrum., 2010. **81**(9): p. 093906.
9. Goncharov, A.F. and J.C. Crowhurst, J. Low Temp. Phys., 2005. **139**(5-6): p. 727-737.
10. Lobanov, S.S., et al., 2013. Nature communications, in press.
11. Socrates, G., *Infrared and Raman Characteristic Group Frequencies: Tables and Charts*. Third ed., 2004, Chichester: John Wiley & Sons. 366.
12. Somayazulu, M.S., et al., Eur. J. Solid State Inorg. Chem., 1997. **34**(7-8): p. 705-713.

A UNIQUE DIAMONDIFEROUS PERIDOTITE XENOLITH FROM UDACHNAYA: EVIDENCE FOR SUBDUCTION

***Logvinova A.M.*[1], *Reutsky V.N.*[1], *Fedorova E.N.*[1], *Wirth R.*[2], *Howarth G.*[3], *Taylor L.A.* [3], *Sobolev N.V.*[1]**

[1] *Institute of Geology and Mineralogy SB RAS, Novosibirsk, Russia,*
[2] *Helmholtz Centre Potsdam, GFZ German Research Centre for Geosci., Potsdam, Germany*
[3] *Department of Earth & Planetary Sciences, University of Tennessee, Knoxville, TN USA*
logv@igm.nsc.ru

Introduction: As our windows into the mantle, kimberlites bring to the surface a variety of samples, particularly diamond as xenocrysts and in xenoliths of their primary host rocks. These xenoliths are divided into mafic (eclogite) and ultramafic (peridotite), and diamondiferous varieties of the latter are quite rare. The Udachnaya kimberlite pipe is dominated by ultramafic rocks; however, it is the diamondiferous eclogites that are most recovered, with precious few diamondiferous peridotites. There are >200 diamond-bearing xenoliths from Udachnaya, described to date, and summarized by **[1-7],** of which only ~5 % relate to ultramafic xenoliths.

We describe here a unique diamondiferous garnet peridotite xenolith U-331, which consists of enstatite grains with small enclosed pyropes. Despite the small size and weight of xenolith (10.5 g), it contains a huge number of colorless diamond microcrystals (>30,000). Most diamonds are sharp-edged octahedra and their intergrowths **(Fig.1),** with varying sizes from 100 to 700 μm. Some diamonds are dark-colored from numerous minute inclusions **(Fig.2).** The diamonds are all euhedral, but many occur in clusters, rather than single crystals.

High-resolution X-ray tomography of this unique xenolith has resulted in various 2-D and 3-D images, wherein the relations of the diamonds and the xenolith minerals are well revealed **(Fig. 3)**. The major minerals seen are the diamonds (9.5 vol%), enstatite (38 vol%), pyrope (35vol%), sulfides (4 vol%), consisting of pyrrhotite, pentlandite, and minor chalcopyrite. The remainder is mainly alteration products, with a few remaining olivine grains.

Mineralogy: *Enstatite* is the main rock-forming mineral of studied xenolith. Enstatite grains are homogeneous in major-elements contents (FeO = 4.81 to 5.1 wt.%; **Mg# = 92.7;** CaO = 0. 55 to 0. 61 wt%; Na_2O = 0.14 to 0.19 wt%; Al_2O_3 = 0.39 to 0.43 wt%; Cr_2O_3 = 0.20 to 0.23 wt%; TiO_2 <0.07 wt%. The *pyrope* grains are chemically homogeneous within grains, but some variations occur between grains: Cr_2O_3 (4.43 to 5.11 wt%); CaO (4.15 to 4.8 wt %); **Mg# (83.6 to 84.1)**; TiO_2 (0.21-0.3 wt%); Na_2O (0.09-0.12 wt%; avg. 0.11 wt%).

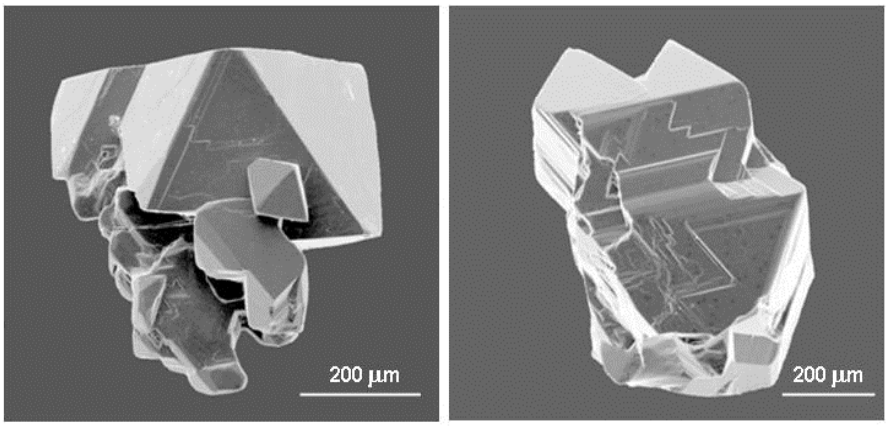

Figure 1. Images of diamonds from peridotite and xenolith Uv-331 from the Udachnaya pipe.

Fine grains (<1 mm) of pyrope are surrounded by a thin kelyphitic rim and enclosed in enstatite. Only a small amount of fresh *olivine* grains remain unaltered and is intergrown with spinel: MgO = 47.5 wt%; FeO = 10.7 wt%; **Mg# = 88.8**. These olivine grains have higher Fe-contents compared to olivine from typical peridotites from Udachnaya (**Mg# 92-94**; **[8]**). The Al-rich *spinel* occurs in the groundmass with olivine of this xenolith: avg.comp. MgO = 22.0 wt%; FeO = 9.57 wt%; Al_2O_3 = 51.1 wt%; Cr_2O_3 = 12.2 wt%. The majority of the interior of the xenolith consists of "spinach" – probably serpentine as highly altered olivine. It is noted that the majority of diamond crystals are confined mainly to this homogeneous interior mass of dark-green material that fills the inter-granular space surrounding the garnet and enstatite.

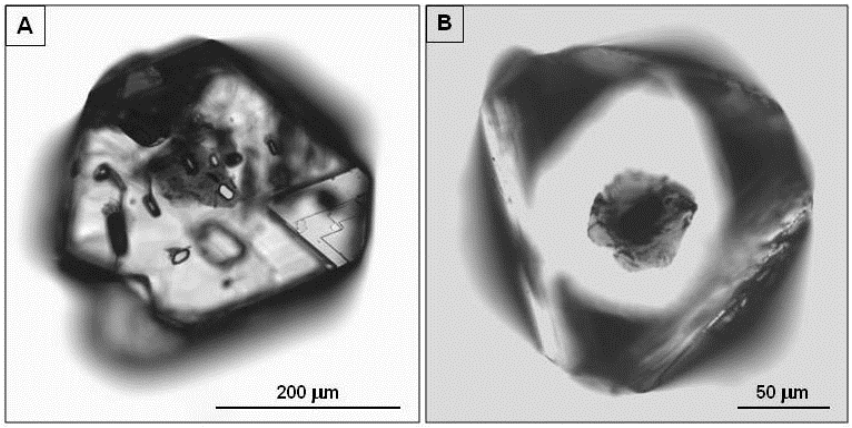

Figure 2. Optical micrographs of mineral (A) and fluid/melt (B) inclusions inside microdiamonds.

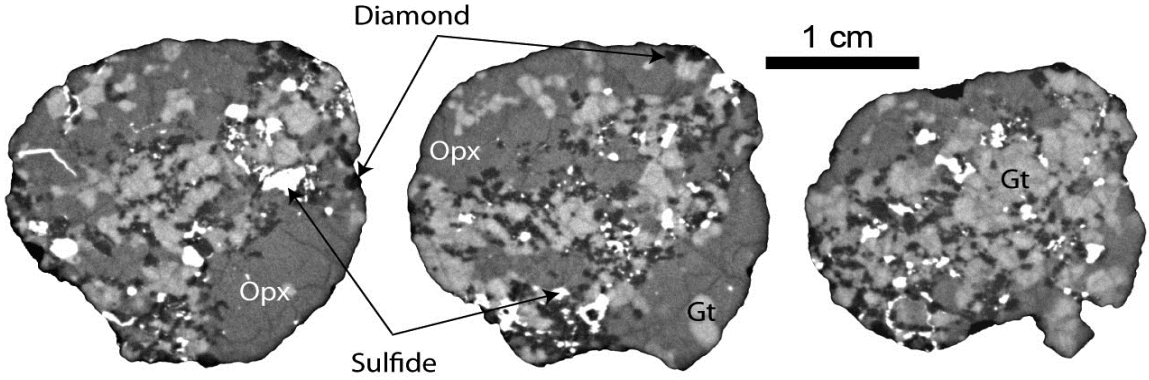

Figure 3. Tomography 2-D slices (out of >600) of diamondiferous peridotite: White = sulfides; Lt-Gray = pyrope; Dk-Gray = Pyroxene; Black = Diamonds. Notice large pyroxenes on the top and bottom, with the "myriad of Diamonds" in between, in a garnet-olivine-serpentine matrix.

Two TEM foils (10x15x0,2 μm) were prepared from the central part of the studied diamonds that contained mineral and fluid inclusions. Using TEM techniques, we have discovered nanometer-scale inclusions, composed of Mg-Al silicate-rich phases, a Ca-carbonate phase, graphite, and fluid. It is assumed that the multiphase associations of micro-inclusions represent mantle fluid that had been captured in the diamond growth process. The composition of the inclusions is similar to that of silicate-carbonate nanoscale inclusions, which were previously described in diamonds from kimberlite pipes of Yakutia **[9].**

The majority of diamonds examined (>150) have nitrogen contents below the detection limit + Type IIa, whereas others have not more than 20 ppm (Type IaB). Most nitrogen impurity

is of the B form that indicates a high-aggregation states (% B defects) of 68 to 94 %. This is considered evidence for long residence of the diamonds at high temperatures under mantle conditions. All diamonds indicate the presence of hydrogen. *The* $\delta^{13}C$ *isotopic composition in these crystals has a value of -22 ‰,* not typical for diamonds of ultramafic paragenesis, which are usually in the narrow range in $\delta^{13}C$ (from -2 to -8 ‰), characteristic of the mantle **[10]**. Diamonds with lighter isotopic composition of carbon, as high as -44 ‰, typical for eclogitic diamonds **[10-11]**, are considered as indicative of subduction of oceanic crust **[12].**

Peridotite xenoliths with kinship to Group A eclogites have typically been explained either by fractionation or by subduction **[13].** However, with this studied peridotite, the non-mantle $\delta^{13}C$ values to the myriad of diamonds, combined with their FTIR-determined nitrogen aggregation values, are considered as supporting evidence for the formation of the diamonds from metasomatic fluids. These deep-seated fluids appear to have had crustal signatures, and highly metasomatized the ultramafic substrate, with its initial crustal signature. Data from this diamondiferous peridotite emphatically demonstrate once again the important role of metasomatic processes in the formation diamonds.

References:

[1] Sobolev N.V. et al. (1984) *Russ. Geol. Geophys., 25,* 63-80;
[2] Sobolev V.N. et al. (1994) *Inter. Geol. Rev., 36*, 42-64;
[3] Sobolev N.V. et al. (1998) *Russ. Geol. Geophys. 39*, 1667-1678;
[4] Snyder G.A. et al (1997) *J.Petrol. 38*, 85-113
[5] Taylor L.A. & Anand M. (2004) *Chemie der Erde-Geochemistry 64*, 74
[6] Shatsky V.S. et al. (2008) *Lithos 105,* 289-300;
[7] Liu Y. et al. (2009) *Lithos, 112,* 1014-1024;
[8] Sobolev N.V. (1977) Deep-Seated Inclusions in Kimberlites and the Problem of the Composition of the Upper Mantle, Publ: AGU, Wash., DC, 279 p;
[9] Logvinova A.M. et al. (2008) *Eur. J. Mineral., 20*, 317-331;
[10] Cartigny P. (2005) *Elements*, 79-84;
[11] Sobolev N.V. et al. (1979) *Dokl. Akad. Nauk SSSR, 249,* 1217-1220;
[12] Sobolev V.S. & Sobolev N.V. (1980) *Dokl. Akad. Nauk SSSR, 250*, 683-685.
[13] Taylor L.A. et al. (2005) *Russ. Geol. Geophys,. 46*, 1198-1206.

Fe-METAL – Mg-Ca-CARBONATE INTERACTION AT 6.5 GPA AND 1000-1600°C

Martirosyan N.S. [1,2]***, Litasov K.D.*** [1,2]***, Shatskiy A.*** [1,2]***, Ohtani E.*** [3]

[1] *V.S. Sobolev Institute of Geology and Mineralogy SB RAS, Novosibirsk, Russia*
[2] *Novosibirsk State University, Novosibirsk, Russia*
[3] *Department of Earth and Planetary Materials Science, Graduate School of Science, Tohoku University, Sendai, Japan*
martirosyanns@gmail.com

The fate of subducted carbonates is an intriguing issue in the deep Earth's dynamics, which is still poorly resolved. Subducted carbonates can be subjected to melting at the island arc depths, in the transition zone, or in the deeper lower mantle [1]. In this case formed alkali carbonatite or carbonate-silicate melt is segregated along slab-mantle interface and forms melt diapir, which can ascent towards the surface by buoyancy forces and dissolution-precipitation mechanism. Indeed, in the deep upper mantle, transition zone and lower mantle Fe-metal-saturated surrounding peridotite can counteract to the carbonated melt mobility and reduces it producing diamond or metal carbide. In the other scenario solid refractory carbonate residues (aragonite, magnesite) after partial melting of the deep slab or formed carbonatite melts can interact with the surrounding reduced mantle and produce the same diamond or metal carbide [2]. The dynamics and kinetics of these processes are extremely important for understanding the carbon behavior and distribution in the deep Earth. The major interacting agents at the slab-mantle interface include carbonate and silicate from subduction slab and silicate with minor Fe-metal from surrounding mantle at depths below 250-300 km [1].

At the first step to study these interactions we considered major reactions between Mg- and Ca- carbonate and Fe-metal at 6.5 GPa and 1000-1600°C. The experiments were conducted using multianvil technique. Carbonate or carbonate+metal starting materials were placed into Fe, MgO or BN capsules. In the Fe-capsules (with Fe-excess) we observed formation of Fe_3C by reaction of $MgCO_3 + 5\ Fe = Fe_3C + 3(Fe_{0.67}Mg_{0.33})O$. In the run products of kinetic experiments we observed significant zone made of magnesiowustite (Fig.1). Carbon migration via this zone can be realized via CO_2 or CO. In the Ca-system we observed similar reaction with the formation of Ca-wustite, but without thick wüstite zone between carbide and unreacted Ca-carbonate. In the MgO and BN capsules at 1673-1873 we observed reactions (Fig.2), such as: $MgCO_3 + Fe = (Mg,Fe)O + (Mg,Fe)CO_3$ (L) + Fe_7C_3 (Fe-C, L) + C and $CaCO_3 + Fe = (Ca,Fe)O + CaCO_3$ (L) + Fe_7C_3 (Fe-C, L) + C (here L is liquid). The minor difference for the Ca-carbonate system in MgO capsule was in the formation of Ca-magnesiowustite due to contamination from MgO capsule.

The results of this study allow providing several important conclusions for carbon behavior in the Earth's mantle. An interaction of carbonates with iron always produces Fe_3C, which is consistent with early thermodynamic prediction for magnesite [3]. This can be different at pressures above 100 GPa, where we can expect formation of alternative crystal structures of carbonates [4] and, in addition, their field of redox stability can be overlapped with IW buffer. Formation of diamond is forbidden in the mantle in the presence of metallic Fe. Therefore fO_2 of diamond-forming media should be at least 1-2 log units above IW buffer or significantly lower than IW buffer in the field of silicide stability.

This work is supported by RF President Grant No MD-500.2013.5, the Ministry of education and science of Russian Federation, Nos 14.B25.31.0032 and 14.B37.21.0457. It is partially supported by RFBR (No 12-05-33008).

References:

[1] Litasov K.D., Shatskiy A.F., Ohtani E., and Yaxley G.M., 2013. Geology, 41(1): 79-82.
[2] Rohrbach, A. and Schmidt, M.W., 2011. Nature, 472: 209-212.

[3] Scott, H.P., Williams, Q., and Knittle, E., 2001. Geophysical Research Letters, 28: 1875–1878.
[4] Oganov, A.R., Ono, S., Ma, Y.M., Glass, C.W., and Garcia, A., 2008. Earth and Planetary Science Letters, 273, 38–47.

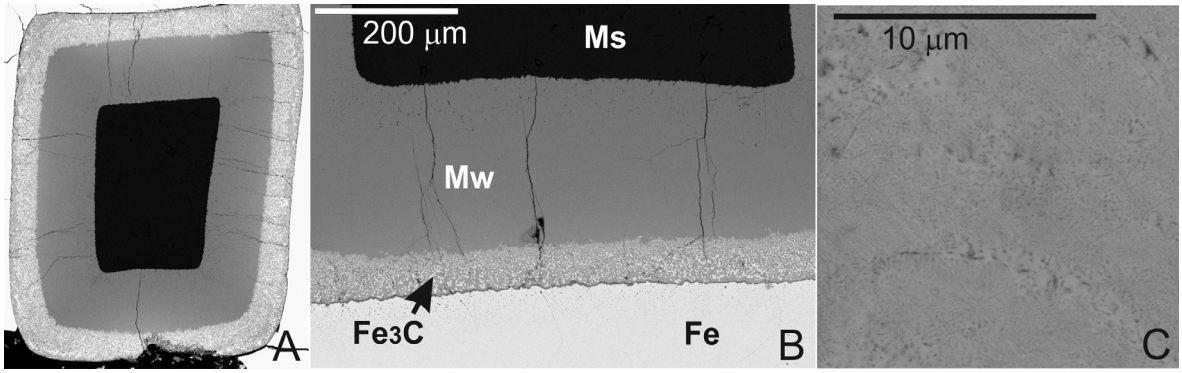

Figure 1. Magnesite interaction with Fe at 6.5 GPa, 1200°C and 120 min. Ms – magnesite, Fe – iron metal, Mw – magnesiowustite. Mw zone contains vermicular net of pores partially filled with carbon materials (C). Starting configuration include magnesite powder placed into Fe-capsule.

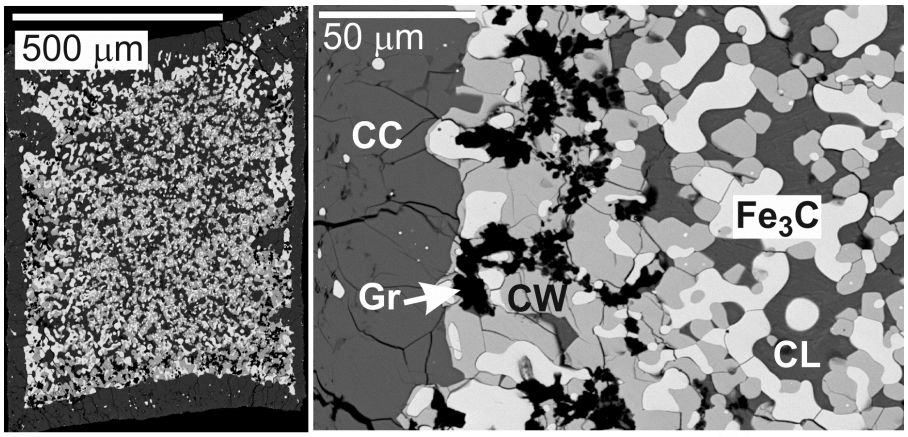

Figure 2. $CaCO_3$ interaction with Fe at 6.5 GPa, BN-capsule 1200°C and 480 min. CC – $CaCO_3$, CW – Ca-wustite, CL – quenched Ca-carbonate liquid, Gr - graphite.

THE FORMATION OF METASTABLE GRAPHITE INCLUSIONS AT DIAMOND CRYSTALLISATION IN MODEL SYSTEMS

Nechaev D.V. [1], ***A.F. Khokhryakov*** [1,2]

[1] *V.S. Sobolev Institute of Geology and Mineralogy, SB RAS, Novosibirsk, Russia*
[2] *Novosibirsk State University, Novosibirsk, Russia*
nechaev@igm.nsc.ru

Graphite often occurs in xenoliths of mantle rocks and as inclusions in diamond **[1, 2]**. Almost all concepts of the genesis of graphite single crystals and graphite macroinclusions in diamond state that graphite can be produced only in the field of its thermodynamic stability before or after the diamond crystallization. Considering the experimental evidence for joint crystallization of diamond and graphite in the diamond stability field **[3]**, the purpose of this work was to study the morphology of metastable graphite inclusions in diamond and liquidus silicate phases produced in silicate-carbonate-fluid and chloride-water systems at 6.3-7.5 GPa and 1400-1600°C.

Graphite inclusions in diamond and liquidus silicate minerals were studied by optical microscopy and Raman spectroscopy. It was established that the graphite in diamond, forsterite and orthopyroxene has a highly ordered structure. Graphite inclusions have hexagonal, round and irregular polygonal shape, depending on the parameters of the experiments. The shape of graphite inclusions correlates with the presence of metastable graphite in products of experiments. Irregular polygonal inclusions of graphite were found only in those experiments in which both diamond and graphite were crystallizing during all time of experiment. These graphite inclusions are oriented parallel to the {111} faces of diamond and they are syngenetic. Angular and irregular polygonal shape of inclusions is formed by contours of growing diamond layers. There are both euhedral and rounded graphite inclusions in the diamond crystals grown in long experiments (40 hours) at 1600°C (Fig.1). However, the capture of various forms of graphite inclusions took place at different stages of diamond growth. The location of euhedral

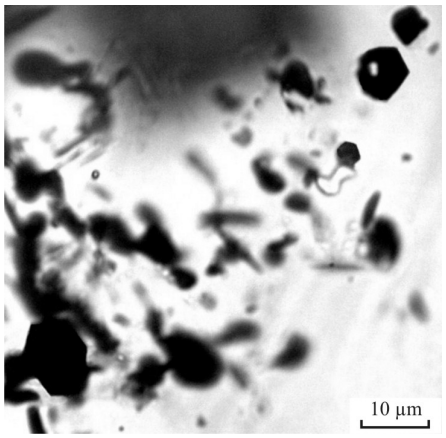

Figure 1. Euhedral graphite inclusions in diamond produced in system SiO_2-H_2O-C at 7.5GPa and 1600°C.

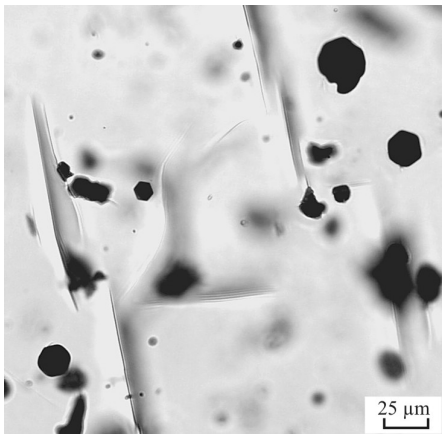

Figure 2. Hexagonal and rounded graphite inclusions in liquidus orthopyroxene grown in system Mg_2SiO_4-Fe_2SiO_4-$MgCO_3$-H_2O at 6.3GPa and 1400°C.

graphite inclusions near the "seed crystal/overgrown layer" indicates that they were captured by the diamond at the early stages of its growth. Rounded inclusions were conserved much later, because arranged close to the {100} and {111} faces of the diamond. The rounded shape of graphite plates and their smaller in size relative to hexagonal inclusions indicates that they are

partially dissolved in the final stages of diamond crystallization in the experiment. One of the features of syngenetic and protogenetic graphite inclusions in diamond are the absence around them of visible stress and cracks. In experiments at 1400°C found only metastable graphite in quenching aggregate and graphite inclusion in liquidus orthopyroxene and forsterite (Fig.2). In the liquidus silicate phases observed joint occurrence of rounded and polygonal graphite inclusions. It can be due to graphite recrystallization in a temperature gradient field of high pressure reaction cell. This is realized dissolution and crystallization of graphite.

Thus, studies graphite inclusions in diamond and liquidus of silicate minerals produced in silicate-carbonate-fluid and chloride-water systems at P=6.3-7.5 GPa and T=1400-1600°C allows the following conclusions.

1. Polygonal graphite inclusions in diamond formation during joint crystallization of diamond and metastable graphite. These inclusions are syngenetic.

2. Rounded graphite inclusions in diamond are protogenetic inclusions. The rounded shape of the graphite plates is associated with instability of graphite and hence its dissolution. The graphite inclusions in natural diamonds can be submitted graphite formed in the graphite stability field at low pressures and metastable graphite formed at the early stages of diamond crystallization.

3. There are no strong stress and cracks around syngenetic and protogenetic graphite inclusions in diamond.

4. The presence of graphite and absence of diamond in natural samples can not be clear evidence of their formation at low pressures, in the graphite stability field. They can form in the diamond stability field, but at relatively low temperatures. To identify the conditions of formation of natural graphite mineral associations need to attract additional research methods.

This work was financially supported by Integration Project 31 from the Siberian Branch of the Russian Academy of Sciences.

References:

[1] Harris J. W. Black material on mineral inclusions and in internal fracture planes in diamond Contr. Miner. Petrol. 1972. V. 35. P. 22-33.

[2] Sobolev, N.V., 1974. Deep Seated Inclusions in Kimberlites and the Problem of the Upper Mantle Composition. Nauka, Novosibirsk. 264 p.

[3] Sokol, A.G., Pal'yanov, Yu.N., Pal'yanova, G.A., Khokhryakov, A.F., Borzdov, Yu.M., 2001. Diamond and graphite crystallization from COH fluids under high pressure and high temperature conditions. Diamond Relat. Mater., 10, 2131-2136.

AN EBSD STUDY OF OLIVINE INCLUSIONS IN SIBERIAN DIAMONDS: CLUES TO SYNGENETIC GROWTH PROCESSES

Neuser, R.D. [1], ***Schertl, H.-P.*** [1], ***Sobolev, N.V.*** [2]

[1] *Ruhr-University Bochum, Institute of Geology, Mineralogy and Geophysics, Bochum, Germany*
[2] *V.S. Sobolev Institute of Geology and Mineralogy,SB RAS, Novosibirsk, Russia*
rolf.neuser@rub.de

It is well accepted that the multitude of natural non-metamorphic diamonds originate from kimberlite and lamproite. But what exactly do we know from the detailed mineralogical and chemical environments of the mantle derived source-material of each respective diamond? Besides e.g. carbon and nitrogen isotope data of diamond itself, studies of mineral and fluid inclusions in diamond offer an enormous potential to the knowledge of its respective source. Already in the late sixties and in the seventies of the last century key studies on such inclusions were made (e.g. **[1], [2], [3], [4]**). **[1]** found numerous peridotitic mineral inclusions (e.g. olivine, chromite, enstatite, pyrope, chromium diopside) in a large quantity of diamonds he studied, and thus he came to the conclusion that ultramafic (U-type environment) inclusions dominate compared to eclogitic (E-type environment) inclusions (Mg-Fe-garnets, omphacite, coesite, kyanite, orthopyroxene, in rare cases sanidine, corundum, phlogopite, biotite, magnetite, ilmenite, rutile – the mineral association of course is dependent on the composition of the eclogite source rock). Due to the use of modern high resolution techniques even more and sometimes quite rare mineral inclusions in diamonds were observed (e.g. carbonates, halides, apatite, hydrous aluminosilicate, ferropericlase, K-Fe sulphides, iron carbide, nitrocarbide).

However, it is still difficult to find an unequivocal evidence for a contemporaneous growth of diamond and the respective mineral inclusion as a hint for syngenetic formation **[5]**. The morphology of phlogopite/biotite inclusions in diamond for instance, which were observed to be cubo-octahedral, would suggest that the inclusion was formed together with the host diamond at the same time (e.g. **[6]**). An epitaxial relationship between host and inclusion, however, provides a particularly strong evidence for a contemporaneous growth (diamond - chromite; see **[7]**).

Here we offer for the first time results on electron backscatter diffraction (EBSD) studies of olivine inclusions within diamond hosts from the Yubileinaya pipe, Siberia (Fig. 1). The forsterite component of these olivine inclusions from Yubileinaya is at average 92.42 mol% with an average amount of 0.376 wt.% NiO **[8]**. Two diamond grains of the samples studied by **[8]** were used in order to get first information on possible crystallographical interrelations between diamond host and olivine inclusion (Fig. 1).

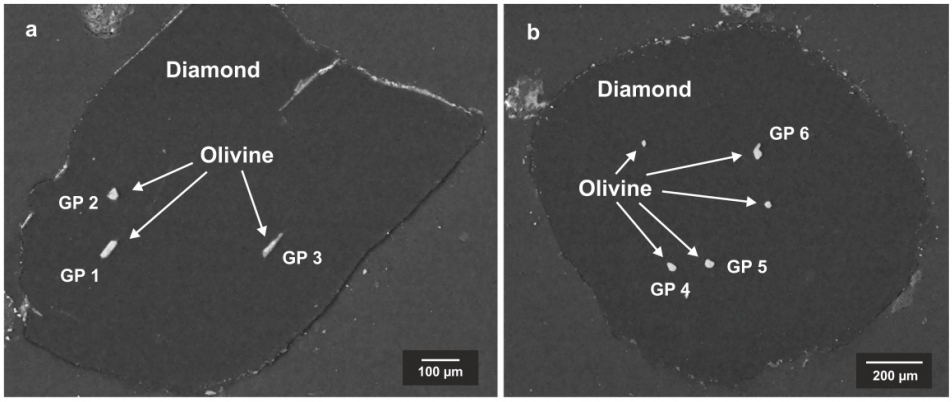

Figure 1. Olivine inclusions in diamond (BSE-images). GP 1 – GP 5 refer to grain pairs shown in Table 1; GP 6: no coincidences observed; inclusions not labeled: not detectable.

Essentially, the stereographic projections observed demonstrate a coincidence of respective normals of {110}, {111}, and {112} lattice planes of diamond with specific normals of olivine lattice planes. Six diamond – olivine pairs were studied. Five of the studied grain pairs show coincidences (see Table 1) whereas in one case no obvious reliable coincidence could be observed. It is important to note, that a coincidence of diamond {100} lattice plane normals with specific normals of olivine lattice planes were not observed. Possibly interrelations of $\{112\}_{diamond}$ with $\{001\}_{olivine}$ also exist which however needs further verification.

normals (diamond)	normals (olivine)		normals (diamond)	normals (olivine)	
{110}	{101}	Grain pair 1	{110}	{001}	Grain pair 4
{110}	{010}		{111}	{110}	
{111}	{100}		{112}	{111}	
{110}	{100}	Grain pair 2	{110}	{001}	Grain pair 5
{110}	{001}	Grain pair 3	{111}	{120}	
{111}	{100}				
{112}	{010}				

Table 1. Crystallographical coincidences of normals of olivine lattice planes and normals of adjacent diamond lattice planes of different grain pairs form the Yubileinaya pipe, Siberia.

Our first study shows, that a crystallographical relationship between diamond host and olivine inclusion from Yubileinaya pipe exists, indicating evidence for a contemporaneous and thus syngenetic growth. EBSD analysis represents an invaluable tool to gain insight into the chemical and mineralogical nature of the formation environment of diamond. We thus recommend a systematic EBSD survey for such diamond host/mineral inclusion pairs, in order to better understand the processes of diamond growth.

References:

[1] Harris, J.W. (1968): Ind. Diamond. Rev. 28:402-410.

[2] Meyer, H.O.A., Boyd, F.R. (1972): Geochim. Cosmochim. Acta, 36:1255-1273.

[3] Sobolev, N.V. (1974): Deep-seated inclusions in kimberlites and the problem of the composition of the upper mantle. Novosibirsk, Nauka Publishing House, 246 p. (in Russian). English translation (1977): Boyd, F.R., ed., Amer. Geophys. Union, Washington D.C., 279 p.

[4] Yefimova, E.S., Sobolev, N.V. (1977): Dokl. Acad. Nauk SSSR, 237:1475-1478 (in Russian).

[5] Shirey, S.B., Cartigny, P., Frost, D.J., Keshav, S., Nestola, F., Nimis, P., Pearson, D.G., Sobolev, N.V., Walter, M.J. (2013): Rev. Mineral. Geochem. 75:355-421.

[6] Sobolev, N.V., Logvinova, A.M., Yefimova, E.S. (2009): Russ. Geol. Geophy.s 50(12):1234-1248.

[7] Wiggers de Vries, D.F., Drury, M.R., de Winter, D.A.M., Bulanova, G.P., Pearson, D.G., Davies, G.R. (2011): Contrib. Mineral. Petrol. 161:565-579.

[8] Sobolev, N.V., Logvinova, A.M., Zedgenizov, D.A., Pokhilenko, N.P., Kuzmin, D.V., Sobolev, A. (2008): Eur. J. Mineral. 20:305–315.

EFFECT OF CRYSTALLIZATION MEDIUM ON GROWTH AND MORPHOLOGY OF DIAMOND

Palyanov Yu.N., Khokhryakov A.F., Borzdov Yu.M., Kupriyanov I.N.

V.S. Sobolev Institute of Geology and Mineralogy, SB RAS, Novosibirsk, Russia
palyanov@igm.nsc.ru

Analysis of data on the diamond morphology **[1,2]** shows that crystals obtained from various deposits are specific and diverse, that allow assuming a considerable range of conditions for diamond formation in the nature. The present work is devoted to experimental study on diamond crystallization in various media at the pressure of 5-7.5 GPa and temperature range of 1200-2000ºC and determining the conditions, affecting the diamond morphology in growth processes.

In the literature concerned with the diamond mineralogy it is traditionally considered that the factors, influencing the morphology of crystals, are the temperature of crystallization **[3]** and supersaturation **[2].** However, according to our data the regular change of diamond morphology in the cube – cubooctahedron – octahedron series with temperature holds only for diamond synthesis in the melts of transition metals and in the S-C system. Experimental data on the effect of supersaturation on the diamond morphology are rather scant.

It is experimentally shown that the composition of the crystallization media is a principal factor, controlling diamond growth and morphology. In the $CaCO_3$-C system, diamond morphology is characterized by tetragon-trioctahedron {533}, {955}, {755}, {211} and {322} faces. The only diamond growth form in sulfide melts is octahedron **[4]**. In the S-C system diamond morphology is determined by {100} and {111} faces with minor development of {411} and {944} ones **[5]**. In ultrapotassic carbonate, carbonate-silicate and carbonate-chloride media principal growth forms are octahedron and cube. In the Mg-C system exceptionally cubic diamonds were synthesized. In carbonate, carbonate-silicate and carbonate-chloride media, modeling composition of inclusions in natural diamonds, it is established that diamond morphology is strongly altered by the addition of H_2O and the only growth form at these conditions is octahedron.

We studied the effect of nitrogen impurities on diamond growth and morphology in metal-carbon systems. The concentration of nitrogen in the growth system was varied by adding nitrogen-containing substances to the charge; the other conditions of the growth were constant: Fe-Ni-C system, P=5.5 GPa, T=1400°C and duration of 65 h **[6]**. It is established, that with an increase in nitrogen concentration the crystallization of diamond proceeds through the following stages: single crystal → block crystal → aggregate of block crystals and twins. An increase in nitrogen concentration in the crystallization medium results in the regular changes in the impurity content, morphology and crystalline perfection of diamond crystals. Concentration of nitrogen impurity in diamonds increases from about 200 to approximately 1100 ppm, with an accompanying growth of the absorption band with a peak near 660 nm, which is responsible for the observed green coloration of nitrogen-doped crystals. The growth form of diamond crystals changes in the following sequence: {111}>{100},{311},{110} → {111}>{100},{311} → {111}>>{100}, that allows to consider nitrogen as an impurity, which stabilize octahedral growth form. The density of dislocations and twin lamellae, as well as anomalous birefringence, caused by internal strains, increases with nitrogen concentration. The stage of growth of aggregates of block crystals and twins occurs at high concentrations of nitrogen in the metal melt and is characterized by the appearance of strong strains, intense micro-twinning, entrapment of inclusions and development of considerable self-deformation phenomena. At nitrogen concentrations in metal melt higher than 0.4 atom. % the nucleation and growth of diamond are terminated and graphite only crystallizes in the field of thermodynamic stability of diamond.

Experiments, modeling diamond growth under the blocking influence of impurity, were performed in metal-carbon systems with addition of water. As a source of water, a mixture of $Mg(OH)_2$ and SiO_2 was used, which reacted under the experimental conditions following the reaction $2Mg(OH)_2+SiO_2=Mg_2SiO_4+2H_2O$ **[7]**. The main experiments were performed in the $Ni_{0.7}Fe_{0.3}$-C system at a pressure of 6 GPa, temperature of 1300-1370 °C, duration of 15 hrs and H_2O concentration (C_{H2O}) ranging from 0 to 0.5 wt.%. It is found that as H_2O content increases from 0 to 0.2 wt.%, diamond morphology changes from bulky octahedra to {111} plate-like crystals and then to {111} dendrites. Further increases in C_{H2O} in the range 0.22-0.4 wt.% result in crystallization of bulky rhombic dodecahedra and then {110} dendrites. At C_{H2O} higher than approximately 0.43 wt.%, nucleation and growth of diamond are completely terminated and graphite only crystallizes. The systematic changes in diamond growth and morphology are accompanied by a decrease in nitrogen impurity concentration in diamond from 220-230 to 40-50 ppm, an increase in the density of micro-inclusions and appearance in IR spectra of a peak at 2840 cm^{-1}, related to hydrocarbons. The anti-skeletal crystal produced in the experiments are morphological analogs of some natural diamonds. The established changes in growth, morphology and main characteristics of diamond are caused by the impurity action.

Thus, our experimental data evidence that the growth and morphology of diamond are largely controlled by the composition of crystallization medium and impurity action.

References:

[1] Orlov Yu.L. The mineralogy of diamond, 1977, John Wiley: New York, 235 p.

[2] Sunagawa I. In Materials Science of the Earth's Interior; Sunagawa I., Ed.; Terra Scientific Publishing Company: Tokyo, 1984; pp 303-330.

[3] Haggerty S.E. Diamond genesis in a multiply constrained model. Nature, 1986, 320, p. 34–38.

[4] Palyanov Yu.N., Borzdov Yu.M., Khokhryakov A.F., Kupriyanov I.N., Sobolev N.V. Sulfide melts-graphite interaction at HPHT conditions: Implications for diamond genesis. Earth and Planetary Science Letters. 2006, v. 250, Iss. 1-2, p. 269-280.

[5] Palyanov Yu.N., Kupriyanov I.N., Borzdov Yu.M., Sokol A.G., Khokhryakov A.F. Diamond crystallization from a sulfur-carbon system at HPHT conditions. Crystal Growth & Design, 2009, v. 9, №6, 2922-2926.

[6] Palyanov Yu.N., Borzdov Yu.M., Khokhryakov A.F., Kupriyanov I.N., Sokol A.G. Effect of nitrogen impurity on diamond crystal growth processes. Crystal Growth & Design, 2010, v. 10, p. 3169-3175.

[7] Palyanov Yu.N., Borzdov Yu.M., Kupriyanov I.N., Khokhryakov A.F. Effect of H_2O on diamond crystal growth in metal-carbon systems. Crystal Growth & Design, 2012. № 11. p. 5571–5578.

CARBONATITE METASOMATISM OF DEPLETED PERIDOTITES IN THE LITHOSPHERIC MANTLE AND ITS RELATION TO THE FORMATION OF DIAMOND AND PRIMARY CARBONATITE-KIMBERLITE ASSOCIATIONS

Pokhilenko N.P. [1], ***Agashev A.M.*** [1], ***Litasov K.D.*** [1,2], ***Pokhilenko L.N.*** [1]

[1] *V.S. Sobolev Institute of Geology and Mineralogy SB RAS, Novosibirsk, Russia*
[2] *Novosibirsk State University, Novosibirsk, Russia*
chief@igm.nsc.ru

A formation of the majority of natural diamonds and variety of kimberlite melts is undoubtedly connected with the processes of carbonatitic metasomatism of the deep lithospheric mantle [**1-3**]. Indeed, the same processes are responsible for changes in geochemical characteristics of pyrope harzburgites in the lithospheric roots and, in an extreme case – for significant wehrlitization and carbonation of these harzburgites [**4-5**].

The evident signatures of the carbonatitic metasomatism are displayed by the Cr-pyrope harzburgite and dunite xenoliths [**4-5**]. These signatures are an increase of Ca-number, amount of LREE and some other incompatible elements accompanied by significant increase of the La/Yb ratio in garnets and bulk rocks. In the deepest xenoliths of refertilized sheared pyrope lherzolites, representing a zone of the lithosphere – asthenosphere interaction, the noticed signs of enrichment are combined with ones of more intense modification of these rocks caused by basanitic melts of sublithospheric origin. This influence result in general basification of depleted peridotites up to their transition to enriched (refertilized) lherzolites [**6-7**].

Significant variations of geochemical characteristics (and sometimes a major elements chemistry, especially Ca) of specific pyrope grains in significant number of megacrystalline Cr-pyrope harzburgite xenoliths, including diamondiferous ones, clearly demonstrate an infiltration character of carbonatitic metasomatism realized by penetration of the low viscosity and highly mobile carbonatitic melts trough the crack system and intergranular space in the megacrystalline olivine matrix [**4-5**]. Diamond in these rocks is formed at the redox conditions corresponding to the CCO buffer at relatively low intensity of carbonatite metasomatism of depleted peridotites. However, higher intensity of metasomatism resulted in the destruction of diamond and further oxidation of the system for several log units above CCO buffer into carbonate stability field. As a result, carbonatite metasomatism leads to wehrlitization and carbonation of initial Cr-pyrope harzburgites of the lithosphere roots. The amount of newly formed carbonates in the rock is usually <1 vol. %. A progressive partial melting of slightly carbonated depleted peridotite at PT-parameters of deep lithosphere (>250 km) generated a primary association of carbonatite (a degree of partial melting is <1 %) and then kimberlite melts with unusual petrochemical and geochemical characteristics, which do not allow to attribute them to known kimberlites group 1 or 2 **[3]**. A secondary enriched lherzolites of the lithosphere roots with the signatures of both carbonatitic and more intensive basanitic metasomatism formed a source for group 1 kimberlite **[7-8]**.

The carbon isotope composition of diamonds associated with the depleted peridotites shows its deep sublithospheric origin. Any significant role of subducted carbonates in the generation of sublithospheric carbonatite melts influencing the depleted peridotites at least during the mid-Archean can be repelled. A stage of mid-Archean carbonatitic metasomatism was anticipated by a relatively short period of the global event (~ 200 Ma, between 3.7 and 3.5 Ga) resulted in the significant increase of lithosphere thickness and growth of the continental crust. The thickness of some blocks of Siberian and Kapvaal cratons at that time exceeded 150 km and PT-parameters of the roots of these blocks were in the diamond stability field. Thus, the lithosphere roots made of depleted peridotite could be affected by carbonatitic metasomatism.

Taking into account the new experimental results on the carbonate stability in the peridotite, eclogite, kimberlite, and carbonatite systems the formation of highly alkaline

carbonatite melts is possible at *PT*-parameters of sublithospheric mantle. The SiO_2 contents of low-degree partial melts in the H_2O-free or H_2O poor experimental systems do not exceed 5-10 wt.% at 6-10 GPa and 1300-1500^oC [9-10]. An important criterion for diamond formation and carbonatite metasomatism would be redox state. Heterogenous oxidation of presumably reduced (below CCO buffer) peridotites in the cratonic roots is connected with variable degree of carbonatite metasomatism, which can cause diamond formation by weak metasomatic influence and carbonation and werhlitization at high degree of metasomatism. The details of these processes can be deciphered by geochemical study of garnet and chromite from metasomatized and diamondiferous megacrystalline peridotites and minerals of sheared refertilized lherzolites.

The work is supported by RFBR Grants # 13-05-00907 and 13-05-12096.

References:

[1] Navon, O., 1999. Proc. 7th. Int. Kimberlite Conf., v. 2, 584-604.
[2] Klein-BenDavid, O., Izraeli, E.S., Hauri, E., Navon. O., 2004. Lithos, 77, 243-253.
[3] Agashev, A.M., Pokhilenko, N.P., Takazawa, E., McDonald, J.A., Vavilov, M.A., Watanabe, T., Sobolev, N.V., 2008. Chemical Geology, v. 255, 318-328.
[4] Shimizu, N., Pokhilenko, N.P., Boyd, F.R., Pearson. D.G., 1999. Proc. 7th Int. Kimberlite Conf., v.2, 773-782.
[5] Pokhilenko, N.P., Sobolev, N.V., Boyd, F.R., Pearson, D.G., Shimizu N., 1993. Geologiya i Geofyzika, 34, 56-68.
[6] Pokhilenko, N.P., Sobolev, N.V., Kuligin, S.S., Shimizu, N., 1999. Proc. 7th Int. Kimberlite Conf., v.2, 689-698.
[7] Agashev A.M., Ionov, D.A., Pokhilenko, N.P., Golovin, A.V., Cherepanova, Yu., Sharygin, I.S., 2013. Lithos, 160-161, 201-215.
[8] Pokhilenko, N.P., 2009. Lithos, 112, 2, 934-941.
[9] Sharygin, I.S., Litasov, K.D., Shatskiy, A.F., Golovin, A.V., Ohtani, E., Pokhilenko, N.P., 2013. Melting experiments on kimberlite of Udachnaya-East pipe at 3-6.5 GPa and 900−1500ºC, Doklady Earth Sciense, 448, 200-205
[10] Ghosh, S., Litasov, K.D., Ohtani, E., 2013. Contributions to Mineralogy and Petrology, in press.

THE IRON CARBIDES AT HIGH PRESSURES STUDIED BY FIRST PRINCIPLES CALCULATIONS: REVISITED

Popov Z.I. [1], ***Fedorov A.S.*** [1], ***Litasov K.D.*** [2], ***Ovchinnikov S.G.*** [1]
[1] *Kirensky Institute of Physics SB RAS, Krasnoyarsk, Russia*
[2] *VS Sobolev Institute of Geology and Mineralogy SB RAS, Novosibirsk, Russia*
zipcool@bk.ru

Structure and elasticity of iron carbides was re-investigated at high pressures using density-functional-theory. Carbon is considered as one of the potential light element in the Earth's liquid outer and solid inner core. It was estimated that core may contain 8–12% of light elements except Fe and Ni [1]. Wood [1] was one of the firsts, who suggested that there might be a significant amount of C in the Earth's core, and the likely stoichiometry of the stable Fe-C compounds at high pressures would be Fe_3C and Fe_7C_3 [1–6].

All calculations were performed in Vienna *ab initio* Simulation Package (VASP 5.2) [7-9] employing the density functional theory (DFT) within the projector-augmented wave (PAW) method [10,11]. The first step of our calculations was geometry optimization of $P6_3mc$ Fe_7C_3, $Pnma$ Fe_3C, $P6_3mmc$ Fe, and $Fd3m$ C at zero pressure and $T = 0$ K. After that, we changed the volume of the unit cell and perform the relaxation energy calculations. The values obtained from the pressure dependence of the energy have been processed using the third-order Birch-Murnaghan equation of state.

We examined the iron carbide forming reactions to identify compounds, preferentially stable along with carbon at high pressures, corresponding to the Earth's inner core.

The enthalpy calculations for the reactions $Fe_3C = 3Fe + C$ and $Fe_7C_3 = 7Fe + 3C$ are presented at Fig.1. It can be seen that Fe_3C is predominantly stable relative to Fe and diamond at pressures above 45 GPa, whereas Fe_7C_3 is stable at pressures above 50 GPa.

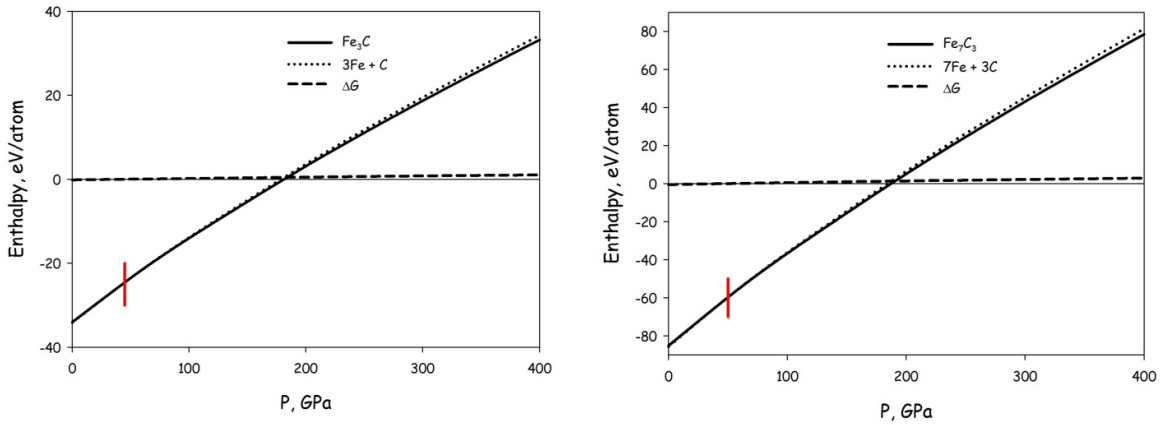

a b

Figure 1. Dependence of formation energy from pressure.

Our calculations of elastic moduli for studied compounds are fairly consistent with the results obtained by Mukherjee et al. [4]. However, we challenged their interpretations for the reaction $3Fe_7C_3 = 7Fe_3C + 2C$, because mass-balance calculations of reaction may not be correct. The balanced energy calculations for this reaction is presented at Fig. 2. The Fe_3C is primarily formed phase at all pressure from zero to 400 GPa. This result contradicts with that of Mookherjee et al. [4], where Fe_7C_3 considered as a preferably stable phase above 200 GPa relative to Fe_3C and C. In addition, we performed spin-polarized calculations for finding point of magnetic collapse. The results of these calculations are presented at Fig.3. It was found that magnetic collapse occurs at around 64 GPa for Fe_3C and at around 80 GPa for Fe_7C_3.

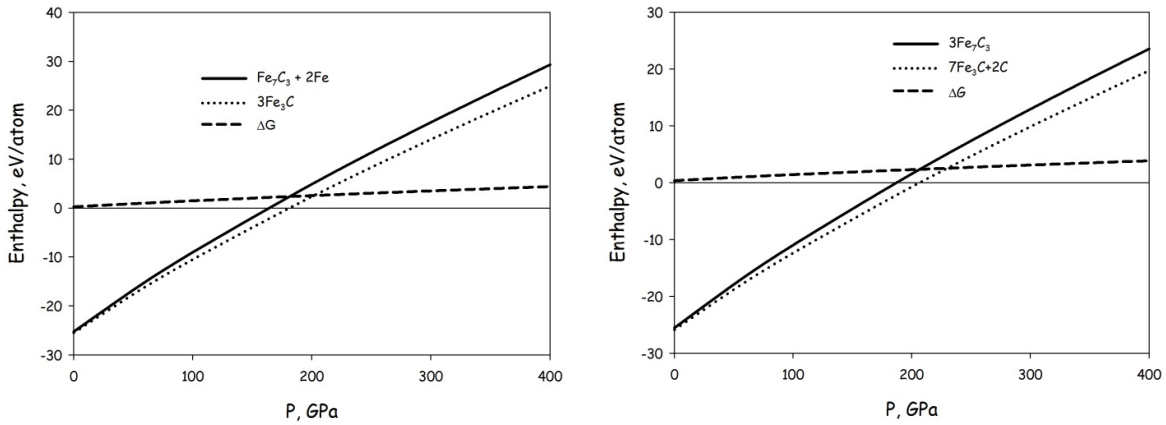

a b

Figure 2. Dependence of formation energy from pressure for the reactions:
a) $3Fe_3C = Fe_7C_3 + 2Fe$; b) $3Fe_7C_3 = 7Fe_3C + 2C$

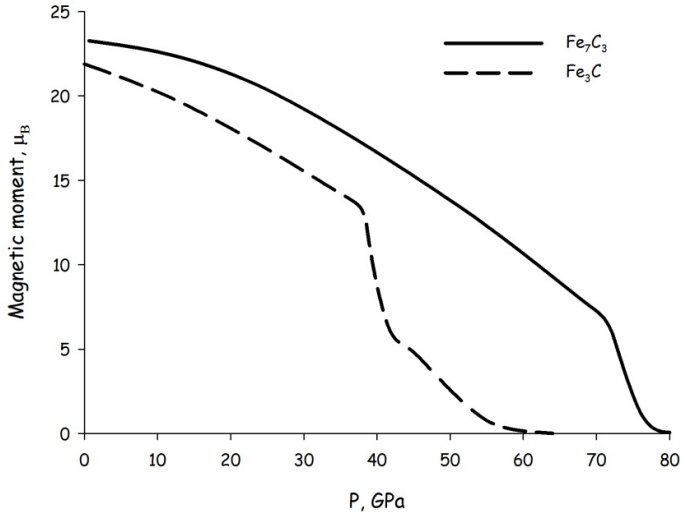

Figure 3. Dependence of magnetic moment of Fe-carbides from pressure.

This work was supported by the Ministry of education and science of Russian Federation, project Nos 14.B37.21.0457 and 14.B25.31.0032, RF President Grant No MD-500.2013.5 It is partially supported by IP SB RAS No 97 and RFBR (No 12-05-33008).

References:

[1] B. J. Wood, Earth Planet. Sci. Lett. 117, 593 (1993).
[2] G. Fiquet et al., Phys. Earth Planet. Int. 172, 125 (2009).
[3] O. T. Lord et al., Earth Planet. Sci. Lett. 284, 157 (2009).
[4] M. Mookherjee et al., J. Geophys. Res. 116, B04201 (2011).
[5] Y. Nakajima et al., Am. Mineral. 96, 1158 (2011).
[6] Gihan L. et al., Phys. Rev. B 84, 174110 (2011).
[7] G. Kresse and J. Hafner, Phys. Rev. B 47, 558 (1993).
[8] G. Kresse and J. Hafner, Phys. Rev. B 49, 14251 (1994).
[9] G. Kresse and J. Furthmueller, Comput. Mater. Sci. 6, 15 (1996).
[10] P. E. Blöchl, Phys. Rev. B 50, 17953 (1994).
[11] G. Kresse and D. Joubert, Phys. Rev. B 59, 1758 (1999).

THE COMPARISON OF GROWTH MEDIA IN ZONAL DIAMONDS FROM NYURBINSKAYA KIMBERLITE PIPE (YAKUTIA)

Ragozin A.L. [1], ***Zedgenizov D.A.*** [1], ***Shatsky V.S.*** [2], ***Kalinina V.V.*** [1], ***Sitnikova E.S.*** [1], ***Pomazansky B.S.*** [3]

[1] *V.S. Sobolev Institute of Geology and Mineralolgy, Novosibirsk, Russia*
[2] *A.P. Vinogradov Institute of Geochemestry, Irkutsk, Russia*
[3] *NIGP CNIGRI ALROSA Co. Ltd, Mirny, Russia*
ragoz@igm.nsc.ru

Due to chemical and physical stability diamond is an ideal "container" for transporting samples of the mineral-forming medium and mantle minerals as primary mineral and fluid/melt inclusions. Studies of high-density fluids (HDF) preserved as microinclusions in cubic, cloudy and coated diamonds provide the unique opportunity to reconstruct the composition and evolution of deep-seated liquids responsible for mantle metasomatism, diamond formation, and partial melting of mantle rocks. Internal structure caused by different distribution of lattice defects in the growth zones and sectors may reflect the separate stages of evolution of the crystals.

Here we present the results of a study of microinclusions in 42 diamonds with pronounced growth zoning from the Nyurbinskaya kimberlite pipe located in the east of Siberian Platform (Nakyn kimberlite field). The Nakyn kimberlite field is located in the east of the Siberian platform, in the Vilyui-Markha deep fault zone. Only two kimberlite pipes (Botuobinskaya and Nyurbinskaya) have been discovered in this region; both are diamondiferous. We studied three types of microinclusion bearing diamonds of different morphologies and internal structures from Nyurbinskaya kimberlite pipe: (1) cuboid diamonds; (2) "cloudy" diamonds; (3) coated diamonds.

Cuboid diamonds (*type 1*) are the crystals of overall cubic morphology. Most of these crystals have typical resorption features, such as tetragonal etch-pits and the rounded edges. Many diamonds we refer to this type have roughly cubic shapes surfaced by repeated small octahedral faces. The diamonds studied here are greyish to almost black due to abundant microinclusions. In most cases there is distinct growth zoning structure revealed by optical microscopy and CL imagery.

So called "cloudy" diamonds (*type 2*) are the crystals having morphology transitional between octahedral and rounded rhombic dodecahedral habit. Morphological features and internal structure are similar to such diamonds described in other Yakutian kimberlite pipes **[1]**. CL imagery have revealed that the re-shaping of diamonds with "cloudy" cuboid cores (microinclusions-rich) occur via generation of numerous octahedral apices on cuboid surfaces and subsequent gradual transformation into regular octahedral morphology.

Coated diamonds (*type 3*) are the gray-yellow crystals of a cubic or cuboctahedral habit with sculptured octahedral faces and rhombic-dodecahedron and cuboid surfaces. The CL images clearly show that the crystals have an intricate internal structure: an octahedral core with a straight zoning contrasts with a fibrous rim with abundant microinclusions. It is concerned that in diamonds with such internal structures at the commencement of the coat an abrupt change to fibrous, radial growth occurs **[2]**.

The samples were polished parallel to (110) and (100) plane into slabs 100–200 μm thick. IR absorption spectra were measured using a FTIR Bruker Vertex 70 spectrometer equipped with a Hyperion-2000 IR microscope. The FTIR spectra obtained from the entire thickness of the slabs reflect the bulk content of all species in the analyzed volume, including absorption from diamond and impurities trapped as lattice defects (nitrogen and hydrogen). The chemical compositions of subsurface microinclusions were determined using a TESCAN MIRA 3 LMU by EDS techniques.

The nitrogen content of studied diamonds varies from 20 to 1850 ppm and in some cases may significantly differ between contrast growth zones. Predominantly cuboids are type IaA (contain only A-centers), only several samples are IaAB with IaB/IaA ratios from 5 to 15%. The nitrogen aggregation state of the cubic cores of "cloudy" diamonds is considerably higher than that of cuboids. Nitrogen content and aggregation states are significantly different in the cores and coats. Coated diamonds have high nitrogen aggregation state in core (up to 45%) and usually contain platelets absorption band (~1370 cm^{-1}). The fibrous coats in these diamonds are always lower aggregated (contain only A-centers).

A comparison of microinclusions in fibrous and cloudy diamonds from worldwide sources reveals a wide range of compositions of HDF between three end-members: (a) a silicic end-member rich in water data and Si, Al, K; (b) a carbonatitic end-member rich in carbonate, Mg, Ca, Fe and K and (c) a saline end-member rich in water, Cl and K. The diamonds from Nyurbinskaya pipe define the range of microinclusions largely from carbonatitic to hydrous-silicic end-members (Fig. 1). Cuboids and coated diamonds and fall in this range. The most of "cloudy" diamonds have microinclusions of predominantly carbonatitic composition. Several "cloudy" diamonds have relatively high content of saline component (K, Na + Cl). Microinclusions in these diamonds are also slightly enriched in water and lie at the starting interval of a continuous trend between carbonatitic and saline end-members of diamond-forming media. From this results may be speculated that the diamond-forming media whose relics were found in the diamonds from Nyurbinskaya pipe might have formed during the low degree partial melting of mantle rocks. The observed variations in the compositions of the diamond-hosted microinclusions within a carbonatitic to hydrous-silicic trend might also be due to fluid/melt fractionation during the crystallization or the mixing of compositionally different parental liquids.

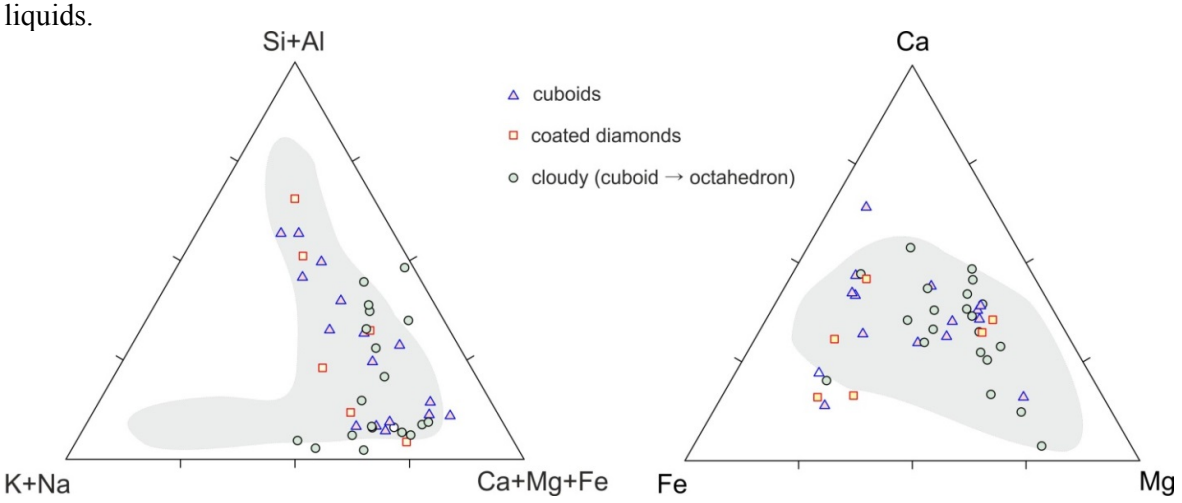

Figure 1. The averaged composition of microinclusions in diamonds from the Nyurbinskaya kimberlite pipe. Each point is the averaged composition of numerous microinclusions (20-40 analysis) in an individual diamond. The shaded areas outline the compositional ranges of worldwide database.

This work is supported by RFBR #12-05-33035 and #13-05-00628.

References:

[**1**] Zedgenizov, D., et al., Directional chemical variations in diamonds showing octahedral following cuboid growth. Contributions to Mineralogy and Petrology, 2006. 151(1): p. 45-57.

[**2**] Kamiya, Y. and A. Lang, On the structure of coated diamonds. Philosophical Magazine, 1965. 11(110): p. 347-356.

CARBON ISOTOPE DISTRIBUTION BETWEEN IRON CARBIDE AND DIAMOND AT HIGH PRESSURE AND HIGH TEMPERATURE

***Reutsky V.*, Borzdov Yu., Palyanov Yu.**

V.S.Sobolev Institute of Geology and Mineralogy SB RAS, Novosibirsk, Russia
reutsky@igm.nsc.ru

Carbides are one of the major host of carbon in reduced part of the Earth's mantle **[1]**. However, not much is known about carbon isotope fractionation during carbide formation. Restricted data on comparison of isotope composition of graphite(diamond) and carbides (cohenite, taenite) in meteorites show difference up to 15‰. Experimental attempts on determination of diamond-carbide isotope effects have been inhibited by the methodological and HPHT technique related uncertainties. On the other hand, diamond-carbide approach not fully adequate for solving the question because both of the crystal phases grown from metal-carbon melt and the difference results from carbide-melt-diamond relationship rather than carbide-diamond fractionation. Here we present results on distribution of carbon isotopes between diamond, iron carbide and quenched rest of Fe-C melt obtained from HPHT crystallization experiments.

Experiments were done at 6.3GPa and 1600^{o}C with slow cooling down to 1400^{o}C during 3 hrs. Initial mix of iron metal (grade 99.998) and graphite ($\delta^{13}C$=-23.0‰) of two compositions: 6.67wt.% of C (Fe_3C stoichiometric composition) and 5.5wt.% of C (a bit lower carbon than peritectic composition) were used. The Fe-C6.67wt.% system gives tiny diamond crystals and Fe_3C crystalline aggregate and Fe-C5.5wt.% system produce Fe_3C aggregate with no diamond. About 20% of Fe-C melt was quenched forming fine iron-carbide aggregate. Diamond crystals were grown first from Fe-C melt at 1600^{o}C within L+Dm stability field. Iron carbide Fe_3C starts to growth at about 1570^{o}C due to peritectic reaction L_1+Dm→L_2+Fe_3C. Some of diamond crystals were trapped within iron carbide aggregate and survive until the quench of the system. The Fe-C5.5wt.% composition did not cross the L+Dm field and stays diamond-free.

Average $\delta^{13}C$ value for diamond crystals (-20,3‰) appear to be higher than initial composition and display sizable isotope effect during diamond crystallization from initial melt. Fe_3C aggregates show measurable isotope trends in directions of growth in both systems also testifies isotope fractionation during Fe_3C crystallization. In the Fe-C6.67wt.% case the carbon isotope composition of Fe_3C changes from -26.2 up to -24.8‰ along direction of growth. In Fe-C5.5wt.% case the trend of $\delta^{13}C$ of Fe_3C starts from -24.8 and goes down to -26.8‰. Accounting the peritectic reaction, both of the trends are result from isotope depletion in accordance with Rayleigh's equations. Direct measurements of $\delta^{13}C$ of iron carbide and quenched Fe-C melt nearby phase's boundary reveal 2.0±0.5‰ enrichment of crystalline phase by ^{13}C isotope.

According to **[1-3]** carbide crystallization at depth relevant to PT-conditions of our experiments is common event. Iron carbides can crystallize during co-called RedOx freezing. Contact (reaction) zones between mantle domains with contrast fO_2 might be consist of iron carbides. Following our experiments, such iron carbide zones will have pronounced carbon isotope gradients if crystallize from Fe-C melt. Further processing of such carbide into diamond as a result of RedOx freezing process highlights the inhomogeneity and leads to isotope trends or zoning in resulting diamond crystals. Because of extremely low carbon isotope diffusion in diamond **[4]**, the isotope inhomogeneity is preserved in geological timescale. Thus, in some cases inner carbon isotope inhomogeneity of natural diamond crystals could be result of iron carbide crystallization form Fe-C melt and have no connection with changing of carbon source.

Work is supported by RFBR research grant #12-05-00846.

References:

[1] Stagno V, Frost D.J., 2010. Carbon speciation in the asthenosphere: Experimental measurements of the redox conditions at which carbonate-bearing melts co-exist with graphite or diamond in peridotite assemblages. Earth Planet. Sci. Lett. 300, 72-84.

[2] Rohrbach, A., Ballhaus, C., Golla-Schindler, U., Ulmer, P., Kamenetsky, V.S., Kuzmin, D.V., 2007. Metal saturation in the upper mantle. Nature. 449, 456-458.

[3] Rohrbach, A., Schmidt, M.W., 2011. Redox freezing and melting in the Earth's deep mantle resulting from carbon-iron redox coupling. Nature. 472, 209-214.

[4] Koga, K.T., Van Ormanb, J.A., Walter, M.J., 2003. Diffusive relaxation of carbon and nitrogen isotope heterogeneity in diamond: a new thermochronometer. Phys. Earth Planet. Inter. 139, 35-43.

POSSIBLE FACIAL P-T AREAS OF CARBON PRECIPITATION IN THE LITHOSPHERE MANTLE UNDER THE INFLUENCE OF MAGMA FLUID FLOWS FROM 'ASTHENOLENSES'

Sharapov V.N.

V.S. Sobolev Institute of Geology and Mineralogy, SB RAS, Novosibirsk, Russia
vik@igm.nsc.ru

Non-isothermal dynamics for metasomatic transformation of homogeneous highly depleted lithosphere mantle has been studied (mole quantities: Si = 6,248; Ti = 0,006; Al = 0,08; Fe = 0,88; Mn =0,02;Mg = 10,7; Ca = 0,11; Na = 0,019; K = 0,006; Cr = 0,034; P = 0,02; H_20 = 0,056; O = 25,52); this transformation is due to magma fluid flows (C-H-O system) coming from 'asthenolenses', having T = 1300^{O}C and P = 30÷35 kbar, and penetrating the permeable zone (K_p= 10^{-13} ÷ 10^{-16} м$^{-2}$, m = 3- 2%). Hydrodynamics for heat and mass exchange is described using the Darcy equation. The dynamics of heterophase interactions is studied using a modification of flow-type reservoir of SELECTOR-C software [3], for the case of P-T dynamics of fluid flow [1]. Variations in fluid compositions depending on mole fraction change have been studied (C = 0,025 ÷2; H = 0,025÷ 2; O = 0,02 ÷ 3, N 0-0,01, S 0-0,1). Possible contents of water, hydrocarbons and hydrogen in gas phase compositions in the heterophase system for the temperature interval 1300^{O}C ÷ 300^{O}C, P = 30 ÷ 1 kbar, and lg pO_2 = 3 ÷ 25 are given in [4]. The results we obtained specify the data [2] on the compositional evolution of gas mixture fluid along the profile for the upper and lithosphere mantle; these data are valid for statistical estimates of P and T of non-isothermal interaction between the upper and lithosphere mantle and lithosphere ultrabasic rocks of the given primary composition. In any spot of the magmatogene convective heterophase system (with constant fluid composition at the entrance of permeable area) the dynamics of interaction between fluid and rock includes two stages: 1) initial, when the interaction is buffered by the rock massif; 2) subsequent, when phase composition change is determined by magma gas composition in magma reservoir. In this case all the consequent interactions along the flow are determined by the processes at the system entrance. We numerically studied heterophase processes for a uniform reactor chain of n = 50, with the lithosphere thickness 100 km. Therefore the relationships for gas mixtures at the system entry can be easily understood for the reactor #1, where T and P are stationary.

Let the primary composition of mantle rock is influenced by a gas of C-H-O-N-S-Cl-F composition, which can extract petrogenic components from the melt during its retrograde boiling. Here we give only the results for the C-H-O system. If we take the rock permeability in the lithosphere mantle as varying, K_p= 10^{-13} ÷ 10^{-16} m, the virtual time for the first stage for the given approximation is about 4 thousand years. In this case the gas phase composition for the reactor R #1 will change as the following: 1) **system C(1)H(1)O(0)** – 1 thousand years C_3H_4O ≈10%, CO_2 ≈ 21%, CH_2O_2 ≈ 14%, H_2O ≈ 2,8%, CHOH ≈ 17%, lg pO2 ≈ -8,8; 2 thousand years C_3H_4O ≈ 51%, $C_{20}H_{42}$ ≈ 48%, H_2 ≈ 0,03%, C_3H_8O ≈ 0,2%, CH_4 ≈ 0,4%, lg pO_2 ≈ -14,0; 3 thousand years $C_{20}H_{42}$ ≈ 90%, C_3H_4O ≈10%, CH_4≈ 0,2%,H_2O ≈ 0,02%, lg pO_2 ≈ -14,8; 4 thousand years $C_{20}H_{42}$ ≈ 96%, C_3H_4O ≈4%, CH_4≈ 0,15%, lg pO_2 ≈ -15,4; equilibrium composition $C_{20}H_{42}$ ≈ 98%, C_3H_4O ≈0,95%, lg pO_2 ≈ -16,6; 2) **system C(1)H(1)O(2),** equilibrium composition of gas mixture C_3H_4O ≈53,6%, CO_2 ≈ 1,5%, CH_2O_2 ≈ 17%, H_2O ≈ 3,5%, CHOH ≈ 21%, lg pO2 ≈ -8,15; 3) **system C(1)H(2)O(1)** - 1 thousand years C_3H_4O ≈25%, CO ≈ 0,3%, CH_2O_2 ≈ 13%, H_2O ≈ 11,6%, CHOH ≈ 16%, lg pO2 ≈ -7,3; 2 thousand years C_3H_4O ≈17%, CO_2 ≈ 5%, CO≈0,4%, CH_2O_2 ≈ 13%, H_2O ≈ 7%, CHOH ≈ 16%, lg pO2 ≈ -9; 3 thousand years C_3H_4O ≈18%, CO_2 ≈ 4,6%, CO≈0,4%, CH_2O_2 ≈ 12,5%, H_2O ≈ 7%, CHOH ≈ 15,5%, lg pO2 ≈ -9; 4 thousand years C_3H_4O ≈18,4%, CO_2 ≈ 4,5%,CO ≈ 0,4%, CH_2O_2 ≈ 17,5%, H_2O ≈ 7,5%, CHOH ≈ 15,7%, lg pO2 ≈ -9; 4) **system C(2)H(1)O(1)** equilibrium composition of gas mixture C_3H_4O ≈12,6%, CO_2 ≈ 20%, CO_2 ≈

1,3%, $CH_2O_{2,5}$ ≈ 8%, H_2O ≈ 1,4%, CHOH ≈ 0,3%, lg pO2 ≈ -8,9.. For the above-mentioned T-P systems the precipitation area for solid carbon phase practically coincides: T ≈ 1215 ÷ 1200 ^{O}C, P ≈ 15 ÷ 16 kbar. The border of carbon precipitation is the widest for the system **C(1)H(1)O(0),** and the narrowest for the system **C(1)H(1)O(2).** For all the studied varieties of gas phase, at the permeable zone entry, the range of carbon precipitation coincides for temperature interval 1270 ÷ 1120^{O}C and pressures P ≈ 25 ÷ 9,5 kbar. In this case the appearance of magnetite for the given P-T interval for a number of systems coincides to the appearance of graphite. Thus, it can be inferred that 1) in convective systems the Chekaluk's 'methane threshold' is spread into rather wide zone of temperature and pressure drops; 2) all magmatogene fluids containing C-H-O in their gas phases have this threshold; 3) the removal of petrogenic components from magma liquid do not change the whole picture substantially, if the system contains S, N, Cl, F; 4) there is no 'prohibited' zone for carbon precipitation if trivalent iron presents; full oxidation of carbon in solid phase corresponds to mineral associations with hematite, at the boundary of magnetite-hematite equilibrium.

This was supported by the Russian Foundation for Basic Research, Grant #12-05-00625.

References:

[1] Bessonova E.P., Sharapov V.N., Cherepanova V.K., Chudnenko K.V. A new model of thermal and physicochemical dynamics for volcanogenic epithermal deposits (Asacha deposit, Kamchatka) // Doklady Earth Sciences, 2010. Vol 431, #2, pp. 453-457

[2] Zubkov V.S. Thermodynamic modeling of C-H-N-O-S system for the upper mantle P-T conditions. Vestnik GeoIGU: Irkutsk, 2005, 177p.

[3] Chudnenko K.V. Thermodynamic modeling in geochemistry: theory, algorithms, software, applications. Novosibirsk, GEO, 2009, 287p.

[4] V.N. Sharapov, K.V. Chudnenko, M.P. Mazurov , Yu.V. Perepechko. Metasomatic zoning of subcratonic lithosphere in Siberia: Physicochemical modeling // Russian Geology and Geophysics, 2009, #12, pp. 1107-1118.

EXPERIMENTAL INVESTIGATION OF REACTION BETWEEN ORTHOPYROXENE AND ALKALINE DOLOMITIC CARBONATITE MELT WITH IMPLICATION FOR KIMBERLITE PETROGENESIS

Sharygin I.S. [1,2], ***Litasov K.D.*** [1,2], ***Shatskiy A.F.*** [1,2], ***Safonov O.G.*** [3], ***Golovin A.V.*** [1], ***Ohtani E.*** [4], ***Pokhilenko N.P.*** [1]

[1] *V.S. Sobolev Institute of Geology and Mineralogy SB RAS, Novosibirsk, Russia*
[2] *Novosibirsk State University, Novosibirsk, Russia*
[3] *Institute of Experimental Mineralogy RAS, Chernogolovka, Russia*
[4] *Department of Earth and Planetary Materials Science, Graduate School of Science, Tohoku University, Sendai, Japan*
igor.sharygin@gmail.com

Kimberlites are the deepest known magma originated at depths > 150 km and during the rapid ascent (10^{-1}–10^{2} km/h) to the surface carried out a large amount of lithosphere-derived xenogenic materials. Peridotite xenoliths are predominant (up to 95 %). The orthopyroxene (Opx) xenocrysts are extremely rare in olivine-dominated (up to 90 vol.%) xenocryst assemblage of kimberlites, whereas in peridotite xenoliths Opx comprises ~ 15-25 vol.%. Accordingly, rapid dissolution of Opx in the kimberlite melt during ascent has been suggested **[1, 2]**. During last decade many evidences for SiO_2-poor alkali-carbonatite compositions of primary kimberlite melts have been offered **[2-4]**, which provide further support for Opx assimilation.

Using experiments at 1 atm and 1000-1100°C Russell et al. **[5]** demonstrated that reaction between Opx and Na_2CO_3 melt leads to decarbonation of carbonatite melt. The authors assumed that this mechanism operates at mantle pressure causing continuous and vigorous degassing which promotes rapid ascent of the kimberlite magma. In order to examine this hypothesis, we conducted high-pressure (H*P*) experiments in the Opx-alkali-dolomitic carbonatite system, which is closer to the natural compositions of kimberlite parental melt.

The H*P* experiments were performed at 3 and 6.5 GPa within reasonable temperature range for kimberlite magma (Fig. 1) using a multianvil high-pressure apparatus at Tohoku University (Sendai, Japan). All experiments were conducted in hermetically welded Pt capsules with preliminarily dried starting mixtures. The starting material were mixture of Opx (60 wt%) and alkali-dolomitic carbonatite (40 wt%): $1.4Na_2CO_3 + 0.6K_2CO_3 + 2CaMg(CO_3)_2$ (in mol.%). Water-free techniques were used for sample preparation to prevent the loss of water-soluble species. The run products were examined by electron-microprobe analyses and Raman spectroscopy.

In our experiments, the Opx was assimilated by the carbonatite melt, but without exsolution of CO_2. Depending on the *P-T* conditions the Opx dissolution in the carbonate melt occurs either congruently or incongruently (Fig. 1) in accordance with the following reactions: $2Opx+CaMg(CO_3)_2$ (melt) = Ol (olivine) + Cpx (clinopyroxene) + $2MgCO_3$ (melt) + SiO_2 (melt) and Opx + $CaMg(CO_3)_2$ (melt) = Cpx + $2MgCO_3$ (melt). At 6.5 and 3 GPa, the melt is essentially carbonatite, it contains 36.4-45.5 wt.% CO_2 likely in the form of carbonate-ion and 5.9-12.6 wt.% SiO_2.

Thus, present H*P* experiments show no voluminous extraction of CO_2 during interaction of the alkali carbonatite melt with Opx within the pressure interval of 3-6.5 GPa. Hence, at depths >100 km, rapid ascent of kimberlite magma through cratonic lithosphere cannot be accelerated by CO_2 extraction as Russell et al. **[5]** suggested. Voluminous extraction of CO_2 from carbonate-rich melt is possible only at lower depths. Decarbonation of carbonatite melt is well constrained in peridotite-CO_2 systems **[6, 7]**. In the alkali-free system **[6]**, the decarbonation occurs only below 2.5 GPa via reaction: $2Opx + CaMg(CO_3)_2$ (melt) = 2Ol + Cpx + $2CO_2$ (Fig. 1). However, the presence of alkalis suppresses the decarbonation to pressures of below 2 GPa **[7]**. In order to clarify the details of decarbonation reactions more experiments are needed at pressures <2 GPa.

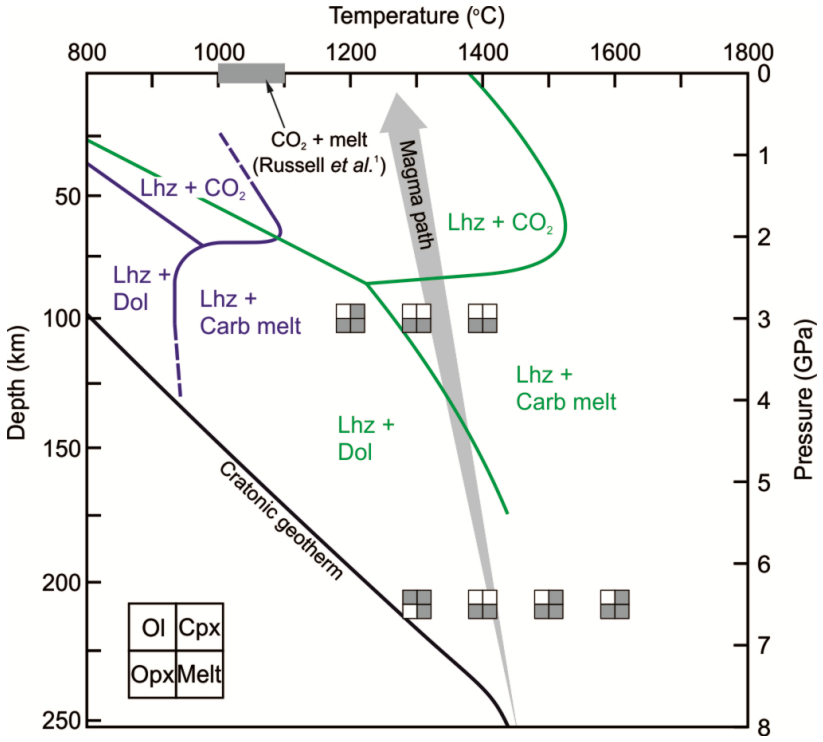

Figure 1. The *P-T* plot showing conditions and phase assemblages in the present experiments and decarbonation reactions in the peridotite-CO_2 systems. *Green and blue lines* show solidi and decarbonation reactions in the alkali-free **[6]** and alkali-bearing **[7]** peridotite-CO_2 systems (Lhz = Ol+Opx+Cpx), respectively. *P-T* path of kimberlite magma ascent is from **[8]**. Cratonic geotherm is from **[9]**.

This work is supported by the Russian Foundation for Basic Research (Grant nos. 12-05-31116-mol-a and 12-05-33008).

References:

[1] Mitchell, R. H., Kimberlites: Mineralogy, Geochemistry and Petrology, Plenum Press, New York, 1986, 442 pp.
[2] Kamenetsky, V. S., Kamenetsky, M. B., Sobolev, A. V., et al., 2009. Lithos, 112: 213-222.
[3] Kamenetsky, V. S., Kamenetsky, M. B., Weiss, Y., et al., 2009. Lithos, 112: 334-346.
[4] Sharygin, I. S., Litasov, K. D., Shatskiy, A. F., et al., 2013. Doklady Earth Sciences, 448: 200-205.
[5] Russell, J. K., Porritt, L. A., Lavallee, Y., Dingwell, D. B., 2012. Nature, 481: 352-356.
[6] Wyllie, P. J., Huang, W. L., Otto, J., Byrnes, A. P., 1983. Tectonophysics, 100: 359-388.
[7] Wallace, M. E., Green, D. H., 1988. Nature, 335: 343-346.
[8] Kavanagh, J. L., Sparks, R. S. J., 2009. Earth and Planetary Science Letters, 286: 404-413.
[9] McKenzie, D., Jackson, J., Priestley, K., 2005. Earth and Planetary Science Letters, 233: 337-349.

EFFECT OF CO_2 CONTENT ON MELTING PHASE RELATIONS IN GROUP I KIMBERLITE AT 6.5 GPA AND 1200-1600ºC: IMPLICATIONS FOR THE PARENTAL MAGMA COMPOSITION

Shatskiy A. [1,2], ***Litasov K.D.*** [1,2], ***Sharygin I.S.*** [1,2], ***Ohtani E.*** [3]

[1]*V.S. Sobolev Institute of Geology and Mineralogy SB RAS, Novosibirsk, Russia.*
[2]*Novosibirsk State University, Novosibirsk, Russia*
[3]*Department of Earth and Planetary Material Science, Graduate School of Science, Tohoku University, Aoba-ku, Sendai, Japan*
anton.antonshatskiy.shatskiy@gmail.com

Kimberlite has in several ways attracted more attention than its relative volume might suggest that it deserves. This is because its industrial importance as a source of mined diamonds. Besides, kimberlite is no less important scientifically because it serves as the deepest probe into Earth's interior. However, our understanding of kimberlite petrogenesis is significantly hampered by uncertainty about the compositions of kimberlite magma. It is generally accepted that the last equilibration of kimberlite magma with surrounding mantle (garnet lherzolite) occurred beneath cratons at 6-7 GPa prior its rapid ascent (~70 km/h) to the Earth's surface. This conclusion is based on the following facts. The deepest (170-220 km depths) and hottest (1200-1500ºC) xenoliths entrapped by kimberlites are sheared garnet lherzolites originating from the lower part of lithospheric mantle. The preservation of deformation features in sheared lherzolites indicates that the rock was undergoing dynamic recrystallization just before it was picked up by the magma and that it reached the surface after less than a few days or even hours in magma rising by crack propagation (Green and Gueguen, 1983; Meyer, 1985; Sparks et al., 2006). Based on our resent study (Sharygin et al., 2012) of melting phase relations in an exceptionally fresh kimberlite group I from Udachnaya-East kimberlite (UEK) pipe at 3.0-6.5 GPa and 900-1500°C, the kimberlite melt had essentially Na-K-Ca carbonatite composition <15 wt.% SiO_2, Na_2O + K_2O = 5-18 wt%, Na/K ≈ 2, Cl >1.5 wt%, and Ca/(Ca+Mg) > 0.5. However, the mineral assemblages obtained in these experiments differ from known mantle parageneses. This may be due to unaccounted CO2 budget missed at shallow depth as a result of decarbonation reactions at 1.5-2.5 GPa. Therefore, in present study we examined the effect of CO_2 content on melting phase relations in synthetic UEK kimberlite system at 6.5 GPa and 1200-1600ºC.

Experiments were conducted using Kawai-type multianvil apparatuses at Tohoku University (Sendai, Japan). Run duration ranged from 8 to 72 hs. Experimental mixtures were loaded in graphite cassettes. Starting compositions are shown in Table 1. Representative images of recovered samples are shown in Fig. 1. Obtained results are summarized in Fig. 2.

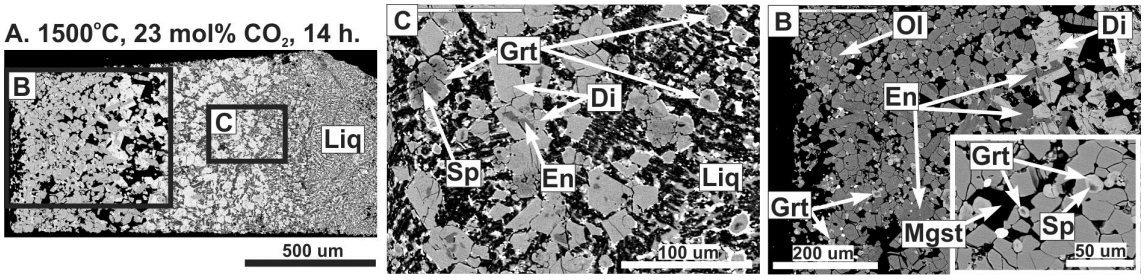

Figure 1. Representative BSE images of kimberlite samples recovered from experiments at 6.5 GPa.

Based on obtained results mineral assemblage equilibrated with kimberlite partial melt gradually changes from peridotite to eclogite paragenesis with increasing its CO_2 content from 13 to 35 mol %. As can be seen at 6.5 GPa kimberlite partial melt (i.e. Na-K-Ca carbonatite melt) becomes equilibrium with garnet lherzolite (i.e. olivine + enstatite + diopside + garnet + FeS + ilmenite assembly) at 1500ºC and 23 mol % (20 wt%) CO_2 (Fig. 1). This value is 10 mol% more than natural abundance of CO_2 in the Udachnaya-East kimberlite rock (group I kimberlite). In other words, the kimberlite magma lost almost half of the CO_2 budget during the eruption.

We greatly thank the Global Center-of-Excellence program at Tohoku University (Sendai, Japan) for the full technical and financial support of this study.

Table 1. Starting compositions of UEK kimberlite system.

#	SiO_2	TiO_2	Al_2O_3	FeO	MgO	CaO	Na_2O	K_2O	P_2O_5	SO_3	Cl	F	CO_2	
1	25.0	1.3	1.6	7.3	43.8	13.3	3.3	0.8	0.4	0.2	1.4	1.5	**0**	mol%
	28.9	2.0	3.1	10.0	33.6	14.2	3.8	1.5	1.1	0.3	0.9	0.6	**0**	wt%
2	21.7	1.2	1.4	6.4	38.1	11.6	2.8	0.7	0.3	0.2	1.2	1.3	**13.0**	mol%
	25.7	1.8	2.8	8.9	29.9	12.6	3.4	1.3	0.9	0.3	0.8	0.5	**11.1**	wt%
3	21.2	1.1	1.4	6.2	37.3	11.3	2.8	0.7	0.3	0.2	1.2	1.3	**15.0**	mol%
	25.2	1.8	2.7	8.7	29.3	12.4	3.3	1.3	0.9	0.3	0.8	0.5	**12.9**	wt%
4	20.2	1.1	1.3	5.9	35.5	10.8	2.6	0.7	0.3	0.2	1.1	1.3	**19.0**	mol%
	24.2	1.7	2.6	8.4	28.1	11.8	3.2	1.2	0.9	0.3	0.8	0.5	**16.4**	wt%
5	19.2	1.0	1.2	5.6	33.8	10.2	2.5	0.6	0.3	0.2	1.1	1.2	**23.0**	mol%
	23.1	1.6	2.5	8.0	26.9	11.3	3.1	1.2	0.8	0.3	0.8	0.4	**20.0**	wt%
6	18.2	1.0	1.2	5.4	32.0	9.7	2.4	0.6	0.3	0.1	1.0	1.1	**27.0**	mol%
	22.1	1.5	2.4	7.6	25.7	10.8	2.9	1.1	0.8	0.2	0.7	0.4	**23.6**	wt%
7	17.2	0.9	1.1	5.1	30.3	9.2	2.2	0.6	0.3	0.1	1.0	1.1	**31.0**	mol%
	21.0	1.5	2.3	7.3	24.4	10.3	2.8	1.1	0.8	0.2	0.7	0.4	**27.3**	wt%
8	16.2	0.9	1.0	4.8	28.5	8.6	2.1	0.5	0.3	0.1	0.9	1.0	**35.0**	mol%
	19.9	1.4	2.1	6.9	23.2	9.8	2.6	1.0	0.7	0.2	0.7	0.4	**31.1**	wt%

#1 UEK composition without CO_2 (shown for comparison). #2 UEK with natural abundance of CO_2, #3-8 UEK with additional CO_2.

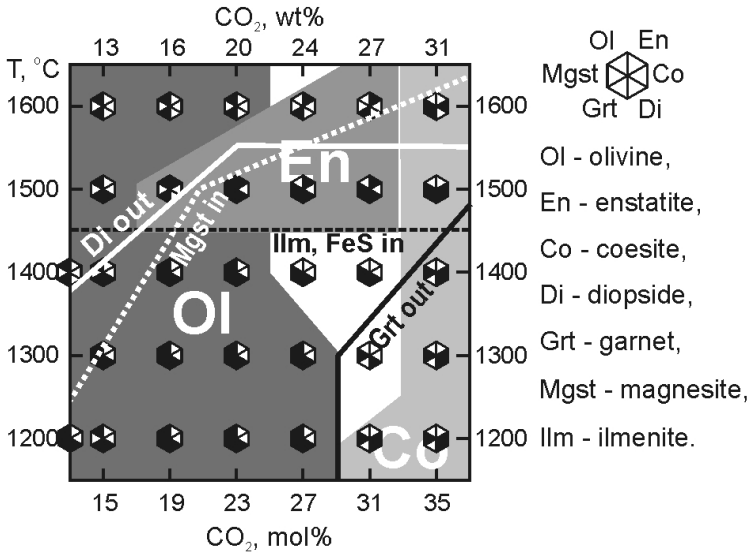

Figure 2. Melting phase relations in Udachnaya-East kimberlite (kimberlite group I) versus temperature and CO_2 content at 6.5 GPa. 13 mol % CO_2 corresponds to the natural abundance of CO_2 in UEK rock.

DEFORMATION-INDUCED DEFECTS IN DIAMONDS: CONTRIBUTION OF SMALL-ANGLE X-RAY SCATTERING AND ATOMIC FORCE MICROSCOPY

Shiryaev A.A.

Institute of Physical Chemistry and Electrochemistry RAS, Moscow, Russia

Diamond is a textbook example of brittle material at ambient conditions. However, the absolute majority of natural diamonds bear traces of plastic deformation. At geologically relevant pressures 4-6 GPa the brittle-to-ductile transition (BDT) occurs at temperatures 900-1100 °C **[1]**. Detailed studies of deformation-induced defects are needed for reconstruction of exact PT and strain conditions of deformation of natural diamonds. Here we review our results of investigation of diamond crystals, deformed both in nature and in High-Pressure High Temperature experiments using several not very common, but complementary techniques: Small-Angle X-ray and neutron Scattering (SAXS and SANS), Atomic force microscopy (AFM) and Transmission Electron Microscopy (TEM). These results show that besides extensive development of dislocation networks, microtwinning is very important mechanism of diamond deformation in broad range of deformation conditions.

The measurements were performed on synthetic and natural diamonds deformed both in nature and in HPHT experiments **[2-4]**. Thermal annealing and/or mechanical deformation cause formation of nanosized planar and 3D defects giving rise to Small-Angle Scattering (fig. 1). The defects are often facetted by crystallographic planes 111, 100, 110, 311, 211 common for diamond. Interestingly, ordering of the defects on scales 15-20 nm is often observed. Analysis of size distribution, shape and of spatial arrangement shows that in many cases the scattering is caused not only by clusters of point defects, but also by boundaries of microtwins.

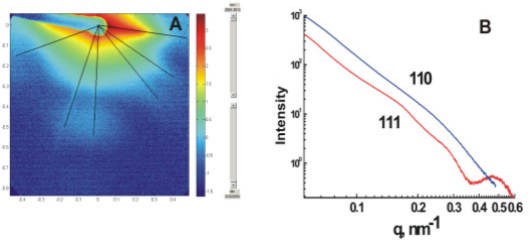

Figure 1: 2D view of SAS pattern and cross-sections along selected crystallographic directions of a type IaB natural diamond; defects ordering is observed.

TEM investigation of diamonds deformed at different PT conditions with variable strain rates **[2; 5]** show that microtwin formation strongly depends exact conditions of deformation. Whereas in some cases only dislocation networks and dislocation trails are present, other experiments produce individual twins of different types or twin colonies of vastly different sizes.

Our AFM study of slightly etched natural diamonds [6] revealed existence of remarkable surface features - "ridges": positive relief forms consisting of long (≤10 mkm), narrow (<2 mkm) features with heights usually below 40 nm. These features are not observable by high resolution optical microscopy (except, perhaps, interferometry) and are very difficult to spot using SEM. Detailed examination of the ridges shape indicate that they represent unelastic twins of different types. The most plausible explanation of the origin of these features is that they represent wedge-shape twins. Remarkably, the height of the observed ridges (≤40 nm) is similar to that observed for deformation lamellae on polished diamonds **[1]**. Tent-shaped twins are also present.

The assignment of the observed features to the twins is supported by analysis of their geometric shape. According to theory **[7]**, the shape of a twin part close to its tip in unloaded crystal should be qualitatively similar to that shown on Fig. 2. Direct measurements of the feature width show very good correspondence to theoretical shape of the twin, thus serving as a sound proof of our suggestion. The tip shapes for both ends of the twin are almost identical, which is logical since the twin shape close to the tip is largely determined by interatomic forces. In the same time, the shape of the intermediate part of a twin depends on elastic fields, which may differ for each side.

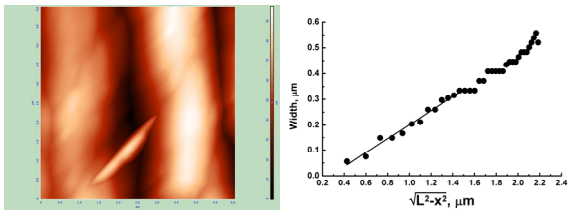

Figure 2. Left - AFM image of a wedge-type twin. Right – width-length correlations show theoretically predicted linear region.

As mentioned above, some of the twins observed are blunted at one end whereas others are symmetrically sharp. Though the statistics is limited, Fourier analysis shows that most blunted twin lamellae are arranged in bands with weakly pronounced periodicity forming twin colony. Individual twins in a colony may be blunted due to long-range stress fields **[8]**. Alternatively, the blunting may be caused by structural defect large enough to serve as an obstacle for twin motion **[7]**.

The twin lamellae are surrounded by twinning dislocations. If the dislocation mobility is low, as is in case of diamond at moderate temperatures, the twin may remain even when the load is removed. In our AFM images the twinning dislocations are manifested in two ways: a) wavy boundary of the blunted twins is likely due to etched dislocation cores and b) a very shallow depression around twins.

Certain types of stacking faults, potentially present at twin boundaries, can be considered as lamellae of hexagonal diamond (h-dia) polytype – lonsdaleite. Raman peak position of h-dia is downshifted from its usual position in cubic diamond. However, despite very high quality of Raman spectra (confocal Raman + AFM; mapping mode) no deviations from spectra of conventional diamond were found. This could be explained either by very small relative volume of the eventual h-dia phase and/or by its absence due to another type of atomic arrangement in the twin boundary.

This work shows that deformation of natural diamond by twinning is much more common than is usually believed. This implies that many diamond crystals were mechanically deformed at temperatures below the BDT point. The majority of previously observed deformation twins (e.g., **[1]**) were macroscopic, often penetrating the whole body of a crystal. Abundant twinning on microscopic scale such observed here and in **[2, 9]** is reported less frequently, probably, due to difficulties in observation. The extent of a twin lamella depends mostly on duration and magnitude of external load **[7]**. Presence of the microtwins without obvious large twin lamellae might indicate transient character of external loading or elastic release of twinning. In case of the elastic release the numeric density of remnant microtwins will depend on concentration of pinning defects.

Remarkably, several completely independent analytical techniques (AFM, Small-Angle Scattering, TEM) give indications that at least in some deformed diamonds extended defects may form fairly regular arrays. The origin of such ordering likely results from superposition of stress fields from several sources (e.g., dislocations).

Some results presented here were obtained with R. Gainutdinov, V. Boyko, Y. Fedourtchouk. The work is partly supported by RFBR grant 12-05-208.

References:

[1] DeVries, 1975, *Mater.Res.Bull.,* **10**, 1193-1200
[2] Shiryaev, 2007, *J.Appl. Cryst.,* 40, 116-120.
[3] Shiryaev et al., 2007, *Diam. Relat. Mater.*, 16, 503-511.
[4] Shiryaev & Boesecke, 2012, *J. Phys.: Conf. Ser.*, 351, 012018
[5] Mussi et al., 2013, *Phys. Stat. Sol. A* 210, 191–194
[6] Gainutdinov et al., submitted.
[7] Boyko, Garber, & Kossevich, 1994, Reversible Crystal Plasticity. AIP ed., New York.
[8] Mitchell & Hirth, 1991, Acta metall. mater., 39(7), 1711-1717.
[9] Titkov et al., 2012, *Miner. Mag.*, **76**, 143-149.

CRYSTALLOGENESIS OF THE MIR KIMBERLITE PIPE CLOUDY DIAMONDS: EVIDENCE FROM THE GROWTH MEDIUM COMPOSITION

Skuzovatov S.Yu. [1], ***Zedgenizov D.A.*** [2]
[1] *A.P. Vinogradov Institute of geochemistry SB RAS, Irkutsk, Russia*
[2] *V.S. Sobolev Institute of geology and mineralogy SB RAS, Novosibirsk, Russia*
skuzovatov@igc.irk.ru

Since first results were obtained by infrared spectra analyses **[1]** and direct determination of HDF composition in coated diamonds **[2]**, it has always been a matter of discussion how diamond-forming fluid/melt originates and evolves during diamond precipitation. Several compositional trends revealed by studies of individual diamonds and diamond populations point to different mechanisms of compositional variations generation, based on fractionational crystallization of silicate and carbonate phases, fluid/melt mixing or liquation **[e.g. 3,4]**. Here we report the first data on microinclusions composition in so-called cloudy diamonds from Mir kimberlite pipe.

Eight diamonds with cloudy core containing numerous microinclusions (fig. 1a) were polished into thin plates (|| {110}) to recover internal structure of crystals and analyze microinclusions. As revealed by transmitted light (fig. 1b) and CL (fig. 1c) imaging the growth of the cuboid core is followed by re-shaping into a cuboctahedra and then to resulting octahedral habit lacking any marks of resorption. It may suggest the continuous growth process without significant interruptions. Nevertheless, in some samples there is a clear boundary between cuboid core and outer octahedral zone. Together with nitrogen aggregation data (a gradual decrease in %B1 towards a crystal periphery or an abrupt drop at the cube/octahedron border) this makes support for at least two different scenarios of growth evolution of these crystals. A gradual decrease of nitrogen content from the start of cuboid growth to the cuboid/octahedron boundary (in the range 410-540 ppm) in most cases is consistent with nitrogen depletion of fluid in the closed system. However in the follow nitrogen content continuously increases up to 560-980 ppm suggesting nitrogen being involved in diamond/fluid fractionation as an incompatible impurity. It is notable that in nitrogen-poor (less than 300 ppm) samples total nitrogen content slightly decreases in octahedral rim suggesting that nitrogen depletion of fluid continues at an octahedral growth stage, and at low N concentration in fluid behaves as a compatible with a diamond. An infrared-active hydrogen (3107 and 1405 cm^{-1}) absorbance is mostly related to an microinclusions-rich cores pointing to its presence of the interfaces of microinclusions or "disc-crack-like" defects common for cuboids **[5]**.

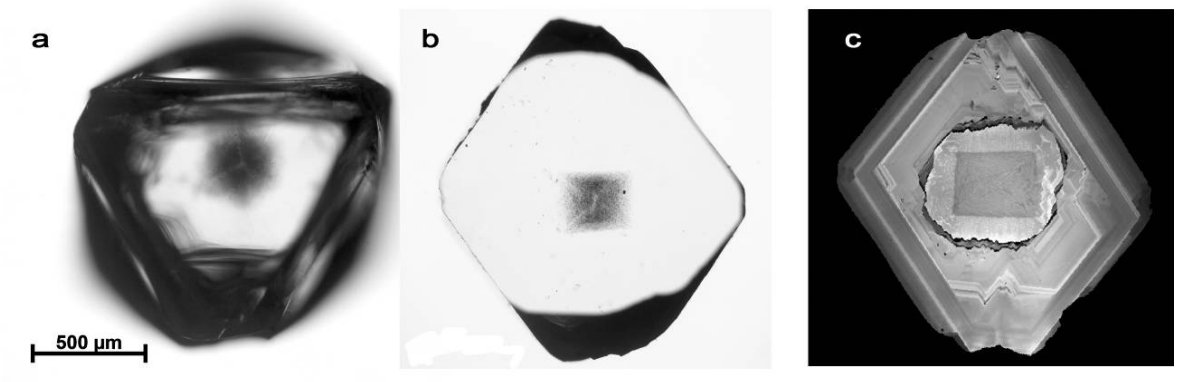

Figure. 1. General habit (a), micrograph of a thin plate (b) and CL image (c) of MS-3 diamond.

Local variations of carbon isotope composition have been analyzed in two samples. Data obtained show the enrichment of octahedral zone with ^{13}C relative to the cuboid core. The $\delta^{13}C$

values in one sample (-5,0÷-5,6‰) are similar to the average mantle and heavier for another (-4,1÷-3,0‰). It assumes their different carbon source or isotope fractionation from a heterogeneous source.

Microinclusions in studied diamonds are characterized by a variety of compositions ranging from carbonate to silicic (fig. 2) with a decrease in chlorine content towards a silica-rich end member. There are two compositional groups: (1) the group having $H_2O/(H_2O+CO_2)$ ratio of 0.04-0.12 and showing strong enrichment in Ca-Mg-Fe with a supporting absorption lines of dolomite (1450 and 880 cm^{-1}) and calcite (1430 and 877 cm^{-1}), low SiO_2 and Al_2O_3, (2) the second one having $H_2O/(H_2O+CO_2)$ up to 0.44 with a strong valence band of molecular water (1660 cm^{-1}) and silicates/quartz (1090, 810, 785 cm^{-1}), the lowest Ca content and high SiO_2 and Al_2O_3. Notably microinclusions of the group I are contained in most of studied diamonds, one of diamonds (MS-2) contain only high-Si microinclusions of group II, but within diamonds microinclusions of both groups show no clear spatial relationship and no intermediate compositions (marked with arrows on fig. 2).

The uncertainties detected in this study may be due to (1) not sufficient diamond population that could fill a compositional "gap" (but could not explain a presence of both silica-rich and carbonatitic microinclusions in the same sample) and/or (2) the process of liquation between hydrous-silicic fluid and carbonatite-silicate fluid/melt **[6]**. The immiscibility model along with the diamond growth from two different HDF's simultaneously goes in conflict with a number of experimental data with the exception of **[7]**, but these data should further be examined carefully. Trace-element patterns of studied microinclusions may give some clues to problem.

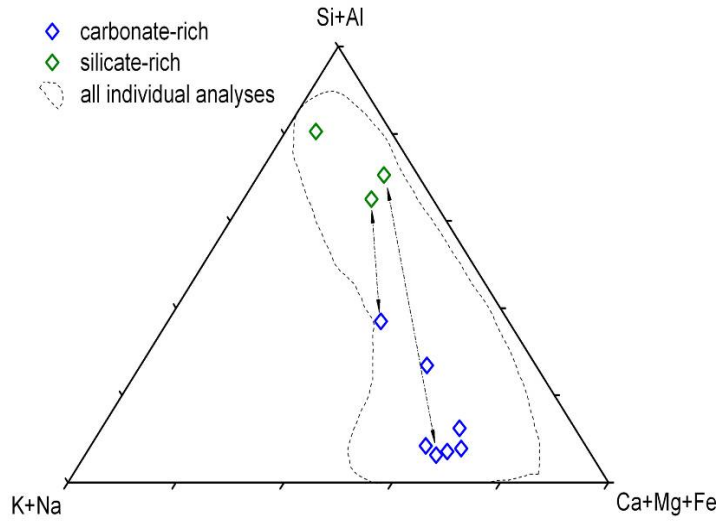

Figure 2. Composition of trapped HDF in studied cloudy diamonds

References:

[1] Chrenko, R.M., McDonald, R.S., Darrow, K.A., 1967. Infra-red spectrum of diamond coat. Nature 213 (5075), 474–476.

[2] Navon, O., Hutcheon, I.D., Rossman, G.R., Wasserburg, G.J., 1988. Mantle-derived fluids in diamond micro-inclusions. Nature 335 (6193), 784–789.

[3] Schrauder, M., Navon, O., 1994. Hydrous and carbonatitic mantle fluids in fibrous diamonds from Jwaneng, Botswana. Geochim. Cosmochim. Acta 58 (2), 761–771.

[4] Klein-BenDavid, O., Izraeli, E.S., Hauri, E., Navon, O., 2004. Mantle fluid evolution — a tale of one diamond. Lithos 77 (1–4), 243–253.

[5] Walmsley, J.C., Lang, A.R., Rooney, M-L.T., Welbourn, C.M., 1987. Newly observed microscopic planar defects on {111} in natural diamond. Philos. Mag. Lett. 55, 209-213.

[6] Rege, S., Griffin, W.L., Pearson, N.J., Araujo, D., Zedgenizov, D., O'Reilly, S.Y., 2010. Trace-element patterns of fibrous and monocrystalline diamonds: Insights into mantle fluids. Lithos 118, 313-337.

[7] Bureau, P., Langenhorst, F., Auzende, A.-L., Frost, D.J., Esteve, I., Siebert, J., 2012. The growth of fibrous, cloudy and polycrystalline diamonds. Geochimica et Cosmochimica Acta 77, 202–214.

THE REDUCED FLUID FLOWS DURING KIMBERLITE-FORMING CYCLES: THEIR CONNECTION WITH MASS EXTINCTION AND HYDROCARBON DEPOSITES

Solov'eva L.V. [1], ***Matveev S.*** [2]

[1] *Institute of Earth Crust SB RAS, Irkutsk, Russia*
[2] *Departament of Earth and Atmospheric Sciences, University of Alberta, Edmonton, Canada*
Solv777@crust.irk.ru

The modern approach considers the correlation between global events such as supercontinents, plumes, rifting, appearance of large igneous provinces (LIP), kimberlite magmatism, global anoxia of athmosphere and ocean, mass extinction [1, 2, 3]. The plume rising, cracking continent by rifting, and powerful flows of subcontinental flood basalt (CFB) caused increasing CO_2, H_2S, CH_4 invasion, developing anoxic environment and mass extinction of sea and overland biota. The hypothesis was confirmed by shift of isotopic values $\delta^{13}C$, $\delta^{34}S$, $\delta^{15}N$, $\delta^{18}O$, $^{87/86}Sr$ and geochemistry features of black shists (claystone, limestone, chert) sedimented during anoxia and mass biota extinction. The Middle-Paleozoic diamondiferous kimberlite cycle was initiated by Yakutian plume rising, tracing by geological features [4] and chemical composition of lithosphere substance [5]. The melts parental for CFB were formed under lithosphere plate base before kimberlite formation and then produced the low-Cr megacryst association and distinctive deep-seated blastomylonites – deformed peridotites [6]. LIPs linking with flood basalt flows appeared also in Pripyat-Dnieper-Donets region and Kola peninsula at Upper-Devonian. At this particular time the mass extinction of living creatures was evident. The most probably these three CFB provinces resulted from secondary plumes deriving from Middle-Paleozoic plume in transition mantle zone.

The lower mantle lithosphere beneath Siberian craton was intensively modified by reduced fluids at the beginning of kimberlite cycle [5]. The fluids were caused reaction metasomatites with graphite. The olivines from prekimberlite reaction metasomatites contain high H_2O concentration (160-300 wt ppm in Ol from metasomatised lherzolites) (Fig. 1) whereas olivines from coarse-grained peridotites without modal metasomatic traces contain 0-15 ppm of H_2O.

The wave spectra of metasomatic olivines refer to 1A 1R group and are similar to spectra of olivines in hydrogenation experiments at annealing and high pressure [7]. According to hydrogenation reaction ($Fe^{3+} + O^{2-} + 1/2H_2 = Fe^{2+} + OH^-$ [8]) H_2 penetration in olivine matrix leads to Fe^{3+} reducing to Fe^{2+}. High-pressure experiments indicate that H_2 is well dissolved in reduced melts and increase the carbon solution in the form of C-H (precursor of CH_4). It may supposed that huge flow of reduced fluids (containing CH_4, H_2, NH_3 and another reduced gases) come from asthenosphere before Middle-Paleozoic basite eruption. On one hand, these fluid flows reduced oxidated gases buried in mantle lithosphere, on another hand the native carbon (in the form of diamond or graphite) was precipitated on the oxidated barrier [5]. Intensive diamond crystallization is thought to occur in boiling melt layer when reduced gases (CH_4, H_2) separating. It is supposed that the global anoxia and mass extinction connect with the reduced gases flows reaching surface before CFB effusion. In addition, total ocean level regression and continental rifting created conditions for anaerobic biota development producing oil maternal beds [10]. The reduced fluid hypothesis is confirmed by the hard-to-explain fact that positive shift $\delta^{13}C_{org}$ at anoxia maximum [3]. The mantle carbon is heavier than organic matter [11]. It is assumed that mantle carbon reach the atmosphere and hydrosphere more later than degasified hydrates, this delay is fixed by maximum $\delta^{13}C$ during anoxia peak. Thus, deposits of kimberlite diamonds and hydrocarbons connected with the same reason and substance (mantle carbon and nitrogen).

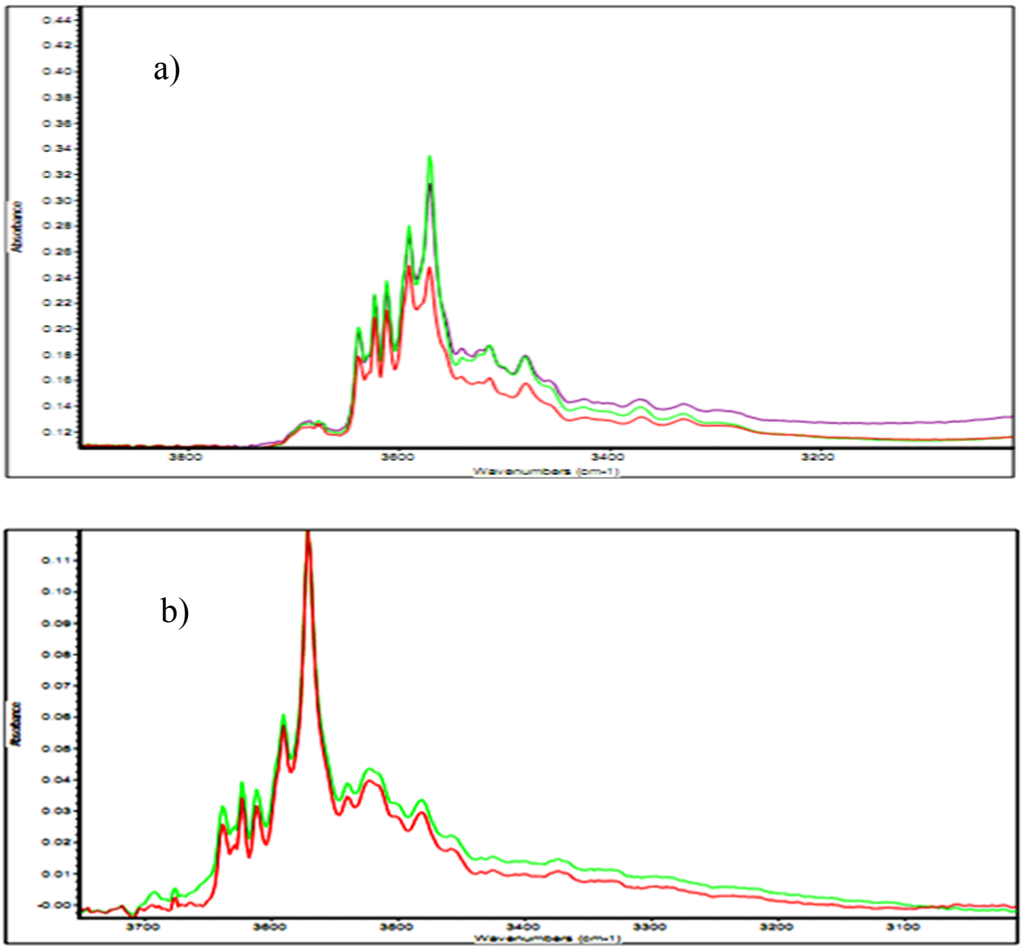

Figure. 1. Representative spectra of three (a) and two (b) olivine grains from metasomatized garnet lerzolithe xenoliths (kimberlite pipe Udachnaya). Group 1A 1R spectra predominate, content OH – group in olivine (a) 300 ± 20 and (b) 160 ± 20 wt. ppm.

References:

[1] Isozaki Y. Journal of Asian Earth Sciences. 2009. V. 36. P. 459-480.
[2] Morgan J.P. et al. Earth Planet. Science. Letters. 2004. V. 217. P. 263 – 284.
[3] Takahashi et al. Palaeogeography, Palaeoclimatology, Palaeoecology. 2010. V. 292. P. 532-539.
[4] Kiselev et al. Journal Asian Earth Sciences. 2012. V. 45. № 2. P. 1 – 16.
[5] Solov'eva L.V. et al. Russian Geology and Geophysics. 2012. V.53. P. 1304-1323.
[6] Solov'eva L.V. Russian Geology and Geophysics. 2008. V. 49. P. 207-224.
[7] Matveev S., Stachel T. Geochim. Cosmochim. Acta. 2007. V. 71. P. 5528 – 5543.
[8] Peslier et al. 2006. 16 annual V.M. Goldschmidt Intern. Conf. (abstr.)
[9] Kadik A. et al. Geochemistry. 2006. №1. P. 38-53.
[10] Hain V.E., Polyakova I.D. Geologiya. 2010. №4. P. 506-509.
[11] Cartigny P. et al. Lithos. 2009. V. 112. P. 852-864.

PHYSICAL PROPERTIES OF DIAMONDS IN ECLOGITE AND PERIDOTITE XENOLITHS FROM THE NYURBINSKAYA KIMBERLITE PIPE, YAKUTIA

***Spetsius Z.V.*, Bogush I.N. and Kovalchuck O.E.**
Scientific Investigation Geology Enterprise, ALROSA Co, Mirny, Russia
spetsiuszv@alrosa.ru

Diamonds from the Nyurbinskaya and other pipes of the Nakynsky fields are unique by their morphology and some physical properties [1, 3]. For the understanding of their growth history from three eclogite and two peridotite xenoliths were taken crystals -4+2 mm and polished plates 0,4-0,7 mm have been made. It was determined photoluminescence (FL) of diamonds, initiated by nitrogen laser LGI-505 and nitrogen content mapping in plates obtained according their IK-spectrum. Plates were analyzed by micro-Fourier transform infrared (FTIR) spectroscopy to determine nitrogen and hydrogen contents, nitrogen aggregation state and. B2-defects (platelets). IR spectra were obtained over the range of 600-4500 cm^{-1} with the use of Vertex 70 FTIR spectrometer and Hyperion 2000 microscope. The spectra resolution was 1 cm^{-1}; the number of points – (800 – 1000). Errors in nitrogen content (N_{FTIR}) and nitrogen aggregation state are estimated to be less than 20% and 5% respectively.

Eclogite Plate N65. Diamond has brightly green photoluminescence with two yellow-green phantoms located in the center of crystal. It is distinguished internal rounding area with the nitrogen content 440 at. ppm (Fig. 1). Second zone is presented by two crystals that were intergrown subsequently. The nitrogen concentration in the time of growth is varies here from 760 to 150 at. ppm and its content in the B-form – from 25 to 15% respectively. This zone is sharply replaced by third zone with high (up to 840 at. ppm) concentration of nitrogen admixture. Intensity of the band B2-defect is changed stepwise from 6 to 0,5 cm^{-1} that correlate with general content of the nitrogen. The coefficient of the absorption of the band on 3107 cm^{-1}, which involve with admixture of the hydrogen, sharply increases up to 17 cm^{-1} at the beginning of the second zone and is falling then up to disappearance. Jump (about 4 cm^{-1}) of the hydrogen concentrations exists at the beginning of third zone (Fig. 1).

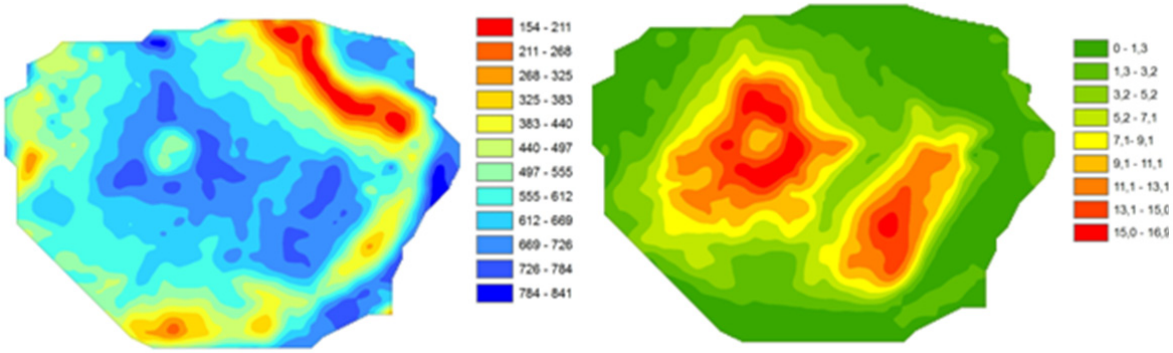

Figure 1. Distribution of nitrogen admixture (at. ppm) and hydrogen (in cm^{-1}) on the plate N65.

Eclogite Plate N60. Diamond has inner phantom with the brightly blue FL that is replaced by the area with the weak luminescence. Concentration of the nitrogen and its aggregation from the center to internal area is lowered from 800 to 60 at. ppm and from 60 to 10% respectively. This area is sharply replaced another with high (up to 830 at. ppm) concentration this admixture and with 25% contents in B1-form and small line B2-defect. The beginning of second area stands out by the narrow band on distribution of hydrogen admixture - stepwise (from 0.3 to 3.0 and again up to 0.1 cm^{-1}). Here is changes line absorption on 3107 cm^{-1}.

Eclogite Plate N1. Diamond has green FL with the dark-green phantom in the center of crystal. By the nitrogen concentration is stands out comparatively uniform internal area with

very small contents of the nitrogen - about 50 at. ppm and with 10-20% in B1-form. This area is sharply replaced by the following zone with high (about 1000 at. ppm) concentrations of main admixture. The intensity of the band B2-defect and position of its maximum also are sharply changed from 0.5 to 3.5 cm^{-1} and from 1360 on 1373 cm^{-1} accordingly. The absorption of the band on 3107 cm^{-1} in central area is not registered, but sharply increases up to 6 cm^{-1} at the beginning of the second zone and falling than up to disappearance to the periphery of the crystal.

Peridotite Plate N98. Diamond has blue FL with lower green phantom in the center of crystal. The concentration of the nitrogen and its aggregation is lowered from the center to periphery of the crystal from 1400 to 370 at. ppm and from 45 to 28% respectively. The line absorption on 3107 cm^{-1} is changed stepwise from 6.0 cm^{-1} (for internal phantom with green FL) before 0.1 cm^{-1} in the field of with blue FL.

Peridotite Plate N95. Diamond has blue FL. Concentration of the total nitrogen and its aggregation from the center to the rim of the crystal is lowered from 450 to 150 at. ppm and from 24 to 16% subsequently. The line absorption on 3107 cm^{-1} in the center is about 1.9 cm^{-1}, then sharply falls before disappearance to the periphery of the crystal.

In the result it is possible to conclude that diamonds from eclogite xenoliths from the Nyurbinskaya pipe often are zonal and have a complex genetic history. The essential difference in nitrogen admixture and degree of the aggregations in separate zone some crystal points to the different times of annealing of these areas, coming from the kinetic of nitrogen aggregations [2].

The given fact it is possible to explain by the discreteness of the diamond formation in several temporary stages that are corresponding to different diamond generation. The general trend installed for probable selected generation, is a consequent reduction of the total nitrogen contents and its aggregations from the center of the crystals to their periphery. For studied crystals from peridotite xenoliths signs of discreteness their formation is not revealed, supposedly, they correspond to one generation. Fixed changes, corresponding to practically united parameter Kt [2], are possible only under a certain increasing of the temperature in process of formation of one zone. By that FL-colour of different areas more depends on the aggregations degree than from concentration of the nitrogen.

The interesting fact is a sharp jump to the concentrations hydrogen admixture at the beginning initially formation of each new zone, corresponding to separate generation. On our opinion, these data are indicative of changing of oxygen-reduction conditions in the course of crystallizations diamond consequent generation. For the beginning of the formation of diamond generations, probably, are typical reducing conditions and comparatively minimal temperatures.

In the whole for the diamond population from the kimberlites of the Nyurbinskaya pipe are typical high nitrogen crystals with small degree of the nitrogen aggregations that points to big contribution to the diamond population of this pipe of late generation growing crystals. The diamonds of this pipe often are zonal and contain inclusions of eclogitic paragenesis [3] that allows expecting the high percent crystals of eclogitic genesis. The number of facts witnesses in the favor of their formation in metasomatic process from the fluid or fluid-melt that has defined typomorphic features of diamonds and has conditioned a high productivity of this pipe.

References:

[1] Bogush I.N.., Mironov V.P, Mitukhin S.I. Characteristics' of diamonds of Nakynsky kimberlite field according to spectroscopic data // Problems of diamonds geology and some ways of their decisions. Voroneg, VGU publ., 2001, p. 359-368. (in Russian).

[2] Evans T., Qi Z. The kinetics of aggregation of nitrogen atoms in diamonds // Proc. Roy. Soc. London, 1982, A381, p. 238-242.

[3] Spetsius Z.V., Mitukhin S.I., Ivanov A.S., Banzeruk S.V., 2005. Paragenesis of inclusions in diamonds from the Botuobinskaya pipe (Nakynsky field, Yakutia). Dokl. Akad. Nauk, v. 403., N 2, p. 248-252 (in Russian).

SYNTHESIS OF HEAVY HYDROCARBONS AT THE EARTH'S UPPER MANTLE TEMPERATURE AND PRESSURE

***Tomilenko A.A.*, Chepurov A.I., Sonin V.M., Bul'bak T.A., Zhimulev E.I.**

V.S. Sobolev Institute of Geology and Mineralogy SB RAS, Novosibirsk, Russia
tomilen@igm.ncs.ru

The Earth's mantle, especially upper mantle, is strongly stratified by the redox conditions [1]. Hence there is a main trend of the mantle against this background – the decrease of oxygen fugacity with the depth. According to the modern view, the stability zone of the oxidized form of carbon (carbonates) gives way to the conditions where the elementary forms of carbon (graphite/diamond) have become stable at a depth of 150 km [2]. At a depth of about 250 km red-ox conditions of the upper mantle correspond to the stability of metallic iron [3, 4]. Considering these data, a possibility of decomposition of carbonates arriving into the mantle in the subduction zones with formation of carbon solid phases (graphite/diamond) and volatiles (hydrocarbons) is of great interest within the concept of the global carbon cycle.

The formation of hydrocarbons is especially topical in the debate on their possible abiotic genesis. In the experiments [5-8] an effort has been made to synthesize hydrocarbons at P-T parameters of the upper mantle from $CaCO_3$ in the presence of H_2O. FeO or metallic Fe have been used as reducing agents. High pressure equipment of different type has been used in the experiments. Decomposition of $CaCO_3$ has been observed in all cases. CH_4 has been observed as a main product. Furthermore, mixture of hydrocarbons (up to C_4H_8 and trace amounts of C_4H_{10}, C_5H_{12}) corresponding in composition to the hydrocarbon part of natural gas has been obtained in [7]. Synthesis of heavy hydrocarbons (HH), which are the components of oil, at temperatures and pressures of the upper mantle has not met with success.

The first results on HH synthesis at high P-T parameters are given in this report. The experiment has been carried out using the multi-anvil high pressure apparatus of "split-sphere" type in the working cell on the basis of ZrO_2 and MgO oxides with tubular graphite heater in the following regime: pressure rise, sample heating and fast cooling (quenching) after the exposure under the given P-T parameters. The details of the experimental procedure are given in the monograph [9]. HH have been synthesized in the system $MgCO_3$ (7.7 mg) – $Ca(OH)_2$ (7.0 mg) - Fe_{metal} (26.0 mg) – SiO_2 (11.1 mg). Crushed and mixed components have been placed into Ti-ampoule (6 mm long, 5.0/3.3 mm in diameter 328.4 in weight) which has been in turn placed into Pt-ampoule. Pt-ampoule was sealed by arc welding. Ti has been used as an absorber of oxygen forming during CO_2 and H_2O reduction because the experiment has been carried out in the closed system (to preserve volatiles). The experimental parameters: 3GPa, 1400^{o}C, 24 hours. After the experiment the volatiles have been analyzed by chromatography mass-spectrometry. Pt-ampoule has been opened with punch in the special attachment. The following composition of volatiles has been found: 1 - permanent gases: Nitrogen (N_2), Carbon dioxide (CO_2), Water (H_2O); 2 - n-alkanes [saturated hydrocarbons (C_nH_{2n+2}) and their derivatives]: Methane (CH_4), Butane (C_4H_{10}), Isobutane (C_4H_{10}), Pentane (C_5H_{12}), Pentane, 3-methyl (C_6H_{14}), Hexane (C_6H_{14}), Heptane (C_7H_{16}), Octane (C_8H_{18}), Nonane (C_9H_{20}), Decane ($C_{10}H_{22}$), Undecane ($C_{11}H_{24}$), Dodecane ($C_{12}H_{26}$), Tetradecane ($C_{14}H_{30}$), Pentadecane ($C_{15}H_{32}$), Hexadecane ($C_{16}H_{34}$); 3 – aldehydes: ($C_nH_{2n+1}COH$, R–COH): Butanal (C_4H_8O), Pentanal ($C_5H_{10}O$), Hexanal ($C_6H_{12}O$), Heptanal ($C_7H_{14}O$), Octanal ($C_8H_{16}O$), Nonanal ($C_9H_{18}O$), Decanal ($C_{10}H_{20}O$); 4 – saturated monohydric alcohols: ($C_nH_{2n+1}OH$, R–O–H): 1-Hexanol, 2-ethyl ($C_8H_{18}O$); 5 – ketones: (R1-CO-R2): 2-Propanone (C_3H_6O), 2-Hexanone ($C_6H_{12}O$).

Microprobe analysis has revealed the following phases in the solid part of the sample: wustite, olivine, periclase, perovskite. Unreacted portion of H_2O has been concentrated in brucite in the interstices between the grains of the main phases.

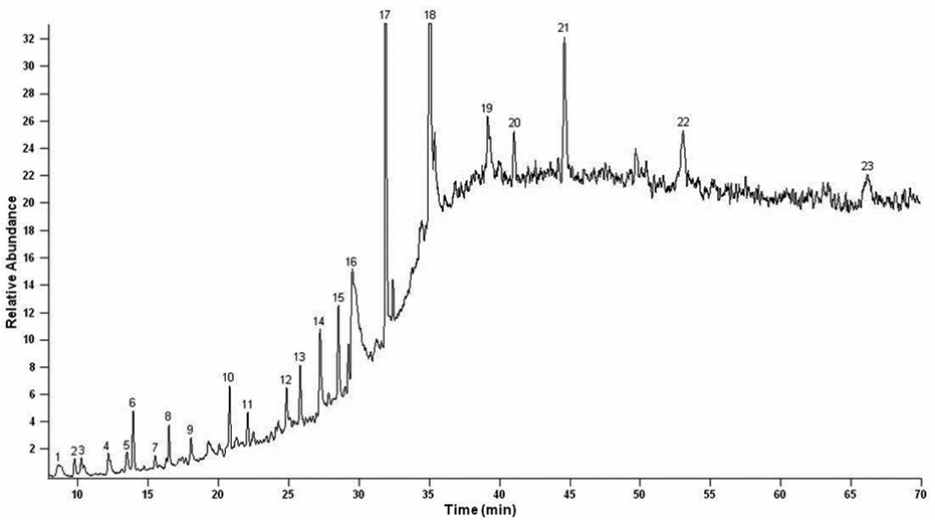

Figure 1. Chromatogram fragment of the volatiles released with the products of the experiment in $MgCO_3$-$Ca(OH)_2$-SiO_2-Fe met. System, when Pt-ampoule has been opened. 1 - Butane (C_4H_{10}); 2 - Isobutane (C_4H_{10}); 3 - Pentane (C_5H_{12}); 4 - Butanal (C_4H_8O); 5 - Pentane, 3-methyl (C_6H_{14}); 6 - Hexane (C_6H_{14}); 7 - 2-Hexanone ($C_6H_{12}O$); 8 - Pentanal ($C_5H_{10}O$); 9 -Heptane (C_7H_{16}); 10 - Hexanal ($C_6H_{12}O$); 11 - Octane (C_8H_{18}); 12 - Heptanal ($C_7H_{14}O$); 13 - Nonane (C_9H_{20}); 14 – non-identified; 15 - Octanal ($C_8H_{16}O$); 16 - 1-Hexanol, 2-ethyl ($C_8H_{18}O$); 17 - Nonanal ($C_9H_{18}O$); 18 - Decanal ($C_{10}H_{20}O$); 19 - Dodecane ($C_{12}H_{26}$); 20 - non-identified; 21 - Tetradecane ($C_{14}H_{30}$); 22- Pentadecane ($C_{15}H_{32}$); 23 - Hexadecane ($C_{16}H_{34}$).

We have thereby synthesized HH at the upper mantle temperature and pressure from magnesium carbonate in the presence of H_2O. In this mode of hydrocarbons formation oxygen binding is the basic challenge. However, with respect to natural inorganic synthesis of heavy hydrocarbons it should be noted that the amount of oxidized CO_2 and H_2O incoming into the mantle with subducting oceanic plates is not comparable with the volume of more reduced Earth's mantle.

References:

[1] Creighton S., Stachel T., Matveev S. et al. // Contrib. Mineral. Petrol. 2009. 157. 491-504.
[2] Stagno V., Frost D.J. // Earth Planet. Sci. Lett. 2010. 300. 72-84.
[3] Rohrbach A., Ballhaus C., Gola-Schindler U. et al. // Nature. 2007. 449. 456-458.
[4] Frost D.J., McCammon C.A. // Annu. Rev. Earth Planet. Sci. 2008. 36. 389-420.
[5] Kenney J.F., Kutcherov V.G., Bendeliani N.A., Alekseev V.A. // PNAS. 2002. 99. 10976-10981.
[6] Scott H.P., Hemley R.J., Mao H. et al. // PNAS. 2004. 101. 1423-1426.
[7] Kutcherov V.G., Kolesnikov A.Yu., Dyuzheva T.I. et al. // Doklady Physical Chemistry. 2010. 433. 132-135.
[8] Chepurov A.I., Sonin V.M., Zhimulev E.I. et al. // Doklady Earth Sciences. 2011. 441. 1738-1741.
[9] Chepurov A.I., Fedorov I.I., Sonin V.M. Experimental modeling of the diamond formation processes. Novosibirsk, Published by SB RAS, SPC UIGGM, 1997. 196p.

HETEROGENOUS CARBON RESERVOIR IN SUBLITHOSPHERIC MANTLE: EVIDENCE FROM LOCAL VARIATIONS OF CARBON ISOTOPIC COMPOSITION IN DIAMONDS FROM SAO-LUIS (BRAZIL)

Zedgenizov D.A. [1], ***Kagi H.*** [2], ***Shatsky V.S.*** [3], ***Ragozin A.L.*** [1]

[1] *V.S.Sobolev Institute of Geology and Mineralogy, Novosibirsk, Russia*
[2] *Tokyo University, Tokyo, Japan*
[3] *A.V.Vinogradov Institute of Geochemistry, Irkutsk, Russia*
zed@igm.nsc.ru

The Juina kimberlite field in Brazil is a well-known source of alluvial sublithospheric diamonds as identified by their properties and mineral inclusions **[1-5]**. Taking advantage of the rather common occurrence of superdeep mineral inclusion assemblages in diamonds from Sao-Luis river alluvial deposits (Juina, Brazil), we carried out a study of variations of C isotope in diamonds from this locality. In this study, we examined any core to rim primary zonation and syngenetic inclusions in 69 diamonds to document the nature of deep mantle compositions, and to interpret evolution of diamond forming media within sublithospheric mantle. The diamonds were polished in order to expose inclusions for analysis and to recover growth history and analyze carbon isotope composition and nitrogen content in different growth zones. Local variations in the carbon isotopic composition were determined by SIMS.

Diamonds from Sao-Luis are characterized by rough morphologies and have complex growth histories. CL imaging displays two or more growth domains in many diamonds. Episodic growth, plastic deformation and breakages are visible in these crystals and most diamonds have experienced a final episode of resorption before exhumation. Total nitrogen content in studied diamonds may reach 1200 ppm and more. There are large variations in some individual diamonds. Only several studied diamonds are nitrogen-free (type II). Some diamonds consist of domains that are also nitrogen-free but other parts may contain nitrogen. Many diamonds have very low (> 10 ppm) but still detectable nitrogen amount. There is an apparent tendency for the hydrogen peak intensity to increase with increasing the nitrogen content. It gives support to the idea that the conditions favouring the incorporation of nitrogen in these diamonds might also favour the incorporation of hydrogen. Extremely high nitrogen aggregation state and overall platelet degradation detected in the majority diamonds from Sao-Luis are suggested they have stored at considerably higher temperatures that are typical for continental lithosphere.

Syngenetic inclusions in 59 diamonds from Sao-Luis were represented by phases of superdeep paragenesis as it was described previously. The dominated inclusions are majoritic garnets, ferropericlases, CaSi- and CaSiTi-perovskites, MgSi-perovskites, TAPP, phases of SiO_2, kyanites, AlSi-phases, olivines and Fe-sulfides. Rare inclusions of clinopyroxenes, KFsp (K-hollandite?), CF, NAL, grossular, native iron, magnesite, $CaCO_3$+$CaMgSi_2O_6$ (composite inclusions) have been found in separate diamonds. All majoritic garnets we found are of metabasic affinity and in some cases associated with omphacitic clinopyroxenes.

The studied diamonds from Sao-Luis display wide variations of carbon isotopic compositions ($\delta^{13}C$) from 2.7 to -25.3 ‰. The diamonds with inclusions of ferropericlase have very narrow range of $\delta^{13}C$ values from -2.1 to -7.7 ‰, which are closely similar to the "normal" mantle values **[6, 7]**. From this observation, it may be suggested that their formation may proceed from isotopically homogeneous mantle reservoir that do not support the model of large primordial isotopic variability of carbon isotopes in primitive Earth's mantle with a predicted "pyrolite" composition. Diamonds with inclusions of majoritic garnet and CaSi- and CaSiTi-perovskites in many cases show marked differences from the expected "normal" mantle values of $\delta^{13}C$ values. Low $\delta^{13}C$ values (-10÷-25‰) have been observed exclusively in a series

superdeep diamonds with calcic-majorite garnets, Ca-silicates, aluminous silicates and SiO_2 from Sao-Luis.

The $\delta^{13}C$ measurements in core–rim traverses within some individual crystals varied substantially, indicating multi-stage growth histories. The variations in $\delta^{13}C$ within individual diamonds may be attributed to either different source of carbon or fractionation effect during diamond growth. No correlation of carbon isotope composition and nitrogen content has been found in an individual diamonds. It therefore appears that the cores and rims of the Sao-Luis diamonds precipitated from different fluids/melts with variable N/C ratios and/or under different growth conditions. The highly negative $\delta^{13}C$ values in the core (-20÷-25 ‰) potentially represent organic matter in sediments or altered basalts, and the lower $\delta^{13}C$ values may represent mixing trends towards "normal" mantle compositions **[5, 8, 9]**. In this study, we have also described a series of diamond which show opposite trend of change carbon source from primordial mantle to subducted/crustal (either biotic or abiotic carbon).

*This work is supported by IP SB RAS No 16 and the Ministry of education and science of Russian Federation, project No 14.B25.31.0032 an*d 14.B37.21.0601.

References:

[1] Harte B., Harris J.W., Hutchison M.T., Watt G.R., Wilding M.C. Lower mantle mineral associations in diamonds from São Luiz, Brazil. // Geochem. Soc. Spec. Publ. 1999. 6. 125-153.

[2] Hayman P.C, Kopylova M.G., Kaminsky F.V. Lower mantle diamonds from Rio Soriso (Juina area, Mato Grosso, Brazil) // Contrib. Miner. Petrol. 2005. 149. 430-445.

[3] Hutchison M.T., Hursthouse M.B., Light M.E. Mineral inclusions in diamonds: associations and chemical distinctions around the 670 km discontinuity // Contrib. Miner. Petrol. 2001. 142. 119-126.

[4] Kaminsky F.V., Zakharchenko O.D., Davies R., Griffin W.L., Khacatryan-Blinova G.K., Shiryaev A.A. Superdeep diamonds from the Juina area, Mato Grosso State, Brazil // Contrib. Miner. Petrol. 2001. 140. 734-753.

[5] Bulanova G.P., Walter M.J., Smith C.B., Kohn S.C., Armstrong L.S., Blundy J., Gobbo L. Mineral inclusions in sublithospheric diamonds from Collier 4 kimberlite pipe, Juina, Brazil: subducted protoliths, carbonated melts and primary kimberlite magmatism // Contrib. Miner. Petrol. 2010. 160. 489-510.

[6] Cartigny P. Stable isotopes and the origin of diamond // Elements. 2005. 1. 79-84.

[7] Stachel T., Harris J.W., Muehlenbachs K. Sources of carbon in inclusion bearing diamonds // Lithos. 2009. 112S. 625-637.

[8] Harte B. Diamond window into the lower mantle // Science. 2011. 334. 51-52.

[9] Schulze D.J., Harte B., Valley J.W., Channer D.M., de R. Evidence for subduction and crust-mantle mixing from a single diamond // Lithos. 2004. 77. 349-358.

DIAMOND CRYSTALLIZATION IN Fe-S-C SYSTEM

Zhimulev E.I.

[1] V.S.Sobolev Institute of Geology and Mineralogy, Novosibirsk, Russia
oda_stk@mail.ru

Sulfides are the most abundant inclusions in natural diamonds **[1]**. This fact raises question about their involvement in diamond genesis. Experimental study of the sulfide melt as possible diamond-forming medium covered a wide range of compositions of sulfur-containing systems – from pure sulfur **[2]** (S-C system) to sulfide-C systems **[3,4]**. It has been found that graphite crystallizes in sulfide melts at 5-6 GPa and 1200-1600^{o}C but higher temperatures and pressures are necessary for diamond synthesis and growth. On the other hand, 5-6 GPa and 900-1400^{o}C are geologically justified pressure and temperature intervals favorable to the diamond formation **[5]**. At the same time the experiments on diamond synthesis and growth didn't cover hypoeutectic area of Fe-S system. Diamond crystals have been obtained in our earlier studies in the systems Fe-Co-S-C and Fe-Ni-S-C at 5.5 GPa and 1300^{o}C in the melts with sulfur content less than 14 wt.%. This work demonstrates the results of studies of diamond growth in the system Fe-S-C with sulfur content of 5 wt.%. The experiments have been carried out on the multi-anvil high pressure apparatus of "split sphere" type at 5.5+0.2 GPa and 1350+25^{o}C during 21-25 hours. Two ampoule-sample assembly with the test and research ampoules has been used in the experiments. After the necessary exposure the sample has been quenched during 2-3 seconds.

Light-yellow or colorless octahedral diamond crystals with additional cube, rhombododecahedral and tetragonal-trioctahedral faces have been experimentally obtained. Metal-sulfide inclusions were present in the crystal volume therefore the crystals were severely cracked and disintegrated into fragments when extracted from the metal-catalyst. The study of two crystal shards has shown low nitrogen content within the accuracy of the instruments (the first ppm units) (Fig. 1). Probably sulfur introduced into the system influences on the nitrogen penetration into the structure.

Graphite, sulfide (pyrrhotite) and carbides (Fe_3C and Fe_7C_3) have been found in the growth charge according to the X-ray phase analysis. The following phases have been determined with the use of scanning electron microscope: carbide, sulfide and iron-carbon alloy.

It should be stressed that graphite crystallization has been observed in all experiments with sulfur addition along with diamond growth, whereas re-crystallized graphite has not been found in the test ampoule. Probably this phenomenon is conditioned by graphite and sulfur competition and as a result, metastable graphite grows. Metastable graphite has been also found in Fe-Ni-S-C and Fe-Co-S-C systems during diamond growth **[6,**7**]**.

It has been determined as a result of this work that diamond crystallizes in Fe-S-C system with 5 wt.% of sulfur at P-T parameters minimal for diamond synthesis and growth also typical of the metal-carbon systems.

Hence iron-sulfide melt is a diamond generating medium at relatively moderate P-T parameters and could participate in the processes of natural diamond formation.

The authors thank Yelisseev A.P. and Babitch Yu.V. for their assistance in the performance of this work. The work was supported by the research project (2013-2016, IGM SB RAS).

References:

[1].Bulanova G.P., Spetsius Z.V., Leskova N.V. Sulfides in diamonds and xenoliths from the kimberlite pipes of Yakutia. Novosibirsk: Nauka, 1990, 120p.
[2].Sato K., Katsura T. //J. Cryst. Growth. 2001. V.223 P.189-194.
[3].Wentorf R.H. // Adv. High-Pressure Res. 1974. P. 249-281.
[4] Shushkanova A.V., Litvin Yu.A.// DAN. 2006. V.409. N3. P. 394-398.
[5]. Boyd F.R., Finnerty A.A. // J. Geophys. Res. 1980. V. 85. P. 6911-6918.

[6] Chepurov A.I., Zhimulev Ye.I., Sonin V.M. et al.// DAN. 2009. V. 428. N1. P. 101-103.
[7] Zhimulev Ye.I., Chepurov A.I., Sinyakova Ey.F. et al.// Geochemistry. 2012. N3. P. 227-239.
[8] Chepurov A.I., Fedorov I.I., Sonin V.M. Experimental modeling of the diamond formation processes. Novosibirsk: RAS Publishing House, NSC UIGGM, 1997. 197 p.

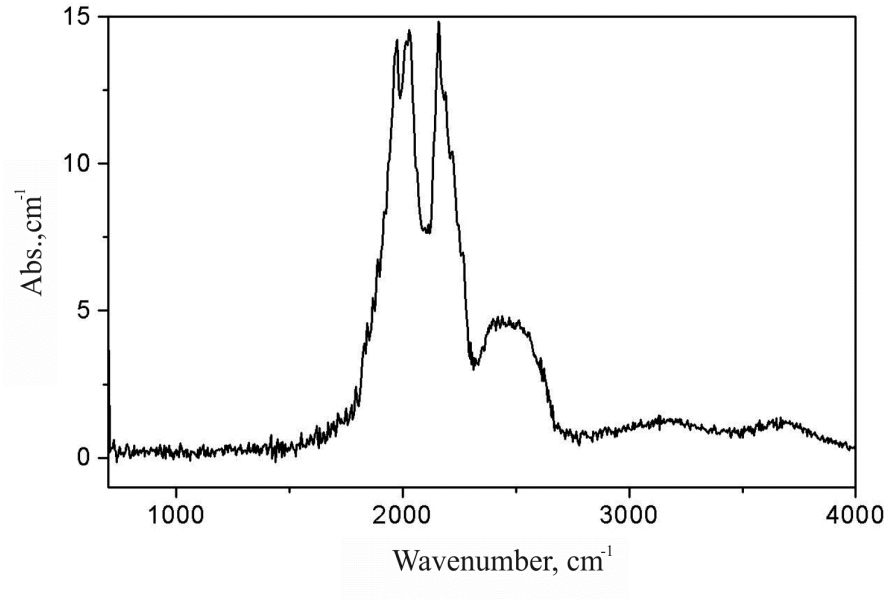

Figure 1. IR spectra of the sample from the experiment N 2-22-10 (FTIR spectrometer Infralum 801 in the mid-IR region).

CHARACTERIZATION AND LIMITS OF SOLID SOLUTIONS IN BINARY SYSTEMS OF THREONINE DIASTEREOMERS ACCORDING TO X-RAY DIFFRACTION DATA

Taratin N.V. [1]***, Binev D.*** [2]***, Lorenz H.*** [2]***, Seidel-Morgenstern A.*** [2]***, Kotelnikova E.N.*** [1]

[1] *St. Petersburg, St. Petersburg State University, Crystallography Department,*
[2] *Magdeburg, Max Planck Institute for Dynamics of Complex Technical Systems*
e-mail: taratinn@gmail.com

Complex mineralogical and crystal-chemical characterization of natural organic matter represents a challenging and unconventional task. Firstly, it should be noted that organic substances often occur in geological environments in disseminated state. Secondly, naturally occurring organic substances generally consist of complex multicomponent mixtures including different compounds, some polymorph modifications, solid solutions, homologues, isomers, stereoisomers, etc. Thirdly, various components of the mixtures can occur in different solid-phase states, for example, as crystalline, amorphous, and rotational-crystalline phases.

A lot of organic molecules have chiral structures. In general chirality results from the fact that a chiral structure contains at least one asymmetrical carbon atom. Usually this atom itself represents a chiral center, exceptions being some rare cases. Other chiral elements can also be the reasons for chirality to occur: for example, a chiral axis (e.g. in an allene molecule), and a chiral plane (e.g. in a cyclohexane molecule). Organic compounds containing chiral molecules can naturally occur and can also be synthesized as various stereoisomers, i.e. enantiomers and diastereomers.

Systematic study of crystalline chiral organic substances and processes of their formation may provide a basis for (1) new fundamental knowledge of structure features of such molecular crystals, and (2) practical implementation of a number of technological processes (in pharmaceutical and cosmetic industries, medicine, agrochemistry, food industry, etc.). Recent publications [1, 2] show that chirality is a subject of great interest for mineralogical-geochemical sciences. Indeed, this phenomenon can cast some light upon origin and subsequent transformations of an organic matter, which underwent various stages of fossilization. In other words, levorotatory (L) and dextrorotary (D) enantiomers and their molecular ratios (L/D) can be used as bio-organogenous markers of various geological environments. Importance of chirality in nature can be shown by the fact that only one out of twenty known proteogenic amino acids is not a chiral compound. All the above demonstrates the significance of simulation analysis of processes occurring during crystallization of chiral organic compounds in various chiral and achiral media [2, 3].

This presentation summarizes results of crystallochemical investigation of an essential amino acid, threonine (*Thr*) HO_2C-$CH(NH_2)$-$CH(OH)$-CH_3. The amino acid molecule contains two different chiral centers, i.e. in accordance with the formula 2^n, where n is a number of chiral centers, threonine may have four different molecular configurations. Due to crucial differences in the locations of the chiral centers, these modifications were divided into threonine (*Thr*) and allothreonine (allo*Thr*) that consequently results in drawing up two enantiomeric systems L-*Thr*—D-*Thr* and L-allo*Thr*—D-allo*Thr*, and four diastereomeric systems: (1) L-*Thr*—L-allo*Thr*, (2) D-*Thr*—D-allo*Thr*, (3) L-*Thr*—D-allo*Thr*, and (4) D-*Thr*—L-allo*Thr*. The diastereomeric systems (1) and (2) are mutually alike, but differ significantly from systems (3) and (4), which are also similar to each other. Hence, it is sufficient to study one system for each of the diastereomeric pairs. Enantiomeric system L-*Thr*—D-*Thr* is characterized by formation of eutectic mixtures [4], while diastereomeric system L-*Thr*—L-allo*Thr* tends to form solid solutions (the present work).

X-ray diffraction patterns of L-*Thr*, L-allo*Thr* and their co-precipitated mixtures were indexed in the space group $P2_12_12_1$. Parameters of orthorhombic cell have been found to depend

upon molecular composition of the mixture (% L-*Thr*), which indicates formation of solid solutions in the system. Figure 1 (left) shows that in the first compositional region L-*Thr* (0 %)→L-*Thr* (55 %) parameter *a* decreases (Δ*a*=0.08 Å), while parameter *b* increases (Δ*b*=0.08 Å); in the second compositional region L-*Thr* (55 %)→L-*Thr* (100 %) values of the parameter *a* remain substantially stable, while the parameter *b* values tend to lower (Δ*b*=0.12 Å). In the whole compositional range (L-allo*Thr*→L-*Thr*), parameter *c* undergoes insignificant *(*Δ*c*=0.03 Å) and non-linear change. The opposite and/or different variations in the parameter values can be the reason of insignificant alteration of the orthorhombic cell volume *V* in the first compositional range and its gradual diminishing in the second compositional region (c and V not shown here).

Mode of shifting the peaks (2Θ) of the pairs *h*00–*hk*0 and *hk*0–0*k*0 in X-ray diffraction patterns and, consequently, dynamics of changing the *a*/*b* ratio, indicate existence of an intermediate compound near equimolar composition of the system. Figure 1 (right) shows that in a wide compositional range characteristic value of *a*/*b* is about √3 (1.732), which is an evidence of formation of a hexagonal cell. This suggests that in the said compositional range there is a possibility for solid solutions based upon an intermediate (hexagonal) compound to exist. The results of thermal X-ray analysis of L-*Thr* also support this conclusion. As a result of the continuous alteration of the orthorhombic cell parameters, at 200 ºC the cell acquires hexagonal symmetry (second-order phase transition). Similar isomorph-polymorph relations are typical for n-paraffins [5].

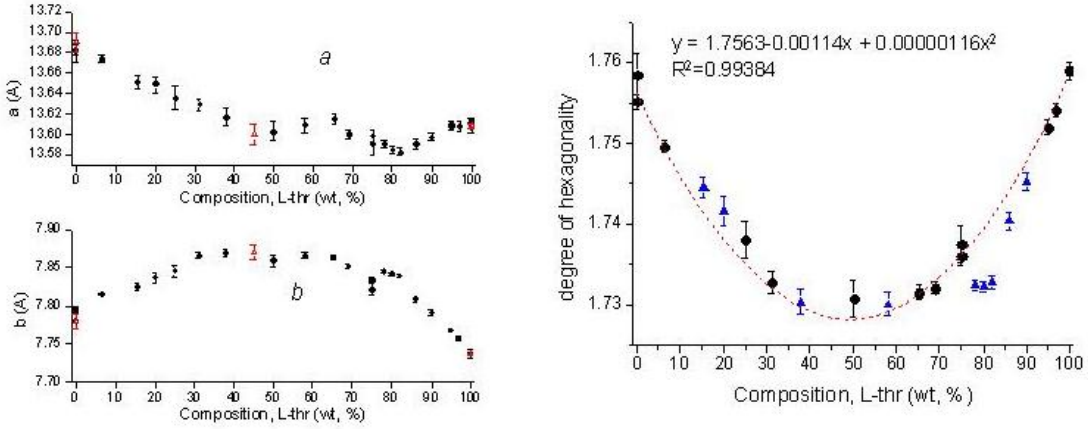

Figure 1. Alteration of parameters *a* and *b* (left) and parameter *a*/*b* or "hexagonality degree" (right) as a function of composition in the diastereomeric systems L-*Thr*—L-allo*Thr*.

Analysis of relative locations of the peaks in the pairs *2*00–110 and 310–020 (Δ2Θ) and hence differences in their interplanar spacing (Δd) forms the basis of a proposed express method allowing to determine single-phase (solid solutions) and two-phase (mixtures of solid solutions) regions in the diastereomeric systems L-*Thr*—L-allo*Thr* and L-*Thr*—D-allo*Thr*, respectively [4].

This work supported by RFBR grant 12-05-00876.

[1] De Torres T., Ortiz J.E., Arribas I., Delgado A., Julià R., Martín-Rubí J.A. Lethaia. 43 (2010), 149-163.

[2] Taratin N.V., Lorenz H., Kotelnikova E.N., Glikin A.E., Galland A., Dupray V., Coquerel G., Seidel-Morgenstern A. Cryst. Growth Des. 12 (2012), 5882-5888.

[3] Binev D., Taratin N., Lorenz H., Kotelnikova E., Seidel-Morgenstern A. (2013) in prep.

[4] Sapoundjiev D., Lorenz H., Seidel-Morgenstern A. Jour. Chem. Eng. Data. 51 (2006), 1526-1566.

[5] Kotelnikova E.N., Filatov S.K. Crystal chemistry of paraffins (Кристаллохимия парафинов). St.-Petersburg: Neva (2002), 352 pp. (Russ).

WHY WE NEED CRYSTALS GROWN BY OPTICAL FLOATING ZONE METHOD

Dabkowska H.A.

BIMR, McMaster University, Hamilton, Ont., Canada
dabkoh@mcmaster.ca

Over the past 60 years **single crystals** have become a key material in the field of computers, optics, optoelectronics, scintillators and information technology. For advanced investigating of physical and chemical properties of new **oxides** it is crucial to have good quality single crystals, since for polycrystalline samples the properties of grain boundaries often show themselves stronger than the properties of the material itself. Growing relatively large single crystals of oxides is possible by many methods like Czochralski, Bridgman, Verneuil or slow cooling, but in the search-for-new materials environment the optical floating zone (OFZ) method has many advantages over the other methods, allowing for growth of crystals which were not achievable before. This crucibles technique, where halogen lamps (or high pressure discharge tubes) are used as a convenient energy source, established itself as a powerful research tool. It is complementary to the conventional oxide crystal growth methods from melt or solution as it extends the range of materials which can be crystallized in different (from reducing to oxidizing) atmospheres and at elevated pressure.

In my talk I will be discussing the basics of the OFZ technique as well as growth and properties of some congruently and incongruently melting oxides obtained and their solid solutions.

References:

Dabkowska H.A., Dabkowski A.B. Crystal Growth of Oxides by Optical Floating Zone Technique. Experimental Approach to Defects Determination" in "Springer Handbook of Crystal Growth, Defects and Characterization", p. 367-392 by Springer-Verlag' Berlin Heidelberg New York Tokyo, 2010

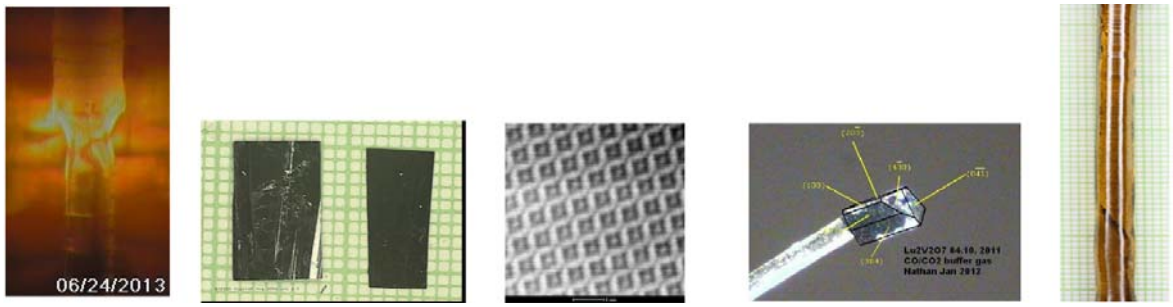

AUTHOR INDEX

TABLE OF CONTENTS

Научное издание

Тезисы докладов 3-й международной конференции
«Кристаллогенезис и минералогия»,
27 сентября – 1 октября 2013 г., Новосибирск

На английском языке

III International Conference “Crystallogenesis and mineralogy”
Abstracts Volume
Novosibirsk, 27 September – 1 October, 2013

Подписано к печати 23.08.2013.
Формат 60 x 84 ⅛.
Бумага офсетная. Печать офсетная. Гарнитура «Таймс».
Усл. печ. л. 41,1. Тираж 180 экз. Заказ №

Издательство СО РАН
630090, Новосибирск, Морской просп., 2
E-mail: psb@sibran.ru
тел. (383) 330-80-50

Отпечатано в Издательстве СО РАН

Partners and Sponsors

SIBERIAN BRANCH OF RUSSIAN ACADEMY OF SCIENCES

RUSSIAN FOUNDATION FOR BASIC RESEARCH

NOVOSIBIRSK STATE UNIVERSITY

INSTITUTE OF SOLID STATE CHEMISTRY
AND MECHANOCHEMISTRY

SAINT PETERSBOURG STATE UNIVERSITY

RUSSIAN MINERALOGICAL SOCIETY

INTERNATIONAL UNION OF CRYSTALLOGRAPHY

INTERNATIONAL MINERALOGICAL ASSOCIATION

MINISTRY OF EDUCATION AND SCIENCE
OF THE RUSSIAN FEDERATION

DEEP CARBON OBSERVATORY

ALROSA

Almax·easyLab
science under pressure

TechnoInfo

OPTEC
Connecting solutions

HUBER
Diffraction and Positioning Equipment